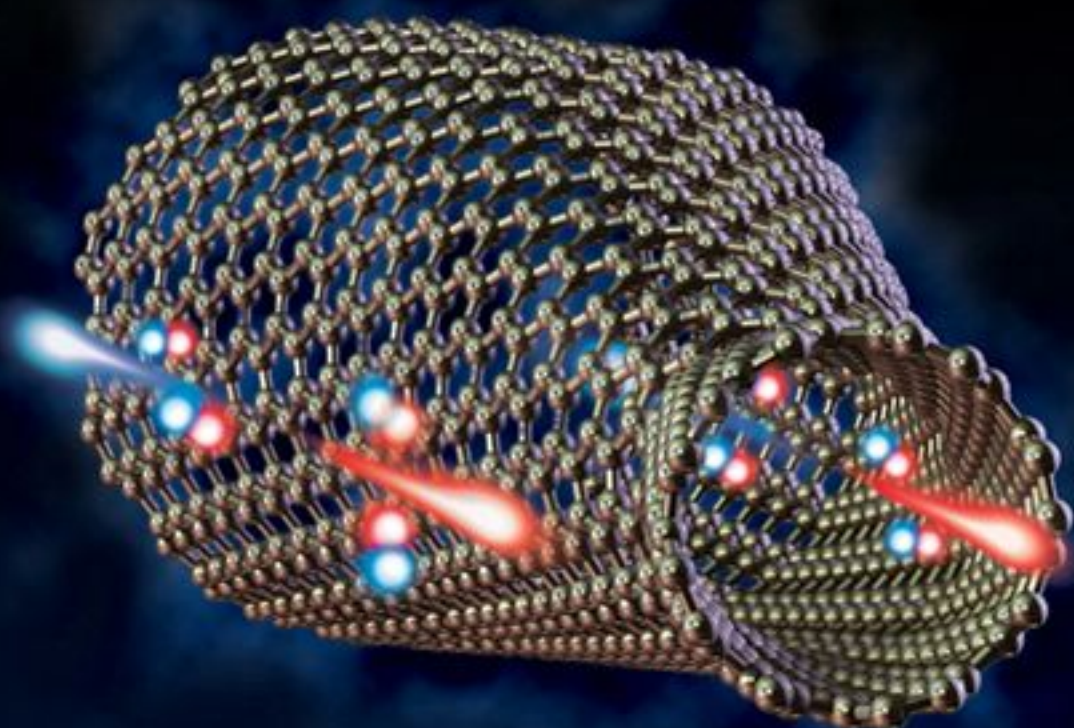


POLYMER NANOTUBE NANOCOMPOSITES

SYNTHESIS, PROPERTIES, AND APPLICATIONS



EDITED BY VIKAS MITTAL

 **WILEY**


Scrivener

This Page Intentionally Left Blank

Polymer Nanotube Nanocomposites

Scrivener Publishing
3 Winter Street, Suite 3
Salem, MA 01970

Scrivener Publishing Collections Editors

James E. R. Couper	Richard Erdlac
Rafiq Islam	Pradip Khaladkar
Vitthal Kulkarni	Norman Lieberman
Peter Martin	W. Kent Muhlbauer
Andrew Y. C. Nee	S. A. Sherif
James G. Speight	

Publishers at Scrivener

Martin Scrivener (martin@scrivenerpublishing.com)
Phillip Carmical (pcarmical@scrivenerpublishing.com)

Polymer Nanotube Nanocomposites

Synthesis, Properties,
and Applications

Vikas Mittal

BASF SE, Polymer Research, Germany



Scrivener



Copyright © 2010 by Scrivener Publishing LLC. All rights reserved.

Co-published by John Wiley & Sons, Inc. Hoboken, New Jersey, and Scrivener Publishing LLC, Salem, Massachusetts.

Published simultaneously in Canada.

No part of this publication may be reproduced, stored in a retrieval system, or transmitted in any form or by any means, electronic, mechanical, photocopying, recording, scanning, or otherwise, except as permitted under Section 107 or 108 of the 1976 United States Copyright Act, without either the prior written permission of the Publisher, or authorization through payment of the appropriate per-copy fee to the Copyright Clearance Center, Inc., 222 Rosewood Drive, Danvers, MA 01923, (978) 750-8400, fax (978) 750-4470, or on the web at www.copyright.com. Requests to the Publisher for permission should be addressed to the Permissions Department, John Wiley & Sons, Inc., 111 River Street, Hoboken, NJ 07030, (201) 748-6011, fax (201) 748-6008, or online at <http://www.wiley.com/go/permission>.

Limit of Liability/Disclaimer of Warranty: While the publisher and author have used their best efforts in preparing this book, they make no representations or warranties with respect to the accuracy or completeness of the contents of this book and specifically disclaim any implied warranties of merchantability or fitness for a particular purpose. No warranty may be created or extended by sales representatives or written sales materials. The advice and strategies contained herein may not be suitable for your situation. You should consult with a professional where appropriate. Neither the publisher nor author shall be liable for any loss of profit or any other commercial damages, including but not limited to special, incidental, consequential, or other damages.

For general information on our other products and services or for technical support, please contact our Customer Care Department within the United States at (800) 762-2974, outside the United States at (317) 572-3993 or fax (317) 572-4002.

Wiley also publishes its books in a variety of electronic formats. Some content that appears in print may not be available in electronic formats. For more information about Wiley products, visit our web site at www.wiley.com.

For more information about Scrivener products please visit www.scrivenerpublishing.com.

Cover design by Russell Richardson.

Library of Congress Cataloging-in-Publication Data:

ISBN 978-0-470-62592-7

Printed in the United States of America

10 9 8 7 6 5 4 3 2 1

Contents

Preface	xiii
1. Carbon Nanotubes: An Introduction	1
<i>V. Mittal</i>	
1.1 Introduction	1
1.2 Properties	4
1.3 Synthesis	8
References	12
2. Overview of Polymer Nanotube Nanocomposites	15
<i>V. Mittal</i>	
2.1 Introduction	15
2.2 Methods of Nanotube Nanocomposites Synthesis	18
2.2.1 Solution Mixing	18
2.2.2 <i>In-Situ</i> Polymerization	20
2.2.3 Melt Mixing	22
2.3 Properties of Polymer Nanotube Nanocomposites	25
2.3.1 Mechanical Properties	25
2.3.2 Thermal and Electrical Properties	34
References	42
3. New Microscopy Techniques for a Better Understanding of the Polymer/Nanotube Composite Properties	45
<i>K. Masenelli-Varlot, A. Bogner, C. Gauthier, L. Chazeau and J.Y. Cavaillé</i>	
3.1 Introduction	46
3.2 Near Field Microscopy	47
3.2.1 Principles of STM and AFM	48
3.2.2 Near Field Microscopy for Nanotubes	50
3.2.3 AFM and CNT Composites	50

3.3	Transmission Electron Microscopy	52
3.3.1	Principles	52
3.3.2	Characterisation of Carbon Nanotubes	56
3.3.3	Characterisation of Polymer/ Nanotube Composites	58
3.4	Scanning Electron Microscopy	67
3.4.1	Overview of the Technique (SEI, BEI, CCI)	67
3.4.2	Application to the Study of Nanotubes	68
3.4.3	For Polymer CNT/Nanocomposites	69
3.4.4	Development of New Imaging Modes	72
3.5	Conclusions	75
	References	77
4.	Polymer Nanocomposites with Clay and Carbon Nanotubes	83
	<i>Qiang Fu, Changyu Tang, Hua Deng and Qin Zhang</i>	
4.1	Introduction	83
4.2	Electrical Properties of Polymer Composites with Clay and CNTs	86
4.3	Mechanical Properties of Polymer Composites with Clay and CNTs	89
4.4	Thermal and Flame Properties of Polymer Composites with Clay and CNTs	100
4.5	Conclusion and Future Outlook	106
	Acknowledgement	108
	References	109
5.	Polyethylene Nanotube Nanocomposites	113
	<i>S. Kanagaraj</i>	
5.1	Introduction	113
5.2	Surface Modification of Carbon Nanotubes	115
5.3	Dispersion of Nanotubes in Polyethylene Matrix	117
5.4	Method of Preparation of CNT-PE Composites	119
5.5	Interfacial Bonding and Load Transfer	123
5.6	Material Characterization	126
5.7	Conclusions	135
	Acknowledgement	136
	References	136

6. Properties of Polyurethane/Carbon Nanotube Nanocomposites	141
<i>Tianxi Liu and Shuzhong Guo</i>	
6.1 Introduction	141
6.2 Preparation of CNT-Based Polyurethane Nanocomposites	144
6.2.1 Melt-Mixing	144
6.2.2 Solution Casting	145
6.2.3 <i>In-Situ</i> Polymerization	146
6.2.4 Sol-Gel Approach	147
6.3 Functionalization, Dispersion Morphology and Micro-/Nano-structures	148
6.4 Physical Properties	151
6.4.1 Mechanical Properties	151
6.4.2 Thermal Conductivity	154
6.4.3 Thermal Stability and Degradation	155
6.4.4 Fire Retardancy	156
6.4.5 Rheological Properties	157
6.4.6 Electrical Conductivity	158
6.4.7 Water Vapor Transport Properties	161
6.4.8 Shape Memory	162
6.4.9 Special Properties Related to Bio-Applications	165
6.4.10 Microwave Absorption	166
6.4.11 UV-Protection	167
6.5 Applications	168
6.6 Conclusions	170
Acknowledgements	171
References	171
 7. Properties of PMMA/Carbon Nanotubes Nanocomposites	 177
<i>R.B. Mathur, Shailaja Pande and B.P. Singh</i>	
7.1 Introduction	177
7.2 Fabrication/Processing of CNT-PMMA Composites	179
7.2.1 Solution Processing	181
7.2.2 Melt-Processing	183
7.2.3 <i>In-Situ</i> Polymerization Processing	185

7.2.4	Coagulation Method	186
7.2.5	Surfactant, Compatibilizers and Co-Solvent Assisted CNT-PMMA Composites	188
7.2.6	Chemical Modification of CNTs for Processing of Nanocomposites	189
7.3	Mechanical Properties of CNT-PMMA Composites	190
7.4	Electrical Properties of CNT-PMMA Composites	198
7.4.1	Electrical Conductivity	198
7.4.2	Electromagnetic Interference (EMI) Shielding	200
7.5	Thermal Properties	204
7.6	Conclusion	216
	References	216
8.	Synthesis of Vinyl Polymer/Carbon Nanotube Nanocomposites Prepared by Suspension Polymerization and Their Properties	221
	<i>P. Slobodian</i>	
8.1	Introduction	221
8.2	Free Radical Polymerization	223
8.3	Suspension and Bulk Polymerization Techniques	225
8.4	<i>In-situ</i> Radical Polymerization in Presence of CNT	228
8.4.1	Polymer Matrix	228
8.4.2	Addition of Radicals onto CNT	229
8.4.3	CNT Degradation	232
8.4.4	Additional Analyses	233
8.5	Polymer/CNT Composite Microspheres	235
8.5.1	CNT Material Adsorbed onto Polymer Microspheres	239
8.6	Electrorheology of Polymer/CNT Nanocomposites Prepared by <i>in-situ</i> Suspension Polymerization	243
	References	246
9.	Polylactide-Based Carbon Nanotube Nanocomposites	249
	<i>Srikanth Pilla, Shaoqin Gong and Lih-Sheng Turng</i>	
9.1	Introduction	249
9.2	Synthesis of PLA	252
9.3	Carbon Nanotubes	254

9.4	Preparation of PLA-CNT Nanocomposites	255
9.5	Viscoelastic Properties	264
9.6	Thermal Properties	268
9.7	Mechanical Properties	269
9.8	Thermal Degradation Properties	272
9.9	Electrical Conductivity Properties	273
9.10	Biodegradability	274
9.11	Applications	275
9.12	Conclusions	275
	Acknowledgements	276
	Note	276
	References	276
10.	Synthesis and Properties of PEEK/Carbon	
	Nanotube Nanocomposites	281
	<i>A.M. Díez-Pascual, J.M. González-Domínguez,</i>	
	<i>Y. Martínez-Rubi, M. Naffakh, A. Ansón, M.T. Martínez,</i>	
	<i>B. Simard and M.A. Gómez</i>	
10.1	Introduction	281
10.2	Poly(ether ether ketone)s: Structure, Synthesis and Properties	283
10.3	Synthesis, Purification and Characterization of the SWCNTs	285
10.3.1	Synthesis of Laser-Grown SWCNTs	285
10.3.2	Synthesis and Purification of Arc-Grown SWCNTs	285
10.3.3	Characterization of the Single-Walled Carbon Nanotubes	287
10.4	Integration of the Carbon Nanotubes in the PEEK Matrix	290
10.4.1	Covalent Grafting in Carbon Nanotube/PEEK Nanocomposites	291
10.4.2	Wrapping of the SWCNTs in Compatibilizing Agents	292
10.4.3	Pre-Mixing Stage and Melt Blending Approach	294
10.5	Characterization of PEEK/Carbon Nanotube Nanocomposites	295

10.5.1 Morphology	295
10.5.2 Thermogravimetric Study	297
10.5.3 Differential Scanning Calorimetry	298
10.5.4 X-ray Diffraction Analysis	303
10.5.5 Mechanical Properties	304
10.5.6 Electrical and Thermal Conductivity	307
10.6 Concluding Remarks	309
Acknowledgements	310
Glossary of Abbreviations	310
References	311
11. Synthesis and Properties of PVA/Carbon Nanotube Nanocomposites	315
<i>C. Mercader, P. Poulin and C. Zakri</i>	
11.1 Introduction	315
11.1.1 Mechanical and Electrical Properties of Carbon Nanotubes	316
11.1.2 Why Use Nanotubes in Nanocomposites?	317
11.1.3 Poly(vinyl) Alcohol	319
11.2 Synthesis Methods and Structural Properties of Nanotubes/PVA Composites	320
11.2.1 Films	320
11.2.2 Fibers	324
11.3 Mechanical Properties of the Composites	327
11.3.1 Reinforcement	328
11.3.2 Stress Transfer Efficiency	331
11.4 Electrical Properties	333
11.5 Other Original Properties of PVA/ Nanotube Composites	335
11.5.1 Energy Absorption	335
11.5.2 Shape Memory Effect	337
11.6 Conclusion	339
References	340
12. Elastomers Filled with Carbon Nanotubes	345
<i>Liliane Bokobza</i>	
12.1 Introduction	345
12.2 Composite Processing	347
12.3 Electrical Properties	350

12.4 Mechanical Properties	355
12.4.1 Tensile and Swelling Behaviors	355
12.4.2 Dynamic Mechanical Analysis (DMA) and Differential Scanning Calorimetry (DSC)	361
12.5 Spectroscopic Characterization	364
12.6 Thermal Stability	367
12.7 Conclusions	369
References	369
13. Specific Interactions Induced Controlled Dispersion of Multiwall Carbon Nanotubes in Co-Continuous Polymer Blends	373
<i>Suryasarathi Bose, Arup R. Bhattacharyya, Rupesh A. Khare and Ajit R. Kulkarni</i>	
13.1 Introduction	373
13.2 Experimental	376
13.2.1 Materials	376
13.2.2 Preparation of the Modifiers	376
13.2.3 Melt Blending	377
13.2.4 Characterization	378
13.3 Results and Discussion	379
13.3.1 Specific Interactions: Spectroscopic and Microscopic Evidences	379
13.3.2 AC Electrical Conductivity Measurements: Assessing the State of Dispersion of MWNTs	381
13.3.3 Phase Morphology and Selective Localization of MWNTs in the Blends	383
13.3.4 Melt-Interfacial Interactions	386
13.4 Summary	387
Acknowledgements	388
References	388
14. Effect of Structure and Morphology on the Tensile Properties of Polymer/Carbon Nanotube Nanocomposites	391
<i>Jingjing Qiu and Shiren Wang</i>	
14.1 Background	391
14.2 Structure and Morphology Characterization	392
14.2.1 Structure and Mechanical Properties of CNTs	392

14.2.2 Characterization of CNTs/Polymer Composites	395
14.2.3 Structure and Tensile Properties of CNTs/ Polymer Composites	396
14.3 Concluding Remarks	417
References	418
15. Polymer Nanotube Composites: Promises and Current Challenges	423
<i>Amal M.K. Esawi and Mahmoud M. Farag</i>	
15.1 Carbon Nanotubes	424
15.1.1 Background	424
15.1.2 Synthesis of CNTs	425
15.1.3 Fabrication of CNT Polymer Composites	426
15.1.4 Electrical Properties of CNT Polymer Composites	429
15.1.5 Mechanical Properties of CNT Polymer Composites	432
15.2 Case Studies	435
15.2.1 Case Study: CNT-Based Strain Sensor	435
15.2.2 Case Study: Technical and Economic Feasibility of Using CNT-Based Composites in Aerospace Applications	440
15.3 Conclusions	445
References	446
Index	449

Preface

Nanotube materials are the one of the best examples of novel nanostructures derived by bottom-up chemical synthesis processes. The chemical composition and atomic bonding configuration present in nanotubes is simple; however, these materials represent diverse structure-property relations among the nano-materials. Since the early discoveries of the nanotube materials, a large number of research studies have been devoted to demonstrate the potential of the nanotubes in improving the mechanical, electrical and thermal properties of materials. Polymer nanotube nanocomposites represent an important class of such hybrid materials where the nanotubes are embedded in the polymer matrices by employing various synthesis methodologies including solution casting, melt blending or *in-situ* polymerization in the presence of nanotubes. Uniform dispersion of nanotubes in the polymer matrix is of utmost importance in order to obtain an optimal improvement in the properties of the polymer at low fractions of nanotubes. Thus it is required to optimize the compatibility between the organic and inorganic phases as well as processing methodologies. The current book intends to assimilate the various polymer nanotube systems reported in the literature to underline the high potential of nanotubes as fillers and to provide pathways for the large scale commercial application of the nanotube nanocomposites.

Chapter 1 describes the properties and synthesis of nanotubes. It is clear from the properties of the nanotubes that tremendous gains in the properties of the composites can be achieved if the nanotubes and polymer phases are optimally mixed. Chapter 2 reviews the numerous polymer nanotube composite systems reporting superior composite properties and thus justifying the ever-increasing use of nanotubes as fillers for composite materials. Chapter 3 deals with the use of electron microscopy methods along with new

advancements in understanding the microstructure of polymer nanotube nanocomposites. Chapter 4 describes the combined use of clay as well as nanotubes as reinforcements in the composite synthesis and the synergistic effects of the two fillers in the property enhancements. Chapter 5 details the non-polar nanocomposites with polyethylene as the polymer. Polar polyurethane nanocomposites with nanotubes is dealt with in Chapter 6. Commercially important PMMA nanotube nanocomposites are described in Chapter 7. Chapter 8 describes the suspension polymerization for the synthesis of vinyl polymer based nanotube nanocomposites. Biodegradable polymer system of polylactide has also been used for the synthesis of nanocomposites and properties of such composites are reported in Chapter 9. Engineering plastics like PEEK have also been reinforced with nanotubes and the microstructure and properties of these composites can be found in Chapter 10. Chapter 11 details the synthesis and resulting properties of polyvinyl alcohol nanotube nanocomposites, whereas Chapter 12 focuses on the reinforcement of elastomers with nanotubes. Controlled dispersion of nanotubes in co-continuous polymer blends are detailed in Chapter 13. Effect of structure and morphology on the tensile properties of polymer nanotube nanocomposites is the focus of Chapter 14. Chapter 15 with the help of case studies sums up the promises and current challenges present in front of the polymer nanotube nanocomposites technology.

At this juncture, I would like to express my gratitude to Scrivener Publishers for their kind support in the project. I dedicate this book to my family, especially to my mother, for being constant source of inspiration without which I would not have achieved this or any goal. Moreover, heartfelt thanks to my wife Preeti for her continuous help in the project from inception till completion.

Vikas Mittal
Ludwigshafen, March 2010.

Carbon Nanotubes: An Introduction*

V. Mittal

BASF SE, Polymer Research, 67056 Ludwigshafen, Germany

Abstract

Carbon nanotubes represent high potential fillers owing to their remarkably attractive mechanical, thermal and electrical properties. The incorporation of nanotubes in the polymer matrices can thus lead to synergistic enhancements in the composite properties even at very low volume fractions. This chapter provides a brief overview of the properties and synthesis methods of nanotubes for the generation of polymer nanocomposites.

Keywords: nanotubes, nanocomposites, electrical, mechanical, vapor deposition, laser, arc.

1.1 Introduction

Carbon nanotubes, which are allotropes of carbon, are regarded as the ultimate carbon fibers (1,2). Their mechanical properties (strength, stiffness) are expected to approach that of an ideal carbon fiber, which has the perfect orientation of defect-free graphene (single layer of graphite) layers along the fiber axis. These graphene layers are also represented to be as thinnest possible layers to form the nanotubes. Nanotube materials are the one of the best examples of novel nanostructures derived by bottom-up chemical synthesis processes (3). The chemical composition and atomic bonding configuration present in nanotubes is simple, however, these materials represent diverse structure-property relations among the nano-materials (2). A single-walled nanotube (SWNT) can be formed by rolling a sheet of graphene into a cylinder along an (m,n) lattice vector in the graphene

*This review work was carried out at Institute of Chemical and Bioengineering, Department of Chemistry and Applied Biosciences, ETH Zurich, Zurich, Switzerland. V. Mittal (ed.) Polymer Nanotube Nanocomposites, (1-14) © Scrivener Publishing LLC

2 POLYMER NANOTUBE NANOCOMPOSITES

plane as shown in Figure 1.1 (3). The (m,n) indices determine the diameter and chirality, which are key parameters of a nanotube. Depending on the chirality (the chiral angle between hexagons and the tube axis), SWNTs can be either metals or semiconductors. As grown, the nanotubes are closed at both ends by a hemispherical cap which is formed by the replacement of hexagons with pentagons in the graphite sheet leading to curvature in the structure.

The credit for realizing the nanotubes in an arc discharge apparatus is given generally to Iijima who could successfully prove the existence of first multi walled carbon nanotubes (MWCNT) mixed with other forms of carbon (4). He observed a graphitic tubular structure

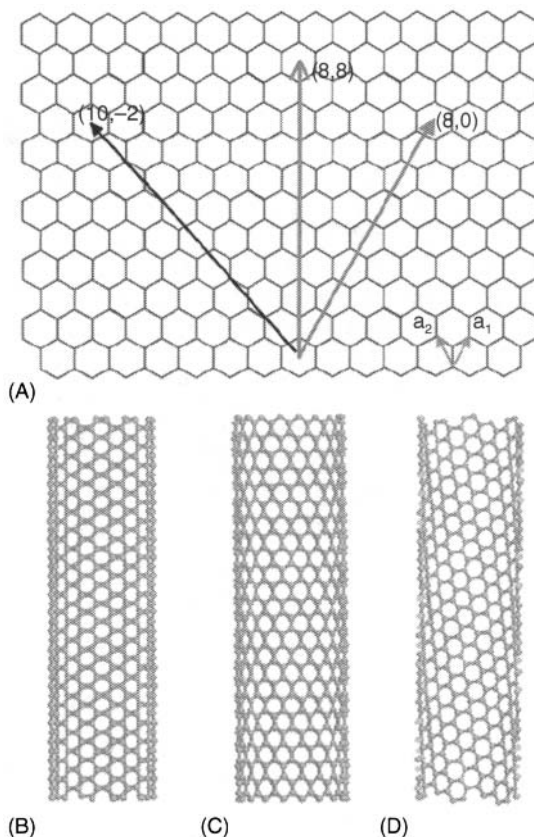


Figure 1.1. (a) Schematic honeycomb structure of a graphene sheet. Single-walled carbon nanotubes can be formed by folding the sheet along lattice vectors. The two basis vectors a_1 and a_2 are shown. Folding of the $(8,8)$, $(8,0)$, and $(10,-2)$ vectors leads to armchair (b), zigzag (c), and chiral (d) tubes, respectively. Reproduced from reference 3 with permission from American Chemical Society.

in an arc discharge apparatus used for the production of fullerenes. Electron diffraction taken from individual nanotubes indicated that the orientation of the top and bottom portions of the individual nanotube cylinders can be different indicating helicity. The identification of these materials as strong structural component for the enhancement of many polymer matrix properties caused an exponential rise in the number of studies dealing with carbon nanotube nanocomposites. Though the existence of these materials was realized earlier also e.g. by Endo in 1976, however, no attention was paid to them (5). MWCNT were classified as either graphite sheets arranged in concentric seamless cylinders or a single sheet of graphite rolled in around itself. The interlayer spacing in the nanotubes is slightly larger than the single crystal graphite because of the existence of the geometrical strain by the formation of concentric seamless cylinders. Outer diameters from 4-50 nm were reported and length of these tubes was also up to few microns, whereas inner tube diameters as small as 2.2 nm were reported. A tremendous activity also in the field of nanotube synthesis followed the initial discoveries and nanotubes with many different methods were generated and characterized (6,7). Subsequently, single wall carbon nanotubes (SWCNT) were discovered in which as mentioned above, one-atom thick sheet of graphite is rolled up into a seamless cylinder. Diameters of the order of a nanometer and length of the order of 1000 nm were achieved depending on the preparation and purification methods (8). Figure 1.2 shows the

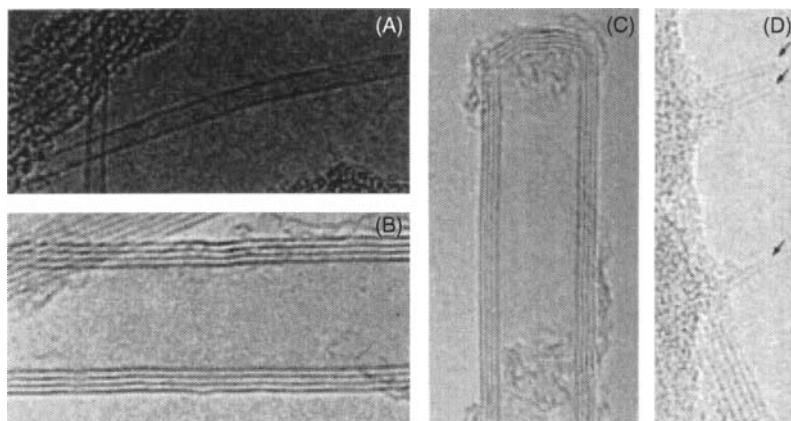


Figure 1.2. High-resolution transmission electron microscopy images of (a) SWNT and (b) MWNT. Closed nanotube tips are also shown in Figure 2C (MWNT tips) and Figure 2D (SWNT tip, shown by arrows).

Reproduced from reference 9 with permission from American Chemical Society.

typical images of the single wall and multiple wall nanotubes (9). One important point to note is that the conventional carbon fibers cannot match the structural perfection achieved in nanotubes and the carbon fibers synthesized by the traditional methods vary significantly in morphology and structure.

1.2 Properties

Carbon nanotubes have unique mechanical, electrical, magnetic, optical and thermal properties as demonstrated in Table 1.1 (10). In some special applications, such as space explorations, high-performance lightweight structural materials are required, and they can be developed by adding CNTs to polymers or other matrix materials to generate nanocomposites. The organic-inorganic nanocomposites can conventionally contain inorganic fillers falling into three

Table 1.1. Theoretical and experimental properties of carbon nanotubes.

Property	CNTs	Graphite
Specific gravity	0.8 g/cm ³ for SWCNT; 1.8 g/cm ³ for MWCNT (theoretical)	2.26 g/cm ³
Elastic modulus	~1 TPa for SWCNT; ~0.3–1 TPa for MWCNT	1 TPa (in-plane)
Strength	50–500 GPa for SWCNT; 10–60 GPa for MWCNT	
Resistivity	5–50 $\mu\Omega$ cm	50 $\mu\Omega$ cm (in-plane)
Thermal conductivity	3000 W m ⁻¹ K ⁻¹ (theoretical)	3000 W m ⁻¹ K ⁻¹ (in-plane), 6 W m ⁻¹ K ⁻¹ (c-axis)
Magnetic susceptibility	22 $\times 10^6$ EMU/g (perpendicular with plane), 0.5 $\times 10^6$ EMU/g (parallel with plane)	
Thermal expansion	Negligible (theoretical)	-1 $\times 10^{-6}$ K ⁻¹ (in-plane), 29 $\times 10^{-6}$ K ⁻¹ (c-axis)
Thermal stability	> 700 °C (in air); 2800 °C (in vacuum)	450–650 °C (in air)
Specific surface area	10–20 m ² /g	

Reproduced from reference 10 with permission from Elsevier.

different categories by the virtue of their primary particle dimensions (11). When all the three dimension of the particles are in the nanometer scale, the inorganic fillers have the form of spherical particles like silica particles (12,13). Fillers with two dimensions in the nanometer scale whereas the third one in the range of micrometers include carbon nanotubes or whiskers (14,15). When the filler has two finite dimensions in the range of micrometers whereas one dimension is in nanometer scale, the fillers include layered silicate (or aluminosilicate) materials (16). Composites with all the three possible filler geometries have been synthesized, however, nanotube composites generate much high end application potential in the nanocomposites as compared to the nanofillers of other geometries. Thus, single and multi walled nanotubes have attracted the interest of scientists and a significant research effort is devoted to the synthesis and characterization of the nanotubes as well as to tune their surface functionalities to compatibilize them with the matrix materials.

Many experimental and theoretical studies have reported the modulus of the nanotubes to be in the same range as graphite fibers and the strength even at least an order of magnitude higher than the graphite fibers (17–21). The single-walled nanotube is supposed to be formed by rolling a graphene sheet and a Young's modulus of about 1 TPa was reported (22) as compared to 300–800 GPa for graphite fibers (17). Another literature study also reported the Young's modulus of 4.7 TPa, which is much higher than any of the filler material known (23). However, some computational studies found that the true moduli of the nanotubes were below the estimated values obtained from the graphene sheet (24). Several kinds of local defects, such as Stone Waals defect and dislocation of carbon atoms may influence the properties of the nanotubes, which have been discussed in some reported computational works (25,26). The big range in the measured and estimated mechanical properties is generally due to the different sizes, lengths and numbers of wall layers. Also, it may be hard to produce identical nanotubes even in the same experiment (8). A typical tensile test for multi-walled nanotubes which was reported by Ruoff and Lorents is shown (27) in Figure 1.3. It has also been observed (24) that the inner walls of a multi walled carbon nanotubes are not effective in taking tensile loads applied at the both ends, and it is only the outmost layer of the nanotubes which takes the entire load. Therefore, failure in such a case starts at the outer wall of the multiwalled carbon nanotube by breaking the bonds among carbon atoms. The simulated version of such a process has been demonstrated in Figure 1.4. The strength

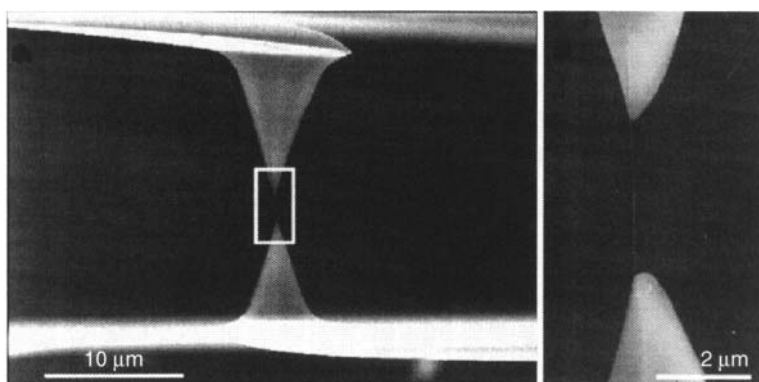


Figure 1.3. Tensile test for the determination of mechanical performance of single nanotube. Reproduced from reference 24 with permission from Elsevier.

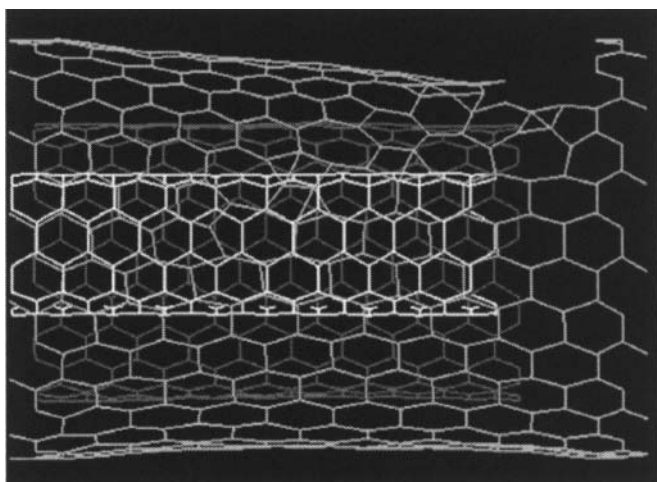


Figure 1.4. Stretching process of a triple-walled carbon nanotube. Reproduced from reference 24 with permission from Elsevier.

of nanotubes also depends on the distribution of defects, interlayer interactions in multi-walled carbon nanotubes as well as bundles of single-walled carbon nanotubes. The defect density is dependant on the growth process. The hollow morphology of the nanotubes has been observed to produce distinct mechanical response thus differing from conventional fibers or other reinforcing materials. Nanotubes can sustain even 40% strain without showing any brittle behavior.

Apart from mechanical properties, electronic properties of nanotubes are equally important and useful. As observed earlier, both metallic and semiconducting nanotubes are generated depending

on the helicity. The measurement of electronic properties directly on a single nanotube is, however, a challenge. Four or more probe measurements have been developed to generate the information on transport properties of individual nanotubes. Multiwalled nanotubes represent more complex transport properties because of the presence of cylinders of different helicity. On the other hand, the transport properties in single walled nanotubes are more uniform in nature. Reports have also suggested that the conductivity in nanotubes can also be altered by suitably doping them which alters their original lattice structure. The conductivity behavior of the nanotubes has also been observed to have similar nature as conducting polymers.

Also, the presence of defects can generate reactive sites on the surface of nanotubes thus making them more reactive compared to graphite counterparts. Figure 1.5 (9) is the simulated representation of such defects which act as electrophilic reaction sites.

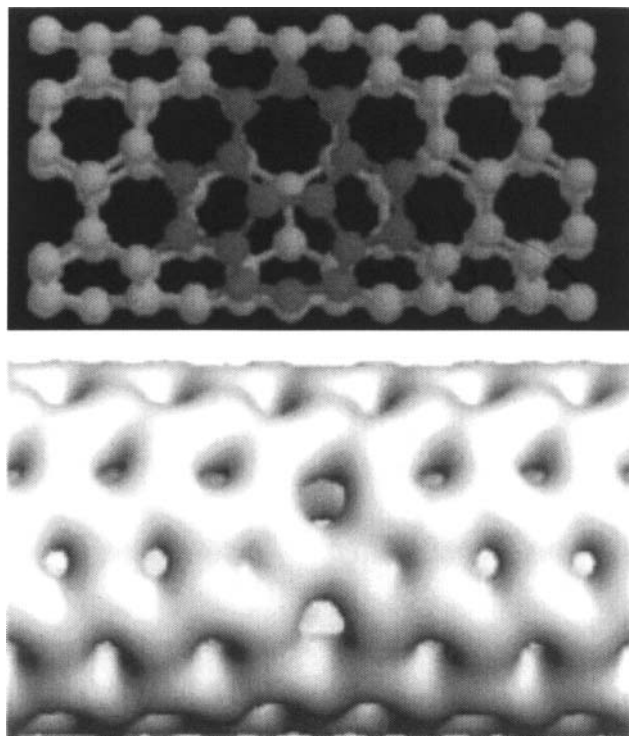


Figure 1.5. Top: ball-and-stick model for a single-walled nanotube with a bond rotation defect (gray atoms). Bottom: corresponding simulated 3D-local density of states image. Reproduced from reference 9 with permission from American Chemical Society.

1.3 Synthesis

The synthesis processes for the nanotubes have been continuously refined in the recent years and today, a number of methods are available to synthesize both single and multiwalled carbon nanotubes. These methods include high temperature evaporation using arc-discharge (28–30), laser ablation (31), chemical vapor deposition etc. (32–34).

In the electric arc method, a DC arc plasma between the two carbon electrodes in an inert atmosphere is generated. The inert atmosphere used is generally helium. A soft, dark black, fibrous deposit forms on the cathode as the anode is consumed. The deposit generally consists of 50 vol% multiwalled carbon nanotubes. It is also possible to grow single walled nanotubes by the arc discharge method using hydrogen.

The laser ablation process uses a graphite target containing small amounts of a metal catalyst. The target is placed in a furnace at roughly 1200°C in an inert atmosphere followed by evaporation using a high power laser. The nanotubes develop on the cooler surface of the reactor, as the vaporized carbon condenses. The yield of nanotube synthesis by this process is roughly 70%. The nanotubes generated by the above mentioned methods are relatively impure, with presence of unwanted carbonaceous impurities. The resulting products are swept from the high temperature zone by using an inert gas and conical copper head (cooled with water) is used to deposit the nanotubes. These methods are also not operated at higher scale, therefore, the overall production costs are high. These methods are, thus, generally not suitable for the generation of large scale cheap production of nanotubes required for the production of polymer nanocomposites.

Chemical vapor deposition method is used as an alternative to circumvent the limitations of the other synthetic methods. In chemical vapor deposition method, a substrate is prepared with a layer of metal catalyst particles, most commonly nickel, cobalt, iron, or a combination of these materials. The diameter of the grown nanotubes is related to the size of the metal particles. The substrate is heated to approximately 700°C. To initiate the growth of nanotubes, two gases are bled into the reactor: a process gas (such as ammonia, nitrogen, hydrogen, etc.) and

a carbon-containing gas (such as acetylene, ethylene, ethanol, methane, etc.). The carbon vapor deposition method generates entangled nanotubes in general; however, more aligned tubes can be generated by using the synthetic conditions which lead to rapid and dense nucleation on the substrates (35–36). The nanotubes in the length range of millimeters have also been synthesized by extending the growth time. A number of commercial CVD routes to SWNT synthesis have been developed, but the so-called ‘HiPco’ method has been widely used. High pressure carbon monoxide is used as a carbon source to generate the gas phase growth of SWNT. Table 1.2 also provides a review of the different methods for the synthesis of carbon nanotubes (37). The quality and yield of the generated nanotubes is significantly affected by the used technique and the synthesis conditions used.

Table 1.2. A summary of the methods for the synthesis of carbon nanotubes.

Short name	Technology of preparation [reference]	Typical mean diameter (nm)	Product description
Laser ablation (PLV)	Ablation from graphite doped with (Fe, Co, Ni, ...) catalyst	1.4 (1–1.8)	High quality, good diameter control, bundled tubes; commercial
dc arc discharge	First reported production. Modified Kratschmer reactor	1.5 (0.9–3.1)	Lesser quality, carbonaceous impurities abundant. CNTs grow bundled
Gas phase decomposition	Decomposition in an oxygen-free environment Typical: HiPco® (high pressure CO decomposition)	1 (0.9–1.3)	Easy purification, commercial, good quality
CCVD	Catalytic chemical vapor deposition. Supported metal catalysts are used	1.5 (1.3–2)	Cheapest, commercial, up-scalable. Most feasible from the application point of view

(continued)

Table 1.2. *(continued)*

Short name	Technology of preparation [reference]	Typical mean diameter (nm)	Product description
Flame pyrolysis	Carbon source + metallocene catalyst, conventional low pressure pyrolysis reactor	2–3	Low yield, bad quality. Still under development. Plant technology available, large commercialization potential
Solar furnace	Solar rays focused on a metal doped graphite target. Growth dynamics similar to PLV	1.4	Good quality CNTs, little amorphous carbon. Spreading not expected in the near future
Inner tubes of DWCNTs	Catalyst free growth from peapods by coalescence of C ₆₀ molecules	0.7 (0.55–1)	Well shielded, best quality CNTs. Separation from outer tubes is very challenging
Zeolite grown	CNTs grow by thermal decomposition of template molecules within zeolite channels	0.45	Monodisperse diameter distribution, oriented tubes. CNTs metastable outside the channels

Reproduced from reference 37 with permission from Elsevier.

Figure 1.6 (3) shows the ordered nanotube arrays synthesized by chemical vapor deposition methodology.

The organic-inorganic nanocomposites generated by the incorporation of the nanotubes in organic materials require optimum dispersion of the nanotubes in order to translate the nanotube and polymer properties synergistically into composite properties. The nanoscale dispersion of nanotubes in the organic materials leads to the generation of large interfacial contacts between the organic and inorganic phases thus generating an altogether different morphology. The nanotubes, however, owing to their inert nature tend to form bundles with each other owing to the van der Waals forces

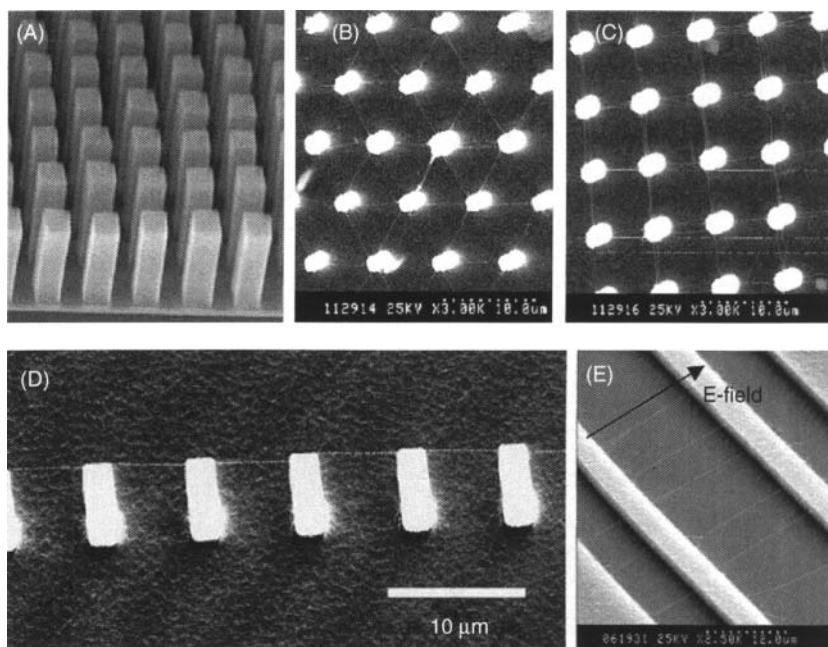


Figure 1.6. Carbon nanotube structures obtained by chemical vapor deposition synthesis. (a) SEM image of self-oriented MWNT arrays. Each tower-like structure is formed by many closely packed multiwalled nanotubes, (b) SEM top view of a hexagonal network of SWNTs (line-like structures) suspended on top of silicon posts (bright dots), (c) SEM top view of a square network of suspended SWNTs, (d) Side view of a suspended SWNT power line on silicon posts (bright) and (e) SWNTs suspended by silicon structures (bright regions). Reproduced from reference 3 with permission from American Chemical Society.

between them and thus do not disperse well in the organic matrices in their pristine state. This hindrance in the optimum dispersion of the nanotubes in the organic matrices is overcome by suitably enhancing the surface of the nanotubes. The surface functionalization makes these nanotubes more organophilic thus facilitating the nanoscale dispersion of the nanotubes in the organic materials. This behavior is similar to the clay based nanocomposites in which the suitable surface modifications of clay surface are required in order to disperse the clay in various polymer systems.

A number of nanotube surface modification approaches have been reported in the recent years. Non-covalent surface modifications aim to physically wrap polymer chains around the nanotubes or adsorb various surfactant molecules on the surface of nanotubes. Thus,

these modification methods retain the structural characteristics of the nanotubes. However, the modifications present on the surface are only physically bound, therefore, they are prone to be removed from the surface or may not be suitable enough for load transfer etc. Covalent means of surface modification of the nanotubes have also been developed. In such methods, polymer chains can either be grafted to the surface or grafted from the surface of the nanotubes.

References

1. P.M. Ajayan, and T.W. Ebbesen, *Reports on Progress in Physics*, Vol. 60, p. 1025, 1997.
2. M.S. Dresselhaus, G. Dresselhaus, and P.C. Eklund, *Science of Fullerenes and Carbon Nanotubes*, New York, Academic Press, 1996.
3. H. Dai, *Accounts of Chemical Research*, Vol. 35, p. 1035, 2002.
4. S. Iijima, *Nature*, Vol. 354, p. 56, 1991.
5. M. Endo, *Ph.D. Thesis*, Japan, Nagoya University, 1978.
6. C. Dekker, *Physics Today*, Vol. 53, p. 22, 1999.
7. M.J. O'Connell, *Carbon Nanotubes: Properties and Applications*, Boca Raton, CRC Taylor & Francis, 2006.
8. P.J.F. Harris, *Carbon Nanotubes and Related Structures: New Materials for the Twenty-First Century*, Cambridge, Cambridge University Press, 2001.
9. P.M. Ajayan, *Chemical Reviews*, Vol. 99, p. 1787, 1999.
10. X.-L. Xie, Y.-W. Mai, and X.-P. Zhou, *Materials Science and Engineering R*, Vol. 49, p. 89, 2005.
11. S. Pavlidoua, and C.D. Papaspyrides, *Progress in Polymer Science*, Vol. 33, p. 1119, 2008.
12. J.E. Mark, *Polymer Engineering and Science*, Vol. 36, p. 2905, 1996.
13. E. Reynaud, C. Gauthier, and J. Perez, *Revue de Metallurgie/Cahiers d'Informations Techniques*, Vol. 96, p. 169, 1999.
14. P. Calvert, in T.W. Ebbesen, ed., *Carbon Nanotubes*; Boca Raton, CRC Press, pp. 277–292, 1997.
15. V. Favier, G.R. Canova, S.C. Shrivastava, and J.Y. Cavaille, *Polymer Engineering and Science*, Vol. 37, p. 1732, 1997.
16. V. Mittal, *Organic Modifications of Clay and Polymer Surfaces for Specialty Applications (PhD Thesis)*, Zurich, Swiss Federal Institute of Technology Zurich, 2006.
17. A. Eitan, F.T. Fisher, R. Andrews, L.C. Brinson, and L.S. Schadler, *Composites Science and Technology*, Vol. 66, p. 1159, 2006.
18. M.-F. Yu, O. Lourie, M. Dyer, K. Moloni, T.F. Kelly, and R.S. Ruoff, *Science*, Vol. 287, p. 637, 2000.
19. M.-F. Yu, B.S. Files, S. Arepalli, and R.S. Ruoff, *Physical Review Letters*, Vol. 84, p. 5552, 2000.
20. M.M.J. Treacy, T.W. Ebbesen, and J.M. Gibson, *Nature*, Vol. 381, p. 678, 1996.
21. G. Gao, T. Cagin, and W.A. Goddard III, *Nanotechnology*, Vol. 9, p. 184, 1998.

22. J.P. Lu, *Journal of Physics and Chemistry of Solids*, Vol. 58, p. 1649, 1997.
23. Z.C. Tu, and Z.C. Ou-yang, *Physical Reviews B*, Vol. 65, p. 233, 2002.
24. K.-T. Lau, C. Gu, and D. Hui, *Composites: Part B*, Vol. 37, p. 425, 2006.
25. T. Belytschko, S.P. Xiao, G.C. Schatz, and R.S. Ruoff, *Physical Reviews B*, Vol. 65, p. 2354, 2002.
26. A. Maiti, A. Svizhenko, and M.P. Anantram, *Physical Review Letters*, Vol. 88, p. 126905, 2002.
27. R.S. Ruoff, and D.C. Lorents, *Carbon*, Vol 33, p. 925, 1995.
28. C. Journet, W.K. Master, P. Bernier, A. Loiseau, M. Lamy de la Chapelle, S. Lefrant, P. Deniard, R. Lee, and J.E. Fischer, *Nature*, Vol. 388, p. 756, 1997.
29. T.W. Ebbesen, and P.M. Ajayan, *Nature*, Vol. 358, p. 220, 1992.
30. D.T. Colbert, J. Zhang, S.M. McClure, P. Nikolaev, Z. Chen, J.H. Hafner, D.W. Owens, P.G. Kotula, C.B. Carter, J.H. Weaver, A.G. Rinzler, and R.E. Smalley, *Science*, Vol. 266, p. 1218, 1994.
31. A. Thess, R. Lee, P. Nikolaev, H. Dai, P. Petit, J. Robert, C. Xu, Y.H. Lee, S.G. Kim, A.G. Rinzler, D.T. Colbert, G.E. Scuseria, D. Tomanek, J.E. Fischer, and R.E. Smalley, *Science*, Vol. 273, p. 483, 1996.
32. H.M. Cheng, F. Li, G. Su, H.Y. Pan, L.L. He, X. Sun, and M.S. Dresselhaus, *Applied Physics Letters*, Vol. 72, p. 3282, 1998.
33. C.N.R. Rao, A. Govindaraj, R. Sen, and B.C. Satishkumar, *Materials Research Innovations*, Vol. 2, p. 128, 1998.
34. R. Andrews, D. Jacques, A.M. Rao, F. Derbyshire, D. Qian, X. Fan, E.C. Dickey, and J. Chen, *Chemical Physics Letters*, Vol. 303, p. 467, 1999.
35. Z.F. Ren, Z.P. Huang, J.W. Xu, J.H. Wang, P. Bush, M.P. Siegel, and P.N. Provenico, *Science*, Vol. 282, p. 1105, 1998.
36. C. Singh, M.S.P. Shaffer, I.A. Kinloch, and A.H. Windle, *Physica B*, Vol. 323, p. 339, 2002.
37. H. Kuzmany, A. Kukovecz, F. Simon, M. Holzweber, Ch. Kramberger, and T. Pichler, *Synthetic Metals*, Vol. 141, p. 113, 2004.

This Page Intentionally Left Blank

Overview of Polymer Nanotube Nanocomposites*

V. Mittal

BASF SE, Polymer Research, 67056 Ludwigshafen, Germany

Abstract

Nanotubes owing to their high mechanical and electrical properties are ideal fillers for the composites generation. Polymer nanotubes nanocomposites are synthesized after achieving suitable surface modifications of the nanotubes using different synthesis methods like melt mixing, *in situ* polymerization and solution mixing. All these methods have their own advantages and limitations and varying degrees of successes in achieving the nanoscale dispersion of the nanotubes as well as significant enhancement in the properties in the composite properties. The tensile modulus is generally reported to significantly enhance on the incorporation of even small amounts of nanotubes. The tensile strength and elongation at break though in many cases are reported to improve, but they are more likely dependant on the morphology of the nanocomposites. The glass transition temperature as well as degradation temperature is also mostly observed to significantly increase owing to the reinforcing effect of nanotubes. Many other properties like electrical conductivity, heat deflection temperature etc. also increase on the addition of nanotubes to the polymer.

Keywords: nanocomposites, dispersion, aspect ratio, *in-situ*, melt, morphology, tensile properties, glass transition temperature, degradation, functionalization, electrical conductivity, resistivity.

2.1 Introduction

Many experimental and theoretical studies have reported the modulus of the nanotubes to be in the same range as graphite fibers

*This review work was carried out at Institute of Chemical and Bioengineering, Department of Chemistry and Applied Biosciences, ETH Zurich, Zurich, Switzerland. V. Mittal (ed.) Polymer Nanotube Nanocomposites, (15–44) © Scrivener Publishing LLC

and the strength even at least an order of magnitude higher than the graphite fibers (1–11). Even if the real mechanical properties of nanotubes are actually somewhat lower than the estimated values, the nanotubes in any such case still represent high potential filler materials for the synthesis of polymer nanocomposites. The surface area per unit volume of nanotubes is also much larger than the other filler fibers, leading to much larger nanotube/matrix interfacial area in the nanotube reinforced composites than traditional fiber-reinforced composites. Figure 2.1 represents such interface polymer fraction in nanotube-reinforced polymers when the ratio of the thickness t of the interphase versus the inclusion radius r_f is plotted with respect to the volume fraction of the inclusion (1). Owing to the interfacial contacts with the nanotubes, the interfacial polymer has much different properties than the bulk polymer. The conversion of a large amount of polymer into interface polymer fraction due to the nanoscale dispersion and high surface area of nanotubes generates altogether different morphology in the nanotube nanocomposites which results into the synergistic improvement in the nanocomposite properties. As mentioned in the earlier chapter, in order to optimize the interfacial interactions between the polymer and nanotubes, it is required to achieve nanoscale dispersion of the filler which necessitates compatibilization of the

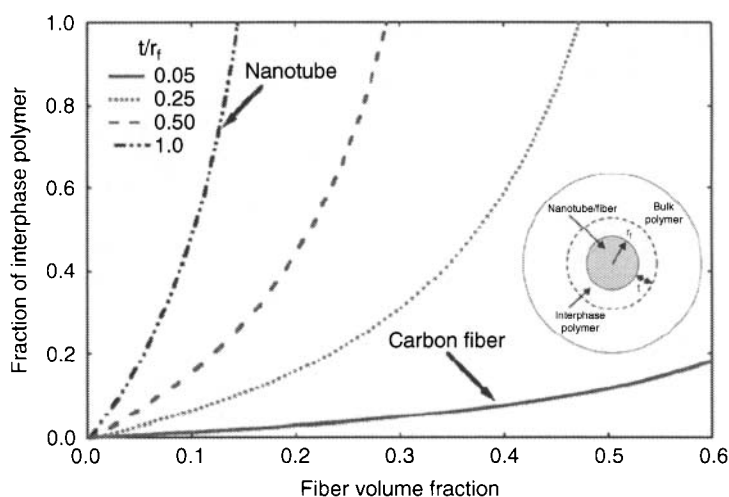


Figure 2.1. Fraction of interphase polymer as a function of volume fraction of fiber inclusion, where t is the interphase thickness and r_f is the radius of the nanotube/fiber inclusion. Reproduced from reference 1 with permission from Elsevier.

polymer and inorganic phases. Therefore, the nanotubes need to be surface modified before their incorporation into the polymer matrix. As CNTs agglomerate, bundle together and entangle, therefore, it may lead to defect sites in the composites subsequently limiting the impact of CNTs on nanocomposite properties. Salvetat et al. (12) studied the effect of CNTs dispersion on the mechanical properties of nanotube reinforced nanocomposites, and it was observed that poor dispersion and rope-like entanglement of CNTs caused significant weakening of the composites. Thus, alignment of CNTs is also equally important to enhance the properties of polymer/CNT composites (13,14). Stress transfer property of the nanotubes in the composites is another parameter which controls the mechanical performance of the composite materials. Many studies reported by using tensile tests on nanotube/polymer nanocomposites the bonding behavior between the nanotubes and the matrix (15,16), in which the interfacial shear strength ranging from 35 to 376 MPa was reported. The values ranged owing to the different diameter of the nanotubes and the number of wall layers. However based on the interfacial compatibility, other behaviors have also been reported. In their study, Lau and Hui (17) observed that most of nanotubes were pulled out during the tensile testing owing to no interaction at the interface.

It has also been reported that in the case of multiwalled nanotubes, the inner layers of nanotubes cannot effectively take any tensile loads applied at the both ends owing to the weak stress transferability between the layers of the nanotubes (8,18). It results into the outmost layer of the nanotubes taking the entire load. As a result, the failure of the multi-walled nanotubes could start at the outmost layer by breaking the bonds among carbon atoms.

Nanotube nanocomposites with a large number of polymer matrices have been reported in the recent years. The composites were synthesized in order to enhance mechanical, thermal and electrical properties of the conventional polymers so as to expand their spectrum of applications. Different synthesis route have also been developed in order to achieve nanocomposites. The generated morphology in the composites and the resulting composite properties were reported to be affected by the nature of the polymer, nature of the nanotube modification, synthesis process, amount of the inorganic filler etc. The following paragraphs review the nanocomposites structures and properties reported in a few of these reports and also stress upon the future potential of nanotube nanocomposites.

2.2 Methods of Nanotube Nanocomposites Synthesis

2.2.1 Solution Mixing

Solution mixing method has the advantage that the viscosity of the system can be controlled to be low so as to achieve higher extents of nanotube dispersion in the polymer systems. Both thermoset and thermoplastic polymers can be employed using this approach to achieve nanocomposites. The disadvantage associated with this method is, however, the requirement of large amount of solvent for the nanocomposite synthesis, which for industrial applications may not be environmentally friendly or cost effective. For thermoset nanocomposites, one can also use the prepolymer to disperse the nanotubes and the prepolymer can then be crosslinked during the evaporation of solvent. Suhr et al. (19) reported the solution mixing approach as shown in Figure 2.2 for the synthesis of polycarbonate nanocomposites.

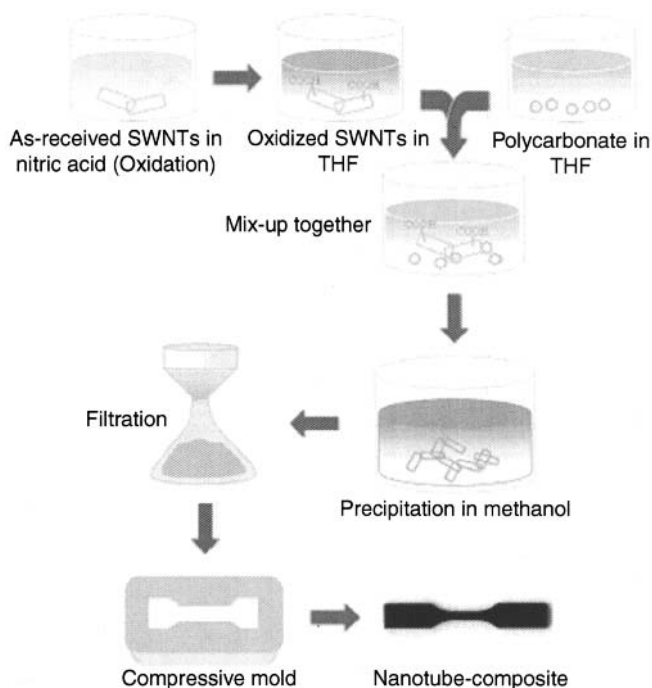


Figure 2.2. Schematic of synthesis of CNT polycarbonate nanocomposites by solution mixing approach. Reproduced from reference 19 with permission from American Chemical Society.

The nanotubes were first oxidized in nitric acid before dispersion as the acidic groups on the sidewalls of the nanotubes can interact with the carbonate groups in the polycarbonate chains. To achieve nanocomposites, the oxidized nanotubes were dispersed in THF and were added to a separate solution of polycarbonate in THF. The suspension was then precipitated in methanol and the precipitated nanocomposite material was recovered by filtration. From the scanning electron microscopy investigation of the fracture surface of nanotubes, the authors observed a uniform distribution of the nanotubes in the polycarbonate matrix as shown in Figure 2.3 (19).

Similarly, Biercuk et al. (20) reported the use of solution mixing approach for the synthesis of epoxy nanocomposites. Epoxy prepolymer was dissolved in solvent in which the CNTs were also uniformly dispersed. The solvent was subsequently evaporated, and the epoxy prepolymer was crosslinked. The resulting nanocomposite was reported to have a good dispersion of nanotubes. In other studies, multi walled nanotubes were mixed to toluene in which polystyrene polymer was dissolved (21,22) to generate polystyrene nanocomposites. The nanocomposites were generated both by film-casting and spin-casting processes. Solution mixing method has also been used to attain alignment of the nanotubes in the composites (23,24). Aspect ratio and rigidity of the nanotubes were reported to be the two factors which affect the alignment of

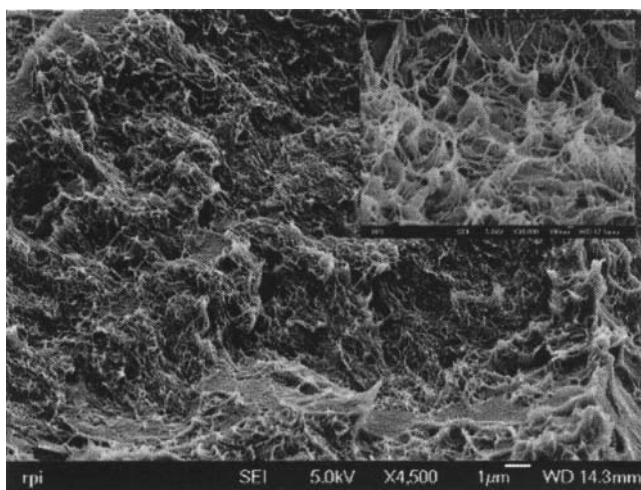


Figure 2.3. Scanning electron microscopy image of the fracture surface of the polycarbonate nanocomposite. Reproduced from reference 19 with permission from American Chemical Society.

the nanotubes. If the nanotubes were longer and more flexible, the alignment of the nanotubes in the composites was observed to deteriorate (25,26). Stretching the casted film of the nanocomposite synthesized by solution mixing method resulted in the improvement of the nanotube alignment (25).

2.2.2 *In-Situ* Polymerization

This mode of nanocomposite synthesis is beneficial owing to the fact that the nanotube dispersion can be achieved in a solvent in which monomer is also dissolved or suspended. The low viscosities encountered during this process lead to better dispersion of nanotubes. The subsequent polymerization of monomer then leads to the uniform intercalation of polymer around the nanotubes. In many instances, the generated polymer can also be chemically grafted to the nanotube surfaces either by the acidic functionalities generated on the surface by chemical treatment or by direct grafting of polymer chains from the surface of the nanotubes by using surface immobilized initiators. Barazza et al. used miniemulsion approach to achieve polystyrene nanocomposites (27). Cetyltrimethylammonium bromide (CTAB) and sodium dodecyl sulphate (SDS) were used to functionalize the nanotubes. Hexadecane was used as a costabilizer and oil-soluble initiator AIBN was used for the polymerization. After the polymerization, the whole reaction contents were poured into a large volume of pure isopropyl alcohol to recover the nanocomposite. The incorporation of nanotubes in the polymer matrix was successfully achieved as demonstrated in Figure 2.4. The incorporation of nanotubes resulted in the black coloration of the nanocomposites materials as well as significant reduction in the electrical resistivity of the composite material. Raman spectra for the composite material also indicated a reduced vibrational freedom of the polymer chains as a consequence of the nanotube incorporation. An adsorbed polymer layer on the nanotube bundles was achieved as shown in Figure 2.4 which was observed to contribute to a better dispersion of the nanotubes.

Velasco-Santos et al. (28) also reported the *in-situ* polymerization of methyl methacrylate with both the treated and untreated nanotubes to generate polymer nanocomposites. The amount of initiator AIBN, reaction time and temperature were controlled to tune the molecular weight of polymer in the composites. The treated nanotubes had COOH and COO⁻ functionalities on the sidewalls

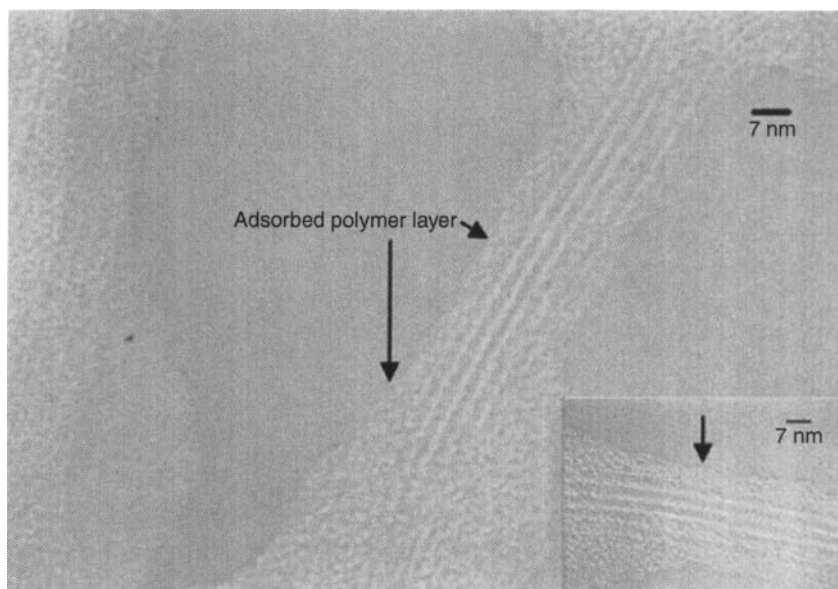


Figure 2.4. TEM micrographs showing nanotube bundles with an adsorbed polystyrene layer in a 8.5% weight SWNT-PS composite. Reproduced from reference 27 with permission from American Chemical Society.

as well as tips and resulted in better property enhancement of the composites as compared to the untreated nanotubes. The authors suggested that the use of *in-situ* polymerization as well as functionalization of the nanotubes lead to the synergistic reinforcement of the organic and inorganic components of the composite.

Some studies on the grafting of the polymer chains from the surface of the nanotubes have also been reported. Qin et al. reported the polymerization of n-butyl methacrylate from the surface of nanotubes by using controlled living polymerization method (29). Gao et al. also followed the similar grafting from the surface approach and polymerized methyl methacrylate on the surface by using atom transfer radical polymerization (30). Figure 2.5 shows the schematic of the process in which an atom transfer radical polymerization initiator was covalently immobilized on the surface of the nanotubes which was subsequently used to graft polymer brushes from the surface. The use of controlled polymerization methods allow the benefits to control the molecular characteristics of the polymer grafts thus allowing to tune the properties of the hybrids. A variety of polymer architectures like block copolymers, multi-arm brushes etc. can also be grafted by using the controlled polymerization mode.

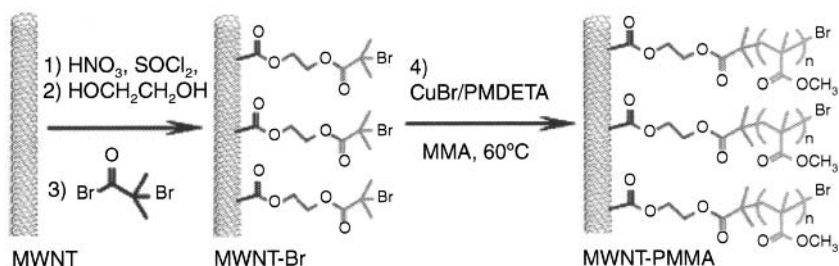


Figure 2.5. Schematic of grafting of PMMA chains from the surface of nanotubes using atom transfer radical polymerization. Reproduced from reference 30 with permission from American Chemical Society.

2.2.3 Melt Mixing

Melt mixing of polymer with the inorganic filler is a very attractive technique to synthesize nanocomposites using a large variety of polymers. This technique has also been exploited in great details for the polymer clay systems and the generated knowledge and experience is applicable also to polymer nanotube nanocomposites in many ways. The advantage of this technique is the direct mixing of the polymer at high temperature with the filler thus requiring no solvent which makes this process more industrially attractive as well as environmentally friendly. The nanotubes have also been reported to have a lesser extent of fiber breakage during compounding in melt (31–32). The dispersion is also generally improved because of the presence of high extents of shear in melt compounding equipments. Longer processing times also lead to better mixing of organic and inorganic phases and alignment of the nanotubes in the composites can also be improved when elongational flow is additionally applied. However, melt mixing may also lead to serious degradation of the polymer if the compounding temperature is too high or very long processing times are used. The organic surface modifications immobilized on the sidewalls of the nanotubes are also prone to thermal damage during the compounding thus requiring an optimal mixing temperature and mixing time which do not cause the thermal damage but are also high and long enough to ensure homogenous mixing.

Pötschke et al. (33) reported the polycarbonate nanocomposites by melt mixing method using twin-screw co-rotating intermeshing extruder. Compounding temperature of 240°C , screw speed of 280 rpm and a feed rate of 980 g/h were used for the composite generation. The SEM investigations of the polymer nanotube masterbatches as shown in Figure 2.6 revealed random orientation of nanotubes and

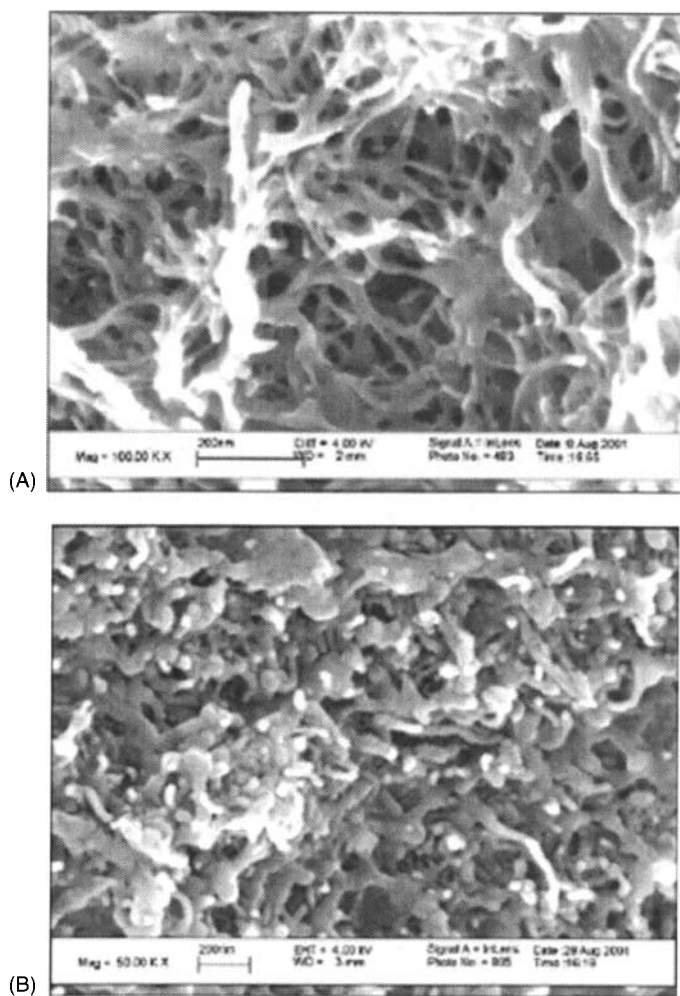


Figure 2.6. SEM micrographs of fracture surfaces of polycarbonate nanotube composites containing (a) 20 wt% filler and (b) 15 wt% filler. Reproduced from reference 33 with permission from Elsevier.

formation of interconnecting structures. The authors also reported that it was not possible to estimate fiber length from the micrographs owing to the complex nanotube network. The diameters of the nanotubes in the composites were observed to be in the range of 10 to 50 nm which is higher than the other studies reporting the diameter in the range of 10 to 15 nm. It was suggested that a thick polycarbonate layer existed on the surface of nanotubes thus increasing the diameter as well as indicating some extents of interphase mixing or phase adhesion.

Shih et al. (34) reported biodegradable poly(butylene succinate) nanocomposites through melt blending in a counter-rotating internal mixer with a rotation speed of 60 rpm for 5 min at 120°C. The authors observed that the generated composites consisted of well-dispersed nanotubes and exhibited enhanced thermal and mechanical properties. Kim et al. (35) reported the thermotropic liquid crystalline polymer (TLCP) nanocomposites prepared by a melt blending process in a Haake rheometer equipped with a twin-screw which was operated in intermeshing co-rotating mode. The temperatures of the heating zone from the hopper to the die were set to 290, 300, 305, and 295°C, and the screw speed was fixed at 40 rpm. The polymer and nanotubes were physically mixed before feeding them to the extruder. The microscopic investigation of the resulting composites, as shown in Figure 2.7, revealed that nanotubes were embedded in the polymer from both the ends, though some of them were pulled out from the matrix. As shown in the image, some nanotubes also broke while still remaining strongly embedded in the polymer matrix thus indicating that CNTs had good interfacial mixing with TLCP matrix owing to positive interfacial interactions. Synthesis of poly(butylene terephthalate) nanotube nanocomposites was also reported using the melt blending in the rheometer equipped with twin-screw (36).

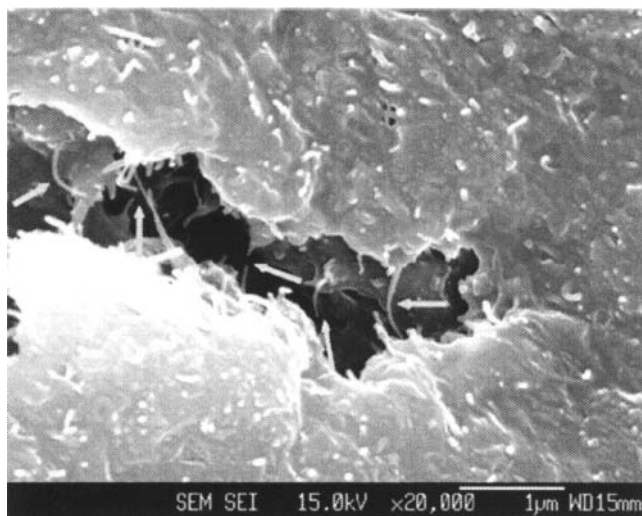


Figure 2.7. SEM image of the fracture surfaces for the nanocomposites containing 0.5 wt% of CNTs. The arrows indicate that the nanotubes were to be broken with their ends still embedded in the polymer matrix or they were bridging the local microcracks in the nanocomposites. Reproduced from reference 35 with permission from Elsevier.

Combination of solution mixing and melt mixing methods has also been reported (37). The nanotubes were dispersed in chloroform to which polyethylene powder was also mixed. The solvent was then evaporated and the mixture was dried in oven. The dry mixture was subsequently melt mixed using a twin-screw extruder with a 30 g bowl. The mixture was blended at a rate of 75 rpm using compounding temperature of 110°C and processing time of 10 min. Giraldo et al. (38) reported the synthesis of nylon nanocomposites using the co-rotating twin screw extruder using for heating zones from 230 to 250°C and a screw speed of 100 rpm. PA 11 nanocomposites incorporating different amounts of nanotubes were also reported by Huang et al. (39) using a twin screw extruder at 220°C and a screw speed of 80 rpm. The cryo-fracture SEM analysis of the composites indicated homogeneous dispersion of nanotubes throughout the PA11 matrix. The authors reported that upon failure, most of the MWNTs were broken apart, while many of them were still in the matrix. This behavior indicated a strong interfacial adhesion between the organic and inorganic components and a sufficient load transfer from the polymer to the nanotubes.

Ferguson et al. (40) and Schwartz and Bryant (41) also reported combined use of kneader and injection molding for the better dispersion of nanotubes in the composites. The authors reported that the CNTs did not break or orient because of their size and geometry, and therefore, conductivity of the nanocomposite was retained even after subsequent processing. The physical properties of the polymer were also retained due to small amount of CNTs present in the matrix. Alignment of nanotubes in the composites was also reported to be tunable by using several melt-mixing methods. Spinning of extruded melt samples was demonstrated as a method to generate the well aligned polypropylene nanocomposites (42).

2.3 Properties of Polymer Nanotube Nanocomposites

2.3.1 Mechanical Properties

Hou et al. (43) reported the poly(vinyl alcohol) nanocomposites using single walled (SWNT), few walled (FWNT) and multi walled (MWNT) nanotubes. The nanotubes were covalently functionalized to generate acid functionalities on the sidewalls. The incorporation

of nanotubes even in the amount of 0.2 wt% in the polymer was observed to enhance the Young's modulus and tensile strength of the polymer significantly. Though all the different types of nanotubes resulted in higher tensile properties, but the FWNTs were observed to be particularly beneficial. The Young's modulus of the composites with 0.2 wt% of the functionalized FWNTs was observed to be 6.33 GPa, which was 1.99 GPa higher than the pure polymer. Similarly, the tensile strength was also much better for the composites with FWNTs as demonstrated in Figure 2.8a. Increasing the amount of nanotubes in the composites also correspondingly enhanced the tensile strength as shown in Figure 2.8b. The authors reported that the FWNTs had diameters in the range of 3–8 nm and length in the range of 20 μm . The higher diameter and thicker wall FWNTs were reported to be much easier to be individually dispersed in solvent or polymer than SWNTs (also confirmed by the electron microscope images of the composite materials).

In polyamide nanocomposites (39), the storage modulus of the composites was reported to increase steadily with increasing the loading of MWNTs. At 2 wt% concentration of the nanotubes, the storage modulus of the nanocomposite was measured to be 1.97 GPa, which is an increase of 54% than the storage modulus of 1.28 GPa for the pure polyamide matrix.

Cao et al. (44) reported nanotube incorporation in Chitosan with medium molecular weight. The polymer, MWNTs and the composites with different fractions of MWNTs were characterized by X-ray diffraction. The MWNTs exhibited a sharp diffraction peak at about 2 θ

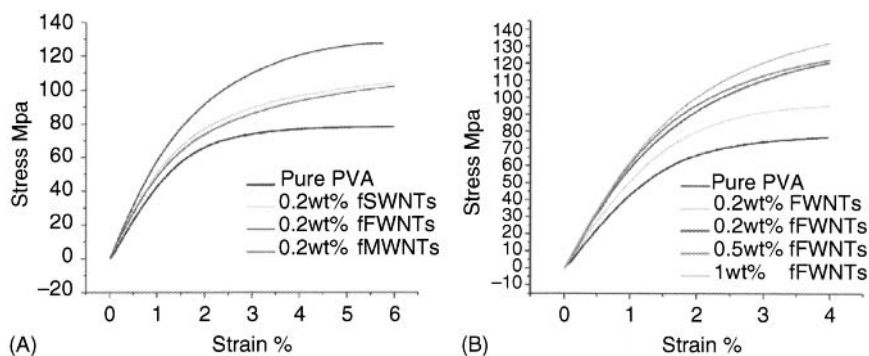


Figure 2.8. Stress-strain curves of nanotube nanocomposites (a) containing 0.2 wt % of different types of functionalized CNTs and (b) containing different concentration of fFWNTs. Reproduced from reference 4 with permission from American Chemical Society.

of 25.8° , which is caused by the regular arrangement of the concentric cylinders of graphitic carbon (45). However, the diffraction peak associated with nanotubes was absent in chitosan nanocomposites which indicated the effective dispersion of nanotubes in the polymer matrix. A small amount of nanotubes were reported to significantly affect the mechanical performance of the nanocomposites. With 3 wt% nanotubes in the composites, the tensile strength and Young's modulus increased from 39.6 MPa and 2.01 GPa for the pure polymer to 105.6 MPa and 4.22 GPa for the composite respectively. The elongation at break was also observed to be only slightly reduced owing to the incorporation of 1 wt% of filler. However, this decrease was much more significant when the filler content was higher than 1 wt% owing to some extent of aggregation of the nanotubes on increasing filler content.

Zhang et al. (46) reported the polyimide nanocomposites with nanotubes containing $\text{CH}_3(\text{CH}_2)_{17}\text{NHCO}$ functional groups on the surface. The microscopic investigation of the composites confirmed the uniform distribution of the nanotubes in the polymer matrix. The nanotubes appeared as an interconnected structure at a loading of 7 wt% or higher indicating a nanotube network. The tensile strength of the pure polymer was measured to be 89 MPa, which increased to 130 MPa at a filler loading of 7 wt%.

However, further increase in the filler fraction in the composites led to a reduction in the tensile strength. The improvement in the tensile strength was suggested to be due to strong interactions between the polymer matrix and the nanotubes. Also, the elongation at break was only gradually decreased with increasing the nanotube fraction. The tensile modulus of the composite was also observed to linearly increase with increasing nanotube content and the modulus of the nanocomposite with 7 wt% filler loading was more than twice the modulus of the pure polymer. The modulus was slightly reduced on further increasing the nanotube fraction.

Polymer nanocomposites with medium density polyethylene were reported with a variety of fluorinated and un-fluorinated nanotubes (37). The nanocomposites consisting of 1 wt% F-SWNT- $\text{C}_{11}\text{F}_x\text{H}_y$ (fluorinated and surface treated nanotubes) nanotubes showed an increase in tensile strength by 52.4%, modulus by 15.9% and elongation by 18.9% as compared to the pure polymer. The composites with 1 wt% F-SWNT- $\text{C}_{11}\text{H}_{23}$ (fluorinated and surface treated nanotubes) had an increase of 28.3% in modulus as compared to the pure polymer. The tensile strength also increased from 4.33 MPa for the pure polymer to 5.01 Mpa for the nanocomposite, the elongation at

break was however observed to decrease. The 1 wt% SWNT (pristine nanotubes) nanotube nanocomposite showed an 11% increase in tensile strength as compared to polymer. The modulus also increased from 637 MPa for the pure polymer to 763 MPa for the nanocomposite. The 1 wt% F-SWNT (fluorinated nanotubes) nanotube composites however showed a decrease in both the tensile strength as well as tensile modulus of the composites as compared to pure polymer.

Poly(butylene terephthalate) (PBT) nanocomposites incorporating different fractions of nanotubes were reported by Kim et al. (36). The storage modulus of the nanocomposites was observed to increase on the incorporation of nanotubes into the PBT matrix which was attributed to the physical interactions between PBT matrix and nanotubes. The nanocomposites also exhibited higher tensile strength and tensile modulus as compared to the pure polymer. At 2 wt% of the filler content in the composites, the tensile strength and tensile modulus were significantly increased by 35.1 and 21.7%, respectively. The enhancement in the mechanical properties was much more significant at the low filler fractions than at higher fractions. The authors suggested that nanotubes at higher concentrations tended to bundle together because of their intrinsic van der Waals attractions between the individual nanotubes in combination with high aspect ratio and large surface area.

Ji et al. (47) reported the poly(acrylonitrile) nanotubes composite nanofiber sheets with high mechanical performance. The tensile strength and modulus of the pure poly(acrylonitrile) terpolymer nanofiber sheet (without nanotubes) were reported to be 71.9 MPa and 2.2 GPa, respectively. On the incorporation of 2.0 wt % functionalized multi walled nanotubes, the tensile strength and modulus was observed to enhance to about 114.8 MPa and 3.2 GPa. The properties were also significantly enhanced after hot stretching processes owing to the alignment and orientation of macromolecular chains. The tensile strength and modulus of the pure terpolymer fiber sheet increased to about 215.9 MPa and 3.6 GPa, respectively. The composite samples with 2 wt % functionalized nanotubes also exhibited marked increases in tensile strength from 114.8 to 302.5 MPa and in modulus from 3.2 to 6.7 GPa owing to the improved alignment of nanotubes. Figure 2.9 shows the mechanical performance of the composites. The experimental values have also been compared to the calculated values of the mechanical properties as a function of increasing the content of nanotubes in the composites. The experimental and theoretical values were observed to match only at low concentrations of

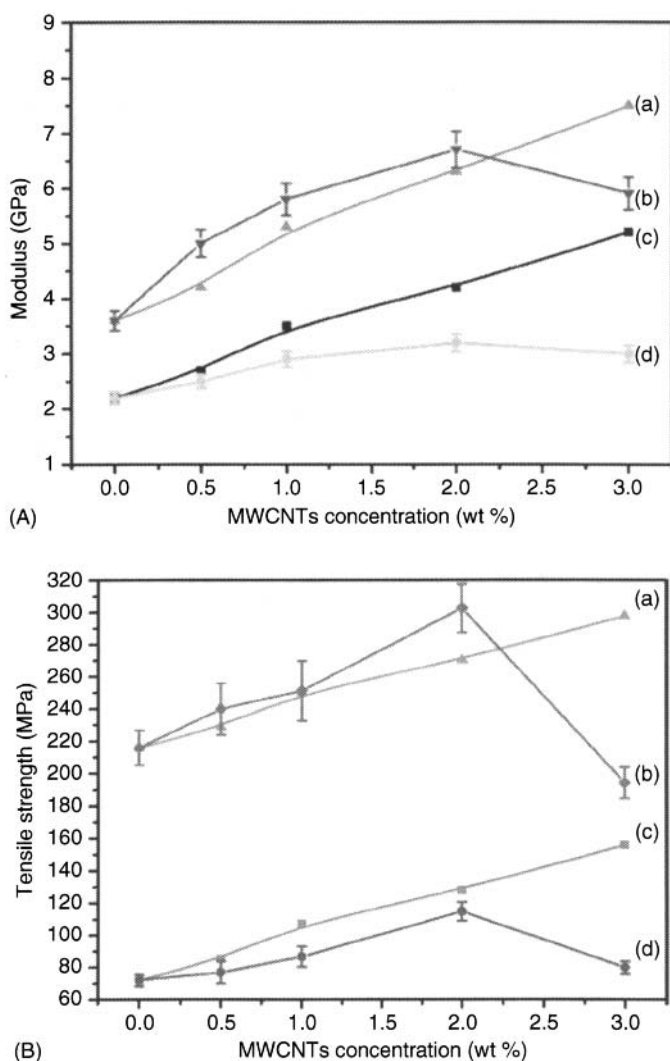


Figure 2.9. (a) and (b) Tensile modulus and strength of PAN nanocomposites. Curves a and c represent theoretical values of hot stretched and original electrospun composites, whereas curves b and d represent the experimental values of these composites. Reproduced from reference 47 with permission from American Chemical Society.

the filler, whereas at high concentrations of filler, these values have significant discrepancies owing to the aggregation of the nanotubes in the composites.

Kim et al. (35) studied the thermotropic liquid crystalline polymer (TLCP) nanocomposites with varying extents of nanotubes. The mechanical performance of the nanocomposites has been demonstrated

in Table 2.1. Increasing the nanotube extent, an increase in both the strength and modulus of the composites as compared to pure polymer was observed. However, these values were always smaller than the calculated values using the Halpin Tsai equations probably owing to incomplete exfoliation and the misalignment of the nanotubes.

Geng et al. (48) reported epoxy nanocomposites with pristine, silane treated and surfactant treated (Triton) nanotubes as a function of increasing the content of nanotubes. The authors observed that both the flexural strength and modulus of the nanocomposites were enhanced with incorporation of nanotubes using differently modified nanotubes. The surfactant treated nanotubes were observed to be much effective than the silane treated or pristine nanotubes in enhancing the composite properties. It was also observed that the flexural properties attained an optimum at roughly 0.1% after which the incorporation of nanotubes was either not effective or the properties even started to degrade as shown in Figure 2.10. The authors explained that the mechanical performance of the nanotubes was a result of two interrelated factors: interfacial adhesion and dispersion of nanotubes in the polymer matrix.

Fragneaud et al. (49) reported polystyrene nanocomposites using as received nanotubes (a-CN_x) and polystyrene grafted nanotubes (PS-g-CN_x). The morphology of the generated composites containing 2.5 vol% of the nanotubes was analyzed through the fracture surfaces and is demonstrated in Figure 2.11. The nanocomposites containing polystyrene grafted nanotubes had better dispersion of the nanotubes within the polymer matrix. Only small extent of aggregation was observed, whereas in the composites containing untreated nanocomposites, larger agglomerations (up to 10 μ m) were observed. This inhomogeneous dispersion of nanotubes in the polymer matrix was observed by the authors to result in a poor

Table 2.1. Mechanical performance of the TLCP nanocomposites

Materials	Experimental results		Theoretically predicted values	
	σ_c (MPa)	E_c (GPa)	σ_c (MPa)	E_c (GPa)
TLCP	83.10	1.96	–	–
TLCP/CNT 0.5	110.23	2.43	118.79	2.46
TLCP/CNT 1.0	114.41	2.55	154.61	2.97
TLCP/CNT 1.5	117.54	2.63	190.55	3.48

Reproduced from reference 35 with permission from Elsevier.

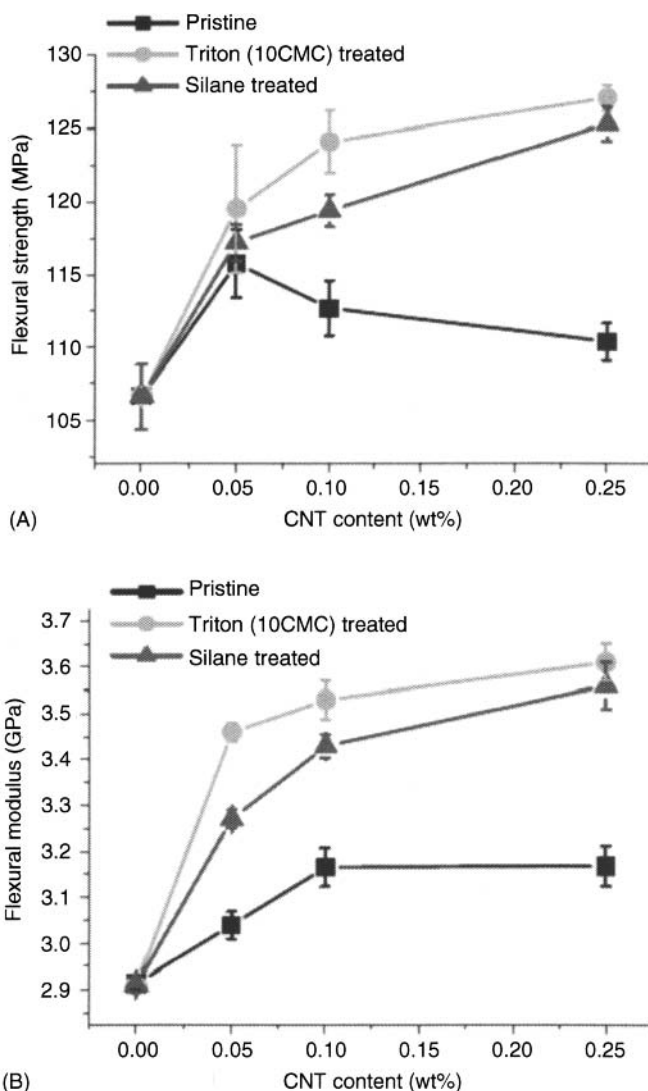


Figure 2.10. (a) Flexural strength and (b) modulus of epoxy nanocomposites as a function of increasing the filler fraction. Reproduced from reference 48 with permission from Elsevier.

interfacial adhesion and lower load transfer. The tensile properties were also significantly impacted similar to morphology by the presence of treated or untreated nanotubes. The tensile modulus of the composites containing 2.5 vol% untreated nanotubes was 2.5 GPa, which is 20% higher than the tensile modulus of 2.20 GPa for the

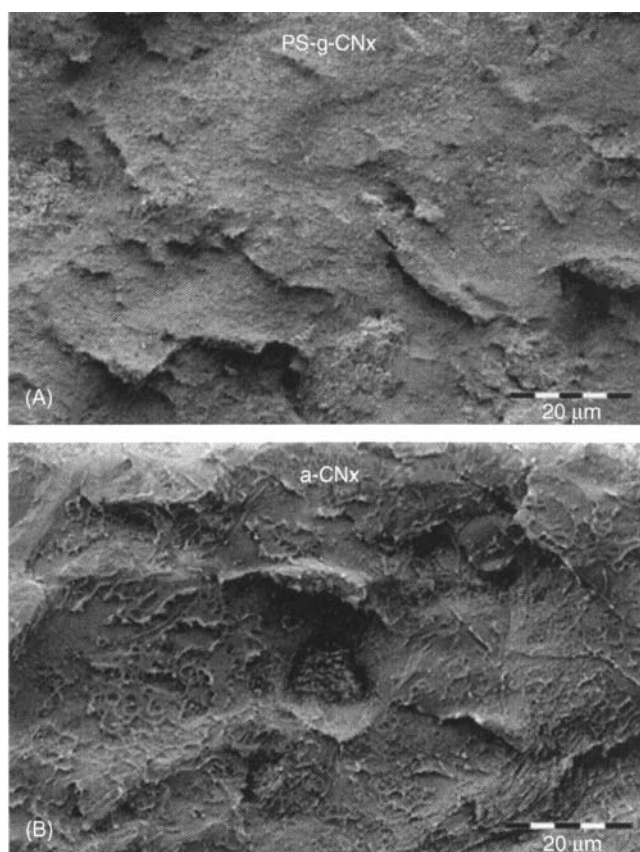


Figure 2.11. SEM micrographs of the nanocomposites containing 2.5 vol% of the (a) polymer grafted nanotubes and (b) as received nanotubes. Reproduced from reference 49 with permission from Elsevier.

pure polymer matrix. When 2.5 vol% of the grafted nanotubes were incorporated in polystyrene matrix, an increase of 33% in tensile modulus as compared to the pure polymer was observed.

Du et al. (50) reported the synthesis of butadiene styrene rubber nanocomposites with halloysite nanotubes. The tensile properties of the composites containing various amounts of nanotubes are depicted in Table 2.2. The tensile properties were observed to significantly increase as a function of increasing amount of nanotubes in the composites. For the maximum loading of the nanotubes, a tensile modulus of 5.56 MPa was observed as compared to 1.52 MPa for the pure polymer.

In the poly(butylene succinate) nanocomposites reported by Shih et al. (34), storage modulus increased with increasing the content

Table 2.2. Mechanical properties of butadiene styrene rubber nanocomposites with halloysite nanotubes

Nanocomposites	Modulus at 100% elongation, MPa	Tensile strength, MPa	Tear strength, kN/m ²	Elongation at break, %	Hardness, Shore A
xSBR	1.52 (0.16)	10.0 (0.44)	19.4 (1.63)	372 (20.0)	55
XSBR2H	2.37 (0.22)	10.4 (0.52)	25.2 (1.25)	236 (18.2)	62
XSBR5H	2.92 (0.30)	11.4 (0.58)	26.0 (0.31)	277 (19.2)	70
xSBR10H	3.48 (0.20)	12.9 (0.09)	32.0 (1.84)	279 (22.2)	75
xSBR20H	5.08 (0.21)	13.6 (0.62)	36.0 (2.15)	259 (21.3)	78
xSBR30H	5.56 (0.19)	15.3 (0.77)	32.0 (0.92)	267 (17.3)	80

Reproduced from reference 50 with permission from Elsevier.

of organically modified nanotubes. Untreated nanotubes were also observed to initially enhance the storage modulus, but after 1.5 wt% content, the storage modulus deteriorated owing to the aggregation of these pristine nanotubes in the polymer. Also, when comparing the two nanotube systems with each other, the enhancements of the mechanical properties of the modified nanotube system at various temperatures were more remarkable than those of the unmodified nanotube system. An increase of 84% in the storage modulus of the composites containing 3 wt% of unmodified nanotubes was observed at 25 °C, whereas this increase was 120% when same amount of modified nanotubes were added to the polymer.

Eitan et al. (1) reported the synthesis of polycarbonate nanocomposites with untreated (as received) and epoxide treated nanocomposites. A 70% increase in the tensile modulus in the nanocomposites as compared to pure polymer with 5 wt% of the untreated nanotubes was observed as shown in Figure 2.12. However, this increase was increased to 95%, when same amount of epoxide treated nanotubes were used thus indicating the significance of interfacial interactions on the composite properties.

In the epoxy nanocomposites containing untreated as well as maleic anhydride grafted nanotubes (51), the tensile strength was observed to increase by 50% at 1 wt% of the modified nanotubes, whereas the untreated nanotubes led to only a slight increase in the tensile strength which subsequently decreased on further addition of these pristine nanotubes. The tensile modulus of the nanocomposites was observed

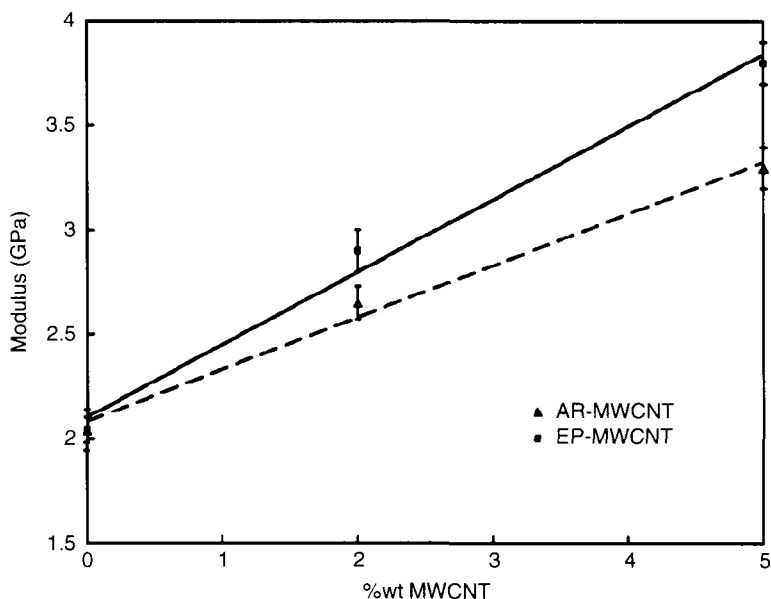


Figure 2.12. Enhancement of the tensile modulus of the polycarbonate nanocomposites as a function of nanotube content in the composites, while using as received (AR) and epoxide treated (EP) multi walled nanotubes. Reproduced from reference 1 with permission from Elsevier.

to increase the filler content of both untreated and treated nanocomposites. However, the extent of increase was much higher in the composites containing modified nanotubes. An increase of 100% in the modulus was observed on the incorporation of 1.0 wt % of modified nanotubes as compared to a 42% increase for the untreated nanotubes. The elongation at break also increased significantly in the composites containing modified nanotubes owing to the better interfacial interaction between the polymer and the nanotube surface.

2.3.2 Thermal and Electrical Properties

Huang et al. (39) reported that in polyamide (PA 11) nanocomposites, the incorporation of nanotubes led to the increase in the peak degradation temperature of the polymer. At an amount of 1 wt% nanotubes in the composites, the peak degradation temperature was enhanced by 20°C. However, the degradation temperature reduced at higher concentrations of nanotubes probably owing to the aggregation of the nanotubes in the composites.

Poly(3-hexylthiophene) (P3HT) nanotube nanocomposites were reported by Saini et al. (52) containing different loadings of MWNTs (0.1 to 10 wt%). The derivative thermogravimetric analysis showed two decomposition temperatures, which originate from the decomposition of either side chains in the polymer or the thiophene rings or main chains in polymer as shown in Figure 2.13a. The decomposition temperature corresponding to the side chains was not affected by the different extents of nanotubes in the composite, whereas the temperature representing the decomposition of the main chain was much more significantly impacted by the addition of nanotubes. At low loadings of filler, this temperature was reported to enhance

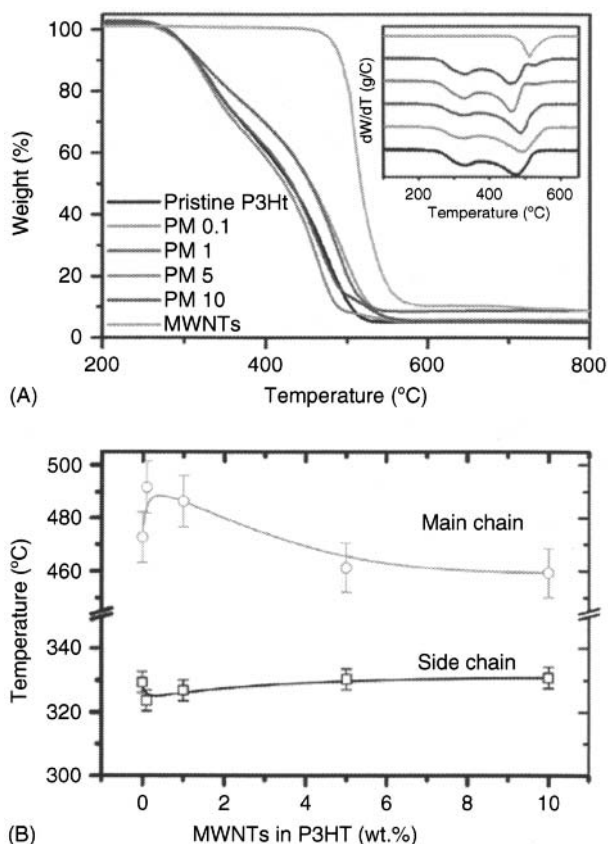


Figure 2.13. (a) TGA thermograms of pristine polymer as well as nanocomposites containing varying amounts of nanotubes and (b) degradation temperatures of side and main chain components of the polymer in the composites. Reproduced from reference 52 with permission from American Chemical Society.

by 20°C owing to the interactions between main chains of P3HT and graphitic walls of MWNTs. However, on increasing the extent of nanotube in the composites, the authors observed that this decomposition temperature decreases owing to only weak interaction between the nanotubes and the polymers due to the poorer dispersion of large amount of nanotubes in the polymer matrix. The poorer dispersion thus leads to reduced interaction between the nanotubes and polymer chains and increases interaction among the nanotubes. This phenomenon is demonstrated in Figure 2.13b.

Onset of degradation as well as peak degradation temperature were reported to shift to higher temperature with increasing MWNT content in the MWNT-polyimide nanocomposites (46). The onset of degradation temperature for the pure polymer was observed to be 570°C which increased to 577, 578 and 580°C for the nanocomposites containing 3, 7 and 10 wt% of the functionalized nanotubes, respectively. Peak degradation temperature of the polyimide polymer was measured to be 599°C, which was enhanced to 602, 619 and 630°C on the incorporation of nanotubes in loadings of 3, 7 and 10 wt%, respectively.

Giraldo et al. (38) reported polyamide 6 nanocomposites in which the crystallization temperature of the polymer was observed to increase with the addition of 2 wt% CNTs. The temperature was 185°C for the pure polyamide which subsequently increased to 190°C. The authors suggested that the nanotubes might serve as the nucleation sites for the polymer crystals to grow which was also confirmed by the reduction of the chain mobility by dynamic mechanical analysis. The thermal stability of the composites was reported to enhance after the incorporation of nanotubes.

Thermal behavior of polyethylene nanocomposites with different nanotubes was reported by Pulikkathara et al. (37). Two peaks at 109.52°C and 111.91°C were observed in differential scanning thermograms of the pure polymer representing an intermediate/amorphous and a crystalline phase, respectively. It was observed that when pristine and alkylated SWNTs were incorporated in the polymer matrix, it resulted in a more phase-compatible morphology of the composites where only one peak was observed in the thermogram. However, when fluorinated SWNTs were added to the polymer, a more distinctively phase-separated morphology was favored where the differential scanning thermograms either exhibited two or three peaks. The thermogravimetric analysis of the nanocomposites also confirmed that the thermal stability of the nanocomposites was

slightly enhanced with the addition of nanotubes irrespective of their type.

The onset of crystallization temperatures in the poly(butylene terephthalate) nanocomposites were reported to significantly increase with the introduction of nanotubes (36). This also indicated the ability of nanotubes to act as strong nucleating agents for the crystallization of polymers. The extent of crystallization of the pure polymer also enhanced in the presence of CNTs. The thermal degradation studies of the pure polymer exhibited only one degradation peak indicating the random scission of the poly(butylene terephthalate) main chain. The thermal degradation behavior of the polymer nanocomposites were also observed to be similar to that of pure polymer indicating that the thermal decomposition of the PBT nanocomposites may primarily stem from PBT. The authors suggested that the nanotubes can effectively act as physical barriers to hinder the transport of volatile decomposed products out of the nanocomposites during thermal decomposition.

The incorporation of nanotubes into thermotropic liquid crystalline polymer (TLCP) was reported to enhance the thermal decomposition temperatures and the residual yields of the nanocomposites (35). It was reported that the nanotubes act as protective barriers in the nanocomposites against thermal decomposition and are likely to retard the thermal decomposition of the TLCP nanocomposites owing to building of barrier to hinder the transport of volatile decomposed products out of the nanocomposites.

Epoxy/nanotube nanocomposites were reported by Geng et al. (48) by using both silane modified as well as surfactant (Triton) modified nanotubes. Much higher increase in the glass transition temperature of the polymer in the composites was observed when surfactant functionalized nanotubes were incorporated in the polymer. The electrical conductivity of the nanocomposites was also observed to increase with increasing surfactant functionalized nanotubes content, presenting a percolating behavior with an associated conductivity surge by more than 10^6 S/cm.

Interesting thermal response of the polystyrene nanocomposites was reported when untreated and polystyrene grafted nanotubes were used for the reinforcement of polymer (49). The glass transition temperature of the pure polystyrene matrix was observed to be 99 °C. Similar transition temperature of 98 °C was observed for the composites containing 2.5 vol% of the untreated nanotubes. The nanocomposites containing polymer functionalized nanotubes

however had a glass transition temperature of 92 °C. The authors observed that the transition in the case of nanocomposites with functionalized nanotubes was much wider than for pure polystyrene matrix. It was opined that if polystyrene grafted layer on the nanotubes acts as a plasticizer in the composite, the matrix near to the interface with the grafted layer should have a lower transition temperature. Also, the matrix far away from the interface with polystyrene grafted layer should not have any change in the transition temperature. The authors suggested that this gradient of molecular mobility results into the DSC thermogram as a wider transition.

Yuen et al. (53) reported silane treated nanotube nanocomposites with polyimide. During the nanotube functionalization, silane was added in different amounts to the nanotube to alter the nature of the nanotube surfaces. These treated nanotubes are named as IPTES-MWNCT-1, 2 and 3 where 1, 2 and 3 represent the weight ratio of 3-isocyanatopropyltriethoxysilane (IPTES) to nanotubes used during the functionalization reaction. As shown in Figure 2.14, incorporation of 6.98 wt% of acid-modified MWNTs in the polymer matrix led to the decrease of surface electrical resistivity of the composites by roughly six orders of magnitude. Similarly, the volume resistivity of the composites also decreased by nine orders of magnitude. The silane modified nanotubes, on the other hand, were much more effective in decreasing the surface and volume resistivity of the nanocomposites. At the same filler content of 6.98 wt%, the surface electrical resistivity decreased by seven orders of magnitude for IPTES-MWCNT-1 and IPTES-MWCNT-2, whereas it decreased by eight orders of magnitude for IPTESMWCNT-3. Similarly, volume

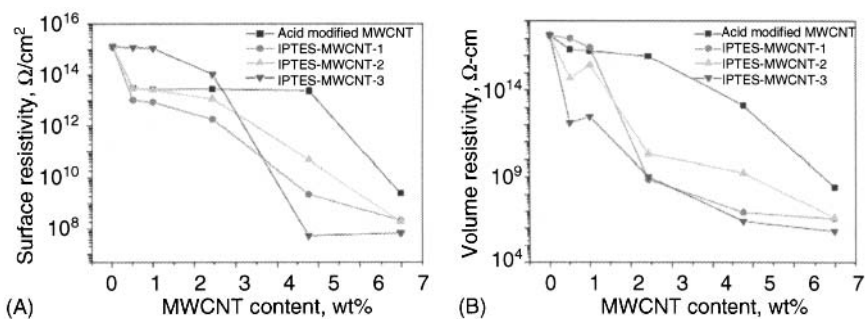


Figure 2.14. (a) Surface and (b) volume resistivity of the polyimide nanocomposites as a function of nanotube content in the nanocomposites. Reproduced from reference 53 with permission from Elsevier.

resistivity was also observed to decrease by eleven orders of magnitude for IPTES-MWCNT-1 and IPTESMWCNT-2 and by twelve orders of magnitude for IPTES-MWCNT-3.

Shih et al. (34) reported in the poly(butylene succinate) nanocomposites that the addition of the nanotubes increased decomposition temperature. The effect was much more significant when the surfactant modified nanotubes were used. The decomposition temperature for the nanocomposites containing 3 wt% of the surface modified nanotubes increased from 367.2 to 379.5 °C, whereas it increased for the nanocomposites containing pristine nanotubes from 367.2 to 374.0 °C. The differential scanning calorimetry analysis on the nanocomposites also exhibited higher re-crystallization temperatures of the nanocomposites as compared to the pure poly(butylene succinate). The temperatures also increased on increasing the nanotube content, indicating that the nanotubes acted as a nucleating agent for the polymer and promoted the crystallization rate of the polymer also observed in the studies mentioned earlier.

Sung et al. (54) reported the electrical conductivity of the polycarbonate multi walled nanotube nanotubes as a function of nanotube content. Nanotubes without treatment as well as after treatment with H_2O_2 (freeze drying or thermal drying) were used for the composite synthesis. For the composites with untreated nanotubes, the electrical conductivity showed the percolation threshold at about 5 wt% of filler content. However, this value was advanced to 2 and 3 wt% of filler content for the composites containing H_2O_2 treated nanotubes by freeze drying and H_2O_2 treated nanotubes by thermal drying. The electrical conductivity values in the composites containing treated nanotubes were also observed to be much higher than the composites containing untreated nanocomposites. It was also reported that the electrical conductivity in the composites with H_2O_2 treated nanotubes with freeze drying was higher than the H_2O_2 treated nanotubes with thermal drying as shown in Figure 2.15.

Tseng et al. (51) reported the epoxy nanocomposites in which the nanotubes were functionalized by maleic anhydride by using plasma treatment. The thermal decomposition temperature was reported to increase with increasing the extent of the nanotubes in the composites as shown in Figure 2.16a. Untreated nanotubes were also used to reinforce the polymer and the increase in the decomposition temperature was also observed in this system as a function of filler content, but the enhancement was more significant using the functionalized nanotubes. This was attributed to

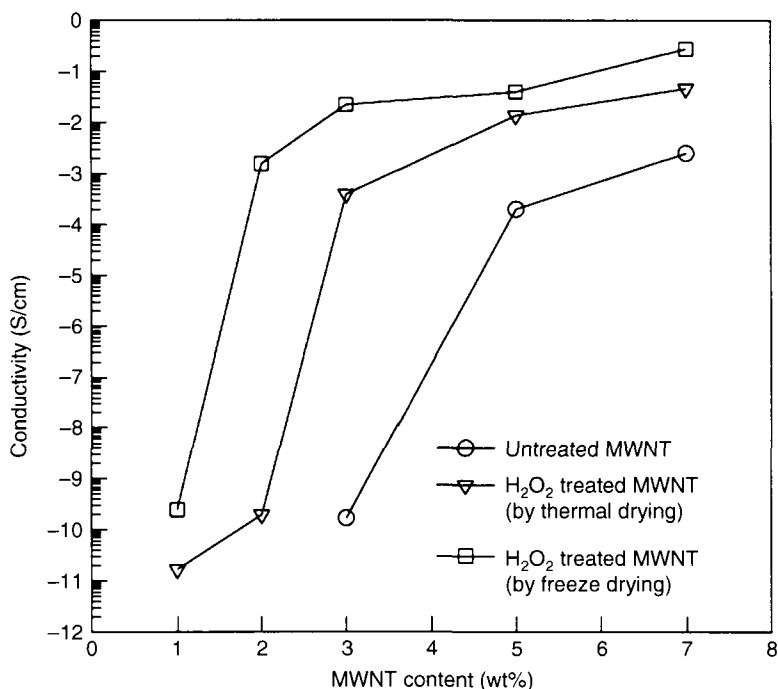


Figure 2.15. Electrical conductivity of polycarbonate nanocomposites by using different fractions of either unmodified nanotubes or H₂O₂ treated nanotubes. Reproduced from reference 54 with permission from Elsevier.

the strong bonding interactions between maleic anhydride modified nanotubes and the epoxy matrix leading to the restriction of the thermal motion of the epoxy molecules thus imparting better thermal stability. Similarly, the glass transition temperature of the composites was also higher as compared to pure polymer and was observed to increase as a function of the filler content. Owing to the similar reasons as stated above, the unmodified nanotubes had much less enhancement of the glass transition temperature as compared to the treated nanotubes as shown in Figure 2.16b.

Numerous other studies on the nanotube nanocomposites have been reported which demonstrate other properties like optical, morphological, fiber surface properties etc. Saini et al. (52) measured the UV absorption spectra of the poly(3-hexylthiophene) (P3HT) and its nanocomposites with varying amounts of nanotubes. The absorption band for pristine P3HT was observed at 505 nm which shifts toward the higher wavelength region on the addition of nanotubes

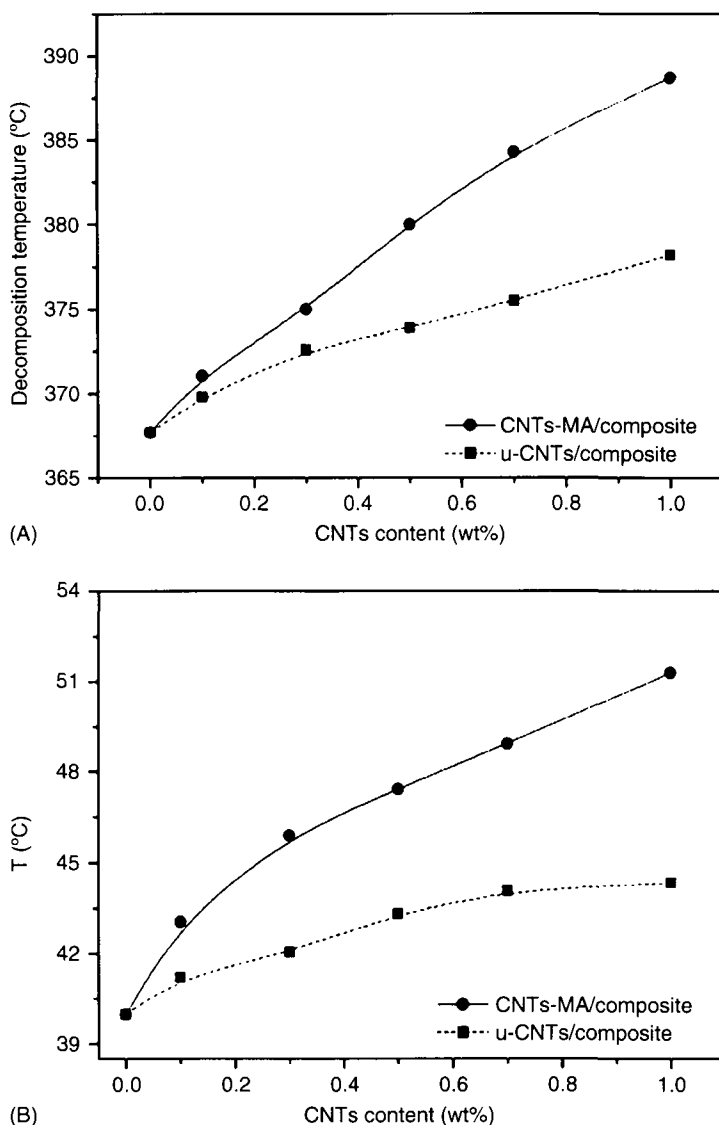


Figure 2.16. Enhancement of (a) decomposition temperature as well as (b) glass transition temperature as a function of filler content in epoxy nanocomposites. Reproduced from reference 51 with permission from American Chemical Society.

indicating a decrease in band gap which is a result of the interaction between P3HT and nanotube. On increasing the MWNT content in the composites, the spectrum broadened suggesting a change in the morphology of spin-coated films. It was reported by Woo et al. (55)

that single walled nanotubes in poly(m-phenylene vinylene-co-2,5-dioctoxy-p-phenylene vinylene) (PmPV) blocked hole transport in the composite by forming hole traps in the polymer matrix induced by image charge effects between SWCNTs and the charge carriers.

References

1. A. Eitan, F.T. Fisher, R. Andrews, L.C. Brinson, and L.S. Schadler, *Composites Science and Technology*, Vol. 66, p. 1159, 2006.
2. M.-F. Yu, O. Lourie, M. Dyer, K. Moloni, T.F. Kelly, and R.S. Ruoff, *Science*, Vol. 287, p. 637, 2000.
3. M.-F. Yu, B.S. Files, S. Arepalli, and R.S. Ruoff, *Physical Review Letters*, Vol. 84, p. 5552, 2000.
4. M.M.J. Treacy, T.W. Ebbesen, and J.M. Gibson, *Nature*, Vol. 381, p. 678, 1996.
5. G. Gao, T. Cagin, and W.A. Goddard III, *Nanotechnology*, Vol. 9, p. 184, 1998.
6. J.P. Lu, *Journal of Physics and Chemistry of Solids*, Vol. 58, p. 1649, 1997.
7. Z.C. Tu, and Z.C. Ou-yang, *Physical Reviews B*, Vol. 65, p. 233, 2002.
8. K.-T. Lau, C. Gu, and D. Hui, *Composites: Part B*, Vol. 37, p. 425, 2006.
9. T. Belytschko, S.P. Xiao, G.C. Schatz, and R.S. Ruoff, *Physical Reviews B*, Vol. 65, p. 2354, 2002.
10. A. Maiti, A. Svizhenko, and M.P. Anantram, *Physical Review Letters*, Vol. 88, p. 126905, 2002.
11. R.S. Ruoff, and D.C. Lorents, *Carbon*, Vol. 33, p. 925, 1995.
12. J.P. Salvetat, A.D. Briggs, J.M. Bonard, R.R. Bacsá, A.J. Kulik, T. Stöckli, N.A. Burnham, and L. Forro, *Physical Review Letters*, Vol. 82, p. 944, 1999.
13. L. Jin, C. Bower, and O. Zhou, *Applied Physics Letters*, Vol. 73, p. 1197, 1998.
14. E.S. Choi, J.S. Brooks, D.L. Eaton, M.S. Al-Haik, M.Y. Hussaini, H. Garmestani, D. Li, and K. Dahmen, *Journal of Applied Physics*, Vol. 94, p. 6034, 2003.
15. D. Qian, E.C. Dickey, R. Andrew, and T. Rantell, *Applied Physics Letters*, Vol. 76, p. 2868, 2000.
16. C.A. Cooper, S.R. Cohen, A.H. Barber, and H.D. Wagner, *Applied Physics Letters*, Vol. 81, p. 3873, 2002.
17. K.T. Lau, and D. Hui, *Carbon*, Vol. 40, p. 1597, 2002.
18. K.T. Lau, M. Chipara, H.Y. Ling, and D. Hui, *Composites: Part B, Engineering*, Vol. 35, p. 95, 2004.
19. J. Suhr, W. Zhang, P.M. Ajayan, N.A. Koratkar, *Nano Letters*, Vol. 6, p. 219, 2006.
20. M.J. Biercuk, M.C. Llaguno, M. Radosavljevic, J.K. Hyun, A.T. Johnson, and J.E. Fischer, *Applied Physics Letters*, Vol. 80, p. 2767, 2002.
21. B. Safadi, R. Andrews, and E.A. Grulke, *Journal of Applied Polymer Science*, Vol. 84, p. 2660, 2002.
22. P.C.P. Watts, W.K. Hsu, G.Z. Chen, D.J. Fray, H.W. Kroto, and D.R.M. Walton, *Journal of Materials Chemistry*, Vol. 11, p. 2482, 2001.
23. O. Breuer, and U. Sundararaj, *Polymer Composites*, Vol. 25, p. 630, 2004.

24. B. Vigolo, P. Launois, M. Lucas, M. Badaire, P. Bernier, and P. Poulin, *Materials Research Society Symposium Proceedings*, Vol. 706, p. 3, 2002.
25. L. Jin, C. Bower, and O. Zhou, *Applied Physics Letters*, Vol. 73, p. 1197, 1998.
26. F. Tsui, L. Jin, and O. Zhou, *Applied Physics Letters*, Vol. 76, p. 1452, 2000.
27. H.J. Barraza, F. Pompeo, E.A. O'Rear, and D.E. Resasco, *Nano Letters*, Vol. 2, p. 797, 2002.
28. C. Velasco-Santos, A.L. Martinez-Hernandez, F.T. Fisher, R. Ruoff, and V.M. Castano, *Chemistry of Materials*, Vol. 15, p. 4470, 2003.
29. S. Qin, D. Qin, W.T. Ford, D.E. Resasco, and J.E. Herrera, *Journal of the American Chemical Society*, Vol. 126, p. 170, 2004.
30. H. Kong, C. Gao, and D. Yan, *Journal of the American Chemical Society*, Vol. 126, p. 412, 2004.
31. J.C. Kearns, and R.L. Shambaugh, *Journal of Applied Polymer Science*, Vol. 86, p. 2079, 2002.
32. C.A. Cooper, D. Ravich, D. Lips, J. Mayer, and H.D. Wagner, *Composites Science and Technology*, Vol. 62, p. 1105, 2002.
33. P. Pötschke, T.D. Fornes, and D.R. Paul, *Polymer*, Vol. 43, p. 3247, 2002.
34. Y.F. Shih, L.S. Chen, and R.J. Jeng, *Polymer*, Vol. 49, p. 4602, 2008.
35. J.Y. Kim, D.K. Kim, and S.H. Kim, *European Polymer Journal*, Vol. 45, p. 316, 2009.
36. J.Y. Kim, *Journal of Applied Polymer Science*, Vol. 112, p. 2589, 2009.
37. M.X. Pulikkathara, O.V. Kuznetsov, I.R.G. Peralta, X. Wei, and V.N. Khabashesku, *Nanotechnology*, Vol. 20, p. 195602, 2009.
38. L.F. Giraldo, B.L. Lopez, and W. Brostow, *Polymer Engineering and Science*, Vol. 49, p. 896, 2009.
39. S. Huang, M. Wang, T. Liu, W.-D. Zhang, W.C. Tjiu, C. He, and X. Lu, *Polymer Engineering and Science*, Vol. 49, p. 1063, 2009.
40. D.W. Ferguson, E.W.S. Bryant, and H.C. Fowler, *SPE ANTEC '98*, p. 1219, 1998.
41. K.K. Schwartz, and E.W.S. Bryant, *SPE ANTEC '95*, p. 1358, 1995.
42. S. Kumar, H. Doshi, M. Srinivasaro, J.O. Park, and D.A. Schiraldi, *Polymer*, Vol. 43, p. 1701, 2002.
43. Y. Hou, J. Tang, H. Zhang, C. Qian, Y. Feng, and J. Liu, *ACS Nano*, Vol. 3, p. 1057, 2009.
44. X. Cao, H. Dong, C.M. Li, and L.A. Lucia, *Journal of Applied Polymer Science*, Vol. 113, p. 466, 2009.
45. O. Zhou, R.M. Fleming, D.W. Murphy, C.H. Chen, R.C. Haddon, and A.P. Ramirez, *Science*, Vol. 263, p. 1744, 1994.
46. Q. Zhang, J. Li, X. Zhao, and D. Chen, *Polymer International*, Vol. 58, p. 557, 2009.
47. J. Ji, G. Sui, Y. Yu, Y. Liu, Y. Lin, Z. Du, S. Ryu, and X. Yang, *Journal of Physical Chemistry C*, Vol. 113, p. 4779, 2009.
48. Y. Geng, M.Y. Liu, J. Li, X.M. Shi, and J.K. Kim, *Composites: Part A*, Vol. 39, p. 1876, 2008.
49. B. Fragneaud, K. Masenelli-Varlot, A. Gonzalez-Montiel, M. Terrones, and J.Y. Cavaillé, *Composites Science and Technology*, Vol. 68, p. 3265, 2008.
50. M. Du, B. Guo, Y. Lei, M. Liu, and D. Jia, *Polymer*, Vol. 49, p. 4871, 2008.

44 POLYMER NANOTUBE NANOCOMPOSITES

51. C.-H. Tseng, C.-C. Wang, and C.-Y. Chen, *Chemistry of Materials*, Vol. 19, p. 308, 2007.
52. V. Saini, Z. Li, S. Bourdo, E. Dervishi, Y. Xu, X. Ma, V.P. Kunets, G.J. Salamo, T. Viswanathan, A.R. Biris, D. Saini, and A.S. Biris, *Journal of Physical Chemistry C*, Vol. 113, p. 8023, 2009.
53. S.-M. Yuen, C.-C.M. Ma, C.-L. Chiang, *Composites Science and Technology*, Vol. 68, p. 2842, 2008.
54. Y.T. Sung, M.S. Han, K.H. Song, J.W. Jung, H.S. Lee, C.K. Kum, J. Joo, and W.N. Kim, *Polymer*, Vol. 47, p. 4434, 2006.
55. H.S. Woo, R. Czerw, S. Webster, D.L. Carroll, J. Ballato, A.E. Strevens, D. O'Brien, and W.J. Blau, *Applied Physics Letters*, Vol. 77, p. 1393, 2000.

New Microscopy Techniques for a Better Understanding of the Polymer/Nanotube Composite Properties

K. Masenelli-Varlot, A. Bogner, C. Gauthier,
L. Chazeau and J.Y. Cavaillé

*Université de Lyon, INSA-Lyon, MATEIS, UMR CNRS 5510, 7 avenue Jean
Capelle, 69621 Villeurbanne cedex, France*

Abstract

The main goal in material science is to provide behaviour laws, i.e. to be able to predict the material properties under given conditions (mechanical, electrical, environmental conditions, temperature, etc.). This requires relating microscopic parameters and local mechanisms to macroscopic behaviours, as there is no other way to express such behaviour laws based on chemical-physical parameters. In other words, the study of materials requires a large part of microstructural observation and analysis.

More specifically with nanocomposite materials, and as noted above, in most of the cases, interface between as received particles and organic matrices are very weak (bad adhesion), and one way to improve it consists in performing chemical grafting on the particle surface. If the chemical reactions are generally classical and work in solution, they can be much more difficult to achieve in heterogeneous media, which is the case for particle grafting. It is thus challenging to check the grafting effectiveness, and microscopy combining spectroscopy is probably the most powerful tool for such purposes.

We describe here three main microscopy techniques, namely local probe microscopy (STM, AFM, etc.), transmission microscopy (TEM) and scanning electron microscopy (SEM).

Keywords: microstructure, microscopy, nanocomposites, properties, microscopic parameters, spectroscopy.

3.1 Introduction

During the last decade, polymer nanocomposites have become one of the most active research fields in polymer science. One of the driving forces of this research is the appearance of new nano-sized objects with interesting properties, like nano-clays, cellulose whiskers and carbon based nanofillers (fullerenes, vapor grown carbon fibers, carbon nanotubes) (1). For instance, carbon nanotubes were first described in 1991 by the electron microscopist Iijima who was studying the arc-evaporation synthesis of fullerenes (2). These long and thin cylinders of carbon can be seen as concentric graphene sheets (a hexagonal lattice of carbon) rolled into cylinders. Just a few nanometer across, these cylinders can be tens of μm long, and each end is “capped” with half of a fullerene molecule (3). Nanotubes can have either a unique cylindrical wall (SWNTs) or multiple walls (MWNTs). Intrinsic mechanical properties of single-wall nanotubes have been theoretically predicted (Young’s Modulus ~ 1 TPa (4,5), maximum tensile strength ~ 30 GPa (6)). Moreover, they have excellent thermal conductivity, they are chemically inert and, depending on the details of their atomic arrangement (chirality), they behave as metals or semiconductors.

Carbon nanotubes have soon appeared as unavoidable candidates as reinforcing fillers in polymer composites. In addition to their intrinsic properties, they indeed display some of the specific features required for reinforcing fillers: one is their huge interfacial area (up to 100 to 1000 m^2 /g of fillers), that is known to favour the short distance filler-filler interaction, to increase the filler matrix interactions and even to modify molecular mobility of an important matrix fraction near the surface. Moreover, their high aspect ratio can lead to the formation of a percolating network at low nanotube content. In addition, the adhesion strength of the nanotube/polymer interface may also be a key factor for reinforcement, which explains that a lot of ongoing works have been focused on understanding the nature of nanotube/polymer matrix interactions and on the grafting of a polymer on nanotube surface (7,8).

Undoubtedly, understanding the reinforcement of carbon nanotubes based nanocomposites requires the characterization of several parameters of the nanotubes like diameters, lengths (and their distribution), structures (SWNT, MWNT). Moreover, after processing, the three-dimensional distribution of nanotubes within the polymer matrix, the presence of agglomerates, the interfacial properties have also to be precisely characterized. However, CNT based

nanocomposites are very difficult to characterize, because they must be observed at a very large scale range, from a few nm (CNT diameter) up to a few μm (CNT length). As a consequence, their characterisation requires the combination of various techniques. The main techniques which intend to characterize the nanocomposite microstructures are, roughly speaking, divided into two groups, namely microscopy and scattering techniques. Scattering techniques lead to information by modelling the interactions between nanoscopic heterogeneities and electromagnetic beams. The obtained information is an average over at least the whole volume in interaction with the beam (often in the order of mm^2). In this chapter, we will rather focus on microscopy techniques, which present the advantage of providing direct and local images.

In the following, we will review several imaging techniques, either based on beam/matter interactions (like electron microscopy either TEM or SEM) or techniques that probe the short distance interactions (like AFM), as they are well suited for the observation of nano-objects and have been extensively used to study nanotubes alone. The principles and the main results on polymer/nanotube composites provided by these imaging techniques (AFM, TEM and SEM) will be presented.

3.2 Near Field Microscopy

By comparison with electron microscopy, the main advantage of near field microscopy is to place a thin probe in the close vicinity of the sample, which avoids working in the propagation regime, and therefore avoids the limitation due to the use of an electromagnetic beam. This probe is located at a given distance from the sample in the nanometer range. To avoid any damage of the probe, a continuous control of the probe-to-sample distance is ensured. Data are processed from the detection of tip – sample interactions (distance, force, current, temperature, etc.). By scanning the sample surface (ensured by a piezoelectric system), a mapping of the chosen physical data can be obtained. Once the type of collected data is chosen, the lateral resolution mainly depends on the tip shape and its distance to the sample. Among the different local probes, two particular techniques have lateral resolutions of 0.1 nm suited to the study of nanocomposites and will therefore be detailed: scanning tunneling microscope (STM) and atomic force microscopy (AFM).

3.2.1 Principles of STM and AFM

The first near-field microscope was a scanning tunneling microscope (STM), invented in 1982. It was based on the tunneling effect which is the occurrence of a current between two conducting or semi-conducting materials at a distance is of few Å through an insulating medium, from the application of a voltage difference between them. The exponential dependence of this current with the tip-to-sample distance leads to the very good resolution of this technique.

Different modes can be used. The continuous current mode consists in keeping the tunneling current constant through a control loop which continually adjusts the sample-to-probe distance. Spectroscopic measurement can also be performed during the sample surface scan. It consists, after adjusting the probe-sample distance, in applying a variable voltage to measure its influence on the tunneling current, which in turn provides information on the chemical characteristics of the sample. The STM technique can also be enriched by *in situ* measurements of the photon emission induced by the de-excitation of atoms from the sample (following the ejection of electrons by interaction with the probe), enabling a fine analysis of the local optical properties.

Atomic force microscopy (AFM) was introduced a few years after as an application of scanning tunneling microscopy. By combining the principles of the STM with that of a profilometer, it enables imaging conductive or non conductive sample surfaces with lateral and vertical resolutions of 30 Å and 1 Å, respectively. The technique is based on the measurement of the interaction force between the tip and the sample surface. The force results from either the interaction potential between the sample and the tip atoms, or friction (during surface scanning). The force may also arise from magnetic or electrostatic interactions, if the tip is conducting or covered by a magnetic material.

The scheme of a typical AFM is presented in Figure 3.1. A cantilever holds the tip at one of its end. The tip position can be accurately measured from the reflection of a laser beam onto a set of four optical detectors. Basically, the relative displacement of the tip from the sample gives either access to the measured value, either to an isovalue surface when the loop controlled feedback adjusts the height of the sample surface to keep constant the value. In addition, the AFM tip can be static or oscillating (via its fixation on a piezoelectric device). Different types of imaging can be obtained depending on whether the tip is in contact or not with the sample, on whether the cantilever is working at its resonance frequency or at zero frequency, and

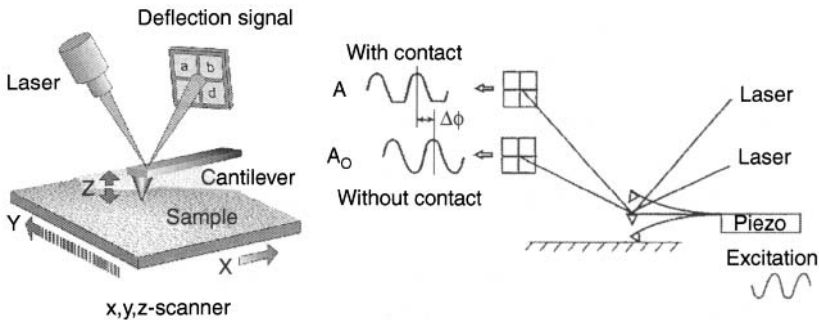


Figure 3.1. Schematic presentation of AFM device.

on whether the sample is vibrating or not. However, three main modes can be distinguished in AFM :

- Contact mode: in this mode, the cantilever is not vibrating. The tip is put in contact with the sample with a controlled load of the order of 10^{-8} N. This mode is similar to that of a classical profilometer. Its drawback is the wear or the deformation of the sample surface it may generate.
- Resonating mode: in this mode the cantilever oscillates with small amplitude at its resonance frequency, “far” from the sample. The gradient of the surface interaction force shifts this resonance frequency towards higher values. Inversely, at a given excitation frequency, the oscillation amplitude is modified and gives information on the local force gradient. This mode is however rarely used for topographical study.
- A tapping mode (also called intermittent contact mode): it is a non linear resonance mode. In this case, the oscillation amplitude is larger and the mean position of the tip is closer to the surface. The tip almost touches the surface at each oscillation. In this mode, friction can be avoided as well as the sample deformation and wear. Adhesion is also avoided thanks to the extremely short time of « contact ». The height of the sample is generally controlled so that the oscillation amplitude remains constant. The phase shift of the oscillation is then characteristic of the system dissipation, which is very useful for characterizing viscoelastic materials.

Other uses have been developed, as for instance the use of AFM tip as a local voltmeter. In that case, AFM becomes an Electrostatic

Force Microscope (EFM). Measurements can be performed under the application of a voltage between the sample and the tip. In the dc-EFM mode, a constant voltage is applied to the sample; the AFM is operating in non contact mode with the cantilever oscillating near its resonant frequency. In the ac-EFM mode, the voltage is oscillating so that the cantilever always oscillates at its resonance frequency.

3.2.2 Near Field Microscopy for Nanotubes

STM has mainly been used to characterize the electronic properties of nanotubes (9). For example, Bachtold et al. used EFM in both ac and dc modes to probe the nature of conduction in SWNTs and MWNTs (10).

The properties of the nanotubes alone have also been studied by AFM. For instance, Duesberg et al. measured the length distribution of nanotube samples and thus studied the influence of a purification process based on size exclusion chromatography (11). Moreover, the AFM device can be used as a nano-manipulator placed in a scanning electron microscope. Applying this idea, the first measurement of the stiffness of arc-MWNT pinned at one end was performed by Wong et al. (12) who gave an average value of 1.28 TPa. They also conducted strength measurements, obtaining an average value of 14 GPa. The modulus was also deduced from bending measurement of an arc-MWNT pinned at each end over a hole, by Salvétat et al. (13). The same type of measurement was also performed by Yu et al. still on MWNTs (14). Experiments on SWNT were performed later by the same authors (6,15).

3.2.3 AFM and CNT Composites

Dispersion studies:

AFM is a surface technique which needs flat surfaces, to avoid tip degradation during scanning. Such flat surfaces can be obtained from the sample surfaces directly after processing or from cryoultramicrotomy. The dispersion of MWNT in PE has thus been studied by AFM by McNally et al. (16). In this example, the image was taken without any sample preparation. The obtained image evidenced the nanotubes alignment along the flow direction during melt compounding. AFM tapping image has also enabled to check the dispersion of PS-grafted SWNT in PS (17) (see Figure 3.2). The contrast between the nanotubes and the polymer matrix can be enhanced by applying a voltage difference between the sample and

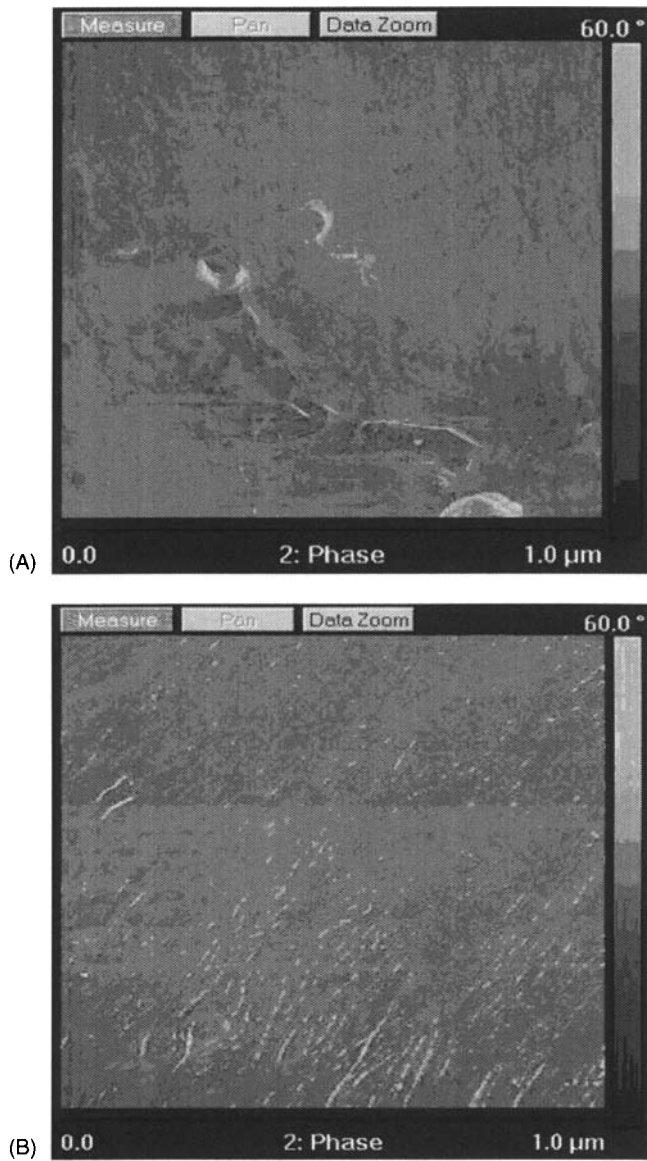


Figure 3.2. AFM image of a (a) a PE and (b) PE with 10 wt% MWCNT. The samples were taken parallel to the extrusion flow direction, with permission from Elsevier (16).

the probe during a scan in tapping mode (dc-EFM), as shown in the study performed by Phang et al. on MWNTs/PA6 composites (18). The same authors also used the AFM in [®]TUNA mode, that is as a STM but the obtained images are much less convincing.

Interfacial studies:

Given the small diameter of the nanotubes, the evaluation of the interfacial shear strength between them and the polymer matrix is very difficult. Fortunately, interactions between nanotubes and polymer can be characterized by the use of the AFM as a nanomanipulator device. For instance, peel tests have been developed by attaching nanotubes on tips and putting them in contact with a polymer substrate. For example, Strus et al. (19) recently studied the peeling of MWNT from epoxy, graphite and polyimide substrate. Shear strength can also be deduced from nano pull-out tests. For instance, Barber et al. mounted an MWNT onto an AFM tip and then pushed it in a heated polymer film of poly(ethylene butene) (22). After cooling, they measured the forces required to pull the tubes out, see Figure 3.3, and deduced stress values between 20 and 90 MPa (20,21). They also studied the pullout behavior a MWNT from an epoxy matrix.

Despite the results presented above, near-field microscopy has not been extensively used to characterize polymer/nanotube composites. However, it can be noticed that AFM is a useful technique to locally probe the mechanical properties of the composites (at the polymer-nanotube interface for example). One possible reason for the small amount of studies by AFM and STM could be that observing the surface only does not permit to obtain much information on the nanotube dispersion state. For that kind of characterization, transmission electron microscopy is a key technique owing to the small nanotube diameter.

3.3 Transmission Electron Microscopy

3.3.1 Principles

Transmission Electron Microscopy (TEM) is an imaging technique, where electrons pass through a very thin sample. The image and the electron gun are on opposite sides relative to the sample, as indicated by the keyword "Transmission". The main advantage of TEM relies in its resolving power. Indeed, resolution in a microscope is limited by diffraction phenomena. Indeed, the image of a small point source will not be a point but a small bright spot, called the "Airy disc", surrounded by less intense bright and dark haloes. The resolving power is directly related to the size of the Airy disc, and thus on the incident beam wavelength. The wavelength associated to electrons

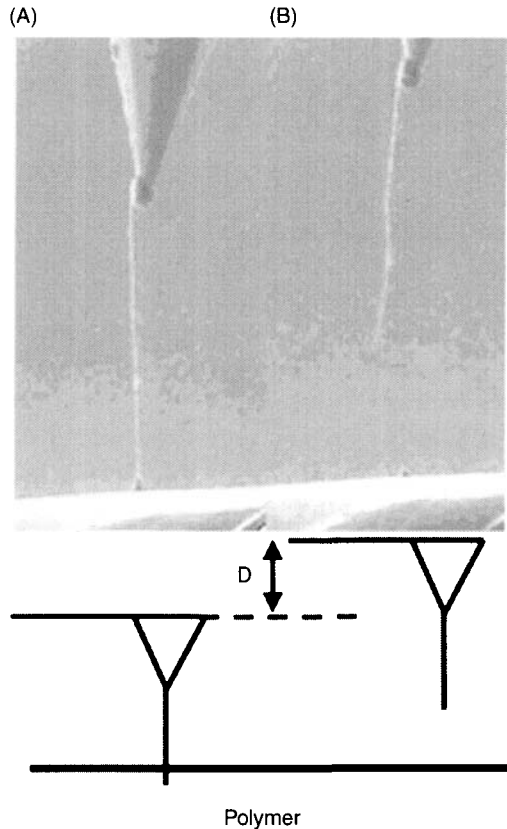


Figure 3.3. SEM images of an AFM cantilever used to calculate nanotube pullout forces. (a) The nanotube is partially embedded within the solid polymer matrix. The AFM chip, containing the AFM cantilever and tip, is then translated away from the polymer surface, resulting in continued bending of the cantilever. The nanotube pulls out of the polymer at a critical bending of the cantilever (b). This bending deflection, D , is calculated from the position of the cantilever before and after the pullout. The nanotube embedded length is calculated by the difference between the nanotube free length in (a) and (b). With permission from Wiley and Sons (22).

in a TEM is so small that fine features can be distinguished, such as atomic columns (23).

The contrast in the image is formed from the interactions between the incident electrons and the matter. The most common operating mode in TEM is the bright field imaging mode. In this mode and in the case of non crystalline materials such as polymers, the contrast is formed directly by absorption of electrons in the sample. Actually, the image is assumed to be a simple two dimensional projection

of the sample down the optic axis, and to a first approximation may be modelled via Beer's law. Experimentally, thicker regions of the sample or regions with a higher atomic number will appear darker. For this reason, heterogeneous polymer samples are often observed after staining by heavy atoms, such as ruthenium or osmium, which selectively reacts with polymers depending on their chemical structure (24).

As far as crystals are concerned, the organised structure leads to diffraction of the incident electrons. In the low magnification images, a contrast arises from the selection of one spot only (in the diffraction plane), which will be used to form the image (see Figure 3.4). Depending on which spot is selected, the image is qualified as "bright-field" or "dark-field" image. In the bright field mode, the central spot, corresponding to no diffraction, is chosen and the regions where crystal planes can give rise to diffraction will appear in dark in the image. On the contrary in the dark field mode, a diffraction spot different from the direct beam is selected and only the regions where planes are in the corresponding Bragg position will appear in bright in the image (23). Diffraction contrast can be used to identify lattice defects in crystals. Indeed, if the sample is

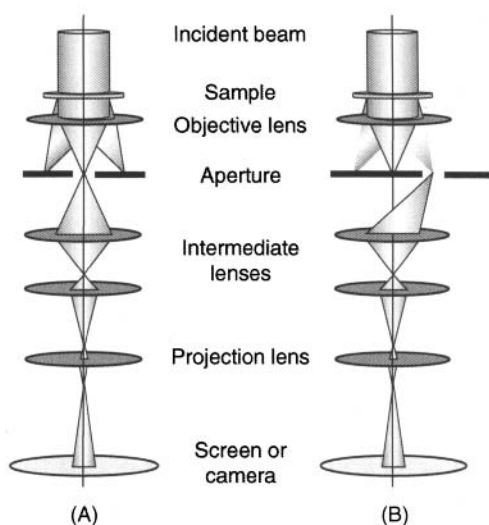


Figure 3.4. Schematic presentation of the TEM a) bright field and b) dark field modes. The difference lies in the position of the aperture: in the bright field mode, the central spot of the diffraction pattern is selected whereas the dark field mode is based on the selection of a diffraction spot.

oriented so that one particular plane is only slightly tilted away its Bragg angle, any distortion of the crystal plane that locally tilts the plane will produce particularly strong contrast variations.

Alternatively, images can be formed with electrons scattered at high angles (HAADF mode, for High Angle Annular Dark Field mode). An annular detector is placed below the sample and the focused electron beam is scanned over the sample. Interestingly, the contrast is not altered by diffraction phenomena and depends both the thickness and the composition (25).

At high magnification, TEM enables the formation of images displaying the atomic structure. It is thus qualified as "High Resolution TEM". The principle is that at least two diffraction spots are selected and the image is the interference pattern of the corresponding waves.

Whereas the TEM images give insight on the materials structure, chemical information can be obtained via two coupled analysis techniques, namely Energy Dispersive Spectroscopy (EDS) and Electron Energy-Loss Spectroscopy (EELS). The EDS signal arises from X-ray photons emitted by the sample after inelastic interactions with the incident electrons. The heavier the atoms in the sample, the more intense the EDS signal. The X-ray photon energy directly depends on the sample composition. Thus, it is possible to determine the local composition (the spatial resolution being that of the microscope), and to acquire maps representing the spatial distribution of elements.

EELS is complementary to EDS since it is better suited to light elements. Indeed, the EELS signal represents the number of incident electrons coming to the detector, as a function of their energies. Since the energy transferred from the incident electrons to the specimen is used to excite atoms from the specimen, the EELS signal contains information not only on the sample composition but also on way atoms are bound to each other (26). For conducting materials, the EELS signal is interpreted in terms of density of states. In the case of polymers, the use of chemical bondings is preferred (27). When a 2D detector is used, images can be formed with electrons that underwent a specific energy loss (EFTEM mode, for Energy Filtered TEM). In that mode, maps can be calculated, representing the spatial distribution of elements (26) or even of chemical bondings (28).

In all modes, TEM provides two-dimensional images, corresponding to projections of the sample structure along the optical

axis. Electron tomography is nowadays available to reconstruct the three-dimensional volume from TEM images of the sample at different tilt angles (29,30). As long as amorphous materials are characterised, the TEM images can be easily acquired in the bright field mode, since the contrast in the image is mass-thickness dependent. However, for crystalline materials such as nanotubes, a contrast may appear due to diffraction, which will hinder the volume reconstruction. Thus, the images have rather to be acquired in the EFTEM or HAADF modes.

The most recent developments in TEM also include the Environmental mode. In dedicated TEM, a differential pumping between the electron gun and the specimen stage allows the specimen to be surrounded by a gaseous atmosphere, with a pressure of a few millibars. Interestingly, the spatial resolution of the TEM is not seriously affected since atomic resolution is still attainable (31) and chemical reactions can be followed *in situ*.

3.3.2 Characterisation of Carbon Nanotubes

Historically, carbon nanotubes were first observed by Transmission Electron Microscopy, see Figure 3.5 (2). Then, nanotubes have gained interest worldwide and led to an incredible number of published papers. It is simply not possible to give an exhaustive list of all studies involving TEM. However, a few ones can be highlighted because they focused on the characterisation of the nanotube intrinsic properties, which in turn will play a great role on the polymer/composite properties.

Nanotube structure:

The first studies after Iijima's paper, presenting TEM micrographs of carbon nanotubes (see Figure 3.5), mainly focused on the nanotube structure (32–35) to determine how the graphene sheets roll themselves up. Once it has been established that the nanotubes were composed by concentric graphene sheets, one of the main issues, especially for single walled nanotubes, was the determination of the nanotube helicity (36–38). At the same time, TEM studies were involved in the development of various elaboration processes (39–42). The *in situ* growth of carbon nanotubes could even be followed in an environmental TEM, giving insights on the growth mechanisms (43).

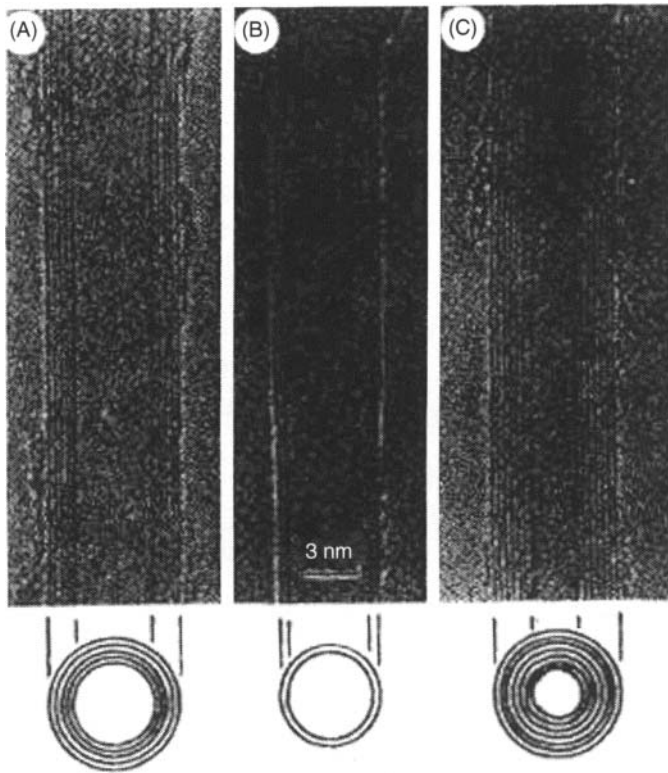


Figure 3.5. First TEM pictures of carbon nanotubes (2), with permission from Nature Publishing Group.

The structure of defects in nanotubes, which occur spontaneously or can be created by doping, has also been extensively studied (44–46). In particular, several teams used EELS to probe the chemical bondings of nitrogen in nitrogen doped carbon nanotubes (47,48).

Quantification of the diameter distribution:

One major issue of the nanotube elaboration processes is to produce nanotubes with controlled dimensions (diameter, length) and without byproducts (catalytic residues, other carbonaceous particles). This is nearly achieved with processes such as catalytic chemical vapour decomposition using supported catalysts. However, the arc discharge method remains the most common one and is perhaps the easiest way to produce the large quantities of nanotubes required for the elaboration of composites (49). The dimensions of

the nanotubes being uncontrolled, it is interesting to measure their distributions (for modelling purposes of the polymer/nanotube mechanical or electrical properties, for example). Unfortunately, the nanotube length cannot be accurately measured by TEM. They are indeed too long to be observed on their whole inside a single mesh of a microscopy grid. Moreover, they are generally so entangled that it is difficult to separate them from each other, especially in the presence of impurities or agglomerates. In a few cases, image analysis of TEM images can still be successfully performed and provide the diameter distribution as well as insights on the wall compacity (50).

Nanotube properties:

Whatever the nanotube production method, understanding the properties of materials filled with nanotubes requires the knowledge of the nanotube properties. As a consequence, many efforts were made to experimentally measure the nanotube Young modulus and intrinsic conductivity. Fortunately in TEM, it was observed that the nanotubes were vibrating when clamped at one end and free at the other one (see Figure 3.6). Thus, the measurement of the mean-square vibration amplitude in function of the temperature allowed the determination of the Young modulus (higher than 1 TPa for bundles of SWNTs) (51).

As far as the nanotube conductivity is concerned, it obviously depends on the nanotube structure (MWNT or SWNT) and also on its helicity (in the case of SWNTs). TEM has also permitted to relate the helicity to the transport properties of nanotubes (52), the helicity being determined from electron diffraction patterns and the transport properties being probed with a dedicated TEM specimen holder.

3.3.3 Characterisation of Polymer/ Nanotube Composites

Once the nanotubes have been characterised and polymer/nanotubes elaborated, their microstructures have to be precisely determined to understand the relations between the process and the nanocomposites macroscopic properties. It is expected that the microstructural parameters that will play major roles (in addition to the filler geometry) are the nanotube dispersion and orientation

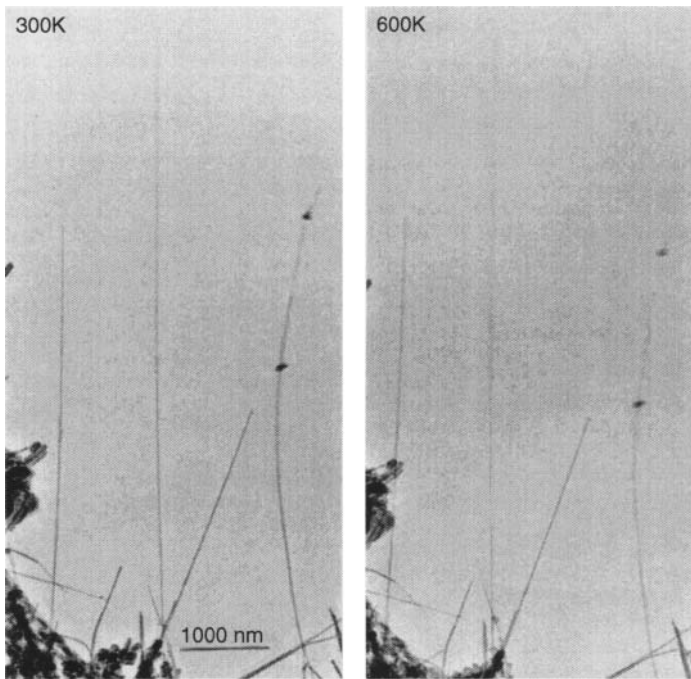


Figure 3.6. TEM micrographs showing the vibration of carbon nanotubes like clamped cantilevers, from (51), with permission from Nature Publishing Group.

state and the polymer/nanotube interfacial adhesion strength. In this section, we present a review of the pieces of information that can be brought by TEM.

Nanotube dispersion state

Obtaining a homogeneous nanotube dispersion state in a polymer matrix is still a major issue. From a general point of view, the dispersion state is influenced from the following parameters (53):

- The nanotube length,
- The nanotube entanglement,
- The nanotube volume fraction,
- The matrix viscosity,
- The tube/tube attraction (mainly for single and double-walled nanotubes).

As a consequence, the nanotube dispersion state has to be characterised at several pertinent scales, including that covered by TEM.

In particular, it can be noticed that in the case of a fine dispersion with very few agglomerates, it is hard to judge the grade of dispersion, because separated CNTs are more difficult to observe in bright-field TEM (agglomerates giving better contrast). However, since alternative methods are not available to estimate the dispersion state, conclusions are always drawn from a few TEM images (53–55).

In some studies, a statistical description of the nanotube dispersion state was obtained from TEM images. For example, Uchida et al. (56) measured the diameter distribution of SWNT bundles in poly(acrylonitrile), with and without a purification treatment involving sonication in methanol. The different bundle diameter distributions (especially the mean diameter) could explain the different composite tensile moduli. Fornes et al. (57) also determined the diameter distribution of SWNTs bundles in a polymer matrix (namely polycarbonate). To improve the contrast in the bright-field TEM images and better measure the bundle diameter, they dissolved the polymer in chloroform and studied the remaining SWNT network.

In order to understand the mechanical and electrical properties, the nanotube dispersion state has to be more precisely determined. Indeed, such properties depend on the formation of a three-dimensional nanotube network. Once such a network has been formed, key parameters include the nanotube curvature and the distance between entanglements. Electron tomography is undoubtedly the most pertinent technique to obtain a three-dimensional view of polymer/nanotube microstructures. For the moment, the published studies presenting electron tomography on polymer/nanotube composites have focused on how to obtain a good contrast between the nanotubes and the polymer matrix. Results have been presented either from bright-field (58,59), HAADF (60) or from energy-filtered images (61,62). The reconstructed volume presented in the study by M.H. Gass et al. (62) and reproduced in Figure 3.7 was obtained from a series of energy-filtered images at every tilt angle. The energy-loss spectrum was then determined at every image pixel. The difference in plasmon energy that exists between the two carbonaceous materials (22 eV for nylon and 28 eV for multiwalled carbon nanotubes) permitted to obtain a 'ratio image' that enhances the signal from the nanotubes. The volume was finally reconstructed from the "ratio" images at every tilt angle. This study emphasized that electron tomography is a powerful technique to study the three-dimensional structure of materials, even those exhibiting a poor contrast in bright field, such as polymer/nanotube composites.

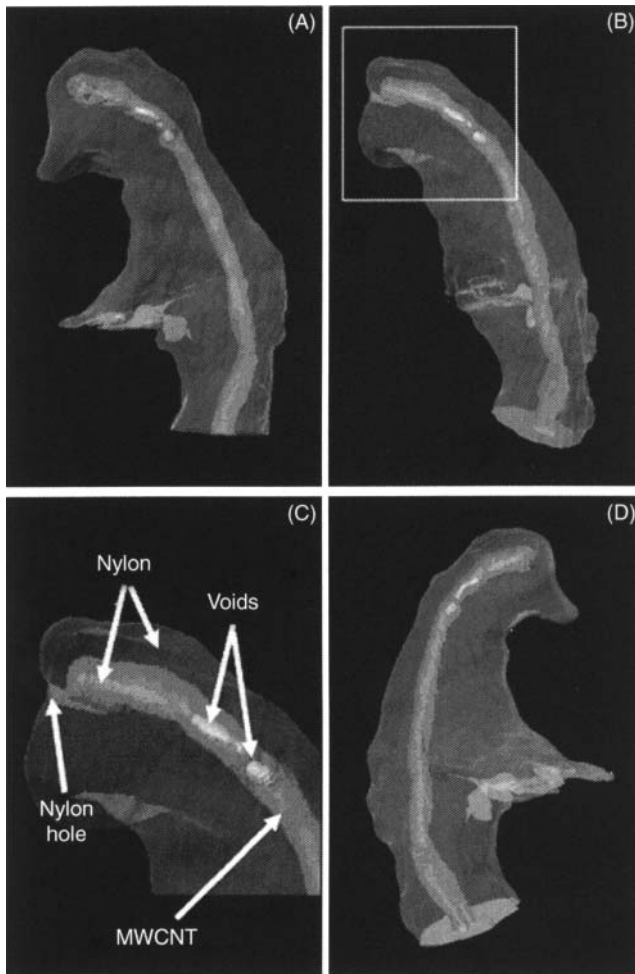
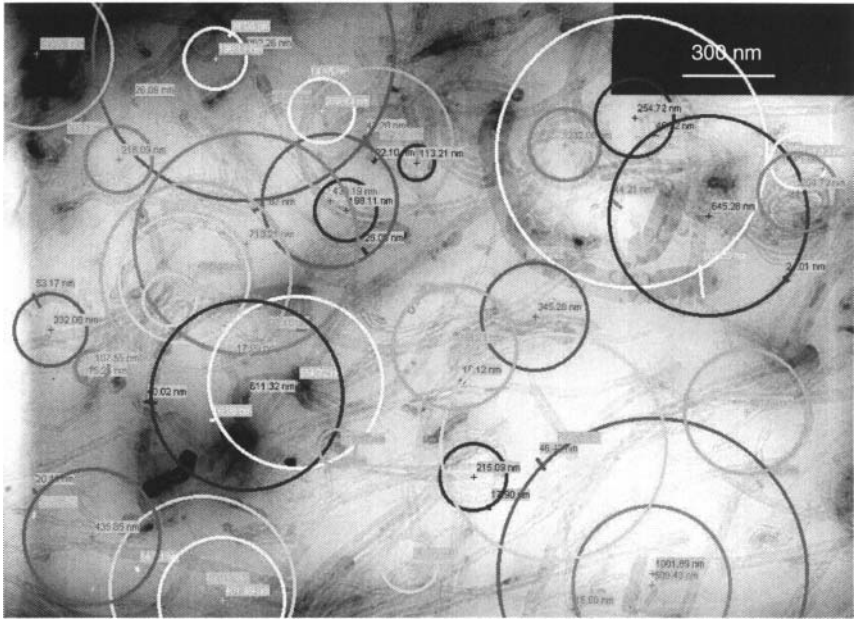


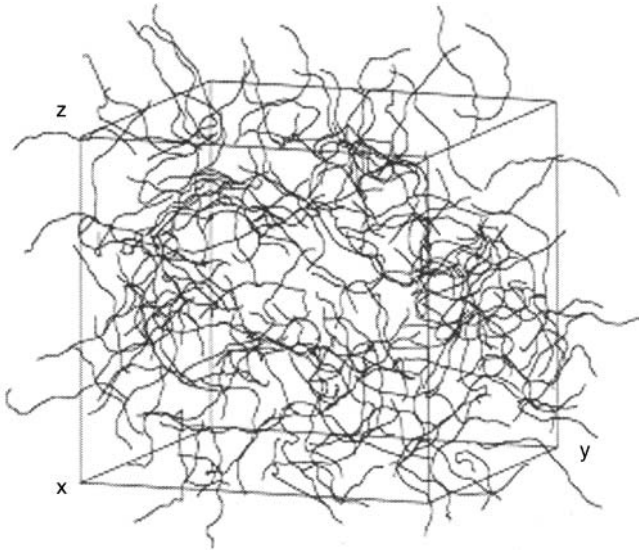
Figure 3.7. Carbon nanotube embedded in a nylon matrix, observed by electron tomography (62), with permission from the Americal Chemical Society.

Unfortunately, no study has yet been published on the carbon nanotube network 3D structure, probably because the thickness of the reconstructed volume is small compared with the expected distance between two successive entanglements.

The nanotube network was successfully investigated in our laboratory by Dalmas et al. (63), in terms of distribution of radius of curvature. Indeed, the 2D apparent nanotube segment curvature radius distribution was then measured on TEM bright field images acquired on the composites (see Figure 3.8). The experimental curvature



(A)



(B)

Figure 3.8. (a) Measurement of the 2D apparent distribution of the nanotube curvature radius in polymer/nanotube composites (63). (b) example of 3D nanotube network (64).

population was then statistically compared to that measured on the projection of the simulated 3D microstructure (simulation of TEM observations). It was then used to model the nanocomposites electrical properties in function of the elaboration process (64).

At this stage, it is worth mentioning that all the previously mentioned studies were performed on homopolymers as matrices. Meincke et al. (65) observed that nanotubes were dispersed in the polyamide-6 phase in blends of polyamide-6, acrylonitrile/butadiene/styrene (ABS). Unfortunately, no further quantification of the nanotube dispersion state has been presented, probably because of the non spherical shape of the polyamide-6 domains. Li et al. (66) used multiwalled carbon nanotubes as fillers in an extruded poly[styrene-*b*-(ethylene-co-butylene)-*b*-styrene] triblock copolymer (SBS). TEM observations confirmed small-angle X-ray scattering experiments: the well-dispersed MWCNTs have a marked effect on the phase separation behaviour of the matrix block copolymer. They inhibit the local phase separation of SEBS, and the MWCNT network impedes the formation of large phase-separated grains. The relationships between the nanocomposites microstructures and properties were investigated. The role of the nanotube network on the mechanical and electrical properties was obvious. However, the change in the copolymer microstructure was not clearly evidenced. Similar nanocomposites were elaborated by Fragneaud et al. (67) but with polystyrene-grafted nitrogen-doped carbon multiwalled carbon nanotubes as fillers. It was also observed in our laboratory that the copolymer structure was altered by the nanotubes, the thinnest tubes being even incorporated into the copolymer polystyrene cylinders (see Figure 3.9). The higher electrical percolation threshold with a SBS matrix compared to that measured with a PS matrix can most probably be attributed to the copolymer structure.

Nanotube orientation state

Although nanotubes tend to align themselves as soon as shear is applied during the nanocomposites elaboration process, very few studies focus on the quantification of the nanotube orientation state. The method proposed by Zhihang et al. (68) is worth mentioning because it can easily be used and the graphical representation allows a rapid understanding. Basically, the orientation of a nanotube can be characterised by a unit vector (collinear to the nanotube), see Figure 3.10. Experimentally, the angles between

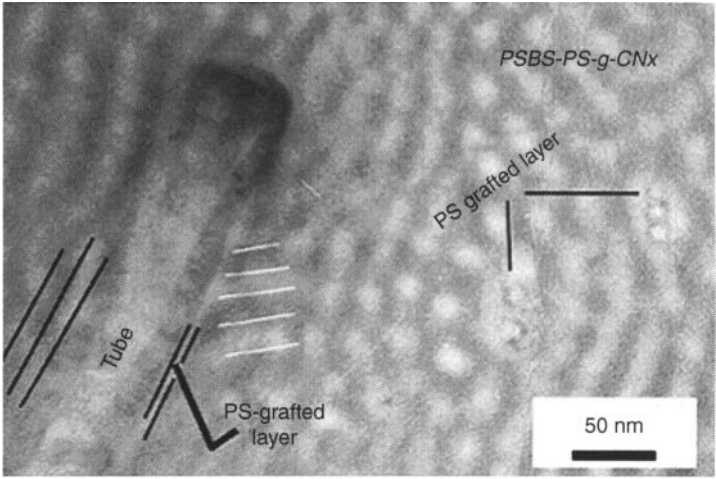


Figure 3.9. TEM bright-field image of a SBS copolymer filled with 2.5 wt.% of polystyrene-grafted nitrogen-doped carbon nanotubes after staining with RuO_4 .

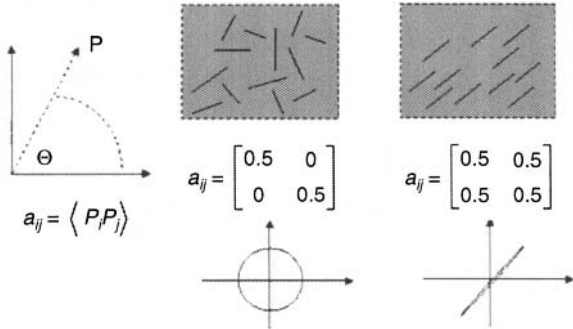


Figure 3.10. Characterization of the nanotube orientation state in one TEM image by a second order tensor and an ellipse, with permission from Elsevier (68).

the unit vectors and a reference direction are measured on TEM images and an ellipse is drawn to graphically gather the orientations of all the unit vectors. In the ellipse, the major axis main in the analysed region. The ratio between the major and minor axes distances of the ellipse represents the degree of orientation in that direction. Thus an elongated ellipse indicates a high degree of alignment in the direction of the major axis, whereas a circle signifies an orthotropic orientation.

Polymer/nanotube interfacial adhesion strength

The interfacial adhesion strength is undoubtedly the most difficult to characterize and over all to quantify. A first method consists in observing the composite behaviour during the preparation of a TEM sample. Thin sections of polymer-based materials are generally prepared by ultramicrotomy, that is by direct cutting with a diamond knife. We observed that raw MWNTs were hardly cut and were instead pulled out from the polystyrene matrix, resulting in holes during observation (see Figure 3.11a). On the contrary, polystyrene-grafted nitrogen-doped multiwalled nanotubes fragments were easily observed in the TEM sample (see Figure 3.11b), which clearly indicates an improvement in the interfacial adhesion strength. The raw nitrogen-doped multiwalled nanotubes were found to be an intermediate case, with observable fragments but still a lot of holes in the sample (69).

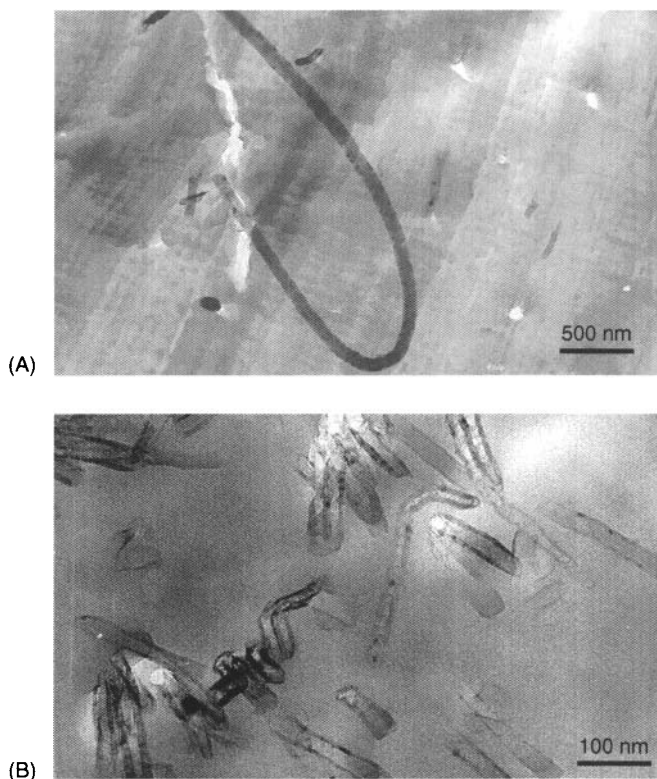


Figure 3.11. TEM bright-field images of composites made of polystyrene and (a) raw and (b) polystyrene-grafted nitrogen-doped multiwalled nanotubes (69).

A second method consists in observing the composite fracture surfaces. For example, in the case of MWNTs in a poly (hydroxy-aminoether) matrix, C. Bower et al. (70) observed a lot of pulled out nanotubes and concluded that the load transfer from polymer to nanotube was not sufficient to fracture the nanotubes. In the same time, a lot of kinked MWNTs were observed, which were believed to be plastically deformed.

Information can also be indirectly obtained by TEM when observing a thin section of the composite. Indeed, damage occurs during observation because of electron-matter interactions, which generally results in strains in the sample. Under certain conditions, deformation of the sample under electron irradiation can be assimilated to local tensile tests. Composites made of polystyrene and MWNTs were studied by D. Quian et al. (71), followed the composite behaviour after crack initiation due to electron irradiation. who estimated that about half of the aligned nanotubes have been broken. In agreement with theoretical calculations of the composite modulus (randomly oriented discontinuous fiber model), it was concluded that with polystyrene, load could be successfully transferred to the nanotubes through the nanotube-polystyrene interface. However, it can be pointed out that the remaining half of the nanotubes were still pulled out from the matrix, which indicates that the load transfer and thus the interfacial adhesion are not the highest possible. As far as SWNTs are concerned, Lourie et al. (72) also concluded that there was a significant interfacial adhesion with epoxy, since the SWNTs were broken instead of pulled out. The absence of pull-out mechanism was attributed to a higher reactivity of the graphene sheets when highly curved into SWNTs.

The poor quality of the interfacial adhesion between polymers and MWNTs was one reason of the development of functionalisation and grafting. The aim is to make chemical bondings (on functionalised nanotubes) or layers of grafted polymer (on grafted nanotubes) appear, that will improve the interfacial adhesion. Two studies involving "tensile tests" under electron irradiation are worth mentioning. In the first one, by Gojny et al. (73), the deformation mechanisms of composites with epoxy and raw or oxidised MWNTs were compared. As the raw nanotubes were pulled out from the epoxy matrix, telescopic pull-outs were observed with functionalised nanotubes. This clearly indicates that the interfacial adhesion was significantly improved. A similar conclusion was drawn by Hwang et al. (74)

when studying poly(methyl metacrylate) (PMMA) filled with PMMA-grafted MWNTs.

At this stage, it is worth mentioning that functionalisation or grafting can also affect the nanotube dispersion state. From a macroscopic point of view, the mechanical and electrical properties are also expected to be modified. A full understanding of these macroscopic properties implies to characterise the nanotube dispersion state, the polymer-nanotube interfacial adhesion strength, more precisely than what has been done in the literature until now. In particular, quantitative data should be deduced from the images, such as the distance between entanglements for example. Moreover, as far as grafted nanotubes are concerned, an evidence of grafting often lacks and it has to be proved that the polymer has been successfully grafted onto the nanotube, instead of a nanotube wrapping. TEM coupled with EELS and EDS is probably the best suited technique to locally investigate the grafted layer. For example, in Fragneaud's work (8), we probed the layer grafted onto nitrogen-doped nanotubes and proved by EELS that it was composed by polystyrene, as expected. Moreover, a peak assigned to bromine was detected on the EDS spectra, indicative of the successful atom-transfer radical polymerisation. Further work is needed but since chemical bondings can also be determined from the EELS spectra, one can also expect quantifying the number of grafted chains.

As was detailed in this section, TEM can bring numerous pieces of information regarding the polymer/nanotube composite microstructure. However, it has to be recalled that nanofillers such as nanotubes easily agglomerates and their dispersion state has to be characterised from the micron to the nanometre scale. This is one reason, among others, why Scanning Electron Microscopy is another widely used to characterise polymer/nanotube composites.

3.4 Scanning Electron Microscopy

3.4.1 Overview of the Technique (SEI, BEI, CCI)

Scanning Electron Microscopy (SEM) is a powerful tool for the surface observation of samples. The scanning of a small electron probe on the surface of the sample induces the emission of several signals. The main imaging mode used in SEM is based on the detection of the secondary electrons (called SEI for Secondary Electrons

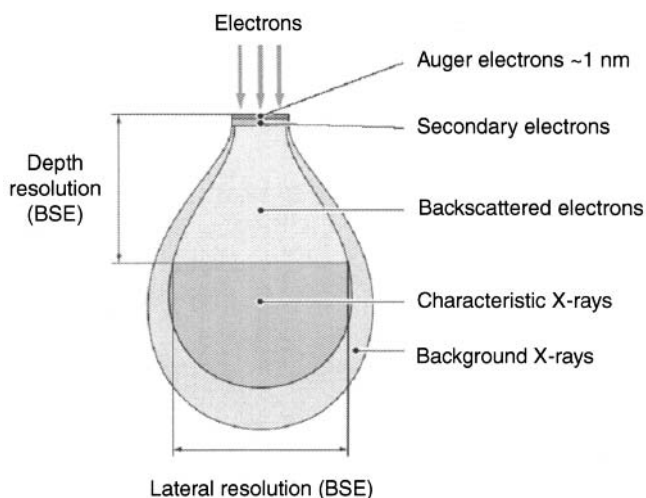


Figure 3.12. Signals detected in SEM, resulting from electrons/sample interaction.

Imaging), giving an idea of the sample topography. Moreover, two other signals resulting from the primary electrons/sample interaction are also often used: backscattered electrons and X-rays, providing information about the topography and/or the composition of the sample (see Figure 3.12).

As SEMs are versatile instruments for relatively low costs, they are largely available in laboratories in the field of biology and materials science. Developed in the 1940's, it has undergone many changes regarding the ease of use, the electron guns and optics, the resolution improvement and the development of specific modes such as transmission (STEM), low-voltage, environmental or variable-pressure, etc.

3.4.2 Application to the Study of Nanotubes

The resolution of SEMs is now suitable for nano-materials characterization. High resolution SEM is a powerful instrument for imaging fine structures of materials and nanoparticles fabricated by nanotechnology. In lens SE, BSE modes, and STEM mode are often performed to check the structure of CNT growths or CNT as delivered by commercial producers, and sometimes coupled with TEM. Even the single-walled carbon nanotubes can easily be observed by HR-SEM (see Figure 3.13). The STEM mode can also be used for free CNT observation (75).

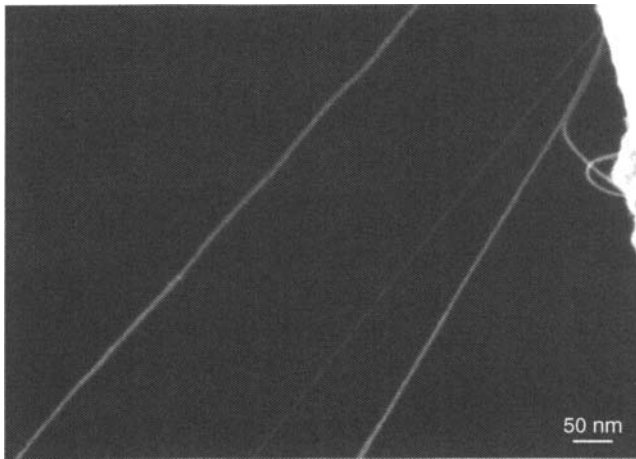


Figure 3.13. SEM image of individual SWNTs and small bundles of SWNTs.

However, the SEM contrast of CNT can be difficult to interpret as it depends on a lot of parameters (76): the primary beam energy landing, the history of imaging, if the CNT are lying on a substrate or suspended, the substrate electrical conductivity and the electron beam induced contamination during imaging. The contrast can for example be linked to potential differences between the CNT and the substrate (77), or to electron beam-induced current on the insulating substrate surface (78).

3.4.3 For Polymer CNT/Nanocomposites

CNT nanocomposites morphological and structural analysis is often done by TEM but an extensive imaging is required then to ensure a representative view of the material. Moreover, carbon based fillers have very low TEM contrast when embedded in a polymer matrix. The application of microscopy techniques is very useful to control the status of CNTs at any time during the preparation process of CNT/polymer nanocomposites, and moreover, to gain insights on parameters important for a better understanding the performance of the final nanocomposite material based on CNTs.

The general approach in SEM is the direct observation of the surface of nanocomposites films or of fracture surfaces performed at ambient temperature or in liquid nitrogen, to check concentration,

alignment and orientation distribution of the fillers, and to have information about the interfacial adhesion strength between the fillers and the matrix (67,79–81), see Figure 3.14. However, SEM of carbon nanotubes embedded in a polymer insulating matrix can be a challenge: traditional gold-coating performed to prevent charging can sometimes mask the nanotubes and the alternatives include lower energies or environmental mode but restrict the resolution (82).

SEM, as others surface-based methods such as scanning probe microscopy (SPM), or more specifically atomic force microscopy (AFM), generally only shows the surface or a cross-section of the three-dimensional arrangement of the CNTs in the polymer matrix. However, the team of Loos et al. has shown that conventional SEM is able to provide (pseudo) three-dimensional morphological

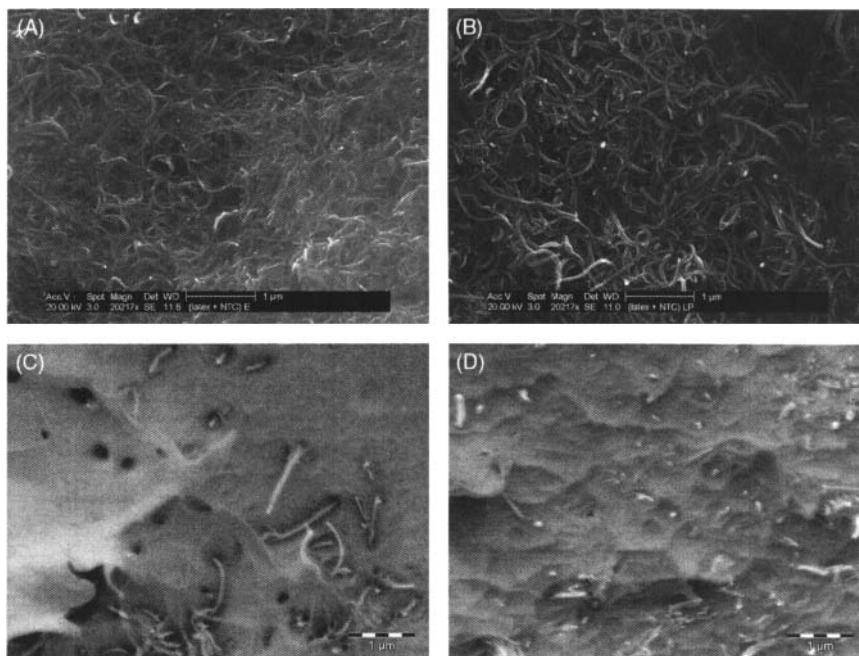


Figure 3.14. CNT/polymer nanocomposites observed in SEM : (a) and (b) P(S-ABu)/MW CNT films surface respectively prepared by evaporation and film formation or freeze-drying and hot-pressing but showing similar fillers distribution; (c) and (d) PS matrix containing ungrafted or PS-grafted N-doped CNT; a fracture performed at ambient temperature highlights the difference in fillers/matrix interface strength. Scale bars: 1 μm .

information on SWNT networks in conductive SWNT/PS nanocomposites at nanometric resolution by monitoring the sample in the charge contrast imaging mode (CCI) (83). This is only observed for nanocomposites above the percolation threshold. With increasing acceleration voltage, the secondary electron yield at the positions of the SWNTs increases and enhances the contrast between SWNTs and the matrix, see Figure 3.15.

As far as transmission is concerned, Reimer et al. have characterized specific samples in various modes and have highlighted a beam broadening through the sample thickness. They have shown that the resolution, directly related to the probe size, is subjected to a top-bottom effect (84). The use of a thin sample thus results in an improved resolution, avoiding the probe broadening through the sample thickness. Moreover, the interaction cross-sections are important at low voltage, for instance the cross section of carbon at 30 kV equals the one of Zn at 100 kV, and the cross section of carbon at 10 kV equals the one of Ta at 100 kV (85). These high values coupled with the high collection angles of our detection configuration can be interpreted as efficient in both the electrons-sample interaction and the scattered electrons detection. This enables for instance polymer/carbon nanotube nanocomposites to be observed with an important contrast between the polymer matrix and the fillers, even if their average atomic numbers are very close (see Figure 3.16). In our STEM configuration, the detection efficiency also contributes to increase the thickness of transparency which can reach several μm (86).

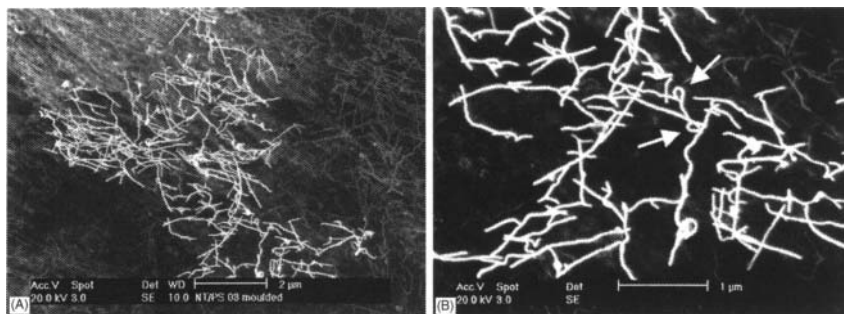


Figure 3.15. Charge-Contrast Imaging in a nanocomposite film of PS containing 0.3 wt% of SW CNT. With permission from Elsevier (83).

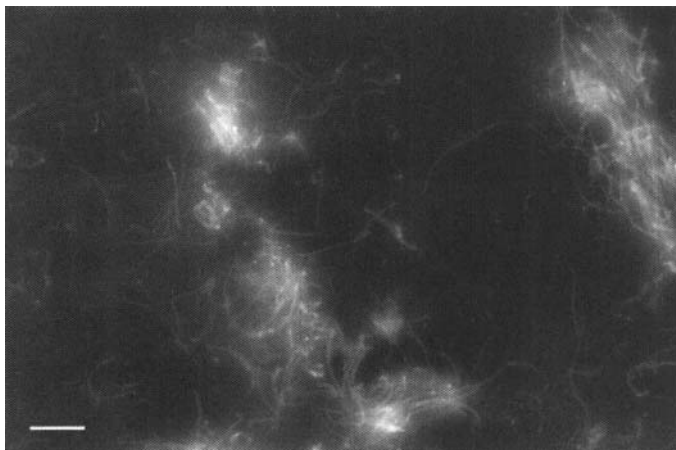


Figure 3.16. STEM image performed in SEM on cryo-ultramicrotomed sections of P(S-ABu)/MWCNT nanocomposites films in annular dark-field conditions at 30 kV; the contrast between the fillers and the matrix is important. Scale bar: 500 nm.

3.4.4 Development of New Imaging Modes

Two specific imaging modes developed in combining ESEM (environmental scanning electron microscopy) and STEM and developed in the MATEIS laboratory can be useful for the characterization of CNT and CNT polymer nanocomposites.

Wet-STEM (86–88)

An imaging mode called “wet-STEM” recently developed in ESEM, and schematically presented in Figure 3.17, allows the observation of nano-objects suspended in a liquid phase, with a few nanometers resolution (87). The idea behind this technique is simply to perform STEM-in-SEM, that is SEM in transmission mode, in an environmental SEM, in the wet state. The ESEM is interesting for the ability to keep samples wet or liquid, and the STEM mode results in high contrast, resolution and thickness of transparency.

At the steps before the elaboration of carbon nanotube nanocomposites, wet-STEM can be used for the characterization of nanotubes dispersed in a liquid (see Figure 3.18), and for polymer latex/nanotubes mixing (before evaporation or freeze-drying to elaborate polymer/carbon nanotube nanocomposites).

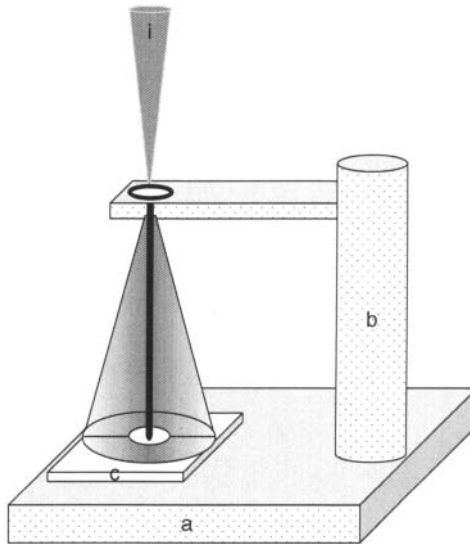


Figure 3.17. Scheme of the wet-STEM imaging mode. a: Peltier cooling stage; b: TEM-grid type sample holder; c: annular detector for transmitted electrons collection; i: incident electron beam.

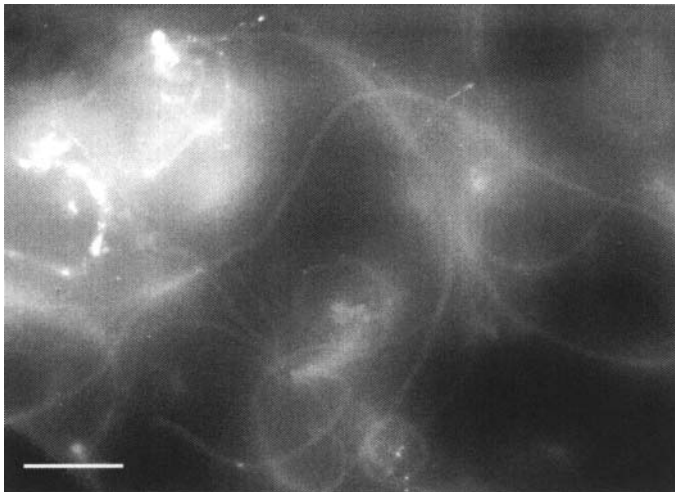


Figure 3.18. Wet-STEM image of MW nanotubes and surfactant dispersed in water.

Three-dimensional characterization: tomo-STEM (89–91)

A new electron tomography technique has been developed in MATEIS, based on STEM configuration in ESEM (see Figure 3.19).

The main interest of this combination to characterize materials 3D structure is linked to the compromise between the resolution level of about ten nm, and the large tomogram size thanks to the important thickness of transparency. It is well adapted for non-conductive samples, and exhibits good contrast even for low-atomic number materials. Taking advantage of the size of the ESEM chamber, the range of tilt angles is not limited by the space around the sample. It has been used for the characterization of free nanowires, and for impact modified polymer composites (see Figure 3.20). Based on the

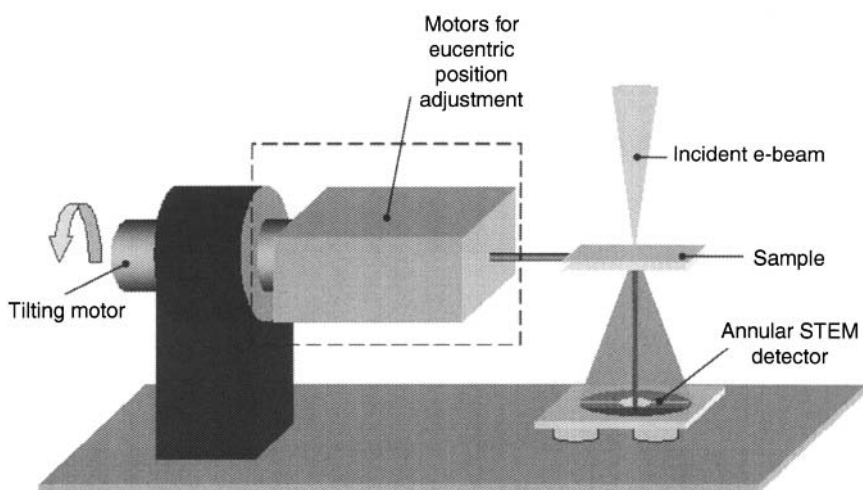
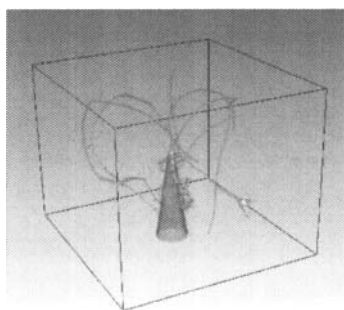
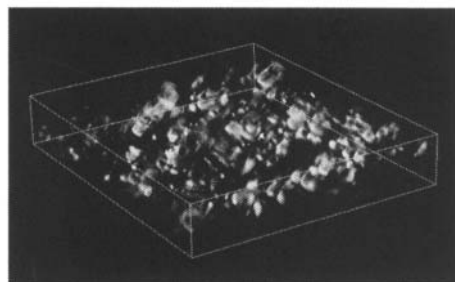


Figure 3.19. The first generation tomo-STEM stage for the new electron tomography technique combining STEM and ESEM.



(A)



(B)

Figure 3.20. Some examples of reconstructed volumes after characterization with tomo-STEM: (a) SiC nanowires grown on a tungsten tip; (b) impact-resistant poly(vinyl chloride) (volume sizes: $41 \times 32 \times 40 \mu\text{m}^3$ and $4.2 \times 4.8 \times 0.8 \mu\text{m}^3$, respectively).

STEM in SEM image obtained on polymer/CNT nanocomposites, experiments are in progress to characterize such sample in 3D with good resolution, contrast and important thickness of transparency, to better characterize entanglements, filler/filler interaction, etc.

3D : FIB slicing

The FIB-SEM approach takes advantage of the recent developments in SEM, providing double gun microscopes. In such instruments, a focused ion beam (FIB) can be used to create a cut at a designated site in the specimen, followed by viewing the newly generated surface with a scanning electron beam focused at the same point (92). This approach can help to better characterize the dispersion and orientation of fillers in polymer nanocomposites. An example of such studies concerns a PET matrix filled with nanoclays: compared to conventional TEM techniques, a wider area of the sample can be observed when using FIB milling and imaging of the milled surface (93).

In FIB-SEM, such milling and imaging can be performed in a sequential manner; thus a series of images (often called “slices”) can be collected at well-defined distances. This opens up the third dimension by making a SEM combined with a FIB a well suited tool for characterizing micron and sub-micron size microstructural features in three dimensions via serial-sectioning procedures (94).

The main drawbacks of this approach are the low availability of such instruments in laboratories, and the fact that many samples are sensitive to ion beam damage, require specific preparation (95), and can induce low contrast. Moreover, the imaging between two milling periods is typically performed in the backscattered electrons mode, which is not always favorable: this is the case for carbon nanotubes in a polymer matrix as the atomic number contrast is low. This is probably the reason why, even if the FIB/SEM approach is used on polymer nanocomposites, it not used in the literature for carbon nanotubes in polymer matrix. In this last application, the tomo-STEM® technique is a good alternative to obtain images of relatively thick samples with high contrast and resolution (91).

3.5 Conclusions

The main goal in material science is to provide behaviour laws, i.e. to be able to predict the material properties under given conditions

(mechanical, electrical, environmental conditions, temperature, etc.). This requires relating microscopic parameters and local mechanisms to macroscopic behaviours, as there is no other way to express such behaviour laws based on chemical-physical parameters. In other words, the study of materials requires a large part of microstructural observation and analysis.

More specifically with nanocomposite materials, and as recalled above, in most of the cases, interface between as received particles and organic matrices are very weak (bad adhesion), and one way to improve it consists in performing chemical grafting on the particle surface. If the chemical reactions are generally classical and work in solution, they can be much more difficult to achieve in heterogeneous media, which is the case for particle grafting. It is thus challenging to check the grafting effectiveness, and microscopy combining spectroscopy is probably the most powerful tool for such purpose.

We have roughly described three main microscopy techniques, namely local probe microscopy (STM, AFM, etc.), transmission electron microscopy (TEM) and scanning electron microscopy (SEM).

It has been pointed out that most of the time, microscopy methods lead to 2D images, either because they provide surface characterisation (local probe and SEM), or because images result from the ability of electrons to cross the sample (TEM). Recent developments allow getting 3D images, by using for instance the classical tomography technique previously developed for X-ray medical applications. It is worthy to note that an old and very tough technique firstly developed to observe in 3D bio-objects –such as viruses– has been recently renewed. Ion beam replaces microtome in producing thin slices and in situ observation by SEM avoids manually changing the samples.

Scanning Probe microscopy techniques are extremely useful for analysing surfaces, but cannot lead to bulk information. They will be used each time surface properties are important, i.e. when surfaces are used for themselves (tribological applications, adhesion, etc.). However, in some cases, the study of transport phenomena (such as thermal or electrical conductivity) by modified AFM may lead to bulk characterisation such as the formation of a percolating nanotube network for instance.

A similar conclusion could be reached for scanning electron microscopy, but two specific features must be underlined. The fact that CNT are good electrical conductors makes easier observations of

CNT nanocomposites, even at low CNT volume fractions, provided they form a percolating network. In such cases, it appears that SEM observations show not only the nanocomposite surface topology, but also the CNT arrangement near the surface within a thickness of even few μm . On the other hand, as for other electron microscopy methods, spectroscopy analysis can be used for imaging purposes.

TEM remains certainly the most powerful technique to get bulk information, but due to the low sample thickness required for observation, in most cases, CNT are cut and it is almost impossible to observe them surrounded by their neighbours and so, to analyse their mutual interactions. However, *in situ* spectroscopy leads to more and more precise data on CNT – matrix interface, which one of the key-point of macroscopic behaviour. It can be noticed that SEM can be performed in transmission, leading to images similar to what can be obtained by TEM. However, in the magnification range covered by both techniques, SEM provides images of thicker samples with a higher contrast, which should provide reliable results on the nanotube dispersion state. However, TEM remains unavoidable to locally characterise the nanotube-matrix interface and the nanotube-nanotube contacts.

To summarize recent improvements which in fact appear as breakthrough, two limits of electron microscopy techniques have been recently bypassed, (i) one related to SEM observation of insulating materials and liquid states by using environmental microscopes, and (ii) the second one related to 3D rather than 2D imaging, by developing tomography techniques in microscopes working in transmission modes or by using micromachining in dual beam microscopes (FIB). We can expect that within few years, it will be possible to answer several questions, as for instance, the effect of nanotubes dispersion on nanocomposite mechanical properties or on electrical properties.

References

1. L. Chazeau, C. Gauthier, G. Vigier and J.-Y. Cavaillé, "Relationships between microstructural aspects and mechanical properties in polymer based nanocomposites", in H.S. Nalwa, ed., *Handbook of Organic-Inorganic Hybrid Materials and Nanocomposites*, American Scientific Publishers, 2003.
2. S. Iijima, *Nature*, Vol. 354, p. 56, 1991.
3. T. Ebbesen, *Carbon Nanotubes: Preparation and Properties*, Boca Raton, CRC Press, 1997.

4. E. Dujardin, T.W. Ebbesen, A. Krishnan, P.N. Yianilos and M.M.J. Treacy, *Physical Reviews B*, Vol. 58, p. 1401, 1998.
5. E.T. Thostenson, Z. Ren and T.W. Chou, *Composites Science and Technology*, Vol. 61, p. 1899, 2001.
6. M.F. Yu, B.S. Files, S. Arepalli and R.S. Ruoff, *Physical Review Letters*, Vol. 84, p. 5552, 2000.
7. M. Dehonor Gomez, K. Masenelli-Varlot, A. Gonzalez-Montiel, C. Gauthier, J.Y. Cavaillé, H. Terrones and M. Terrones, *Chemical Communications*, p. 5349, 2005.
8. B. Fragneaud, K. Masenelli-Varlot, A. Gonzalez-Montiel, M. Terrones and J.Y. Cavaillé, *Chemical Physics Letters*, Vol. 419, p. 567, 2006.
9. L.C. Venema, J.W.G. Wildoer, C. Dekker, G.A. Rinzler and R.E. Smalley, *Applied Physics A*, Vol. 66, p. S153, 1998.
10. A. Bachtold, M.S. Fuhrer, S. Plyasunov, M. Forero, E.H. Anderson, A. Zettl and P.L. McEuen, *Physical Review Letters*, Vol. 84, p. 6082, 2000.
11. G.S. Duesberg, J. Muster, V. Krstic, M. Burghard and S. Roth, *Applied Physics A*, Vol. 67, p. 117, 1998.
12. E.W. Wong, P.E. Sheehan and C.M. Lieber, *Science*, Vol. 277, p. 1971, 1997.
13. J.P. Salvetat, A.J. Kulik, J.M. Bonard, G.A.D. Briggs, T. Stockli, K. Metenier, S. Bonnamy, F. Beguin, N.A. Burnham and L. Forro, *Advanced Materials*, Vol. 11, p. 161, 1999.
14. M.F. Yu, O. Lourie, M.J. Dyer, K. Moloni, T.F. Kelly and R.S. Ruoff, *Science*, Vol. 287, p. 637, 2000.
15. J.P. Salvetat, G.A.D. Briggs, J.M. Bonard, R.R. Bacsá, A.J. Kulik, T. Stockli, N.A. Burnham and L. Forro, *Physical Review Letters*, Vol. 82, p. 944, 1999.
16. T. McNally, P. Potschke, P. Halley, M. Murphy, D. Martin, S.E.J. Bell, G.P. Brennan, D. Bein, P. Lemoine and J.P. Quinn, *Polymer*, Vol. 46, p. 8222, 2005.
17. G. Viswanathan, N. Chakrapani, H.C. Yang, B.Q. Wei, H.S. Chung, K.W. Cho, C.Y. Ryu and P.M. Ajayan, *Journal of the American Chemical Society*, Vol. 125, p. 9258, 2003.
18. I.Y. Phang, T.X. Liu, W.D. Zhang, H. Schonherr and G.J. Vancso, *European Polymer Journal*, Vol. 43, p. 4136, 2007.
19. M.C. Strus, C.I. Cano, R.B. Pipes, C.V. Nguyen and A. Raman, *Composites Science and Technology*, Vol. 69, p. 1580, 2009.
20. A.H. Barber, S.R. Cohen, S. Kenig and H.D. Wagner, *Composites Science and Technology*, Vol. 64, p. 2283, 2004.
21. A.H. Barber, S.R. Cohen and H.D. Wagner, *Applied Physics Letters*, Vol. 82, p. 4140, 2003.
22. A.H. Barber, S.R. Cohen, A. Eitan, L.S. Schadler and H.D. Wagner, *Advanced Materials*, Vol. 18, p.83, 2006.
23. L. Reimer and H. Kohl, *Transmission Electron Microscopy: Physics of Image Formation*, Springer Series in Optical Science, Vol. 36, Springer, 2008.
24. L.C. Sawyer and D.T. Grubb, *Polymer Microscopy*, Chapman & Hall, 1996.
25. S. Pennycook, *Ultramicroscopy*, Vol. 30, p. 58, 1989.
26. R.F. Egerton, *Electron Energy-Loss Spectroscopy in the Electron Microscope*, 2nd Edition, Kluwer Academic/Plenum Publishers, 1996.

27. K. Varlot, J.M. Martin, D. Gonbeau and C. Quet, *Polymer*, Vol. 40, p. 5691, 1999.
28. J.M. Martin, B. Vacher, L. Ponsonnet and V. Dupuis, *Ultramicroscopy*, Vol. 65, p. 229, 1996.
29. P.A. Midgley and M. Weyland, *Ultramicroscopy*, Vol. 96, p. 413, 2003.
30. P.A. Midgley, E.P.W. Ward, A.B. Hungria and J.M. Thomas, *Chemical Society Reviews*, Vol. 36, p. 1477, 2007.
31. [http://www.hitachi-hhta.com/sites/default/files/technotes/E-TEM-MicroscopyToday-XF06\(2\).pdf](http://www.hitachi-hhta.com/sites/default/files/technotes/E-TEM-MicroscopyToday-XF06(2).pdf)
32. X.D. Fan and L.A. Bursill, *Philosophical Magazine A*, Vol. 72, p. 139, 1995.
33. S. Xie, N. Li, Z. Zhang, W. Liu, G. Wang, S. Qian and C. Fu, *Journal of Materials Science*, Vol. 30, p. 2291, 1995.
34. S. Wang and D. Zhou, *Chemical Physics Letters*, Vol. 225, p. 165, 1994.
35. D. Ugarte, *Microscopy Microanalysis Microstructures*, Vol. 4, p. 505, 1993.
36. M. Liu and J.M. Cowley, *Carbon*, Vol. 32, p. 393, 1994.
37. L.C. Qin, S. Iijima, H. Kataura, Y. Maniwa, S. Suzuki and Y. Achiba, *Chemical Physics Letters*, Vol. 268, p. 101, 1997.
38. L. Henrard, A. Loiseau, C. Journet and P. Bernier, *Synthetic Metals*, Vol. 103, p. 2533, 1999.
39. A. Loiseau, J. Gavillet, F. Ducastelle, J. Thibault, O. Stéphan, P. Bernier and S. Thair, *C.R. Physique*, Vol. 4, p. 975, 2003.
40. P. Chen, H.B. Zhang, G.D. Lin, Q. Hong and K.R. Tsai, *Carbon*, Vol. 35, p. 1495, 1997.
41. P.M. Ajayan, J.M. Lambert, P. Bernier, L. Barbedette, C. Colliex and J.M. Planeix, *Chemical Physics Letters*, Vol. 215, p. 509, 1993.
42. K. Hernadi, A. Fonseca, P. Piedigrosso, M. Delvaux, J.B. Nagy, D. Bernaerts and J. Riga, *Catalysis Letters*, Vol. 48, p. 229, 1997.
43. S. Helveg, C. López-Cartes, J. Sehested, P.L. Hansen, B.S. Clausen, J.R. Rostrup-Nielsen, F. Abild-Pedersen and J.K. Nørskov, *Nature*, Vol. 427, p. 426, 2004.
44. S. Amelinckx, A. Lucas and P. Lambin, *Reports on Progress in Physics*, Vol. 62, p. 1471, 1999.
45. D. Cherns, W.T. Young and F.A. Ponce, *Materials Science and Engineering B*, Vol. 50, p. 76, 1997.
46. O. Stephan, P.M. Ajayan, C. Colliex, P. Redlich, J.M. Lambert, P. Bernier and P. Lefin, *Science*, Vol. 266, p. 1683, 1994.
47. R. Czerw, M. Terrones, J.C. Charlier, X. Blase, B. Foley, R. Kamalakaran, N. Grobert, H. Terrones, D. Tekleab, P.M. Ajayan, W. Blau, M. Ruehle and D.L. Carroll, *Nano Letters*, Vol. 1, p. 457, 2001.
48. M. Glerup, M. Castignolles, M. Holzinger, G. Hug, A. Loiseau and P. Bernier, *Chemical Communications*, p. 2542, 2003.
49. A. Loiseau, X. Blase, J.C. Charlier, P. Gadelle, C. Journet, C. Laurent and A. Peigney, 'Synthesis methods and growth mechanisms', in *Understanding Carbon Nanotubes. From Basics to Application*, Lecture Notes in Physics 677, Springer, 2006.
50. C. Gommès, S. Blacher, K. Masenelli-Varlot, C. Bossuot, E. McRae, A. Fonseca, J.B. Nagy and J.P. Pirard, *Carbon*, Vol. 41, p. 2561, 2003.
51. M.M. Treacy, T.W. Ebbesen and J.M. Gibson, *Nature*, Vol. 381, p. 678, 1996.

52. M. Kociak, K. Suenaga, K. Hirahara, Y. Saito, T. Nakahira and S. Iijima, *Physical Review Letters*, Vol. 89, p. 155501, 2002.
53. B. Fiedler, F.H. Gojny, M.H.G. Wichmann, M.C.M. Nolte and K. Schulte, *Composites Science and Technology*, Vol. 66, p. 3115, 2006.
54. K.P. Ryan, M. Cadek, V. Nicolosi, D. Blond, M. Ruether, G. Armstrong, H. Swan, A. Fonseca, J.B. Nagy, W.K. Maser, W.J. Werner and J.N. Coleman, *Composites Science and Technology*, Vol. 67, p. 1640, 2007.
55. P. Pötschke, A.R. Bhattacharyya and A. Janke, *European Polymer Journal*, Vol. 40, p. 137, 2004.
56. T. Uchida and S. Kumar, *Journal of Applied Polymer Science*, Vol. 98, p. 985, 2005.
57. T.D. Fornes, J.W. Baur, Y. Sabba and E.L. Thomas, *Polymer*, Vol. 47, p. 1704, 2006.
58. J. Yu, K. Lu, E. Sourty, N. Grossiord, C.E. Koning and J. Loos, *Carbon*, Vol. 45, p. 2897, 2007.
59. K. Masenelli-Varlot, L. Chazeau, C. Gauthier and J.Y. Cavaillé, *Composites Science and Technology*, Vol. 69, p. 1533, 2009.
60. G.B. Thompson, M. Abdalla and D. Dean, *Microscopy and Microanalysis*, Vol. 12, p. 1578, 2006.
61. C. Sealy, *Materials Today*, Vol. 9, p. 10, 2006.
62. M.H. Gass, K.K. Koziol, A.H. Windle and P.A. Midgley, *Nano Letters*, Vol. 6, p. 376, 2006.
63. F. Dalmas, Ph-D thesis, Institut National Polytechnique de Grenoble, 2005, available online at : <http://hal.archives-ouvertes.fr/tel-00012111/>
64. F. Dalmas, R. Dendievel, L. Chazeau, J.Y. Cavaillé and C. Gauthier, *Acta Materialia*, Vol. 54, p. 2923, 2006.
65. O. Meincke, D. Kaempfer, H. Weickmann, C. Friedrich, M. Vathauer and H. Warth, *Polymer*, Vol. 45, p. 739, 2004.
66. Y. Li and H. Shimizu, *Macromolecules*, Vol. 42, p. 4287, 2009.
67. B. Fagneaud, K. Masenelli-Varlot, A. González-Montiel, M. Terrones and J.Y. Cavaillé, *Chemical Physics Letters*, Vol. 444, p. 1, 2007.
68. F. Zhihang and S.G. Advani, *Polymer*, Vol. 46, p. 5232, 2005.
69. M. Dehonor Gomez, Ph-D thesis, Instituto Potosino de Investigacion Cientifica y Tecnologica (Mexico) and Institut National des Sciences Appliquées de Lyon (France), 2007. Available online at http://docinsa.insa-lyon.fr/these/pont.php?id=dehonor_gomez
70. C. Bower, R. Rosen, L. Jin, J. Han and O. Zhou, *Applied Physics Letters*, Vol. 74, p. 3317, 1999.
71. D. Qian, E.C. Dickey, R. Andrews and T. Randell, *Applied Physics Letters*, Vol. 76, p. 2868, 2000.
72. O. Lourie and H.D. Wagner, *Applied Physics Letters*, Vol. 73, p. 3527, 1998.
73. F.H. Gojny, J. Nastalczyk, Z. Roslaniec and K. Schulte, *Chemical Physics Letters*, Vol. 370, p. 820, 2003.
74. G.L. Hwang, Y.T. Shieh and K.C. Hwang, *Advanced Functional Materials*, Vol. 14, p. 487, 2004.
75. C. Probst, R. Gauvin and R.A.L. Drew, *Micron*, Vol. 38, p. 402, 2007.
76. W. K. Wong, A. Nojeh and R.F.W. Pease, *Scanning*, Vol. 28, p. 219, 2006.

77. T. Brintlinger, Y.F. Chen, T. Durkop, E. Cobas, M. S. Fuhrera, J.D. Barry and J. Melngailis, *Applied Physics Letters*, Vol. 81, p. 2454, 2002.
78. Y. Homma, S. Suzuki, Y. Kobayashi, M. Nagase and D.Takagi, *Applied Physics Letters*, Vol. 84, p. 1750, 2004.
79. F. Dalmas, L. Chazeau, C. Gauthier, K. Masenelli-Varlot, R. Dendievel, J.-Y. Cavaillé and L. Forró, *Journal of Polymer Science, Part B: Polymer Physics*, Vol. 43, p. 1186, 2005.
80. F. Dalmas, J.-Y. Cavaillé, C. Gauthier, L. Chazeau and R. Dendievel, *Composites Science and Technology*, Vol. 67, p. 829, 2007.
81. B. Fragneaud, K. Masenelli-Varlot, A. González-Montiel, M. Terrones and J.-Y. Cavaillé, *Composites Science and Technology*, Vol. 68, p. 3265, 2008.
82. W. Chen and X. Tao, *Applied Surface Science*, Vol. 252, p. 3547, 2006.
83. J. Loos, A. Alexeev, N. Grossiord, C. E. Koning and O. Regev, *Ultramicroscopy*, Vol. 104, p. 160, 2005.
84. P. Gentsch, H. Gilde and L. Reimer, *Journal of Microscopy*, Vol. 100, p. 81, 1974.
85. A. Takaoka and T. Hasegawa, International Microscopy Congress 16 Sapporo, Japan (2006).
86. A. Bogner, P.-H. Jouneau, G. Thollet, D. Basset and C. Gauthier, *Micron*, Vol. 38, p. 390, 2007.
87. A. Bogner, G. Thollet, D. Basset, P.-H. Jouneau and C. Gauthier, *Ultramicroscopy*, Vol. 104, p. 290, 2005.
88. A. Bogner, PhD thesis, INSA-Lyon, MATEIS Lab. (2006), download link: <http://csidoc.insa-lyon.fr/these/pont.php?id=bogner>
89. P. Jornsano, G. Thollet, K. Masenelli-Varlot and C.Gauthier, FR Patent 06-09-708, 2006.
90. P. Jornsano, PhD thesis, INSA-Lyon, MATEIS Lab. (2008), download link: <http://csidocinsa.insa-lyon.fr/these/pont.php?id=jornsano>
91. P. Jornsano, G. Thollet, J. Ferreira, K. Masenelli-Varlot, C. Gauthier and A. Bogner, *Ultramicroscopy*, in press.
92. B.J. Inkson, M. Mulvihill and G. Möbus, *Scripta Materialia*, Vol. 45, p. 753, 2001.
93. R.S. Rajeev, E. Harkin-Jones, K. Soon, T. McNally, G. Menary, C.G. Armstrong and P.J. Martin, *Materials Letters*, Vol. 62, p. 4118, 2008.
94. A.J. Kubis, G.J. Shiflet, D.N. Dunn and R. Hull, *Metallurgical and Materials Transactions A*, Vol. 35 A, p. 1935, 2004.
95. D.J. Stokes, F. Morrissey and B.H. Lich, *Journal of Physics: Conference Series*, Vol. 26, p. 50, 2006.

This Page Intentionally Left Blank

Polymer Nanocomposites with Clay and Carbon Nanotubes

Qiang Fu, Changyu Tang, Hua Deng and Qin Zhang

*College of Polymer Science and Engineering, Sichuan University,
State Key Laboratory of Polymer Materials Engineering,
Chengdu 610065, China*

Abstract

In recent years, nano-particles with different dimensions are frequently used together to prepare multi-component polymer nanocomposites, to study the synergistic effects of different nano-particles. In this chapter, we select some interesting examples to demonstrate the importance and synergies of using CNTs and clay together for the preparation of polymer nanocomposites. The property enhancements including mechanical, electrical, thermal, and fire retardant properties have been reported. The relationships between these properties and the morphological structure of clay/CNTs, particularly, possible formation of filler network constructed by clay and CNTs are discussed. Finally, we point out that the study on ternary polymer nanocomposites containing clay and CNTs is still at its primary stage. But promising results have already been generated by assembling two types of nanoparticles to break the limitation of single nanofiller.

Keywords: polymer nanocomposite, clay, CNTs, synergistic effect, network.

4.1 Introduction

During the past nearly one hundred years, the purpose of using inorganic fillers for the modification of polymers in industries have experienced a revolutionary change from decreasing the product cost to producing high performance and multifunctional composites. The appearance of nano-sized fillers opens a large window of

opportunity because nano-scaled fillers have less structure defects and higher aspect ratio than their micrometer-sized counterparts (1,2). Nanofillers used in nanocomposites have a versatile shape and size, which could be classified into zero-dimensional (atomic clusters, e.g., silica), 1D (one-dimensional; e.g., carbon nanotubes), 2D (nanoscale layered structure, eg., clay platelets), and 3D (filler networks and hybrid filler) nanostructure (Figure 4.1) (2–7). Among these nanofillers with different morphologies, carbon nanotube (CNT) as a novel low-dimensional (1D) nano-material has been currently paid intensive attention in different academic and industry fields, where unique mechanical, electrical, optical, electrochemical, and catalyst properties have been reported (8–15). Fabrication of polymer nanocomposites is one of the most important applications of CNTs. Since the first report of polymer nanocomposite based on carbon nanotubes from Ajayan et al. in 1994 (16), polymer nanotube composites have been studied extensively by other researchers in the world. Integration of CNTs with excellent mechanical, thermal, electrical properties into facile processing, flexible polymers (including synthetic and natural polymers) becomes a greatly appealing route for fabricating various advanced materials.

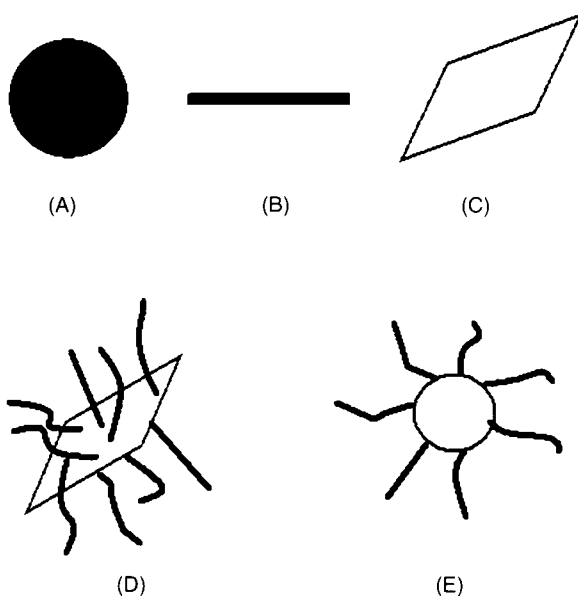


Figure 4.1. Schematic of nanofillers with different dimensions: (a) 0-dimensional filler, (b) 1-dimensional filler, (c) 2-dimensional filler, (d, e) 3-dimensional filler.

Those composites with unique properties can be widely used for chemical and biological sensors, cell electrodes, super-capacitors, heat dissipation films, and ultra-strong engineering plastics (17–25). However, poor CNT dispersion and weak interface interaction between CNTs and matrix lead to achievement of limited improvements in various properties, and the unique properties of CNTs can not be efficiently utilized in nanocomposites (26–30). For instance, the mechanical properties of polymer nanocomposites containing CNTs saturate at a low CNTs content due to aggregation of CNTs at higher loadings (31,32). The interface interaction between CNTs and polymer matrix are also subjected to the limited enhancement even if a lot of surface modification methods are used inside or on surface of CNTs (33). For the electrical properties, very high amount of CNTs are often added into polymer, but the improvement of electrical conductivity in composites is still limited due to poor dispersion and random distribution of CNTs (30). Therefore, wide application of much expensive CNTs in industry has not been realized at present.

In recent years, some literature studies have reported that the properties of polymer nanocomposites are greatly affected by the different dimensions of nanofillers, which can affect the dispersion, interface, and distribution of nanofiller in polymer matrix (34,35). In fact, because of their differences in shape and element component, each nanoparticle has its own unique ability. It is therefore not possible to replace one nanoparticle with another. For example, CNT is considered as an excellent conductive filler for polymer matrix, but its thermal stability and barrier properties are not as good as sheet-like clay. Furthermore, multi-functional high performance polymer composites are desperately needed, which are difficult to be achieved by incorporating single type of nanoparticle. For this reason, multiphase polymer/CNT nanocomposites created by adding another inorganic nanoparticle family are increasingly investigated (36–42). Positive synergistic effects of these nanoparticles for improving the properties of polymer matrix are expected. Multiphase system means that at least three phases exist in the polymer composites. Actually, the enhancement of polymer properties by adding different types of nanofillers into one system is not a new concept. For example, synergistic effect was found regarding elastic modulus in rubber where carbon black and silica were used as fillers (43,44). It is one of the most important engineering composite materials in the 20th century. The only difference in our

description is that conventional multiphase systems are based on various micro-scaled fillers. Then, the key issue is to create synergistic effects between different types of nanoparticles in the polymer matrix. Good nanoparticle dispersion and strong interfacial interactions between nanoparticle and matrix are still the key issues in the nanocomposites containing multi-particles. In contrast to conventional nanocomposites, the particle/particle interaction will be considered as a new factor influencing the structure and properties of composites in addition to the interaction between nanoparticle and matrix in this unique system. In this case, one type of nanoparticle will affect the dispersion and distribution of another one, which may lead to new nanofiller synergistic effects in nanocomposites.

In the previous several years, various nanoparticles have been assembled into pairs to fabricate polymer nanocomposites, such as clay/silica (45), clay/carbon black (43), CNTs/clay (41,42), and CNTs/Titanium (38). Polymer/CNTs/clay ternary composite is one of most important multiphase systems with interesting synergistic effect, where sodium based montmorillonite (MMT) are the most commonly used layered clay. In this chapter, we will select some typical examples to demonstrate the importance and synergies of using CNTs and clay together in the preparation of polymer nanocomposites.

4.2 Electrical Properties of Polymer Composites with Clay and CNTs

Conductive polymer composites (CPCs) containing conductive particles have a wide range of industrial applications, such as antistatic materials, self-regulating heaters, over-current and over-temperature protection devices, and materials for electromagnetic radiation shielding (46). Despite these advantages, large amounts of conductive fillers (e.g. carbon black > 25%) are often required to achieve desired electrical property in insulating polymer matrix (47). A conductive filler content at which the composites electrical conductivity shows a sudden jump is known as the percolation threshold. Carbon nanotubes are considered as ideal conductive filler, which could be used to prepare CPCs with low percolation threshold due to their large aspect ratio and unique graphite structure. However, carbon nanotubes quite often form bundles due to strong intertubular van der Waals attractions and physical entanglement between them,

which usually lead to high percolation (2-10%) (48,49). Chemical modification can be used to improve the overall dispersion/exfoliation of CNTs (50), but it degrades the mechanical and electronic performance of the nanotubes.

Recently, Grunlan et al. prepared epoxy/clay/CNTs composite with high electrical conductivity and low percolation by using solution blending method without any additional chemical modification to CNTs (41). Clay as a solid dispersant was introduced into SWNT/epoxy composites to improve nanotube dispersion. Unlike surfactant or polymer dispersants, clay is mechanically rigid and can be used to enhance the properties (e.g., modulus, gas barrier, and flame retardation) of polymer composites (7). For epoxy composite with 0.05 wt% SWNT, electrical conductivity was increased by more than four orders of magnitude (from 10^{-9} to 10^{-5} S/cm⁻¹) with the addition of 0.2 wt% clay (Figure 4.2). Furthermore, the percolation threshold of these nanocomposites was reduced from 0.05 wt% to 0.01 wt% with the addition of clay. They also found that the conductivity of composites decreased slightly while clay content was more than 0.2 wt%. It is likely that higher loadings of clay (> 0.2 wt%) are somewhat less effective at improving conductivity due to their interference with the conductive network once its concentration dramatically exceeds that of the SWNTs.

Figure 4.3 shows optical microscope images of epoxy samples containing SWNT and clay. In the absence of clay, poorly dispersed and highly aggregated nanotubes are observed (Figure 4.3a). An effective three-dimensional CNTs network cannot be formed

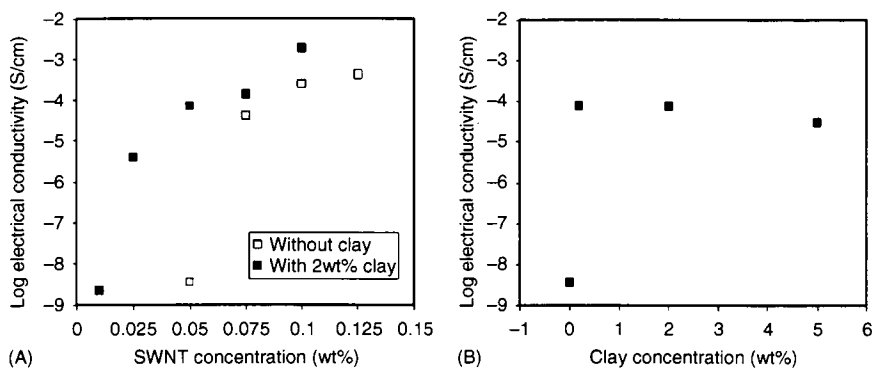


Figure 4.2. Electrical conductivity as a function of (a) SWNT concentration for composites with and without 2 wt% clay; (b) clay concentration for composites with 0.05 wt% SWNT. Reprinted with permission from ref (41).

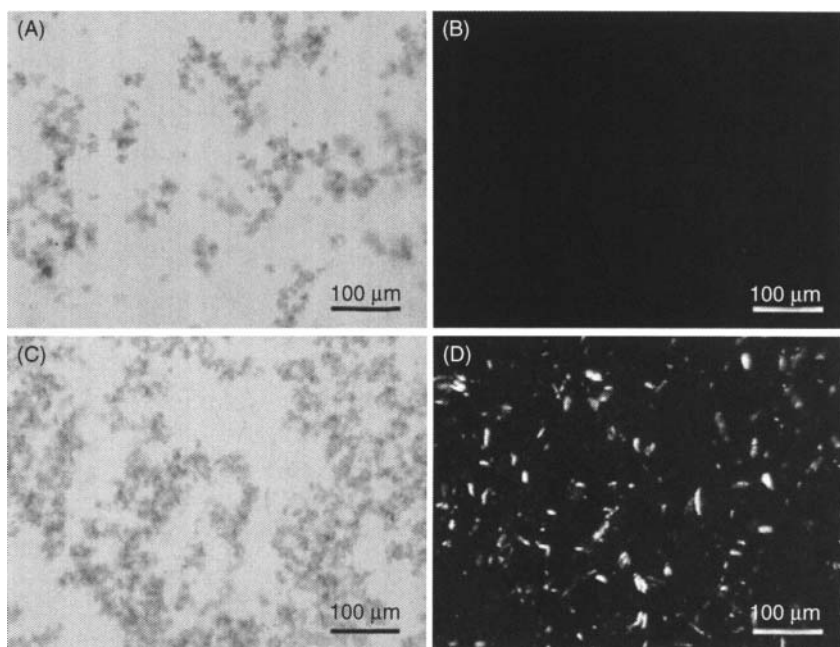


Figure 4.3. Bright field optical microscope images for epoxy composites containing: 0.05 wt% SWNT (a), 0.05 wt% SWNT, and 2 wt% clay (c), images (b) and (d) are the same respective positions, but under cross-polarized light condition. Reprinted with permission from ref (41).

because of the poor connection among the aggregates. By incorporating 2 wt% clay into the polymer matrix, SWNT dispersion is significantly improved. It is shown by the observation of more SWNT rich area (dark area) with the same SWNT concentration (see Figure 4.3c). Simultaneously, the SWNT network became better connected, as indicated by increased conductivity. It is noted that clay clusters as crystallites are not visible under optical microscope in bright field conditions, but cross-polarized light can be applied to resolve them as well-dispersed bright aggregates.

The mechanism of improvement in the formation of SWNT network and electrical conductivity induced by clay in these composites could be understood as following: firstly, the addition of clay increases the viscosity of the composite before curing, which makes it more difficult for nanotubes to migrate and re-aggregate during sonication. Secondly, the excluded volume created by the micron-scale clay clusters effectively creates a segregated network of CNTs. Finally, the nanotubes seem to interact more strongly with clay than

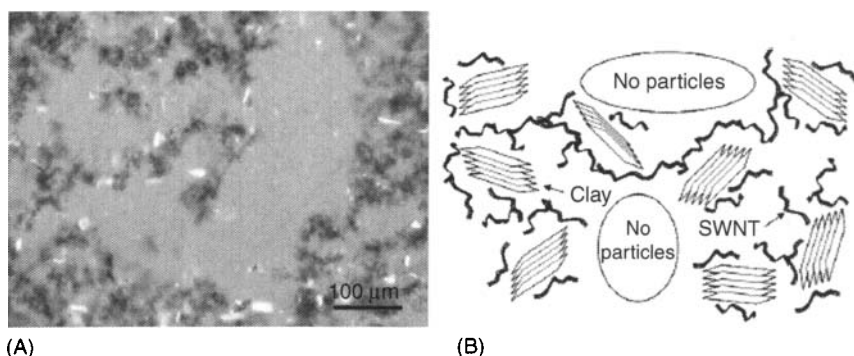


Figure 4.4. Optical microscope image for composites containing 0.05 wt% SWNT and 2 wt% clay under partial polarized light condition (a) and schematic illustration for clay assisted dispersion of SWNT (b). Reprinted with permission from ref (41).

epoxy. This SWNT-clay interaction can be visualized using partially polarized light in an optical microscope (as shown in Figure 4.4). Under these conditions, the epoxy matrix is gray in color, while clay is seen as bright clusters and SWNT is black. Nearly all of the clay aggregates are surrounded by a sea of SWNTs in this image (Figure 4.4a), which suggests that there is a strong affinity between these two particle systems. In this system, no synergistic effect of clay and SWNTs on mechanical properties is obtained. This is probably due to lack of adequate clay exfoliation providing large aspect ratio for stress load transfer. Therefore, using organically modified clays could provide the system with better dispersion and synergistic effect on mechanical properties could be produced by adding extra SWNTs. Moreover, a further reduction in the electrical percolation threshold may be found.

4.3 Mechanical Properties of Polymer Composites with Clay and CNTs

Generally, realizing effective reinforcement of CNTs in polymer needs two factors (21): (1) good dispersion in matrix, and (2) strong interface strength between CNTs and polymer. Dispersion is probably a more fundamental issue. Nanotubes must be uniformly dispersed as isolated nanotubes and individually coated with polymer. This results in a more uniform stress distribution and minimizes the presence of stress-concentrated centers. Furthermore, strong interface between CNTs and polymer leads to efficient stress transfer

from matrix to nanotubes, which allows polymer/CNT composites to afford higher stress load. Although a lot of work has been done to improve the interfacial interactions between CNTs and matrix by applying surface modification to CNTs (50), the extent of enhancement in mechanical properties in polymer nanocomposite is still not ideal due to limited enhancement in interface strength. Therefore, introducing clay into polymer/CNT composites can be a new route for solving above issue.

Chitosan, poly- β (1,4)-2-amino-2-deoxy-D-glucose, is the deacetylated product of chitin, the second abundant natural polymers on earth. Chitosan has been widely studied for biosensors, tissue engineering, separation membrane, water treatment and so on because of its good biocompatibility, biodegradability, and multiple functional groups (51). However, its low mechanical properties and poor thermal stability restricts its application. On one hand, the modified CNTs containing hydrophilic groups such as -COOH and -OH can be well dispersed in water. On the other hand, the amino group in chitosan can be protonated to NH_3^+ in acid media, which promotes the intercalation of polymer chains into clay by means of a cationic exchange process. Thus a good dispersion of clay and CNTs in chitosan solution is expected. Fu et al. reported that an obvious synergistic effect between clay platelets and CNTs on reinforcing biopolymer chitosan matrix. The composites were prepared by a simple solution blending method (42). By incorporating 3 wt% clay and 0.4 wt% CNTs into the system, the tensile strength and Young's modulus of the nanocomposites were improved by 171 and 124%, respectively (see Figure 4.5). Both tensile strength and Young's modulus of chitosan/CNT-clay composites are much higher than that of binary nanocomposites containing chitosan/clay (72 and 2753 MPa) or chitosan/CNTs (73 and 2682 Mpa). The increase of mechanical properties are usually "saturated" with increasing filler content due to the filler (clay or CNTs) aggregation and limited interfacial strength at higher filler loadings. Thus, it is difficult to further improve the mechanical properties of a polymer by using CNTs or clay alone (52,53). However, the saturated mechanical properties of chitosan nanocomposite with increasing CNTs content is further improved by synergistic effect between clay platelets and CNTs as demonstrated by Fu et al. (42).

Figure 4.6 shows the XRD patterns of pure clay (sodium montmorillonite), neat chitosan, chitosan/clay, chitosan /CNTs and chitosan/CNT-clay composite. Neat chitosan film shows weak crystalline

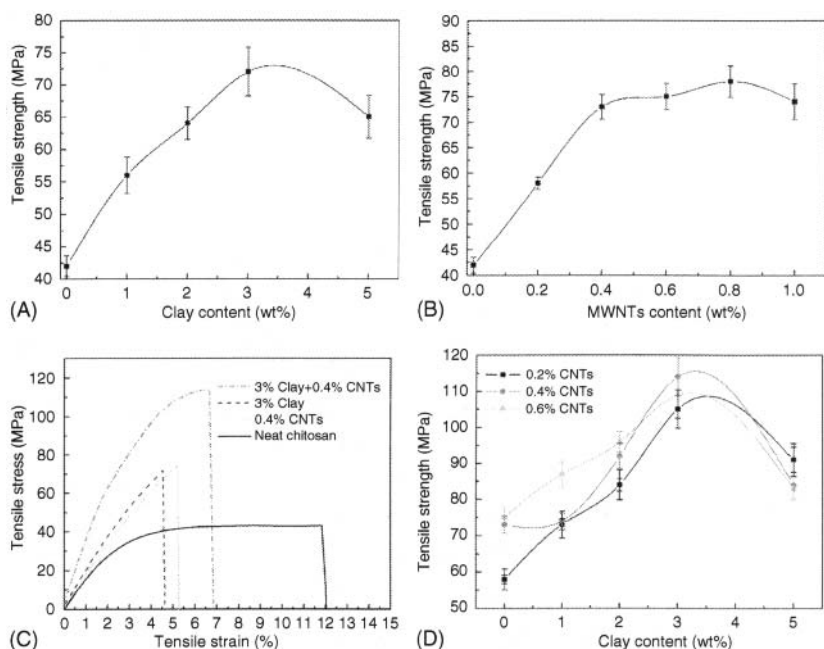


Figure 4.5. (a) Tensile strength of chitosan/clay nanocomposite as a function of clay content; (b) tensile strength of chitosan/CNTs nanocomposite as a function of CNT content; (c) stress-strain behavior for neat chitosan, chitosan/0.4% CNTs, chitosan/3% clay, and chitosan/3%clay/0.4% CNTs composites; (d) tensile strength of chitosan/clay/CNTs nanocomposite as a function of clay content. Reprinted with permission from ref (42).

peaks around $2\theta=11.3^\circ$, 18.2° , 23° in XRD spectrum. These crystalline peaks become stronger and sharper once desired amounts of CNTs or clay is added into chitosan. It is also accompanied by a new peak at about 8.5° . The result suggests an enhanced crystallinity or denser packing in the main chain in comparison with neat chitosan. The characteristic peak of clay disappears in the X-ray diffraction spectrum for both chitosan/clay and chitosan/CNT-clay composite when clay content is less than 5 wt %, which indicates the formation of exfoliated clay structure. In the case of chitosan/5%clay/0.4%CNTs composite, a new lower broaden peak around $2\theta=4^\circ\sim 6^\circ$ appears due to the formation of intercalated structure with some exfoliation. This work also indicates that the presence of CNTs will not affect the exfoliation of clay in chitosan. TEM characterization of the system (Figure 4.7) shows the existence of individual nanotubes, and no aggregates of CNTs are observed.

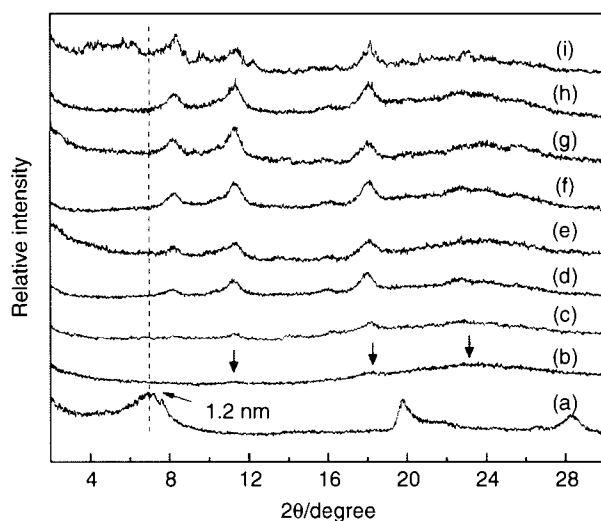


Figure 4.6. XRD pattern of neat chitosan, clay, and nanocomposites with different contents of CNTs and clay: (a) pure clay; (b) neat chitosan; (c) chitosan/0.4% CNTs; (d) chitosan/1% clay; (e) chitosan/2% clay; (f) chitosan/2% clay/0.4% CNTs; (g) chitosan/3% clay; (h) chitosan/3% clay/0.4% CNTs; (i) chitosan/5% clay/0.4% CNTs. Reprinted with permission from ref (42).



Figure 4.7. TEM images of chitosan/3% clay/0.4% CNTs composite. Reprinted with permission from ref (42).

Based on the XRD and TEM results, it can be concluded that the chitosan/CNT–clay nanocomposites containing exfoliated clay structure and well dispersed CNTs have been successfully prepared through a simple solution-intercalation/mixing method. A strong electrostatic interaction and hydrogen-bond could also be formed between chitsoan and these two nanofillers, which facilitate the dispersion and interfacial adhesion. CNTs can be inserted into clay network, as indicated by arrows in Figure 4.7. A part of CNTs located in clay platelet regions is seen to be connected with clay platelets to form a new type of clay-CNTs network. In this unique fillers network, clay platelets probably impede the motion of CNTs in chitsoan matrix during deformation, which could enhance the interaction between chitosan chains and fillers.

Schematic illustration of clay and CNTs morphology in chitosan nanocomposites is shown in Figure 4.8. In the composites based on chitosan/CNTs containing 0.4 wt % CNTs, nanotubes can be well dispersed in chitosan, but no filler network could be formed due to its low concentration (Figure 4.8a). In the composites based on chitosan/clay containing 3 wt % clay, formation of 2D clay platelets network is possible (Figure 4.8b). In chitosan/clay-CNTs ternary nanocomposites, 1D CNTs are confined in 2D clay platelets network, which results in a much jammed and conjugated 3D clay-CNTs network (Figure 4.8c). The interactions and networks in the system can be divided into: (1) clay-clay network, (2) clay-CNTs network, (3) CNTs-polymer-clay bridging, (4) polymer-polymer network. The formation of different networks and interactions could be the main reason for the observed synergistic reinforcement of CNT and clay

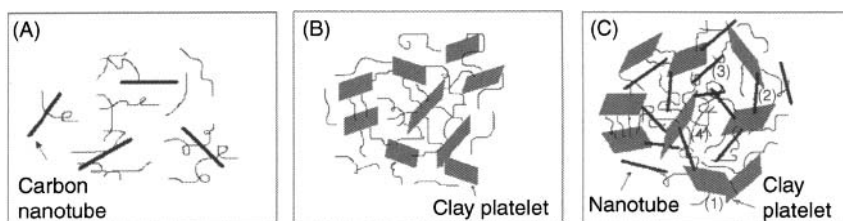


Figure 4.8. Schematic illustration of morphology of clay and CNTs in chitosan nanocomposites: (a) chitosan/0.4% CNTs; (b) chitosan/3% clay; (c) chitosan/3% clay/0.4% CNTs. The interaction and networks in the system could include: (1) clay-clay network; (2) clay-CNTs network; (3) CNTs-polymer-clay bridging; (4) polymer-polymer network. Reprinted with permission from ref (42).

on chitosan, as they are in favor of the stress transfer of chitosan onto clay and CNTs.

An obvious synergistic effect of clay sheets and pristine MWNTs in improving mechanical properties was also observed in poly(ethylene oxide) (PEO) nanocomposite (see Figure 4.9) (54). Yield strength, tensile strength, and strain at break for composites based on PEO/MMT/MWNTs were the highest among all the composites prepared (PEO/MWNTs, PEO/MMT, and PEO/MMT/MWNTs) containing the same total filler content. In contrast, the improvements in mechanical properties are moderate for the composites based on PEO/MWNTs comparing with pure PEO. Poor stress transfer between PEO and pristine CNTs might be responsible for this. In this work, MWNTs/MMT hybrids have been pre-established through mixing pristine MWNTs in MMT aqueous dispersion under ultrasonication. In the aqueous suspensions of MWNTs/MMT, the Na^+ ion on the MMT sheets/water surface can interact with the negatively charged MWNTs. The upshift of the G-band in MWNTs/MMT dispersions in the Raman spectra represents a strong interaction between MMT sheets and carbon atoms due to the structural integrity of the sp^2 hybridization. Figure 4.10 shows TEM images of the cross section of PEO/MMTs/MWNTs 97.9/1.6/0.5 (wt. %) nanocomposite and its parental binary nanocomposites prepared by solution mixing PEO with the suspension of

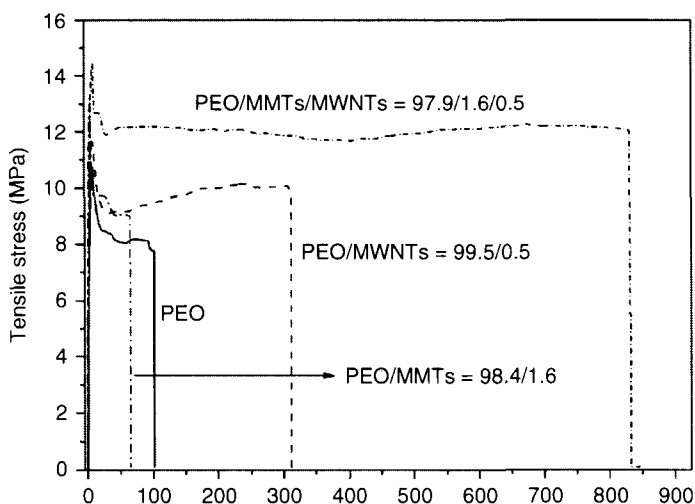


Figure 4.9. Stress-Strain behaviors of neat PEO and its nanocomposites. Reprinted with permission from ref (54).

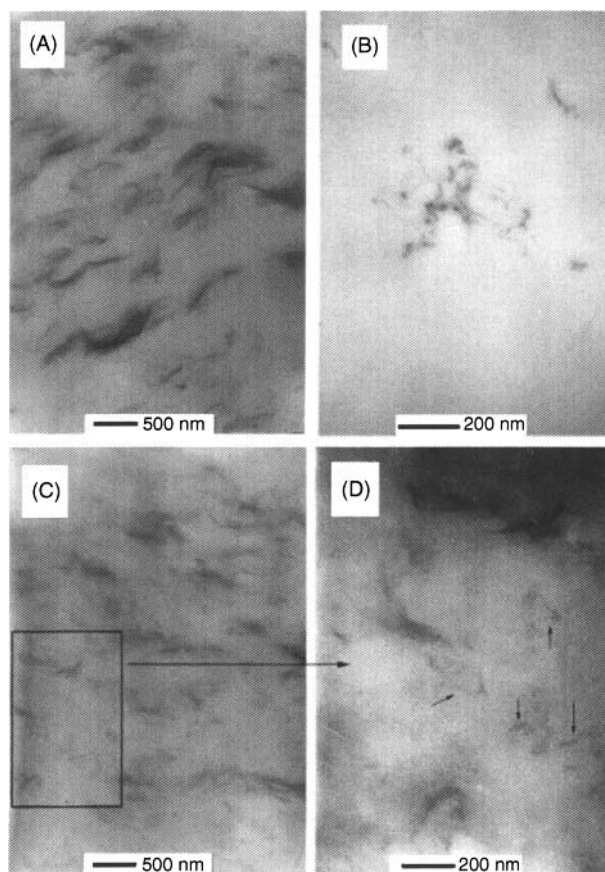


Figure 4.10. TEM images of PEO nanocomposites: (a) PEO/MMTs=98.4/1.6; (b) PEO/MWNTs=99.5/0.5; (c) PEO/MMTs/MWNTs=97.9/1.6/0.5 (all by weight); and (d) high magnification of panel c. Reprinted with permission from ref (54).

nanomaterials. MWNTs are dispersed as individual nanotubes in PEO/MMTs/MWNTs nanocomposites (see Figure 4.10d). Meanwhile, the size of MMT phase in this ternary nanocomposite is smaller than that in the PEO/MMTs nanocomposite (see Figure 4.10 a and c). It is clear that strong interaction between MMT sheets and MWNTs prevents the formation of larger aggregates of MMTs or MWNTs. More importantly, the network-like structure of nanofillers can be observed due to improved MMTs and MWNTs dispersion (Figure 4.10c). Therefore, the synergistic reinforcement of PEO is caused by this special nanofillers network combining MWNTs with clay. Interestingly, the enhanced interaction between polymer

matrix and nanofillers are realized by controlling the filler morphology and dispersion rather than any complex surface modification of fillers. Creating more exfoliated MMT platelets in this system may be favorable for improving the mechanical properties of PEO nanocomposites.

In addition to creating a synergistic reinforcing effect of nanofillers by using individual clay and CNTs, clay-CNTs hybrid (Figure 4.1d and 4.11) prepared by catalytic decomposition of acetylene over iron-catalyst centers supported on montmorillonite surfaces by ion-exchange is used as reinforcement in polymer matrix, which is another effective method to prepare polymer nanocomposite with high mechanical properties. The unique hybrid filler as a whole has some advantages for making high performance polymer nanocomposite: 1) the clay is exfoliated to well-separated nanoplatelets by intercalation with iron (oxide) followed by the growth of CNTs, with large aspect ratio, 2) the interaction between CNTs and clay are much stronger than that between mixture of clay and CNTs, which is favorable for stress transfer between polymer and fillers, 3) the as-prepared CNT-clay hybrid is the combination of a 2D nano-clay platelet and several 1D nanotubes; this effectively promotes the homogeneous dispersion of both clay platelets and nanotubes in the polymer; 4) the polymer chains are entangled and wrapped around the 3D nano-structured filler, the interaction between polymer chains and hybrid filler is much stronger than that with the smooth CNTs or clay platelets alone.

Recently, Zhang et al. have successfully grown carbon nanotubes on clay platelet to form 3D nanostructured filler (55). This hybrid

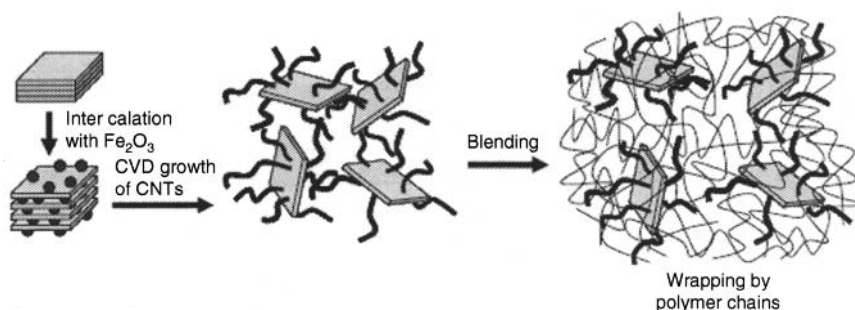


Figure 4.11. Schematic illustration showing the procedure for growth of carbon nanotubes on clay platelets and incorporation of CNT-clay hybrid filler into PA6 matrix for making the PA6/CNT-clay composite. Reprinted with permission from ref (55).

filler was added into nylon-6 (PA6) by melt blending as shown in Figure 4.11. The tensile modulus and the tensile strength of the PA6 composite were greatly improved, by about 290% and 150 %, respectively. It was achieved by incorporating only 1 wt % CNT–clay hybrid filler and the enhancements were attributed to the synergistic effect between CNTs and clay platelets and their homogeneous dispersion and strong interaction with the polymer matrix. The enhancement of mechanical properties upon incorporation of 1 wt% hybrid filler (i.e., 0.4 wt% CNTs) was even higher than that of composites containing 1 wt% neat CNTs alone, where the improvements in tensile modulus and tensile strength were about 115% and 120%, respectively (56). Therefore, the results in this study clearly demonstrate the benefit of using CNT–clay hybrid filler. The observation that most CNTs are broken upon failure rather than just pulled out of the matrix is a clear evidence of strong interfacial adhesion between CNT–clay hybrid fillers and the PA6 matrix (Figure 4.12). The TEM image clearly exhibits the intimate adhesion of CNTs and clay platelets with the matrix, and the combination of CNT–clay fillers with the polymeric matrix. Therefore, the finely dispersed CNT–clay filler throughout the polymeric matrix and the strong interaction between the hybrid filler and PA6 matrix are responsible for the significant reinforcement of the mechanical properties of the composite prepared.

Furthermore, CNT–clay hybrid filler can also be used to prepare polymer nanocomposites by solution based method. Hydrophilic

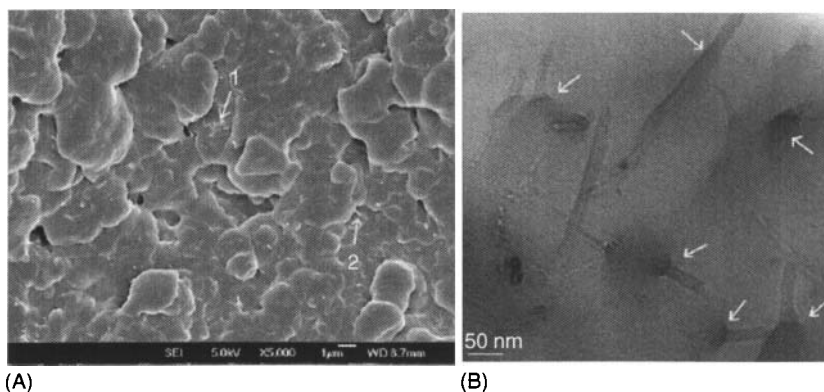


Figure 4.12. (a) SEM image showing typical morphology of the failure surface for PA6 nanocomposite containing 1 wt% CNT–clay hybrid. (b) TEM image of a thin section of the composite. Reprinted with permission from ref (55).

clay can form stable suspension in water, which leads to good dispersion of its hybrid (clay-CNTs) in water despite the fact that CNTs are highly hydrophobic. So clay-CNTs hybrid can be dispersed well in water soluble polymers such as poly(vinyl alcohol) (PVA) (57) and poly(ethylene oxide) in water (58). Zhao et al. prepared clay-CNT hybrid /PVA nanocomposite films with different clay-CNT content by this method (59). They reported that the thermal stability and dynamic mechanical properties of PVA were remarkably enhanced by incorporating clay-CNTs into PVA matrix (59). The storage modulus was significantly improved by 133% at 508°C, when 7 wt% clay-CNTs was added into PVA matrix.

Moreover, this novel CNTs-clay hybrid also can be used to improve the mechanical properties of composites based on thermoset polymer systems, such as epoxy. This resin exhibits many desirable properties, such as high thermal stability and excellent electric properties. However, epoxy resin is generally brittle due to its highly cross-linked structure. Therefore, improving the toughness of this resin is very important for epoxy technology (60). Li et al. used highly exfoliated clay-CNTs hybrid (E-MMT) as filler to improve the mechanical properties of epoxy (EP) (61). Epoxy composites containing 1 wt% organically modified MMT were observed to have an impact strength of 24.3 kJ/m², showing 20% increase over neat EP. More interestingly, the impact strength of composites demonstrated an increase from 20.2 to 42.6 kJ/m² by adding 1 wt% E-MMT/EP into epoxy, and it equals to nearly 110% enhancement by 1 wt% filler. Figure 4.13 shows the SEM micrographs of impact failure surfaces of the pristine EP and their nanocomposites. In Figure 4.13 a and b, the failure surfaces are generally flat and featureless, suggesting a typical brittle-fracture behavior of the pristine EP and composites containing 1 wt% Na-MMT/EP. Figure 4.13d exhibits a much rougher failure surface for epoxy nanocomposite containing 1 wt% E-MMT. The increased surface roughness indicates that the path of the crack is distorted by adding E-MMT into epoxy composites, making crack propagation more difficult. Therefore, the presence of E-MMT might cause perturbations along the crack front and consequently alter the propagating crack path. Meanwhile, the Vicker's hardness of the E-MMT/EP nanocomposites (when incorporating only 1 wt% E-MMT) were greatly improved by 36.4% compared with pristine EP. The hardness values of 1 wt % Na-MMT/epoxy composites (Na-MMT/EP) were lower than the pristine epoxy (pristine EP), which may come from inhomogeneous dispersion

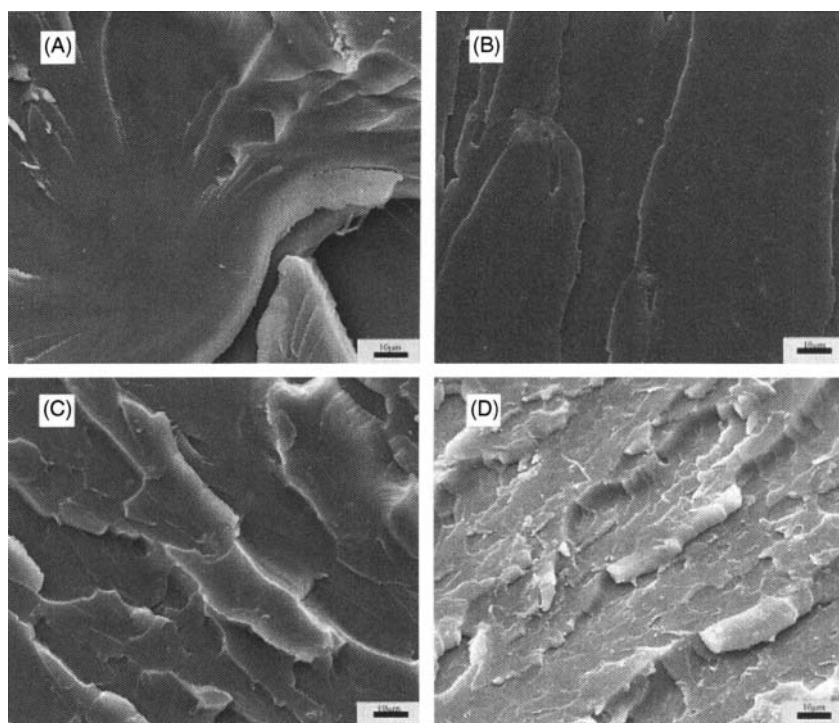


Figure 4.13. SEM images of fracture surface for pristine EP (a), Na-MMT/EP (b), CTAB-MMT/EP (c) and E-MMT/EP (d) nanocomposites. Reprinted with permission from ref (61).

and poor interfacial bonding between Na-MMT and epoxy matrix. Organically modified MMT/epoxy composites (organic-MMT/EP) only show moderate hardness increase of 13.5%. Obviously, the exfoliated clay-CNTs hybrid performs better than traditional filler in terms of hardness enhancement in epoxy matrix. The considerable improvement is attributed to the *in-situ* growth of CNTs on clay layers, which promotes clay exfoliation process in epoxy matrix, as well as mechanical interlocking within the matrix. In the study performed by Lau et al., they reported that the epoxy composite containing clay-supported CNTs (clay-CNTs hybrid) shows more improvement in hardness than the epoxy composite containing only clay or CNTs (Table 4.1). Meanwhile, they compared the effective reinforcement of clay-CNTs hybrid with a simple mixture of clay and CNTs in epoxy (62). Although the hardness of the composites containing the mixture of CNT/clay was higher than those

Table 4.1. Average Vicker's hardness and percent improvement of 2 wt% NT-NC/epoxy composites with different NT-NC concentration. Reprinted with permission from ref (62).

Sample	Average Vicker's hardness no.	Percent improvement (%)
Pure epoxy	10.8	0
2 wt.% NT/epoxy	12.9	19
2 wt.% NC/epoxy	12.5	16
2 wt.% NT-NC composite/epoxy	15.1	40
2 wt.% NT/NC mixture/epoxy	13.1	21

based on nanotubes or nanoclay alone, the reinforcement effect was still not considered as significant due to poor interaction between nanotubes and nanoclay in the mixture.

4.4 Thermal and Flame Properties of Polymer Composites with Clay and CNTs

Organoclay is commonly used nanoscale filler to obtain thermal stability and flame retardation in polymers as it acts as a superior insulator of mass transport of the volatile products generated during decomposition (7). Some groups also report that incorporation of CNTs can enhance the thermal stability of polymer matrix by hindering the flux of degradation product and speed up the formation of char (63–65). In recent years, the synergistic effect between CNT and clay in thermal stability and flame retarding performance was also investigated.

Dubois et al. prepared ethylene–vinyl acetate (EVA) copolymers nanocomposite with commercial organo-modified clays (organo-clays) and multi-walled carbon nanotubes (MWNTs) via direct melt blending (66). Interestingly, a synergistic effect arising from the combination of MWNTs and organoclays has been evidenced in enhancement of thermal degradation stability and flame retardant properties. In binary nanocomposites with the same filler content, clay-based materials displayed slightly larger shifts in the temperature with the maximum rate of degradation in TGA test, than

those based on purified MWNTs. The largest delay (as high as 56°C) was observed for the composites based on a filler combination of 3 wt% of Cloisite 30B and 1 wt% of purified MWNTs (Figure 4.14). The best result for binary systems corresponds to a shift by 52°C for the nanocomposite based on 5 wt% of organo-modified clay. Compared to neat EVA, heat release rate (370 kw/m²) for ternary nanocomposite containing clay and CNTs was lower than that for binary nanocomposites (470 kw/m² for clay based composite and 405 kw/m² for CNTs based composite). The char formed during the

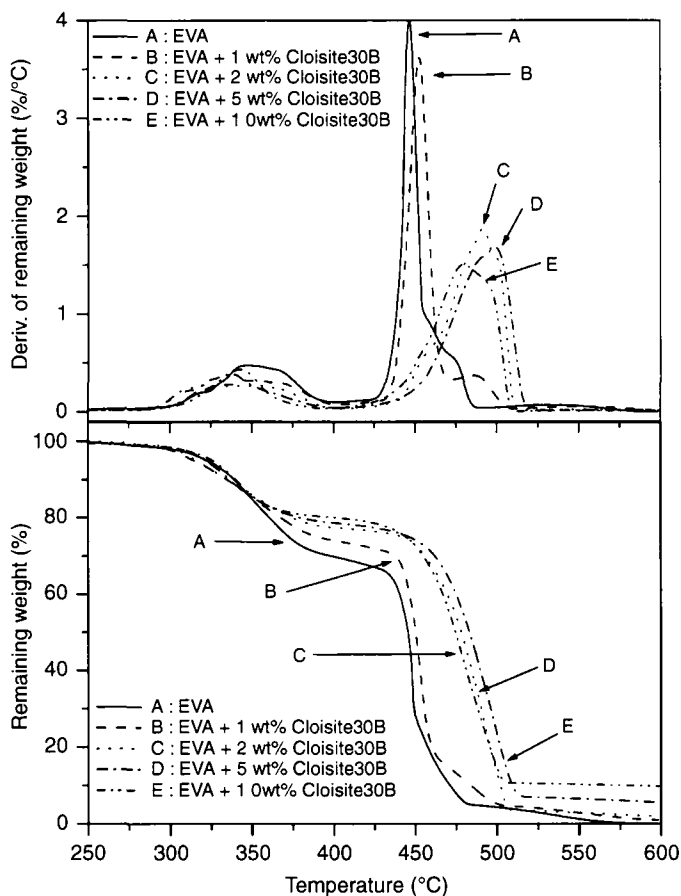


Figure 4.14. Thermogravimetric analysis of EVA nanocomposites filled with 3 wt% Cloisite 30B and either 0, 0.5 or 1.0 wt% purified MWNTs under air flow at 20 K/min (unfilled EVA matrix is shown for sake of comparison). Reprinted with permission from ref (66).

degradation (and responsible for the reduction of the PHRR) was much less cracked in ternary compositions compared to those from corresponding binary systems. The formation of uniform crust on top of the burning sample strongly limits heat diffusion. Gao et al. investigated the roles of MWNTs and clay on the fire retardant properties of ethylene vinyl acetate copolymer (EVA) nanocomposites (67). It was found that nanotubes played an important role in the reduction of heat release rate peak by forming low permeability char containing graphitic carbon. The oxidation resistance of the char is a function of the degree of graphitisation. By adding clay into nanotube/EVA composite, the trend of graphitic carbon formation is enhanced. Nanotubes also have the function of reducing surface cracks of chars to increase barrier resistance to the evolution of flammable volatiles and the oxygen ingress to the condensed phase. Figure 4.15 shows that nanotube-enhanced EVA is almost burnt out while an integrated char structure is retained in the clay/EVA nanocomposite. For the composite containing both clay and carbon nanotubes (clay/MWNT/EVA), similar char morphology is obtained in both natural burning and muffle furnace tests. The chars formed have an integrated structure with moderate surface cracks.

Most of the previous studies on flame retardation of polymer nanocomposites are focused on the relationship between macroscopic morphologies of chars and the flammability properties. Fang et al. studied the relationship between evolution of the microstructure, viscoelasticity and graphitization degree of chars and the flammability of polymers during combustion (68). The flame retardancy of ABS/clay/MWNTs nanocomposites was strongly affected by the formation of a network structure. Flammability properties

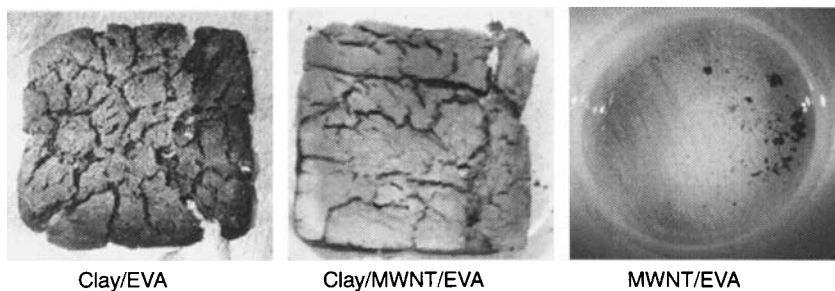


Figure 4.15. The morphology of the chars produced from clay/EVA, clay/MWNT/EVA and MWNT/EVA nanocomposites following the burning at 600°C for 20 min. Reprinted with permission from ref (67).

measured by a cone calorimeter revealed that incorporation of clay and MWNTs into ABS resin significantly reduced the peak heat release rate (PHRR) and slowed down the whole combustion process comparing to individually filled system based on clay or MWNTs (Figure 4.16). The construction of a nanoparticle network can be demonstrated by the variation in rheological properties. The G' in the low frequency regime significantly depends on the addition of clay and MWNTs, which can reflect the relaxation and motion of the polymer chain. As shown in Figure 4.17, it is observed that the terminal slope of $G'-\omega$ curves decreases with the addition of clay and MWNTs, indicating that a percolated filler network is established where the free movement of ABS chains is restricted by the spatially confined geometry. The coexistence of clay and MWNTs in the composites forms a more effective confined space and enhances the network structure, which could be responsible for the improved flame retardant property in this study. For ABS/clay/MWNTs nanocomposites, the complex viscosity increases by at least one order of magnitude comparing with pure ABS matrix when the temperature is higher than 240°C (see Figure 4.17c). As the coexistence of clay and MWNTs induces an effective confined geometry, a network structure is formed at lower temperatures to protect the polymer matrix more efficiently. The authors observed

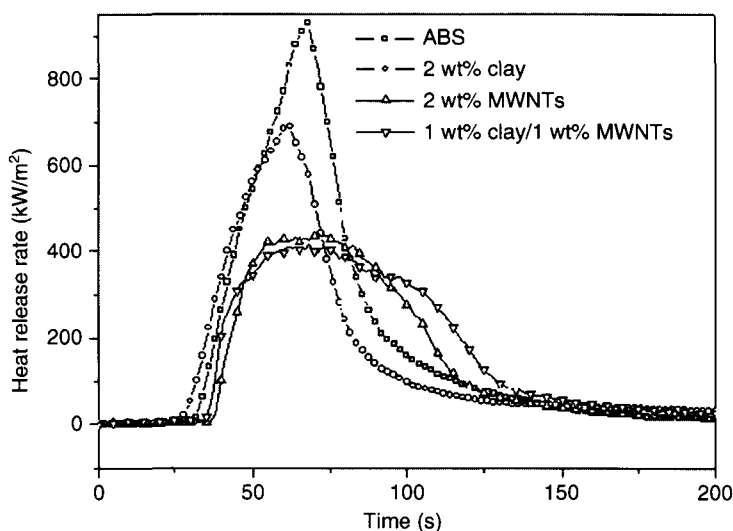


Figure 4.16. Heat release rate versus time measured with a cone calorimeter (heat flux: 35 kW m^{-2}) for ABS nanocomposites. Reprinted with permission from ref (68).

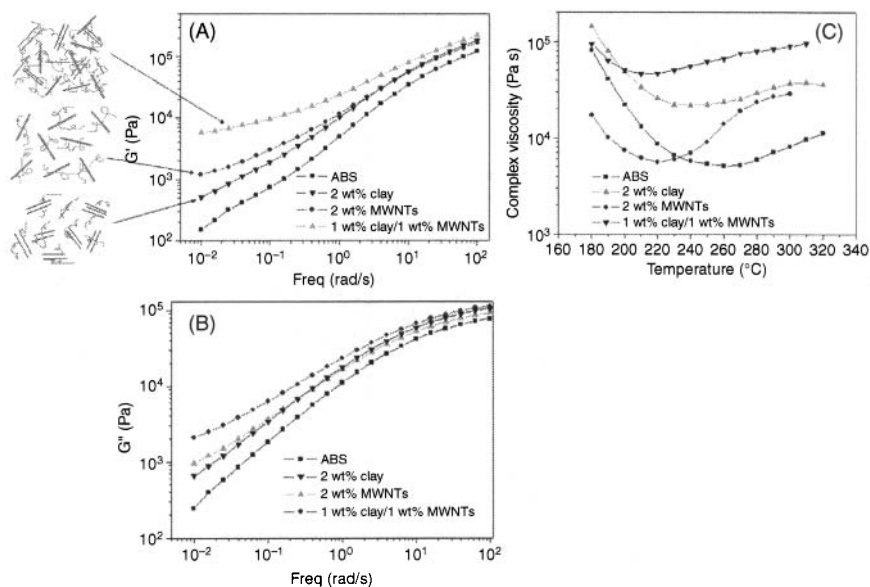


Figure 4.17. Linear melt-state rheological properties as a function of oscillatory frequency: (a) storage modulus, G' and (b) loss modulus, G'' ; (c) Dependence of complex viscosity on temperature for ABS nanocomposites. Reprinted with permission from ref (68).

that some MWNTs run across between clay layers by examining chars of ABS/clay/MWNTs nanocomposites. It indicates a strong interaction between clay and MWNTs. Moreover, the existence of clay enhances the graphitization degree of MWNTs during combustion. As clay assists the process of elimination of dislocations and defects, and induces the rearrangement of crystallites, Al_2O_3 , as one of the components of clay, acts as the catalyst of graphitization.

In addition to the enhanced mechanical properties of chitosan by adding clay and CNTs as discussed above, a great synergistic effect between 2D clay platelets and 1D CNTs (chitosan/2% clay/1% CNTs) for improved thermal stability of chitosan matrix has also been observed (69). The surface morphology of the char for chitosan nanocomposites is shown in Figure 4.18. For chitosan/3% CNT composites, some microcracks and large holes are observed in the char layer, which indicate high weight loss of degradation product. The degradation temperature of chitosan/clay is higher than that of chitosan/CNTs and the former demonstrates a relatively dense and small pore structure in char. The char is denser with fewer cracks for the composites containing both clay and CNTs as shown in Figure 4.18c. The formation of 3D conjugated filler network with

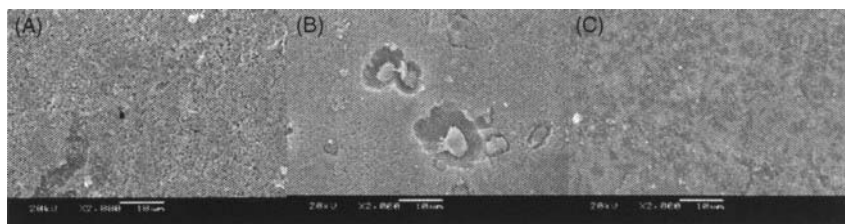


Figure 4.18. SEM images of the char of chitosan nanocomposites after TGA tests: (a) chitosan/3% clay; (b) chitosan/3% CNT; (c) chitosan/2% clay/1% CNT composites. Reprinted with permission from ref (69).

1D CNTs inserted in the 2D clay platelet network is believed to be responsible for this, as this unique nanostructure provides larger tortuosity and obstacle for the heat transport. The large improvement in thermal stability of chitosan may arise from following two reasons: (1) good heat barrier properties of CNTs and clay for polymer matrix during formation of chars and (2) formation of carbonaceous layer.

In previous studies, most researchers investigated the relationship between morphology of nanoparticles (clay and CNTs) and flame retardancy (or thermal stability) of polymer composites without considering the thermal degradation as a kinetic process. However, the thermal degradation of hydrogenated nitrile-butadiene rubber (HNBR)/clay and HNBR/clay/CNTs nanocomposites was investigated with thermogravimetric analysis (TGA) by Zhang et al. (70), where the kinetic process of thermal degradation was taken into account. The activation energy sequence of HNBR and its nanocomposites was HNBR/clay/CNTs > HNBR/clay > HNBR. HNBR/clay/CNTs nanocomposites had higher char yield at 600°C than HNBR/clay, which was attributed to the interactions between clay and CNTs. The activation energies of HNBR and HNBR nanocomposites had a sharp increase in low conversion degree area and a slow increase in high conversion degree area. The gases involved during thermal degradation in nitrogen atmosphere were studied by Fourier transform infrared spectroscopy coupled with TGA. The composites based on HNBR/clay/CNTs had a lower thermal degradation rate than HNBR/clay composites. This effect is caused by the formation of clay-CNTs filler network which reduced the diffusion speed of degradation products. The coexistence of clay and CNTs could form compact char layers with better barrier property and thus the thermal stability of HNBR was improved.

In comparison with the studies on flame behavior of homopolymers, Pack et al. (71) reported the synergistic effect of clay and CNTs on enhancing flame retardancy in polymer blends (PS/PMMA). The thermal properties of the blend system can be very complicated as phase separation occurs continuously with different temperatures during thermal degradation. The combination of nanoparticles can achieve a synergy which minimizes the total amount of fillers, and therefore, preserves the mechanical properties of polymer blends. The authors found that the flame retardant (FR) particles segregate to MWNTs preferentially, thereby allowing clay to segregate to the blend interfaces. In this manner both phase stabilization and good dispersion could be achieved. The addition of all types of nanoparticles, including standard FR formulations, decreased the time to ignition. Furthermore, the combination of s-MWNT and clay significantly reduced the heat release rate (HRR) and mass loss rate (MLR) compared with compounds containing only one type of nanoparticle. Electron microscopy images of the nanocomposites and chars showed that s-MWNTs were able to diffuse and form a distinct phase in the nanocomposites after heating. The exclusion process of clay allows s-MWNTs to achieve better physical contacts, thereby improving the thermal conductivity. In contrast, l-MWNTs were entangled and therefore unable to move. However, clays formed a barrier between tube contacts which results in an increase in the specific heat and HRR and MLR compared to unfilled or compound containing only clay. It was concluded that one must consider the organization of nanoparticles, as well as their chemical nature when designing flame retardant nanocomposites, since specific synergies may be established which can reduce the overall filler concentration.

4.5 Conclusion and Future Outlook

In this chapter, we discussed some interesting studies on ternary polymer composites containing both clay and CNTs. Synergistic effect is observed in composites as improvements in various properties (such as mechanical, electrical and thermal stability properties) are obtained. This effect between clay and CNTs in polymer composites indicates that the nanofillers with different dimensions can greatly cooperate with each other in certain way to improve the properties of the composites rather than work independently. More importantly, the improvement is more than a simple sum of

the property of individual component which is determined by the mutual influence (including direct and indirect influence) between two types of nanoparticles

Two methods are reported to produce synergistic effect between clay and CNTs on the properties of polymer: (1) one way is to add clay and CNTs simultaneously in polymer matrix to fabricate nanocomposite. In these systems, the interaction between clay platelets and CNTs is relatively weak. The key is to create a filler network by combining clay and CNTs to produce synergistic effect between nanofillers in order to improve the mechanical properties and thermal stability of the composites. Perfect and jammed clay-CNTs network is in favor of the stress transfer from polymer onto clay and CNTs, and the formation of intact char layers to hinder heat and substance loss during high temperature degradation. In addition, incorporation of clay may also affect the dispersion and distribution of CNTs, which can lead to a change in electrical properties of the nanocomposites; (2) another method to fabricate polymer nanocomposite is adding synthesized clay-CNTs hybrid produced by CVD method as filler into polymer matrix. In these systems, the interaction between clay platelets and CNTs is stronger than previous method due to stronger connection between clay and CNTs. This strong interaction can greatly enhance the composite mechanical properties. Moreover, this 3D clay-CNTs hybrid filler has unique structure owing to its highly exfoliated clay platelets structure and good dispersability of CNTs, thus, it can be used as novel filler for various polymer matrices. However, these hybrid fillers appears to be obviously efficient only in reinforcing polymer matrix, the application is not flexible due to their special filler structure. For example, it is not possible to use them in highly conductive polymer systems as the attached clay platelets with CNTs may break down the conductive CNTs networks. Since the interaction and morphology of clay and CNTs can be tailored by varying process conditions and filler surface modification, it looks like a promising way to fabricate multifunctional polymer composites, which show great potential in a wide range of applications, including flame retardancy, mechanical, electrical and thermal properties.

Currently, the study on ternary polymer composites containing both clay and CNTs is still at its primary stage, but it is promising and exciting to assemble two types of nanoparticles to break the limitation of single nanofiller in composites. Furthermore, we would like to propose some issues that should be addressed in future work in this field:

- (1) The properties of polymer nanocomposites are influenced by numerous factors including nanofillers type, purity, and the match between clay and CNT dimensions (length and diameter). These factors should be taken into account in the preparation of polymer nanocomposite, as well as in process of reporting and interpreting the experimental data.
- (2) The effect of clay and CNTs on the melt temperature, crystallization temperature, glass transition temperature and crystallinity of polymer matrix should be carefully investigated, as they are often related to different properties of the composites.
- (3) Synergistic reinforcement mechanism between clay and CNTs are still not clear in terms of improving various properties of polymer matrix. More understanding of the synergistic mechanism can help tailor the morphology and structure of the nanofillers to obtain desired properties in nanocomposites. Currently, the subject of addition of clay and CNTs to enhance thermal properties and flame retardancy of polymers is better understood compared to other properties. As creating a nanofiller network of clay and CNTs is commonly considered to produce synergistic effect in polymer composites, thus, tailoring the interaction and promotion of the formation of an effective morphology of nanofiller network in polymers by various methods should be one of the most important aspects of future research.
- (4) So far, utilization of as-prepared clay-CNTs hybrid in polymer composites exhibits good properties, especially mechanical properties. However, the versatile structure of this hybrid synthesized by different processing conditions lead to different composites properties. So the effect of fabrication method and process parameters on final properties of polymer composites should be investigated more systematically. For example, the density and length (or diameter) of CNTs on clay platelets may affect the properties of hybrid. It is interesting to enhance the connection between clay and CNTs in order to obtain higher mechanical properties for the hybrid filler and composites.

Acknowledgement

We would like to express our sincere thanks to the National Natural Science Foundation of China for Financial Support (50533050, 20874064 and 50873063).

References

1. H.D. Wagner, *Nature Nanotechnology*, Vol. 2, p. 742, 2007.
2. P.M. Ajayan, L.S. Schadler, and P.V. Braun, *Nanocomposite Science and Technology*, WILEY-VCH, 2003.
3. H. Zou, S.S. Wu, and J. Shen, *Chemical Reviews*, Vol. 108, p. 3893, 2008.
4. A.P. Philipse, *Colloid and Polymer Science*, Vol. 266, p. 1174, 1988.
5. S. Iijima, *Nature*, Vol. 354, p. 56, 1991.
6. P. Calvert, *Nature*, Vol. 399, p. 210, 1999.
7. S.S. Ray and M. Okamoto, *Progress in Polymer Science*, Vol. 28, p. 1539, 2003.
8. E.W. Wong, P.E. Sheehan, and C.M. Lieber, *Science*, Vol. 277, p. 1971, 1997.
9. J.P. Lu, *Journal of Physics and Chemistry of Solids*, Vol. 58, p. 1649, 1997.
10. A. Bachtold, P. Hadley, T. Nakanishi, and C. Dekker, *Science*, Vol. 294, p. 1317, 2001.
11. S. Joseph, R.J. Mashl, E. Jakobsson, and N.R. Aluru, *Nano Letters*, Vol. 3, p. 1399, 2003.
12. G.B. Blanchet, C.R. Fincher, and F. Gao, *Applied Physics Letters*, Vol. 82, p. 1290, 2003.
13. S.M., Bachilo, M.S. Strano, C. Kittrell, R.H. Hauge, R.E. Smalley, and R.B. Weisman, *Science*, Vol. 298, p. 2361, 2002.
14. J. Lefebvre, Y. Homma, and P. Finnie, *Physical Review Letters*, Vol. 90, p. 217401, 2003.
15. C. Lau, M.J. Cooney, and P. Atanassov, *Langmuir*, Vol. 24, p. 7004, 2008.
16. P.M. Ajayan, O. Stephan, C. Colliex, and D. Trauth, *Science*, Vol. 265, p. 1212, 1994.
17. J.B. Lu, B. Kumar, M. Castro, and J.F. Feller, *Sensors and Actuators B-Chemical*, Vol. 140, p. 451, 2009.
18. Q.J. Wan, X.W. Wang, F. Yu, X.X. Wang, and N.J. Yang, *Journal of Applied Electrochemistry*, Vol. 39, p. 785, 2009.
19. D.W. Kim, S.R. Sivakumar, D.R. MacFarlane, M. Forsyth, and Y.K. Sun, *Journal of Power Sources*, Vol. 180, p. 591, 2008.
20. Q.F. Xiao, and X. Zhou, *Electrochimica Acta*, Vol. 48, p. 575, 2003.
21. J.N. Coleman, M. Cadek, R. Blake, V. Nicolosi, K.P. Ryan, C. Belton, A. Fonseca, J.B. Nagy, Y.K. Gun'ko, and W.J. Blau, *Advanced Functional Materials*, Vol. 14, p. 791, 2004.
22. R. Andrews, D. Jacques, M. Minot, and T. Rantell, *Macromolecular Materials and Engineering*, Vol. p. 287, 2002.
23. O. Meincke, D. Kaempfer, H. Weickmann, C. Friedrich, M. Vathauer, and H. Warth, *Polymer*, Vol. 45, p. 739, 2004.
24. J. Gao, M.E. Itkis, A. Yu, E. Bekyarova, B. Zhao, and R.C. Haddon, *Journal of the American Chemical Society*, Vol. 127, p. 3847, 2005.
25. M.J. Biercuk, M.C. Llaguno, M. Radosavljevic, J.K. Hyun, A.T. Johnson, and J.E. Fischer, *Applied Physics Letters*, Vol. 80, p. 2767, 2002.
26. P.M. Ajayan, and J.M. Tour, *Nature*, 2007, Vol. 447, p. 1066.
27. T. McNally, P. Potschke, P. Halley, M. Murphy, D. Martin, S.E.J. Bell, G.P. Brennan, D. Bein, P. Lemoine, and J.P. Quinn, *Polymer*, Vol. 46, p. 8222, 2005.

28. W.K. Park, J.H. Kim, S.S. Lee, J. Kim, G.W. Lee, and M. Park, *Macromolecular Research*, Vol. 13, p. 206, 2005.
29. J. Chen, R. Ramasubramaniam, C. Xue, and H. Liu, *Advanced Functional Materials*, Vol. 16, p. 114, 2006.
30. M. Moniruzzaman, and K.I. Winey, *Macromolecules*, Vol. 39, p. 5194, 2006.
31. E.M. Moore, D.L. Ortiz, V.T. Marla, R.L. Shambaugh, and B.P. Grady, *Journal of Applied Polymer Science*, Vol. 93, p. 2926, 2004.
32. J.C. Kearns, and R.L. Shambaugh, *Journal of Applied Polymer Science*, Vol. 86, p. 2079, 2002.
33. W.J. Ma, L.Q. Liu, Z. Zhang, R. Yang, G. Liu, T.H. Zhang, X.F. An, X.S. Yi, Y. Ren, Z.Q. Niu, J.Z. Li, H.B. Dong, W.Y. Zhou, P.M. Ajayan, and S.S. Xie, *Nano Letters*, Vol. 9, p. 2855, 2009.
34. S.T. Knauert, J.F. Douglas, and F.W. Starr, *Journal of Polymer Science, Part B: Polymer Physics*, Vol. 45, p. 1882, 2007.
35. D.W. Schaefer, and R.S. Justice, *Macromolecules*, Vol. 40, p. 8501, 2007.
36. H.D. Bao, Z.X. Guo, and J. Yu, *Polymer*, Vol. 49, p. 3826, 2008.
37. Z.H. Chang, F. Guo, J.F. Chen, L. Zuo, J.H. Yu, and G.Q. Wang, *Polymer*, Vol. 48, p. 2892, 2007.
38. J. Sumfleth, L. Prado, M. Sriyai, and K. Schulte, *Polymer*, Vol. 49, p. 5105, 2008.
39. W. Zhang, T. Yang, D.M. Huang, K. Jiao, and G.C. Li, *Journal of Membrane Science*, Vol. 325, p. 245, 2008.
40. Y. Konishi, and A. Cakmak, *Polymer*, Vol. 47, p. 5371, 2006.
41. L. Liu, and J.C. Grunlan, *Advanced Functional Materials*, Vol. 17, p. 2343, 2007.
42. C.Y. Tang, L.X. Xiang, J.X. Su, K. Wang, C.Y. Yang, Q. Zhang, and Q. Fu, *Journal of Physical Chemistry B*, Vol. 112, p. 3876, 2008.
43. N. Rattanasom, T. Saowapark, and C. Deeprasertkul, *Polymer Testing*, Vol. 26, p. 369, 2007.
44. M.J. Wang, *Rubber Chemical Technology*, Vol. 71, p. 520, 1997.
45. T.S. Yu, J.P. Lin, J.F. Xu, T. Chen, S.L. Lin, and X.H. Tian, *Composites Science and Technology*, Vol. 67, p. 3219, 2007.
46. J.H. Yang, T. Xu, A. Lu, Q. Zhang, and Q. Fu, *Journal of Applied Polymer Science*, Vol. 109, p. 720, 2008.
47. J.C. Grunlan, A.R. Mehrabi, M.V. Bannon, and J.L. Bahr, *Advanced Materials*, Vol. 16, p. 150, 2004.
48. Y.T. Sung, M.S. Han, K.H. Song, J.W. Jung, H.S. Lee, C.K. Kum, J. Joo, and W.N. Kim, *Polymer*, Vol. 47, p. 4434, 2006.
49. P. Petra, R.B. Arup, J. Andreas, *Polymer*, Vol. 44, p. 8061, 2003.
50. D. Tasis, N. Tagmatarchis, A. Bianco, M. Prato, *Chemical Reviews*, Vol. 106, p. 1105, 2006.
51. N.V. Majeti, and R. Kumar, *Reactive and Functional Polymers*, Vol. 46, p. 1, 2000.
52. S.F. Wang, L. Shen, W.D. Zhang, and Y.J. Tong, *Biomacromolecules*, Vol. 6, p. 3067, 2005.
53. Y.X. Xu, X. Ren, and M.A. Hanna, *Journal of Applied Polymer Science*, Vol. 99, p. 1684, 2006.
54. Z. Wang, X.Y. Meng, J.Z. Li, X.H. Du, S.Y. Li, Z.W. Jiang, and T. Tang, *Journal of Physical Chemistry C*, Vol. 113, p. 8058, 2009.

55. W.D. Zhang, I.Y. Phang, and T.X. Liu, *Advanced Materials*, Vol. 18, p. 73, 2006.
56. T.X. Liu, I.Y. Phang, L. Shen, S.Y. Chow, and W.D. Zhang, *Macromolecules*, Vol. 37, p. 7214, 2004.
57. K.A. Carrado, P. Thiagarajan, and D.L. Elder, *Clays and Clay Minerals*, Vol. 44, p. 506, 1996.
58. R.A. Vaia, B.B. Sauer, O.K. Tse, and E.P. Giannelis, *Journal of Polymer Science, Part B: Polymer Physics*, Vol.35, p. 59, 1997.
59. Y.Q. Zhao, K.T. Lau, Z. Wang, Z.C. Wang, H.Y. Cheung, Z. Yang, and H.L. Li, *Polymer Composites*, Vol.30, p. 702, 2008.
60. M. Ochi, K. Takemiya, O. Kiyohara, and T. Nakanishi, *Polymer*, Vol. 41, p.195, 2000.
61. Z.C. Wang, C.L. Xu, Y.Q. Zhao, D.D. Zhao, Z. Wang, H.L. Li, and K.T. Lau, *Materials Science and Engineering, A: Structural Materials Properties Microstructure and Processing*, Vol. 490, p. 481, 2008.
62. M. Lu, K.T. Lau, W.Y. Tam, and K. Liao, *Carbon*, Vol. 44, p. 383–386, 2006.
63. R. Xu, E. Manias, A.J. Snyder, and J. Runt, *Macromolecules*, Vol. 34, p. 337, 2001.
64. T. Kashiwagi, F. Du, J.F. Douglas, K.I. Winey, R.H. Harris, and J.R. Shields, *Nature Materials*, Vol. 4, p. 928, 2005.
65. B. Schartel, P. Potschke, U. Knolland, and M.A., Goad, *European Polymer Journal*, Vol. 41, p. 1061, 2005.
66. S. Peeterbroeck, M. Alexandre, J.B. Nagy, C. Pirlot, A. Fonseca, N. Moreau, G. Philippin, J. Delhalle, Z. Mekhalif, R. Sporken, G. Beyer, and P. Dubois, *Composites Science and Technology*, Vol. 64, p. 2317, 2004.
67. F.G. Gao, G. Beyer, and Q.C. Yuan, *Polymer Degradation and Stability*, Vol. 89, p. 559, 2005.
68. H.Y. Ma, L.F. Tong, Z.B. Xu, and Z.P. Fang, *Nanotechnology*, Vol. 18, p. 375602, 2007.
69. C.Y. Tang, N.X. Chen, Q. Zhang, K. Wang, Q. Fu, and X.Y. Zhang, *Polymer Degradation and Stability*, Vol. 94, p. 124, 2009.
70. S.G. Chen, H.Y. Yu, W.T. Ren, and Y. Zhang, *Thermochimica Acta*, Vol. 491, p. 103, 2009.
71. S. Pack, T. Kashiwagi, D. Stemp, J. Koo, M. Si, J.C. Sokolov, and M.H. Rafailovich, *Macromolecules*, Vol. 42, p. 6698, 2009.

This Page Intentionally Left Blank

Polyethylene Nanotube Nanocomposites

S. Kanagaraj

*Department of Mechanical Engineering
Indian Institute of Technology Guwahati,
North Guwahati 781 039, Assam, India*

Abstract

Carbon-nanotubes (CNTs) have been used with polymers from the date of their inception to make composites having remarkable properties. In order to prepare CNT-polyethylene nanocomposites, different manufacturing techniques such as *in-situ* polymerization, solution mixing, and melt blending have been followed. Many attempts have been carried out to modify the surface of the CNTs to have homogeneous dispersion of CNTs in polymer matrix, which can produce good bonding between CNT and polyethylene. A significant improvement on mechanical and tribological properties of polyethylene was observed when the concentration of CNT was increased. The composite reinforcement shows a good load transfer effect and interface link between CNT and polyethylene, which were confirmed by Raman spectroscopy. It is also found that the Young's modulus of CNT-PE composites can be predicted using Halpin-Tsai and modified series models which provide good agreement with experimental results.

Keywords: CNTs, HDPE, UHMWPE, characterization, nanocomposites, surface modification.

5.1 Introduction

The discovery of CNTs offers exciting opportunities for a number of applications in most areas of science and engineering due to their remarkable properties. Both theoretical and experimental results suggest enormous properties of CNTs (1–3), which are compiled in

Table 5.1. Properties of carbon nanotubes, Xie et al. (3)

Property	Values
Specific gravity	0.8 g/cc for SWCNT; 1.8 g/cc for MWCNT
Elastic modulus	~1 TPa for SWCNT; ~0.3–1 TPa for MWCNT
Strength	50–500 GPa for SWCNT; 10–60 GPa for MWCNT
Resistivity	5–50 $\mu\Omega$ cm
Thermal conductivity	3000 W/m-K
Thermal stability	>700 °C in air; 2800 °C in vacuum
Specific surface area	10–20 m ² /g

Table 5.1. Carbon nanotubes have a high potential to improve the mechanical, physical and electrical properties of polymers, as stated by Thostenson et al. (4). They exhibit an exceptionally high aspect ratio in combination with low density, as well as high strength and stiffness (Coleman et al. (5)), which make them a potential candidate for the reinforcement of polymeric materials.

High density polyethylene (HDPE) is a polymeric material having the largest tonnage in the world with respect to production. HDPE possesses excellent properties in addition to its low cost, ability to be recycled, good processability, non-toxicity, bio-compatibility, and low production cost. It is one of the simplest and among the well-studied polymers with a known crystal structure and has a wide range of applications including orthopedic implants, automobile parts, consumer goods, durable equipment and industrial machinery. However, due to the inherent chemical nature, both its stiffness and low temperature toughness are not satisfactory and thus HDPE needs to be improved to extend its engineering applications (Incarnato et al. (6)). To utilize and enhance the properties of HDPE, especially to improve its stiffness, wear resistance and rigidity, CNT-HDPE composites are being prepared and the effects of CNT loading on mechanical properties are investigated.

Ultrahigh molecular weight polyethylene (UHMWPE) is an engineering plastic which has a wide spectrum of applications, particularly as a material for orthopedic prostheses due to its high strength, high resistance to chemicals and physical abrasion, high wear

resistance, biocompatibility and low coefficient of friction. Despite the success of total joint arthroplasty, wear is a major obstacle limiting the long-term performance of UHMWPE implants. It has been estimated that billions of particles are produced yearly from the surface of a total hip replacement (Kurtz et al. (7)). Although UHMWPE components are in no imminent danger of wearing during a patient's lifetime, osteolysis and loosening of implants are attributed to the debris generated from the articulating surface. The poor processability of UHMWPE restricts its extensive applications. Moreover, the mechanical and physical properties of UHMWPE still need to be improved; in particular, enhancing friction and wear resistance can satisfy the material requirement in joint replacement surgery (Jacobs et al. (8)). Many attempts have been made to improve the wear resistance and mechanical properties by incorporating CNTs into UHMWPE through composite technology.

5.2 Surface Modification of Carbon Nanotubes

The effective utilization of nanotubes in composites depends on the ability to disperse CNTs homogeneously throughout the matrix without or destroying less their integrity. Prior to the mixing of CNTs in a matrix, it is required to modify the surface of CNTs, since a better interfacial bonding between CNT and polymer and also the enhancement of load transfer are believed to occur. When CNTs are added into a polymer, a high specific surface area of CNTs encourages the formation of agglomerates due to intermolecular interactions, such as van der Waals forces. In order to suppress the agglomeration, a control of surface polarity and resulting interactive forces between CNTs and matrix are required, which can be achieved by controlling the polarity of the surface. A chemical functionalization of the CNT surface enables the formation of polar interaction between matrix and CNT, which influences the interfacial strength in the composite and the dispersibility of the CNTs during manufacturing. Besides the chemical interaction among the nanotubes and the matrix, the geometrical effects, CNT-length and curvature, are important parameters influencing the properties of nanocomposites (Fisher and co-workers (9–10)).

Many physical and chemical methods were used to functionalize CNTs for enhancing interactions between CNTs and polymer (11–12). Three general approaches have been adopted to modify the surface of CNTs to promote the interfacial interactions: chemical,

electrochemical and plasma treatment. Santos et al. (13) placed different organo-functional groups on multi-walled carbon nanotubes (MWCNTs) using an oxidation and silanization process. The chemical surface functionalization of CNTs is reported to be a key issue in developing CNT-polymer composites (Fiedler et al. (14)). The chemical functionalization of nanotubes is achieved by an oxidative treatment of the nanotubes to develop carboxylic acid groups. The generation of the functional groups is combined with opening of the CNT cap and the terminal carbons could be converted into carboxylic acids by oxidation in concentrated sulfuric or nitric or mixed acids (Park et al. (15)), which would enable a direct bonding of the tube ends via the carboxylic groups to the matrix. Boiling of CNTs in nitric acid has two purposes (Xue et al. (16)): one purpose is the purification of the nanotubes and the other one is the grafting of functional polar groups on the CNT surface in order to promote the CNT-matrix interaction. In the process, the CNTs may be cracked and peeled and thus the aspect ratio of the CNTs and their reinforcing effect could be reduced. A reduction of the agglomerate size in the polymer matrix can also be achieved with the functionalization process (Gojny et al. (17)). Bubert et al. (18) modified the surface of CNTs using low-pressure oxygen plasma treatment. Several other methods such as polymer wrapping (Connell et al. (19)), electrochemical (Bahr et al. (20)), and mechanochemical (Konya et al. (21)), plasma treatment (Yu et al. (22)) etc. were applied for functionalization of CNTs. Another common method to assimilate the polarity of CNT and matrix is the use of surfactants. Due to physical adhesion of the surfactant, it does not reduce the structural quality of CNTs, whereas a covalent integration of functional groups is always related to structural changes. Xie et al. (23) confirmed that maleic anhydride grafted styrene-(ethylene-co-butylene)-styrene copolymer is an effective compatibilizer to enhance the dispersion of CNTs in the UHMWPE matrix. An active carboxylic acid group was also introduced onto the surface of CNTs with an aid of a surfactant by Eitan et al. (24). To improve single walled carbon nanotubes (SWCNT) dispersion in HDPE, the tubes could also be dispersed with an aid of sodium dodecyl sulfate surfactant by Zhang et al. (25). Li et al. (26) reported a polymer crystallization method to modify CNTs and nanofibers with semicrystalline polymers in a periodic manner, leading to a novel 'nanohybrid shish-kebab' superstructure. Zou et al. (27) proposed a "roping and wrapping" method to disperse MWCNTs by non-covalently wrapping with linear polymers. Liang et al. (28) used molding processing technique to modify

the surface of MWCNTs, which is a convenient way for the enhancement of interfacial adhesion in MWCNT-polymer composites.

5.3 Dispersion of Nanotubes in Polyethylene Matrix

Dispersing nanotubes individually and uniformly into the polymer matrix without or less destruction of the integrity of the CNTs seems to be a fundamental concern when producing polymer composites with enhanced and reproducible properties. The properties of CNT-polymer composites are directly related to aspect ratio of CNT and interfacial strength between CNT and matrix. CNTs exhibit an enormous surface area being several orders of magnitude larger than the surface of conventional fillers and the surface area acts as an interface for stress transfer. It is also responsible for the strong tendency of the CNTs to form agglomerates, which make dispersion of CNTs in polymer difficult. Agglomerates of CNTs can act as stress concentration points and reduce the mechanical properties of the matrix. Overcoming the 'clumping' of nanotubes is a critical issue in the fabrication of CNT-polymer composites (29,30). There are two fundamental issues associated with transferring the properties of CNTs into a matrix. Firstly, the nanotubes must be uniformly distributed throughout the matrix, and secondly, there must be enhanced interfacial interaction between the polymer and the nanotubes. Any load applied to the polymer matrix should be transferred to the nanotubes which depend on the interfacial stress transfer at the polymer-nanotube interface, which tends to be polymer dependent (Barber et al. (31)). Adhesion of the CNTs to the surrounding matrix has been another key issue (Jin et al. (32)). Efforts to address the adhesion and dispersion issues have led to the use of polymer-wrapped CNTs and functionalized CNTs producing distinct interphase regions between matrix and CNTs (Wagner et al. (33)).

The following factors are to be considered while dispersing CNTs into a matrix: length of the tubes, their entanglement, volume fraction, the high matrix viscosity and the tube/tube attraction. With increasing the CNT length, the resulting interactive forces similar to the influence of the molecular weight (chain length) hinder the separation of the tubes. The degree of CNT entanglement prior to dispersing has been shown to severely limit the homogeneity of dispersion. The shear forces are introduced into the suspension in order

to separate the agglomerates and to disperse the individual CNTs. Nanotubes are known to increase the viscosity of fluids due to their large aspect ratio, high stiffness, and ability to form entangled networks (34). Therefore, achieving high loadings of CNTs in polymer melts is difficult. The factors affecting the quality of the dispersion are the amount of dispersive energy input into system, the degree of entanglement of the bulk CNT, and the interaction of the CNT surface with the matrix. The first factor was investigated by Andrews et al. (35) in melt mixing of CNTs into various thermoplastics. Dispersion quality was assessed via optical microscopy at relatively large areas of the composites, and the observed homogeneity was correlated to the amount of mechanical energy input by the shear melt mixer. CNT shortening is an unavoidable result in all dispersive processes, and the forces help to enhance the dispersability of the CNTs as the ability of CNTs to entangle is dependent on their aspect ratio.

A good dispersion of CNTs in polymer matrices can be achieved by the following techniques:

Sonication: Ultrasonic devices generate a high impact of energy but introduce low portion of shear forces, hence this method is only suitable for very low viscous matrix materials and small volumes. Sonication can be provided in two forms, mild sonication in a bath or high-power sonication using a tip or horn. The high power dispersion methods, such as ultrasound and high speed shearing, are the simplest and most convenient way to improve the dispersion of CNTs in a polymer matrix. Sonication process uses high frequency sound waves to induce cavitation in low viscosity solvents in the presence of CNT agglomerates. Ultrasonic instruments using a frequency of 20 kHz have been shown to disperse CNTs very well (Weisenberger et al. (36)). Higher frequency sonication instruments, such as ultrasonic cleaning baths at 40 kHz, have also shown to be effective (Kearns et al. (37)) and they reported an optimum sonication time of 2 hrs for a nanotube loading of 1 wt%. The energy released upon cavity collapse breaks up CNT agglomerates, thus, dispersing the nanotubes into the solvent. The local introduction of the energy also leads to a rupture and damage of CNTs by reducing the overall aspect ratio (Lu et al. (38)). The efficiency of ultrasonic dispersion depends upon an inverse relationship between frequency and CNT size. Thus, the progressively increasing frequency is required to sequentially reduce bulk agglomerates of CNTs into individual tube.

Stirring: It is a common technique to disperse particles in liquid systems and can be used to disperse nanotubes. Size and shape of the propeller and the mixing speed control the dispersion result. After intensive stirring of CNTs in epoxy resin, a relative fine dispersion could be achieved (Sandler et al. (39)).

Calendering: The application of a mini-calender to disperse of CNTs in a matrix is a promising technique (Gojny et al. (40)). Besides the improved dispersion results, the efficient manufacturing of larger amounts of nano-composites is also possible.

5.4 Method of Preparation of CNT-PE Composites

Most of the methods used for the preparation of nanocomposites have focused on improving nanotube dispersion by some mechanism that minimizes or prevents the high driving force of the CNT to aggregate. Currently, there are four commonly used methods for incorporating CNTs into a polymer matrix (Jin et al. (41)): direct mixing (Sandler et al. (39)), *in-situ* polymerization of CNT-polymer monomer mixture, solution mixing of suspensions of CNTs in dissolved polymer and melt processing of CNTs with polymers. While direct mixing generally applies only to thermosetting polymers, all the other methods can be used for thermoplastic polymers. During the process of *in-situ* polymerization (42,43), CNTs are added to an un-polymerized solution containing the polymer monomer and thus a stable solution with well dispersed nanotubes in polymer is obtained by the mechanical dispersion. The nanotubes are locked into the polymer matrix by curing or polymerization and they become chemically attached to the polymer chains.

In case of solution processing of composites, the nanotubes and polymer are mixed in a suitable solvent before evaporating the solvent to form a composite (32,44–46). Dispersion of nanotubes in a solvent or polymer solution and mixing of nanotubes and polymer in a solution by energetic agitation and the controlled evaporation of solvent generates a composite film. The advantage is that agitation of the nanotubes in a solvent facilitates nanotube de-aggregation and dispersion. For a chemically resistant polymer such as HDPE, only a few toxic solvents (toluene and xylene) can dissolve it at elevated temperatures with low solubility. The dispersion and interaction among solvent, SWCNT and PE relies on the choice of the solvent, which is a key factor to circumvent the strong van der Waals

interactions among them. SWCNT-HDPE composites were also fabricated by rapidly quenching a hot solution containing polyethylene and well dispersed SWCNT in 1,2-orthodichlorobenzene (1,2-DCB) (Jeon et al. (47)). SWCNTs were first added to 1,2-DCB, and sonicated for 3 hrs using a tip sonicator. The temperature of the solution increased gradually during sonication, reaching a value of 130°C after 3 hrs. In a separate vessel, polyethylene was dissolved in 1,2-DCB at 130°C stirring the solution for 20 min. The hot sonicated SWCNT solution was added to the HDPE solution at 130°C and thoroughly mixed with a teflon magnetic stirrer for an additional 20 min. Finally, the hot solution was quickly poured into methanol at 6°C and kept at 4°C for 12 hrs. The supernatant liquid was transparent, and the precipitate lacked black lump aggregates, indicating that the SWCNTs were incorporated in the HDPE matrix. Ruan et al. (48) used magnetic stirring and sonication to disperse the nanotubes which were purified by the procedure developed by Esumi et al. (49) and they were dispersed in xylene by magnetic stirring for 2 hrs followed by a 2 hrs of ultrasonic vibration at room temperature. The CNT-xylene mixture was then poured into the UHMWPE-xylene solution refluxed at 140°C for 3 hrs and the whole mixture was further refluxed for 30 min. in order to disperse the CNTs into the UHMWPE solution. Thus the composite films were prepared by solution casting.

While solution processing is a valuable technique for both nanotube dispersion and composite formation, it is completely unsuitable for many polymers that are insoluble or the possible solvents are toxic or environmentally unfriendly. Melt processing is a common alternative, which is particularly useful for dealing with thermoplastic polymers, which soften when heated. As an effective processing method, the twin-screw extruder can play an important role in preparation of nanocomposites with uniform microstructure (Bledzka et al. (50)). Advantages of this technique are its speed and simplicity, free of any contamination, compatibility with standard industrial techniques (Andrews et al. (35)). In melt processing, CNTs are mechanically dispersed into a polymer melt using a mixer or a compounder, (35,41,45,51–53). The idea is to use fluid shear forces to break nanotube aggregates and prevent their formation. This approach is simple and compatible with existing polymer processing techniques. Thus, the melt blending method becomes a promising technique to produce CNT-polymer composites.

Xue et al. (16) prepared UHMWPE-HDPE and UHMWPE-HDPE-CNT blends by mixing the melt in a kneader and then hot pressing into plates. The addition of HDPE reduced the melt viscosity of

UHMWPE, which can be processed in a conventional twin-screw extruder. Moreover, the lower viscosity eased the dispersion of the CNTs in the matrix. The UHMWPE-HDPE nanocomposites with different loadings of untreated and pretreated CNFs were prepared using a twin-screw extruder which can provide the high shear compounding for polymer melts by Sui et al. (54). The specimens from the extruder were pelletized into granules which were compression molded at 200°C to obtain the test specimens. It was observed from different studies (25,52,55) that the mixing time of 20 min. was found to yield good dispersion of CNTs in HDPE. Zou et al. (27) found that CNT-HDPE composites fabricated at higher screw speed give uniform dispersion of CNT in HDPE. Kanagaraj et al. (56) followed both dispersion and melt mixing techniques to prepare nanocomposites. The chemically treated CNTs were sonicated for 1 hr to have a homogeneous dispersion of CNTs in water, which was then mixed with HDPE pellets. This mixture was heated and magnetically stirred continuously to have a uniform coating of CNTs on the HDPE pellets. HDPE was melted at the plasticized unit of the injection moulding machine which was kept at 200°C to induce sufficient softening of polymer to mix with CNTs. Tong et al. (43) have modified SWCNTs with polyethylene (PE) where the surface of the SWCNTs was initially functionalized with a catalyst ($\text{MgCl}_2/\text{TiCl}_4$), and then ethylene monomer was polymerized thereby giving PE grafted SWCNTs, which were mixed with commercial PE by melt blending. A new method to prepare composites, spraying aqueous solution with SWCNTs on the surface of HDPE, was developed to disperse CNTs in a matrix and then to prepare composites by melt processing technique, Zhang et al. (25). During spraying, the substrate with a thin layer of HDPE was shaken to ensure that the SWCNT solution was uniformly absorbed on the polymer particles. The sample was extruded using a micro compounder with a co-rotating twin-screw using a mixing time of about 20 min at 160°C.

Tang et al. (52) fabricated CNT-HDPE composite film by the following technique: the first step was the preparation of a precursor material in the form of CNT-HDPE composite pellets. The pellets of neat HDPE and CNTs were combined in a beaker and heated in an oven at 200°C for 10 min. Then the mixture was mechanically stirred to mix the CNTs into the melt and to form a viscous suspension. The dough-like suspension was then compressed and cooled to form a solid plate. The plate was then chopped into smaller pieces, which were fed into a twin-screw extruder. In the extruder, the temperature was maintained

at 170°C to re-melt the composite pellets to form a thermoplastic suspension containing CNTs. This suspension was further mixed for 6 min through the shearing action of the rotating screws and then extruded through a slit die. The extrudate strip was placed between heated aluminum plates, and compressed together to form a thin MWCNT-HDPE film. The same procedure was followed by Johnson *et al.* (55) and the method of sample preparation is schematically shown in Figure 5.1.

Zou *et al.* (27) combined solution mixing technique and melt processing technique in order to prepare CNT-PE composites. Firstly, polyethylene glycol (PEG) and 3-(trimethoxysilyl) propyl methacrylate were dissolved in ethanol, CNTs were added to the solution, and sonicated for 1 hr in a low power ultrasonic bath. Then, SiO₂ was added and mixed by mechanically stirring then sonicated for 30 min., and then more SiO₂ was added. Finally, the mixed filler was dried in a vacuum oven at 60°C for 36 hrs to remove ethanol, and broken into small pieces, which were mixed with HDPE and 0.1 wt% of paraffin wax. The above mixture was then extruded with a co-rotating inter-meshing twin-screw compounding extruder at higher screw speed. Finally the composite was dried in an oven at 70°C for 6 hrs.

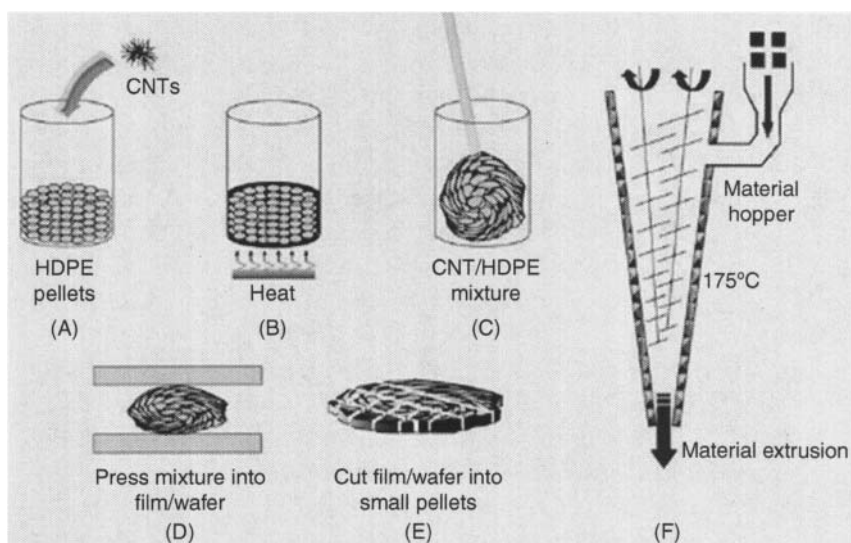


Figure 5.1. Manufacturing of precursor materials, Johnson *et al.* (55).

Process a: The pellets of neat HDPE and CNTs were mixed in a beaker. Process b: Mixed materials was heated. Process c: Mixture was mechanically stirred to form dough like suspension. Process d: Viscous suspension was compressed to form a plate. Process e: Plate was cut into smaller pieces. Process f: Processing of composite film

Xiao et al. (57) prepared CNT-low density PE composites where both were mixed at 140°C for 20 min using a mechanical mixer. The mixed samples were then compressed in a mold under 8 MPa pressure at 140°C for 5 min. The resultant composite was broken into small pieces, mixed, and then molded again for 10 times in order to improve the dispersion of the nanotubes in the matrix. Kuan et al. (58) proposed to synthesize CNT-linear low density PE nanocomposite via water-crosslinking reaction. Vinyltriethoxysilane and benzoyl peroxide were used to modify the surface of CNT by a free radical reaction. Compared to functionalized CNT by acid treatment, covalently functionalized CNT by the addition of free radicals is particularly useful for large-scale synthesis and provides functional groups for further application (Ying et al. (59)). Bakshi et al. (60) used electrostatic technique to prepare CNT-UHMWPE composite film. The UHMWPE powder was mixed with 5 wt% of CNT in a jar mill for 4 hrs in order to distribute the CNTs evenly throughout the powder. The powders were then sprayed onto a teflon coated substrate using an electrostatic powder coating system. Spraying with the electrostatic spray system leads to a uniform deposition of CNT-UHMWPE powder with negligible overspray and loss of CNT. The teflon substrate with the spray deposited layer was heated in an oven at 180°C for 30–40 min for consolidating the composite film.

5.5 Interfacial Bonding and Load Transfer

The effective techniques used to understand the load transfer and failure of nanotubes are Raman spectroscopy, Schadler et al. (61) and a Kelly–Tyson approach to measure the interfacial shear stress (Wagner et al. (33)). These techniques have given some evidences for good load transfer between the polymer and CNTs. The well dispersion of CNTs and the CNT-polymer interfacial adhesion are the two main issues for warranting excellent properties of nanocomposites. Due to high aspect ratio of the nanotubes, large interfacial areas are available for matrix to CNT stress transfer, but an adequate interfacial adhesion is necessary in order to achieve a good load transfer. Interfacial failure may compromise the reinforcement effect and then the full potential of CNTs may not be realized. Therefore, it is of great importance to understand the interfacial characteristics of nanocomposites. Barber et al. (31) performed pull-out experiments of individual carbon nanotubes embedded in a polymer matrix with

a specially developed test setup in order to evaluate the interfacial shear strength of the nanotube polymer system. Raman spectroscopy provides a cost-effective way to analyze functionalization effectiveness in improving load-transfer of nanocomposites. Compared to the Raman spectrum of the purified CNTs, the incorporation of CNTs into PE matrix resulted in a further peak shift, which means the CNTs were subjected to compressive stress (Siesler (62)), which is attributed to the contraction of PE matrix during cooling. Wood et al. (63) suggested that Raman spectroscopy can be used to measure the strain of nanocomposites by measuring the peak signal shift of Raman spectra. When strain is applied to nanocomposites, the interatomic distances change, and thus the vibrational frequencies of some of the normal modes change causing a Raman peak shift which is used to monitor the deformation of CNTs in the polymer matrix. There are two possible explanations: (a) there is a poor bonding between the matrix and the outermost nanotubes layer; or (b) the outermost nanotube is loaded, but because of the relatively weak bonding between the nanotube layers, load is not transferred to the inner layers. Instead the inner tubes may slip with respect to the outer tubes. Since an increase in the modulus is observed for the composite due to good interfacial strength (Wagner et al. (33)), the second hypothesis is expected to occur. In compression, the load transfer occurs to the inner layers of the MWCNT through easy buckling and bent sections of the nanotubes. Slippage of nanotube layers in compression is prevented because of the seamless structure of the tubes and the geometrical constraint of the outer layers imposed on the inner layers.

Wang et al. (64) developed an experimental method to evaluate the interface between functionalized CNT and matrix through Raman spectra under thermal-loading. A considerable improvement of the tensile strength of nanocomposites suggests that functionalization of SWCNTs enhances interfacial bonding and load-transfer. Both the method and degree of functionalization seem to show significant effects on interface improvement. The mismatch in the coefficient of thermal expansion between CNT and polymer leads to a compressive radial residual stress along the tube when the polymer is cooled down from its melt which suggests good intercalation of UHMWPE chains into MWCNT clusters and load transfer between the two (Bakshi et al. (60)). The same reason could also be valid in case of thermal load applied on the nanocomposites where large thermal stresses develop at the interface. The strong interfacial bonding leads to large stresses on the nanotubes, which would

cause noticeable Raman peak shift; otherwise, there is minor shift or no observable shift. The up-shifting of the D and G bands is also a consequence of strong compressive forces associated with PE chains on MWCNTs (McNally et al. (53)). An up-shift of the G band can be explained by the disentanglement of the MWCNTs and subsequent dispersion in the PE matrix as a consequence of polymer penetration into the CNT bundles during melt mixing. The slope of this shift as a function of strain is proportional to the nanotube modulus with a proportionality factor reported to be in the region of $-0.2 \text{ GPa}/\text{cm}^{-1}$ (Cooper et al. (65)). Significant shifts in the line position shows efficient stress transfer. It is well-known that the position of the Raman D* band (located around 2662 cm^{-1}) is sensitive to stress in the nanotubes and a function of strain, (48,65). The positions of Raman modes at 1060 cm^{-1} and 1130 cm^{-1} (C–C stretches) are also sensitive to stress on the polymer backbone. While the position of both modes shifted significantly as a function of strain for the neat polymer, the shift was less pronounced for the composite. Again, this indicates that stress has been transferred from the polymer to the nanotubes for a given strain. Ruan et al. (48) characterized both the embedded MWCNTs and the matrix indicating 4 regions of strain which are shown in Table 5.2. The Raman shift corresponding to UHMWPE, MWCNT and composite at the draw ratio of 1 is shown in Figure 5.2 where peak shift by the addition of CNT in UHMWPE is clearly observed.

There are three main mechanisms of load transfer from a matrix to a filler (Schadler et al. (66)). The first is micromechanical interlocking;

Table 5.2. Raman Shift (2691 cm^{-1}) vs. percent tensile strain in CNT/ UHMWPE composites Ruan et al. (48)

Region	% strain	Shift	Interpretation
1	0–1	Clear shift down	Tensile loading of MWCNTs Elastic response
2	1–10	Much less apparent or intense shift down	Interfacial ‘stick and slip’ yielding matrix
3	10–15	Somewhat more apparent shift down	Tensile loading of MWCNTs” MWCNT knots preventing further PE chain stretching
4	> 15	A shift up	Compressive loading of MWCNTs Elastic recovery from local matrix failure

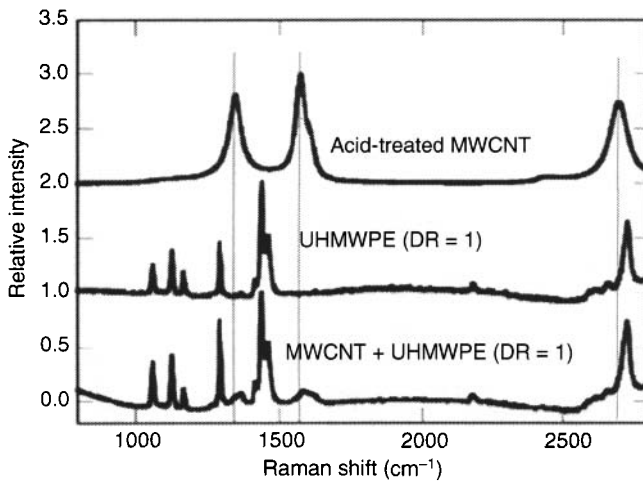


Figure 5.2. Purified MWCNTs and the undrawn pure UHMWPE and the undrawn 1 wt% MWCNT-UHMWPE film, Ruan et al. (48).

this could be difficult in nanotube composites due to their atomically smooth surface. The second is chemical bonding between the nanotubes and the matrix. The third mechanism is a weak van der Waals bonding between the CNT and the matrix. Wagner et al. (33) found that the polymer/CNT interfacial shear stress is of the order of 500 MPa, which is much larger than traditional fiber composites which suggests good bonding between CNTs and matrix.

5.6 Material Characterization

The requirements for mechanical reinforcement in any nanocomposites are the optimum aspect ratio, good dispersion, alignment of CNT and interfacial stress transfer between CNT and polymer. If the aspect ratio is high, Young's modulus will also be high. In case of homogenous dispersion, nanotubes must be uniformly dispersed to the level of isolated nanotubes individually coated with polymer which has an efficient load transfer to the CNT network and results in a more uniform stress distribution and minimizes the stress concentration area. If any agglomeration of CNTs occurs in the polymer, it acts as a stress concentration area and it leads to decrease in strength and modulus of the composites. In case of alignment, the difference between random orientation and perfect alignment is a factor of five in composite modulus, (Thostenson et al. (67)). However, the

composite becomes an anisotropic material which is not beneficial in case of bulk materials. In case of interfacial stress transfer, the external stresses applied to the composite are efficiently transferred to the nanotubes, allowing them to take a disproportionate share of the load resulting in high performance in composites. At some point of stress, either the matrix in the vicinity of the interface or the interface bond between CNT and matrix will rupture. This stress is termed as interfacial stress which governs the maximum stress transfer to the CNT.

Tang et al. (52) studied mechanical properties of composites by a small punch test which was adopted by Kurtz and co-workers (68–69). Since the loading configuration involves lateral bending and large biaxial deformation, the experimental results do not directly yield the usual mechanical properties. Focusing on the small deformation region, experimental results of the elastic modulus were obtained by comparing the initial slope of the force-displacement curve and the results are shown in Table 5.3. Lozano et al. (70) observed the enhancement of 220% in elongation, 60% in modulus and 290% in toughness over HDPE in nanofibre-HDPE composites. It was also observed that randomly oriented NF/NT reinforced polymers have increase of at least 20,000% in toughness and 16,000% in strain to failure. Ruan et al. (48) reported an increase of tensile strength by 25%, strain energy density by 150%, ductility by 140% due to the enhanced chain mobility in UHMWPE induced by 1 wt% of MWCNTs. The enhancement in tensile strength is most likely due to the load bearing effect by the embedded CNTs similar to the taut-tie molecules in polyethylene (Schadler et al. (61)). The nano-scale dispersion of CNTs in the composite film and good interfacial bonding with the neighboring polyethylene enable the CNTs to act as nucleating centers for PE crystal growth. The secondary crystals, Shish-kebab, observed in the composites which nucleated from MWCNTs were attributed a higher mobility under stress

Table 5.3. Mechanical properties of CNT/HDPE composites, Tang et al. (52) & Johnson et al. (55).

MWCNT weight content (%)	Stiffness increase (%)	Peak load increase (%)	Work to failure increase (%)
1	3.62	5.4	1.64
3	5.08	8.61	3.22
5	7.88	12.92	4.95

than PE crystals which lead to a significantly enhanced ductility and strain energy in the nanocomposites. Significant increases in the Young's modulus of nanotubes-polymer composites have been associated with the formation of an ordered polymer layer coating on the nanotubes. Bakshi et al. (60) observed that the stiffness of UHMWPE increases by 82% by incorporating 5wt.% MWCNT. The poor dispersion and rope-like entanglement of CNTs led to drastic weakening of the composites. Thus, alignment of CNTs in the matrix has a predominant role on the mechanical and functional properties of CNT-polymer composites (Jin et al. (32)).

Ruan et al. (71) prepared thick and flexible composite films of UHMWPE reinforced with MWCNTs by a novel route and observed the improvement in mechanical properties which were very close to commercially available fibers like Kevlar. However, Wang et al. (72) reported insignificant increase in the tensile strength and modulus even by adding 3 wt% MWCNT in UHMWPE. Xue et al. (16) reported moderate increase in the yield strength from 25 to 30 MPa and Young's modulus from 1187 to 1495 MPa for 2 wt% MWCNT addition with UHMWPE+20%HDPE. Yang et al. (73) used PE-grafted MWCNTs as reinforcing agent for PE in order to have well dispersion of nanotubes in the PE matrix, which resulted in an improvement of MWCNT-PE interfacial adhesion and thus enhanced mechanical properties of composites. Tang et al. (52) observed enhancement of mechanical properties of HDPE composite films with increasing MWCNT content. With the addition of 5 wt% CNTs, the overall material stiffness increased by 8%, the maximum load to failure by 13% and the work to failure by 5% (Johnson et al. (55)). Zoo et al. (74) hypothesized that the improvement in properties of CNT-UHMWPE was due to increased shear strength of the UHMWPE caused by addition of CNTs. Kanagaraj et al. (75) studied CNT-UHMWPE composites where the raw materials were prepared at different milling time and the processed composites were cooled by different cooling media such as air, water and liquid nitrogen. It was concluded that water cooling technique and 45 min of milling time for CNT and UHMWPE powder produces an optimum characteristic nanocomposites and the comparison of results is given in Table 5.4.

Kanagaraj et al. (56) observed the enhanced mechanical properties with an increase of CNT concentration, which is believed to be due to good interface between polymer and CNT thus transferring load from the polymer to CNT and it is depicted in Table 5.5. It is observed from Figure 5.3 that the experimental relation between stiffness and

Table 5.4. Mechanical properties of UHMWPE-0.2 wt% CNT composites, Kanagaraj et al. (75)

Sample specification	Young's modulus		Tensile strength		Toughness		Breaking elongation	
	GPa	% of increment	MPa	% of increment	J/g	% of increment	%	% of increment
UHMWPE	0.718	0	21.2	0	50.84	0	280.7	0
15 min.	0.736	2.5	23.4	10.4	58.99	16.0	295.6	5.3
30 min.	0.744	3.6	23.9	12.7	65.30	28.4	338.0	20.4
45 min.	0.754	5.0	26.0	22.7	68.53	34.8	354.7	26.3
60 min.	0.746	3.9	24.2	14.3	68.47	34.7	344.4	22.7
75 min.	0.780	8.6	22.9	8.0	58.36	14.8	340.2	21.2
LN2	0.778	8.4	24.1	13.7	61.39	20.7	326.6	16.3
Water	0.754	5.0	26.0	22.7	68.53	34.8	354.7	26.3
Air	0.912	27.0	24.7	16.8	58.92	15.9	288.4	2.7

Nanocomposites
(ball milling time)Cooling
technique

Table 5.5. Increase of Young’s modulus, strain and toughness of CNT/ HDPE composites, Kanagaraj et al. (56)

Volume fraction of CNT (%)	% increment of Young’s modulus	% increment of strain	% increment of toughness
0.11	6.74	9.86	17.15
0.22	12.13	13.34	19.18
0.33	17.56	18.19	22.34
0.44	22.23	23.82	32.77

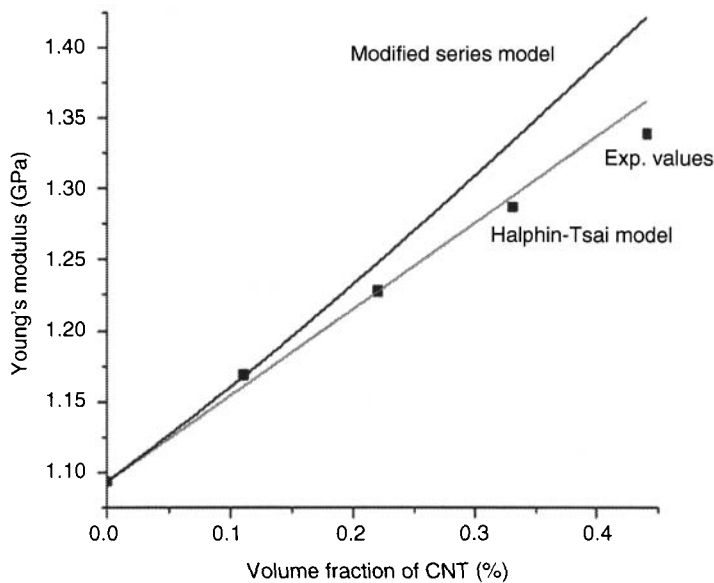


Figure 5.3. Comparison of experimental and theoretical values of Young’s modulus of CNT–HDPE composites, Kanagaraj et al. (56).

volume fraction of CNTs shows good agreement with modified series model and Halpin-Tsai (HT) model where a linear increase of modulus with volume fraction of CNTs is observed which confirms a good measure of reinforcement. The comparison between experimental and HT model results gives a close agreement within 2% which indicates that the assumptions made to derive the equations were closely agreeing with experimental conditions, like tensile loads were successfully transmitted to the nanotubes across the CNT–HDPE interface. In case of modified series equation, the experimental results closely follow the predicted values within the maximum relative error of 4%.

It is observed from Sui et al. (54) that the tensile strength and modulus of UHMWPE/HDPE blend were improved by the addition of the untreated CNFs which possesses intrinsically high tensile strength and modulus, which are shown in Table 5.6. But they were decreased at 3 wt% content. The enhancement in tensile strength containing 0.5 wt% pretreated CNFs was four times higher than that of the nanocomposites containing untreated CNFs of the same loading over that of the pure polymer, but its tensile modulus exhibited a slightly lower value owing to the reduced degree of crystallinity. It is observed from Figure 5.4 that around 1 wt% of MWCNT, the elongation of composites shows the transition from decreasing trend to increasing trend. However, tensile strength and modulus of composites are showing a transition from sharp increasing trend to slowly decreasing trend (Zou et al. (27)). McNally et al. (53) measured the mechanical properties of the nanocomposites as a function of MWCNT loading and the results are shown in Figure 5.5. It was observed that the yield stress increased slightly as the loading of MWCNTs was increased up to 10 wt%. However, both the ultimate tensile strength and the elongation at break decreased.

Xue et al. (16) observed that the wear rate of the UHMWPE/HDPE blend can be significantly reduced by adding CNTs, which can be correlated with an increase of the Young's modulus. The addition of 0.5 wt% CNTs to the UHMWPE/HDPE blend caused about 50% reduction of the wear rate, which is shown in Table 5.7. Besides, the composites reinforced with untreated CNTs had a better wear performance than the composites with pre-treated CNTs and the graphical

Table 5.6. Modulus and strength of UHMWPE/HDPE + CNFs, Sui et al. (54)

Materials	Gain in strength (%)	Gain in modulus (%)
UHMWPE/HDPE	0	0
UHMWPE/HDPE + 0.5 wt% Untreated CNFs	8	10
UHMWPE/HDPE + 1.0 wt% Untreated CNFs	16	20
UHMWPE/HDPE + 3.0 wt% Untreated CNFs	10	17
UHMWPE/HDPE + 0.5 wt% pretreated CNFs	32	7

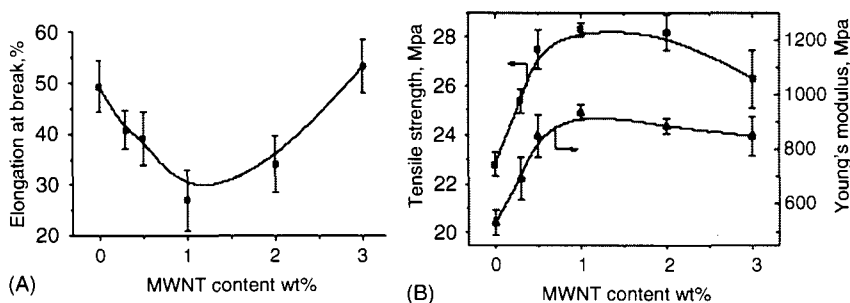


Figure 5.4. (a) Elongation at break, and (b) tensile strength and modulus of HDPE/2%Polyethylene glycol/ 2%SiO₂/ MWCNT composites versus MWCNT content, Zou et al. (27).

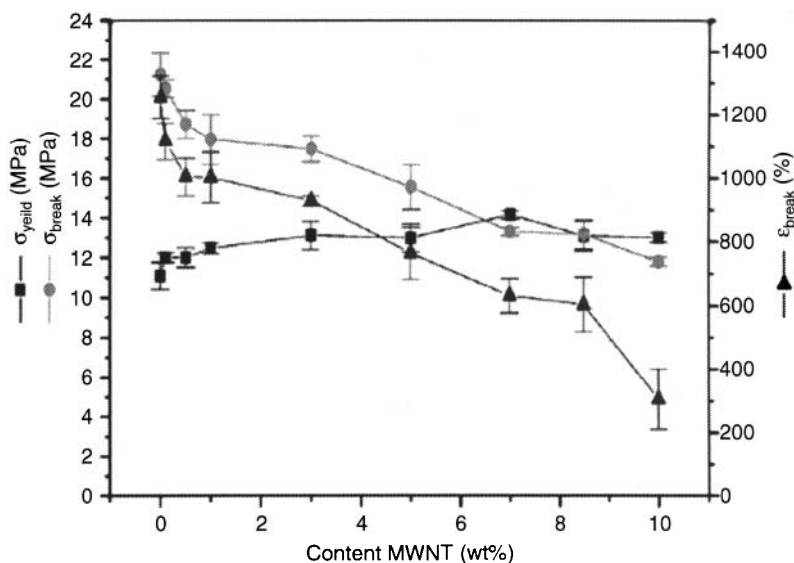


Figure 5.5. Mechanical properties of PE and MWCNT-PE nanocomposites as a function of MWCNT loading, McNally et al. (53).

representation of the results are shown in Figure 5.6. In UHMWPE/HDPE composites, HDPE can improve the creep resistance of UHMWPE due to its higher crystallinity compared to metal and bone (Jacobs et al. (8)), but reduces the wear performance because of its lower wear resistance compared to UHMWPE. Kanagaraj et al. (75) observed that the wear volume of UHMWPE against sliding distance can be decreased by adding CNTs. The decrease of wear volume is due to enhanced interfacial strength between polymer and CNTs and other mechanical properties, resulting in a good load

Table 5.7. Properties of UHMWPE+20%HDPE+MWCNT composites, Xue et al. (16)

Material	Yield stress (MPa)	Tensile strength (MPa)	Strain at break (%)	Young's modulus (MPa)	Specific wear rate 10^{-8} (mm ³ /Nm)
UHMWPE	25.0	24.7	109	1187	40.8
80%UHMWPE +20%HDPE (UH-HD)	28.4	27.8	26	1493	44.3
UH-HD + 0.2% pre treated MWCNT	29.6	29.7	34	1578	33
UH-HD + 0.5% pre treated MWCNT	27.6	26.2	31	1610	20
UH-HD + 1.0% pre treated MWCNT	28.8	25.5	32	1603	21
UH-HD + 2.0% pre treated MWCNT	30.8	28.7	29	1613	19
UH-HD + 0.2% un treated MWCNT	27.3	27.9	31	1508	...
UH-HD + 0.5% un treated MWCNT	26.2	24.7	30	1576	18
UH-HD + 1.0% un treated MWCNT	29.9	29.0	28	1594	16
UH-HD + 2.0% un treated MWCNT	29.9	28.0	30	1495	14

transfer effect to the nanotube network from polymer. When CNTs were introduced into UHMWPE matrix, it helps to enhance surface hardness, ploughing and cutting resistance of UHMWPE and prevent easy removal of the wear particles. The interesting phenomenon is the restriction of plastic displacement of the composite by the counter face which occurred due to plasticity index and plastic contact between the composite and counterface. The wear volume and the wear coefficient of UHMWPE and MWCNT-UHMWPE composites against sliding distance are shown in Figure 5.7. Wear coefficient of CNT-HDPE composites as a function of CNTs concentration was studied by Kanagaraj et al. (76). It is observed that the wear volume decreases with an increase of CNT concentration upto 0.5 wt% of CNTs. It is also observed that 0.5 wt% of CNT with

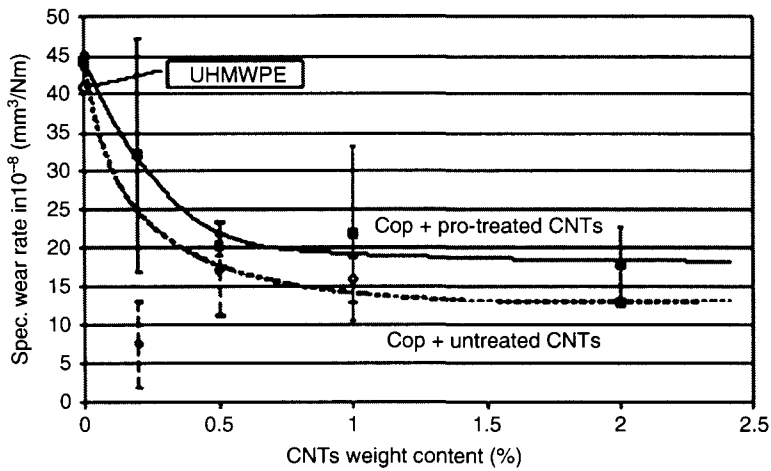


Figure 5.6. Steady state wear rates of materials tested against X5CrNi18-10, [Cop = 80% UHMWPE and 20% HDPE, Cop 2%p = Cop + 2% MWCNT (pre-treated), Cop 2%u = Cop + 2% MWCNT (un-treated), Xue et al., (16)].

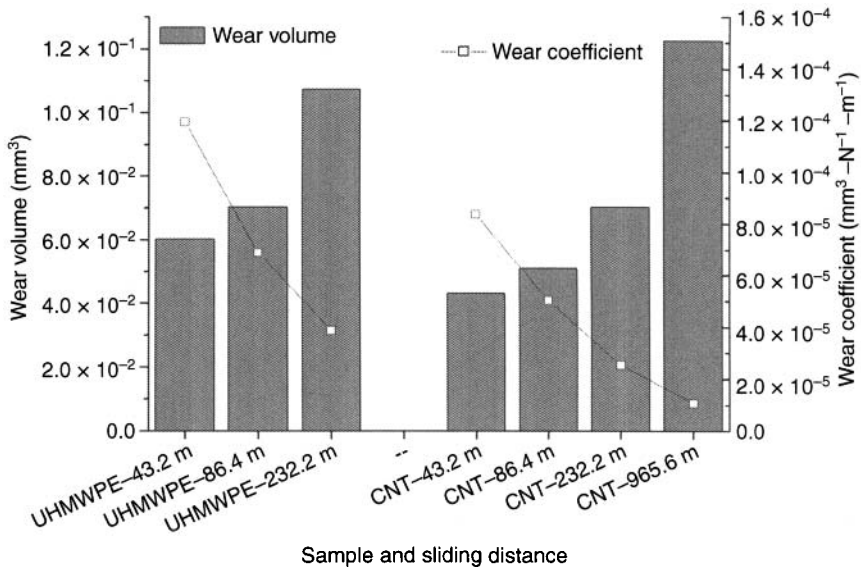


Figure 5.7. Variation of wear volume and wear coefficient of UHMWPE and composites against sliding distance, Kanagaraj et al. (75).

HDPE composite has critical characteristics concerning tribological behaviour. Johnson et al. (55) also confirmed that the addition of nanotubes to HDPE decreases the wear rate of the composites. Table 5.8 shows average wear rates and the decrease in wear rates

Table 5.8. Average wear rate of CNT/HDPE nanocomposites, Johnson et al. (55)

CNT weight fraction (%)	Average wear rate (mm/million cycles)	% decrease of linear wear rate compared to HDPE
0	0.1546	0
1	0.0840	45.7
3	0.0798	48.4
5	0.0637	58.5

for increased CNT content. The wear resistance and frictional properties of HDPE were also improved by the addition of CNTs. The wear tests showed that the addition of 5 wt% CNTs decreased the overall wear rate by up to 50% and friction coefficients decreased by at least 12%. It was also seen that the addition of CNTs to HDPE could bring wear rates down to the level seen in UHMWPE, the material currently in common use for artificial joint implants.

Bakshi et al. (60) observed that the addition of the MWCNT reduces the crystallinity of PE, which is consistent with studies of McNally et al. (53). They reported a decrease in crystallinity in MWCNT-PE composites from 32.5% to 27.6% for 10 wt% MWCNT addition which is due to higher cooling rate experienced by the melt during solidification leading to lower time for arrangement of the chains to form crystallites. This has also been observed by Turrel et al. (77) who subjected UHMWPE melt at 170 °C to different crystallization conditions and found that isothermal crystallinity at 120 °C resulted in a crystallization of 52% while quenching in liquid nitrogen resulted in a crystallinity of 34.6%. Other reason could be that nanotubes act as obstacles and decrease the mobility of the chains leading to lower amount of crystallization. It can be seen that CNTs provide huge surface area and can enhance the nucleation of polymer crystals in thermoplastic materials resulting in increased mechanical properties by changing the polymer morphology.

5.7 Conclusions

From the above study, it may be concluded that CNT-PE composites show a good enhancement of mechanical and tribological properties with an increase of CNT loading. The measure of reinforcement

increases with an increase of CNT content because of good load transfer effect and interface link between CNT and polymer. The overall views and developments concerning techniques for preparing CNT-PE composites, surface treatment of CNTs, dispersion techniques and interface stress transfer of carbon nanotubes in polyethylene composites have been studied and discussed in detail.

Acknowledgement

Author kindly acknowledges the research work carried by scientists whose works are referred.

References

1. C. Goze, P. Bernier, L. Henrard, L. Vaccarini, E. Hernandez, and A. Rubio, *Synthetic Metals*, Vol. 103, p. 2500, 1999.
2. P. Kim, L. Shi, A. Majumdar, and P.L. McEuen, *Physica B: Condensed Matter*, Vol. 323, p. 67, 2002.
3. X-L. Xie, Y-W. Mai, and X-P. Zhou, *Materials Science and Engineering*, Vol. R 49, p. 89, 2005.
4. E.T. Thostenson, Z. Ren, and T.W. Chou, *Composites Science and Technology*, Vol. 61, p. 1899, 2001.
5. J.N. Coleman, U. Khan, W.J. Blau, and Y.K. Gun'ko, *Carbon*, Vol. 44, p. 1624, 2006.
6. L. Incarnato, P. Scarfato, L. Scatteia, and D. Acierno, *Polymer*, Vol. 45, p. 3487, 2004.
7. S.M. Kurtz, O.K. Muratoglu, M. Evans, and A.A. Edidin, *Biomaterials*, Vol. 20, p. 1659, 1999.
8. O. Jacobs, M. Kazanci, D. Cohn, and G. Marom, *Wear*, Vol. 253, p. 618, 2002.
9. F.T. Fisher, R.D. Bradshaw, and L.C. Brinson, *Composites Science and Technology*, Vol. 63, p. 1689, 2003.
10. R.D. Bradshaw, F.T. Fisher, and L.C. Brinson, *Composites Science and Technology*, Vol. 63, p. 1705, 2003.
11. J.L. Stevens, A.A.Y. Huang, H. Peng, I.W. Chiang, V.N. Khabashesku, and J.L. Margrave, *Nano Letters*, Vol. 3, p. 331, 2003.
12. F. Liang, A.K. Sadana, A. Peera, J. Chattopadhyay, Z. Gu, R.H. Hauge, and W.E. Billups, *Nano Letters*, Vol. 4, p. 1257, 2004.
13. C.V. Santos, A.L. M-Hernandez, M. L-Cassou, A. A-Castillo, and V.M. Castano, *Nanotechnology*, Vol. 13, p. 495, 2002.
14. B. Fiedler, F.H. Gojny, M.H.G. Wichmann, M.C.M. Nolte, and K. Schulte, *Composites Science and Technology*, Vol. 66, p. 3115, 2006.
15. S.J. Park, S.T. Lim, M.S. Cho, H.M. Kim, J. Joo, and H.J. Choi, *Current Applied Physics*, Vol. 5, p. 302, 2005.
16. Y. Xue, W. Wu, O. Jacobs, and B. Schadel, *Polymer Testing*, Vol. 25, p. 221, 2006.

17. F.H. Gojny, J. Nastalczyk, Z. Roslanic, and K. Schulte, *Chemical Physics Letters*, Vol. 370, p. 820, 2003.
18. H. Bubert, S. Haiber, W. Brandl, G. Marginean, M. Heintze, and V. Bruser, *Diamond Related Materials*, Vol. 12, p. 811, 2003.
19. M.J. Connell, P. Boul, L.M. Ericson, C. Huffman, Y. Wang, E. Haroz, C. Kuper, J. Tour, K.D. Ausman and R.E. Smalley, *Chemical Physics Letters*, Vol. 342, p. 265, 2001.
20. J.L. Bahr, E.T. Mickelson, M.J. Bronikowski, R.E. Smalley, and J.M. Tour, *Chemical Communications*, Vol. 2, p. 193, 2001.
21. Z. Konya, I. Vesselenyi, K. Niesz, A. Kukovecz, A. Demortier, A. Fonseca, J. Delhalle, Z. Mekhalif, J. B. Nagy, A.A. Koos, Z. Osvath, A. Kocsonya, L.P. Biro, and I. Kiricsi, *Chemical Physics Letters*, Vol. 360, p. 429, 2002.
22. K. Yu, Z. Zhu, M. Xu, Q. Li, and W. Lu, *Chemical Physics Letters*, Vol. 373, p. 109, 2003.
23. X.L. Xie, K. Aloys, X.P. Zhou, and F.D. Zeng, *J. of Thermal Analysis and Calorimetry*, Vol. 74, p. 317, 2003.
24. A. Eitan, K. Jiang, D. Dukes, R. Andrews, and L.S. Schadler, *Chemistry of Materials*, Vol. 15, p. 3198, 2003.
25. Q. Zhang, S. Rastogi, D. Chen, D. Lippits, and P.J. Lemstra, *Carbon*, Vol. 44, p. 778, 2006.
26. L. Li, Y. Yang, G.L. Yang, X.M. Chen, B.S. Hsiao, and B. Chu, *Nano Letters*, Vol. 6, p. 1007, 2006.
27. Y. Zou, Y. Feng, L. Wang, and X. Liu X, *Carbon*, Vol. 42, p. 271, 2004.
28. S. Liang, K. Wang, D. Chen, Q. Zhang, R. Du, and Q. Fu, *Polymer*, Vol. 49, p. 4925, 2008.
29. K.T. Lau, and D. Hui, *Carbon*, Vol. 40, p. 1605, 2002.
30. X. Gong, J. Liu, S. Baskaran, R. Voise, and J. Young, *Chemistry of Materials*, Vol. 12, p. 1049, 2000.
31. A.H. Barber, S.R. Cohen, and H.D. Wagner, *Applied Physics Letters*, Vol. 82, p. 4140, 2003.
32. L. Jin, C. Bower, and O. Zhou, *Applied Physics Letters*, Vol. 73, p. 1197, 1998.
33. H. Wagner, O. Lourie, Y. Feldman, and R. Tenne, *Applied Physics Letters*, Vol. 72, p. 188, 1998.
34. S. Kanagaraj, J. Ponmozhi, F.R. Varanda, J.A.L. Silva, A. Fonseca, M.S.A. Oliveira and J.A.O. Simões, *Proc. of 19th National & 8th ISHMT-ASME HMT Conference*, Hyderabad, India, paper no. NFF-7, p. 1, 2008.
35. R. Andrews, D. Jacques, M. Minot, and T. Rantell, *Micromolecular Material Engg.*, Vol. 287, p. 395, 2002.
36. M.C. Weisenberger, E.A. Grulke, D. Jacques, T. Rantell, and R. Andrews, *Journal of Nanoscience and Nanotechnology*, Vol. 3, p. 535, 2003.
37. J.C. Kearns, and R.L. Shambaugh, *Journal of Applied Polymer Science*, Vol. 86, p. 2079, 2002.
38. K.L. Lu, M. Lago, Y.K. Chen, M.L.H. Green, P.J.F. Harris, and S.C. Tsang, *Carbon*, Vol. 34, p. 814, 1996.
39. J. Sandler, M. Shaffer, T. Prasse, W. Bauhofer, K. Schulte, and A.H. Windle, *Polymer*, Vol. 40, p. 5967, 1999.
40. F.H. Gojny, M.H.G. Wichmann, U. Kopke, B. Fiedler, and K. Schulte, *Composites Science and Technology*, Vol. 64, p. 2363, 2004.

41. Z. Jin, K.P. Pramoda, S.H. Goh, and G. Xu, *Material Research Bulletin*, Vol. 37, p. 271, 2002.
42. C. Park, Z. Ounaies, K.A. Watson, R.E. Crooks, J.J. Smith, S.E. Lowther, J.W. Connell, E.J. Siochi, J.S. Harrison, and T.L.S. Clair, *Chemical Physics Letters*, Vol. 364, p. 303, 2002.
43. X. Tong, C. Liu, H-M. Cheng, H. Zhao, F. Yang, and X. Zhang, *Journal of Applied Science*, Vol. 92, p. 3697, 2004.
44. M.S.P. Schaffer, and A.H. Windle, *Advanced Materials*, Vol. 11, p. 937, 1999.
45. R. Haggennmuller, H.H. Gonmas, A.G. Rinzler, J.E. Fischer, and K.I. Winey, *Chemical Physics Letters*, Vol. 330, p. 219, 2000.
46. B. Safadi, R. Andrews, and E.A. Grulke, *Journal of Applied Polymer Science*, Vol. 84, p. 2660, 2002.
47. K. Jeon, L. Lumata, T. Tokumoto, E. Steven, J. Brooks, and R.G. Alamo, *Polymer*, Vol. 48, p. 4751, 2007.
48. S.L. Ruan, P. Gao, X.G. Yang, and T.X. Yu, *Polymer*, Vol. 44, p. 5643, 2003.
49. K. Esumi, M. Ishigami, A. Nakajima, K. Sawada, and H. Honda, *Carbon*, Vol. 34, p. 279, 1996.
50. A.K. Bledzkie, M. Letmana, A. Viksneb, and L. Rence, *Composites: Part A*, Vol. 36, p. 789, 2005.
51. P. Potschke, A.R. Bhattacharyya, and A. Janke, *Carbon*, Vol. 42, p. 965, 2004.
52. W. Tang, M.H. Santare, and S.G. Advani, *Carbon*, Vol. 41, p. 2779, 2003.
53. T. McNally, P. Potschke, P. Halley, M. Murphy, D. Martin, S.E.J. Bell, G.P. Brennan, D. Bein, P. Lemoine, and J.P. Quinn, *Polymer*, Vol. 46, p. 8222, 2005.
54. G. Sui, W.H. Zhong, X. Ren, X.Q. Wang, and X.P. Yang, *Mat. Chemistry and Physics*, Vol. 115, p. 404, 2009.
55. B.B. Johnson, M.H. Santare, J.E. Novotny, and S.G. Advani, *International Journal of Mechanics of Materials*, Vol. 41, p. 1108, 2009.
56. S. Kanagaraj, F.R. Varanda, T.V. Zhil'tsova, M.S.A. Oliveira, and J.A.O. Simoes, *Composites Science and Technology*, Vol. 67, p. 3071, 2007.
57. K.Q. Xiao, L.C. Zhang, and I. Zarudi, *Composites Science and Technology*, Vol. 67, p. 177, 2007.
58. C-F. Kuan, H-C. Kuan, M. Ma, C-H. Chen, and H-L. Wu, *Materials Letters*, Vol. 61, p. 2744, 2007.
59. Y.M. Ying, R.K. Saini, F. Liang, A.K. Sadana, and W.E. Billups, *Organic Letters*, Vol. 5, p. 1471, 2003.
60. S.R. Bakshi, J.E. Tercero, and A. Agarwal, *Composites: Part A*, Vol. 38, p. 2493, 2007.
61. L.S. Schadler, C. Giannaris, and P.M. Ajayan, *Applied Physics Letters*, Vol. 12, p. 750, 2000.
62. H.W. Siesler, *Infrared and Raman spectroscopy of polymers*, Marcel Dekker, Inc; 1980.
63. J.R. Wood, Q. Zhao, and H.D. Wagner, *Composites Part A*, Vol. 32, p. 391, 2001.
64. S. Wang, R. Liang, B. Wang, and C. Zhang, *Chemical Physics Letters*, Vol. 457, p. 371, 2008.
65. C.A. Cooper, R.J. Young, and M. Halsall, *Composites: Part A*, Vol. 32, p. 401, 2001.

66. L.S. Schadler, S.C. Giannaris, and P.M. Ajayan, *Applied Physics letters*, Vol. 73, p. 3842, 1998.
67. E.T. Thostenson, and T.W. Chou, *Journal of Physics D: Applied Physics*, Vol. 35, p. L77, 2002.
68. S.M. Kurtz, J.R. Foulds, C.W. Jewett, S. Srivastav, and A.A. Edidin, *Biomaterials*, Vol. 18, p. 1659, 1997.
69. A.A. Edidin, and S.M. Kurtz, *Functional Biomaterials*, Vol. 198, p. 1, 2001.
70. K. Lozano, S. Yang, and R.E. Jones, *Carbon*, Vol. 42, p. 2329, 2004
71. S. Ruan, P. Gao, and T.X. Yu, *Polymer*, Vol. 47, p. 1604, 2006.
72. Y. Wang, R. Cheng, L. Liang, and Y. Wang, *Composites Science Technology*, Vol. 65, p. 793, 2005.
73. B.X. Yang, K.P. Pramoda, G.Q. Xu, and S.H. Goh, *Advanced Functional Materials*, Vol. 17, p. 2062, 2007.
74. Y.S. Zoo, J.W. An, D.P. Lim, and D.S. Lim, *Tribology Letters*, Vol. 16, p. 305, 2004
75. S. Kanagaraj, M.T. Mathew, A. Fonseca, L.A. Rocha, M.S.A. Oliveira and J.A.O. Simões, *International Journal of Surface Science and Engineering* 2010 (in press).
76. S. Kanagaraj, M.T. Mathew, A. Fonseca, L.A. Rocha, M.S.A. Oliveira, and J.A.O. Simões. *Proc. of International Conference on Industrial Conference, New Delhi, India*, Article No.11, p. 1, 2008
77. B. Turrel and B. Anuj, *Biomaterials*, Vol. 25, p. 3389, 2004.

This Page Intentionally Left Blank

Properties of Polyurethane/Carbon Nanotube Nanocomposites

Tianxi Liu and Shuzhong Guo

*Key Laboratory of Molecular Engineering of Polymers of Ministry of Education,
Department of Macromolecular Science,
Fudan University, Shanghai 200433, P. R. China*

Abstract

We review the research on preparation, morphology, especially physical properties and applications of polyurethane (PU)/carbon nanotube (CNT) nanocomposites. First, we provide a brief introduction about the preparation of PU/CNT nanocomposites. Then, the functionalization and the dispersion morphology of CNTs as well as the structures of the nanocomposites are also introduced. After that, we discuss in detail the effects of carbon nanotubes on the physical properties (including mechanical, thermal, electrical, rheological and other properties) of PU/CNT nanocomposites. The potential applications of these nanocomposites are also addressed. Finally, the challenges and the research that needs to be done in the future for achieving high-performance polyurethane/carbon nanotube nanocomposites are prospected.

Keywords: polyurethane, carbon nanotubes, nanocomposites, properties.

6.1 Introduction

Polyurethane, IUPAC abbreviation PUR, but commonly abbreviated PU, is any polymer consisting of a chain of organic units joined by urethane (carbamate) links. Polyurethane polymers are formed through step-growth polymerization by reacting a monomer containing at least two isocyanate functional groups with another monomer containing at least two hydroxyl (alcohol) groups in the presence of a catalyst.

Polyurethanes were initially synthesized by Bayer (1), and have been known to users for nearly 60 years now, predominantly as

elastomers and foams. The first polyurethane, Perlon U, was obtained in 1937, by the reaction of 1,6-diisocyanatohexane and 1,4-butanediol (1). Polyurethane products were introduced into the market in late 1940s and they quickly established a strong position there, mostly as elastomers and foamed materials. The essential distinguishing criterion for polyurethanes against other plastics is density of the former. Polyurethane plastics belong now to the group of important materials applicable in numerous fields of engineering (2). If the volumes of polyurethane products and raw materials needed for the production are considered, PU shall be put among the prime polymeric materials, and namely PU polymers are ranked 5th, after the unquestionably dominant polyolefins (such as polyethylene, polypropylene), poly(vinyl chloride), polystyrene and diene rubber.

Polyurethane is a unique material that offers the elasticity of rubber combined with the toughness and durability of metal. PU is composed of polyether or polyester soft segments and diisocyanate-based hard segments. The linear structure of segmented PU takes the form of $(A-B)_n$. The soft segment part B represents the polyester or polyether macrogel with molecular weight ranging from 1000 to 3000, and the hard segment part A is consisted of a low-molecular weight diol or diamine reacting with diisocyanate. Figure 6.1 is a typical representation of segmented PU (3). Because of the incompatibility

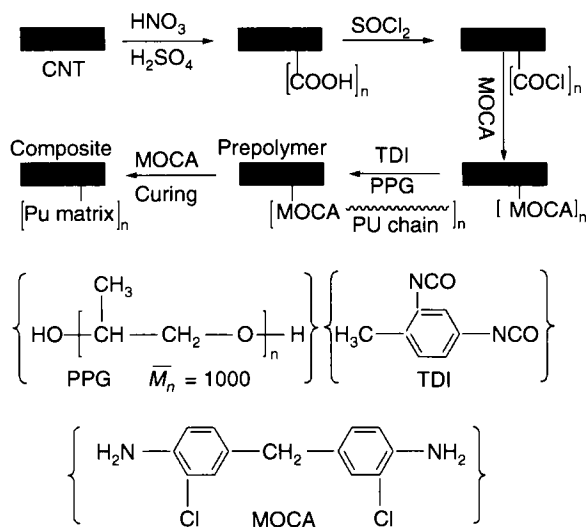


Figure 6.1. Chemical route for the modification of CNTs and the fabrication of PU/CNT composites. Reprinted from Xiong et al. (19) with permission from the Elsevier.

between the hard segments and the soft segments, thermoplastic PU (TPU) undergoes microphase separation resulting in a hard-segment domain, soft-segment matrix, and urethane-bonded interphase. The hard-segment domains act as physical crosslinks in the soft-segment matrix. The primary driving force for phase separation is the strong intermolecular interaction of the urethane units, which are capable of forming intermolecular hydrogen bonds. Owing to such interactions, interconnected or isolated hard segments remain distributed in the soft segment matrix, though the soft domain may contain some hard segments dissolved in it, which is evident from the hydrogen bonding of the urethane-NH groups with the oxygen of the ether or ester linkages (3,4).

Polyurethane formulations cover an extremely wide range of stiffness, hardness, and densities. The performance properties of polyurethane can be widely modified by selecting appropriate raw materials, catalysts and auxiliary compounds, by employing various production methods and /or by employing various methods for further processing and /or for shaping the final products. Therefore, polyurethanes have wide applications such as elastomer, coating, adhesive, foam, and leather.

Since their discovery in 1991 (5), carbon nanotubes (CNTs) have generated huge activity in most areas of science and engineering due to the unique mechanical, electrical, magnetic, optical and thermal properties (6–9). CNTs consist of graphitic sheets that have been rolled into cylindrical shape and the ends of the cylinders may or may not be capped by hemifullerenes. The properties of nanotubes depend on atomic arrangement, the diameter and length of the tubes, and the morphology or nanostructure. Depending on the arrangement of the hexagon rings along the tubular surface, CNTs can be metallic or semiconducting. There are two types of CNTs: multi-walled carbon nanotubes (MWNTs) and single-walled carbon nanotubes (SWNTs). The former consists of two or more concentric cylindrical shells of graphene sheets coaxially arranged around a central hollow core with interlayer separations as in graphite. In contrast, SWNTs comprise a single graphene cylinder. Both SWNTs and MWNTs have high aspect ratios of 1000 or more, because carbon nanotubes can have diameters ranging from 1 to 100 nm and length of up to millimeters (10–12). There are varying reports in the literature on the exact properties of carbon nanotubes, theoretical and experimental results on individual SWNTs show extremely high tensile modulus (640 GPa to 1 TPa) and tensile strength (150–180 GPa). In addition

to the exceptional mechanical properties, they also possess superior thermal and electric properties: thermally stable up to 2800°C in vacuum, thermal conductivity about twice as high as diamond, electric-current-carrying capacity 1000 times higher than copper wires (9). Theory predicts that SWNTs exhibit large phonon mean free path lengths that result in high thermal conductivity (theoretically $>6000 \text{ W}/(\text{m}\cdot\text{K})$) (9,13,14). Because of these extraordinary properties of isolated carbon nanotubes, great enthusiasm exists among researchers around the world as they explore the immense potential of these nanofillers. It is not surprising that the CNT-based polyurethane nanocomposites have been intensively studied.

6.2 Preparation of CNT-Based Polyurethane Nanocomposites

Fabrication methods have overwhelmingly focused on improving nanotube dispersion because better nanotube dispersion in polyurethane matrix has been found to improve the properties of the nanocomposites. The dispersion extent of CNTs in the polyurethane matrix plays an important role in the properties of the polymer nanocomposites. Similar to the case of nanotube/solvent suspensions, pristine nanotubes have not yet been shown to be soluble in polymers, illustrating the extreme difficulty of overcoming the inherent thermodynamic drive of nanotubes to bundle. Therefore, CNTs need to be surface modified before the composite fabrication process to improve the load transfer from the polyurethane matrix to the nanotubes. Usually, the polyurethane/CNT nanocomposites can be fabricated by using four techniques: melt-mixing (15), solution casting (16–18), *in-situ* polymerization (19–21), and sol gel process (22).

6.2.1 Melt-Mixing

Melt processing is a common alternative that is particularly useful for dealing with thermoplastic polymers and holds great interest because of the ease with which the process could be scaled up to industrial standards. Thermoplastic polyurethane nanocomposites can be fabricated by melt compounding of CNTs with polymer resin. Melt processing makes use of the fact that thermoplastic polymers soften when heated. Amorphous polymers like elastomer

can be processed above their glass transition temperature (T_g) while semi-crystalline polymers need to be heated above their melt temperature to form viscous liquid. Carbon nanotubes can be mixed into the polymer melt by shear mixing. It is important that processing conditions are optimized, not just for different nanotube types, but for the whole range of polymer-nanotube combinations. Melt blending is sometimes less effective at dispersing nanotubes in polymers because nanotubes can affect melt properties such as viscosity, resulting in unexpected polymer degradation under conditions of high shear rates.

A representative example of composite fabricated via a twin-screw extrusion method with significant improvement in Young's modulus and tensile strength is reported in (15). The Young's modulus of the unfilled PU fiber is 4.96 MPa, while the composite fiber with the highest loading of nanotubes (17.7 wt%) shows a modulus of 135.1 MPa. This corresponds to a great increase of 27 folds. Results indicated a homogeneous dispersion of MWNTs throughout PU matrix and strong interfacial adhesion between them. The shear force of the melt mixing was favorable for this homogeneous dispersion of MWNTs.

6.2.2 Solution Casting

Perhaps the most common method for preparing polymer-nanotube composites has been to mix the nanotubes and polymer in a suitable solvent before evaporating the solvent to form a composite film. One of the benefits of the solution casting method is that agitation of the nanotube powder in a solvent facilitates nanotube de-aggregation and dispersion. Almost all solution processing methods are variations on a general theme which can be summarized in three major steps:

- (1) Dispersion of nanotubes in either a solvent or polymer solution by energetic agitation;
- (2) Mixing of nanotubes and polymer in solution by energetic agitation;
- (3) Controlled evaporation of solvent leaving a composite film.

In general, de-aggregation and dispersion of carbon nanotubes are provided by magnetic stirring, shear mixing, reflux, or, most commonly, ultrasonication. Sonication can be provided in

two forms: mild sonication in a bath or high-power sonication using a tip or horn. Note that high-power ultrasonication for a long period of time shortens the nanotube length, i.e., reduces the aspect ratio, which is detrimental to the composite properties (23).

An early example of solution based composite formation is described by Chen et al. (16). In this work, SWNTs produced by chemical vapor deposition were dispersed in TPU/THF solution. The solution was then sonicated for 5 min using a high-power sonic tip (200 W) followed by a mild sonication for 2 h in a sonic bath. After careful mixing of TPU solution with carbon nanotubes followed by subsequently casting and controlled solvent evaporation, free-standing TPU/SWNT composite films were obtained by peeling off from the Teflon disk. Solvent-polymer interactions that induce the orientation of soft chain segments during the swelling and moisture curing stage are believed to serve as a driving force for the macroscopic alignment of the carbon nanotubes. Scanning electron microscopy (SEM) clearly exhibits the orientation distribution of the SWNTs in the composite films. At a 0.5-wt% nanotube loading, a 1.9-fold increase in Young's modulus was achieved for PU/SWNT nanocomposites due to the alignment of the nanotubes (16).

It should be pointed out that this method relies on the efficient dispersion of nanotubes in the relevant solvent. The choice of solvent is generally made based on the solubility of the polymer. However, pristine nanotubes usually cannot be well dispersed in most solvents. To get around this problem, Xia et al. (17) compared the dispersion of MWNT-graft-PU, MWNT-OH and raw MWNTs in 0.2% aqueous solution of sodium lauryl sulfate. The results showed that MWNT-graft-PU has a better dispersion stability compared to MWNTs and MWNT-OH. The incorporation of polyurethane-grafted carbon nanotubes had a better reinforcing effect compared to the raw carbon nanotubes. This should be attributed to the improved interfacial interaction between polyurethane matrix and carbon nanotubes.

6.2.3 *In-Situ* Polymerization

Over the past decade, *in-situ* polymerization, where inorganic nanoparticles are dispersed in an appropriate monomer, followed by heat or other treatment of the reaction mixture to induce polymerization, has been used to prepare nanocomposites. *In-situ* polymerization can be performed not only during the radical polymerization, but also during condensation polymerization. The main advantage of

this method is that it enables uniform CNT dispersion in monomers, and polymer chains may also be grafted onto the convex walls of carbon nanotubes during the *in-situ* polymerization process, thus CNTs can be homogeneously dispersed in polymer matrix. What's more, *in-situ* polymerization is particularly important for the preparation of insoluble and thermally unstable polymer composites, which can not be processed by solution or melt processing. For the preparation of polymer composites with high nanotube loading, *in-situ* polymerization is also a very convenient processing technique and provides very good miscibility with almost any types of polymers. Note that as polymerization progresses and the viscosity of the reaction medium increases, the extent of *in-situ* polymerization reactions might be limited. Noteworthy extensions of *in-situ* polymerization include infiltration methods in which the reactive agents are introduced into a nanotube structure and subsequently polymerized (24–26).

Methylene-bis-ortho-chloroaniline (MOCA), an excellent cross-linker widely used to prepare cured PU elastomers with high performance, was used to modify multi-walled carbon nanotubes (19). PU/CNT nanocomposites were prepared by incorporating the MOCA-grafted CNTs into PU matrix. Figure 6.1 is a typical example of *in-situ* polymerization. Nanocomposites synthesized by this way have covalent bonds between CNTs and polymer matrix. Chemically functionalized CNTs could react with raw material to form covalent bonds, which was proved to be effective in improving both the dispersion and nanotube-matrix compatibility which provide excellent properties of CNT-based polymer nanocomposites. In comparison with neat PU, the glass transition temperature of the PU composite containing 5.0 wt% CNTs was increased by more than 20°C.

6.2.4 Sol-Gel Approach

The sol-gel process is a wet-chemical technique (chemical solution deposition) widely used recently in the fields of materials science and ceramic engineering. Such methods are used primarily for the fabrication of materials (typically a metal oxide) starting from a chemical solution which acts as the precursor for an integrated network (or gel) of either discrete particles or network polymers. Typical precursors are metal alkoxides and metal chlorides, which undergo various forms of hydrolysis and polycondensation reactions.

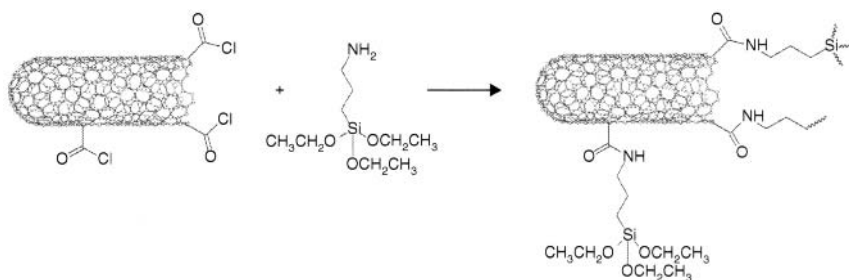


Figure 6.2. Amination of MWNTs with APES. Reprinted from Xu et al. (22) with permission from the American Chemical Society.

The formation of a metal oxide involves connecting the metal centers with oxo (M-O-M) or hydroxo (M-OH-M) bridges, therefore generating metal-oxo or metal-hydroxo polymers in solution. Sol-gel process was proved to be an effective way to synthesize nanocomposites with applications in biosensors and biomaterials. Xu et al. modified the MWNTs with coupling agent amino-propyl-tri-ethoxy-silane (APES), as shown in Figure 6.2 (22). MWNTs were then introduced into the polyurethane-urea system by chemical linkages, and thus a series of novel self-crosslinkable PU/MWNT composites were then prepared using typical sol-gel process. The obtained PU/MWNT composites with various MWNT contents, which are homogeneous and transparent materials, showed good optical limiting properties. The normalized extinction increased and the optical limiting threshold decreased with the increase of the contents of MWNTs. Thus, it was possible to change the required transmittance and transmitted energies by changing the MWNT contents in composites.

Several main synthesis methods widely applied to produce carbon nanotube-polyurethane nanocomposites were summarized above. In addition, latex technology (27), thermally induced phase separation (28), electrospinning (29,30) and many other methods also show their own advantages and promises, however, these methods will not be discussed here.

6.3 Functionalization, Dispersion Morphology and Micro-/Nano-structures

It is difficult to fully utilize the mechanical or electrical properties of CNTs in their polyurethane nanocomposites due to the difficulty

in achieving efficient dispersion of nanotubes. This difficulty is primarily due to the non-reactive surface of CNTs. Intrinsic van der Waals interaction among tubes, in combination with their high surface area agglomeration, made it difficult to transfer the superior properties of the CNTs to the polymer matrix. A number of studies have focused on dispersion of CNTs in polymer matrices, and it was found that there are three main methods to achieve good CNT/polymer compatibility: mechanical methods (31–33), covalent functionalizing of CNTs (34,35), and noncovalent adsorption or wrapping of various functional molecules, such as using surfactants, onto the nanotubes (36–39). It is known that mechanical dispersion methods, such as ultrasonication and high shear mixing, separate nanotubes from each other, but can also fragment the nanotubes, thus decreasing their aspect ratio (40). Exfoliation of CNT bundles into individual tubes can also be successfully achieved using surfactants. However, the individual tubes obtained by the mechanical methods are usually shortened to lengths of about 80–200 nm and the dispersion strategies using surfactants require the presence of surfactant to obtain aqueous solutions of individual CNTs (36,41–43), while the majority of the polymerization processes employ organic solvents. Though aggressive chemical functionalization such as the use of neat acids at high temperatures, might introduce structural defects thus resulting in inferior properties for the nanotubes, it can significantly improve their chemical compatibility and reduce their tendency to agglomerate (44). Therefore, chemical functionalization is the most convenient and effective method for dispersion of individual CNTs in organic solvents.

Different methods have been used in fabricating homogeneous CNT dispersed polyurethane nanocomposites. The mostly used and effective method is using functionalized CNTs. Sahoo et al. prepared MWNT/polyurethane nanocomposites by adding acid-treated CNTs to PU solution (45). A homogeneous dispersion of MWNTs was successfully achieved in PU matrix as evidenced by SEM. It may be attributed to the hydrogen bonds existing between C=O groups of hard segments of PU chains and COOH groups on the acid-treated MWNT-COOH. The polyurethane-grafted SWNTs were obtained by Xia et al. through the following two steps (46): SWNT-OH and polyTDI (i.e., tolylene 2,4-diisocyanate terminated poly(propylene glycol)) were mixed and kept for 24 h in DMF. Then, the SWNT-g-polyTDI were mixed with poly(ϵ -caprolactone) (PCL) diol to form SWNT-g-PU. SWNT-g-PU/PU composites

were thus prepared via *in-situ* polymerization. It was also found that both acid-treated MWNTs and polyurethane-modified MWNTs were effectively dispersed in the polyurethane matrix. The remarkable reinforcing effects were found for SWNT-g-PU/PU system: At 0.7 wt% SWNT-g-PU concentration, the Young's modulus was improved by ~278% compared to the blank PU, and by ~188% compared to 0.7 wt% ungrafted pristine SWNT/PU. SWNT-g-PU may be related to better dispersion of SWNT-g-PU and stronger interfacial interactions between the PU matrix and SWNTs. This study could open up a new route for the preparation of high performance polyurethane/SWNT composites.

The core-shell structure of PU-functionalized MWNTs was found via transmission electron microscopy (TEM) by Chen et al. (47). Ultra-high resolution TEM indicated that a layer of an amorphous structure with a thickness in the range of 2 to 5 nm was formed on the surface of the MWNT-PU. Functionalized MWNT samples could be dispersed very well in highly polar solvents and formed a homogenous solution, which was stable even after 10 days. Neither sedimentation nor aggregation of the MWNT bundles was observed.

Besides modified by acid, amine and functional groups which can react with raw materials of polyurethane (48,49), the CNTs can also be functionalized to obtain new properties. MWNTs were modified with self-crosslinkable coupling agent like APES to change the required transmittance and transmitted energies by changing the MWNT contents in composites (22). Yang et al. prepared photoresponsive azobenzene polyurethane-functionalized multiwalled carbon nanotubes (AzoPU-MWNTs) by *in-situ* polycondensation of azobenzene monomer containing bis-hydroxyl (AzoM) with two types of diisocyanates (50), an aliphatic diisocyanate (hexamethylene diisocyanate, HDI) as soft monomer and an aromatic diisocyanate (TDI) as rigid monomer, in the presence of MWNTs with terminated multi-hydroxyl groups (MWNT-OH). To improve the surface hydrophobicity of poly(etherurethane) (PEU), MWNTs were surface grafted by 3,3,4,4,5,5,6,6,7,7,8,8,8-tridecafluoro-1-octanol (TDFOL) and used as reinforcing agent for PU (51).

Besides covalent functionalization of carbon nanotubes, non-covalent interaction between CNTs and polyurethane can also help fabricate uniform CNT dispersion nanocomposites. A dominant improvement in the dispersion of MWNTs in hyperbranched polyurethane (HBPU) matrix was found, and good solubility of

HBPU-MWNT nanocomposites in organic solvents was shown by Rana et al. (52). Surfactants or other reagents were used during the fabrication of polyurethane nanocomposites to help disperse CNTs and thus obtain better performance materials. Sodium dodecyl sulfate (SDS) was used by Cai et al. to improve the dispersion of MWNTs in water (27), and then the PCL-based PU/MWNT composites were prepared. During the preparation of waterborne polyurethane (WPU), ionic bonding can be formed between the amine functionalized CNTs and the chain extender with COOH groups like dimethylol-propionic acid (DMPA) (53). Thus, the nanocomposites prepared through this approach have a homogeneous dispersion of CNTs. However, all the three methods described above can only help improve the dispersion of CNTs, and can not obtain fully dispersed CNT nanocomposites. As so many researchers are studying in this field, better CNT dispersion methods were anticipated in the future.

There are many different methods which can be used to characterize the dispersion of CNTs in PU nanocomposites. High-resolution electron microscopy and energy-filtered TEM imaging methods were used to examine nanotube reinforced polyurethane composites (19,27,52–55). The use of atomic force microscopy is also a promising technique for characterizing the dispersion of nanotubes in a high performance polyurethane matrix (56–59). In addition, polarized Raman spectroscopy, near-edge X-ray absorption, X-ray diffraction and scattering, have also been used for the characterization of CNT dispersion and alignment (60,61).

The dispersion of carbon nanotubes in PU matrix can also be affected by the synthetic methods as well as the tensile stress etc. Xiong et al. found that the CNTs in the composites after tensile testing could easily take an ordered orientation along with the tensile direction on the cross-section perpendicular to the pressure direction, whereas the arrangement of the CNTs has not almost changed on the cross-section parallel to the pressure direction (62). The phenomenon that the SWNTs near the film substrate interface are driven to self-organize to a more ordered structure was discovered by Chen et al. (16).

6.4 Physical Properties

6.4.1 Mechanical Properties

From virtually the moment carbon nanotubes were discovered, it was expected that they would display outstanding mechanical properties by analogy with graphite. Since C-C covalent bonds are among the strongest bonds in nature, a structure based on a perfect arrangement of these bonds oriented along the axis of the nanotubes produces a very strong material with an extremely high strength-to-weight ratio (63,64). The extreme small size of nanotube makes it rather suitable to be embedded into light-weight and soft materials such as polymers as reinforcements to form strong and light nanocomposites. Thus carbon nanotube (especially SWNTs) has been well recognized as the "ultimate" carbon fiber as a reinforcing phase for polymer matrices.

The mechanical properties of various types of carbon nanotubes have been extensively studied by both theoretical and experimental studies. In 1993, Overney et al. firstly calculated the rigidity of short SWNTs and the calculated Young's modulus was estimated to be about 1500 GPa, similar to that of graphite (65). Then a range of studies predicted that the Young's modulus of carbon nanotubes was approximately 1 TPa (66). The tensile strength of SWNTs was also estimated from molecular dynamics simulation to be 150 MPa (67).

In general, the tensile modulus and strength of polyurethane/nanotube composites are found to increase with nanotube loading, dispersion, and alignment in the matrix (68). However, the results at low nanotube concentrations typically remain far behind the idealized theoretical predictions. At higher nanotube loadings, the extent of improvement in mechanical properties might be limited by the agglomerations of CNTs, the high viscosity of the composites and the resulting void defects (69,70).

The gap between the predictions and experimental results arises from imperfect dispersion of carbon nanotubes and poor load transfer from the matrix to the nanotubes. Even modest nanotube agglomeration impacts the diameter and length distributions of the nanofillers and overall is likely to decrease the aspect ratio. In addition, nanotube agglomeration reduces the modulus of the nanofillers relative to that of isolated nanotubes because there are only weak dispersive forces between the nanotubes. Schadler et al. (71) and Ajayan et al. (72) concluded from Raman spectra that slippage occurs between the shells of MWNTs and within SWNT ropes and may limit stress transfer in nanotube/polymer composites. Thus, good dispersion of CNTs and strong interfacial interactions between CNTs and PU chains contribute to the dramatic improvement of the mechanical properties of the

composites. Functional moieties on nanotubes typically provide better interfacial load transfer via bonding and/or entanglements with the polymer matrix. Molecular simulation by Frankland et al. (73) predicted that chemical bonding between SWNTs and the polymer matrix with only ~0.3% grafting density can increase the shear strength of a polymer-nanotube interface by over an order of magnitude.

Kwon et al. compared WPU/MWNT with WPU/nitric acid treated multiwalled carbon nanotube (A-CNT) composites (20). The tensile strength and modulus of the WPU/A-CNT composites were higher than those of the WPU/MWNT composites with the same CNT content. The better mechanical properties of WPU/A-CNT composites can perhaps be attributed to higher content of polar groups of A-CNTs thus inducing higher interfacial interactions between A-CNTs and WPU chains.

Stronger interfacial interactions between PU and carbon nanotubes and better reinforcing effects of carbon nanotubes may be achieved by incorporation of polyurethane modified carbon nanotubes. Polycaprolactone (PCL)-PU grafted single-walled carbon nanotubes (SWNT-g-PU) were synthesized from hydroxyl functionalized single-walled carbon nanotubes (SWNT-OH) through a two-step reaction by Xia et al. (46) Based on SWNT-g-PU, PCL-PU/SWNT nanocomposites were prepared by further *in-situ* polymerization. SWNT-g-PU had a more remarkable effect on Young's modulus of the nanocomposites compared with pristine SWNTs. At 0.7 wt% SWNT-g-PU concentration, the Young's modulus was improved by ~278% compared to the blank PU, and by ~188% compared to 0.7 wt% ungrafted pristine SWNT/PU. Usually, the aggregation of MWNTs in polyurethane at a higher content often has a downside effect on the mechanical properties. A three-step surface treatment of MWNTs was used to obtain MWNT grafted with isophorone diisocyanate (IPDI) (MWNT-IPDI) (74), then the prepared MWNT-IPDI was incorporated into PU membranes. It was observed that the sample with 0.3 wt% MWNT-IPDI showed the highest tensile strength (42 MPa) and the largest elongation (1280 %).

Generally, polymer nanocomposites improve their mechanical properties such as tensile strength, initial modulus with sacrificing the toughness and flexibility. This is a common phenomenon even in commercial composites but might be particularly problematic while trying to modify elastomers. A promising result from Xu et al. reported the fabrication of polyurethane-urea system by chemical linkages with APES functionalized MWNTs (22), where they found

that the tensile modulus and strength are significantly increased in these composites without loss of elongation.

6.4.2 Thermal Conductivity

Nanocomposites with good thermal conductivity (κ) have potential applications in printed circuit boards. The thermal conductivity of connectors is in the order of 10^3 W/(m·K), while typical thermoplastics have $\kappa \sim 0.1$ W/(m·K). A theoretical model was proposed by Nan et al. to predict the thermal conductivity of CNT-based composites (75,76). Theoretically, the thermal conductivity of the composites filled with 0.1 wt% MWNTs can be six times that of neat polymers.

Xia et al. prepared and compared CNT/polyurethane nanocomposites based on both SWNTs and MWNTs (21). In their study, the thermal conductivities of PU and PU-carbon nanotube composites were determined by modulated differential scanning calorimetry. The incorporation of carbon nanotubes enhances the thermal conductivity of PU matrix. At 1 wt% carbon nanotube loading, the thermal conductivities of PU-MWNT and PU-SWNT composites were improved by $\sim 21\%$ and $\sim 42\%$, respectively, compared to blank polyurethane. SWNTs had a better effect on the improvement of thermal conductivity compared to MWNTs. The limitation of CNTs in extensive improvement of thermal conductivity of polymers is still not very clear. Huxtable et al. (77) opined that the increase in thermal conductivity appears rather limited by a large thermal resistance across the nanotube-matrix interface even for the case with ultrahigh intrinsic thermal conductivity and aspect ratio of embedded carbon nanotubes. Interfacial resistance happens when the frequencies are different, and the heat energy has finds difficulty taking the leap from one element to the next. This was attributed to a reduction in phonon scattering length rather than changes in the vibration frequencies of the carbon atoms in the nanotubes, which has been commonly considered as the biggest bottleneck limiting the thermal transport in CNT/polymer composites (78).

Cai et al. proposed a new route to reduce the interfacial phonon scattering (27). Semicrystalline PU dispersions were used as latex host to accommodate MWNTs following the colloidal physics

method. The thermal conductivity was found to increase by ~210%, from $0.15 \text{ W} \cdot \text{m}^{-1} \cdot \text{K}^{-1}$ to $0.47 \text{ W} \cdot \text{m}^{-1} \cdot \text{K}^{-1}$, as the addition of the MWNTs increases to 3 wt%. The continuous nanotube-rich phase existing in the interstitial space among the latex particles and the crystallites nucleated at the nanotube-polymer interface were the main factors for the effective reduction of interfacial phonon scattering.

6.4.3 Thermal Stability and Degradation

Thermal decomposition of segmented PUs is a multi-stage process and its complexity is dependent on the presence of rigid segments (79). The first degradation stage is fast and initiated predominantly within hard segments. After the first stage of decomposition, i.e. when the weakest bonds in the polymer have been used up, the second and third stages, depending on the content of soft segments, are much slower. More stable urethane groups connected to aliphatic radicals undergo decomposition during the second degradation stage. The most stable structures such as ester groups present in the soft segments are damaged at the third degradation stage. The higher the content of soft segment in a polymer is, the more stable the polymer is at elevated temperatures and the lower the initial rate of its degradation is.

Using thermogravimetric analysis (TGA), several research groups have reported the improved thermal stability in carbon nanotube/polyurethane composites relative to the neat polymers. Specifically, the onset decomposition temperature, T_{onset} , and the temperature of maximum weight loss rate, T_{peak} , are higher in the nanocomposites. A number of mechanisms have been suggested to explain the enhancement of thermal stability for CNT/PU composites. Dispersed nanotubes might hinder the flux of degradation products and thereby delay the onset of degradation. Polymers near the nanotubes might degrade more slowly, which would shift T_{peak} to higher temperatures. Another possible mechanism attributes the improved thermal stability to the effect of higher thermal conductivity in the nanotube/polymer composites that facilitates heat dissipation within the composite (80).

Xia et al. found that the incorporation of MWNTs and SWNTs did not improve the first degradation temperature, but did improve the second degradation temperature (21). This indicates that carbon nanotubes may preferably interact with the soft segment in polyurethane structure. There were no significant differences between

SWNTs and MWNTs series. At 1 wt% of SWNT or MWNT loading, the second degradation temperature was delayed by $\sim 5^{\circ}\text{C}$.

Generally, covalent bond between carbon nanotubes and PU chains facilitate the improvement of thermal stability. Kuan et al. (48) prepared WPU nanocomposite with modified carbon nanotubes compatibilized with waterborne polyurethane via covalent bonding or ionic bonding. Consequently, the thermal degradation of both the systems was significantly improved, and covalent bonding system exhibited better outcome in enhancing the thermal stability of nanocomposite. PU nanocomposites were prepared through conventional and *in-situ* methods with MWNTs functionalized with poly(ϵ -caprolactone) by Jana et al. (81). The degradation temperature of the *in-situ* nanocomposites was better than that of the conventional nanocomposites with the same loading of MWNTs. Such higher thermal stability of the *in-situ* nanocomposites was ascribed to covalent bond formation between MWNTs and PU chains, which could result in better nanotube dispersion in the PU matrix for the *in-situ* nanocomposites.

Generally, the thermal stability of the composites was improved by the addition of the CNTs, which may be attributed to the following combined effects: (1) the uniformly dispersed carbon nanotubes presumably provided thermo-oxidative stability to the polymers in the vicinity of the tube surfaces; (2) the enhanced thermal conductivity of the composite can facilitate heat transport and thus increase its thermal stability (81); (3) it is possible that the formation of compact chars of CNTs and polymer matrix during the thermal degradation is beneficial to the improvement of thermal stability of the composites (82).

Moreover, Mondal et al. observed that MWNT could act as a thermal conductor as well as a filler. The thermal stability declined at low MWNT loading (0.25 and 0.50 wt%) (83). This may be due to the increase in the thermal conductivity property of PU by the incorporation of MWNTs which helps the flow of heat to the internal structure of TPU and breaks the bonds of TPU structure. And a further increase of MWNTs improves the thermal stability of TPU due to the filling effect of MWNTs into the TPU matrix.

6.4.4 Fire Retardancy

Polymeric materials are commonly used in everyday life with increased fire hazards and therefore flame retardants are very often incorporated into them to limit their flammability (84,85).

The application of polyurethane, which is combustible, leads to an increase in fire risks. Therefore, the studies on flame retardant PU nanocomposites are worthwhile. Bourbigot et al. mixed the TPU with MWNTs (1 and 2 wt%) at 180 °C using a Brabender mixer (84). The incorporation of MWNTs in TPU permits to decrease the PHRR (peak of heat release rate) by 50% compared to the neat TPU. The good dispersion of MWNTs in TPU matrix might explain the excellent flame retardancy properties. The mode of action of CNTs as flame retardant was investigated by Kashiwagi et al. (86–88). They found that the shape of carbon particles appears to be important for effectively reducing the flammability (by comparing carbon black vs. MWNTs) and that the flame retardant performance is achieved through the formation of a relatively uniform network-structured floccule layer covering the entire sample surface without any cracks or gaps. A network layer is then formed by acting as a heat shield to slow the thermal degradation of the polymer.

6.4.5 Rheological Properties

The viscoelastic properties of carbon nanotube/polymer composites have both practical importance related to composite processing and scientific importance as a probe of the composite dynamics and microstructure. The viscosity for CNT/PU dispersion at mixing is also very important for *in-situ* formation of polyurethane nanocomposite. Lower viscosity means a better flow ability and more homogenous mixing with isocyanate. Furthermore, low viscosity is very helpful to remove the bubbles before curing, which is a key step for polyurethane preparation.

Normally, the incorporation of carbon nanotubes increases the melt viscosity of polyurethane nanocomposites, thus the processability of polyurethane composites with high carbon nanotube loading is hindered. Meng et al. prepared shape-memory polyurethane/multiwalled carbon nanotube (SMP-MWNT) fibers with various MWNT contents by melt spinning (55). SEM images indicate that the surface of the SMP-MWNT fibers becomes rough and coarse with increasing MWNT content. When the nanotube content is increased from 3 to 5 wt%, the fiber surface becomes very coarse and has bad hand feeling. Correspondingly, the melt flow index of the composites decreased with increasing MWNT content. When the MWNT content was increased to 8 wt%, the rheological properties of the composite deteriorated completely. Thus, the fibers

could not be spun. This can be ascribed to two factors: first, with increasing MWNT content, the continuity of the polymer matrix is destroyed, and second, the filter screens inside the spinneret are more readily blocked because of the high MWNT content.

Addition of the carbon nanotube, on the one hand, can increase the melt viscosity of polyurethane nanocomposite (48), on the other hand, the viscosity variation can be reduced by adding carbon nanotube thus benefiting from the stabilization of viscosity during polymer melting. For both MWNT/WPU nanocomposites in which carbon nanotubes were modified to compatibilize with waterborne polyurethane via covalent bonding (system 1) or ionic bonding (system 2), the melt viscosity was increased and the viscosity variation was decreased for both systems. After melting, however, some of carbon nanotubes aggregate again and the phase separation phenomenon of nanocomposite appears in system 2. High processing temperature destroys the ionic bonding, which diminishes the interface between carbon nanotubes and waterborne polyurethane, thus leading to the phase separation of nanocomposite.

Homogeneous dispersion of polymer functionalized carbon nanotubes could increase the wetting properties of carbon nanotubes and thus acquire better lower viscosity compared with the nanocomposites with raw carbon nanotubes. Poly(propylene glycol)-grafted-MWNT/polyurethane composites were synthesized based on the hydroxyl functionalized MWNTs through an *in-situ* polymerization by Xia et al. (17). The viscosity for polyol/1 wt% MWNT-graft-polyol dispersion was much lower than that for 1 wt% raw MWNT/polyol system. This suggests that grafting polyol on MWNTs can improve the rheological behavior during the processing, compared with the raw MWNTs (21,46).

6.4.6 Electrical Conductivity

A common characteristic of most polymeric materials is their high electrical resistivity, which accounts for the insulating character of these materials. While for many applications this feature is highly desirable, there are also numerous applications for which an electrically conducting behavior would be advantageous. Elastomers with high electrical conductivity are critical for applications ranging from seals between pipes used for transferring flammable gases, electrostatic automotive painting and electromagnetic shielding for mobile electronics. Traditionally, conductive fillers,

such as carbon black, chopped carbon fibers or metallic flakes are used. Conductivity is established by percolative network formation of the conductive fillers and limited by carrier transport (hopping or tunneling) between filler particles. Thus the extent of filler dispersion, aspect ratio of the filler, and wettability of the filler by the elastomeric medium are key morphological characteristics in determining the conductivity of the system. In order to obtain materials with high conductivity, high loading level of conductive filler is often needed. The large volume fractions, however, not only negatively impact deformability, processability, surface finish, and limit the ability to maintain desired conductivity at extreme deformations ($> 100\%$), but also often impair the mechanical properties of the materials.

Recently, CNTs have been shown to be attractive fillers for achieving electrical conductivity of polymers at relatively low CNT contents. Amounts lower than 1 wt% CNTs are reported to be sufficient to get conductive polymer composites which is much less as compared to carbon black. The broad availability of carbon nanotubes with large aspect ratios (usually > 1000) and high electrical conductivity (σ 18,000 S/cm along tube axis) have led to a resurgence of applied and fundamental investigations of filled polymers, driven by the potential to address limitations of classic conductive fillers. In addition, mechanical properties may be enhanced due to the fiber or tube like shape of the filler. Thus, it is also promising to use CNTs as additives in polyurethanes for electrically conductive or antistatic applications. A variety of applications are being pursued using these conductive composites: electrostatic dissipation, electrostatic painting, electromagnetic interference (EMI) shielding, printable circuit wiring, transparent conductive coating, and so on (89). Composites containing conducting fillers in insulating polymers become electrically conductive when the filler content exceeds a critical value, known as a percolation threshold. The carbon nanotube/polymer composites usually exhibit very low percolation threshold for electrical conductivity because of the large aspect ratio and the nanoscale dimension of nanotubes. The percolation threshold is characterized by a sharp jump in the conductivity by many orders of magnitude which is attributed to the formation of a three-dimensional conductive network of the fillers within the matrix. Pötschke et al. prepared thermoplastic polyurethane filled with MWNTs via melt mixing (56). Using small scale melt mixing, electrical percolation of as extruded strands could be

reached at concentrations as low as 1.5 wt% (<1 vol %). Electrically conductive composites were obtained starting at 2 wt% addition of industrial crude MWNTs which has an excellent dispersibility and led to quite homogeneous dispersion.

WPU/(pristine) CNT and WPU/A-CNT (acid-treated CNT) composites were prepared through *in-situ* polymerization by Kwon et al. (53). The conductivity of the PU/acid treated CNT system was found higher compared with that of the WPU/CNT system, probably due to the smaller particle size and higher dispersibility of A-CNTs thus homogeneous dispersion in WPU matrix. For instance, the electrical conductivities of the WPU/CNT1.5 and WPU/A-CNT1.5 composites (containing 1.5 wt% CNTs) were measured to be 8.0×10^{-4} and 1.1×10^{-3} S/cm, respectively, which were nearly 8 and 9 orders of magnitude higher than that of neat WPU (2.5×10^{-12} S/cm). Maximum surface electrostatic potential V_{\max} and the half-life of the electrostatic charge ($\tau_{1/2}$) values of the neat WPU film were 57 kV and 110 s, respectively, indicating that WPU was a typical insulating polymer. With increasing pristine CNT and A-CNT contents from 0.01 to 1.5 wt%, the values of V_{\max} and $\tau_{1/2}$ for both systems exponentially decreased. Generally, polymers with $\tau_{1/2}$ values lower than 10 s are considered materials with good antistatic properties. The antistatic properties of the WPU/A-CNT composite were better than those of the WPU/CNT composite with the same CNT content. The $\tau_{1/2}$ values of the WPU/CNT0.1 and WPU/A-CNT0.07 composites were 10 and 4.2 s, respectively. From a comparison of the results in this study with those in the previous study (20), Kwon et al. found that the *in-situ* polymerization system was found to be a more effective process for improving the conductivity of the composites in comparison with the blending system (53).

However, excessive acid treatment could damage the crystalline structure of CNTs, thus resulting in poor electrical behavior of the composites despite good MWNT dispersion in the polymer matrix. MWNTs were purified by Jang et al. at 80°C in 40% aqueous solutions of either nitric acid or a mixture of nitric and sulfuric acids (90). The degree of crystallinity, as obtained from Raman spectroscopy measurements, shows a maximum for the MWNTs treated for 2 h in the mixture acid solution. The MWNTs with the maximum degree of crystallinity enables the PU/MWNT composites to present a lower percolation threshold and the highest electrical conductivity in the region of the conductive network formation for the given composite systems. Excessive acid treatment, on the contrary,

leads to the decrease of electrical conductivity. Since the MWNTs obtained via insufficient acid treatment are not well dispersed in the matrix or sufficiently purified such that the end tips of the MWNTs remain unopened, the composites also exhibit low conductivity and high percolation threshold. Therefore, the acid treatment condition applied to the MWNTs must be controlled to purify effectively the impurities in the MWNT bundles and to maintain the crystalline structure of the MWNTs without further damage for ensuring superior electrical properties of the polymer composites.

Zhang et al. studied the effect of conductive network formation in a polymer melt on the conductivity of MWNT/TPU composite systems (91). An extremely low percolation threshold of 0.13 wt% was achieved in hot-pressed composite film samples, whereas a much higher CNT concentration (3–4 wt%) is needed to form a conductive network in extruded composite strands. This was explained in terms of the dynamic percolation behavior of the CNT network in the polymer melt. The conductivity of extruded strand showed a hopping resistivity dominated behavior at low concentrations and a dynamic percolation induced network dominated behavior at higher concentrations. It was shown that a higher temperature can reduce the filler concentration required for the dynamic percolation to take effect.

6.4.7 Water Vapor Transport Properties

Segmented polyurethanes (SPU) can present micro-phase separated structure due to the thermodynamic incompatibility between the constituent segments (92). Phase transition at T_g or melting point temperature (T_m) of soft segment crystals accompanies a great change in thermomechanical property of the SPU. In addition to the change of thermomechanical property of SPU, it was observed that SPU also has a large change in moisture permeability above and below the T_g/T_m s (93,94). This significant change of water vapor transport behavior will be useful for SPU-coated textile that could provide thermal insulation at cold temperature and high permeability above T_g/T_m s.

Mondal et al. investigated the influence of functionalized MWNTs on microstructure and water vapor transport properties of SPU membranes (95). The presence of MWNT was expected to decrease the permeability due to the more tortuous path for the diffusing molecules that must bypass through impermeable nanoparticles. Experimental results revealed that there were about 20% reductions

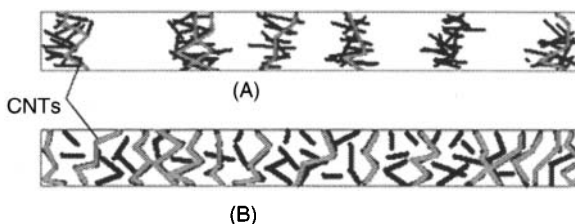


Figure 6.3. The sketch of the dispersion of raw MWNTs (a) and MWNT-IPDI (b) in PEU. The red line represents end-connected CNTs. Reprinted from Deng et al. (74) with permission from the Elsevier.

of water vapor permeability (WVP) of coated fabrics as compared with uncoated fabrics at all temperatures. However, Chen and Sholl (96) theoretically predicted that the diffusion of some gas molecules such as CH_4 in carbon nanotubes was extremely rapid compared to other known nanoporous materials. Therefore, Kim et al. (97) suggested that carbon nanotubes could be an attractive additive for universally enhancing the gas permeability of polymers.

Meng et al. reached the opposite conclusion against Mondal that incorporation of MWNTs increases the WVP of polyurethane/MWNT composite membranes (54). The increase of WVP with increasing MWNTs (above 0.25 wt% MWNT content) may be due to two reasons: first, the MWNTs constrain the formation of more ordered soft segment crystalline structure; secondly, these filled straight MWNTs with large aspect ratios may offer a straight “free” pathway for the diffusion of water molecules on the surface of MWNTs or inside MWNTs (74). Deng et al. gave a more reasonable explanation when dealing with such contradiction: the water vapor conduction was improved due to the dramatically increased paths along or inside the tubes of MWNTs when the dispersion of CNTs is good. However, raw MWNTs could not have such wonderful path for the water vapor because of their poor dispersion, thus leading to the reduction of water vapor conduction (Figure 6.3) (74).

6.4.8 Shape Memory

Shape memory polymers are defined by their ability to store and recover strains when subjected to a particular thermo-mechanical cycle. Shape-memory polymers can recover their original shape by being heated above their transition temperature, which are defined by different phases in the materials. In particular, the shape-

memory effect of segmented polyurethane block copolymers has been extensively studied because of its superior material properties, which arises from the phase-separated structure of its hard and soft segments. The hard segments form physical crosslinks arising from polar interactions, hydrogen bonding, and crystallization in the hard domain, while the soft segments form the reversible phase because of molecular motion in a rubbery state (98,99). This shape-memory effect is usually induced by thermal stimulation by heating above the transition temperature of the polymers, such as the glass transition temperature or melting temperature. And more and more reports about linear, phase-segregated polyurethane block copolymers being used in thermoresponsive shape memory polymers can be found. The high strain recovery and the high degree of chemical control over the softening/retraction temperature allow a broad range of applications (100–103). Moreover, some other stimulating sources, such as pH, electric field, and chemicals, may also be available for actuating polymers with shape memory.

The hard-segment phase has a higher thermal transition temperature (T_{perm}), whereas the soft-segment phase has a transition temperature, the glass-transition temperature or melting temperature that acts as a switching temperature (T_{trans}). When shape-memory polyurethane is deformed at a high temperature (T_{high}) between T_{trans} and T_{perm} (thermal draw) or at a temperature below T_{trans} (cool draw), the temporary deformation can be fixed once the shape-memory polyurethane is cooled to (or kept at) a low temperature (T_{low}) below T_{trans} . If it is heated to a temperature above T_{trans} , it recovers to the original shape by releasing the internal stress stored among the physically crosslinked hard segments during deformation. In the shape memory polyurethane, the hydrogen bonded hard segment phase is responsible for shape recovery, while the soft segment phase plays the major role in shape fixity.

Shape-memory MWNT fibers were prepared through melt spinning by Meng et al. (55). The recovery ratio of the shape-memory MWNT fiber was higher at 1.0 and 3.0 wt% MWNTs than that of the neat shape-memory fiber (SMF). For the shape-memory polyurethane (SMP) system, the homogenously in-plane aligned MWNTs have high interaction with polyurethane chains particularly with the hard segment regions during membrane deformation at or above melting transition temperature of the soft segment. When the soft segment phase is “melted”, the stress is effectively transferred to the high modulus MWNTs, providing higher shape-

recovery force to the composite. Therefore, in one aspect, the MWNTs help storing internal stress; in another aspect, the MWNTs restrict the slippage of hard segments and consequently protect the hard segment network. Therefore, the shape recovery ratios increase with increasing MWNT content. However, at 7.0 wt% MWNTs, first, the aggregated MWNTs degrade the fiber shape-recovery effect; secondly, the degree of phase separation in polyurethane decreases greatly. Thus the shape-memory ratio is much lower than that of the neat SMF (24). Polyurethane/MWNT composite membranes were synthesized via *in-situ* pre-polymerization by Meng et al. (104). The authors found the increase of recovery ratios below 2.0 wt% of MWNTs. However, when the MWNT content reaches 3.0 wt%, the shape recovery ratios decreased prominently. It was also observed that the MWNTs were preferentially aligned in the fiber axial direction during the spinning. Accordingly, the shape recovery ratio and recovery force were prominently improved by the aligned MWNTs, and the self-aligned MWNT shape memory fibers recovered the original length more quickly.

Better dispersion of MWNTs in the polymer matrix caused by the formation of the chemical bonds leads to uniform stress distribution and enhanced shape memory (23). Jana et al. prepared nanocomposites of PU and MWNTs via *in-situ* polymerization and conventional method (105). PU nanocomposites obtained via an *in-situ* method with PCL-g-MWNTs showed better shape recovery, compared to conventional nanocomposites.

In some applications such as remote control of material shape, voltage-triggering is a more convenient method than the thermal heating method. In order to get rid of external heaters, thermoresponsive SMP composites incorporated with conductive carbon nanotubes have been developed. In the study by Sahoo et al. (106), electroactive shape-memory composites were synthesized using conducting PU composites and acid-treated multi-walled carbon nanotubes (A-MWNTs) as surface modified MWNT content increases the conductivity (an order of $10^{-3} \text{ S}\cdot\text{cm}^{-1}$ was obtained in samples with 5 wt% modified MWNTs). Electroactive shape recovery was observed for the surface modified MWNT composites with an energy conversion efficiency of 10.4%. Electroactive shape-memory polyurethane block copolymer/MWNT nanocomposite coated with polypyrrole (PPy) was also prepared by Sahoo et al. (106). The electrical conductivity was the highest for the MWNT-PU composites coated with PPy on the film surface. The conductivity of 0.098

S/cm in this composite was sufficient to show electroactive shape recovery by heating above a transition temperature of 40–48 °C. A good shape recovery in the 90–95% range could be obtained during a shape recovery test when a voltage of 25 V was applied. Hence, PU-CNT composites may prove promising candidates for use as smart actuators. An electroactive shape memory fiber was fabricated through incorporating MWNTs by Meng et al. (107). At 6.0 wt% MWNT content, the shape recovery ratio of the prepared shape memory fiber was 75% and the fixing ratio was 77%.

Goo et al. investigated the actuation durability of a conducting shape memory polyurethane/MWNT (CSMPU) actuator and concluded that the number of cycles at breaking decreased, as the actuation temperature increased (108). The possible reason is that more material degradation of CSMPU can be induced due to rapid and large movement of polymer chains as the actuation temperature increases. For a CSMPU actuator, the authors confirmed that an actuation temperature that is higher than the transition temperature produces a rapid response but low durability.

6.4.9 Special Properties Related to Bio-Applications

The exceptional combination of good mechanical properties of special PU elastomers with their high hydrolytic stability and biological stability makes it possible to use polyurethanes as highly specialized biomedical materials. They can be utilized to produce endoprostheses, cardiac valves and/or regenerative membranes for damaged internal organs because they do not induce any inflammatory condition of tissues, do not undergo any destruction by body fluids, and no blood components are deposited on them (109,110).

Growth behaviors of fibroblast cells on the non-woven membrane composed of single-walled carbon nanotubes were studied and it was found that the scaffold enhanced the cell adhesion and proliferation significantly in 3 weeks (111). It was also reported that the mats of multiwalled carbon nanotubes could support cell growth including neuron (112) and bone (113,114), implying the application potentials in tissue engineering. In addition to enhanced mechanical strength, incorporation of functionalized CNTs has the potential to alter the surface chemistry and modify the nanoscale architecture of nanocomposite materials. This ability to tailor surface chemistry, create nanoscale architectures and potentially match the mechanical

properties (modulus) of tissues makes nanocomposites particularly attractive for biomedical applications, where they have been advocated as novel biomaterials and as scaffolds for tissue-engineering applications.

TPU/MWNT foams were manufactured by thermally induced phase separation (28). Some CNTs are trapped perpendicularly to the pore surface creating a rough, nanotextured surface. The surface character of the nanocomposites became more acidic with increasing the loading fraction of oxidized CNTs. The biological properties revealed that increasing MWNT loading fraction did not cause osteoblast cytotoxicity or detrimental effects on osteoblast differentiation or mineralization. However, osteoblast production of the potent angiogenic factor VEGF (vascular endothelial growth factor) increased in proportion to CNT loading (after 3 days in culture). Nanofibrous scaffold of MWNT/PU composite with aligned topography was fabricated by electrospinning for the growth of endothelium cells (115). The scaffold with nanofibrous architecture and carbon nanotube component provided friendly micro-environment for endothelial cell proliferation. The studies by Meng et al. demonstrated the scaffold with the nanofibrous architecture and MWNT component significantly enhanced the cell adhesion, proliferation, migration and aggregation, and secretion (116). CNTs were deposited on the surfaces of polyurethane foams by electrophoretic deposition. Zawadzak et al. found that CNTs can act as a template for nucleation and growth of nanosized and weakly crystalline calcium phosphate particles (117).

Liu et al. have demonstrated that the direct electron transfer reactivity of the immobilized hemoglobin (Hb) can be effectively enhanced by the addition of MWNTs into the PUE film (118). Biosensors based on the direct electron transfer of the immobilized proteins show good analytical performance, including high sensitivity, acceptable fabrication reproducibility, and storage stability.

6.4.10 Microwave Absorption

Microwave-absorbing materials are currently in high demand for many expanded EMI shielding and radar cross section reduction applications with both commercial and defense purposes. The nanostructured materials have attraction for microwave radiation absorbing and shielding materials in the high-frequency range due

to their many unique chemical and physical properties. Particularly, the unique structure and many excellent properties of CNTs have prompted intensive studies for many potential engineering, including EMI shielding, applications.

Processable composites of SWNTs with soluble crosslinked polyurethane (SCPU) were prepared at various loadings of SWNTs (0–25 wt%) (119), and they exhibited strong microwave absorption in the microwave range of 2–18 GHz. SCPU composite with 5 wt% loading of SWNTs had a strong absorbing peak at 8.8 GHz and achieved a maximum absorbing value of 22 dB. The absorbing peak position moved to lower frequencies with increasing SWNT loading. The microwave absorption of these composites can be mainly attributed to the dielectric loss rather than magnetic loss.

6.4.11 UV-Protection

UV radiation, which is harmful to the skin, is well known. A UV-ray, like visible light, is a segment of the electromagnetic spectrum with a wavelength ranging from 100 to 400 nm, and it is subdivided into three bands: UVA (320 or 315 to 400 nm), UVB (290 to 315 or 320 nm), and UVC (100–290 nm). The terrestrial solar UV consists of only UV with wavelength of 290–400 nm, because UVC and some UVB are absorbed by the stratospheric ozone in the earth's atmosphere. Any effective protection of the skin from the damaging effects of undue exposure to sunlight clearly needs to include means for absorbing both UV-A and UV-B components of sunlight before they reach the skin surface. Traditionally, most of the natural and synthetic textile fabrics, whether undyed or dyed, are usually at least partially permeable to UV radiation. Therefore, the mere wearing of clothing does not afford adequate protection of the skin from damage induced by UV radiation. Remedy will be possible here by incorporating UV absorbers in textile fabrics maybe by means of coating. Condensation is of particular interest in the discussion of the merits of coated fabrics when they are used as the outermost layer of any kind of clothing for outdoor activities. The polyurethane garments which have a high capacity for water vapor transmission, so that the forming perspiration can evaporate and be transmitted from the body to the environment can provide wearing comfort to the wearer.

The discovery of CNTs gives new direction for the use of CNTs in polymeric materials to improve several properties, including UV protection. Mondal et al. have coated the cotton fabrics with

different quantities of MWNTs containing hydrophilic polyurethane (HPU) and without MWNTs containing HPU (95). MWNTs were dispersed in HPU solution by functionalization of MWNTs. The nanotube containing HPU coating shows excellent protection against UV radiation, with only 1 wt% of MWNTs, a UV protection factor (UPF) of 174 and with 2.5 wt % of MWNTs a UPF of 421 was obtained, which stated excellent protection (UPF ≥ 50) according to the Australian/New Zealand standards. The coated fabrics maintained very good water vapor permeability, hence confirming the wearing comfort. Room temperature (20–23 °C) range soft segment crystal melting of HPU enhanced the permeability of coated fabrics.

6.5 Applications

The principal issues for the materials technology related to the basic properties for polyurethane/CNT composites were already presented in previous sections. It provided the correlation between the structural factors and the properties resulting therefrom. This section, however, is going to present a review of the latest trends in applications for the materials based on polyurethane/CNT composites.

Photoresponsive

Two kinds of photoresponsive azobenzene polyurethane functionalized multiwalled carbon nanotube (AzoPU-MWNT) composites were synthesized by *in-situ* polycondensation (50). Core-shell structures with MWNTs as hard core and polymer layer as soft shell were formed and the average thickness of the grafted polymers was about 7–10 nm. The AzoPU-MWNT composites showed reversible photoisomerism behavior.

Vapor Sensitive Response

Luo et al. have fabricated a conductive polyurethane/MWNT composite thin film with a selective vapor-induced sensing performance through *in-situ* dispersion polymerization (120). This kind of thin films yielded higher responsivity to some solvent vapors like benzene, toluene, acetone and chloroform than others such as carbon tetrachloride, cyclohexane, methanol and formaldehyde.

Electromagnetic Interference

PU composites with well-dispersed SWNTs were prepared using a simple physical mixing method and an EMI shielding effectiveness of ~17 dB was achieved at the SWNT loading of 20 wt% (121). Oxidized MWNTs and silver powder were filled in polyurethane matrix by Kim et al. (122). The EMI shielding effectiveness of the composites could be controlled from about 60 dB to more than 80 dB at an extremely low loading level of both the MWNTs and the Ag flakes in the frequency range from 10 to 1000 MHz. Together with excellent properties and wide applications of PU, the EMI shielding properties endowed by CNTs as a filler shall make these composites one of the ideal candidates for EMI application.

Nanowebs

PU and PU/MWNT nanocomposite nanofibers created via an electrospinning process from PU/dimethylformamide (DMF) solution were successfully prepared with average diameter around 350 nm (29). During the electrospinning, the so-called nanowebs with diameters of 20-40 nm were observed in PU/MWNT nanofiber structures containing PU fibers. The existence of these structures could be based on the occurrence of strong secondary electric fields, which were created between individual conducting MWNTs (distributed in the PU/MWNT nanocomposites), which started to behave as the local moving nanoelectrodes promoting the creation of additional very fine nanowebs during the electrospinning processes.

Tissue Engineering Scaffolds

Tissue-engineering scaffolds play important roles in cell growth and tissue formation. Biodegradable polyurethanes are interesting materials for tissue engineering scaffolds. They are expected to be suited for applications ranging from soft tissue engineering requiring the use of flexible elastic material to cartilage and bone regeneration requiring rigid scaffolds. Carbon nanotubes are being increasingly considered in tissue engineering strategies to enhance the properties and function of scaffolds. It has been reported that composites of carbon nanotubes and polyurethane exhibited promising biocompatibility and enhance the cell adhesion, proliferation, migration and aggregation, and secretion, implying the application

potentials in tissue engineering (28,29,115–123). A MWNT-PU composite was prepared through a controlled co-precipitation by Meng et al. (116). It was demonstrated that platelets activation and red blood cell disruption in MWNT-PU composite were remarkably reduced compared to neat PU, and the strength and elasticity of PU improved slightly. The composite exhibited promising application potentials in cardiac vascular surgery and other blood-contact environments.

6.6 Conclusions

The above analysis takes the synthesis methods, the performance affected by the dispersion of CNTs, enhanced physical properties and the latest applications of carbon nanotube/polyurethane composites described in literature reports as the reference point. In the interest of brevity, this is not a comprehensive review, however, it goes through numerous research reports and applications which have been learned and described in the recent years. Despite that, there are still many opportunities to synthesize new carbon nanotube/polyurethane systems and to modify carbon nanotubes with new functional groups. The possibility of producing modern biomedical and shape memory materials in that way makes the challenge of the near future.

The unique two-phase structures of polyurethane that offers the elasticity of rubber combined with the toughness and durability of metal make them one of the most extensively studied and frequently used materials in carbon nanotube related nanocomposites. The main difficulty in developing CNT based polyurethane nanocomposites was how to achieve uniform and homogeneous CNT dispersion. Further investigations on the interactions between carbon nanotubes and two-phase structures are critical for the wider applications of carbon nanotube/polyurethane composites.

With the development of polymer science and technology, the main idea in materials science is to develop high-performance and multifunctional materials. It is known to us all that the alignment of CNTs in polyurethane matrices is of vital importance in fabricating high-performance and advanced polyurethane nanocomposites. However, there were few reports investigating the CNT alignment in polyurethane matrices in detail. The orientation of CNTs in polyurethane matrices can significantly improve the mechanical,

electrical and thermal conductivity properties. We believe that the CNT alignment in polyurethane matrices especially by electrical and magnetic fields may be an important and interesting field to be studied.

In summary, carbon nanotube/polyurethane composites offer both great potential and great challenges, marking it as a vibrant area of work for years to come. The improvement and applications of these composites will depend on how effectively we can handle the challenges. The significant progress in the understanding of these composite systems within the past few years points toward a bright future.

Acknowledgements

This work was supported by the National Natural Science Foundation of China (20774019; 50873027).

References

1. O. Bayer, *Angewandte Chemie*, Vol. 71, p. 26, 1947.
2. G. Oertel, *Polyurethane Handbook*, Munich, Hanser Publishers, 1994.
3. Z. Wirpsza, *Poliuretany Chemia Technologia Zastosowanie*, Warsaw, Wydawnictwo Naukowo-Techniczne, 1991.
4. M.S. Sanchez-Adsuar, E. Papon, J.J. Villenave, *Journal of Applied Polymer Science*, Vol. 76, p. 1596, 2000.
5. S. Iijima, *Nature*, Vol. 354, p. 56, 1991.
6. J.P. Salvetat, G.A.D. Briggs, J.M. Bonard, R.R. Bacsá, A.J. Kulik, T. Stockli, N.A. Burnham, L. Forro, *Physical Review Letters*, Vol. 82, p. 944, 1999.
7. M.F. Yu, B.S. Files, S. Arepalli, R.S. Ruoff, *Physical Review Letters*, Vol. 84, p. 5552, 2000.
8. B.Q. Wei, R. Vajtai, P.M. Ajayan, *Applied Physics Letters*, Vol. 79, p. 1172, 2001.
9. Z.K. Tang, L.Y. Zhang, N. Wang, X.X. Zhang, G.H. Wen, G.D. Li, J.N. Wang, C.T. Chan, P. Sheng, *Science*, Vol. 292, p. 2462, 2001.
10. D.S. Bethune, C.H. Kiang, M.S. Devries, G. Gorman, R. Savoy, J. Vazquez, R. Beyers, *Nature*, Vol. 363, p. 605, 1993.
11. S. Iijima, T. Ichihashi, *Nature*, Vol. 363, p. 603, 1993.
12. P. Calvert, *Nature*, Vol. 399, p. 210, 1999.
13. S. Berber, Y.K. Kwon, D. Tomanek, *Physical Review Letters*, Vol. 84, p. 4613, 2000.
14. M.A. Osman, D. Srivastava, *Nanotechnology*, Vol. 12, p. 21, 2001.

15. W. Chen, X. Tao, Y. Liu, *Composites Science and Technology*, Vol. 66, p. 3029, 2006.
16. W. Chen, X. Tao, *Applied Surface Science*, Vol. 252, p. 3547, 2006.
17. H.S. Xia, M. Song, J. Jin, L. Chen, *Macromolecular Chemistry and Physics*, Vol. 207, p. 1945, 2006.
18. F. Buffa, G.A. Abraham, B.P. Grady, D. Resasco, *Journal of Polymer Science Part B: Polymer Physics*, Vol. 45, p. 490, 2007.
19. J.W. Xiong, Z. Zheng, W.H. Song, D.S. Zhou, X.L. Wang, *Composites Part A: Applied Science and Manufacturing*, Vol. 39, p. 904, 2008.
20. J. Kwon, H. Kim, *Journal of Polymer Science Part A: Polymer Chemistry*, Vol. 43, p. 3973, 2005.
21. H.S. Xia, M. Song, *Soft Matter*, Vol. 1, p. 386, 2005.
22. M. Xu, T. Zhang, B. Gu, J.L. Wu, Q. Chen, *Macromolecules*, Vol. 39, p. 3540, 2006.
23. S. Badaire, P. Poulin, M. Maugey, C. Zakri, *Langmuir*, Vol. 20, p. 10367, 2004.
24. N.R. Raravikar, L.S. Schadler, A. Vijayaraghavan, Y. Zhao, B. Wei, P.M. Ajayan, *Chemistry of Materials*, Vol. 17, p. 974, 2005.
25. W. Feng, X.D. Bai, Y.Q. Lian, J. Liang, X.G. Wang, K. Yoshino, *Carbon*, Vol. 41, p. 1551, 2003.
26. F.M. Du, C. Guthy, T. Kashiwagi, J.E. Fischer, K.I. Winey, *Journal of Polymer Science Part B: Polymer Physics*, Vol. 44, p. 1513, 2006.
27. D. Cai, M. Song, *Carbon*, Vol. 46, p. 2107, 2008.
28. G. Jell, R. Verdejo, L. Safinia, M.S.P. Shaffer, M.M. Stevens, A. Bismarck, *Journal of Materials Chemistry*, Vol. 18, p. 1865, 2008.
29. D. Kimmer, P. Slobodian, D. Petras, M. Zatloukal, R. Olejnik, P. Saha, *Journal of Applied Polymer Science*, Vol. 111, p. 2711, 2009.
30. M.T. Hunley, P. Pötschke, T.E. Long, *Macromolecular Rapid Communications*, Published Online: Sep 1 2009 12:34PM, DOI: 10.1002/marc.200900393, 2009.
31. C. Park, Z. Ounaies, K.A. Watson, R.E. Crooks, J. Smith, S.E. Lowther, J.W. Connell, E.J. Siochi, J.S. Harrison, T.L.S. Clair, *Chemical Physics Letters*, Vol. 364, p. 303, 2002.
32. T. Lin, V. Bajpai, T. Ji, L. Dai, *Australian Journal of Chemistry*, Vol. 56, p. 635, 2003.
33. K. Mukhopadhyay, C.D. Dwivedi, G.N. Mathur, *Carbon*, Vol. 40, p. 1373, 2002.
34. M. Holzinger, J. Abrahams, P. Whelan, R. Graupner, L. Ley, F. Hennrich, M. Kappes, A. Hirsch, *Journal of American Chemical Society*, Vol. 125, p. 8566, 2003.
35. D.E. Hill, Y. Lin, A.M. Rao, L.F. Allard, Y.P. Sun, *Macromolecules*, Vol. 35, p. 9466, 2002.
36. M.F. Islam, E. Rojas, D.M. Bergey, A.T. Johnson, A.G. Yodh, *Nano Letters*, Vol. 3, p. 269, 2002.
37. L. Vaisman, H.D. Wagner, G. Marom, *Advances in Colloid and Interface Science*, Vol. 37, p. 128-130, 2006.
38. A. Star, Y. Liu, K. Gant, L. Ridvan, J.F. Stoddart, D.W. Steuerman, M.R. Diehl, A. Boukai, J.R. Heath, *Macromolecules*, Vol. 36, p. 553, 2003.

39. S.A. Curran, P.M. Ajayan, W.J. Blau, D.L. Carroll, J.N. Coleman, A.B. Dalton, A.P. Davey, A. Drury, B. McCarthy, S. Maier, A. Strevens, *Advanced Materials*, Vol. 10, p. 1091, 1998.
40. K.L. Lu, R.M. Lago, Y.K. Chen, M.L.H. Green, P.J.F. Harris, S.C. Tsang, *Carbon*, Vol. 34, p. 814, 1996.
41. N.I. Kovtyukhova, T.E. Mallouk, L. Pan, E.C. Dickey, *Journal of American Chemical Society*, Vol. 125, p. 9761, 2003.
42. M.J. O'Connell, S.M. Bachilo, C.B. Huffman, V.C. Moore, M.S. Strano, E.H. Haroz, K.L. Rialon, P.J. Boul, W.H. Noon, C. Kittrell, J.P. Ma, R.H. Hauge, R.B. Weisman, R.E. Smalley, *Science*, Vol. 297, p. 593, 2002.
43. J.I. Paredes, M. Burghard, *Langmuir*, Vol. 20, p. 5149, 2004.
44. J. Hilding, E.A. Grulke, Z.G. Zhang, F. Lockwood, *Journal of Dispersion Science and Technology*, Vol. 24, p. 1, 2003.
45. N.G. Sahoo, Y.C. Jung, H.J. Yoo, J.W. Cho, *Macromolecular Chemistry and Physics*, Vol. 207, p. 1773, 2006.
46. H.S. Xia, M. Song, *Journal of Materials Chemistry*, Vol. 16, p. 1843, 2006.
47. X.H. Chen, X.J. Chen, M. Lin, W.B. Zhong, X.H. Chen, Z.H. Chen, *Macromolecular Chemistry and Physics*, Vol. 208, p. 964, 2007.
48. H.C. Kuan, C.C.M. Ma, W.P. Chang, S.M. Yuen, H.H. Wu, T.M. Lee, *Composites Science and Technology*, Vol. 65, p. 1703, 2005.
49. J.W. Xiong, Z. Zheng, X.M. Qin, M. Li, H.Q. Li, X.L. Wang, *Carbon*, Vol. 44, p. 2701, 2006.
50. Y.K. Yang, X.T. Wang, L. Liu, X.L. Xie, Z.F. Yang, R.K.Y. Li, Y.W. Mai, *Journal of Physical Chemistry C*, Vol. 111, p. 11231, 2007.
51. J.N. Deng, J. Cao, J.H. Li, H. Tan, Q. Zhang, Q. Fu, *Journal of Applied Polymer Science*, Vol. 108, p. 2023, 2008.
52. S. Rana, N. Karak, J.W. Cho, Y.H. Kim, *Nanotechnology*, Vol. 19, p. 495707, 2008.
53. J.Y. Kwon, H.D. Kim, *Journal of Applied Polymer Science*, Vol. 96, p. 595, 2005.
54. Q.H. Meng, J.L. Hu, S. Mondal, *Journal of Membrane Science*, Vol. 319, p. 102, 2008.
55. Q.H. Meng, J.L. Hu, Y. Zhu, *Journal of Applied Polymer Science*, Vol. 106, p. 293, 2007.
56. P. Potschke, L. Haussler, S. Pegel, R. Steinberger, G. Scholz, *KGK-Kautschuk Gummi Kunststoffe*, Vol. 60, p. 432, 2007.
57. H. Koerner, W.D. Liu, M. Alexander, P. Mirau, H. Dowty, R.A. Vaia, *Polymer*, Vol. 46, p. 4405, 2005.
58. V. Bliznyuk, S. Singamaneni, R. Kattumenu, M. Atashbar, *Applied Physics Letters*, Vol. 88, p. 164101, 2006.
59. H.J. Yoo, Y.C. Jung, N.G. Sahoo, J.W. Cho, *Journal of Macromolecular Science Part B: Physics*, Vol. 45, p. 441, 2006.
60. Y. Yan, M.B. Chan-Park, Q. Zhang, *Small*, Vol. 3, p. 24, 2007.
61. L.M. Dai, A. Patil, X.Y. Gong, Z.X. Guo, L.Q. Liu, Y. Liu, D.B. Zhu, *ChemPhysChem*, Vol. 4, p. 1150, 2003.
62. J.W. Xiong, D.S. Zhou, Z. Zheng, X.H. Yang, X.L. Wang, *Polymer*, Vol. 47, p. 1763, 2006.
63. B.T. Kelly, *Physics of Graphite*, London, Applied Science Inc., 1981.
64. J.P. Lu, *Journal of Physical Chemistry of Solids*, Vol. 58, p. 1649, 1997.

65. G. Overney, W. Zhong, D. Tomanek, *Zeitschrift fur Physik D - Atoms Molecules and Clusters*, Vol. 27, p. 93, 1993.
66. M.M.J. Treacy, T.W. Ebbesen, J.M. Gibson, *Nature*, Vol. 381, p. 678, 1996.
67. B.I. Yakobson, M.P. Campbell, C.J. Brabec, J. Bemholc, *Composite Materials Science*, Vol. 8, p. 341, 1997.
68. R. Sen, B. Zhao, D. Perea, M.E. Itkis, H. Hu, J. Love, E. Bekyarova, R.C. Haddon, *Nano Letters*, Vol. 4, p. 459, 2004.
69. X. Chen, J. Wang, J. Zou, X. Wu, X. Chen, F. Xue, *Journal of Applied Polymer Science*, Vol. 114, p. 3407, 2009.
70. J. Zhu, H.Q. Peng, F. Rodriguez-Macias, J.L. Margrave, V.N. Khabashesku, A.M. Imam, K. Lozano, E.V. Barrera, *Advanced Functional Materials*, Vol. 14, p. 643, 2004.
71. L.S. Schadler, S.C. Giannaris, P.M. Ajayan, *Applied Physics Letters*, Vol. 73, p. 3842, 1998.
72. P.M. Ajayan, L.S. Schadler, C. Giannaris, A. Rubio, *Advanced Materials*, Vol. 12, p. 750, 2000.
73. S.J.V. Frankland, A. Caglar, D.W. Brenner, M. Griebel, *Journal of Physical Chemistry B*, Vol. 106, p. 3046, 2002.
74. J.N. Deng, X.Q. Zhang, K. Wang, H. Zou, Q. Zhang, Q. Fu, *Journal of Membrane Science*, Vol. 288, p. 261, 2007.
75. C.W. Nan, Z. Shi, Y. Lin, *Chemical Physics Letters*, Vol. 375, p. 666, 2003.
76. C.W. Nan, G. Liu, Y. Lin, M. Li, *Applied Physics Letters*, Vol. 85, p. 3549, 2004.
77. S.T. Huxtable, D.G. Cahill, S. Shenogin, L.P. Xue, R. Ozisik, P. Barone, M. Usrey, M.S. Strano, G. Siddons, M. Shim, P. Keblinski, *Nature Materials*, Vol. 2, p. 731, 2003.
78. F.H. Gojny, M.H.G. Wichmann, B. Fiedler, I.A. Kinloch, W. Bauhofer, A.H. Windle, K. Schulte, *Polymer*, Vol. 47, p. 2036, 2006.
79. W. Kim, R. Wang, A. Majumdar, *Nanotoday*, Vol. 2, p. 40, 2007.
80. A. Koscielicka, *Polimery*, Vol. 30, p. 187, 1985.
81. R.N. Jana, J.W. Cho, *Journal of Applied Polymer Science*, Vol. 108, p. 2857, 2008.
82. B.M. Ginzburg, L.A. Shibaev, V.L. Ugolkov, V.P. Bulatov, *Journal of Macromolecular Science Part B: Physics*, Vol. 42, p. 139, 2003.
83. S. Mondal, J.J. Hu, *Journal of Elastomers and Plastics*, Vol. 38, p. 261, 2006.
84. S. Bourbigot, S. Duquesne, G. Fontaine, S. Bellayer, T. Turf, F. Samyn, *Molecular Crystals and Liquid Crystals*, Vol. 486, p. 1367, 2008.
85. C. J. Hilado, *Flammability Handbook for Plastics*, CRC, 1998.
86. T. Kashiwagi, E. Grulke, J. Hilding, K. Groth, R. Harris, K. Butler, J. Shields, S. Kharchenko, J. Douglas, *Polymer*, Vol. 45, p. 4227, 2004.
87. T. Kashiwagi, F.M. Du, K.I. Winey, K.M. Groth, J.R. Shields, S.P. Bellayer, H. Kim, J.F. Douglas, *Polymer*, Vol. 46, p. 471, 2005.
88. T. Kashiwagi, F.M. Du, J.F. Douglas, K.I. Winey, R.H. Harris, J.R. Shields, *Nature Materials*, Vol. 4, p. 928, 2005.
89. R.H. Baughman, A.A. Zakhidov, W.A. de Heer, *Science*, Vol. 297, p. 787, 2002.
90. P.G. Jang, K.S. Suh, M. Park, J.K. Kim, W.N. Kim, H.G. Yoon, *Journal of Applied Polymer Science*, Vol. 106, p. 110, 2007.

91. R. Zhang, A. Dowden, H. Deng, M. Baxendale, T. Peijs, *Composites Science and Technology*, Vol. 69, p. 1499, 2009.
92. S. Velankar, S.L. Cooper, *Macromolecules*, Vol. 33, p. 382, 2000.
93. S. Hayashi, N. Ishikawa, C. Giordano, *Journal of Coated Fabric*, Vol. 23, p. 74, 1993.
94. H.M. Jeong, B.K. Ahn BK, B.K. Kim, *Polymer International*, Vol. 49, p. 1714, 2000.
95. S. Mondal, J.L. Hu, *Journal of Applied Polymer Science*, Vol. 103, p. 3370, 2007.
96. H.B. Chen, D.S. Sholl, *Journal of Membrane Science*, Vol. 288, p. 261, 2007.
97. S. Kim, T.W. Pechar, E. Marand, *Desalination*, Vol. 192, p. 330, 2006.
98. A. Lendlein, S. Kelch, *Angewandte Chemie International Edition*, Vol. 41, p. 2034, 2002.
99. B.S. Lee, B.C. Chun, Y.C. Chung, K.I. Sul, J.W. Cho, *Macromolecules*, Vol. 34, p. 6431, 2001.
100. Y. Lai, E.T. Quinn, P.L. Valint, *Journal of Polymer Science Part A: Polymer Chemistry*, Vol. 33, p. 1767, 1995.
101. T. Takahashi, N. Hayashi, S. Hayashi, *Journal of Applied Polymer Science*, Vol. 60, p. 1061, 1996.
102. J.W. Cho, Y.C. Jung, Y.C. Chung, B.C. Chun, *Journal of Applied Polymer Science*, Vol. 93, p. 2410, 2004.
103. T. Takahashi, N. Hayashi, S. Hayashi, *Journal of Applied Polymer Science*, Vol. 60, p. 1061, 1996.
104. Q. Meng, J. Hu, *Composites Part A: Applied Science and Manufacturing*, Vol. 39, p. 314, 2008.
105. R.N. Jana, H.J. Yoo, J.W. Cho, *Fibers and Polymers*, Vol. 9, p. 247, 2008.
106. N.G. Sahoo, Y.C. Jung, H.J. Yoo, J.W. Cho, *Composites Science and Technology*, Vol. 67, p. 1920, 2007.
107. Q.H. Meng, J.L. Hu, L. Yeung, *Smart Materials Structure*, Vol. 16, p. 830, 2007.
108. N.S. Goo, I.H. Paik, K.J. Yoon, *Smart Materials Structure*, Vol. 16, p. 23, 2007.
109. L. Poussard, F. Burel, J.P. Couvercelle, Y. Merhi, M. Tabrizian, C. Bunel, *Biomaterials*, Vol. 25, p. 3473, 2004.
110. J.H. Wang, C.H. Yao, W.Y. Chuang, T.H. Young, *Journal of Biomedical Materials Research*, Vol. 51, p. 761, 2000.
111. J. Meng, L. Song, J. Meng, H. Kong, G.J. Zhu, C.Y. Wang, L.H. Xu, S.S. Xie, H.Y. Xu, *Journal of Biomedical Materials Research Part A*, Vol. 79, p. 298, 2006.
112. L.P. Zanello, B. Zhao, H. Hu, R.C. Haddon, *Nano Letters*, Vol. 6, p. 562, 2006.
113. M.P. Mattson, R.C. Haddon, A.M. Rao, *Journal of Molecular Neuroscience*, Vol. 14, p. 175, 2000.
114. K. Matsumoto, C. Sato, Y. Naka, A. Kitazawa, R.L. Whitby, N. Shimizu, *Journal of Bioscience and Bioengineering*, Vol. 103, p. 216, 2007.
115. Z.Z. Han, H. Kong, J. Meng, C.Y. Wang, S.S. Xie, H.Y. Xu, *IFMBE Proceedings: APCMBE 2008: 7th Asian-Pacific Conference on Medical and Biological Engineering*, Vol. 19, p. 194, 2008.

116. J. Meng, H. Kong, Han ZZ, C.Y. Wang, G.J. Zhu, S.S. Xie, H.Y. Xu, *Journal of Biomedical Materials Research Part A*, Vol. 88A, p. 105, 2009.
117. E. Zawadzak, M. Bil, J. Ryszkowska, S.N. Nazhat, J. Cho, O. Bretcanu, J.A. Roether, A.R. Boccaccini. *Biomedical Materials*, Vol. 4, p. 015008, 2009.
118. S.Q. Liu, B.P. Lin, X.D. Yang, Q.Q. Zhang, *Journal of Physical Chemistry B*, Vol. 111, p. 1182, 2007.
119. Z.F. Liu, G. Bai, Y. Huang, F.F. Li, Y.F. Ma, T.Y. Guo, X.B. He, X. Lin, H.J. Gao, Y.S. Chen, *Journal of Physical Chemistry C*, Vol. 111, p. 13696, 2007.
120. Y.L. Luo, C. Wang, Z.Q. Li, *Synthetic Metals*, Vol. 157, p. 390, 2007.
121. Z.F. Liu, G. Bai, Y. Huang, Y.F. Ma, F. Du, F.F. Li, T.Y. Guo, Y.S. Chen, *Carbon*, Vol. 45, p. 821, 2007.
122. Y.J. Kim, K.J. An, K.S. Suh, H.D. Choi, J.H. Kwon, Y.C. Chung, W.N. Kim, A.K. Lee, J.I. Choi, H.G. Yoon, *IEEE Transactions on Electromagnetic Compatibility*, Vol. 47, p. 872, 2005.
123. R. Verdejo, G. Jell, L. Safinia, A. Bismarck, M.M. Stevens, M.S.P. Shaffer, *Journal of Biomedical Materials Research Part A*, Vol. 88A, p. 65, 2009.

Properties of PMMA/Carbon Nanotubes Nanocomposites

R.B. Mathur, Shailaja Pande and B.P. Singh

*Carbon Technology Unit, Division of Engineering Materials,
National Physical Laboratory (CSIR), New-Delhi-110012, India*

Abstract

Carbon nanotubes (CNT) – polymer composites have been the focus of immense interest in recent years. Carbon nanotubes possess novel material properties which make them ideal filler for reinforcing polymer matrices to obtain light-weight advanced nanocomposites with high mechanical, electrical, thermal and multi-functional properties. Amongst the various polymers, polymethylmethacrylate (PMMA) has been extensively investigated as the matrix material to develop nanocomposites for both structural and electrical applications. This chapter provides a comprehensive review of the recent studies conducted on CNT-PMMA nanocomposites. Various composite processing methods for fabricating CNT-PMMA composites have been described particularly solvent casting, melt-mixing and *in-situ* polymerization. The mechanical, electrical and thermal properties of the resulting composites have been discussed. Finally, challenges associated with the processing and applications of CNT-PMMA nanocomposites and some novel techniques to improve upon the existing methods have been proposed.

Keywords: carbon nanotubes, PMMA, dispersion, interface, composites, strength, electrical conductivity, EMI shielding.

7.1 Introduction

Polymer composites consisting of polymers reinforced with various additives such as carbon fibers, graphite fibers, glass fibers, or Kevlar fibers and carbon black are increasingly being used in

defense, aerospace, automobile, sports and electronics sectors as light-weight, high strength and high electrical and thermal conducting materials (1–6). In recent years, nanocomposites, in which the reinforcing additive has nanoscale dimensions have attracted both scientific and technological interest to meet the growing demand for materials with improved properties and challenging applications (7,8). Carbon nanotubes (CNT) have particularly led the research in the development of advanced polymer nanocomposites due to their unique material properties that comprises of extraordinarily high mechanical, electrical and thermal properties (9–11). They have been shown to possess extremely high elastic modulus $> 1\text{TPa}$ and strength ranging from 63 GPa to 600 GPa which is many times higher than the steel at a fraction of its weight (high strength to weight ratio) (12–15). In addition to this, these tubes possess electrical current-carrying capacity which is 1000 times higher than copper wires, thermal conductivity about twice as high as diamond and thermal stability up to 2800°C in vacuum or inert atmosphere (16). Carbon nanotubes, both single-walled carbon nanotubes (SWCNT) with diameters 1–2 nm and multi-walled carbon nanotubes (MWCNT) with diameters 10–100 nm, have very high aspect ratio and therefore very large surface area (12,13,17). This suggests that small amounts of CNT can significantly change the properties of polymer in terms of imparting strength and conductivity to a composite system (18).

The most promising and challenging areas of carbon nanotube based nanocomposites research is the development of light-weight, high-strength structural composites. In recent years, many studies have been carried out towards the enhancement of mechanical properties of CNT-polymer composites (12,16,19,20). Different polymers, both thermoplastics [PMMA (polymethylmethacrylate) (21–28), polystyrene (29–31), polycarbonate and polypropylene (12)] and thermosets [phenolic (32), polyimide (16,33) and epoxy (34–38)] have been investigated as matrices to make CNT-reinforced polymer composites. However, unlike conventional polymer composites such as carbon fibre-reinforced polymer composites, the bulk mechanical properties of CNT-polymer composites are significantly lower than that predicted by theory. The studies have led to identify two important challenges, a homogeneous dispersion of CNTs within the polymer matrix and strong interfacial adhesion between CNTs and polymer matrix to translate the unique nanoscale properties of CNTs into the macroscale properties of polymer composites (39,40).

The use of CNTs as a conductive additive for plastics in the electronic, automotive and aerospace sectors with potential uses as electromagnetic interference (EMI) shielding materials, coatings for enclosures, electrostatic discharge (ESD) and antistatic materials, conductive coatings, etc. is also emerging as a major application area (8,13,17). Compared to conventional metal-based EMI shielding materials, carbon-based conducting polymer composites are becoming attractive due to their light-weight, resistance to corrosion, flexibility and comparative ease of processability. Amongst the carbon fillers (e.g. graphite, carbon black, or carbon fibers) carbon black is commonly used as conducting filler in polymer composites (15,17). In using carbon black as filler, a major disadvantage is the high amount of carbon black that is required up to 30–40% to achieve desired conductivity levels, which results in deterioration in the mechanical properties of the polymer. A major advantage of using CNTs over carbon black is that conductive composites can be formed at low loading of CNTs due to low percolation thresholds (the point at which a long continuous chain of conducting particles first appears) resulting from higher intrinsic conductivity and higher aspect ratio of CNTs (17). High mechanical strength and lower loading levels of CNTs also show promise for developing effective, light-weight and mechanically strong EMI shielding materials (13). Several studies have been reported on the electrical and EMI shielding properties of CNT-polymer composites (21,22,24,30,37,38,41–50).

The chapter focuses on the studies that have been carried out on the processing and properties of CNT-PMMA composites. The various composite fabrication methods used by different researchers have been described followed by a discussion of the mechanical, electrical and thermal properties of CNT-PMMA composites. The key issues of CNT dispersion and interfacial adhesion between CNT and polymer matrix that are essential to develop these advanced composites have also been discussed. Some new ideas in this direction have also been proposed.

7.2 Fabrication/Processing of CNT-PMMA Composites

PMMA is an interesting polymer which is widely used in architecture, railway, aerospace, automobile and biomedical sectors due to its good mechanical and optical properties (1,51). The low cost,

ease of availability and processability makes PMMA an interesting material of choice to develop CNT-PMMA composites with improved mechanical properties and to also develop conductivity in an otherwise non-conducting matrix for newer applications such as ESD and EMI shielding materials. Most of the studies on CNT-PMMA composites have used the conventional polymer processing methods available in the plastic industry.

As-synthesized MWCNT and SWCNT exist as bundles or ropes and tend to agglomerate due to strong van der Waals forces (13) (Figure 7.1). Unless the CNTs are separated in to individual tubes and dispersed in the polymer matrix, the interactions of the nanotubes with the polymer will be weak. The mechanical failure of such composites will occur due to slippage of the tubes in the bundle that are not bonded to the matrix. In addition, the aggregates or bundles reduce the aspect ratio of the reinforcement which affects electrical properties as well (15). Because of these factors the first step will be to open up these bundles to separate individual tubes by using different techniques to increase the volume of interface between the CNT and the matrix (40).

A second important criterion to effectively exploit properties of CNTs in composites is a strong interfacial bonding (physical or chemical bonds) with the polymer matrix (12,15,40). This is

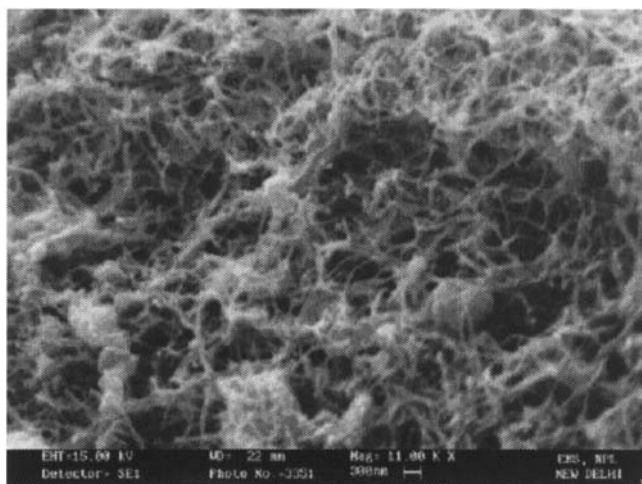


Figure 7.1. SEM image of as-synthesized MWCNT. Reprinted with permission from John Wiley & Sons, Inc (25).

crucial for load transfer to the CNTs across the CNT-matrix interface and enhanced interfacial shear strength. Since CNTs have a relatively smooth surface, various surface modification methods are employed to increase the wetting between the CNT and the polymer matrix by using surfactants, compatibilizers or chemical treatments (12,19 40,52). These functional groups may differ for different polymer systems. The chemical treatment of CNT surface generally involves oxidation in air /oxygen or using strong inorganic acids. Generally, carboxylic acid and hydroxyl groups are formed on the surface or open ends of CNTs during oxidation process by air, oxygen, concentrated nitric acid and concentrated sulphuric acid and their mixture (40). The advantage with acid treatments is not only to introduce functional groups and provide active sites for further chemical functionalization but also to disentangle and shorten the nanotubes and to remove undesirable side-products such as amorphous carbon, graphitic nanoparticles and metal catalyst co-produced along with CNTs. This improves the processability of CNTs through improved dispersion and better chemical interactions with the polymer matrix and efficient load transfer to the nanotubes. However extensive chemical treatment of CNTs may be detrimental to the final composite properties since it may introduce defects in the CNT structure and also significantly shorten its length.

CNT-PMMA composite processing methods may broadly fall under the following four categories:

- solution based methods such as solvent casting, drop casting and spin casting
- melt-processing such as melt blending, shear mixing
- *in-situ* polymerization
- coagulation method

7.2.1 Solution Processing

In solvent casting or solution mixing, CNTs are first dispersed in a suitable solvent and then mixed with a polymer solution to obtain a suspension of nanotubes in the polymer. The mix is then poured into suitable die molds and the solvent is allowed to evaporate to leave behind nanocomposite film. Solution based methods offer advantages of lower viscosities which facilitate uniform mixing and dispersion. Ultrasonication or magnetic stirring is typically used to separate and disperse CNTs uniformly in different solvents or

polymer systems (12,13). Deagglomeration of the CNTs in a solvent can also be carried out using high shear processors e.g. in a microfluidizer (Microfluidics, USA). The solvent used for CNT dispersion may be same as that used to prepare PMMA solution or it may be a different solvent than used for PMMA (24). Polymethylmethacrylate is polar and hydrophobic in nature and is soluble in common organic solvents such as chloroform, toluene, DMF etc. Mathur et al. (24) used solvent casting technique to prepare MWCNT-PMMA composite films with different concentrations (0.1 to 10 vol. %) of MWCNT. While PMMA was dissolved in chloroform, nanotubes were dispersed in toluene by ultrasonication. After mixing the two the suspension was again ultrasonicated and cast into MWCNT-PMMA composite film. The scanning electron microscopy (SEM) image of the composite film shows a homogeneous dispersion of CNTs in PMMA (Figure 7.2) with no aggregation of nanotubes even with 10% loading which suggests that ultrasonication is quite useful in dispersion of the tubes in PMMA. The composites showed enhanced electrical properties though little improvement in tensile strength was observed. Even higher loading levels up to 40 wt% of CNT have been achieved by Kim et al. (42) and the resulting composite films particularly those prepared from raw MWCNT showed high electrical conductivity and EMI shielding properties.



Figure 7.2. SEM of 10 vol. % MWCNT-PMMA composite film showing MWCNT dispersion in PMMA. Reprinted with permission from Springer Science and Business Media (44).

Dispersion characteristics of CNTs in PMMA could vary with the type of solvent, e.g. nitromethane, the most polar amongst the other solvents has been found to be most effective for dispersion of SWCNT in PMMA cast films (53).

Solvent evaporation during casting is however, a slow process and in some studies it has been found to cause CNT agglomeration (21). Spin casting and drop casting are two techniques that reduce solvent evaporation time and minimize re-aggregation of CNTs (15). In spin casting, CNT/PMMA suspension is poured on a rotating substrate and solvent evaporates within seconds. In drop casting, the suspension is dropped on a hot substrate so that solvent evaporates quickly.

Benoit et al. (41) obtained electrically conductive nanocomposites by dispersing SWCNT and PMMA in toluene, followed by drop casting the mixture on substrates. Thin films of SWCNT-PMMA composites for different CNT concentration were produced by spin casting by Chapelle et al. (54) and Stephan et al. (55). They characterized these nanocomposites by Raman spectroscopy to study interactions between nanotubes and PMMA and found that PMMA tends to intercalate between the CNTs thereby increasing the distance between the nanotubes in the film.

7.2.2 Melt-Processing

Melt-processing is a simple and industrially used solvent-free technique especially for thermoplastic polymeric materials (12,13). In this method, solid polymer is first melted into a viscous liquid before adding CNTs. This is followed by shear mixing of the blend resulting into dispersion of CNTs in the polymer (56). Generally twin-screw extruders are used to produce high shear forces that help in dispersion. After mixing, composites can be fabricated by compression molding, extrusion etc. In fact, melt-blending is a commonly used method to prepare CNT-polymer composite fibres with aligned nanotubes (28,56). Nanotube damage by shear forces needs to be analysed before using it as a fabrication technique. Melt-processing requires proper optimization of the processing conditions such as extruder temperature, screw speed and residence time (28). The processing can be carried out on available systems e.g. laboratory mixing molder (Atlas USA), high shear mixer cum twin screw extruder (Haake, Germany; DACA Instruments, Goleta, CA), and also by calendering approach with pure shearing in commercial roll mill (Exakt 80E, Exakt Technologies Inc.).

Jin et al. (26) used melt blending to fabricate MWCNT-PMMA composites with different CNT loadings varying from 0 to 26 wt%. They used a laboratory mixing molder to disperse MWCNT in PMMA at 200°C followed by compression molding at 210°C. Their TEM studies revealed good dispersion even at high MWCNT concentration. The composites showed enhanced mechanical and thermal properties.

Gorga et al. (28) performed studies on the effect of melt-processing conditions on the dispersion of SWCNT in PMMA and determined the optimum extrusion conditions for nanotube dispersion. No apparent PMMA degradation or damage to the nanotubes during extrusion was observed and the counter-rotating twin-screw extruder was found to be most effective in dispersing SWCNT. In their subsequent studies, the authors dispersed different amounts of MWCNT in PMMA at 230°C for 10 mins at 100 rpm using counter-rotating screw configuration followed by extrusion through a cylindrical die to obtain as-extruded composites. Aligned composites were further obtained by melt-drawing the extruded rods. Mechanical properties such as tensile strength, modulus and toughness of the resulting MWCNT-PMMA nanocomposites were improved.

Combination of solvent casting followed by compression molding is also one of the approaches to fabricate CNT-PMMA composites (21,24,57). Slobodian et al. (57) fabricated MWCNT-PMMA composites by this technique and studied electrical conductivity of composites obtained after two-time compression molding. Different percolation thresholds were found for different solvent systems. Mathur et al. (24) also reported improvement in the mechanical properties of the CNT-PMMA composite over the one prepared by simple solvent casting. The reason attributed is the removal of any solvent trapped in the cast films.

A more rigorous process of multi-step melt mixing followed by Haggenmueller et al. (21) shows each subsequent melt mixing step improved quality of dispersion as exhibited in the optical micrographs obtained after different melt-mixing cycles (Figure 7.3). The as-cast composite films were broken into pieces, stacked together between two polished metal plates and hot pressed at 180°C and 3000 lb for 3 min. This melt mixing procedure was repeated as many as 25 times. The superior quality films obtained after using the combined methods of solvent casting and melt-mixing showed high electrical conductivity and were subsequently extruded through a cylindrical die and drawn under tension to form composite fibers that exhibited high mechanical properties.

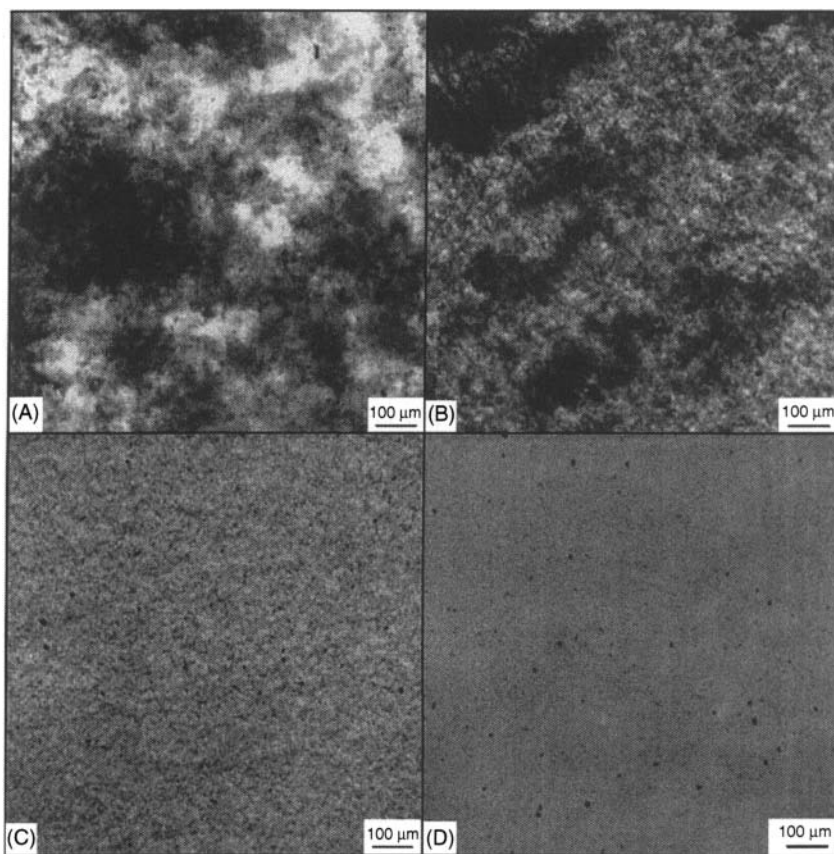


Figure 7.3. Optical micrographs of SWCNT-PMMA nanocomposite having 1 wt% purified soot: (a) as-cast film (b) after 1 cycle; (c) after 5 cycles; (d) after 20 cycles. Reprinted with permission from Elsevier (21).

7.2.3 *In-Situ* Polymerization Processing

In-situ polymerization methods have been used to fabricate CNT-PMMA composites by incorporating CNTs during the course of polymerization of MMA to improve dispersion and integration between the two phases (12,13). The basic starting materials for *in-situ* polymerization are nanotubes and MMA monomer. *In-situ* free radical polymerization method involves polymerization of the monomer using a radical initiator such as 2,2'-azobisisobutyronitrile (AIBN). Generally polymerization is carried out up to a prepolymer stage before adding CNTs. The CNTs are dispersed

through ultrasonication in the prepolymer. Adding CNTs at this stage ensures good dispersion in the low viscosity of the prepolymer. As the polymerization progresses in the presence of dispersed CNTs the viscosity of the solution increases and the polymer grows and wraps around the dispersed CNTs (Figure 7.4 a, b) (23). *In-situ* methods can achieve higher interfacial strengths since CNTs interact with the growing polymer and can therefore form stronger CNT-polymer bonds via non-covalent or covalent interactions (12,58). Composites with enhanced mechanical, electrical and tribological properties were obtained (18,23,25,27,59).

Park et al. (60) studied dispersion characteristics of MWCNT-PMMA composites synthesized by *in-situ* bulk polymerization using AIBN as free radical initiator. In their method, CNTs in varying amounts such as 0.001, 0.01 and 0.1 wt% with respect to MMA were first dispersed in MMA monomer by ultrasonication before polymerization. Experimental evidence such as molecular weight of free PMMA prepared via *in-situ* polymerization with and without CNTs, diameter of pristine MWCNT and diameter of MWCNT in composite, FTIR and SEM studies confirmed the role of AIBN and MWCNT in polymerization. The induced radicals on MWCNT by AIBN were found to trigger grafting of PMMA on to CNT surface. Solvent cast film of the composite was transparent and showed a better nanoscopic dispersion without aggregates compared to the cast film prepared from direct mixing of MWCNT and PMMA.

Shang et al. (61) used microemulsion polymerization to synthesize MWCNT-PMMA composites for gas sensor applications. Better dispersion, enhanced electrical conductivity and better sensor response was observed for *in-situ* fabricated composites compared to composites prepared by solution mixing. Ma et al. (62) performed *in-situ* polymerization of MWCNT-PMMA composites in the presence of an AC electric field to study dispersion and alignment of MWCNT in PMMA matrix induced by the electric field. Experimental evidences from *in-situ* optical microscopy, Raman spectroscopy, SEM and electrical conductivity showed that both dispersion and alignment qualities were significantly enhanced for oxidized MWCNT compared to pristine MWCNT.

7.2.4 Coagulation Method

Coagulation method can be used to fabricate SWCNT-PMMA composites with uniform dispersion (15,22,63,64). First a well-dispersed

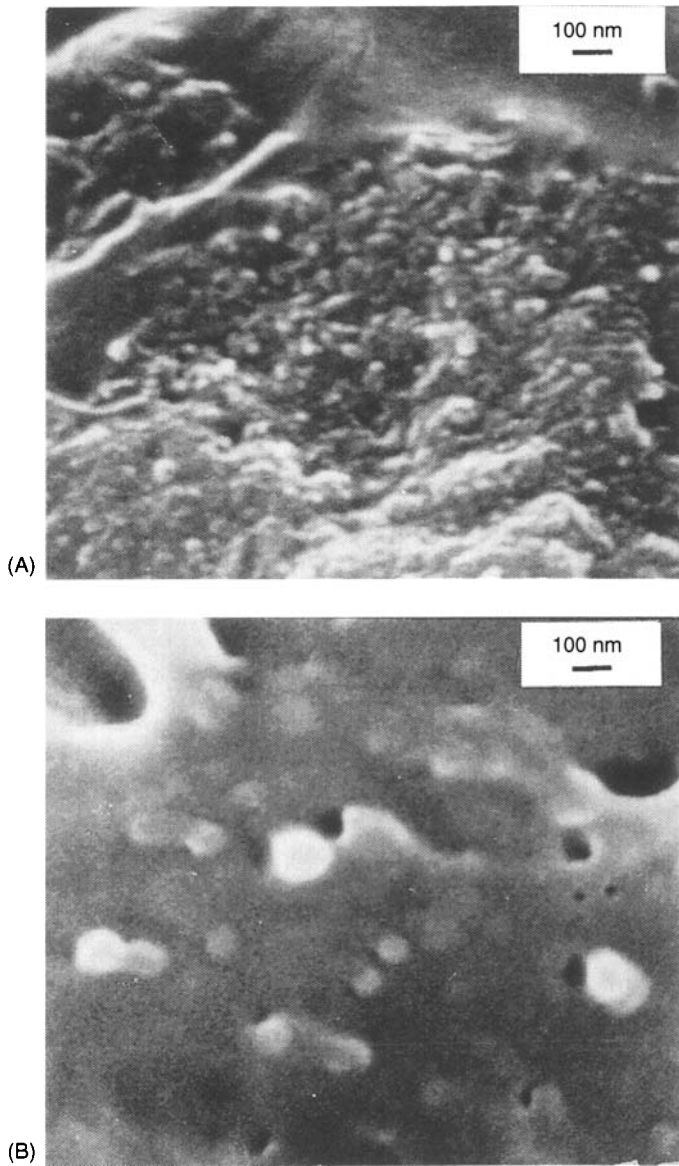


Figure 7.4. Microstructure of the *in-situ* fabricated MWCNT-PMMA composite (a) using untreated tubes, (b) treated tubes and improved *in-situ* process. The bright masses are CNTs wrapped with PMMA layers. Reprinted with permission from Elsevier (23).

CNT/PMMA suspension in DMF is obtained by sonication. The suspension is poured into an excess of non-solvent e.g. distilled water. The polymer rapidly precipitates in the non-solvent simultaneously entrapping the nanotubes giving apparently no time for CNT re-aggregation. Optical and SEM micrographs show no obvious aggregates indicating a uniform dispersion of CNTs within the PMMA matrix (22). The technique is useful for drawing aligned CNT-PMMA composite fibres with improved mechanical properties. According to Du et al. (22), this technique is superior to the multi-step melt-mixing technique.

7.2.5 Surfactant, Compatibilizers and Co-Solvent Assisted CNT-PMMA Composites

In the majority of the methods discussed above, CNTs are directly mixed with PMMA using ultrasonication or shear forces. Another approach which has been studied to improve quality of dispersion of CNTs in PMMA is third component assisted dispersion of CNTs (65–67). In this method, a third component such as a surfactant or a compatibilizer is added to assist the dispersion of CNTs in a solvent before mixing with the polymer solution (40). This is an effective non-covalent functionalization technique.

Jin et al. (65) used poly(vinylidene fluoride) (PVDF) as a compatibilizer to assist dispersion of CNTs in PMMA. Multi-walled carbon nanotubes were first coated with PVDF and then melt-blended with PMMA. Poly(vinylidene fluoride) served as an adhesive to improve wetting of CNTs by PMMA and to increase the interfacial adhesion resulting in improved mechanical properties of MWCNT-PMMA composites.

Kim et al. (66) used poly(3-hexylthiophene) (P3HT)-graft-PMMA as a compatibilizer to prepare MWCNT-PMMA composites by solution blending. The CNT content was varied from 0.01 to 0.1 wt%. The resulting composites showed improved tensile strength and modulus.

Chen et al. (67) reported the use of trifluoroacetic acid (TFA) as a co-solvent with tetrahydrofuran (THF) to improve dispersion and processability of the nanocomposites. They prepared MWCNT-PMMA composite films with varying CNT content by solvent casting method using 10 vol % TFA as a co-solvent with tetrahydrofuran (THF). SEM and optical microscopy revealed a good dispersion of nanotubes in solvent and PMMA. The composites showed low percolation

thresholds of electrical conductivity. Using a conjugated polymer poly(3-hexylthiophene) (P3HT) (0.5 wt% with respect to PMMA) they fabricated a ternary composite of MWCNT-P3HT-PMMA in the presence of TFA which also served as a doping agent for P3HT. The resulting composite films showed enhanced conductivity compared to the binary composite MWCNT-PMMA. After material processing, TFA being high volatile solvent could be evaporated leaving no or minimum additives in the composites. The X-ray photoelectron spectra of MWCNT treated with TFA revealed that chemical structure of TFA-treated nanotubes remained intact without oxidation and TFA effectively purified the carbon nanotubes by dissolving out the impurities like carbonaceous particles and metal catalysts.

7.2.6 Chemical Modification of CNTs for Processing of Nanocomposites

A number of studies on CNT-polymer composites have focused on improving the dispersion and load transfer efficiency in other words the compatibility between the CNTs and polymer matrix through covalent chemical functionalization of CNT surface (12,40). Many of the studies reported above have used acid-functionalized CNTs to fabricate MWCNT-PMMA composites with improved mechanical properties using different processing methods (24,25,27,62). Yang et. al (68) modified the acid functionalized CNTs with octadecylamine (ODA) to obtain ODA-functionalized CNTs. These CNTs were reinforced in a copolymer P(MMA-co-EMA) to form composites with improved dispersion and mechanical properties.

Hwang et al. (69) studied grafting reactions of PMMA polymer chains onto MWCNT and used PMMA-grafted MWCNT to reinforce commercial PMMA. In their work, PMMA was first grafted to MWCNT via emulsion polymerization of MMA monomers in the presence of MWCNTs in micelles. Then PMMA/PMMA-grafted MWCNTs composites were prepared by solvent casting method by using various amounts of commercial PMMA and PMMA-grafted MWCNT using chloroform as the solvent. The weight percents of PMMA-grafted MWCNT added into the composites varied from 0 to 20%. The dynamic mechanical properties of the composites were significantly enhanced.

A new approach has been adopted by Yuen et al. (70) wherein they prepared silane-modified MWCNT-PMMA composites by bonding MWCNTs modified with 3-isocyanato-propyltriethoxysilane

(IPTES) (Si-MWCNT) with crosslinkable PMMA prepared from MMA monomer and vinyltriethoxysilane (VTES) (PMMA-VTES). The resulting Si-MWCNT/PMMA-VTES composites showed enhanced thermal conductivity and thermal stability.

Although the approach of covalent functionalization of CNT surface is an effective means to obtain a homogeneous dispersion of CNTs in polymer matrix and a strong interfacial interaction with the polymer, it inevitably destroys the intrinsic properties of CNTs such as the unique π -electron system of pristine CNTs is affected due to formation of covalent bonds and shortening of length of CNTs during chemical treatments (70).

7.3 Mechanical Properties of CNT-PMMA Composites

The unique structure of carbon nanotubes, low density and exceptional mechanical properties make CNTs the ultimate filler material for mechanical reinforcement in composites. Their tensile strength is an order of magnitude higher than current high strength carbon fibers and their moduli are superior to all carbon fibers. Their density (1.3–1.5 g/cc) is also lower than the density of commercial carbon fibers (1.8–1.9 g/cc) (12,13). These properties of CNTs combined with their high surface area compared to carbon fibers suggests that substituting commercial carbon fibers with CNTs will result in significant weight reduction for structural composites used in aerospace, sporting goods and other high-performance applications. Currently about 50–70 vol% carbon fiber is used as reinforcement in composite materials.

The previous sections described mainly the processing methods of CNT-PMMA composites. Important properties such as tensile strength, elastic modulus, fracture toughness, flexural strength, flexural modulus, storage modulus etc. have been shown to be improved in several of these studies. Figure 7.5 and Figure 7.6 respectively show the plots for the strength and modulus of composites as a function of CNT loading. In almost all the studies, the value of the modulus increases with CNT concentration in the PMMA matrix. However, the strength values do not show consistent improvement with increasing amount of CNTs. There is either no improvement in strength or only a moderate improvement especially for untreated randomly oriented CNT composites. The composites based on surface modified tubes as reinforcement, however,

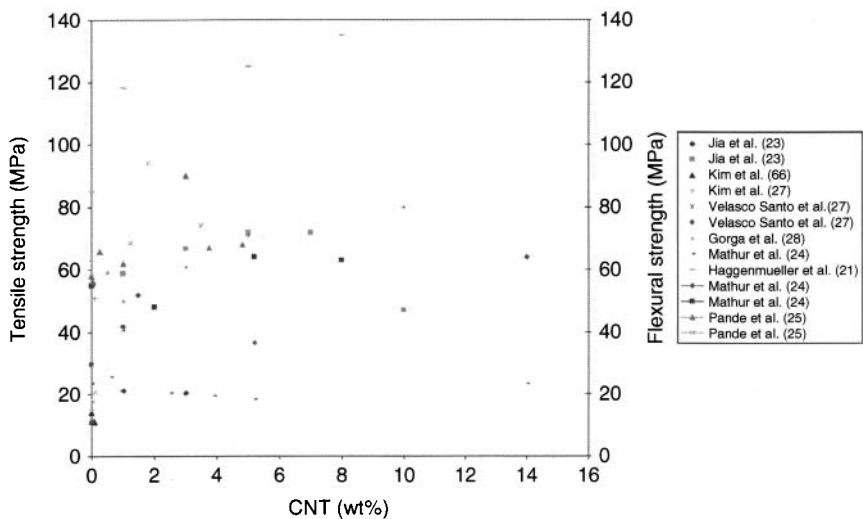


Figure 7.5. Variation in strength of CNT-PMMA composites with different CNT loadings. Two results from same author represents composites prepared by improved techniques. (Horizontal lines shown in the legend represent secondary Y-axis).

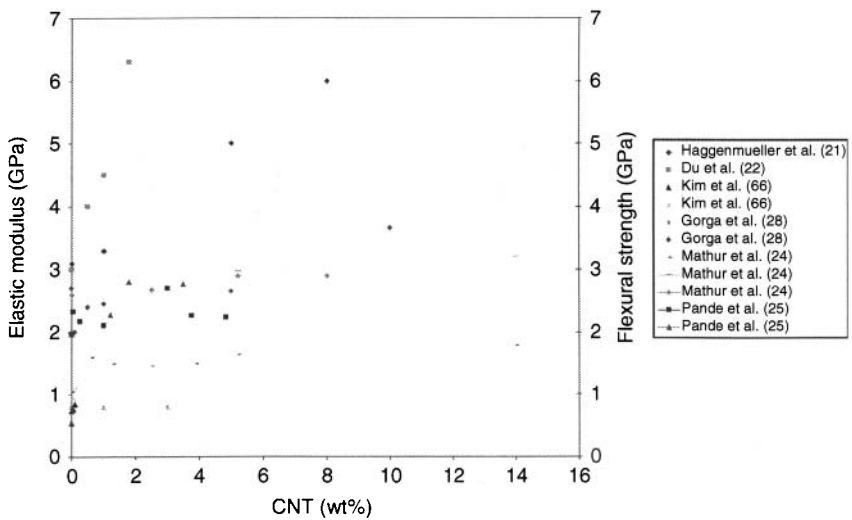


Figure 7.6. Variation in modulus of CNT-PMMA composites with different CNT loadings. Two results from same author represents composites prepared by improved techniques. (Horizontal lines shown in the legend represent secondary Y-axis).

show better properties. A significant improvement in the tensile strength could be achieved for aligned CNT reinforced composite fibres (21). However, there is no study which could co-relate the improved CNT-polymer fibre properties into bulk aligned composites. The SEM, TEM, optical microscopy, FTIR spectroscopy, Raman spectroscopy, TGA etc. have been used to obtain useful information regarding dispersion, interfacial interactions and reinforcement mechanisms such as load transfer between CNTs and PMMA which influence the mechanical properties of nanocomposites.

Haggenmueller et al. (21) found that the elastic modulus of SWCNT-PMMA composite fibres increased from 3.1 GPa for pure PMMA to 6 GPa (8 wt% SWCNT) for composite fibre. The yield strength of fibres increased with draw ratio (Figure 7.7). Significant increase in elastic modulus was reported by Du et al. (22) for SWCNT-PMMA composite fibres where the modulus of fibres (6.3 GPa) at 2 wt% loading was about 90% higher than pure PMMA. Gorga et al. (28) have shown statistically significant increase in modulus and strength only at 10 wt% MWCNT loading in aligned composite fibres wherein the modulus and yield strength increased from about 2.7 to 3.7 GPa (38% increase) and about 64 MPa to 80 MPa

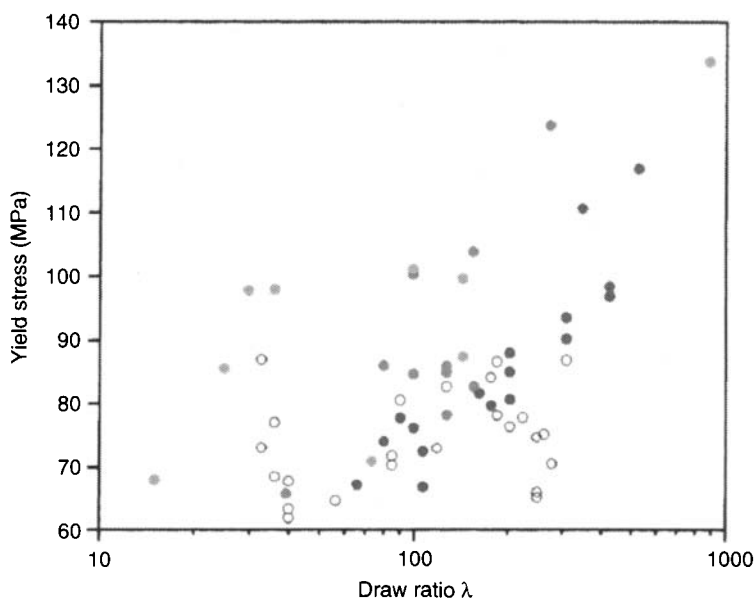


Figure 7.7. Yield stress vs draw ratio ' λ ' for SWCNT-PMMA melt spun fibers containing 0 wt% (white), 1 wt% (blue), 5 wt% (red), or 8 wt% (green) of purified soot, Reprinted with permission from Elsevier (21).

(25% increase) respectively. They also observed that the alignment of MWCNT in PMMA was the only way to toughen the nanocomposite. A loading of only 1wt% CNT in oriented composites resulted in 170% increase in toughness over oriented PMMA.

In their studies on the development of MWCNT-PMMA composite films with random orientation of MWCNT, Mathur et al. (24) found that the tensile strength of composite films showed marginal improvement in properties over neat PMMA. Tensile strength increased by 9% from 23.5 MPa in the pure polymer to 25.6 MPa at 0.5 vol% loading. The strength, however, did not improve further even at 10 vol% loading. Tensile modulus on the other hand improved by 70% from 1.04 GPa in neat PMMA to 1.78 GPa in 10 vol% MWCNT-PMMA composite. The SEM of the cross-section of the fractured surface of composite film after tensile test shows that CNTs are well-dispersed in the PMMA matrix (Figure 7.8a). Failure of the CNT-matrix interface indicates weak bonding between the matrix and CNTs which leads to poor load transfer to the CNTs resulting in separation between the surfaces of polymer and nanotube. The image shows CNT pull-outs and also matrix crack bridging. By using the two-step method i.e. solvent casting followed by compression molding they found an improvement in mechanical properties even at high CNT concentration. The flexural strength of 10 vol% MWCNT-PMMA composite using as-synthesized MWCNT (a-MWCNT) was about 64 MPa which was 16% higher than pure PMMA (21, 44). The SEM of the fractured surface of the bulk composite shows a homogeneous dispersion and a stronger CNT-matrix interaction (Figure 7.8b). By using functionalized nanotubes (f-MWCNT) a flexural strength value of 64 MPa was obtained at only 5 vol% CNT loading as compared to only 35 MPa for a-MWCNT-PMMA composite at this loading.

Jia et al. (23) observed that using treated (functionalized and ball milled) CNTs and an improved *in-situ* polymerization method, the strength of MWCNT-PMMA composites increased from 55 to 72 MPa at 5–7 wt% CNT loading. This was also accompanied by improvements in fracture toughness and hardness. Following FTIR studies it was concluded that this improvement in the properties was due to formation of covalent bonds between CNT and polymer matrix. They showed that the CNTs could be initiated by AIBN to open their π -bonds and therefore participate in PMMA polymerization to form a strong interface between CNTs and the matrix. The SEM images of fractured surfaces of composites prepared by improved *in-situ* polymerization method reveal a good dispersion and thicker PMMA layers wrapping the CNTs (Figure 7.4a,b).

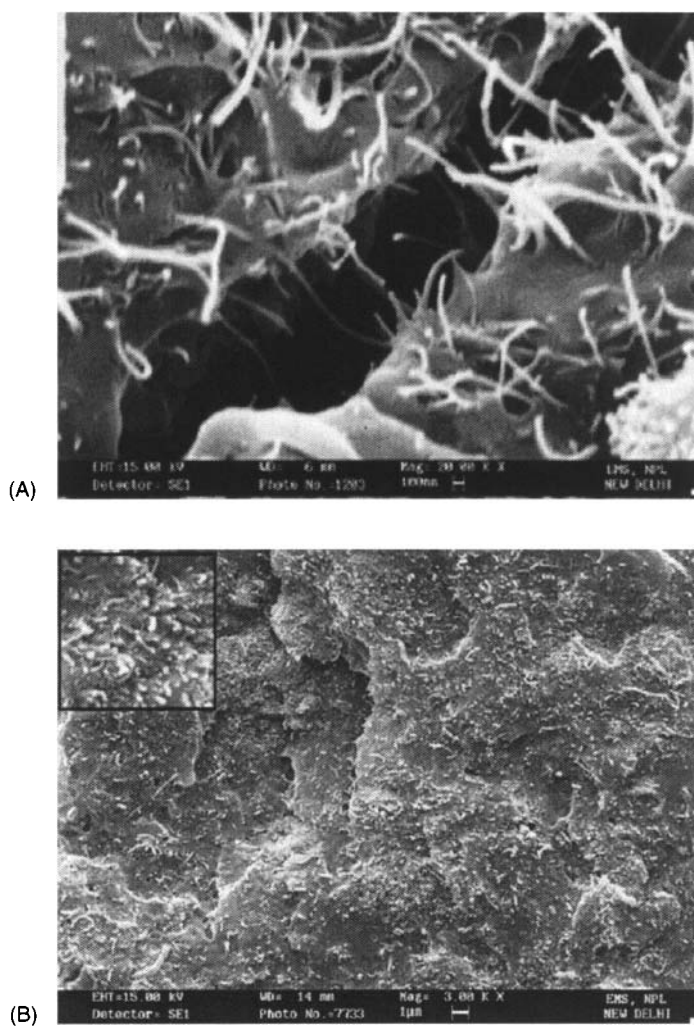


Figure 7.8. Fracture surface of 10 vol% MWCNT-PMMA (a) as-cast film. Reprinted with permission from John Wiley & Sons, Inc (24), (b) bulk Composite. Reprinted with permission from Springer Science and Business Media (44).

Pande et al. (25) also reported significant improvements in the flexural properties of MWCNT-PMMA composites prepared by *in-situ* polymerization method. They observed a maximum reinforcing effect of CNTs at 3 wt% for a-MWCNT and at 1.8 wt% for f-MWCNT. The flexural strength for the two cases was about 90 MPa as compared to about 64 MPa from two step method

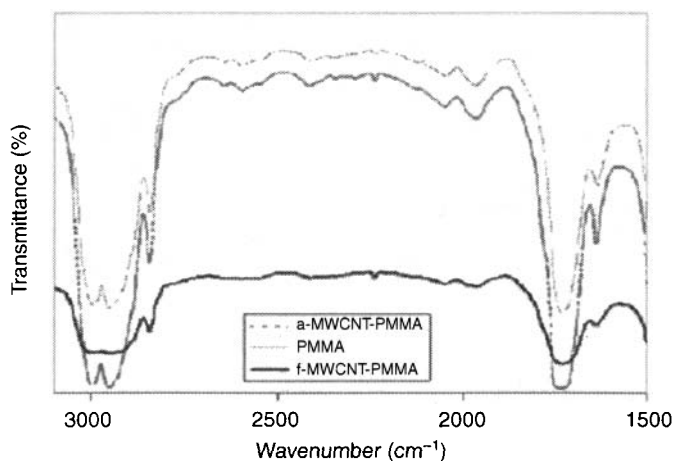


Figure 7.9. FTIR spectra of MWCNT-PMMA composites. Reprinted with permission from John Wiley & Sons, Inc (25).

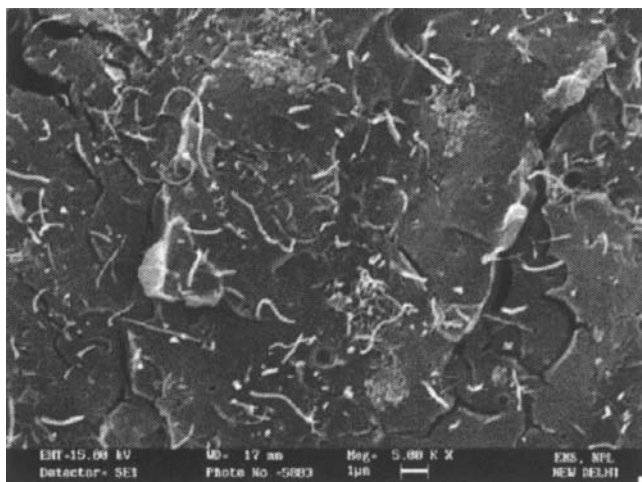


Figure 7.10. Microstructure of the 3.0 wt% *in-situ* fabricated a-MWCNT-PMMA composite. Reprinted with permission from John Wiley & Sons, Inc (25).

discussed earlier. The FTIR studies revealed hydrogen-bonding interactions between acid-functionalized CNTs and PMMA (Figure 7.9). The SEM studies also confirmed a stronger CNT-polymer matrix interface in the f-MWCNT-PMMA composites (Figure 7.10, Figure 7.11).

Tensile mechanical properties of MWCNT-PMMA composites were shown to be improved by using P3HT-g-PMMA as a

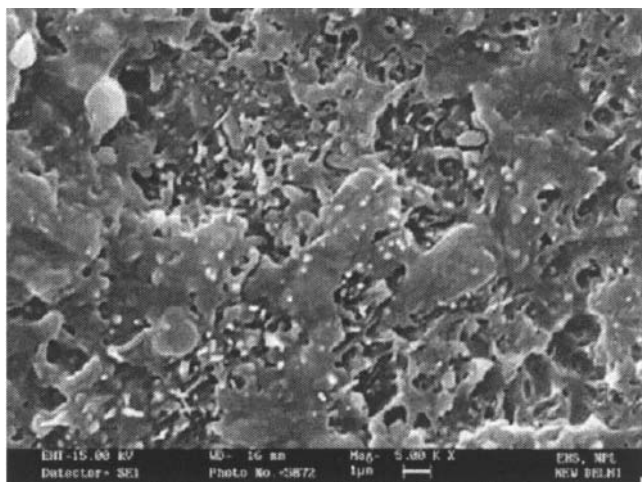


Figure 7.11. Microstructure of the 1.8 wt% f-MWCNT-PMMA composite. Reprinted with permission from John Wiley & Sons, Inc (25).

compatibilizer (66). By incorporating 0.1 wt% MWCNT in PMMA in the presence of compatibilizer tensile strength increased from 11.3 ± 0.8 MPa in neat PMMA to 21 ± 0.6 in PMMA/MWCNT/P3HT-g-PMMA composite. Young's modulus increased from 541 ± 16 MPa to 1104 ± 17 MPa. Fluorescence emission and Raman spectra of composites revealed interactions of compatibilizer with CNT surface through π - π interactions. The strong π - π interactions between MWCNT and P3HT-g-PMMA and the miscibility of compatibilizer in PMMA result in a homogeneous dispersion of MWCNT and a good interfacial adhesion.

In some studies dynamic mechanical behavior of CNT-PMMA composites has been investigated to assess the mechanical properties (26,27,65,69). Jin et al. (26) found that the storage modulus of MWCNT-PMMA composites increased with CNT loading particularly at high temperature due to stiffening effect of CNTs. The modulus increased by a factor of 1.6–2.0 at 40°C whereas it showed a 5–27 fold increase at 120°C. The $\tan \delta$ and glass transition temperature also increased by incorporation of CNT suggesting that nanotubes delay the onset of thermal degradation of the polymer. In another study using PVDF as a compatibilizer they found that the storage modulus of composite containing 0.5 wt% PVDF was almost twice as that of MWCNT-PMMA without PVDF at 50 °C (65).

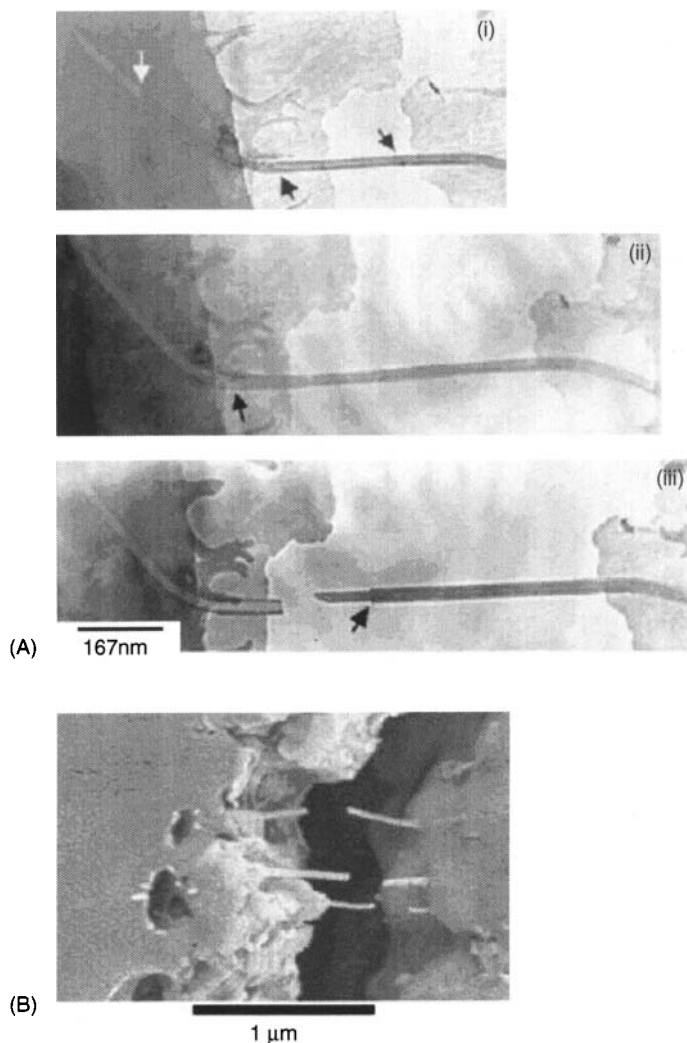


Figure 7.12. (a) TEM images of a MWCNT-containing PMMA thin film taken at different times (i) $t = 0$, (ii) $t = 4$, and (iii) $t = 10$ min and (b) SEM image of the g-MWCNT-PMMA composite. Reprinted with permission from Wiley VCH (69).

Velasco Santos et al. (27) measured both the dynamic mechanical behavior and tensile mechanical properties of MWCNT-PMMA composites. They observed 1135% increase in storage modulus at 90°C and increase in glass transition temperature by 40°C over neat PMMA with only 1 wt% functionalized nanotubes. The tensile

strength increased from 30 MPa for pure PMMA to about 50 MPa using 1.5 wt% functionalized CNTs which was also accompanied by increased elastic modulus and toughness. They demonstrated by the use of IR and Raman spectra the presence of chemical interactions between acid functionalized CNTs and PMMA through -COOH and -COO- groups on CNT surface, which improve effectively the mechanical load transfer from the matrix to the CNTs.

Hwang et al. (69) reported for the first time use of PMMA-grafted MWCNT (g-MWCNT) as reinforcement for commercial PMMA. They observed an increase in storage modulus of the composites with increasing concentration of g-MWCNTs. The storage modulus increased from 2.5 GPa for pure PMMA to 31 GPa at 20°C (by 29 GPa or 1110%) for composite containing 20 wt% g-MWCNT. The dramatic increase in storage modulus shows that the interactions between PMMA matrix and g-MWCNTs are strong enough to allow a very efficient load transfer to MWCNT, providing high mechanical strengths. Scanning electron microscopy and TEM images reveal a homogeneous dispersion and strong interaction of g-MWCNT with PMMA matrix (Figure 7.12a,b).

7.4 Electrical Properties of CNT-PMMA Composites

High electrical conductivity and high aspect ratio of carbon nanotubes make them ideal for conductive filler applications in composites since the critical loading level reduces significantly by using CNTs (8,17). This is important not only in terms of saving weight but the use of CNTs will also ensure good mechanical stability of the composite. Many potential applications exist for CNT based conductive thermoplastics and amongst them EMI shielding for electronics and defense applications has gained immense research interest (8,13,15–17,24,42–44).

7.4.1 Electrical Conductivity

The studies on electrical properties of CNT-PMMA composites show that electrical conductivity of these composites follow the classical percolating behavior though values of percolation threshold vary from one study to another (22,24,41,57).

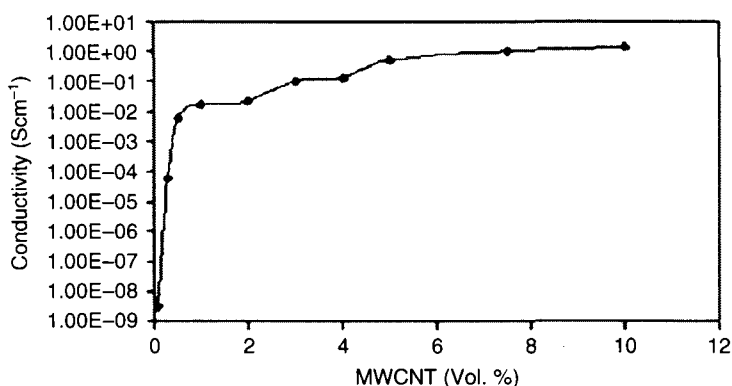


Figure 7.13. Electrical conductivity of MWCNT-PMMA composites as a function of CNT loading. Reprinted with permission from John Wiley & Sons, Inc (24).

The addition of MWCNT to insulating PMMA matrix transforms it to conductive plastic (24) as shown in Figure 7.13. Conductivity increased by almost 9 orders of magnitude with increase in MWCNT loading from 0.1 to 10 vol%. Addition of only 1 vol% of MWCNT to PMMA resulted in high conductivities up to $1.64 \times 10^{-2} \text{ Scm}^{-1}$. Conductivities as high as 1.5 Scm^{-1} were achieved with 10 vol% loading of MWCNT in PMMA. The conductivity increased in a classical percolating way, with a percolation threshold of about 0.5 vol%. Benoit et al. (41) reported an increase in electrical conductivity by 9 orders of magnitude from 0.1 to 8 % mass fraction with a threshold of 0.33 % for SWCNT soot-PMMA composite film. Percolation phenomenon was observed at room temperature with no significant effect of impurities like amorphous carbon, catalysts etc on the transport process.

Haggenmueller et al. (21) measured electrical conductivity of melt-processed SWCNT-PMMA films. They found that conductivity increased from 1.18×10^{-3} to 0.115 Scm^{-1} from 1.3 to 6.6 wt% CNT along flow direction of melt-processing but relatively lower values of conductivity were obtained perpendicular to the flow direction. The effect of nanotube orientation on electrical conductivity of CNT-PMMA composites was studied by Du et al (22,63,64). They observed an increase in electrical conductivity up to 10^{-4} Scm^{-1} at and beyond 2 wt% SWCNT loading in PMMA for unaligned SWCNT-PMMA composite (22). The percolation threshold was about 1%. Alignment of SWCNT decreased the electrical conductivity significantly ($>10^{-10} \text{ Scm}^{-1}$ at 2 wt% loading) and increased the

percolation threshold since there are fewer contacts between the nanotubes when they are aligned. On the contrary, in a randomly distributed system there are greater chances of contacts between the nanotubes resulting in the formation of a conducting network at low filler loadings.

In another study Slobodian et al. (57) found that the percolation threshold for electrical conductivity of MWCNT-PMMA composites depends on the solvent used. The lowest percolation threshold was achieved for toluene where percolation was found to be at 4 wt% of MWCNT, for chloroform at 7 wt% and for acetone at 10 wt%. The highest conductivity was obtained at 20 wt% of MWCNT at values around $4 \times 10^{-5} \text{ Scm}^{-1}$ for composite prepared from toluene solution. They observed that the Hansen solubility parameters of individual solvent play an important role in the dispersion of MWCNT in PMMA.

Chen et al. (67) studied the effect of a conjugated conducting polymer (P3HT) on the electrical conductivity and percolation threshold of MWCNT-P3HT-PMMA ternary composite. They found percolation threshold at less than 0.006 wt% MWCNT and the electrical conductivity of 10^{-4} Scm^{-1} . For many electronics and packaging applications a good conductivity at low filler loading is desired which suggests that the above ternary composite system may find use for applications such as electrostatic dissipation and electrostatic painting.

7.4.2 Electromagnetic Interference (EMI) Shielding

Electromagnetic interference shielding is very important in today's world of electronic devices and components. Typically, metals, graphite, carbon fibers and conducting polymers have been used for EMI shielding (42,71–74). Enhanced electrical properties of CNT-PMMA composites show potential applications of these nanocomposites for electronics applications, such as electrostatic charge dissipation, anti-static charge dissipation applications, electrostatic painting etc and EMI shielding (8,13,17,75). Electromagnetic interference shielding is one of the most promising applications of MWCNT-PMMA composites (17).

Mathur et al. (24) and Pande et al. (44) studied the effect of MWCNT content on the EMI shielding properties of MWCNT-PMMA composite films in the X-band (8.2–12.4 GHz). The MWCNT-PMMA nanocomposites with higher MWCNT content exhibit greater EMI shielding effectiveness (SE) (Figure 7.14).

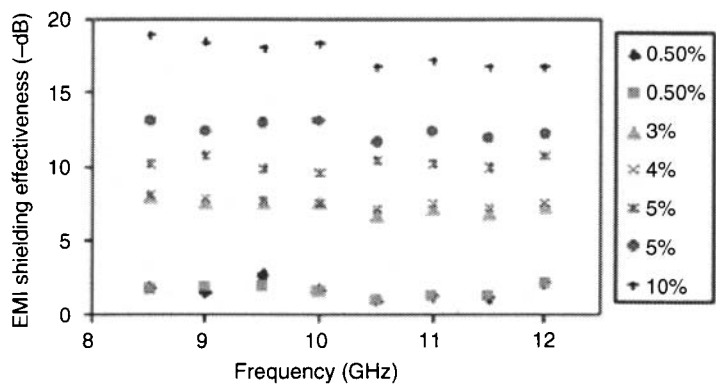


Figure 7.14. EMI shielding effectiveness of MWCNT-PMMA composites with different CNT loading. Reprinted with permission from John Wiley & Sons, Inc (24).

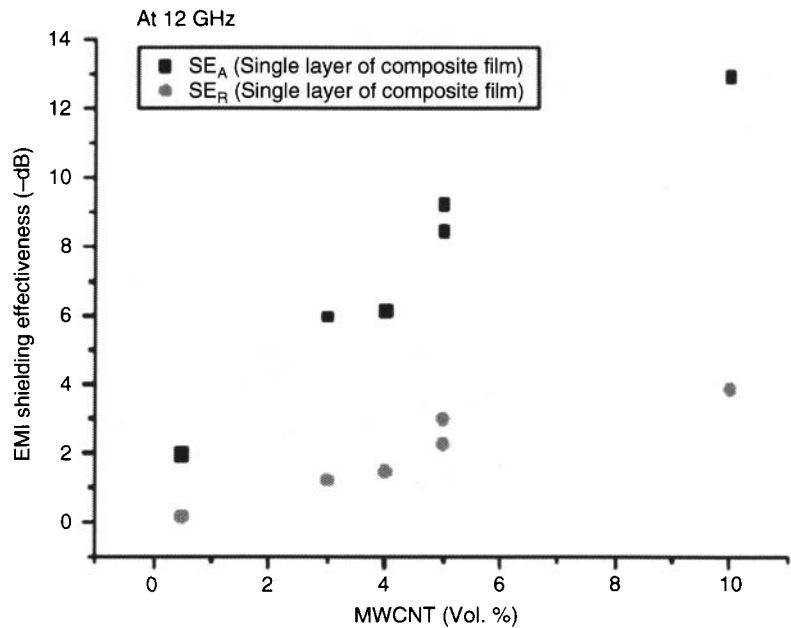


Figure 7.15. Effect of MWCNT content on SE_R and SE_A of MWCNT-PMMA composite film at 12 GHz. Reprinted with permission from Springer Science and Business Media (44).

Electromagnetic interference shielding effectiveness of about 18 dB was achieved with 10 vol% MWCNT-PMMA film which was found to be primarily an EMI absorbing composite material. Figure 7.15 shows the variation of EMI shielding effectiveness due to reflection

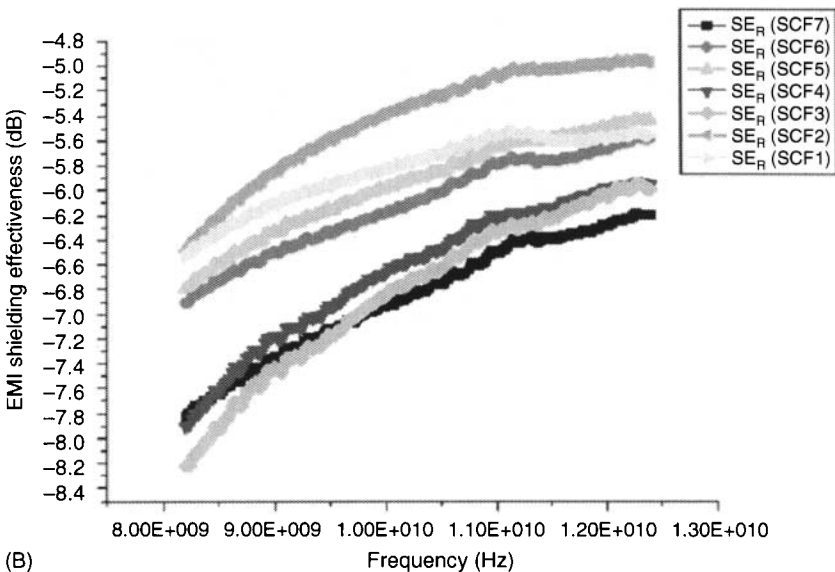
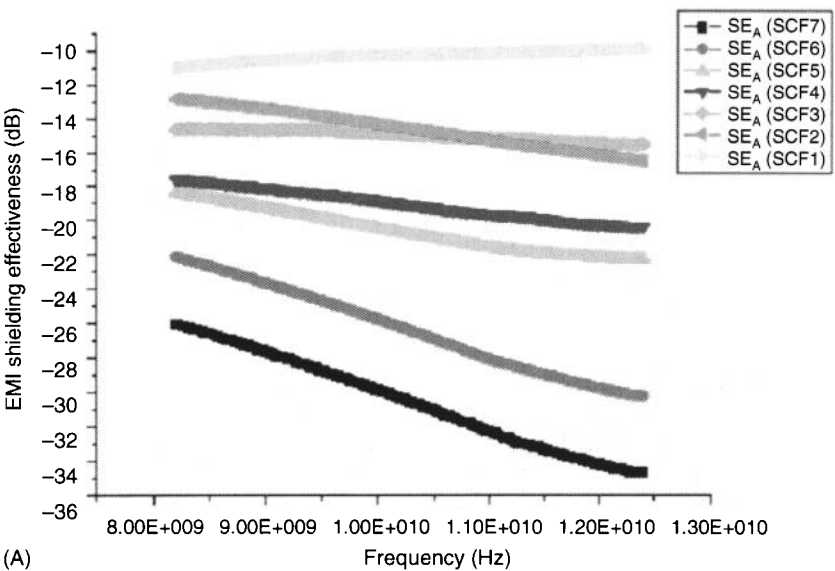


Figure 7.16. (a) Variation in the SE_A of multi layered MWCNT-PMMA composite films in the X-band, (b) variation in the SE_R of multi layered MWCNT-PMMA composite films in the X-band and (c) variation in the SE_{Total} of multi layered MWCNT-PMMA composite films in the X-band. Reprinted with permission from Springer Science and Business Media (44).

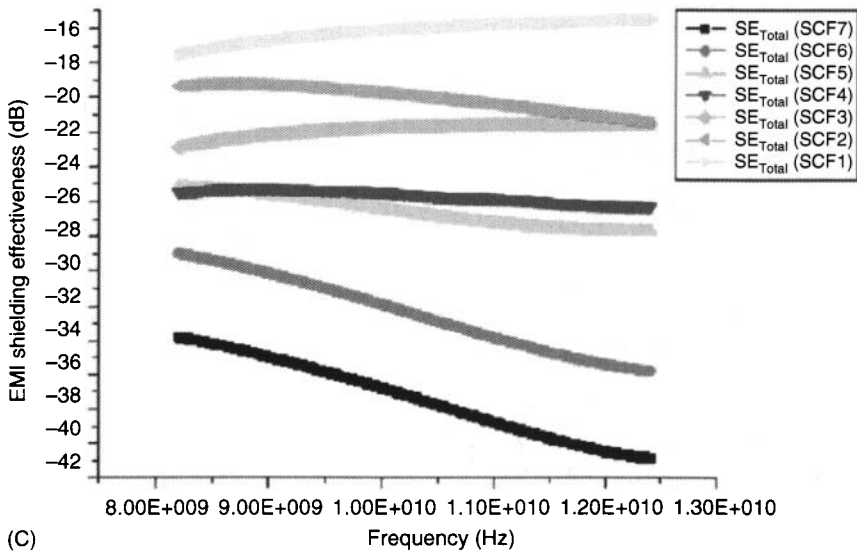


Figure 7.16. (continued)

(SE_R) and absorption (SE_A) at 12 GHz with increasing MWCNT loadings. The difference between SE_A and SE_R increases as CNT content increases, suggesting that the absorption contribution to the total electromagnetic shielding (SE_{Total}) increases with increase in CNT loading. In a further study, Pande et al. (44) observed that a EMI shielding effectiveness up to 40 dB was achieved with seven layers of stacked composite films (SCF7) compared to 30 dB achieved with two layers of bulk composite (SCB2) of the same thickness (Figure 7.16a,b,c, Figure 7.17). The stacking of thin film layers of the network over one another acts as a conducting mesh to intercept electromagnetic radiation resulting in multiple reflection and absorption phenomena within the layers. The layered structure increases the absorption component of the shielding effectiveness and hence the total EMI SE of the composite.

Kim et al. (42) studied EMI shielding properties of MWCNT-PMMA composites in the range 50 MHz–13.5 GHz and reported up to 27 dB shielding effectiveness at a high (40 wt%) loading of raw MWCNT in PMMA matrix. The contribution of absorption to the total EMI SE was more than that of reflection. They suggested commercial use of these composites in far-field EMI shielding. Because of the presence of iron in the raw MWCNT (as evidenced from

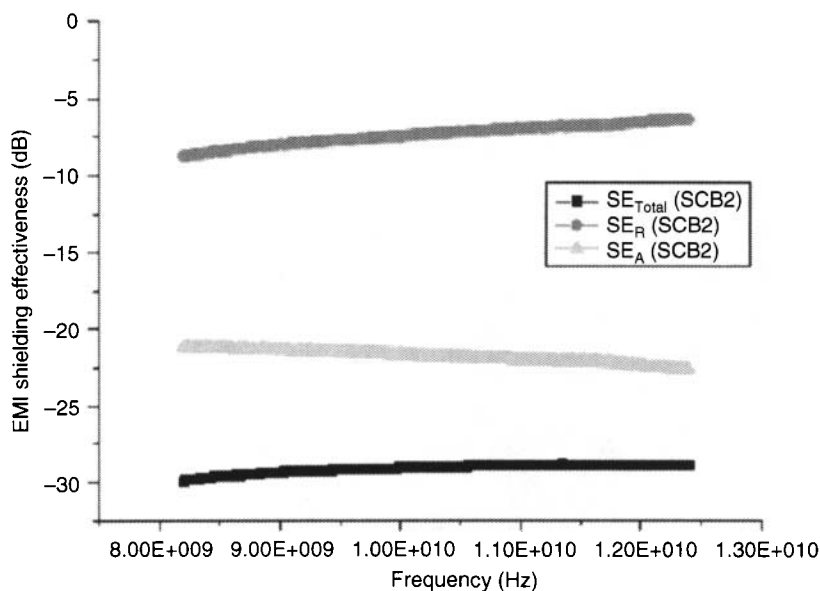


Figure 7.17. Variation in SE_A , SE_R and SE_{Total} of layered bulk composites in the X-band. Reprinted with permission from Springer Science and Business Media (44).

magnetic permeability studies), they suggested the use of these composites for near-field EMI shielding also.

Yuen et al. (43) studied effect of processing conditions on the EMI shielding properties (between 2 and 18 GHz) of MWCNT-PMMA composites prepared by *in-situ* polymerization and ex-situ fabrication methods. They found that shielding effectiveness was higher for *in-situ* fabricated composites and also found that the EMI shielding effectiveness of composites prepared by stacking ten layers of MWCNT-PMMA films was higher than a single thick piece of bulk 4.76 wt. % MWCNT-PMMA composite suggesting the composite stacking process as a better fabrication method. The maximum shielding effectiveness of the ten layers of *in-situ* prepared MWCNT-PMMA composite was 58.73 dB at 14.84 GHz compared to the 32.06 dB at 2.18 GHz for bulk MWCNT-PMMA composite.

7.5 Thermal Properties

Exceptionally high thermal conductivity of CNTs is expected to impart high thermal conductivity to the polymer composites (13,15).

Thermal conductivity depends on the adhesion between the CNTs and the polymer matrix. Strong covalent bonding will facilitate heat transport by phonon transfer or phonon-phonon couplings. In the absence of strong covalent bonds the thermal energy contained in high frequency phonon modes within the CNT needs efficient phonon-phonon couplings at the interface to overcome high interfacial thermal resistance in nanotube/polymer composites. Yuen et al. (70) prepared Si-MWCNT/PMMA-VTES nanocomposites wherein the silane modified carbon nanotubes were chemically bonded to PMMA-VTES via SiOx covalent bonds. Thermal conductivity increased by 87.5% by adding 0.99 wt% of modified CNTs to the neat PMMA-VTES.

Addition of CNT to PMMA has also been found to increase the thermal stability of these composites (22,24–26,70). These studies have shown an increase in the temperature for the onset of thermal degradation of the polymer matrix by incorporation of different concentrations of CNTs in PMMA to enable it for high temperature applications (Figure 7.18).

Consolidated data on the mechanical, electrical and thermal performance of these composites reported by different authors is compiled in Table 7.1.

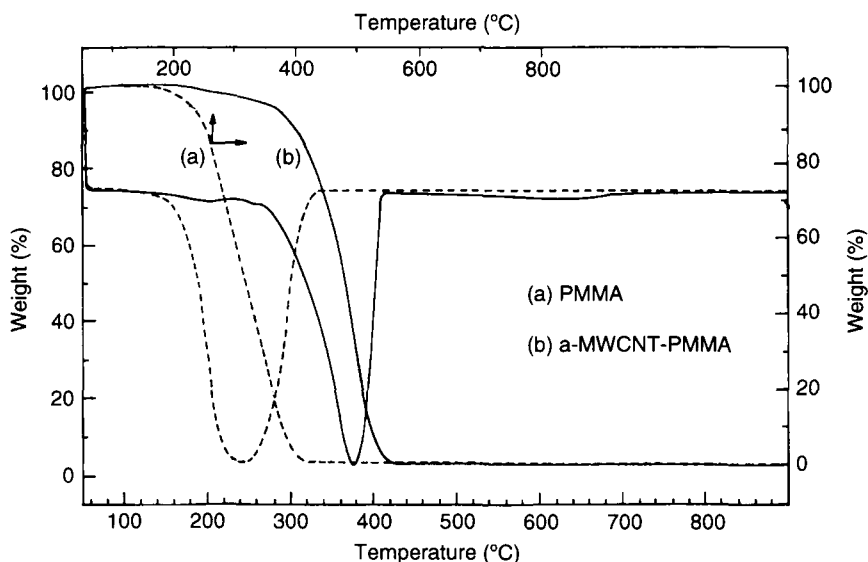


Figure 7.18. TGA of (a) PMMA and (b) 4.8 wt% a-MWCNT-PMMA. Reprinted with permission from John Wiley & Sons, Inc (25).

Table 7.1. Properties of MWCNT-PMMA composites

Group	CNT Type	CNT Synthesis Method	As-Synthesized/ Treated	Composite Fabrication Method	Composite Type	Mechanical Properties	Electrical Properties	Thermal Properties	Remarks
Haggenmueller et al. 2000 (21)	SWCNT	Laser Ablation (Rice University)	As-grown soot Purified soot Tubes@ Rice Material	Combination of solvent casting and Melt mixing Melt spinning CNT Loading levels 1 to 8 wt%	Film Fiber	Fibers: Elastic Modulus and yield strength increased with CNT loading and draw ratio Modulus: WT% GPa 0 3.1 8 6.0	Film: Conductivity Along flow Direction of melt-pressing 0.118 Sm^{-1} for 1.3 wt% 11.5 Sm^{-1} for 6.6 wt%	Optical microscopy revealed the improvement in dispersion as the melt-mixing cycles increased	
Du et al. 2003 (22)	SWCNT	HiPco Method (Rice University)	Purified SWCNT	Coagulation Method Melt Spinning CNT Loading levels 0.1 to 7 wt%	Unaligned and aligned Composite Fibers	Elastic Modulus of fibers increased with loading Modulus ~90% higher than pure PMMA	Percolation threshold 1% for unaligned composite At 2 wt% loading Conductivity Unaligned Composite 10^{-4}Sm^{-1} Aligned Composite 10^{-10}Sm^{-1}	Increased thermal Stability Decomp. temp. increased by 61°C	Increased viscosity resulting from improved dispersion prevented melt spinning fiber composite beyond 2 wt%

Jin et al. 2001 (26)	MWCNT	Arc-Discharge	As-synthesized	Melt-Blending CNT Loading levels 4 to 26 wt%	Film	Storage Modulus: Increased with CNT loading particu- larly at high temperature tan δ and lg increased with loading	TGA: Decomp. Range 320–430°C for PMMA 350–430°C for 26 wt% composite	TEM showed well dispersed tubes with no apparent damage or breakage to tubes
Jin et al. 2002 (65)	MWCNT	Arc-discharge	As-synthesized	Melt-blending Using PVDF as compatibilizer CNT Loading levels 1.5 to 2.6 wt%	Film	Storage Modulus of com- posite containing 0.5 wt% PVDF was almost twice that of composite without PVDF at 50°C	PVDF improved wetting of CNTs by PMMA SEM, TEM confirms wrapping of PVDF on MWCNT and dis- persed of MWCNT in PVDF PVDF was effective when added in optimum amount and its beneficial effect dimin- ishes at higher temperature	
Jia et al. 1999 (23)	MWCNT	CVD	Untreated tubes Treated tubes	In situ polymerization Improved In situ polymerization CNT Loading levels 1 to 10 wt%	Tensile Strength, fracture toughness and hardness increased with CNT loading from 0 to 7 wt% using treated tubes and improved method Tensile Strength Untreated tubes Treated tubes In situ poly. Improved In situ poly. Wt% MPa Wt% MPa 0 54.9 3 66.8 1 21.2 5.7 71.7 3 20.3 10 47.2		FTIR and SEM studies revealed CNT participation in PMMA polymerization and presence of a strong interface between CNTs and PMMA	

(continued)

Table 7.1. (continued)

Group	CNT Type	CNT Synthesis Method	As-Synthesized/Treated	Composite Fabrication Method	Composite Type	Mechanical Properties	Electrical Properties	Thermal Properties	Remarks
Velasco Santos et al. 2003 (27)	MWCNT	Arc-discharge MER Corp.	Functionalized	In situ polym. followed by casting CNT Loading Levels 1 to 1.5 wt%	Cast Composites	Tensile strength, Modulus and toughness increased Tensile Strength MPa 0 29.67 1 41.87 1.5 52.0 Storage Modulus at 90°C increased by 1135% and $\tan \delta$ increased by 40°C using 1 wt% funct. CNTs			FTIR, Raman studies revealed chemical interactions between CNT and PMMA via acid functional groups $-\text{COOH}$, $-\text{COO}^-$ functional groups on CNT
Mathur et al. 2008 (24)	MWCNT	CVD	As-synthesized As-synthesized (a-MWCNT) And Functionalized (f-MWCNT)	Solvent Casting CNT Loading Levels 0.1 to 10 vol. % Casting followed by compression molding Loading levels 5 to 10 vol. %	Film Bulk Composites	Elastic modulus increased with CNT loading Vol. % 0 1.04 1 1.5 4 1.64 10 1.78 GPa	Percolation threshold at 0.5 vol. % Electrical Conductivity of 10 vol. % MWCNT-PMMA was 1.5 S/cm	Thermal stability of composite increased by 65°C	SEM showed homogeneous dispersion of MWCNT in PMMA matrix but fracture surface after tensile test revealed weak CNT-matrix interface

Table 7.1. (continued)

Group	CNT Type	CNT Synthesis Method	As-Synthesized/ Treated	Composite Fabrication Method	Composite Type	Mechanical Properties	Electrical Properties	Thermal Properties	Remarks
Pande et al. 2009 (25)	MWCNT	CVD	As-synthesized and functionalized	In situ polymerization CNT Loading levels 0.06 to 4.8 wt%	Bulk Composites	A maxima was observed in flexural strength for both a-CNT-PMMA and f-CNT-PMMA composites Flexural Strength Modulus Wt.% MPa 0 58 1.97 a-3 90 2.7 f-1.8 94 2.8		Thermal stability increased by 65°C by adding CNT FTIR revealed presence of H-bonding interactions between PMMA and -COOH groups present in f-MWCNT	
Pande et al. 2009 (44)	MWCNT	CVD	As-synthesized	Solvent casting CNT Loading level 10 vol.% Two-step method loading levels CNT 10 vol.%	Film Bulk Composites	EMI SE in X-Band Layered composite (7 layers of 0.3 mm thickness film) ~ 40 dB Bulk composite (2 layers of 1.1 mm thickness bulk specimen) ~30 dB		Contribution of SE _A and SE _K to SE _{total} was studied SE dominated by absorption Stacking method results in increased multiple reflections and absorptions for layered composite	
Gorga et al. 2004 (28)	MWCNT	Plasma enhanced-CVD Method Nano-Lab Brighton, MA	As-obtained	Melt-processing CNT Loading levels 0.1 to 10 wt%	Unoriented and oriented composites	Tensile toughness of unoriented composites was less than PMMA and modulus of composites was same as PMMA. For oriented composites tensile toughness was maximum at 1 wt%, modulus increased by 38% at 10 wt% and yield strength increased by 25% at 10 wt% CNT loading		Toughening of brittle PMMA by bridging cracks that developed during tensile test	

Kim et al. 2008 (66)	MWCNT	Jeico Co.	As-received	Solution Blending using P3HT-g-PMMA as a compatibilizer CNT Loading lev- els 0.01 to 0.1wt%	Film	Wt% Young's Modulus Tensile Strength (MPa) (MPa) 0 541±16 11.3± 0.8 MWCNT-PMMA 0.10 850± 38 11.0± 0.2 MWCNT-P3HT-g-PMMA-PMMA 0.10 1104±17 21.0±0.6	Fluorescence emission and Raman Spectra provide evidence of strong π - π interactions of P3HT part of the compatibil- izer with the surface of MWCNT
Hwang et al. 2004 (69)	MWCNT	Arc Discharge	PMMA-grafted MWCNT	Solvent Casting CNT Loading lev- els 3 to 20 wt%	Film	Various amounts of PMMA- grafted MWCNT were used to reinforce commercial PMMA Storage modulus at 20°C of composite containing 20 wt% PMMA-grafted MWCNT increased by ~29 GPa (1100%) from 2.5 GPa in pure PMMA to 31 GPa in the composite	SEM and TEM data showed evidence of strong MWCNT- matrix interactions and efficient load transfer
Park et al. 2003 (60)	MWCNT	CVD Iljin Nanotec Co., Korea	Purified	In situ Bulk Polymerization CNT Loading levels 0.001 to 0.1 wt%	Film	SEM studies showed good wetting, uniform dispersion and strong interfacial adhesion between CNT and matrix	

(continued)

Table 7.1. (continued)

Group	CNT Type	CNT Synthesis Method	As-Synthesized/Treated	Composite Fabrication Method	Composite Type	Mechanical Properties	Electrical Properties	Thermal Properties	Remarks
Yang et al. 2004 (68)	MWCNT	CVD Sun Nanotech Co. Ltd. (Nanchang, China)	Purified p-MWCNT Octadecylamine (ODA)-functionalized s-MWCNT	Solution Mixing and Melt-mixing CNT Loading levels 1 to 10 wt%	Bulk strips	Young's modulus of 10 wt% s-MWCNT composite (2.32 GPa) showed 135% increase over neat PMMA-co-EMA and 9.2% increase over 10 wt% p-MWCNT composite	Tensile strength (73.4 MPa) of 10 wt% s-MWCNT composites showed 49% increase over neat P(MMA-co-EMA) and 12.8% increase over 10 wt% p-MWCNT composite	Decomposition temp. increased by about 110°C from 160°C to 270°C for the onset temperature of degradation when s-MWCNT were added	Surface modified CNTs i.e. s-MWCNT showed homogeneous dispersion and better interfacial bonding resulting in increased load transfer from matrix to MWCNT
Yang et al. 2005 (59)	MWCNT	CVD	Purified	In situ polymerization CNT Loading levels 0.05 to 2.5wt%	Block Specimens	Microhardness increased, friction coefficient decreased and wear rate decreased with increasing CNT content	Tg increased from 89 to 106°C for 10 wt% s-MWCNT composite	SEM analyses of worn surfaces of PMMA showed the positive effect of CNTs on tribological behavior of composites	
Yuen et al. 2007 (70)	MWCNT	Nanotech Port Company, Shenzhen, China	Silane-modified MWCNT (Si-MWCNT)	Solution mixing CNT Loading levels 0.5 to 3.85 wt% Used a copolymer PMMA-VTES as cross-linkable PMMA to Si-MWCNT	Surface and volume electrical resistivity decreased with increasing content of Si-MWCNT	Thermal conductivity increased by 87% at 0.99wt% Si-MWCNT loading	Thermal stability increased substantially by adding Si-MWCNT due to the presence of Si-O-Si groups	SEM and TEM revealed that Si-MWCNT was completely dispersed in the polymer matrix	

Benoit et al. 2001 (41)	SWCNT	Arc Discharge	As-synthesized	Casting CNT Loading lev- els 0.1 to 8 wt%	Film	Electrical conductivity increases with CNT content by 9 orders of magnitude from 0.1 to 8% mass fraction with percolation threshold 0.33 wt%.	Temperature dependence of resistivity for 0.2 to 8 wt% SWCNT composite films showed that percolating network is affected at low temperature, enhancing the relative resistivity
Kim et al. 2004 (42)	MWCNT	CVD Iijin Nanotech Co. Ltd.	Raw and Purified	Solvent Casting CNT loading lev- els 0.1 to 40 wt%	Film	Electrical Conductivity increases with increasing CNT content EMI SE (50 Mz to 13.5 GHz) increases with CNT content Highest EMI SE for raw MWCNT-PMMA composite was 27 dB at 40 wt% MWCNT EMI SE for purified MWCNT-PMMA at 20 wt% loading was 7 dB	Use of raw MWCNT-PMMA composites is good for EMI SE for far field and near field applications.
Yuen et al. 2008 (43)	MWCNT	CVD CNT Company, Incheon, Korea	As-received	In situ method Ex situ method CNT Loading levels 0.25 to 4.76 wt%	Film Bulk Film Bulk	Electrical Conductivity Percolation threshold 0.25 wt% for in situ prepared composites Percolation threshold 0.74 wt% for ex situ prepared composites EMI SE (2-18 GHz) 32.06 dB at 2.18 GHz for bulk composite prepared by in situ method & 58.73 dB at 14.84 GHz for 10 layers of stacked composite film prepared by in situ method	Higher EMI shielding effectiveness of layered composite attributed to energy loss by multi- reflections in the layered composites

(continued)

Table 7.1. (continued)

Group	CNT Type	CNT Synthesis Method	As-Synthesized/Treated	Composite Fabrication Method	Composite Type	Mechanical Properties	Electrical Properties	Thermal Properties	Remarks
Slobodian et al. 2007 (57)	MWCNT	Sun Nanotech Co. Ltd.	Purified	Solvent Casting Followed by compression molding CNT loading levels 2 to 20 wt%	Bulk Composites	Percolation threshold Solvent Toluene 4 Chloroform 7 Acetone 10	Percolation threshold MWCNT (wt%)	Hansen solubility parameters were used as a guide to characterize percolation thresholds:	
Shang et al. 2009 (61)	MWCNT	Purified		Microemulsion polymerization CNT Loading levels 1 to 15 wt%	MWCNT-PMMA composites prepared by microemulsion polymerization at 8 wt% loading showed high sensor responses to different organic vapors such as acetone, toluene, THF, chloroform, acetonitrile, benzene			They suggested the use of these composites for gas sensor applications	
Chen et al. 2007 (67)	MWCNT	Aldrich Type 1 Nano-Lab Type 2	Purified Type 1 As-received Type 2	Solvent Casting Binary Composites MWCNT-PMMA 10 vol. % TFA as a co-solvent Loading levels 0.12 to 1.5 wt% Ternary composites MWCNT-P3HT-PMMA where P3HT is a conjugated polymer (0.5 wt%) 10 vol. % TFA as a co-solvent Loading levels 0.006 to 0.5 wt%	Film	For binary composites percolation threshold was found at 0.65 wt% for type 1 and 0.12 wt% for type 2 MWCNT At 0.2 wt% loading of type 2 MWCNT electrical conductivity reached 10^{-3} S/cm For ternary composite by using conjugated polymer percolation threshold was decreased to 0.006 wt% (electrical conductivity about 10^{-4} S/cm at this loading level)		TFA is a good co-solvent to assist dispersion and a doping agent for P3HT which results in promoting π - π interactions between conjugated polymer and CNT. Applications as electrostatic dissipation and electrostatic painting	

Putz et al. 2004 (18)	SWCNT	Laser Ablation NASA Johnson Space Center	Purified	In situ polymerization CNT Loading levels 0.0001 to 0.014 wt%	Bulk Composites	Addition of 0.014 wt% SWCNT increased low temperature modulus by 10% beyond that of pure PMMA.	Raman spectroscopy was used to assess degree of MWCNT alignment
Ma et al. 2008 (62)	MWCNT	CVD	Pristine Oxidized	In situ polymer- ization under AC electric field to induce alignment of CNT CNT Loading levels 0.1wt%	Pristine aligned rapidly under electric field but reagglomerated. Oxidized CNTs remained aligned and stable without reaggregating Electrical conductivity (parallel and perpen- dicular to the direction of electric field) was 4 orders of magnitude higher for oxidized CNT than pristine CNTs due to better dispersion		
Chapelle et al. 1999 (54) Stephan et al. 2000 (55)	SWCNT	Arc- discharge	As-produced	Spin casting CNT loading levels 1 to 20 wt%	Raman spectroscopy was used to characterize interaction between SWCNT and PMMA The introduction of PMMA into bundles increases the distance between nanotubes and the interactions between themselves decrease and bundles are destroyed for low concentrations (<2.5 wt%). For higher concentrations (10 wt%) the presence of a high quantity of nanotubes does not allow intercala- tion by PMMA		
Liu et al. 2005 (53)	SWCNT	HiPCO nano- tubes Carbon Nano- technologies, Inc.	As-received	Solvent casting CNT Loading levels 10 wt% 8 different solvents with different solubility parameters were used	Analyzed the role of solvent in obtaining uniform SWCNT dispersion in PMMA Stressed the importance of the polar component of the solubility parameter Raman spectroscopic analysis of SWCNT-PMMA samples exhibiting different degrees of dispersion (homogeneous and heterogeneous) were consistent with the qualitative dispersion observations obtained from optical and scanning electron microscopy		

7.6 Conclusion

The CNT-PMMA composites have been developed with improved mechanical properties but for actual structural applications these have to compete with the existing carbon fibre based composites (tensile strength ~1200 MPa for UD and ~600 MPa for 2D composites). The existing values of about 70–90 MPa for bulk CNT-PMMA isotropic composites and 130–140 MPa for aligned composites are far below the expectations to actually use them exclusively for structural applications. The vast amount of information now available on the dispersion and interfacial behaviour of CNTs in the PMMA matrix can be used to select the best combination of parameters such as type of CNT (SWCNT or MWCNT), their synthesis methods, aspect ratio, purity, surface characteristics and the composite fabrication techniques. Surface modification of CNTs and *in-situ* polymerization techniques seems to hold a lot of promise. More efforts are needed in the development of aligned CNT-PMMA composites. Quite encouraging results have already been reported on this aspect with other polymer systems (16). Carbon nanotube- carbon fibres-PMMA hybrid composites could be an exciting area for further studies to achieve the desired mechanical properties. Such type of studies have already been undertaken on different polymer systems and results are quite promising (76).

So far as electrical properties are concerned CNT-PMMA composites have shown lot of promise as an effective EMI shielding material at very low loadings together with improved mechanical strength. In conclusion, significant progress has been made in the processing of CNT-PMMA composites and the efforts should be made to push these composites for commercial applications. The sectors such as aerospace, automobile, sports can benefit most from these composites.

References

1. R.B. Seymour, *Polymeric Composites*, VSP, The Netherlands, 1990.
2. P. Morgan, *Carbon Fibers and their Composites*, CRC Press, Taylor and Francis Group, 2005.
3. J.A.H. Hult, and F.G. Rammerstorfer, *Engineering Mechanics of Fibre Reinforced Polymers and Composite Structures*, Springer Verlag, 1994.
4. M. Sittig, *Carbon and Graphite Fibers: Manufacture and Applications*, Noyes Data Corporation, 1980.

5. H. Marsh, E.A. Heintz, and F. Rodriguez-Reinoso, *Introduction to Carbon Technologies*, University of Alicante Press, 1997.
6. E. Fitzer and L.M. Manocha, *Carbon Reinforcements and Carbon/Carbon Composites*, Springer-Verlag, 1998.
7. K. Friedrich, S. Fakirov, and Z. Zhang, *Polymer Composites: from Nano-to-Macro-scale*, Springer, 2005.
8. S. Advani, *Processing and Properties of Nanocomposites*, World Scientific, 2006.
9. S. Iijima, *Nature*, Vol. 354, p. 56, 1991.
10. M.S. Dresselhaus, G. Dresselhaus, and P. Avouris, *Carbon Nanotubes: Synthesis, Structure, Properties, and Applications* Springer-Verlag, 2001.
11. P.M. Ajayan, J.-C. Charlier, and A.G. Rinzler, *PNAS*, Vol. 96, p. 14199, 1999.
12. J.N. Coleman, U. Khan, W.J. Blau, and Y.K. Gunko, *Carbon*, Vol. 44, p. 1624, 2006.
13. O. Breuer, and U. Sundararaj, *Polymer Composites*, Vol. 25, p. 630, 2004.
14. E.T. Thostenson, Z. Ren, and T-W. Chou, *Composites Science and Technology*, Vol. 61, p. 1899, 2001.
15. Y. Gogotsi, *Carbon Nanomaterials*, CRC Press, Taylor and Francis Group, 2006.
16. J.-H. Du, J. Bai, and H.-M. Cheng, *eXPRESS Polymer Letters*, Vol. 1, p. 253, 2007.
17. D.T. Colbert, *Plastics Additives and Compounding*, January/ February 2003.
18. K.W. Putz, C.A. Mitchell, R. Krishnamoorti, and P.F. Green, *Journal of Polymer Science, Part B: Polymer Physics*, Vol. 42, p. 2286, 2004.
19. J.N. Coleman, U. Khan, and Y.K. Gunko, *Advanced Materials*, Vol. 18, p. 689, 2006.
20. E.T. Thostenson, C. Li and T.-W. Chou, *Composites Science and Technology*, Vol. 65, p. 491, 2005.
21. R. Hagenmueller, H.H. Commans, A.G. Rinzler, J.E. Fischer, and K.I. Winey, *Chemical Physics Letters*, Vol. 330, p. 219, 2000.
22. F. Du, J.E. Fischer, and K.I. Winey, *Journal of Polymer Science, Part B: Polymer Physics*, Vol. 41, p. 3333, 2003.
23. Z. Jia, Z. Wang, C. Xu, J. Liang, B. Wei, D. Wu, and S. Zhu, *Materials Science and Engineering A*, Vol. 271, p. 395, 1999.
24. R.B. Mathur, S. Pande, B.P. Singh, and T.L. Dhami, *Polymer Composites*, Vol. 29, p. 717, 2008.
25. S. Pande, R.B. Mathur, B.P. Singh, and T.L. Dhami, *Polymer Composites*, Vol. 30, p. 1312, 2009.
26. Z. Jin, K. P. Pramoda, G. Xu, and S.H. Goh, *Chemical Physics Letters*, Vol. 337, p. 43, 2001.
27. C. Velasco-Santos, A.L. Martinez-Hernandez, F.T. Fisher, R. Rouff, and V.M. Castano, *Chemistry of Materials*, Vol. 15, p. 4470, 2003.
28. R.E. Gorga, and R.E. Cohen, *Journal of Polymer Science, Part B: Polymer Physics*, Vol. 42, p. 2690, 2004.
29. D. Qian, E.C. Dickey, R. Andrews, and T. Rantell, *Applied Physics Letters*, Vol. 76, p. 2868, 2000.
30. B. Safadi, R. Andrews, and E.A. Grulke, *Journal of Applied Polymer Science*, Vol. 84, p. 2660, 2002.
31. E.T. Thostenson, and T.-W. Chou, *Journal of Physics D: Applied Physics*, Vol. 61, L77, 2002.

32. R.B. Mathur, B.P. Singh, T.L. Dhami, Y. Kalra, N. Lal, R. Rao, and A.M. Rao, *Polymer Composites*, Vol. 31, p. 321, 2010.
33. B.P. Singh, D. Singh, R.B. Mathur, and T.L. Dhami, *Nanoscale Research Letters*, Vol. 3, p. 444, 2008.
34. X.Y. Gong, J. Liu, S. Baskaran, R.D. Voise, and J.S. Young, *Chemistry of Materials*, Vol. 12, p. 1049, 2000.
35. M.J. Biercuk, M.C. Llaguno, M. Radosavljevic, J.K. Hyun, A.T. Johnson, and J.E. Fischer, *Applied Physics Letters*, Vol. 80, p. 2767, 2002.
36. K.T. Lau, S.-Q. Shi, L.-M. Zhou, and H.-M. Cheng, *Journal of Composite Materials*, Vol. 37, p. 365, 2003.
37. A. Allaoui, S. Bai, H.M. Cheng, and J.B. Bai, *Composites Science and Technology*, Vol. 62, p. 1993, 2002.
38. Y.S. Song, and J.R. Youn, *Carbon*, Vol. 43, p. 1378, 2005.
39. R.H. Baughman, A.A. Zakhidov, and W.A. de Heer, *Science*, Vol. 297, p. 787, 2002.
40. X.-L. Xie, Y.-W. Mai, and X.-P. Zhou, *Materials Science and Engineering R*, Vol. 49, p. 89, 2005.
41. J.-M. Benoit, B. Corraze, S. Lefrant, W.J. Blau, P. Bernier, and O. Chauvet, *Synthetic Metals*, Vol. 121, p. 1215, 2001.
42. H.M. Kim, K. Kim, Y. Lee, J. Joo, S.J. Cho, H.S. Yoon, D.A. Pejakovic, J.W. Yoo, and A.J. Epstein, *Applied Physics Letters*, Vol. 84, p. 589, 2004.
43. S.-M. Yuen, C.-C. M. Ma, C.-Y. Chuang, K.-C. Yu, S.-Y. Wu, C.-C. Yang, and M.-H. Wei, *Composites Science and Technology*, Vol. 68, p. 963, 2008.
44. S. Pande, B.P. Singh, R.B. Mathur, T.L. Dhami, P. Saini, and S.K. Dhawan, *Nanoscale Research Letters*, Vol. 4, p. 327, 2009.
45. Y. Yang, M.C. Gupta, K.L. Dudley, and R.W. Lawrence, *Nano Letters*, Vol. 5, p. 2131, 2005.
46. Y. Yang, M.C. Gupta, K. L. Dudley, and R.W. Lawrence *Journal of Nanoscience and Nanotechnology*, Vol. 5, p. 927, 2005.
47. Y. Yang, M.C. Gupta, and K.L. Dudley, *Nanotechnology*, Vol. 18, p. 345701, 2007.
48. Z. Liu, G. Bai, Y. Huang, Y. Ma, F. Du, F. Li, T. Guo, and Y. Chen, *Carbon*, Vol. 45, p. 821, 2007.
49. N. Li, Y. Huang, F. Du, X. He, X. Lin, H. Gao, Y. Ma, F. Li, Y. Chen, and P.C. Eklund, *Nano letters*, Vol. 6, p. 1141, 2006.
50. Y. Huang, N. Li, Y. Ma, F. Du, F. Li, X. He, X. Lin, H. Gao, and Y. Chen, *Carbon*, Vol. 45, p. 1614, 2007.
51. H. Zweifel, R.D. Maier and M. Schiller, *Plastics Additives Handbook*, 6th Edition, Hanser Publications, 2009.
52. J.H. Rouse, *Langmuir*, Vol. 21, p. 1055, 2005.
53. J. Liu, T. Liu, and S. Kumar, *Polymer*, Vol. 46, p. 3419, 2005.
54. M.L. de la Chapelle, C. Stephan, T.P. Nguyen, S. Lefrant, C. Journet, P. Bernier, E. Munoz, A. Benito, W.K. Maser, M.T. Martinez, G.F. de la Fuente, T. Guillard, G. Flamant, L. Alvarez, and D. Laplaze, *Synthetic Metals*, Vol. 103, p. 2510, 1999.
55. C. Stephan, T.P. Nguyen, M.L. de la Chapelle, S. Lefrant, C. Journet, and P. Bernier, *Synthetic Metals*, Vol. 108, p. 139, 2000.
56. R. Andrews, D. Jacques, M. Minot, and T. Rantell, *Macromolecular Materials and Engineering*, Vol. 287, p. 395, 2002.

57. P. Slobodian, A. Lengalova, P. Saha, and M. Slouf, *Journal of Reinforced Plastics and Composites*, Vol. 26, p. 1705, 2007.
58. J.U. Park, S. Cho, K.S. Cho, K.H. Ahn, S. J. Lee, and S.J. Lee, *Korea-Australia Rheology Journal*, Vol. 17, p. 41, 2005.
59. Z. Yang, B. Dong, Y. Huang, L. Liu, F.-Y. Yan, and H.-L. Li, *Mater. Lett.*, Vol. 59, p. 2128, 2005.
60. S.J. Park, M.S. Cho, S.T. Lim, H.J. Choi, and M.S. Jhon, *Macromolecular Rapid Communications*, Vol. 24, p. 1070, 2003.
61. S. Shang, L. Li, X. Yang, and Y. Wei, *Composites Science and Technology*, Vol. 69, p. 1156, 2009.
62. C. Ma, W. Zhang, Y. Zhu, L. Ji, R. Zhang, N. Koratkar, and J. Liang, *Carbon*, Vol. 46, p. 706, 2008.
63. F. Du, R.C. Scogna, W. Zhou, S. Brand, J.E. Fischer, and K.I. Winey, *Macromolecules*, Vol. 37, p. 9048, 2004.
64. F. Du, J.E. Fischer, and K.I. Winey, *Physical Review B*, Vol. 72, p. 121404(R), 2005.
65. Z. Jin, K.P. Pramoda, S.H. Goh, and G. Xu, *Materials Research Bulletin*, Vol. 37, p. 271, 2002.
66. K.H. Kim, and W.H. Jo, *Composites Science and Technology*, Vol. 68, p. 2120, 2008.
67. H. Chen, H. Muthuraman, P. Stokes, J. Zou, X. Liu, J. Wang, Q. Huo, S.I. Khondaker, and L. Zhai, *Nanotechnology*, Vol. 18, p. 415606, 2007.
68. J. Yang, J. Hu, C. Wang, Y. Qin, and Z. Guo, *Macromolecular Materials and Engineering*, Vol. 289, p. 828, 2004.
69. G.L. Hwang, Y.-T. Shieh, and K.C. Hwang, *Advanced Functional Materials*, Vol. 14, p. 487, 2004.
70. S.-M. Yuen, C.-C.M. Ma, C.-L. Chiang, J.-A. Chang, S.-W. Huang, S.-C. Chen, C.-Y. Chuang, C.-C. Yang, and M.-H. Wei, *Composites, Part A: Applied Science and Manufacturing*, Vol. 38, p. 2527, 2007.
71. X. Luo, and D.D.L. Chung, *Carbon*, Vol. 34, p. 1293, 1996.
72. X. Luo, and D.D.L. Chung, *Composites, Part B: Engineering*, Vol. 30, p. 227, 1999.
73. D.D.L. Chung, *Carbon*, Vol. 39, p. 279, 2001.
74. P. Saini, V. Choudhary, B.P. Singh, R.B. Mathur, and S.K. Dhawan, *Materials Chemistry and Physics*, Vol. 113, p. 919, 2009.
75. P.M. Ajayan, and J.M. Tour, *Nature*, Vol. 447, p. 1066, 2007.
76. R.B. Mathur, S. Chatterjee, and B.P. Singh, *Composites Science and Technology*, Vol. 68, p. 1608, 2008.

This Page Intentionally Left Blank

Synthesis of Vinyl Polymer/ Carbon Nanotube Nanocomposites Prepared by Suspension Polymerization and Their Properties

P. Slobodian

Tomas Bata University in Zlín, Faculty of Technology, Zlín, Czech Republic

Abstract

In-situ radical polymerization technique of vinyl-type monomers in presence of carbon nanotubes (CNT) is a potential way of improvement of final polymer/CNT nanocomposites properties. The product usually shows better CNT dispersion and advanced matrix/filler interfacial properties, which very probably result from good homogeneity of monomer/CNT dispersion achieved by applying ultrasound as mixing agent (often also during polymerization). The radicals from initiator, growing polymeric macroradicals or radicals produced in polymer degradation triggered by applied ultrasound create covalent bonds between organic molecules and carbon nanotubes surface. On the other hand, chemical/mechanical loading from ultrasound leads to significant destruction of CNT particles, mainly due to their shortening. Typical products of such suspension polymerization are microspheres with CNT material situated both on the surface and inside the spheres. The presence of CNT significantly modifies electrical properties of polymer/CNT microspheres, which find their application, among others, in electrorheology.

Keywords: Carbon nanotube, nanocomposite, radical polymerization, suspension polymerization, *in-situ* polymerization, electrorheology.

8.1 Introduction

Carbon nanotubes, CNT, are considered a very prospective material with incredibly broad future applications. They can be of various

types: beside the principal types - SWCNT (single-wall carbon nanotubes), DWCNT (double-wall carbon nanotubes) or MWCNT (multi-wall carbon nanotubes) - there are many other forms of carbon, such as nanohorns, nanoscrolls, onion-like carbon or graphene sheets. They have a great potential because of excellent Young modulus (reaching values of about $\sim 0.3\text{--}1$ TPa) together with a very high aspect ratio (as much as $10^3\text{--}10^4$ recently even 10^5 (1)), and also their excellent electrical and thermal conductivities, low density or large specific surface area are promising.

Their unique properties predestine them for both very specific applications and broad use in the field of polymer composites. They not only enhance mechanical properties but also electrical and thermal properties, act as flame retardants, etc. Thus their positives can be successfully exploited from simple or advanced polymer matrix reinforcement, through electronic devices, sensors and actuators, to electrorheological fluids, to name just the most important applications.

Although carbon nanotubes have already been practically used for some time, substantial technological problems still remain. First of them is the fact that in mixing it is very difficult to individualize single nanotubes from their aggregates and disperse them well in polymeric matrix. This is caused by CNT insolubility in organic materials on the one hand and their strong tendency to agglomerate on the other hand (2,3). Actually, CNT are produced in the form of bundles or bundle aggregations consisting of 50 to a few hundred individual tubes or ropes, or alternatively as a network of individual tubes, either SWCNT (4) or MWCNT (5). It is very difficult to de-aggregate CNT bundles using conventional methods of polymer melt processing, so usually nanotube agglomerates of the size of micrometer or even larger can be observed in polymer matrix, which may be polypropylene (6), poly(methylmethacrylate) (7), high-density polyethylene (8), polyamide 6 (9) or others. Further, the aggregates of CNT considerably reduce the aspect ratio of the tubes, and thus the reinforcing effect is far from the expected (7). Also load transfer can be limited because of the bundles of nanotubes: when some of the nanotubes are not bonded to the matrix, they slip within the bundles, and it is easier for them to slide out of the bundle than to break (10,11).

Another critical point relevant to polymer/CNT composites seems to be good adhesion between the polymer matrix and nanotube surface. However, contemporary literature does not offer any

reliable rules for predicting the compatibility between CNT and polymer matrix which would enable to avoid poor load transfer at nanotube/polymer interface (12–14).

From the above it is clear that polymer/CNT nanocomposites call for further development and innovation of preparation methods. Commonly used techniques, such as mixing in polymer melt, are currently being replaced by more efficient methods, e.g. using ultrasound as a stirring element or high-speed shearing. Another effective way of preparation of high-performance polymer/CNT composites with better filler distribution and compatibility can be chemical or chemical-physical modification of the filler by the method of covalent or non-covalent CNT functionalization, and some effort can also be seen in modification of conventional polymerization techniques: bulk (15–17), suspension (16,18–21) or mini- or micro-emulsion polymerizations (22–24). In brief, the polymerization techniques referred above can be viewed as polymerization in the presence (16,18,19,22) or in the absence of CNT (20–23). The most progressive method seems to be the process of CNT oxidation (25,26) leading to creation of carboxyl and hydroxyl groups, which become binding elements for different polymeric molecules (27–32).

8.2 Free Radical Polymerization

Vinyl monomers, such as styrene, methyl methacrylate, vinyl acetate, vinyl chloride or acrylonitrile are preferably polymerized by chain polymerization techniques initiated by free radicals. Suitable free radicals can be handily achieved from unstable chemicals like peroxides (benzoyl peroxide, dicumyl peroxide) or di-azo reagents (e.g. 2,2'-azo-bis-isobutyronitrile, AIBN) which are dissolved in monomer and usually thermally decompose at temperature range of 40–120°C. Alternatively, suitable radicals for polymerization can also be activated without addition of external initiators, by just applying ultraviolet light (wave length 200–350 nm) or ultrasound (15,33,34) onto monomer.

In both cases, free radical polymerization has three major kinetic steps: initiation, propagation and termination (35,36). When external initiators are used, in the initiation step they provide free radicals which become active sites of following reactions. At the

beginning of the process, they attract the first molecule of monomer. For a successful product the number of active sites should not be very high, they must sustain for sufficient time and be active while polymer chain can achieve required length. For the same reason any impurities which can react with active sites must be cleared away from the system.

Initiation is followed by the propagation step of the reaction, when monomer molecules are rapidly added, step by step. In a fraction of a second, the macroradical reaches 2000–10000 monomer units. On the addition of each monomer unit the active site moves to the end of the growing polymer chain. The last step, termination, can act as recombination of two growing polymer chains (macroradicals) or by disproportionation, when hydrogen is transferred from one chain to another.

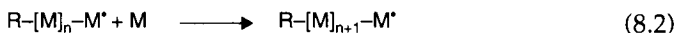
The principle of radical chain polymerization can be schematically illustrated by the following reaction scheme:

1. Initiation

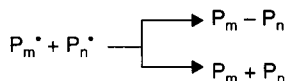


where M represents a monomer unit and R is a radical from the initiator;

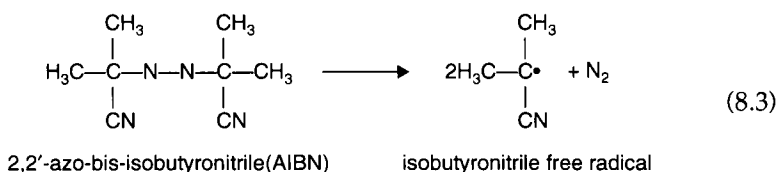
2. Propagation:



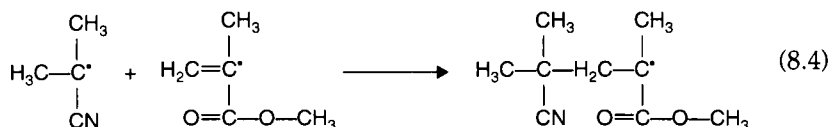
3. Termination by recombination and disproportionation, respectively:



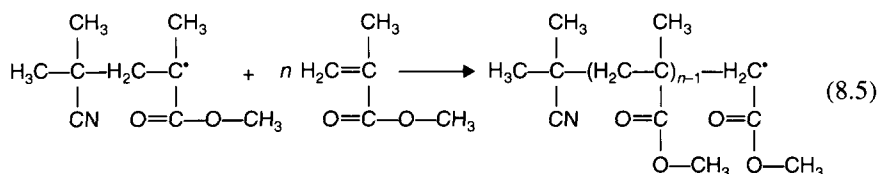
An example of initiation can be thermal decomposition of the above mentioned di-azo reagents represented by AIBN. Heat supplies the energy needed for splitting the molecule into two isobutyronitrile radicals (plus a molecule of nitrogen). Each free radical has an unpaired electron further acting as an active site for propagation.



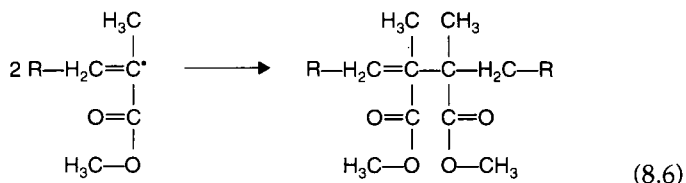
As written above, initiation in radical polymerization usually includes the addition of the first molecule of monomer (in the following example it is a molecule of methyl methacrylate):



Then the process continues in propagation



and is terminated by recombination of macroradicals:



8.3 Suspension and Bulk Polymerization Techniques

The preparation of polymers through free radical polymerization can be carried out in several ways, both in laboratory and industrial scales. Among the techniques, bulk, suspension, emulsion and solution polymerization methods are of the most practical importance.

In the case of bulk polymerization, the initiator is dissolved in the monomer and the viscosity of the system increases with progressing polymerization from liquid, through the state of gel ("gel-effect") to solid polymer. This polymerization technique has many disadvantages, among others the transfer of exothermic reaction heat from the system is very complicated. The reaction heat reaches values as high as 85 kJ/mol, and because polymers are poor heat conductors, this may cause the temperature of the system to reach the boiling point of monomer and consequently the polymer is foamed by vapours of monomer.

These troubles can be eliminated using suspension polymerization method. Here, the monomer with dissolved initiator is dispersed in

fluid medium (usually water; the monomer is not soluble in the fluid medium) in the form of small spherical beads so that the reaction heat can be easily removed. The size of beads depends on a number of properties and variables including the character of reaction mixture and set up of the process, such as viscosity, surface tension, geometry of the reactor or intensity of stirring. From the kinetics point of view, suspension polymerization is identical with bulk polymerization. In the course of suspension polymerization also, viscosity of liquid monomer increases up to the gel state and finally to solid polymer. The products of this polymerization technique are polymer spheres with a typical diameter of $50\text{ }\mu\text{m}$ - 2 mm . At some point of polymerization process, the beads usually shows tendency to stick with each other to form bigger agglomerates.

To ensure the suspension stability, stabilizers and dispersive agents are usually added into the reaction system. They can be both organic and inorganic materials. The former are usually represented by polymers (polyvinyl alcohol, polyvinyl pyrrolidone, soluble cellulose derivates, polyelectrolytes or gelatin) which modify the viscosity of fluid medium and only allow creation of smaller beads. The latter include water insoluble fine inorganic powders (e.g. BaSO_4 , MgO , $\text{Ca}_3(\text{PO}_4)_2$), which coat the beads to prevent them from sticking together, and also change surface tension because coated beads are less wettable. However, this way has also disadvantages - it is very difficult to wash the stabilizer away from the polymer without any residues and one has to count them in the final product. On the other hand, an advantage of the method is very simple separation of the polymer from the reaction system. In general, suspension polymerization has big practical significance.

Figure 8.1 shows a schematic view of suspension polymerization technique.

The increasing scope of applications often requires smaller polymer beads together with narrower size distribution. In order to meet both requirements, the conventional suspension polymerization techniques can be modified, so the resulting technique may be, for example two-step polymerization in microsuspension (38, 39), typical product is shown in Figure 8.2. The microsuspension is prepared at high shear agitation and then polymerization is carried out under slow stirring. The mechanism of polymerization is the same as in conventional suspension polymerization described above. The disadvantage of this technique, however, is simultaneous formation of a significant amount of emulsion particles adhered onto surface of microbeads, as shown in Figure 8.2.

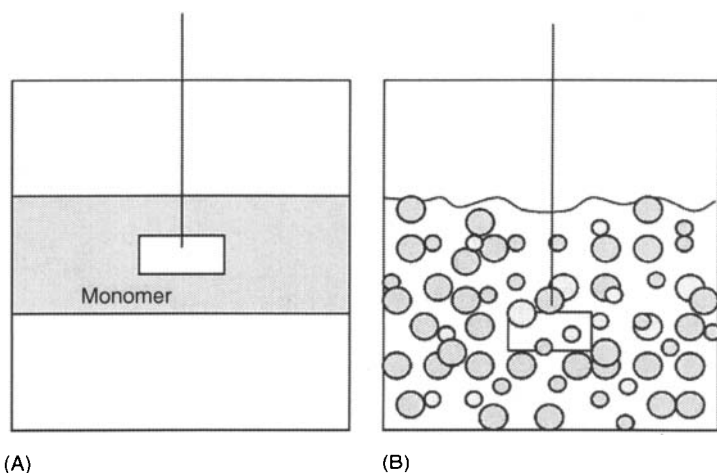


Figure 8.1. Schematic illustration of dispersion polymerization reactor, (a) two layers of immiscible liquids - monomer and dispersion fluid (e.g. water), and (b) monomer dispersion achieved by agitation (37).

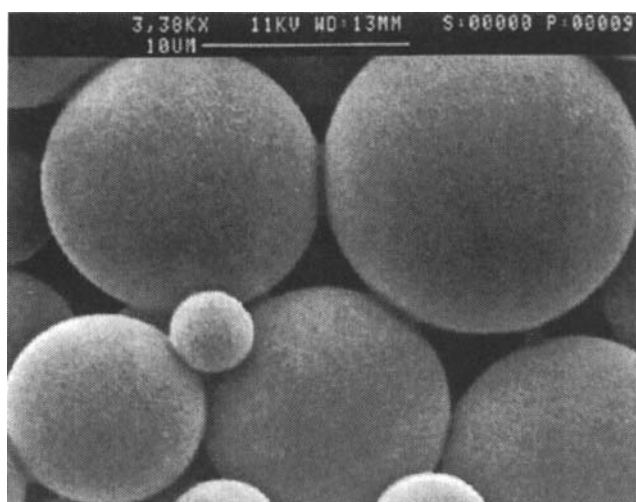


Figure 8.2. SEM analysis of PS-DVB (polystyrene-co-divinylbenzene) microspheres prepared by two-step microsuspension polymerization method, particle diameter 2–20 μm (39).

Micron-size particles can also be prepared by polymerization of monomer dispersion in organic solvents (e.g. alcohol) in which the emerging polymer is not soluble. At the beginning of the process, the reaction mixture is homogenous but during the reaction, stabilized polymer particles precipitate. This method offers uniform particles with a diameter of 2–15 μm (40).

A similar principle is applied in dispersion polymerization in ionic liquids; produced particles are in sub-micron range (41,42). The monomer, initiator and colloidal stabilizer are soluble in the liquid medium, but the obtained polymer is not. Different kinds of ionic liquids may be used, such as for styrene 1-butyl-3-methylimidazolium tetrafluoroborate or N,N-diethyl-N-methyl-N-(2-methoxyethyl)ammonium bis(trifluoromethanesulfonyl)imide. In general, radical polymerization in ionic liquids provides higher polymerization rate and higher molecular weights than the process in bulk or organic solvents (homogenous system).

As mentioned earlier, polymerization techniques can also be used in the presence of nanotubes for preparation of polymer/CNT nanocomposite materials. In these, *in-situ* radical polymerization techniques of polymerization in the presence of CNT filler under or without applied ultrasound. Both new factors (presence of CNT and ultrasound) can affect reaction kinetics, stability of suspension or the size of prepared particles. For example, ultrasound waves can open C=C bond of monomer, which starts polymerization initiation. Thus vinyl monomers (styrene, methyl methacrylate or vinyl acetate) can be polymerized without addition of initiator, only by application of ultrasound. This is called sonochemical polymerization method (15,33,34).

8.4 *In-situ* Radical Polymerization in Presence of CNT

8.4.1 Polymer Matrix

One of the potential ways how to improve CNT dispersion in polymer matrixes is *in-situ* polymerization of monomers in presence of nanotubes. Monomers have very small shear viscosity in orders of about 10^{-4} – 10^{-3} Pa.s, compared to relatively high viscosity of polymer melts, 10^3 – 10^6 Pa.s. This low viscosity helps to better impregnation and wetting of CNT material, which leads to more efficient dispersion and debundling of the nanotubes aggregates, especially when ultrasound is used as a dispersing agent.

However, literature sources very often claim that the presence of CNT in the reaction mixture significantly changes reaction kinetics of radical polymerization. This can be seen as consumption of free radicals, for example isobutyronitrile radicals from thermally decomposed initiator AIBN (43). It leads to increase of molecular weight of the resulting polymer, as shown in Table 8.1 for PMMA

Table 8.1. The influence of CNT content in polymerization mixture during *in-situ* radical polymerization on molecular weight of polymers and polydispersity index

Polymer matrix	CNT type	CNT content (wt%)	M_w [kg/mol]	M_n [kg/mol]	Polydispersity index, M_w/M_n
PMMA (17)	MWCNT	–	300	50	6.00
		0.001	330	72	4.58
		0.01	370	60	6.17
		0.1	410	62	6.61
PS (15)	MWCNT	–	45.9	23.0	1.99
		0.05	46.3	21.2	2.18
		0.1	64.8	20.6	3.14
		0.2	90.6	18.0	5.03
PS (35)	MWCNT	–	271.6	105.0	2.59
		0.1	323.9	117.7	2.75
		0.5	375.8	127.7	2.94
		1.0	427.1	137.0	3.45

(17) and for PS (15,35) initiated by AIBN. In the case of PS also significant broadening of molecular weight distribution can be observed with increasing amount of MWCNT.

8.4.2 Addition of Radicals onto CNT

The presence of CNT in polymerization system not only changes properties of the polymer matrix but also has a significant impact onto carbon nanotubes; they can be functionalized on the surface by the radicals. Functionalized nanotubes are on the one hand better individualized from the bundles and aggregates (44), but on the other hand they are shorter and can possess some open ends (43).

CNT functionalization during radical polymerization represents creating of new covalent bonds between the nanotube surface and organic material from the reaction mixture. Here the free radicals (both fresh - created from the initiator - and growing polymer macro-radicals) are capable of chemical reaction with CNT structure, opening the π -bonds in carbon nanotubes and creating a covalent bond between CNT and the radical (15–19,43–45). The process is expressed for single-walled nanotubes (SWNTs) and AIBN in the following equation, Figure 8.3:

The way in which modification affects the properties of nanotubes can be detected for instance by thermogravimetric measurements.

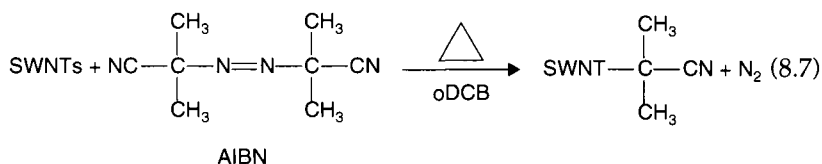


Figure 8.3. Reaction scheme for radical functionalization of SWNT with AIBN performed in 1,2-dichlorobenzene at the temperature of thermal decomposition of AIBN (44).

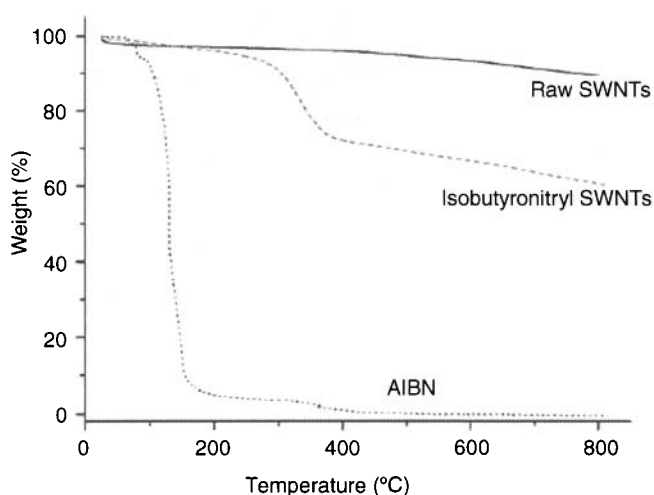


Figure 8.4. TGA of raw SWCNTs and those functionalized with isobutyronitrile and AIBN (44).

Figure 8.4 shows thermal decomposition of three types of single-walled carbon nanotubes, SWCNT (raw nanotubes and those modified in two ways - by radical initiator AIBN and functionalized), which was measured at a heating rate of $10^\circ/\text{min}$ in helium atmosphere. As can be seen, raw SWCNTs show only little mass loss in the course of heating up to 800°C , while the other two materials display significant decomposition events. The AIBN initiator has the main decomposition events. The AIBN initiator has the main decomposition temperature at about 75°C , at higher temperatures it completely degrades, as the curve shows. In the other case, the mass loss corresponding to the decomposition of isobutyronitril covalently attached onto SWCNT surface (not washed enough) has a maximum rate at around 350°C and what is more, the total weight loss is about 20% with respect to raw SWCNTs. It means that one isobutyronitril group is proportional to approximately 23 carbon atoms of SWCNT (44).

A typical experimental procedure suitable for functionalization was described in (44). It includes sonication of SWCNT dispersion in organic solvent (1,2-dichlorobenzene) together with dissolved AIBN for 5 min, which is followed by stirring of reaction mixture for a certain time (1–5 hours) at 75°C.

Opening of CNT π -bonds by AIBN can also lead to generating of radicals on the tube surface, which become active sites from which polymer chain starts to grow (16,18). It has lately been announced that chemical reaction with CNT (somewhere called radical addition (46,47)) can be performed also by macroradicals, which originate during propagation step of radical polymerization (15).

In both cases, i.e. presence of initiator radical or polymer macroradical, covalent C-C bonds between CNTs and polymer can be created. A suitable method which should prove the existence of such covalent bonds between polymer and CNTs is FT-IR spectra. For example, PMMA/CNT composite materials (16–18,43,48) show the existence of a new peak at around 1665 cm^{-1} (43) 1650 cm^{-1} (17,48) or 1630 cm^{-1} (16), here demonstrated in Figure 8.5.

As said before, another way of CNT functionalization is by polymer macroradicals using methods of ultrasonic sonochemistry. The macroradicals are generated by the degradation effect of ultrasonic waves applied onto polymer solutions, e.g. those prepared of poly(methyl

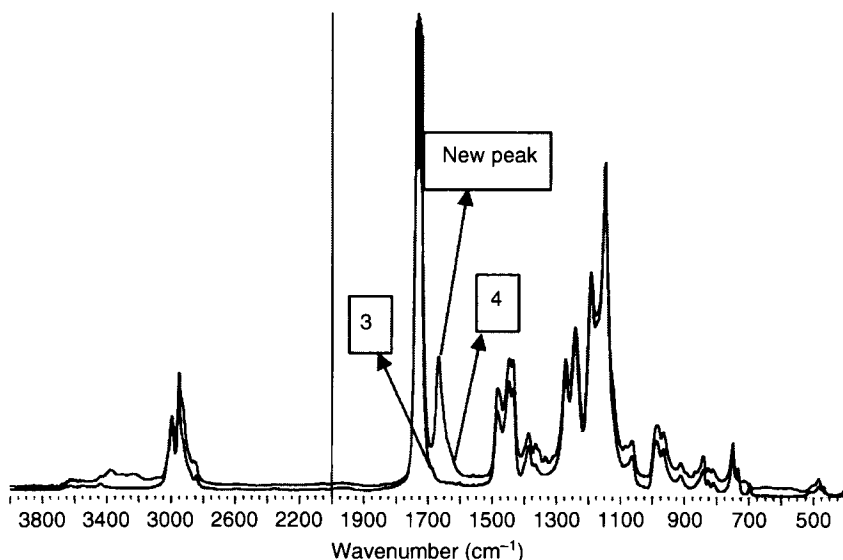


Figure 8.5. Infrared transition spectra of PMMA (3) and PMMA/CNT composite containing 20 wt% of CNTs prepared by *in-situ* polymerization (adapted from (43)).

methacrylate), PMMA, polystyrene, PS, polyvinylacetate, PVAc, and polyvinylpyrrolidone, PVP (49–52). Sonication causes disruption of macromolecular C-C bonds forming long-chain polymer radicals. It has been proved that macroradicals formed by sonochemical degradation of polymer chains can lead to polymer-grafted CNTs (52).

8.4.3 CNT Degradation

In-situ polymerization techniques play an important role in nanotubes modification, significantly improving CNT properties like dispersibility, individualization of tubes from CNT bundles and ropes or stronger CNT/polymer matrix interface. On the other hand, it must be mentioned that the process can also have a negative effect on the structure and properties of concrete carbon nanotubes - significant degradation of the structure can be observed as an effect of ultrasonication-induced nanotube cutting (52,53). This effect is demonstrated in Figure 8.6, which represents TEM analysis of multi-walled CNT, before (a-b) and after (c-f) functionalization (grafting) by PVP with the help of ultrasound (52). As can be seen, the original MWCNTs create entangled bundles and have a large aspect ratio. A different situation occurs after sonication of

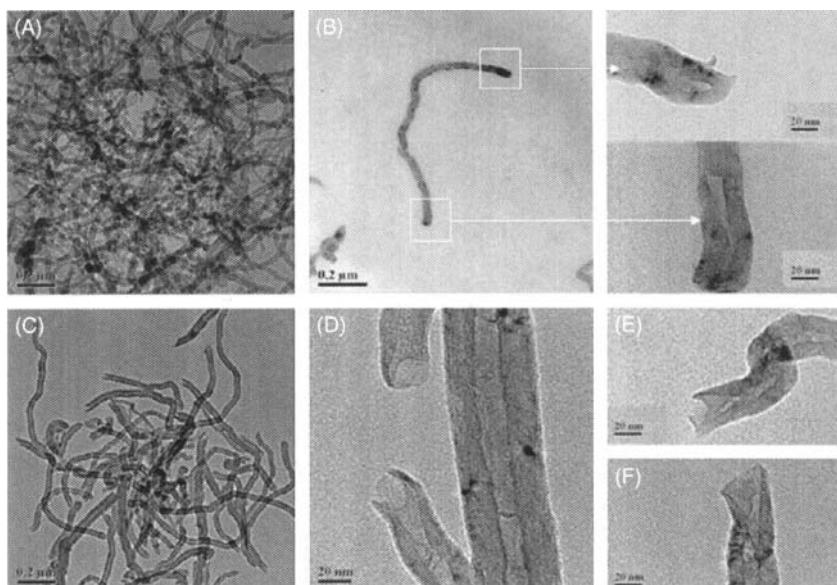


Figure 8.6. TEM images of pure MWCNTs (a-b) and nanotubes exposed to ultrasonic functionalization (grafting) by PVP (52).

CNT dispersion in PVP water solution. The PVP-grafted MWCNT aggregates seem to be reduced, which is most probably the effect of the mentioned polymer grafting onto CNT surface and better dispersibility of nanotubes. On the other hand, it is certainly due to the degradation of CNT that the nanotubes are shorter than before, with a lower aspect ratio, which results from the damaging effect of high-energy ultrasound. The original MWCNTs bundles are several microns to tens of microns long, with only few ends of nanoropes, and as the detailed view shows, their ends are closed, while many more nanorope ends can be found in PVP-grafted MWCNTs and they are opened by CNT cutting (Fig. 8.6 e-f).

8.4.4 Additional Analyses

Another possible evidence of grafted organic/polymeric molecules onto CNT surface can be achieved by microscopy analyses using both principal types of electron microscopy - transition electron microscopy, TEM, or scanning electron microscopy, SEM (15,19,24,44,45,47). Such analyses are usually performed after careful extraction of the polymer from tubes by polymer solvents, performed several times by a reflux procedure with an excess of solvent; therefore it is supposed that only covalently attached molecules remain fixed at CNT surface. High Resolution mode of TEM analysis shows the evidence of amorphous material on nanotubes surface (15).

Another important property - wettability was followed by SEM analysis on PS/MWCNTs nanocomposite prepared by *in-situ* bulk-suspension polymerization (54). Figure 8.7 presents a micrograph of fracture surface of the prepared nanocomposite. The picture very clearly evidences that the nanotubes are covered by a thick layer of polystyrene. Parts of original nanotubes can be identified at the end of the fracture; noteworthy is also the smaller diameter at the end of tubes.

The improved properties of modified CNTs achieved by polymerization technique, e.g. better polymer-CNT interaction, can be also detected by other techniques. As an example, we present here behavior of solutions of the prepared composites. Figure 8.8 represents photomicrographs of two different SWCNT/PS samples dissolved in toluene (right parts) and optical transmission microscopy of casted PS thin films from two different dispersions. The first one (a) represents PS solution in toluene where raw SWCNTs were only added and dispersed by ultasonication for two hours. The second (b) is

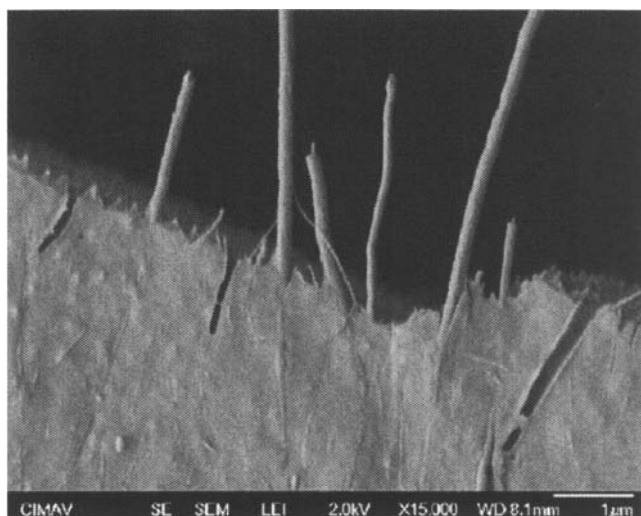


Figure 8.7. Evidence of wettability of polystyrene matrix on the surface of MWCNT nanocomposite prepared by *in-situ* polymerization with assistance of sonication (54).

the PS/SWCNT product of suspension *in-situ* polymerization, again dissolved in toluene. The concentration of SWCNT in both cases was approximately the same. Although the first dispersion (a) was very dark immediately after sonication, nearly all carbon material sedimented within next 48 hours, as apparent in the beaker. On other hand, the second dispersion, prepared from polystyrene grafted SWCNT (b), remained homogenous and dark even for longer than a month. This indicates that there is strong interaction between polystyrene chains and SWCNTs (19). To form stable dispersion, each individual nanotube must be stabilized by grafting PS molecules to its surface; this helps to solvate them and avoid tubes aggregation. The same tendency can be also observed on thin films prepared from the dispersions after sonication (left part). It is clearly visible that in case (b), i.e. for filler treated by *in-situ* polymerization, the dispersion was much better than in case (a), where large aggregates can be identified.

The state of prepared polymer/CNT nanocomposites can be adventurously characterized through an indirect method - rheological measurements. Rheological behaviour reflects the more effective transfer of forces due to enhanced interfacial bonding strength and good dispersion (45,55,56). Generally, any particles added into polymer melt will result in increase of shear viscosity. However, if there is good interaction between the particles and polymer, the

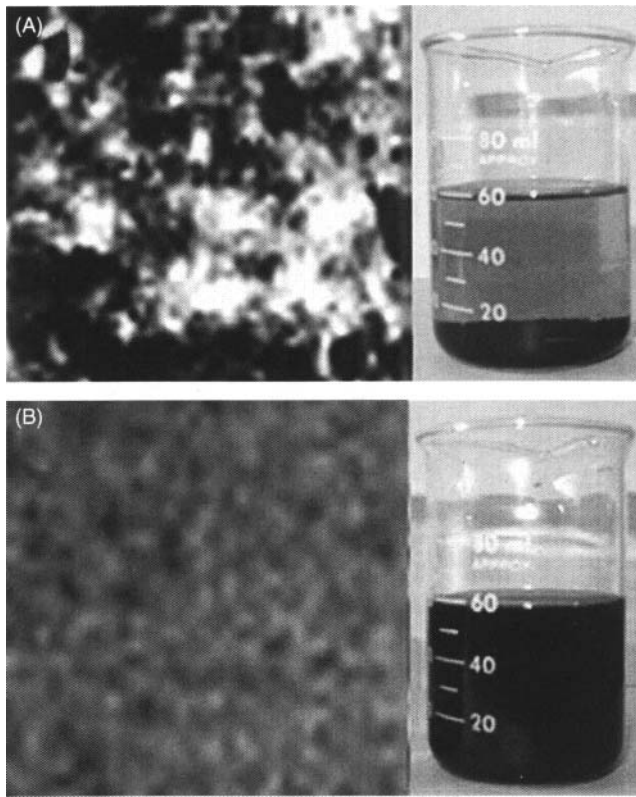


Figure 8.8. Polystyrene solution in toluene with SWCNTs (right) three weeks after sonication, and transmission light micrographs of 30 μm PS films produced by film casting technique of dispersion (left). Part (a) represents samples prepared by only mixing of raw SWCNT with PS solution, and part (b) is for SWCNTs treated by *in-situ* polymerization (19).

system also shows a significant effect of CNT content on its elasticity (recoverable shear). As a consequence, increase in the CNT loading in polymer matrix leads to increased polymer melt elasticity. The surface-modified nanotubes enhance the melt elasticity more significantly than the filler without modification (55). From this point of view, surface modification might be a good tool to improve the interaction between CNT and polymer matrix.

8.5 Polymer/CNT Composite Microspheres

Typical products of suspension polymerization techniques are polymer beads or spheres with a diameter of 50 μm - 2 mm. The

advantage of suspension polymerization in general is that it is a single batch process. In the case of polymerization well executed in all steps, the final product is very attractive for practice. Produced micro-sized monodisperse polymeric particles find their applications in different areas, such as toners, instrument calibration standards, column packing materials for chromatography, spacers for liquid crystal displays, and biomedical or biochemical analysis (57). However, recently also some novel uses have been reported, e.g. crosslinked polystyrene/multi-walled nanotube spheres prepared by *in-situ* suspension polymerization technique can be applied as conductive microfiller into PS matrix, where it enhances electrical conductivity and mechanical properties (58). Common polymers are insulators but the prepared composites can be semi- or conductive materials, which is also the case of polymer/CNT composite. The resulting microspheres with modified electrical conductivity can be advantageously applied also as electrorheological fluids.

Presence of conductive carbon nanotubes can significantly change the composite particles properties. One example is documented in Figure 8.9 (16): MMA suspension polymerized together with MWCNT.

Part (a) presents carbon nanotubes purified by acid-treatment (leading also to shortening of tubes), and part (b) shows PMMA spherical particles together with individualized MWCNT tubes, which seem to connect particles (16,18).

In consequent experiments, the authors (16) innovated the preparation procedure in order to improve the quality of prepared PMMA/MWCNT particles; they profitably used a steric stabilizer, poly(vinyl pyrrolidone) (PVP) (48). PVP has both hydrophobic and hydrophilic

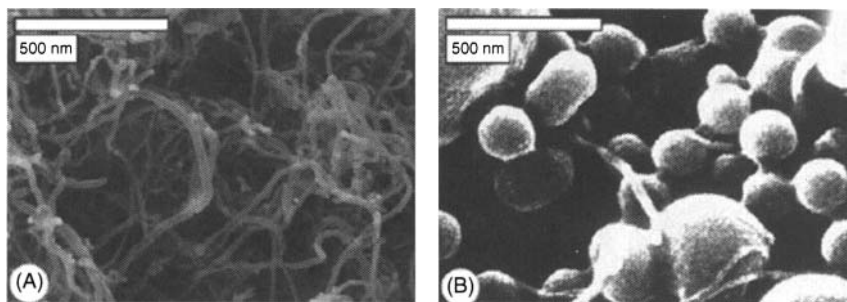


Figure 8.9. MWCNT after acid-treatment procedure to achieve their purity (e.g. removing of metallic catalysts) (a), and product of *in-situ* suspension polymerization of MMA monomer in presence of MWCNT (b) (16).

groups and can act as a surfactant contributing to better dispersion of nanotubes. CNT material in the experiment was subjected to strong acid treatment (mixture of H_2SO_4 and HNO_3 3:1) before use in polymerization. This chemical procedure leads to better MWCNTs disentanglement during polymerization process (under mechanical stirring) but even more during ultrasonic dispergation of CNT in reaction medium before suspension polymerization. In such chemical treatment the tubes are oxidized, which leads to their shortening and creating open ends. New functional groups synthesized by oxidation (mainly carboxyl but also carbonyl, hydroxyl and other groups (59)) are formed preferably at the end of the tubes, but also side-wall functionalization of CNT is possible. The functional groups on the tubes surface are capable to push tubes apart from each other. This, simultaneously with CNT shortening, leads to their more effective dispersing in polymer matrix, i.e. to dispersion with smaller aggregates of tubes and finally to individualized tubes. On the other hand, such drastic treatment leads to reversing of advantageous CNT characteristics like mechanical properties (mainly due aspect ratio reduction) or electrical conductivity (by increased number of defect sides on CNT walls).

The product of the innovated polymerization procedure described above shows a uniform size distribution of spherical particles, with spheres size of $\sim 8 \mu\text{m}$, contrary to polydispersed MWCNT/PMMA particles $\sim 1\text{--}12 \mu\text{m}$ in diameter. The polydispersity may originate from the presence of MWCNT particles (48), and the size of final MWCNT/PMMA spheres depends on MWCNT concentration and size and also on the level of MWCNT aggregation and the number of individual MWCNTs involved in the formation of composite particles. The presence of nanotubes in PMMA/MWCNT composites was confirmed by SEM analysis, which identified a large amount of MWCNTs at the surface of the composite spheres. Some of them are just adhered on PMMA spheres surface but others come into bulk of PMMA matrix. It was also confirmed by TEM analysis that nanotubes are well embedded in the surface of PMMA particles and even more, they are present inside individual PMMA/MWCNT particles.

The above cited authors further modified the procedure (57) by applying ultrasonication during the whole polymerization time; the resulting pure PMMA and composite particles are presented in Figure 8.10. Figure 8.10(a) represents PMMA microparticles prepared under mechanical stirring. As can be seen, the particles pose uniform size distribution, with a slightly smaller diameter ($\sim 6 \mu\text{m}$) than in the previous paper (48). The other two pictures present

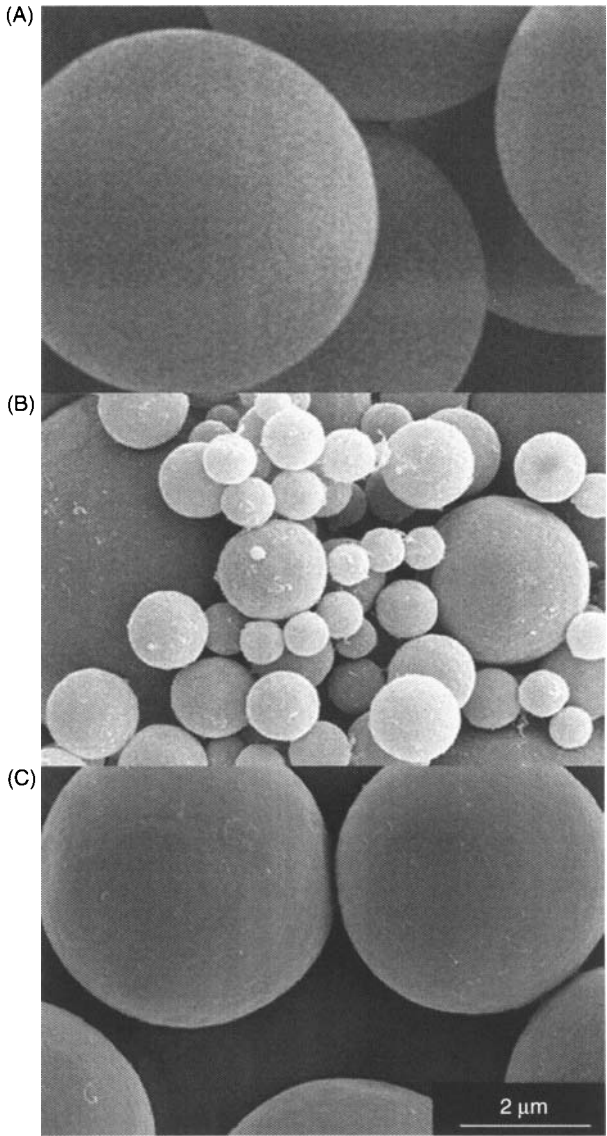


Figure 8.10. PMMA (a) and PMMA/MWCNT particles (b and c) prepared by *in-situ* suspension polymerization under stirring (b), and under ultrasonication (c) (57).

products of MMA polymerization together with MWCNT. In case of (b) only mechanical stirring was applied, which led to polydisperse particles of PMMA/MWCNT, in case of (c) batch sonication was used during the polymerization process.

It was discovered that sonication of the mixture during reaction results in PMMA/MWCNT particles with a uniform size distribution, which indicates that size distribution of composite spheres is strongly dependent on proper dispersion of the nanotubes in the reaction mixture, in this case caused by permanent sonication. Again, SEM analysis proved the presence of MWCNT on the surface of MWCNT/PMMA particles (nanotubes strongly and thickly adhered to the surface).

A similar experiment is reported in (60): *in-situ* polymerization of PMMA in presence of MWCNT at analogous experimental conditions (in methanol, using PVP as stabilizer and AIBN as initiator) produced monodisperse PMMA/MWCNT microspheres only with the help of mechanical stirring. The spheres diameters decreased from about 11.6 μm to 6.0 μm as the content of MWCNT increased from 0 to 0.03 wt%. Additional analyses identified carbon nanotubes to be present both in the interior and on the surface of the particles.

The process and properties of PS/MWCNT particles prepared by *in-situ* suspension polymerization are presented in (21). Here, however, the presence of CNT material coming into or out from spheres or adsorbed on their surfaces was not spotted on SEM images, although some differences in the size and the structure of particles can be identified between pure PS and PS/MWCNT composite.

The following TEM microscopy analysis observed the cross sections of ultra-thin cuts through PS/MWCNT and pure PS spheres. In Figure 8.11, it can be seen that the structure of the composite sphere is made of smaller particles with distinct boundaries creating somewhere only contact of smaller particles (arrows 1) or creating some space between them with new heterogeneous phase (arrows 2). The interface between particles is significantly disturbed in PS/MWCNT composite (arrows 2). No nanotubes were found in the volume of particles assembling basal spheres. It seems that nanotubes are situated in the space between sintered PS particles.

8.5.1 CNT Material Adsorbed onto Polymer Microspheres

The suspension polymerization method has become very popular because of its simplicity and the wide variety of monomers which can be effectively polymerized. Prepared spherical particles are applied in different areas of science and technology. It is also the case of polymer/CNT nanocomposite microspheres produced by the modified

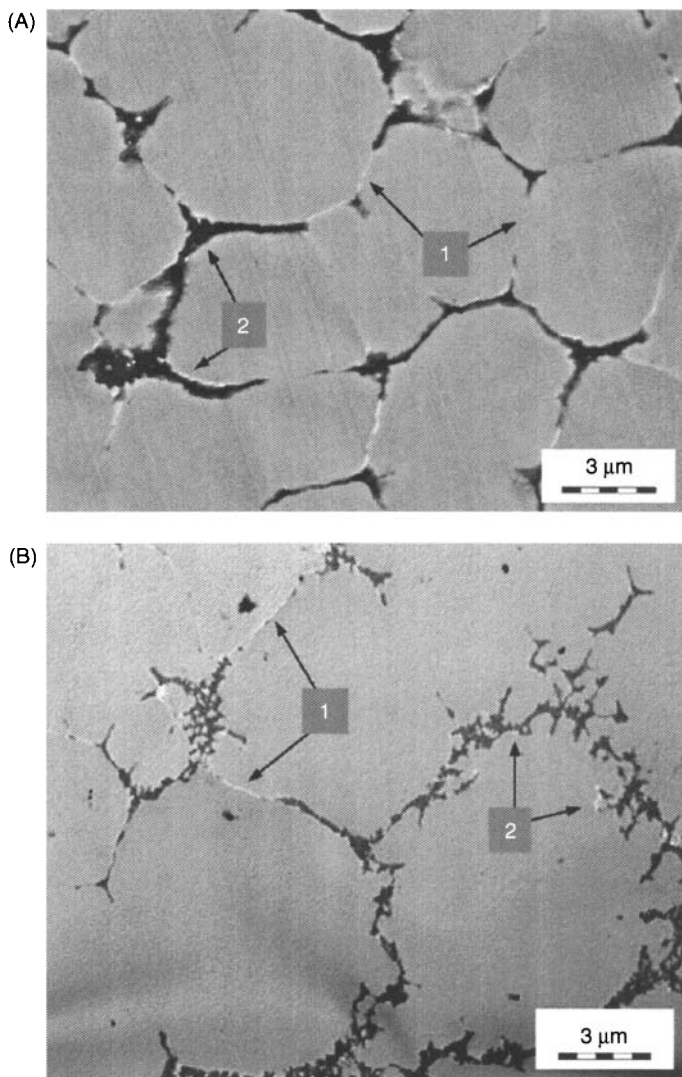


Figure 8.11. TEM analysis of ultra-thin cross-sections of PS (a) and PS/MWCNT containing 0.3 wt% MWCNT (b) microspheres prepared by *in-situ* suspension polymerization (21).

version of suspension polymerization, which can be advantageously applied for example as electrorheological fluids (16,18,20,21).

The interest in electrorheology has stimulated development of a new method of preparation of particles for such fluids. In this technique, polymeric microspheres are produced separately, which is

followed by controlled CNT adsorption on their surface (20,61–63). It means, in the first step CNT aqueous dispersion is prepared and polymer microspheres polymerized (PS, PMMA) separately. The nanotubes dispersion is prepared with the help of suitable surfactants and ultrasound. Proper surfactants for stable aqueous CNT dispersions are, for instance, anionic sodium dodecyl sulfate (SDS) and sodium dodecylbenzene sulfonate (NaDDBS), cationic cetyl trimethylammonium bromide (CTAB), and nonionic Triton X-100. In the second step, polymer microspheres water dispersion is slowly dropped into CNT/surfactant dispersion. After some time the nanotubes are adsorbed on the surface of microspheres, which causes their slow sedimentation and changes supernatant of the nanotube dispersion into a clear solution. The surface morphology of the resulting microspheres can be observed after particles removing, washing of the rest of surfactant and drying. A suitable method for the analysis is field emission scanning electron microscopy (FESEM) (20), as presented in Figure 8.12. Here, part (a) represents PMMA microspheres prepared by suspension polymerization and stabilized by poly(vinyl pyrrolidone). Then aqueous MWCNT dispersion was prepared by sonication, with the help of CTAB, the surfactant concentration being approximately 0.3 wt% and the nanotubes concentration about 0.02 wt%. In the procedure, PMMA microspheres water dispersion was dropped into nanotube dispersion using a syringe pump at a rate of 0.5 ml/min. The product of this second step is presented in part (b). As can be seen, carbon nanotubes are heavily adsorbed onto the surface of PMMA microspheres. The origin of such good adhesion can be explained by hydrophobic interaction between PMMA and MWCNT (63).

The same experimental group continued the research (61) by adsorption of carbon nanotubes onto both PS and PMMA particles in the same method, with four different surfactants. Finally, the prepared PS microspheres with adsorbed nanotubes were sonicated in deionised water to test the durability of their association. It was found that individual tubes remain strongly adhered to the PS microspheres surfaces even after exposition to ultrasound.

The amount of adsorbed carbon nanotubes onto PS and PMMA microspheres was measured (61), and the results are presented in Table 8.2. It was found that the type of surfactant considerably affects the amount of adhered CNT. As can be seen, the best results, i.e. the highest CNT amount, were achieved for CTAB and NaDDBS. The influence of the used surfactants and polymer

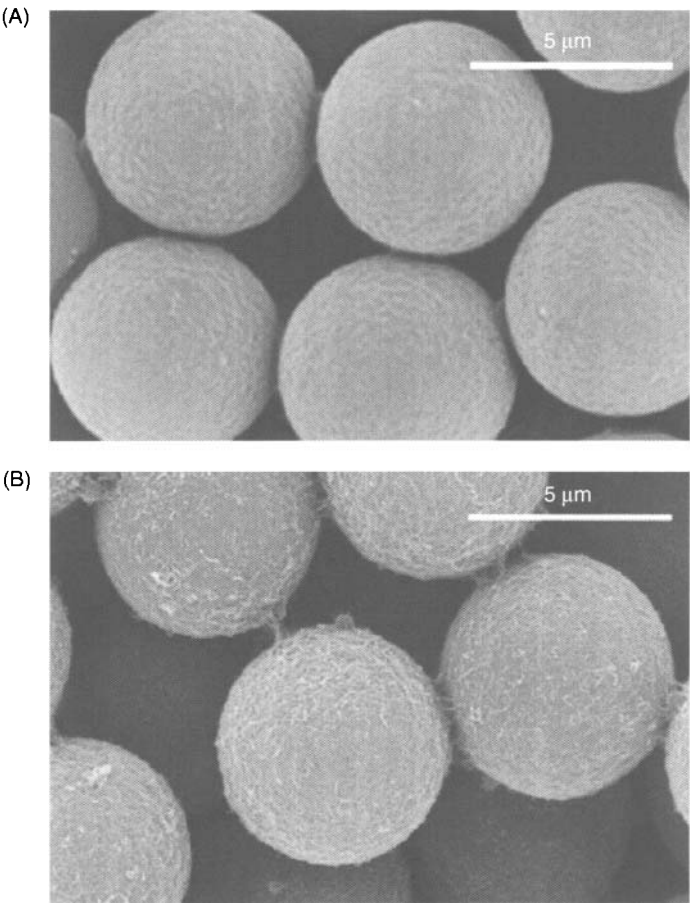


Figure 8.12. FESEM analysis of (a) PMMA microspheres prepared by suspension polymerization, and (b) PMMA microspheres with adsorbed MWCNT particles (20).

Table 8.2. The amount of adsorbed carbon nanotubes on the surface of suspension polymers PS and PMMA with various surfactants, and electrical conductivities of prepared compression moulded discs-type specimens (61)

Surfactant	Amount (wt%) of CNT coated on microspheres		Conductivities [S/cm]	
	PS	PMMA	PS	PMMA
CTAB	5.9	3.9	1.9×10^{-4}	6.3×10^{-4}
NaDDBS	4.7	3.6	2.9×10^{-5}	5.2×10^{-5}
SDS	1.8	2.1		
Triton X-100	2.3	1.6		

matrix on electrical conductivity was also studied, which was studied on discs-type specimens produced from polymer/CNT microspheres by compression (20,61).

8.6 Electrorheology of Polymer/CNT Nanocomposites Prepared by *in-situ* Suspension Polymerization

As mentioned above, one of the possible applications of composites prepared by *in-situ* dispersion polymerization is their use in electrorheological (ER) fluids (16,18,20,21,57,61,63). This area has been lately going through intensive development, with promising applications. Electrorheology employs the fact that when external electric field (both DC and AC) in the order of $\text{kV}\cdot\text{mm}^{-1}$ is applied, suitable ER fluids dramatically change their viscosity in a very short time (milliseconds) (64). The particles become polarized, direct themselves along the lines of the field and join into chains or columns spanning the gap between the electrodes. This change in structure reflects in a steep increase in viscosity (several orders of magnitude) or even solidification of the fluid. The strength of the structure created is assessed by yield stress, which is the value of stress above which the material starts to flow. When the electric field is switched off, polarization of particles disappears, the particles return to random positions and viscosity restores to its original level.

Electrorheological phenomenon is demonstrated in Figure 8.13 on optical microscope images of two different types of CNT microspheres. Both are based on PMMA matrix but in the first case the particles were prepared by *in-situ* suspension polymerization in presence of MWCNT (57) and in the second by MWCNT adsorption on separately prepared PMMA microspheres (20). Particles were dispersed in silicon oil and placed between two parallel electrodes. Figure 8.13(a) represents the state without and Figure 8.13(b) with applied electric field. In the figure, typical ER fibril structures can be observed for both principal materials when external electric field is applied; the dispersed PMMA/MWCNT microspheres form chain structures.

Electrorheological properties of fluids, in this case PS/MWCNT suspensions in silicone oil, can be demonstrated in the form of flow curves obtained from measurements on a rotational rheometer in the absence and presence of external electric field (21). The flow curves expressing shear stress vs. shear rate dependence are

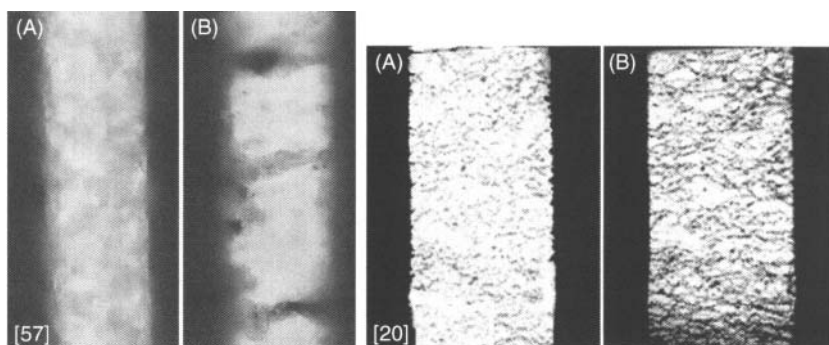


Figure 8.13. Optical microscope image of silicone oil dispersions of PMMA/MWCNT microspheres (left part) (57) and of MWCNT particles adsorbed on PMMA microspheres (right part) (20), in both cases without (a) and with applied electric field (b).

shown in Figure 8.14. For this demonstration, composite particles containing 1 wt% MWCNT were chosen because the observed ER effect was strongest for this concentration, but in general all the investigated samples showed very similar trends. In the absence of electric field, the fluid shows Newtonian behaviour: the shear stress increases linearly with the shear rate, with a slope of 1.0. In the presence of electric field, the suspension displays an obvious ER effect - the shear stress rapidly increases with increasing electric field strength, and the fluid shows Bingham behaviour.

The dynamic yield stress (extrapolated to zero shear rates, Figure 8.15) becomes greater with stronger field, indicating the increase of attractive forces between the polarized particles with applied electric field. This phenomenon is attributed to columnar or fibrillar structure formed by the particles as a response to electrostatic interactions induced by electric field. The stronger the field, the larger shear rate is needed to destroy the structure.

Beside the strength of electric field, the dynamic yield stress significantly depends on the amount of MWCNT in the composite particles. As can be seen in Figure 8.15, for different field strength the yield stress goes up with rising concentration in different ways. While for 1 and 2 kV/mm, it continuously increases with nanotubes content, at 3 kV/mm a saturation effect can be observed. The presence of MWCNT enhances the conductivity of the composite particles and thus influences their ability to be polarized. If the conductivity of the particles is above a certain limit, the current density in the

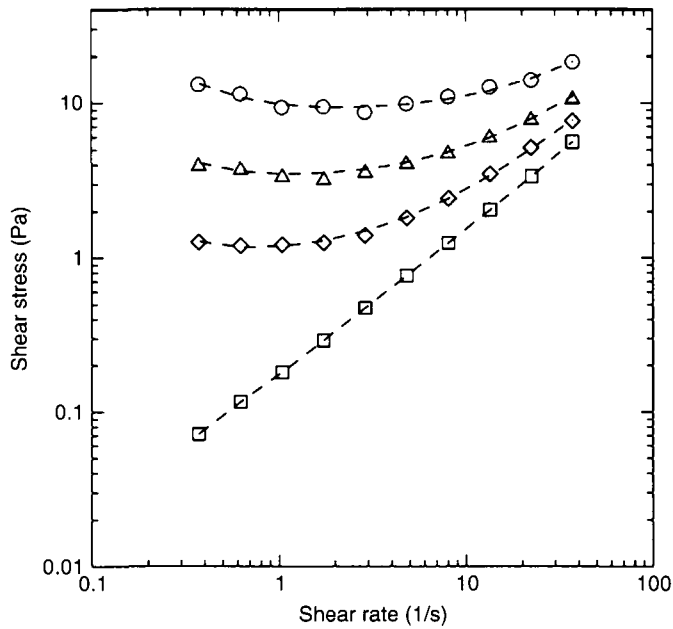


Figure 8.14. Dependence of shear stress on shear rate at various electric field strengths for 9 wt% PS/MWCNT in silicone oil (MWCNT content 1 wt%). Electric field strengths (kV/mm): 0 (\square), 1 (\diamond), 2 (Δ), 3 (O) (21).

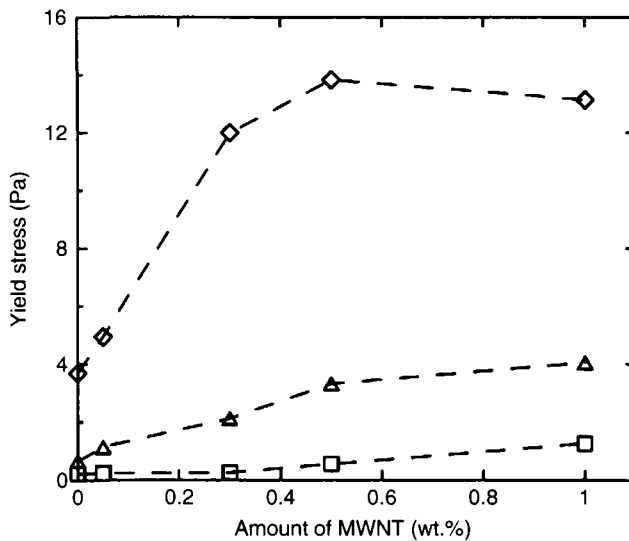


Figure 8.15. Dependence of yield stress on MWCNT content in particles at various electric field strengths. E (kV/mm): 1 (\square), 2 (Δ), 3 (\diamond) (21).

fluid increases and even shortcut may appear. Thus suspensions containing too conductive particles are not suitable ER fluids.

As the chapter has shown, suspension polymerization in the presence of carbon nanotubes can be an efficient tool for the preparation of materials suitable for a broad spectrum of applications. As the properties of the resulting material can be to a certain level tailored to the requirements, it is a promising area for research and industry.

References

1. Q. Cheng, J. Bao, J.G. Park, Z. Liang, C. Zhang, and B. Wang, *Advanced Functional Materials*, Vol. 19, p. 1, 2009.
2. H.T. Ham, Y.S. Choi, and I.J. Chung, *Journal of Colloid and Interface Science*, Vol. 286, p. 216, 2005.
3. K.A. Narh, L. Jallo, and K.Y. Rhee, *Polymer Composites*, Vol. 29, p. 809, 2008.
4. A. Thess, R. Lee, P. Nikolaev, H.J. Dai, P. Petit, J. Robert, C.H. Xu, Y.H. Lee, S.G. Kim, A.G. Rinzler, D.T. Colbert, G.E. Scuseria, D. Tomanek, J.E. Fischer, and R.E. Smalley, *Science*, Vol. 273(5274), p. 483, 1996.
5. H. Kathyayini, I. Willems, A. Fonseca, J.B. Nagy, and N. Nagaraju, *Catalysis Communications*, Vol. 7(3), p.140, 2006.
6. M.A.L. Manchado, L. Valentini, J. Biagiotti, and J.M. Kenny, *Carbon*, Vol. 43, p. 1499, 2005.
7. P. Slobodian, A. Lengálová, M. Šlouf, and P. Sáha, *Journal of Reinforced Plastics and Composites*, Vol. 26, p. 1705, 2007.
8. W.Z. Tang, M.H. Santare, and S.G. Advani, *Carbon*, Vol. 41, p. 2779, 2003.
9. O. Meincke, D. Kaempfer, H. Weickmann, C. Friedrich, M. Vathauer and H. Warth, *Polymer*, Vol. 45, p. 739, 2004.
10. P.M. Ajayan, L.S. Schadler, C. Giannaris, and A. Rubio, *Advanced Materials*, Vol. 12, p. 750, 2000.
11. L.S. Schadler, S.C. Giannaris, and P.M. Ajayan, *Applied Physics Letters*, Vol. 73, p. 3842, 1998.
12. K. Schulte, and H. Windle, *Composites Science and Technology*, Vol. 67, p. 777, 2007.
13. X.L. Xie, Y. W. Mai, and X.P. Yhou, *Materials Science and Engineering R*, Vol. 49, p. 89, 2005.
14. L.S. Schadler, S. C. Giannaris, and P.M. Ajayan, *Applied Physics Letters*, Vol. 73, p. 3842, 1998.
15. S.T. Kim, H.J. Choi, and S.M. Hong, *Colloid and Polymer Science*, Vol. 285, p. 593, 2007.
16. S.J. Park, S.T. Lim, M.S. Cho, H.M. Kim, J. Joo, and H.J. Choi, *Current Applied Physics*, Vol. 5, p. 302, 2005.
17. S.J. Park, M.S. Cho, S.T. Lim, H.J. Choi, and M.S. Jhon, *Macromolecular Rapid Communications*, Vol. 24, p. 1070, 2003.
18. S.J. Park, M.S. Cho, S.T. Lim, H.J. Choi, and M.S. Jhon, *Macromolecular Rapid Communications*, Vol. 26, p. 1563, 2005.
19. Z. Wang, M. Lu, H.L. Li, and X.Y. Guo, *Materials Chemistry and Physics*, Vol. 100(1), p. 77, 2006.

20. I.S. Lee, S.H. Yoon, H.J. Jin, and H.J. Choi, *Diamond and Related Materials*, Vol. 15, p. 1094, 2006.
21. P. Slobodian, V. Pavlínek, A. Lengálová, and P. Sáha, *Current Applied Physics*, Vol. 9, p. 184, 2009.
22. H.T. Ham, Y.S. Choi, M.G. Chee, and I.J. Chung, *Journal of Polymer Science, Part A: Polymer Chemistry*, Vol. 44 (1), p. 573, 2006.
23. Y. Xu, B. Higgins, and W.J. Brittain, *Polymer*, Vol. 46, p. 799, 2005.
24. P. Slobodian, D. Králová, A. Lengálová, R. Novotný, and P. Sáha., *Polymer Composites*, Vol. 31, no. 3, p. 452, 2010.
25. A. Rasheed, J.Y. Howe, M.D. Dadmun, and P.F. Britt, *Carbon*, Vol. 45, p. 1072, 2007.
26. K. Hernadi, A. Siska, L. Thien-Nga, L. Forro, and I. Kiricsi, *Solid State Ionics* 141 (2001) 203.
27. T. Ramanathan, H. Liu, L.C. Brinson, *Journal of Polymer Science, Part B: Polymer Physics*, Vol. 43, 3269, 2005.
28. M.H. Kim, C.K. Hong, S. Choe, and S.E. Shim, *Journal of Polymer Science, Part A: Polymer Chemistry*, Vol. 45, p. 4413, 2007.
29. J.U. Ha, M. Kim, J. Lee, S. Choe, I.W. Cheong, and S.E. Shim, *Journal of Polymer Science, Part A: Polymer Chemistry*, Vol. 44, p. 6394 (2006).
30. J.W. Xiong, Z. Zheng, X.M. Qin, M. Li, H.Q. Li, and X.L. Wang, *Carbon*, Vol. 44, p. 2701, 2006.
31. T. Ramanathan, F.T. Fisher, R.S. Ruoff, and L.C. Brinson, *Chemistry of Materials*, Vol. 17, p. 1290, 2005.
32. D. Kimmer, P. Slobodian, D. Petráš, M. Zatloukal, R. Olejník, and P. Sáha P, *Journal of Applied Polymer Science*, Vol. 111(6), p. 2711, 2009.
33. H.J. Choi, K. Zhang, and J.Y. Lim, *Journal of Nanoscience and Nanotechnology*, Vol. 7(10), p. 3400, 2007.
34. K. Zhang , B.J. Park, F.F. Fang , and H.J. Choi, *Molecules*, Vol. 14(6), p. 2095, 2009.
35. L.H. Sperling, *Introducing to Physical Polymer Science*, John Wiley and Sons., Lehigh University, Bethlehem, Pennsylvania, 1985.
36. J. Mleziva and J. Kálal, *Základy makromolekulární chemie*, Praha, SNTL-nakladatelství technické literatury, 1986.
37. F. Jahanzad, S. Sajjadi, M. Yianneskis, and B. W. Brooks, *Chemical Engineering and Science*, Vol. 63(17), p. 4412, 2008.
38. Y. Almong. and M. Levy, *Journal of Polymer Science, Part A: Polymer Chemistry*, Vol. 18(1), p. 1, 1980.
39. L. Danicher and P. Gramain, *Reactive Polymers*, Vol. 20, p. 111, 1993.
40. Y. Almong., S. Reich, and M. Levy, *British Polymer Journal*, 14(4) 1982, 131–136.
41. H. Minami, K. Yoshida, and M. Okubo, *Macromolecular Rapid Communications*, Vol. 29(7), p. 567, 2008.
42. H. Minami, K. Yoshida, and M. Okubo, *Macromolecular Symposia*, Vol. 281, p. 54, 2009.
43. Z.J. Jia, Z.Y. Wang, C.L. Xu, J. Liang, B.Q. Wei, D.H. Wu, and S.W. Zhu, *Materials Science and Engineering, A*, Vol. 271(1–2), p. 395, 1999.
44. X.B. Wang, S.Q. Li, Y. Xu, L. Wan, H.J. You, Q. Li, and S.M. Wang, *Applied Surface Science*, Vol. 253(18), p.7435, 2007.

45. J.U. Park, S. Cho, K.S. Cho, K.F. Ahn, S.J. Lee, and S.J. Lee, *Korea-Australia Rheology Journal*, Vol. 17(2), p. 41, 2005.
46. S. Banerjee, T. Hemraj-Benny, and S.S. Wong, *Advanced Materials*, Vol. 17(1), p. 17, 2005.
47. P. Liu, *Journal of Nanoparticles Research*, Vol. 11(4), p. 1011, 2009.
48. S.T. Kim, J.Y. Lim, B.J. Park, and H.J. Choi, *Macromolecular Chemistry and Physics*, Vol. 208(5), p. 514, 2007.
49. M. Tabata, and J. Sohma, *Chemical Physics Letters*, Vol. 73(1), p. 178, 1980.
50. M. Tabata, and J. Sohma, *European Polymer Journal*, Vol. 16(7), p. 589, 1980.
51. Q.Y. Li, G.Z. Wu, Y.L. Ma, and C.F. Wu, *Carbon*, Vol. 45(12), p. 2411, 2007.
52. Q. Li, Y. Ma, C. Mao, and C. Wu, *Ultrasonics Sonochemistry*, Vol. 16(6), p. 752, 2009.
53. K.B. Shelimov, R.O. Esenaliev, A.G. Rinzler, C.B. Huffman, and R.E. Smalley, *Chemical Physics Letters*, 282(5–6), p. 429, 1998.
54. E.A. Zaragoza-Contreras, E.D. Lozano-Rodríguez, M. Román-Aguirre, W. Antunez-Flores, C.A. Hernández-Escobar, S. G. Flores-Gallardo, and A. Aguilar-Elguezabal, *Micron*, Vol. 40(5–6), p. 621, 2009.
55. R. Olejník, L. Pengbo, P. Slobodian, M. Zatloukal, and P. Saha, AIP Conference Proceedings (Novel Trends in Rheology III), Zlín, Czech Republic, p. 204, 2009.
56. P. Potschke, T.D. Fornes, and D.R. Paul, *Polymer*, Vol. 43(11), p. 3247, 2002.
57. H.J. Choi, J.Y. Lim, and K. Zhang, *Diamond and Related Materials*, Vol. 17(7–10), p. 1498, 2008.
58. S.M. Kwon, H.S. Kim, S.J. Myung, and H.J. Jin, *Journal of Polymer Science, Part A: Polymer Physics*, Vol. 46(2), p. 182, 2008.
59. J. Zhang, H.L. Zou, Q. Qing, Y.L. Yang, Q.W. Li, Z.F. Liu, X.Y. Guo, and Z.L. Du, *Journal of Physical Chemistry B*, Vol. 107, p. 3712, 2003.
60. S.M. Kwon, H.S. Kim, D.Y. Kim, Y.S. Yun, and H.J. Jin, *Journal of Applied Polymer Science*, Vol. 110 (6), p. 3737, 2008.
61. H.J. Jin, H.J. Choi, S.H. Yoon, S.J. Myung, and S.E. Shim, *Chemistry of Materials*, Vol. 17(16), p. 4034, 2005.
62. K. Zhang, J.Y. Lim, B.J. Park, H.J. Jin, and H.J. Choi, *Journal of Nanoscience and Nanotechnology*, Vol. 9(2), p. 1058, 2009.
63. J.H. Sung, H.S. Kim, H.J. Jin, H.J. Choi, and I.J. Chin, *Macromolecules*, Vol. 37(26), p. 9899, 2004.
64. V. Pavlinek, P. Saha, J. Stejskal, and O. Quadrat, *Journal of Rheology*, Vol. 43, p. 1547, 1999.

Poly lactide-Based Carbon Nanotube Nanocomposites

Srikanth Pilla¹, Shaoqin Gong^{1,2,3}
and Lih-Sheng Turng⁴

¹*Department of Mechanical Engineering and*

²*Department of Materials, University of Wisconsin-Milwaukee,
Milwaukee, WI 53211, USA*

³*Department of Biomedical Engineering, University of Wisconsin-Madison,
Madison, WI 53706, USA*

⁴*Department of Mechanical Engineering, University of Wisconsin-Madison,
Madison, WI 53706, USA*

Abstract

There has been growing interest in developing biodegradable and biobased materials in recent decades due to concerns about the impact of petroleum-based plastics on the environment, as well as depleting fossil fuels. Polylactide (PLA) is one of the most widely studied biodegradable and biobased polymers due to its unique material properties and commercial availability at a reasonable price. PLA is an aliphatic polyester, which has many potential applications in areas such as packaging, automobiles, and medical devices. To further modify the material properties of PLA, PLA composites with different types of fillers, including carbon nanotubes (CNTs), were investigated. CNTs have excellent mechanical properties and good thermal and electrical properties; thus, when blended with PLA, the resulting PLA-CNT nanocomposites exhibit a set of unique properties. This chapter reviews this new class of materials, viz. their preparation, properties, and potential applications.

Keywords: biodegradable, biobased, polyester, polylactide, mechanical properties, dispersion, environmentally friendly.

9.1 Introduction

Human society has benefited tremendously from the use of petroleum-based plastics due to their versatility and ease of manufacturability;

however, this prosperity comes at the price of adverse effects on the environment and depleting fossil fuels. To minimize these undesirable consequences, scientists have been developing biobased plastics that are sustainable and biodegradable. Biobased plastics can reduce our dependency on depleting fossil fuels and help to control the emission of CO₂. Some representative biobased plastics include polylactide (PLA), polyhydroxyalkanoates (PHAs), starch plastics, and polytrimethylene terephthalate (PTT). PLA is one of the most widely studied biodegradable and biobased polymers due to its unique material properties and commercial availability at a reasonable price (1).

PLA was first produced by Pelouze (2), in 1845, through condensation polymerization of lactic acid. Although PLA was first synthesized more than 160 years ago, its commercial feasibility and usefulness has not been prominent until recently, when an economical way of manufacturing the monomer for PLA was discovered and commercialized (3).

Table 9.1 provides the physical and rheological properties of PLA. Due to its biodegradability and biocompatibility, PLA is used in medical applications such as surgical implants (4–6), tissue engineering (7) and wound closures (8), and in commodity applications such as food packaging (9). Although PLA greatly interests many scientists and engineers, its inferior properties such as brittleness, low heat distortion temperature, and high gas permeability limit its application in areas that are currently dominated by petroleum-based plastics. Additionally, biobased polymers, including PLA, tend to have narrow processing windows, which further limit their widespread application. Therefore, over the last few years, many researchers around the world have

Table 9.1. Physical properties of PLA (35)

Property	Unit	Value
Density	kg/m ³	1.25
Molecular weight	kg/mol	100–300
Degree of crystallinity	%	10–40
Melting temperature	°C	130–200
Glass transition temperature	°C	55–70
Melting enthalpy, ΔH_m	J/g	8.1–89.1

been investigating ways to enhance the material properties and processability of PLA.

To improve the properties of PLA, plasticizers, special additives such as chain-extenders, polymer blends, and composites are commonly investigated. Martin and Averous (10) have studied the effects of various plasticizers on the properties of PLA. Pilla et al. (11–12) have investigated the effects of chain-extenders on the foaming properties of PLA. In addition, a vast number of studies have been conducted to enhance the properties of PLA by blending it with various polymers such as polyethylene oxide (PEO), polypropylene oxide (PPO), polyvinyl acetate, polyolefins, polystyrene, HIPS (high impact polystyrene), polyacetals, polycarbonate, and acrylonitrile butadiene styrene (ABS) (13–26).

For polymer composites, various types of fillers have been studied, including inorganic fillers (e.g., nanoclay (27), hydroxyapatite (28)), natural fibers (both wood and plant fibers) (29–34), and other types of fillers such as carbon nanotubes (CNTs) (35). In general, adding fillers to polymers will improve properties such as tensile strength and modulus, melt strength, thermal stability, and gas barrier properties. Of the fillers reported, nanofillers show great promise in designing eco-friendly, biobased nanocomposites (36). Such nanocomposites can match certain properties of conventional composites (with 40–50 wt% of filler) at a much lower filler loading level (≤ 5 wt%) due to the nanoparticles' high surface area-to-volume ratio and frequently high aspect ratio (27). This makes nanocomposites lighter in weight than conventional composites and an obvious choice in automotive and aerospace applications where a reduction in weight leads to less fuel consumption. Also, these types of bio-nanocomposites are well suited for biomedical applications such as fracture fixation (37). Among the various PLA nanocomposites reported, this chapter focuses on PLA-carbon nanotube (CNT) nanocomposites. Carbon nanotubes (CNTs) possess excellent mechanical properties and high electrical and thermal conductivity, making them desirable additives for high-performance, multifunctional nanocomposites (38).

This chapter first presents a brief discussion on the synthesis of PLA, then, it gives an overview of various processing techniques used to fabricate PLA nanocomposites, with a special focus on the microcellular technology. Lastly, the chapter discusses various viscoelastic, thermal, mechanical, thermal degradation, electrical

conductivity and biodegradability properties and potential applications of composites.

9.2 Synthesis of PLA

PLA is a linear, aliphatic, thermoplastic polyester made from bio-based and renewable resources such as corn, and is readily biodegradable and compostable (8,39). Figure 9.1 shows different manufacturing methods to produce high-molecular weight PLA from lactic acid. The first method is condensation polymerization of lactic acid, which yields a glassy, low-molecular weight polymer that is not suitable for many applications. To increase the molecular weight, chain coupling agents (or chain-extenders) such as isocyanates, acid chlorides, anhydrides, epoxides, thiirane, and oxazoline or esterification-promoting adjuvants such as bis(trichloromethyl) carbonate dicyclohexylcarbodiimide, and carbonyl diimidazole are added, which increases the cost and complexity of producing PLA (40–54).

The second method is azeotropic condensation polymerization of lactic acid, which produces high-molecular weight PLA without using chain-extenders or esterification-promoting adjuvants. This type of polymerization needs high reaction rates and thus uses catalysts; however, due to the use of catalysts, the PLA produced by this method is not suitable for some applications, such as medical, since any residual catalyst offers toxicity within the polymer, which is harmful for medical applications. In addition to toxicity, residual catalyst degrades PLA in further processing (39). On the other hand, the level of residual catalyst can be reduced with the use of sulphuric acid (55,56).

The third method, which has become very popular in recent years, is ring opening polymerization of lactide, the cyclic dimer of lactic acid (α -hydroxy acid). The first successful high-molecular weight PLA produced by ring opening polymerization of lactide was demonstrated by DuPont in 1954 (57). First, a low-molecular weight PLA was obtained by condensation polymerization of lactic acid. This low-molecular weight pre-polymer was then depolymerized under reduced pressure to obtain a mixture of isomers of lactide, namely, L-lactide, D-lactide, or *meso*-lactide (Figure 9.2). The lactide monomer then went through ring opening polymerization to form high-molecular weight PLA.

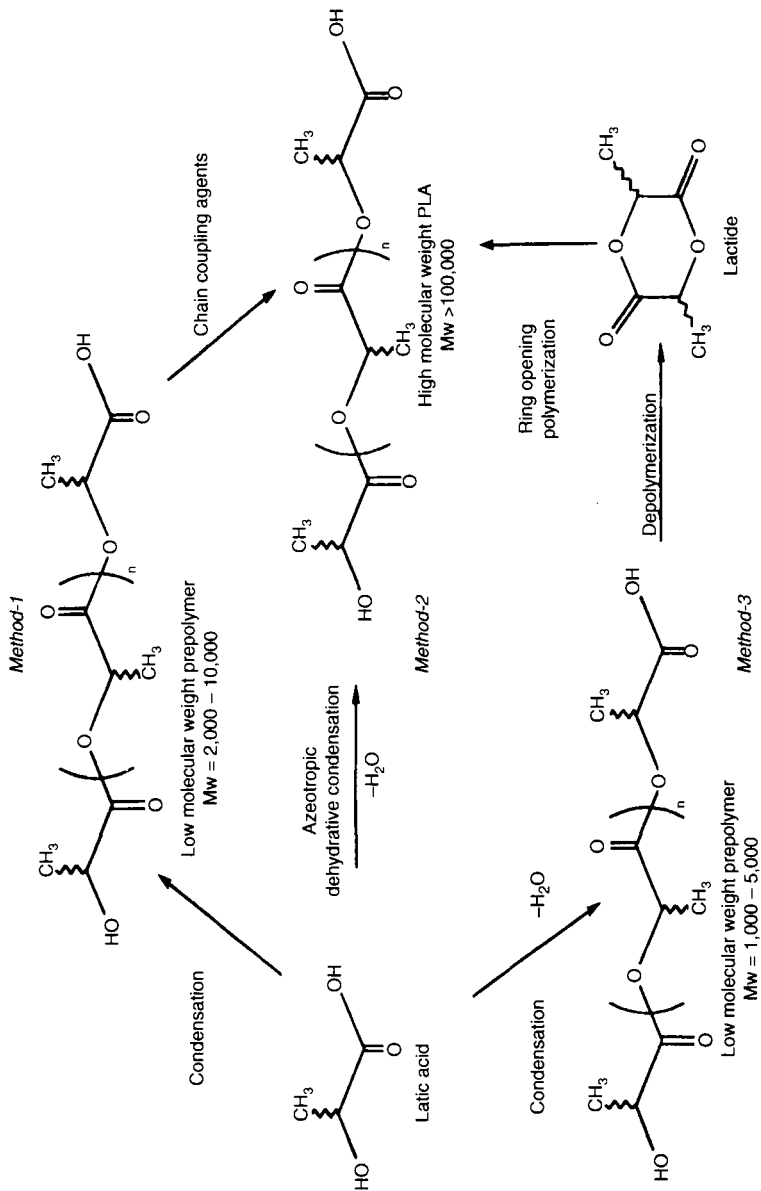


Figure 9.1. Manufacturing methods to produce high-molecular weight PLA from lactic acid. Reprinted with permission from J. Lunt, *Polymer Degradation and Stability*, Vol. 59, p. 145, 1998, © 1998, Elsevier Science Ltd.

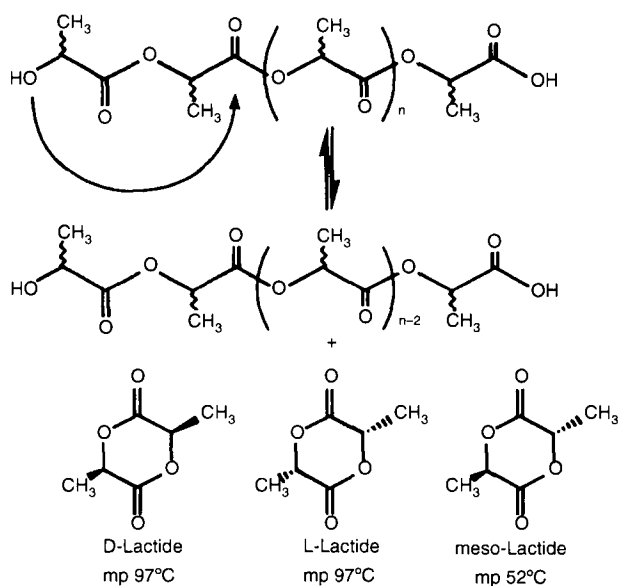


Figure 9.2. Lactide ring formation by depolymerization of low-molecular weight PLA. Reprinted with permission from J. Lunt, *Polymer Degradation and Stability*, Vol. 59, p. 145, 1998, © 1998, Elsevier Science Ltd.

9.3 Carbon Nanotubes

Carbon nanotubes (CNTs) have been one of the most outstanding scientific discoveries of the 20th century. Ever since they were discovered by Iijima in 1991 (58), CNTs have been attracting researchers due to their extraordinary physical properties. CNTs are half as dense as aluminum; have high elastic modulus and tensile strength, and good electric conductivity and current carrying capacity; they also transmit heat twice as well as pure diamond (59). For instance, the elastic modulus of CNTs can be as high as 1000 GPa and their strength can be 100 times as that of steel. Due to these outstanding properties, CNTs are used in a variety of applications such as field emission tips, mechanical memory, chemical and genetic probes, ultra-fine sensors, hydrogen and ion storage, scanning probe microscope tips, and structural composites for aerospace and automotive industries (59).

CNTs consist of graphite sheets rolled into a cylinder. CNTs have diameters in the range of 1–10 nm. CNTs can be categorized into two types: single-walled carbon nanotubes (SWCNTs) and multi-walled carbon nanotubes (MWCNTs). SWCNTs can be thought of as a single

graphite sheet rolled into a cylinder, while MWCNTs consist of multiple layers of graphite sheets rolled into a cylindrical shape.

9.4 Preparation of PLA-CNT Nanocomposites

Among the applications discussed in this chapter, the most prominent in recent years is CNT-reinforced polymer nanocomposites. The use of CNTs in polymers can provide superior mechanical properties (60). For instance, the addition of 1% CNTs might increase the stiffness of polymers by 10% and increase their resistance to fracture; however, improvements in the properties of CNT-reinforced polymers largely depend on the dispersion of CNTs within the polymer matrix and the polymer-CNT interfacial properties. The following section highlights several studies regarding the processing of PLA-CNT nanocomposites.

The first study on the preparation of PLA-CNT nanocomposites was reported by Moon et al. in 2005 (61). They used a two-step method to prepare the PLA-MWCNT nanocomposite films. In the first step, 10 wt% solution of PLA in chloroform (CHCl_3) was prepared and combined with already-dispersed MWCNTs (at 0.5, 3, 5, and 10 wt%) and was sonicated for six hours. These mixtures were then poured into Teflon dishes and dried at room temperature for one week. Later, they were vacuum-dried at 80°C for eight hours to ensure complete evaporation of the solvent. In the second step, the dried composite films created in the first step, were cut into small pieces of approximately $0.5 \sim 1.0 \text{ cm}^2$ in dimension and stacked between two metal plates. This stack was then pressed at approximately 200°C and 150 kgf/cm^2 for 15 minutes, which resulted in $100 \sim 200 \text{ }\mu\text{m}$ -thick films. This methodology yielded uniformly dispersed MWCNTs within PLA matrix, as confirmed by the TEM images (see Figure 1 in (61)). A similar methodology was also adopted by Krul et al. (62) and Tsuji et al. (63); however, Tsuji et al. casted PLLA and SWCNT films and then melt-compounded (discussed later) them for further mixing. After the melt-compounding, the nanocomposite was extruded and then compressed for further characterization.

Chen et al. used a "grafting to" technique to synthesize PLLA-MWCNT nanocomposites (64). In this study, MWCNTs were first treated with acid to yield the carboxylic-acid-functionalized MWCNTs (MWCNT-COOH), which subsequently reacted with

excess SOCl_2 to yield acyl-chloride-functionalized MWCNT (MWCNT-COCl). The MWCNT-COCl was then added to chloroform and the resulting mixture was sonicated to create a homogeneous dispersion. Next, PLLA under nitrogen was introduced to the mixture and the reactor was immersed in an oil bath with mechanical stirring to remove the solvent. The resulting reaction medium was then dissolved in excess chloroform and vacuum-filtered through a polycarbonate membrane to yield MWCNT-g-PLLA hybrids.

To understand the effect of the molecular weight of PLLA on the properties of nanocomposite, Chen et al. prepared different MWCNT-g-PLLA hybrids with varying molecular weights of PLLA, viz., 1000, 3000, 11000, and 15000. For detailed experimental conditions, refer to Chen et al. (64). The extent of PLLA grafting on MWCNTs was examined by both SEM and TEM (Figure 9.3 and Figure 9.4, respectively). TEM studies revealed that the degree

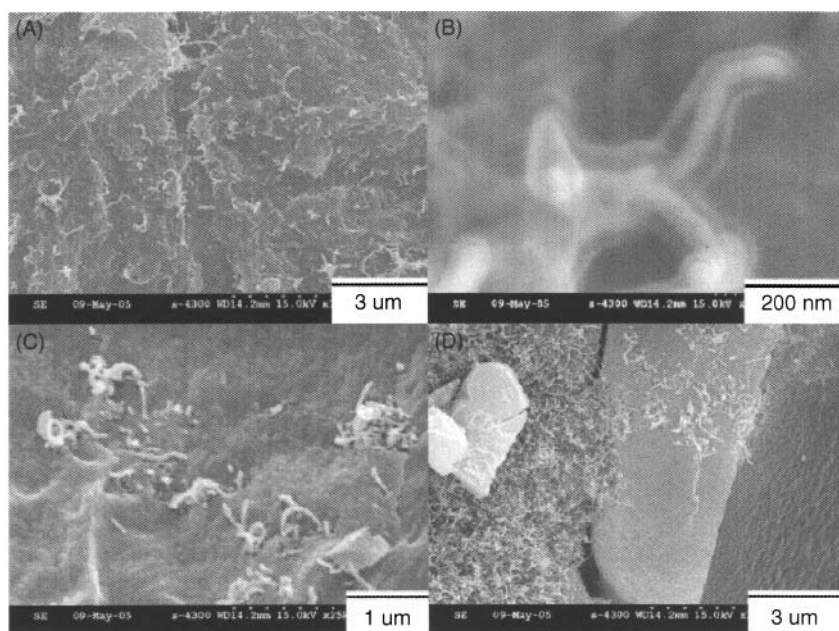


Figure 9.3. SEM images of MWCNT-g-PLLA (3000)/PLLA nanocomposite at (a) lower and (b) higher magnifications; (c) MWCNT-g-PLLA (15000)/PLLA nanocomposite and (d) PLLA-MWCNT-COOH nanocomposite. Reprinted with permission from G. Chen et al., *Journal of Polymer Chemistry*, Vol. 109, p. 22237, 2005, © 2005, Elsevier Science Ltd.

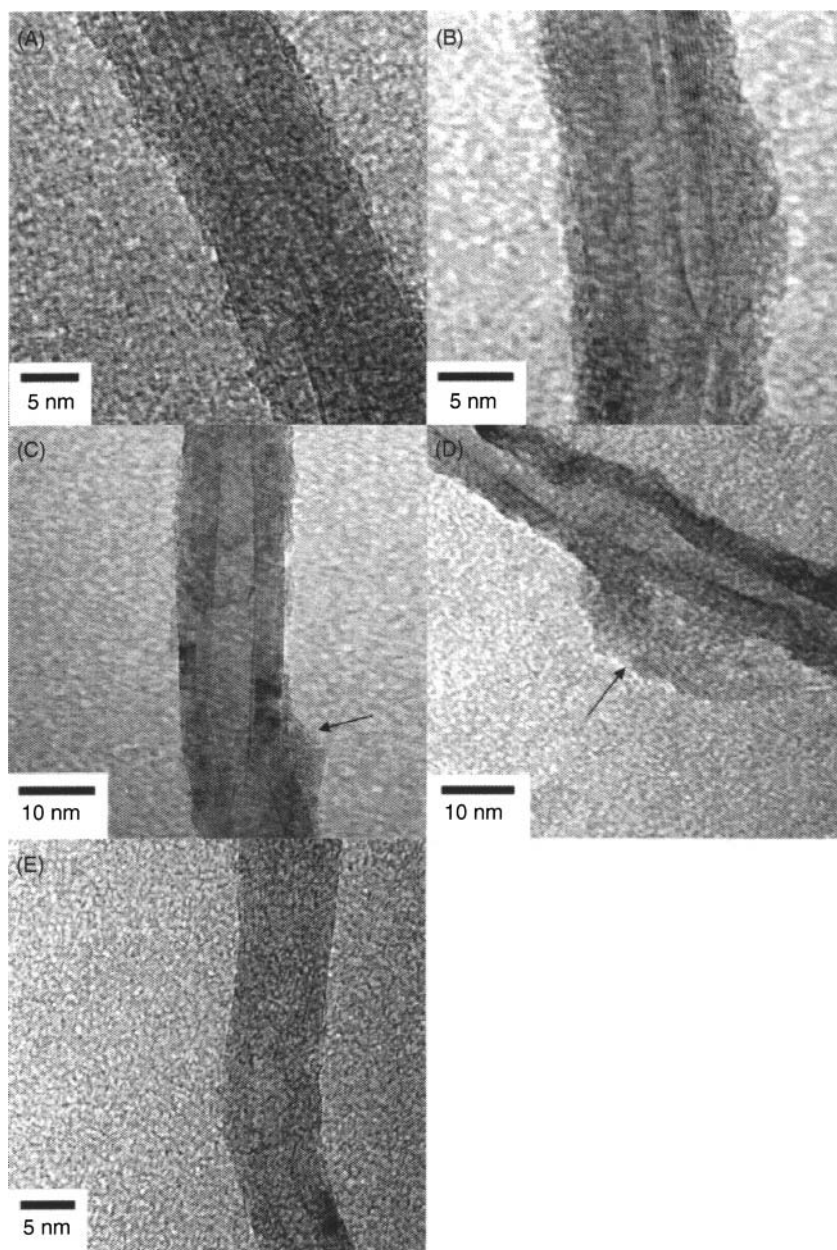


Figure 9.4. TEM images of (a) MWCNT-COOH and MWCNT-g-PLLA (15000) at (b) lower and (c) higher magnifications. Reprinted with permission from G. Chen et al., *Journal of Polymer Chemistry*, Vol. 109, p. 22237, 2005, © 2005, Elsevier Science Ltd.

of PLLA grafting strongly depended on the molecular weight of PLLA. Initially, as the molecular weight of PLLA increased from 1000 to 3000, the PLLA coating on MWCNTs became thicker and more uniform; however, when the molecular weight was further increased to 11000 and 15000, it was found that PLLA grafting did not cover the whole MWCNT surface.

Zhang et al. (65) prepared PLLA-MWCNT nanocomposites by solution-mixing and precipitation method. First, 50g MWCNTs were suspended in 1mL DMF. This suspension was stirred overnight in a round-bottom flask along with purified PLLA at 110°C under N₂. The resultant mix was poured into excess methanol, filtered, washed with methanol, and dried at 100°C under vacuum overnight, which yielded a fluffy black solid (226 mg, 90% yield). SEM and TEM (Figure 9.5) were used to visually examine the degree of dispersion and the extent of absorption of PLLA on the surface of

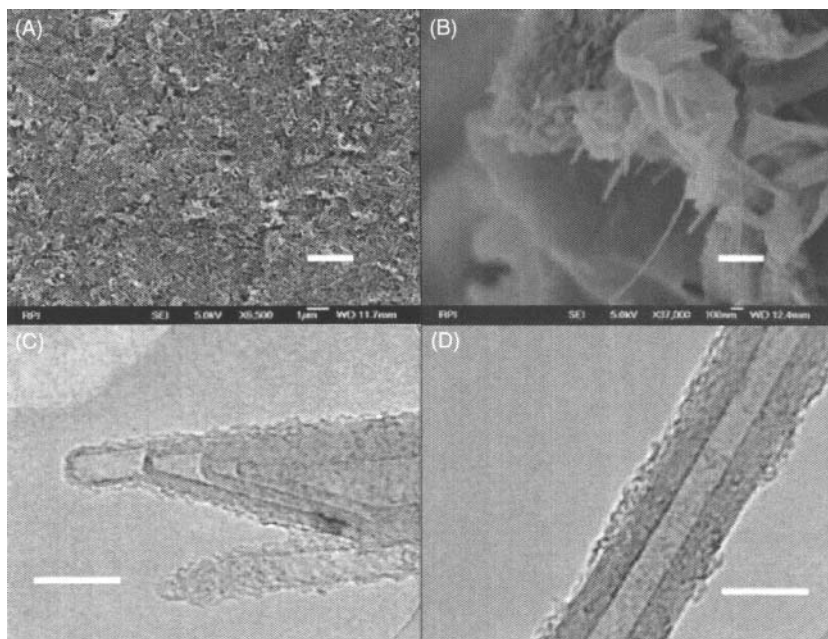


Figure 9.5. (a) SEM image of PLLA-MWCNT nanocomposites with 3wt% MWCNT loading; (b) magnified SEM image of PLLA-MWCNT nanocomposite with 3wt% MWCNT loading; (c,d) TEM images of PLLA-MWCNT (7wt%) nanocomposite showing PLLA absorbed on the MWCNT surface. Reprinted with permission from D. Zhang et al., *Journal of Physical Chemistry B*, Vol. 110, p. 12910, 2006, © 2006, American Chemical Society.

MWCNT. A uniform dispersion with good absorption of PLLA on the surface of MWCNT was observed.

Pilla et al. (35) prepared PLA-MWCNT nanocomposites using melt-compounding. First, 10% (w/v; w/v = weight/volume, g/mL) MWCNTs were sonicated in ethanol for five minutes to break up the CNT agglomerates. Afterwards, PLA pellets were added to the sonicated MWCNT solution and stirred to coat the PLA pellets with an even distribution of MWCNTs. The PLA-MWCNT mixture was then left to dry at room temperature and at atmospheric pressure to remove any excess ethanol, followed by vacuum-drying at 50 °C overnight. Finally, the PLA neat resin and PLA-MWCNT mixture were extruded using a co-rotating twin screw extruder at 200 rpm to create a PLA-MWCNT nanocomposite with an MWCNT concentration of 1.5 wt% in PLA. The extruded material was then chopped into small pellets using a pelletizer and the pellets were injection-molded using both conventional (non-foamed) and microcellular processing technology.

Microcellular processing technology was first reported during 1970s and 1980s by Skripov (66) and Suh (67). The microcellular process uses environmentally benign supercritical fluids (SCFs) such as N₂ or CO₂ as the blowing agents in contrast with conventional foaming technology that uses chemical blowing agents, which may present environmental concerns. Compared with conventional foamed plastic, microcellular-foamed plastics offer larger cell densities and reduced cell sizes at the same weight reduction, thereby improving material properties (68,69).

Figure 9.6 shows an SEM image of the microstructure of a representative microcellular plastic. In addition to reducing the density (weight) of the molded components, the microcells can act as crack arrestors by blunting the crack tip, thereby increasing the energy requirement for crack propagation. Furthermore, the SCF used in the microcellular process serves as a plasticizer by reducing the viscosity due to its presence between polymer molecules (70). This allows the materials to be processed at a lower temperature, which is significant for biobased polymers that are sensitive to high temperatures and moisture. The microcellular injection-molding process uses the thermodynamic instability phenomena to nucleate bubbles (or cells). The foaming process takes place in three steps: nucleation, cell growth, and cell stabilization. First, a large amount of SCF (under high pressure) is dissolved into a polymer melt to form a single-phase polymer-gas solution. Then, the pressure

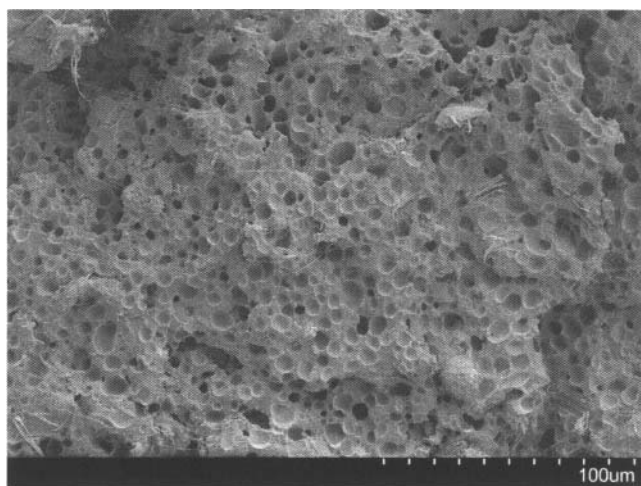


Figure 9.6. A representative image of microcellular PLA-MWCNT nanocomposite produced via microcellular injection-molding.

is suddenly lowered to below the saturation pressure, creating a phase separation and initiating cell nucleation. The nucleated cells then start to grow until they stabilize. A detailed description about microcellular processing is given in (71).

The structure of the solid¹ and microcellular nanocomposites was studied using TEM (Figure 9.7). Although a high degree of uniform dispersion of MWCNTs was not achieved in either process, nanocomposites fabricated via the microcellular process showed better dispersion compared with that made via the conventional process. This is attributed to the use of supercritical N_2 in the microcellular process, which helped to further disperse the MWCNTs due to its rapid plasticization effect.

A similar procedure for melt-compounding was adopted by Kuan et al. (72) and Wu et al. (73,74), but none of these studies used microcellular foaming for further processing. Kuan et al. molded maleic anhydride-grafted MWCNT and PLA nanocomposites using the conventional injection-molding process. Wu et al. (73) used melt compounding to blend PLA and three different types of MWCNT, viz., pure MWCNTs, carboxylic-acid-functionalized MWCNTs, and hydroxyl-functionalized MWCNTs (Figure 9.8). The resultant mixtures were compression-molded for further characterization. The order of the degree of dispersion was: carboxylic-acid-functionalized MWCNT > hydroxyl-functionalized

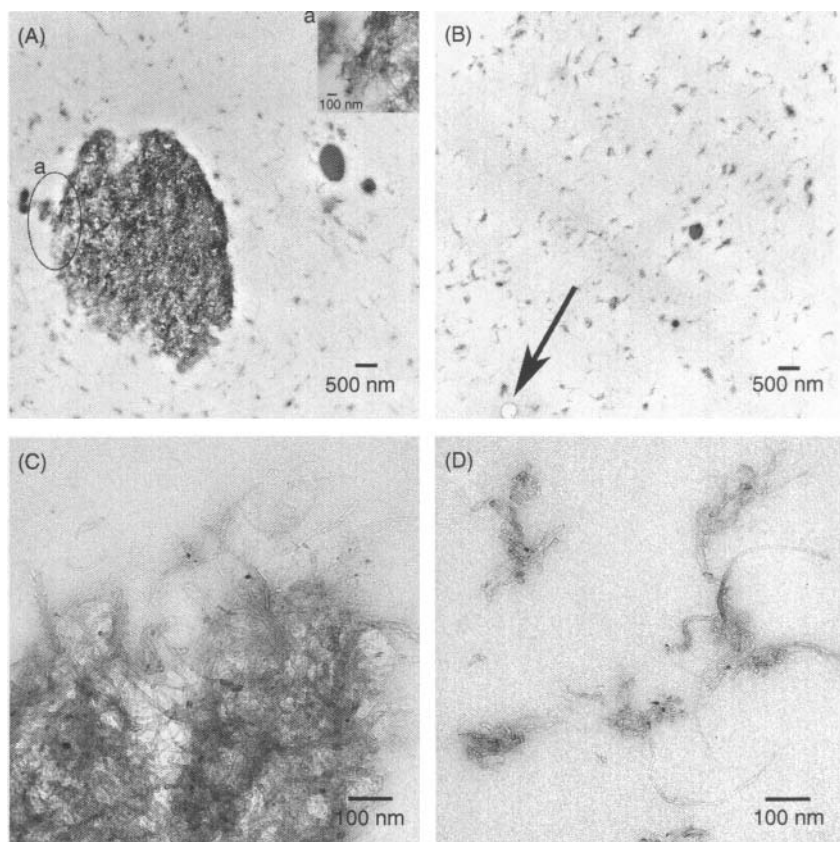


Figure 9.7. TEM Images of (a) Solid PLA-MWCNT Nanocomposite at 500 nm (Inset-a: magnified view of agglomerated MWCNTs at 100 nm); (b) Microcellular PLA-MWCNT Nanocomposite at 500 nm (arrow indicates micro cell formed during microcellular injection-molding); (c) Solid PLA-MWCNT Nanocomposite at 100 nm; and (d) Microcellular PLA-MWCNT Nanocomposite at 100 nm. Reprinted with permission from S. Pilla et al., *International Polymer Processing*, XXII, p. 418, 2007, © 2007, Polymer Processing Society.

MWCNT > pure MWCNTs. Wu et al. (74) have molded PCL/PLA-MWCNT ternary composites using melt-compounding and injection-molding with both carboxylic-acid-functionalized and non-functionalized MWCNTs. Although no discussion was presented related to dispersion of MWCNTs, it was observed that the carboxylic-acid-functionalized MWCNTs-filled nanocomposites showed better properties compared with non-functionalized ones.

Wu and Liao (75) also used melt-compounding to process PLA-MWCNT nanocomposites similar to other studies listed above;

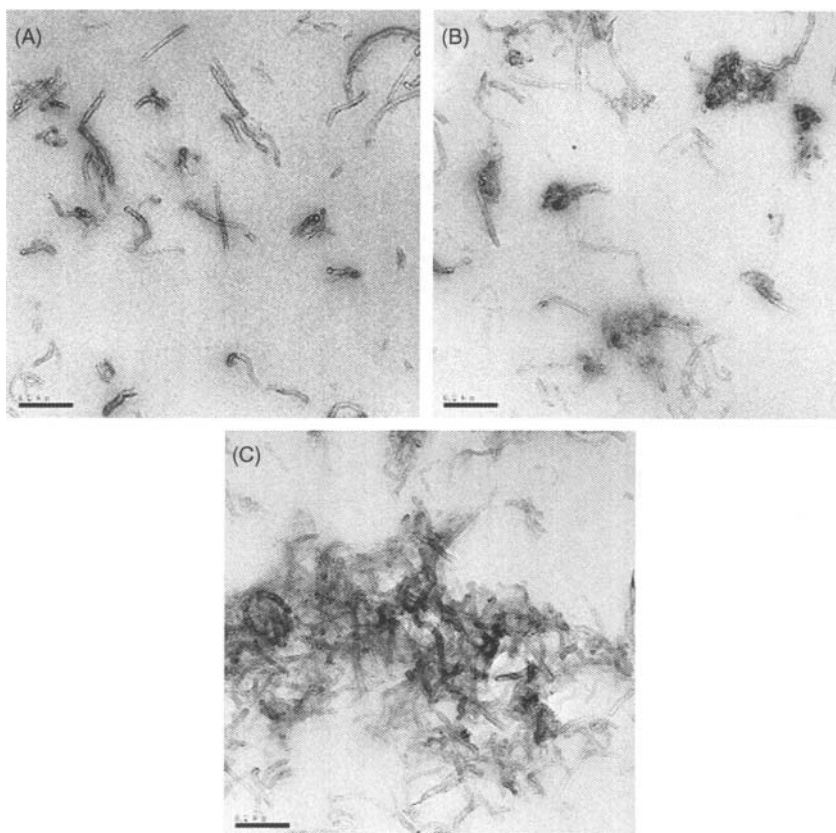


Figure 9.8. TEM images of (a) PLLA-carboxylic-acid-functionalized MWCNTs; (b) PLLA-hydroxyl-functionalized MWCNTs PLA and (c) PLLA-MWCNTs nanocomposites at a magnification of 596000. Reprinted with permission from D. Wu et al., *Polymer Degradation and Stability*, Vol. 93, p. 1577, 2008, © 2008, Elsevier Science Ltd.

however, unlike those studies, Wu and Liao used a synthesis route to enhance the reactivity of MWCNTs, as shown in Figure 9.9. First, the MWCNTs were chemically oxidized with 3:1 concentrated H_2SO_4 and HNO_3 mixture at 130–135 °C for one day to create carboxylic groups onto them. These acid-treated MWCNTs were then stirred in SOCl_2 at 65–70 °C for 24 hours under reflux; this converts the carboxylic groups into acyl chlorides. Then, the acyl-chloride-functionalized MWCNTs reacted with 1,6-hexanediol at 115–120 °C for 48 hours to produce hydroxyl-functionalized MWCNTs. These were then washed and filtered and dried overnight in a vacuum oven. The dried hydroxyl-functionalized MWCNTs were

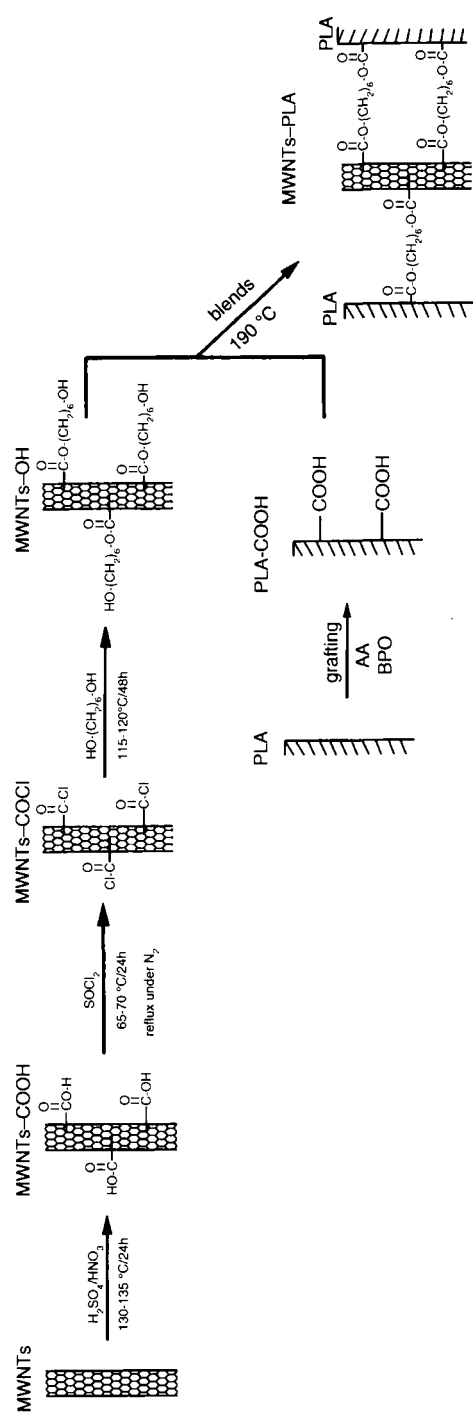


Figure 9.9. Synthesis route to enhance the reactivity of MWCNTs. Reprinted with permission from C-S. Wu and H-T. Liao, Polymer, Vol. 48, p. 4449, 2007, © 2007, Elsevier Science Ltd.

then blended along with acrylic acid grafted PLA in a mixer and compression-molded to make nanocomposites. The morphological study conducted using TEM revealed that the dispersion was uniform at a lower MWCNT ratio (1 wt%) but small agglomerates were observed at a higher ratio (3 wt%).

In addition, Song et al. (76) used a one-step condensation synthesis method to prepare the PLA-MWCNT nanocomposites. For detailed experimental conditions, refer to Song et al. (76). The nanocomposites were prepared using pure and carboxylic-acid-functionalized MWCNTs. As with the other studies, the carboxylic-acid-functionalized MWCNTs dispersed better in PLA compared with non-functionalized MWCNTs. Overall, it can be inferred from the studies described in this section that the functionalization of MWCNTs is a very important step in the process of making a nanocomposite, as it will help to disperse the nanotubes uniformly, which will eventually create the superior properties of the resulting nanocomposite. In addition, among the currently available methods for functionalization, carboxylic-functionalization is the best for uniform dispersion.

9.5 Viscoelastic Properties

The viscoelastic properties such as storage modulus, loss modulus, and $\tan \delta$ are measured using a dynamic mechanical analyzer (DMA) and/or a rheometer.

Pilla et al. (35) investigated the dynamic mechanical properties of PLA-MWCNTs nanocomposites using DMA from TA instruments (model Q800). The specimens were tested in a single-cantilever mode and under a liquid nitrogen atmosphere. The specimens were heated at a rate of 3 °C/min from 0 °C to 85 °C with a frequency of 1 Hz and pre-strain of 0.02%, which is in the linear viscoelastic region as determined by a strain sweep. A declining trend was observed for the storage modulus (G') with increasing temperature (Figure 9.10), with the most rapid reduction occurring at approximately 69 °C, corresponding with the glass transition temperature of PLA. It was also observed that the addition of MWCNTs did not seem to affect the storage modulus significantly for both the solid and microcellular specimens. The storage modulus of the microcellular components (for both the PLA and PLA-MWCNT nanocomposites) was found to be higher than their solid counterparts for temperatures

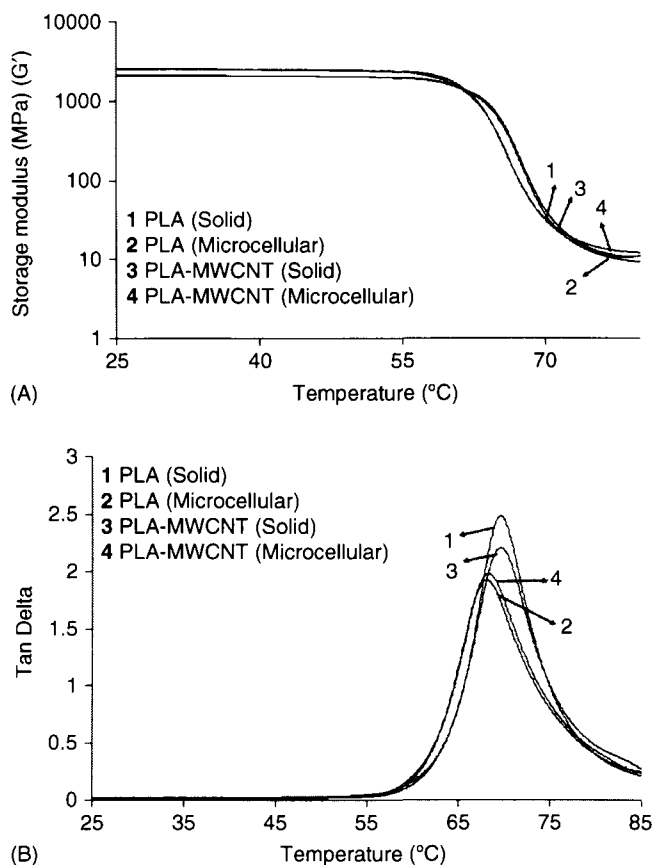


Figure 9.10. Viscoelastic Properties of Solid and Microcellular PLA and PLA-MWCNT nanocomposites: (a) Storage Modulus as a Function of Temperature; (b) Loss Factor (Tan- δ) as a Function of Temperature. Reprinted with permission from S. Pilla et al., *International Polymer Processing*, XXII, p. 418, 2007, © 2007, Polymer Processing Society.

below T_g (Figure 9.10). This may be attributed to the introduction of microcells in the microcellular components that made the polymeric material systems exhibit more elastic behavior.

In addition, it was found that the area integration under the tan δ curve (Figure 9.10) for microcellular specimens was less than that of their solid counterparts, indicating less damping in the microcellular components. For solid samples, the area under the Tan- δ peak decreased slightly with the addition of MWCNTs, as shown in the Figure 9.10. Also, the addition of MWCNTs had shifted the peak

of $\text{Tan-}\delta$, towards a slightly higher temperature for both solid and microcellular specimens, indicating that MWCNTs have meagerly influenced the chain mobility of PLA (79).

Wu and Liao (75) used DMA (TA analyzer Model 2080) to evaluate the viscoelastic properties of PLA-hydroxyl-functionalized MWCNTs nanocomposites. The tests were performed at a frequency of 1 Hz, a pre-strain level of 0.075%, and at a temperature range from -30 to 200°C with a heating rate of $3^\circ\text{C}/\text{min}$. Similar to Pilla et al. (35), Wu and Liao observed that the peak of $\text{tan } \delta$ shifted to higher temperature with the addition of 0.5 wt% hydroxyl-functionalized MWCNTs (Figure 9.11). Moreover, by increasing the amount of hydroxyl-functionalized MWCNTs to 1 wt%, the $\text{tan } \delta$ shifted to further higher temperatures. The shifting of $\text{tan } \delta$ peak to higher temperatures is an indication of good adhesion between PLA and hydroxyl-functionalized MWCNTs (75).

Wu et al. (73) studied the viscoelastic properties, viz. storage modulus (G') and complex viscosity (η^*) with respect to frequency (ω) of PLA-carboxylic-acid-functionalized MWCNTs nanocomposites using a rheometer (HAAKE RS600, Thermo Electron Co., USA). The dynamic frequency sweep measurements were carried out at the pre-strain level of 1%. They observed that the addition of carboxylic-acid-functionalized MWCNTs weakened the dependence of G' on ω , especially at higher loading levels (Figure 9.12). This indicates

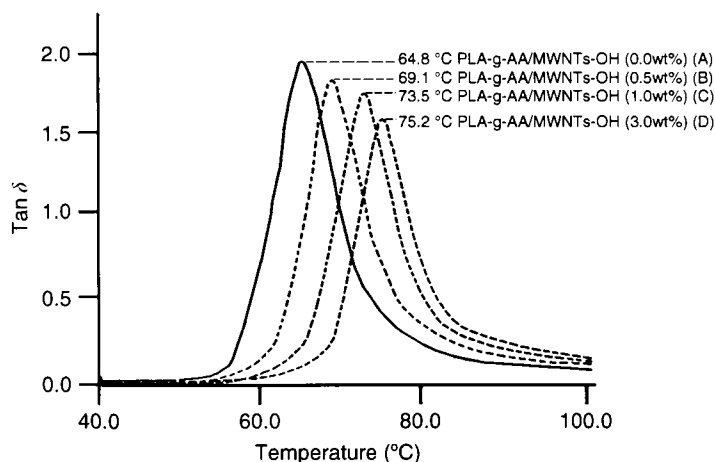


Figure 9.11. Variation of the $\text{Tan-}\delta$ with temperature for acrylic acid grafted PLA and its nanocomposites with different contents of hydroxyl-functionalized MWCNTs. Reprinted with permission from C.-S. Wu and H.-T. Liao, *Polymer*, Vol. 48, p. 4449, 2007, © 2007, Elsevier Science Ltd.

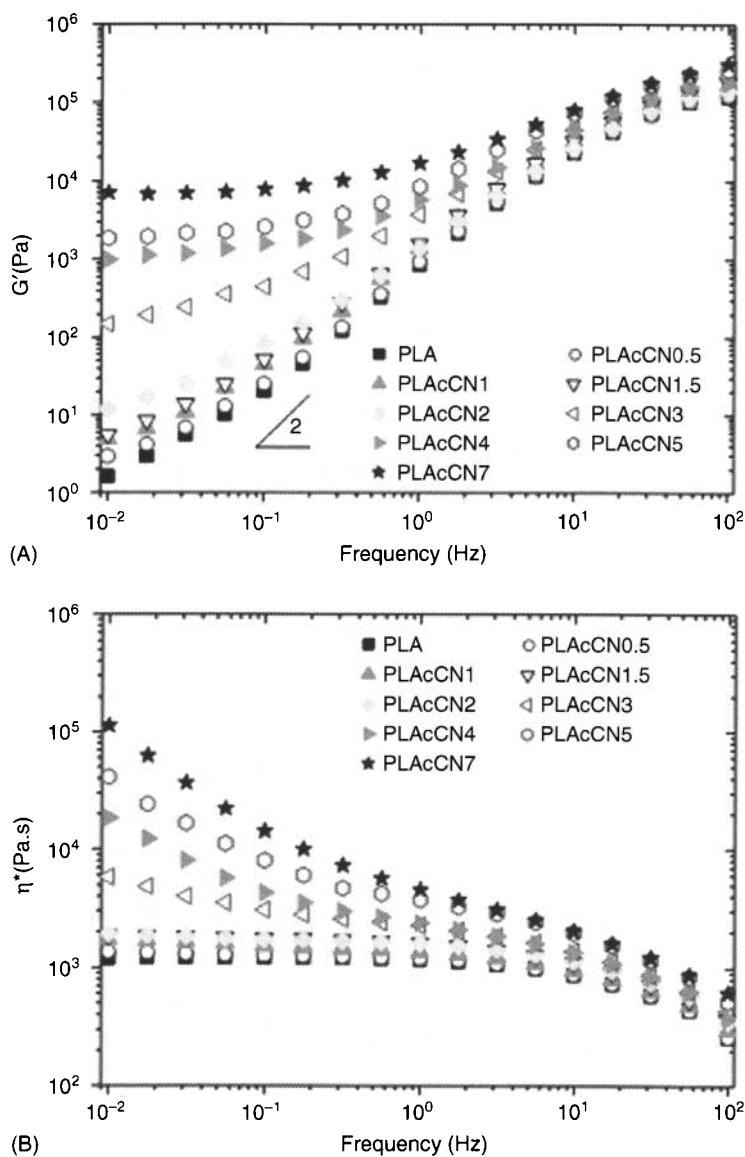


Figure 9.12. (a) Dynamic storage modulus (G') and (b) complex viscosity (η^*) for pure PLA and PLA-carboxylic-acid-functionalized MWCNTs nanocomposites obtained in dynamic frequency sweep. Reprinted with permission from D. Wu et al., *Polymer Degradation and Stability*, Vol. 93, p. 1577, 2008, © 2008, Elsevier Science Ltd.

that MWCNTs effectively restrained the relaxations of the large-scale polymer chains (80–88), which also increased η^* at lower frequencies. Moreover, the network formed by the MWCNTs within the nanocomposite also affects the η^* and G' . Thus, by increasing the content of the MWCNTs, the particle-particle interactions will become dominant and this will have an effect on the viscoelastic behavior of the nanocomposite. Hence, the content of MWCNTs in the nanocomposites needs to be optimized in order to tailor the properties for a particular application.

Similar to Wu and Liao (75), Wu et al. (74) used a DMA (Model –242C, NETZSCH Co.) and a rheometer (HAAKE RS600, Thermo Electron Co.) to evaluate the viscoelastic behavior of the carboxylic-acid-functionalized MWCNTs reinforced PCL/PLA blend. Using DMA, it was observed that, with the increase of MWCNT loading, the T_g of the blend system shifted to higher temperatures. This agrees with the results obtained from the other studies discussed above and indicates the MWCNTs are compatible with the blend. The viscoelastic properties observed via rheometer were similar to those by Wu et al. (73), discussed above.

9.6 Thermal Properties

This section discusses the thermal properties, including the glass transition temperature, melting temperature and crystallization temperature, of PLA-CNT nanocomposites as studied by differential scanning calorimetry (DSC). The thermal property studies performed by Wu and Liao (75) on non-functionalized and hydroxyl-functionalized MWCNTs filled acrylic acid-grafted PLA revealed that T_g increased in both cases with the addition of MWCNTs, although the T_g 's of hydroxyl-functionalized MWCNTs filled nanocomposites was found to be higher than that of non-functionalized MWCNTs. This was attributed to the good interfacial adhesion between hydroxyl-functionalized MWCNTs and acrylic acid-grafted PLA. However, T_g plateaued beyond certain level of MWCNT loading (1 wt%), which was attributed to fewer available reactive functional groups between the hydroxyl-functionalized MWCNTs and the acrylic acid-grafted PLA. The T_m of hydroxyl-functionalized MWCNT-filled nanocomposites was found to be lower than PLA filled with non-functionalized MWCNTs.

In the thermal studies conducted by Song et al. (76), the T_g increased modestly with the addition of pure and carboxylic-functionalized MWCNTs in PLA matrix. Also, the T_c and T_m of the nanocomposites were found to be lower than pure PLLA. Tsuji et al. (63) also observed the same trend of decreasing T_c in the nanocomposites compared with pure PLA; however, here the nano-fillers are SWCNTs. In addition, several studies reported the T_g of the nanocomposites was lower than that of pure PLLA (61, 63, 65).

Pilla et al. (35) have observed that the degree of crystallization of PLA in both solid and microcellular specimens increased with the addition of MWCNTs, thereby increasing the degree of crystallinity.

9.7 Mechanical Properties

The static mechanical properties such as tensile modulus, strength, strain-at-break, and toughness are measured using a tensile testing machine. Moon et al. (61) studied the tensile properties (Young's modulus and strain-at-break) measured using a Shimadzu Autograph SD-100-C tensile testing machine. Moon et al. observed that Young's modulus increased with MWCNTs loading; however, with the addition of MWCNTs, the stain-at-break decreased due to the development of brittle fracture mode in the nanocomposites (Figure 9.13).

On the other hand, Krul et al. (62) found that adding MWCNTs increased the tensile strength. Wu and Liao (75), Kuan et al. (72) and Wu et al. (74) have also observed similar effects of increased tensile strength with the addition of MWCNTs. In the case of Wu and Liao (75),

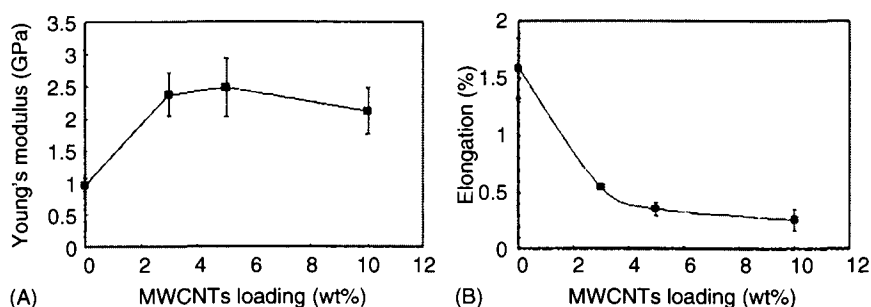


Figure 9.13. (a) Young's modulus and (b) elongation at break of PLLA-MWCNTs nanocomposites plotted versus the MWCNTs contents. Reprinted with permission from S. Moon et al., *Macromolecular Symposia*, Vol. 224, p. 287, 2005, © 2005, Wiley InterScience Ltd.

the tensile strength improved significantly up until 1wt% of MWCNTs, beyond which it plateaued. This might be due to the formation of agglomerates at a higher loading of MWCNTs (>1 wt%). Also the tensile strength of hydroxyl-functionalized MWCNT-filled nanocomposites was found to be higher than non-functionalized MWCNT-filled nanocomposites. This shows the significance of functionalization in the improvement in the tensile strength of nanocomposites. Kuan et al. (72) also observed that functionalization improved the tensile strength significantly compared with non-functionalized nanocomposites. Additionally, it was observed that the strength of low-crystalline PLA-MWCNTs nanocomposites was higher than that of high-crystalline PLA-MWCNTs nanocomposites, which was attributed to the better dispersion of MWCNTs in the low-crystalline nanocomposites compared with the high-crystalline nanocomposites (72).

Pilla et al. (35) conducted tensile tests to study the static mechanical properties of both solid and microcellular components. The properties studied include energy-to-break (specific toughness), strain-at-break, specific modulus, and specific strength. These specific properties were obtained by taking into account the reduced density of the microcellular components compared with solid ones. Pilla et al. found that, with the addition of 1.5 wt% MWCNTs, the specific toughness, specific strength, and strain-at-break decreased for both solid and microcellular specimens, while no change was observed for the specific modulus (Table 9.2). The reduction in the specific toughness and strain-at-break observed with the PLA-MWCNT nanocomposites in both solid and microcellular specimens was attributed to 1) the relatively poor dispersion of the CNTs, which might act as stress concentrators, and 2) the much higher crystallinity observed with the PLA-MWCNT nanocomposites.

There was a greater decrease in the specific strength for the solid PLA-MWCNT specimens compared with microcellular PLA-MWCNTs. The higher decrement in strength observed in the solid specimen compared with the microcellular specimen with the addition of MWCNTs was attributed to two factors: 1) the MWCNTs were dispersed more uniformly in the microcellular specimens than the solid specimens due to the presence of SCF; 2) the addition of MWCNTs in the microcellular components led to smaller cell sizes. Also, in general, the specific strength of microcellular samples was found to be less than their solid counterparts. This was attributed to certain large voids that occurred due to the dynamic nature of microcellular injection-molding (89). These larger voids were much larger than naturally

Table 9.2. Specific mechanical properties of solid and microcellular PLA and PLA-MWCNT nanocomposites (35)

Sample ↓	Property →	Specific Toughness	Strain at Break	Specific Young's Modulus	Specific Tensile Strength
	Units →				
PLA (Solid)		[MPa/(kg/m ³)]	[%]	[Mpa/(kg/m ³)]	[Mpa/(kg/m ³)]
		1.957E-3 ± 2.293E-4	5.476 ± 0.384	1.648 ± 0.743	5.43E-2 ± 3.1E-4
PLA (Microcellular)		1.844E-3 ± 4.427E-4	5.661 ± 0.959	1.629 ± 0.286	4.49E-2 ± 6.4E-4
PLA-MWCNT (Solid)		1.258E-3 ± 2.321E-4	4.285 ± 0.461	1.577 ± 0.236	4.82E-2 ± 2.7E-4
PLA-MWCNT (Microcellular)		1.089E-3 ± 3.208E-4	3.932 ± 0.764	1.808 ± 0.337	4.36E-2 ± 7.1E-4

occurring voids in the solid components and may become regions of stress concentrations, thereby decreasing mechanical properties.

9.8 Thermal Degradation Properties

This section discusses the thermal degradation studies conducted using a thermogravimetric analyzer (TGA). In general, the thermal stability of filled composites is better than pure polymers due to the presence of fillers, which act as stabilizing agents (73). In particular, the addition of CNTs present superior thermal stability for composites compared with neat polymers (90–92).

Moon et al. (61) showed from the mass loss curves for the degradation of PLLA and PLLA-MWCNT nanocomposites that PLLA degraded without forming any residue, but the nanocomposites left a residue of about 3–10% (Figure 9.14). Additionally, the decomposition temperature (T_d), at 10% weight loss, was found to increase with the MWCNT loading by 10–20%. Rapid weight loss also took place at around 300 °C in both PLA and PLA nanocomposites. Similar results were also obtained by (64,73,75,76).

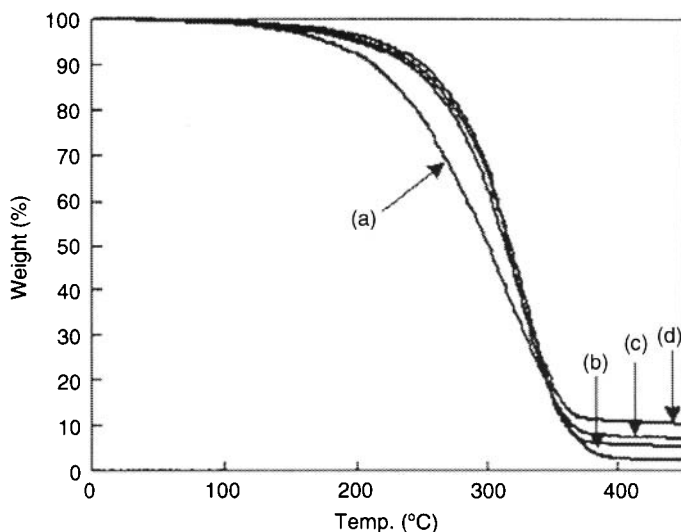


Figure 9.14. TGA curves of PLLA-MWCNTs nanocomposites with various MWCNTs contents: (a) PLLA; (b) PLLA-3wt% MWCNTs; (c) PLLA-5wt% MWCNTs and (d) PLLA-10wt% MWCNTs. Reprinted with permission from S. Moon et al., *Macromolecular Symposia*, Vol. 224, p. 287, 2005, © 2005, Wiley InterScience Ltd.

9.9 Electrical Conductivity Properties

CNTs possess good electrical conductivity; thus, when impregnated in a non-conducting polymer, they can greatly enhance the electrical conductivity of the composites when the CNT loading level is above its electrical percolation threshold. As shown in Figure 9.15, the conductivity of the PLLA-MWCNTs nanocomposites increased with the MWCNTs loading level (72). A similar effect was observed in (61,63,65,74). Tsuji et al. (63) observed that among many different nano-fillers such as SWCNTs, carbon nanohorn, carbon nanoballoon, and carbon black, blended in PLLA, SWCNT-based nanocomposites showed the lowest resistivity (Figure 9.16). This is because of the needle-like (fiber-like) structure of SWCNTs (higher aspect ratio) compared with the spherical-like structure of other fillers that makes them have an effective contact to each other, thereby lowering the resistance values. Also, CNTs have many π -bonds (C=C bonds) and electrons transfer through the π -bonds, which result in good conductivity (72). Thus, it can be inferred that CNTs can be promising fillers to enhance the conductivity of PLLA-based materials.

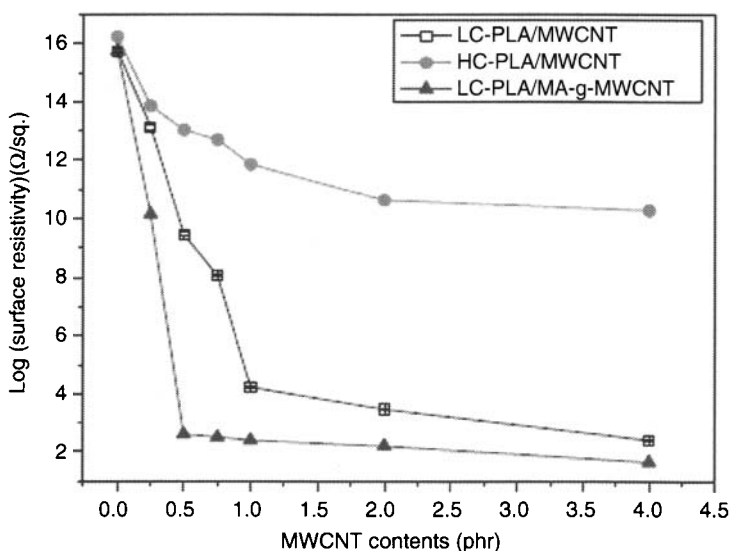


Figure 9.15. Effect of MWCNTs contents on the surface resistance of PLA-MWCNTs nanocomposites. Reprinted with permission from C-F. Kuan et al., *Journal of Physics and Chemistry of Solids*, Vol. 69, p. 1395, 2008, © 2008, Elsevier Science Ltd.

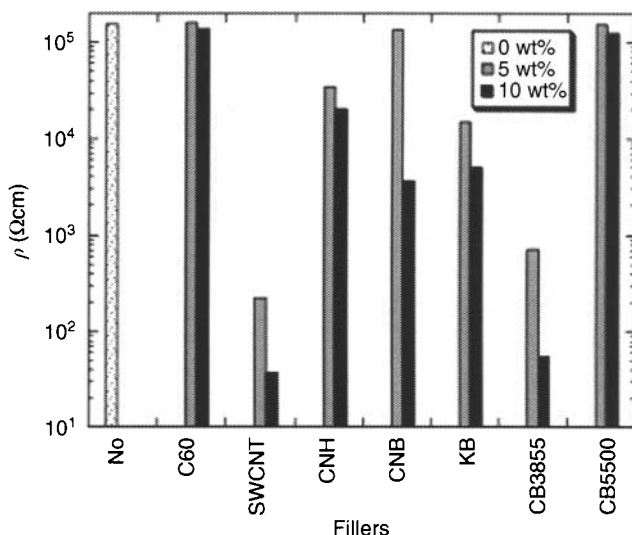


Figure 9.16. Resistivity (ρ) of PLLA films with different carbon fillers at 5 and 10wt%. Reprinted with permission from H. Tsuji et al., *Polymer*, Vol. 48, p. 4213, 2007, © 2007, Elsevier Science Ltd.

9.10 Biodegradability

Biodegradability, or the rate of biodegradation, depends on many factors such as the structure of polymers, biodegradation conditions, the hydrophobicity of polymers, filler type and content, the presence of additives and substituents, crystallinity, and the stereo-configuration of polymers (93,94). Therefore, appropriate measures need to be taken before designing a composite.

PLA has a slow rate of degradation compared with other biopolymers such as poly(ϵ -caprolactone), poly[(R)-3-hydroxybutyrate] (95). Biodegradation of PLA is well established; however, its allied blends and composites, especially nanocomposites, have yet to be explored in detail. Tsuji et al. (63) have investigated the K-catalyzed enzymatic biodegradation of PLLA-SWCNTs nanocomposites, which is the only study on the biodegradation of PLA-based CNT nanocomposites that has been identified thus far. In general, the K-catalyzed degradation rate is determined by concentration, shape, dimension, type, dispersion and the adhesion of fillers for a specific type of polymer nanocomposites (93–94). In their study, Tsuji et al. (63) observed that SWCNTs accelerated the rate of enzymatic biodegradation. This was attributed to the enhanced diffusibility of proteinase K between PLLA and SWCNTs, and the

porous structure created in the nanocomposites during the enzymatic degradation process due to the weak interfacial adhesion between PLLA and SWCNTs, as they were not functionalized (96).

9.11 Applications

Due to their extraordinary properties, CNTs have been incorporated in PLA, a biobased, biocompatible, and biodegradable polymer, to produce PLA-CNT bio-nanocomposites that can be used in a wide variety of applications such as medicine, surgery, and pharmaceuticals. Especially, PLA-CNT nanocomposites are used in applications such as structural components, advanced packaging, vascular grafts, catheters, ligament repair materials, prosthetic devices, biosensors, drug and vaccine delivery vehicles, tissue engineering, and electrically conductive polymers. With advancements, it is foreseen that PLA-based CNT nanocomposites will emerge as a new class of bio-nanocomposites for a wide range of applications.

9.12 Conclusions

Poly lactide-based carbon nanotube nanocomposites are a recent development and a new addition to the field of bio-nanocomposites. Its history spans less than a decade. Due to their versatile and outstanding properties together with its renewable, biocompatible and biodegradable nature, PLA-based CNT bio-nanocomposites have raised a great deal of interest among academicians and scientists around the world, led to novel research in biomaterials, and paved the way to discovering innovative products for a wide variety of applications. This chapter has presented various routes for synthesizing and processing PLA-CNT nanocomposites, and then analyzed the viscoelastic, thermal, mechanical, thermal degradation, electrical conductivity, and biodegradability properties of these bio-nanocomposites. Finally, this chapter has shown that simple variations in the type of materials and processing scheme can achieve different properties for these bio-nanocomposites. This opens a new challenge and a new direction for research in this field to explore novel materials for varied applications. With continuous advancements in science and up-to-date progress in research, the day is not far when all the fruitful research in PLA-CNT nanocomposites will be commercialized for the benefit of humankind.

Acknowledgements

The authors acknowledge the financial support from the National Science Foundation (CMMI-0734881).

Note

1. Samples fabricated by conventional injection-molding (non-foamed) process.

References

1. P. Gruber and M. O'Brien, "Polyesters III applications and commercial products", in Y. Doi and A. Steinbuchel, eds., *Biopolymers*, Wiley-VCH, Vol. 4, pp. 235, 2002.
2. J. Pelouze, *Annali di Chimica*, Vol. 13, p. 257, 1845.
3. E.T.H. Vink, K.R. Rabago, D.A. Glassner, and P.R. Gruber, *Polymer Degradation and Stability*, Vol. 80, p. 403, 2003.
4. V. Krikorian, and D.J. Pochan, *Chemistry of Materials*, Vol. 15, p. 4317, 2003.
5. M.S. Taylor, A.U. Daniels, K.P. Andriano, and J. Hiller, *Journal of Applied Biomaterials*, Vol. 5, p. 151, 1994.
6. S.H. Hyon, F. Jin, S. Tsutsumi, and T. Kanamoto, *Macromolecular Symposia*, Vol. 197, p. 355, 2003.
7. A.G. Mikos, M.D. Lyman, L.E. Freed, and R. Langer, *Biomaterials*, Vol. 15, p. 55, 1994.
8. S. Singh, S.S. Ray, *Journal of Nanoscience and Nanotechnology*, Vol. 7, p. 2596, 2007.
9. R.G. Sinclair, *Journal of Macromolecular Science: Pure & Applied Chemistry*, Vol. 33, p. 585, 1996.
10. O. Martin, and L. Averous, *Polymer*, Vol. 42, p. 6209, 2001.
11. S. Pilla, A. Kramschuster, L. Yang, S. Gong, A. Chandra, and L-S. Turng, *Materials Science and Engineering: C*, Vol. 29, p. 1258, 2009.
12. S. Pilla, S.G. Kim, G.K. Auer, S. Gong, and C.B. Park, *Polymer Engineering and Science*, Vol. 49, p. 1653, 2009.
13. J. Ren, O. Urakawa, K. Adachi, *Nihon Reorogi Gakkaishi*, Vol. 32, p. 161, 2004.
14. M. Sheth, R.A. Kumar, V. Dave', R.A. Gross, and S. P. McCarthy, *Journal of Applied Polymer Science*, Vol. 66, p. 1495, 1997.
15. A.M. Gajria, V. Dave, R.A. Gross, and S.P. McCarthy, *Polymer*, Vol. 37, p. 437, 1996.
16. J.W. Park, and S.S. Im, *Polymer*, Vol. 44, p. 4341, 2003.
17. Y.F. Kim, C.N. Choi, Y.D. Kim, K.Y. Lee, and M.S. Lee, *Fibers and Polymers*, Vol. 5, p. 270, 2004.
18. K.S. Anderson, and M.A. Hillmyer, *Polymer*, Vol. 45, p. 8809, 2004.
19. G. Biresaw, and C.J. Carriere, *Journal of Polymer Science Part B: Polymer Physics*, Vol. 40, p. 2248, 2002.

20. H. Ome, S. Kumasawa, and J. Kumaki, Poly(lactic acid)/polyacetal resin compositions and heat-resistant high-strength moldings therefrom with good surface appearance and dimensional stability, Japanese patent 2003342460 A2, assigned to Toray Industries, Inc., December 3, 2003.
21. T. Ochi, Y. Maeda, and H. Ohme, Polymer alloy fibers with good biodegradability and abrasion resistance consisting of blends comprising poly(lactic acid) and polyacetals, Japanese patent JP 2003227037 A2, assigned to Toray Industries, Inc., Japan, August 15, 2003.
22. H. Ohme, S. Kumazawa, and J. Kumaki, Heat-resistant poly(lactic acid)-polyacetal blend with good processability, mechanical strength, and transparency for plastic moldings, films, and fibers, WO 2003014224 A1, assigned to Toray Industries, Inc., Japan, February 20, 2003.
23. G. Zhang, J. Zhang, S. Wang, and D. Shen, *Journal of Polymer Science, Part B: Polymer Physics*, Vol. 41, p. 23, 2002.
24. J.L. Eguiburu, J.J. Iruin, M.J. Fernandez-Berridi, and J. Roman, *Polymer*, Vol. 39, p. 6891, 1998.
25. T. Kamisawa and M. Kimura, Poly(lactic acid)-type polymer drawn films with increased stiffness at high temperatures and good transparency, comprising poly(lactic acid) compositions containing (meth)acrylate polymers, Japanese Patent 2005036054 A2, assigned to Toray Industries, Inc., Japan, February 10, 2005.
26. 'Fujitsu, "Toray Develops PLA Notebook Housing", *Modern Plastics*, 2005, March, p. 11.
27. S.S. Ray, and M. Okamoto, *Progress in Polymer Science*, Vol. 28, p. 1539, 2003.
28. Y. Shikinati, and M. Okuno, *Biomaterials*, Vol. 20, p. 859, 1999.
29. S. Pilla, S. Gong, E. O'Neill, R.M. Rowell, and A.M. Krzysik, *Polymer Engineering and Science*, Vol. 48, p. 578, 2007.
30. A. Kramschuster, S. Pilla, S. Gong, A. Chandra, and L.-S. Turng, *International Polymer Processing*, Vol. XXII, p. 436, 2007.
31. S. Pilla, S. Gong, L. Yang, E. O'Neill, and R.M. Rowell, *Journal of Applied Polymer Science*, Vol. 111, p. 37, 2009.
32. S. Pilla, A. Kramschuster, J. Lee, G.K. Auer, S. Gong, and L.-S. Turng, *Composite Interfaces*, (DOI:10.1163/092764409X12477467990283), 2009.
33. M.S. Huda, L.T. Drzal, A.K. Mohanty, and M. Misra, *Composites Science and Technology*, Vol. 68, p. 1753, 2008.
34. M.S. Huda, L.T. Drzal, A.K. Mohanty, and M. Misra, *Composites Science and Technology*, Vol. 66, p. 1813, 2006.
35. S. Pilla, A. Kramschuster, S. Gong, A. Chandra, and L.-S. Turng, *International Polymer Processing*, Vol. XXII, p. 418, 2007.
36. E.P. Giannelis, *Advanced Materials*, Vol. 8, p. 29, 1996.
37. N.C. Bleach, S.N. Nazhat, K.E. Tanner, M. Kellomaki, and P. Tormala, *Biomaterials*, Vol. 23, p. 1579, 2002.
38. J.K.W. Sandler, M.S.P. Shaffer, T. Prasse, W. Bauhofer, K. Schulte, A.H. Windle, *Polymer*, Vol. 40, p. 5967, 1999.
39. D. Garlotta, *Journal of Polymers and the Environment*, Vol. 9, p. 63, 2001.
40. B. Buchholz, Process for preparing polyesters based on hydroxycarboxylic acids, US Patent 5302694, assigned to Boehringer Ingelheim GmbH, April 12, 1994.

41. L. Cotarca, P. Delogu, A. Nardelli, and V. Sunjic, *Synthesis*, Vol. 5, p. 553, 1996.
42. J. Seppala, J. F. Selin and T. Su, European Patent 593,271, 1993.
43. J. Seppala, J. F. Selin, T. Su, Method for producing lactic acid based polyurethane, U.S. Patent 5380813, assigned to Neste Oy, January 10, 1995.
44. M. Harkonen, K. Hiltunen, M. Malin, and J. V. Seppala, *Journal of Macromolecular Science-Pure and Applied Chemistry A*, Vol. 32(4), p. 857, 1995.
45. P. V. Bonsignore, Production of high molecular weight polylactic acid, US Patent 5470944, assigned to ARCH Development Corporation, November 28 1995.
46. M. Spinu, L-D polylactide copolymers with controlled morphology, US Patent 5270400, assigned to Maria Spinu, December 14, 1993.
47. A. C. Ibay and L. P. Tenney, Polymers from hydroxy acids and polycarboxylic acids, US Patent 5206341, assigned to Southern Research Institute, November 21, 2011.
48. J. Kylma, M. Harkonen, and J. V. Seppala, Abstracts of the Fourth International Workshop on Biodegradable Polymers, Poster 38, 1995.
49. H. Inata, and S. Matsumura, *Journal of Applied Polymer Science*, Vol. 30, p. 3325, 1985.
50. S. M. Aharoni, and T. Largman, Process for preparing graft and block copolymers, US Patent 4417031, assigned to Allied Corporation, November 22, 1983.
51. C.D. Dudgeon, *Bis-Orthoesters as Polymer Intermediates*, Thesis, University of Massachusetts, 1976.
52. S.M. Aharoni, and D. Masilamani, Process for preparing extended chain polyesters and block or graft copolyesters, US Patent 4568720, assigned to Allied Chemical Corporation, February 4, 1986.
53. S.M. Aharoni, C.E. Forbes, W.B. Hammond, D.M. Hindenlang, F. Mares, K. O'Brien, and R.D. Sedgwick, *Journal of Polymer Science, Part A: Polymer Chemistry Edition*, Vol. 24, p. 1281, 1986.
54. A.J. Pennings, and S. Gogolewski, *Rapid Communications*, Vol. 3, p. 839, 1982.
55. M.H. Hartmann, "High Molecular Weight Polylactic Acid Polymers", in D.L. Kaplan, ed., *Biopolymers from Renewable Resources*, Springer-Verlag, Berlin, pp. 367-411, 1998.
56. H. Suizu, M.A. Takagi, A. Yamaguchi, and M. Ajioka, Purification process of aliphatic polyester, U.S. Patent 5496923, assigned to Mitsui Taotsu Chemicals, Mar 5, 1996.
57. C.E. Lowe, Preparation of high molecular weight polyhydroxyacetic ester, US Patent 2668162, assigned to DuPont, February 2, 1954.
58. S. Iijima, *Nature*, Vol. 354, p. 56, 1991.
59. P.G. Collins, and P. Avouris, *Scientific American*, Vol. 282, p. 62, 2000.
60. E.T. Thostenson, Z. Ren, and T.W. Chou, *Composites Science and Technology*, Vol. 61, p. 1899, 2001.
61. S. Moon, F. Jin, C.J. Lee, S. Tsutsumi, and S.H. Hyon, *Macromolecular Symposium*, Vol. 224, p. 287, 2005.
62. L.P. Krul, A.I. Volozhyn, D.A. Belov, N.A. Poloiko, A.S. Artushkevich, S.A. Zhdanok, A.P. Solntsev, A.V. Krauklis, and I.A. Zhukova, *Biomolecular Engineering*, Vol. 24, p. 93, 2007.

63. H. Tsuji, Y. Kawashima, H. Takikawa, and S. Tanaka, *Polymer*, Vol. 48, p. 4213, 2007.
64. G.X. Chen, H.-S. Kim, B.H. Park, and J.-S. Yoon, *Journal of Physical Chemistry B*, Vol. 109, p. 22237, 2005.
65. D. Zhang, M.A. Kandadai, J. Cech, S. Roth, and S.A. Curran, *Journal of Physical Chemistry B*, Vol. 110, p. 12910, 2006.
66. G.B. Okonishnikov, E.I. Blednykh, and V.P. Skripov Mekh, *Polimerov*, Vol. 2, p. 370, 1973.
67. J.E. Martini, F.A. Waldman, and N.P. Suh, in SPE ANTEC Technical Papers, Vol. 28, p. 674, 1982.
68. S. Gong, M. Yuan, A. Chandra, H. Kharbos, A. Osorio, L.-S. Turng, *International Polymer Processing*, Vol. 20, p. 202, 2005.
69. J. Throne, in N.P. Suh and N. Sung, eds., *Science and Technology of Polymer Processing*, MIT Press, pp. 77, 1979.
70. A.K. Bledzki, O. Faruk, H. Kirschling, J. Kuhn, and A. Jaszkievicz, *Polimery*, Vol. 51, p. 697, 2006.
71. S. Gong, M. Yuan, A. Chandra, H. Kharbas, A. Osorio, and L. S. Turng, *International Polymer Processing*, Vol. XX, p. 202, 2005.
72. C.-F. Kuan, H.-C. Kuan, C.-C.M. Ma, and C.-H. Chen, *Journal of Physics and Chemistry of Solids*, Vol. 69, p. 1395, 2008.
73. D. Wu, L. Wu, M. Zhang, and Y. Zhao, *Polymer Degradation and Stability*, Vol. 93, p. 1577, 2008.
74. D. Wu, Y. Zhang, M. Zhang, and W. Yu, *Biomacromolecules*, Vol. 10, p. 417, 2009.
75. C.-S. Wu, and H.-T. Liao, *Polymer*, Vol. 48, p. 4449, 2007.
76. W. Song, Z. Zheng, H. Lu, and X. Wang, *Macromolecular Chemistry and Physics*, Vol. 209, p. 315, 2008.
77. H.E. Naguib, C.B. Park, and N. Reichelt, *Journal of Applied Polymer Science*, Vol. 91, p. 2661, 2004.
78. S. Gong, L.-S. Turng, C.B. Park, and L. Liao, "Microcellular Polymer Nanocomposites for Packaging and Other Applications", in A. Mohanty, M. Misra and H.S. Nalwa, eds., *Packaging Nanotechnology*, American Scientific Publishers, 2008.
79. S.S. Ray, and M. Bousmina, *Progress in Materials Science*, Vol. 50, p. 962, 2005.
80. F.M. Du, R.C. Scogna, W. Zhou, S. Brand, J.E. Fischer, and K.I. Winey, *Macromolecules*, Vol. 37, p. 9048, 2004.
81. P. Potschke, T.D. Fornes, and D.R. Paul, *Polymer*, Vol. 43, p. 3247, 2002.
82. P. Potschke, M. Abdel-Goad, I. Alig, S. Dudkin, and D. Lellinger, *Polymer*, Vol. 45, p. 8863, 2004.
83. Y.T. Sung, M.S. Han, K.H. Song, J.W. Jung, H.S. Lee, C.K. Kum, J. Joo, and W.N. Kim, *Polymer*, Vol. 47, p. 4434, 2006.
84. Y.S. Song, *Polymer Engineering and Science*, Vol. 46, p. 1350, 2006.
85. Y.S. Song, *Rheologica Acta*, Vol. 46, p. 231, 2006.
86. G.G. Hu, C.G. Zhao, S.M. Zhang, M.S. Yang, and Z.G. Wang, *Polymer*, Vol. 47, p. 480, 2006.
87. D.F. Wu, L. Wu, Y.R. Sun, and M. Zhang, *Journal of Polymer Science Part B: Polymer Physics*, Vol. 45, p. 3137, 2007.
88. D.F. Wu, L. Wu, and M. Zhang, *Journal of Polymer Science Part B: Polymer Physics*, Vol. 45, p. 2239, 2007.

89. A. Kramschuster, S. Gong, T. Li, T. Li, and L.-S. Turng, Society of Petroleum Engineers - 5th International Conference on Thermoplastic Foam, FOAMS 2006, p. 59–63, 2006.
90. B.B. Marosfoi, A. Szabo, G. Marosi, D. Tabuani, G. Camino, and S. Pagliari, *Journal of Thermal Analysis and Calorimetry*, Vol. 86, p. 86, 2006.
91. G. Gorrasi, M. Sarno, B. Di, D. Sannino, P. Ciambelli, and V. Vittoria, *Journal of Polymer Science Part B: Polymer Physics*, Vol. 45, p. 597, 2007.
92. H-S. Kim, B.H. Park, J.S. Yoon, and H.J. Jin, *European Polymer Journal*, Vol. 43, p. 1729, 2007.
93. N. Fukuda, H. Tsuji, and Y. Ohnishi, *Polymer Degradation and Stability*, Vol. 78, p. 119, 2002.
94. N. Fukuda, and H. Tsuji, *Journal of Applied Polymer Science*, Vol. 96, p. 190, 2005.
95. H. Tsuji, and K. Suzuyoshi, *Polymer Degradation and Stability*, Vol. 75, p. 347, 2002.
96. H. Tsuji, and S. Miyauchi, *Biomacromolecules*, Vol. 2, p. 597, 2001.

Synthesis and Properties of PEEK/Carbon Nanotube Nanocomposites

A.M. Díez-Pascual^{1,*}, J.M. González-Domínguez², Y. Martínez-Rubi³, M. Naffakh¹, A. Ansón², M.T. Martínez², B. Simard³ and M.A. Gómez¹

¹*Departamento de Física e Ingeniería de Polímeros. Instituto de Ciencia y Tecnología de Polímeros, CSIC, c/ Juan de la Cierva 3, 28006 Madrid, Spain*

²*Departamento de Nanotecnología. Instituto de Carboquímica, CSIC, c/ Miguel Luesma Castan 4, 50018 Zaragoza, Spain*

³*Steacie Institute for Molecular Sciences, NRC, 100 Sussex Drive, Ottawa, Canada*

Abstract

This review describes the development and characterization of high-performance poly(ether ether ketone) (PEEK) based nanocomposites incorporating different types of single-walled carbon nanotubes (SWCNTs). The influence of the preparation and processing conditions, presence of a compatibilizing agent as well as SWCNT loading on the structure, morphology, thermal, electrical and mechanical properties of the resulting materials is analyzed in detail. Experimental results indicate a remarkable improvement in the thermal stability, electrical and thermal conductivity, storage modulus and glass transition temperature of the matrix by the incorporation of the carbon nanotubes. The overall performance of these composites is suitable for potential use in the aeronautic industry.

Keywords: nanocomposites; PEEK; carbon nanotubes; compatibilizer; thermal stability; crystalline structure; mechanical properties.

10.1 Introduction

Polymer nanocomposites including nanoscaled carbon fillers such as single and multi-walled carbon nanotubes have attracted a lot of

* Corresponding author. E-mail address: adiez@ictp.csic.es

V. Mittal (ed.) Polymer Nanotube Nanocomposites, (283–314) © Scrivener Publishing LLC

attention over recent years (1,2). These nanocomposites, easily processed due to the small diameter of the carbon nanotubes (CNTs), exhibit unique properties (3,4), such as enhanced modulus and tensile strength, high thermal stability and good environmental resistance. This behavior, combined with their low density makes them suitable for a broad range of technological sectors such as telecommunications, electronics (5) and transport industries, especially for aeronautic and aerospace applications where the reduction of weight is crucial in order to reduce the fuel consumption. However, because of high cost and limited availability of CNTs, to date only a few practical applications in industrial fields, such as microelectronic devices, have evolved. Nowadays, one of the main challenges in aircraft research and technology is the development of cost-effective techniques for manufacturing nanocomposites at large scale, so that they can be used in structural components, such as wing panels, horizontal and vertical stabilizers, landing gear doors and some sections of the fuselage. For this purpose, materials easily processed by continuous methods should be employed; poly (ether ether ketone) (PEEK) carbon nanotube reinforced composites seem to be highly suitable candidates due to the thermal environment and mechanical requirements of these parts.

In the literature there are many reports related to the integration of CNTs into polymer matrices, but only a few papers deal with such composites with a PEEK matrix; the most relevant are those published by Shaffer et al. (6,7), working with carbon nanofibre/PEEK composites, Deng et al. (8), dealing with multi-walled carbon nanotube (MWCNT)/PEEK nanocomposites, and Song et al. (9), who prepared sandwich like buckypaper/PEEK composites. Recently, Díez-Pascual and co-workers (10,11) reported the synthesis and characterization of single-walled carbon nanotube (SWCNT)/PEEK nanocomposites. They developed strategies to efficiently incorporate the nanotubes into the polymer matrix without destroying the integrity of the nanotubes as uniform CNT dispersion and improved nanotube-matrix interfacial adhesion are critical issues in the processing of these composites in order to achieve efficient load transfer across the interface, a necessary condition to enhance the mechanical properties of polymer composites. Fundamental work in processing, characterization, and analysis/modelling is required before this new class of nanocomposites can be applied in commercial applications.

This review provides the reader with background knowledge on polymer composites with a clear example of the strong

influence of the preparation and processing conditions, as well as SWCNT type and concentration on the morphology, thermal, electrical and mechanical properties of the resulting nanocomposite materials. A complete characterization at nano(micro)scopic and macroscopic scales is fundamental to obtain information on the structural and functional changes induced in the polymer with the addition of SWCNTs.

10.2 Poly(ether ether ketone)s: Structure, Synthesis and Properties

Poly(aryl ether ketone)s (PAEKs), such as (PEEK) (Figure 10.1) are an important class of high-performance engineering thermoplastics displaying a unique combination of thermal stability, chemical and solvent resistance, excellent mechanical properties over a wide temperature range and good fire resistance (12,13). These polymers can be fabricated by conventional techniques, such as extrusion and compression moulding, and can be applied as matrix resins for high-performance reinforced composites. Compared to poly(arylene ether sulfone)s, which are usually amorphous polymers and subject to attack by solvents, PAEKs are semicrystalline polymers and therefore resistant to solvents, which is a critical factor in an aerospace environment. However, due to their insolubility and high melting points (generally above 300°C), these polymers need to be prepared under specific reaction conditions. PAEKs are generally synthesized by an aromatic nucleophilic substitution reaction of activated aryl dihalides with aromatic diphenolates or by Friedel-Crafts acylation of aryl ethers.

In 1962, Bonner (14) at DuPont was the first one who reported the synthesis of wholly aromatic poly(ether ketone ketone)s (PEKK) by Friedel-Crafts acylation. Isophthaloyl chloride was condensed with diphenyl ether using nitrobenzene as solvent and aluminum trichloride as a catalyst.

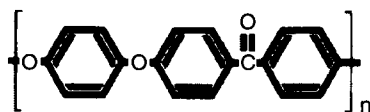


Figure 10.1. Chemical structure of PEEK.

Johnson *et al.* (15) reported the first attempt to synthesize PEEK by polycondensation of bisphenolate with activated dihalides using DMSO as a solvent and NaOH as a base. High molecular weight polymers were difficult to obtain due to the crystallinity and the resulting insolubility of polymers in DMSO. To circumvent the solubility problem, Attwood and Rose (16) used diphenyl sulfone as a solvent, and the polymerization was carried out close to the melting point. *Victrex* PEEK was commercialized by the British company ICI in 1982 using this method. Since its commercialization, this thermoplastic polymer has been used in a wide range of applications, from medicine to the electronic, telecommunications and transport industries (automobile, aeronautic and aerospace) (17,18).

Over the last decades many studies have been reported on the structural (19), thermal (20) and mechanical (21) characterization of this linear aromatic polymer. This high-performance material exhibits the following characteristics:

- Chemical and hydrolysis resistance: insoluble in all common solvents, has excellent resistance to most of organic and inorganic liquids. It can be used in steam or high pressure environment without any degradation in properties.
- Wear resistance: excellent tribological properties under a wide range of conditions.
- Radiation resistance: exceptional resistance to gamma radiation at high dose levels.
- High temperature performance: excellent mechanical properties retained at temperatures up to 300°C.
- Flammability and gas emission: V-0 flammability rating down to 1.45 mm without the use of additives. The levels of smoke and toxic acid gas released during combustion are extremely low.
- Electrical: excellent electrical behaviour that remains stable over a wide range of temperatures and frequencies.

Victrex PEEK is available in different viscosity grades suitable for extrusion processes, powder coating and compression moulding. PEEK 150P ($M_w \sim 40000$ g/mol, $d_{25^\circ\text{C}} = 1.32$ g/cm³, $T_g = 147^\circ\text{C}$, $T_m = 345^\circ\text{C}$), a coarse powder, presents the lowest viscosity grade and is the most suitable for potential aircraft applications.

10.3 Synthesis, Purification and Characterization of the SWCNTs

SWCNTs exhibit unique physical and chemical properties that make them very attractive candidates for the production of new materials. Carbon nanotubes are made by wrapping up single sheets of graphite, known as graphene, upon themselves to form hollow, straw-like structures. Traditionally, SWCNTs have been prepared by electric arc-discharge, laser ablation and chemical vapor deposition (CVD) methods; these techniques produce significant quantities of impurities, such as amorphous and graphitic forms of carbon and encapsulated catalytic metal nanoparticles.

10.3.1 Synthesis of Laser-Grown SWCNTs

Laser-grown SWCNTs can be synthesized using an approach to the two-laser synthesis method (22), in an electric tube-furnace heated to a temperature of 1450 K. A flowing gas environment composed of argon and carbon monoxide at a constant pressure of 500 Torr is established inside a 45 mm diameter quartz tube; a cylindrical graphite target doped with 0.6 at.% each of cobalt and nickel powders is mounted in an axially rotating stage at the center of the furnace. A 25 mm diameter quartz tube was placed coaxially inside the larger tube and positioned approximately 4 mm from the exposed face of the target. The vaporization laser (nanosecond-pulsed Nd:YAG) operating at 1064 nm and 30 Hz is controlled with a programmable actuator attached to a steering mirror. The excitation laser (continuous wave Nd:YAG) operates at a wavelength of 1064 nm defocused to a spot 13 mm in diameter and average power of 75 W. The role of this excitation laser was to alter the rate of cooling of the condensing plume generated by the vaporization laser through thermal excitations and not to contribute to the removal of material from the target.

10.3.2 Synthesis and Purification of Arc-Grown SWCNTs

In 1997 Journet *et al.* (23) described a method to obtain high yields of SWCNTs by means of electric arc-discharge, using a transition metal mixture (Nickel and Yttrium) as catalyst. In a typical arc reactor,

the electric discharge is generated between two electrodes under inert atmosphere. The cathode is made by a graphite rod, while the anode is prepared by drilling a hole in a graphite rod and filling it with the metals and graphite powder mixture. Then a 100A current is applied and a voltage drop of 30V is continuously maintained between the electrodes, by progressively approaching the electrodes with a crank system. While the electric arc is held, the anode is progressively consumed and the SWCNTs are deposited in the inner walls of the reactor. The highest SWCNT yield (~80 wt%) was found with the 4.2:1 (Ni:Y atomic ratio) mixture.

The treatment of arc-discharge SWCNTs at moderate temperatures under oxidant environment, such as air or ozone, followed by reflux in inorganic acids (e.g. HNO_3 or H_2SO_4), centrifugation and water rinsing leads to highly purified materials (24,25) with a metal content reduced in a yield between 88–95%. The further annealing treatment at very high temperature ($\geq 1000^\circ\text{C}$) under inert atmosphere removes defects and amorphous carbonaceous material. Furthermore, the combination of the oxidative step with the nitric acid treatment performed in a microwave reactor (26) leads to a more effective removal of the metal impurities. During these treatments, oxygenated groups covalently grafted onto the surfaces of the SWCNTs are generated. These functional groups are mainly reported to be carboxylic acids (COOH) and seem to have preference for SWCNT tips and sidewall defects, where reactivity is known to be higher. The formation of COOH groups provides anchoring sites for further covalent functionalization throughout common synthetic routes.

A milder route to remove impurities from arc-discharge SWCNT materials is the interaction with surface active molecules which non-covalently interact with the SWCNTs; this interaction often implies a wrapping process which releases the tubes from their surrounding impurities, without damaging, shortening or oxidizing the material. Obtaining arc-purified SWCNTs without alteration of their structure or electronic properties is critical for specific applications such as nanoelectronic devices. The purification throughout surfactants (e.g. Sodium Dodecyl Sulfate, SDS (27)) or polymers should be combined with ultrasonication and centrifugation stages. Recently, González-Domínguez et al. (28) have reported that the wrapping process of Pluronic F68 block copolymer over arc-discharge SWCNTs ends up in the almost complete elimination of graphitic impurities.

10.3.3 Characterization of the Single-Walled Carbon Nanotubes

The as-produced and purified SWCNTs are characterized by Raman spectroscopy, transmission electron microscopy (TEM), scanning electron microscopy (SEM), UV-Visible-NIR absorption spectroscopy and thermogravimetric analysis (TGA). The results obtained from the different techniques are summarized in Table 10.1. Quantitative data for metal content and thermal stability can be obtained from TGA under air atmosphere. Higher oxidation temperatures are always associated with less defective materials (29). The temperatures of maximum weight loss ranged between 459°C, for as-produced arc-SWCNTs, to 541°C for arc-purified SWCNTs. Although highly purified and defect-free SWCNTs would oxidize at temperatures of 700°C or more, it has been shown (30) that the presence of carbon impurities can induce SWCNT oxidation at lower temperatures. Moreover, the amount and morphology of the metal catalyst particles and other carbon based impurities also affect strongly the degradation temperatures of the CNT samples. As-grown laser-SWCNTs, with a lower metal content, exhibit higher thermal stability than raw arc-SWCNTs (see Table 10.1); arc-purified nanotubes present the lowest metal content and the highest decomposition temperatures.

Images from TEM are mostly used to monitor the surface texture of individual ropes and qualitative determine the impurities of the material. SEM micrographs indicate the bundle diameter and the degree of agglomeration of the samples. Figure 10.2 shows

Table 10.1. Characteristics of the SWCNTs used for the preparation of the composites

SWCNT type (preparation method)	Metal (%) (TGA)	T _{mr} (°C) (TGA)	G/D ratio (Raman)	Purity (%) (NIR)	D (nm) SEM
Arc (as-grown)	12.7	459	5.6	35.7	21.8
Arc (HNO ₃ treated)	3.2	541	14.3	50.4	20.4
Laser (as-grown)	3.9	493	7.2	38.8	39.8
Laser (PEI dispersed)	4.1	488	3.8	—	33.6
Arc (PEI dispersed)	3.3	532	2.5	—	19.9

T_{mr} corresponds to the temperature of maximum rate of weight loss under air atmosphere at a heating rate of 5°C/min, and D to the average bundle diameter obtained by SEM micrographs. Polyetherimide (PEI) is the compatibilizing agent.

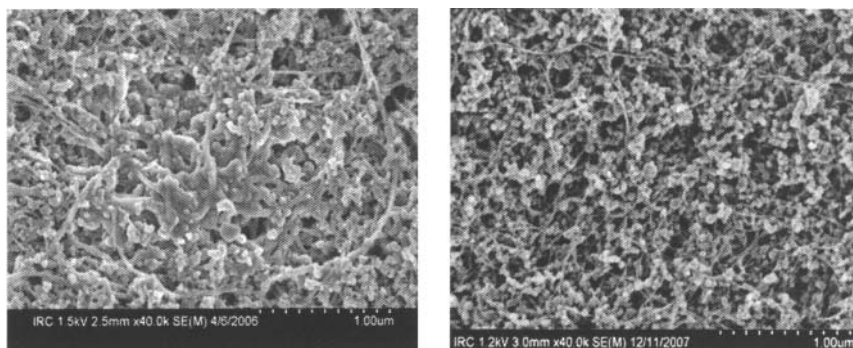


Figure 10.2. SEM images of as-produced laser-grown (left) and arc-grown (right) SWCNTs.

representative SEM images of raw arc-grown and laser-grown SWCNTs. Their average bundle diameters are 21 and 39 nm, respectively. Both types of nanotubes appear quite agglomerated, with a non-homogeneous size distribution of the diameters. Residual impurities could be observed in the micrographs, which were effectively removed after the purification process.

Raman spectroscopy is a powerful tool for characterization of SWCNTs. Figure 10.3 shows the Raman spectrum of SWCNTs

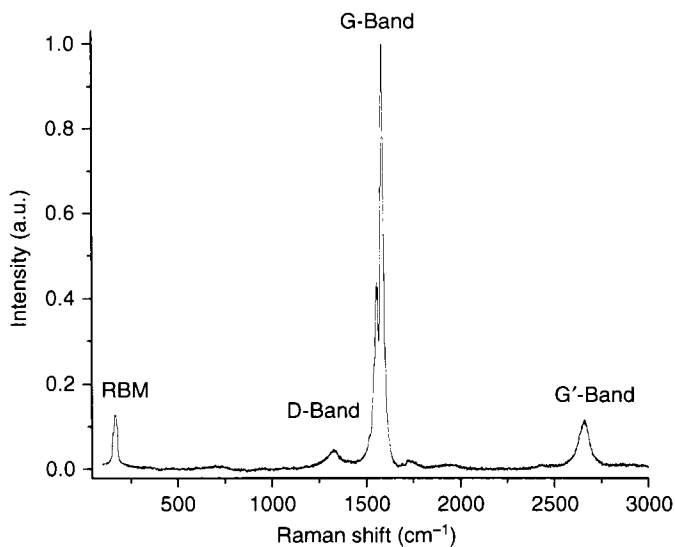


Figure 10.3. Raman spectrum of laser-grown SWCNTs measured with a 514.5 nm laser focused to $\sim 1 \mu\text{m}$ through a 50x objective. Laser power density was maintained below $3 \text{ kW}/\text{cm}^2$ to avoid heating.

synthesized by the laser method; the most characteristic bands are: (1) The radial breathing modes (RBM), low-frequency peaks ($<200\text{ cm}^{-1}$) assigned to vibrations of the carbon bonds moving in-phase in the radial direction; (2) The tangential modes or G-band, near 1600 cm^{-1} , where neighboring atoms are moving in opposite directions along the surface of the tube; (3) the dispersive disorder induced D-band around 1300 cm^{-1} and; (4) its second-order related harmonic G'-band around 2600 cm^{-1} . The Raman shift of the RBM is inversely proportional to the SWCNT diameter and has been shown to closely follow the relationship (31) $\omega_{\text{RBM}} (\text{cm}^{-1}) = 223.5/d + 12.5$, where d is the tube diameter expressed in nm. The calculated (d) values for raw arc-grown and laser-grown SWCNTs range between 1.2 and 1.7 nm.

The G-band is an intrinsic feature of carbon nanotubes that is closely related to vibrations in all sp^2 carbon materials, and allows distinguishing whether the nanotube is semiconducting or metallic. The profile shown in Figure 10.3 reveals the semiconductor character of these CNTs. The intensity of the G-band can be related to the SWCNT concentration in the sample. Although is not a quantitative measurement it can be used as a relative indicator of the sample purity. The D-band usually creates ambiguities whether to be assigned to disordered carbon forms (purity) or to SWCNT defects (quality). Nevertheless, the relative strength and width of the D-band has been used as qualitative measurement of the fraction of defects present in the sample. The quality/purity of the SWCNTs can be evaluated by the G/D intensity ratio; values obtained for the different SWCNTs are listed in Table 10.1.

NIR spectroscopy is an efficient tool to semi-quantitatively evaluate the carbonaceous purity of bulk SWCNT samples. Their absorption spectrum in the VIS-NIR region consists of semiconducting (S_{nn}) and metallic (M_{nn}) SWCNT interband transitions and the π -plasmon. Sample purity can be evaluated by NIR spectroscopy, following the method described by Itkis *et al.* (32). The NIR spectrum of laser SWCNTs dispersed in DMF is shown in Figure 10.4. The S_{11} peak for arc-produced SWCNTs is typically located between 5000 and 7000 cm^{-1} (33); the high-energy edge of this absorption peak is just visible in the spectrum. The S_{22} transition of semiconducting SWCNTs can be clearly observed. The ratio between the S_{22} peak area after baseline correction and the S_{22} total area can be used as an indicator of relative purity; calculated values are included in Table 10.1. Acid-treated SWCNTs show higher purity than as-produced arc-grown SWCNTs; this evidences the effectiveness of the purification step.

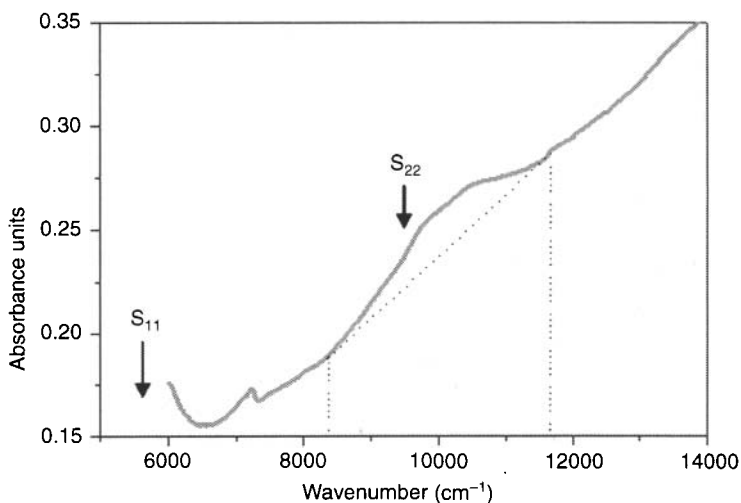


Figure 10.4. NIR spectrum of laser-grown SWCNTs dispersed in DMF (0.01 mg/mL). Reprinted with permission from ref 10. Copyright 2009 Elsevier.

10.4 Integration of the Carbon Nanotubes in the PEEK Matrix

In the literature, several methods for the preparation of polymer/CNT composites have been reported (34,35), including solution mixing, sonication, melt compounding and *in-situ* polymerization. The melt blending approach presents two main advantages: firstly, it is environmentally sound, due to the absence of organic solvents; secondly, it is compatible with conventional industrial processes, such as extrusion, injection and blow moulding, thus being easily implemented. However, generally it is difficult to achieve homogeneous dispersion of CNTs by this procedure. To improve their distribution throughout the matrix, nanotubes have been purified, ball milled, functionalized, surface treated with plasma and dispersed in compatibilizing agents (36). Generally, compatibilizers are block or graft copolymers, chemically identical to or having affinity with the matrix, which possesses segments capable of interaction with each blend component. Acting as polymeric surfactants, these reduce the interfacial tension, thus promoting interfacial adhesion between the matrix and the dispersed phase, which results in improved mechanical properties of the composites.

The melt blending process seems to be the most suitable for the integration of CNTs in the PEEK matrix. The following sections

explain in detail the strategies employed to efficiently incorporate the different types of nanotubes into this polymer, including covalent functionalization, wrapping in compatibilizers and pre-mixing stages in organic solvents.

10.4.1 Covalent Grafting in Carbon Nanotube/PEEK Nanocomposites

Conventional methods for integration of nanotubes into polymer matrices usually lead to poor adhesion, which limits the load transfer, hence the improvement in the mechanical properties of the composites. An efficient way to solve this issue is the covalent attachment of carbon nanotubes to the polymer matrix. To date very few studies have been undertaken to address this approach. Moreover, the works developed in this area have mostly been carried out with multi-walled carbon nanotubes (MWCNTs). The very first attempt to create nanocomposites with polyetherketone (PEK) covalently anchored to carbon nanotubes was based on *in situ* polymerization of the polymer chains. The synthesis process (electrophilic substitution reaction) is initiated onto the surface of the nanotubes by an AB or AB₂ monomer derivated from phenoxy benzoic acids, in the presence of polyphosphoric acid (PPA) and P₂O₅ (37). The experimental process is carried out under a flow of inert gas and continuous high torque mechanical stirring. The participation of P₂O₅ as a dehydrating agent allows the Friedel-Crafts reaction with PPA to undergo more efficiently. PPA is an acid and viscous medium, which promotes the protonation of the nanotubes and avoids their reaggregation. The resulting material, a MWCNT-PEK nanocomposite, exhibits high processability. Conventional moulding techniques and wet-spinning can be successfully applied to obtain test samples. Besides, by tuning the initiating monomer, different PEK chain morphologies (linear, hyperbranched) and compositions (carboxylated (38), oxyethylene spaced (39)) can be grafted.

Another approach to covalently attach carbon nanotubes is based on the chemical modification of a PEEK matrix which allows further covalent interaction with functionalized carbon nanotubes. In 2007 Babaa et al. (40) proposed a route to covalently graft commercial MWCNTs by using this approach. The process initiates by dissolution of PEEK in concentrated H₂SO₄, leading to functionalization yields of 70%. MWCNTs covalently functionalized with

terminal amine groups were grafted to sulfonated PEEK (s-PEEK) by prolonged stirring of both components in DMF at 40°C. The reaction generates sulfoamide groups that link MWCNTs to the PEEK matrix. This covalent anchoring is demonstrated by near edge X-ray absorption fine structure spectroscopy (NEXAFS) and X-ray photoelectron spectroscopy (XPS).

10.4.2 Wrapping of the SWCNTs in Compatibilizing Agents

The incorporation of compatibilizing agents is an alternative method to the covalent functionalization, which is expected to improve the interfacial adhesion between the reinforcement and the matrix, hence the load transfer. Compatibilizers should be chosen based on their affinity to the matrix and the fillers. Polyetherimide (PEI), an amorphous amber-coloured thermoplastic polymer miscible and structurally similar to PEEK (41,42), is an effective compatibilizing agent to introduce SWCNTs into this polymer matrix (11). The bisphenol-A and phenyl moieties of the compatibilizer interact strongly with the matrix chains, due to their chemical similarity, as well as with SWCNTs due to π - π interactions of its aromatic rings with the sp^2 -bonded carbon hexagonal networks. Moreover, the imide rings of PEI have high polarity and are able to undergo polar interactions (e.g. hydrogen bonds) with the oxygen groups of the SWCNTs, either generated in their synthesis or induced by acid treatments. The aforementioned selective affinities enhance the interfacial adhesion between the SWCNTs and the matrix, hence the resulting properties of the nanocomposites.

The wrapping process is typically carried out in liquid medium; a PEI chloroform solution (1.5% w/w) is mixed with the SWCNTs under intense stirring. The blend is then treated with an ultrasonic tip for ~1 h at 50% oscillation amplitude and 50% cycle time. The resulting dispersion is subsequently filtered using a 0.2 μ m pore size PTFE membrane and dried under vacuum at 60°C to assure total evaporation of the solvent. The wrapped SWCNTs can be characterized by different techniques, and some results are included in Table 10.1. Figure 10.5 shows TEM images of acid-treated SWCNTs dispersed in the compatibilizer. Small nanotube bundles shrouded in PEI can be visualized in the micrographs.

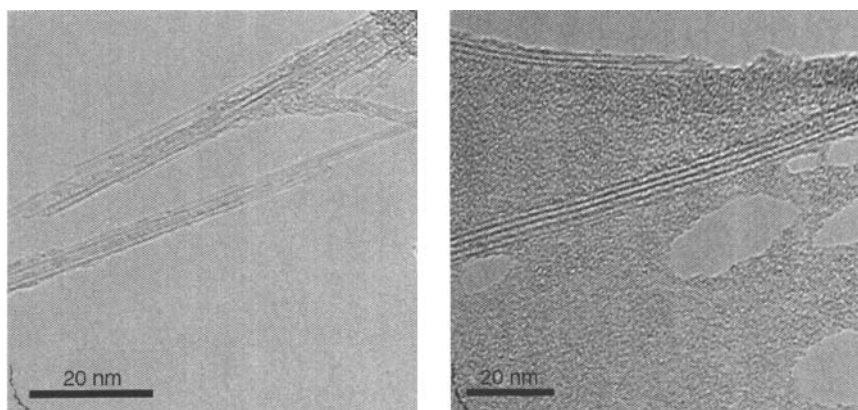


Figure 10.5. TEM images of acid-treated arc-SWCNTs wrapped in PEI.

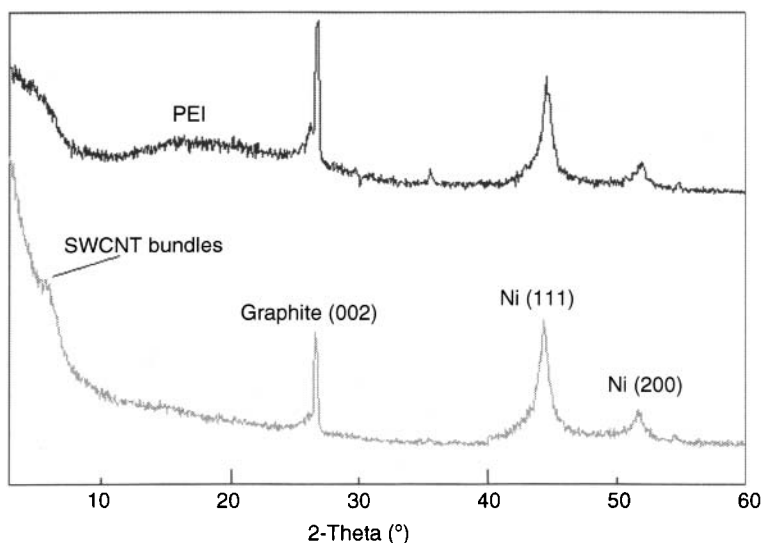


Figure 10.6. X-ray diffractograms of pristine (bottom) and PEI-wrapped (top) arc-grown SWCNTs.

X-ray diffractograms for pristine and PEI-wrapped arc-SWCNTs are presented in Figure 10.6. The peak corresponding to SWCNT bundles (appearing at low diffraction angles (43°), $2\theta = 6^\circ$) disappear after the purification and wrapping processes. Raman spectroscopy can also be applied to characterize these dispersions. The G/D ratio decreases drastically for the shrouded carbon nanotubes after the wrapping process (see Table 10.1), attributed to an increase in the

disordered material content and a change in the vibrational modes of the nanotubes.

10.4.3 Pre-Mixing Stage and Melt Blending Approach

To improve the distribution of the CNTs in the matrix, nanocomposites are prepared following a procedure based on mechanical treatments in alcohol media (Figure 10.7):

- The polymer is ground with a ball mill in order to reduce its particle size, vacuum dried at 120°C for 4 h and stored in a dry environment before blending.
- PEEK fine powder is manually mixed with the SWCNTs.
- PEEK/SWCNT mixture is dispersed in a small volume of ethanol and subsequently sonicated in an ultrasonic bath for 30 min.
- The dispersion is partially dried under vacuum (70 mbar) at 50°C for 5 min, sonicated for another 30 min and heated in an oven until the ethanol is eliminated.

The melt compounding is performed in a thermo-extruder (e.g. Haake MiniLab System) at 380°C, with a rotor speed of 150 rpm. Mixing times of 20 min are applied to attain an adequate mixture.

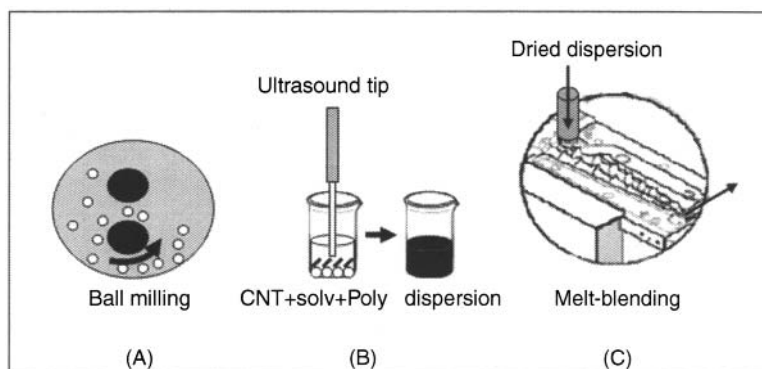


Figure 10.7. Different stages of the processing route employed for the preparation of PEEK/SWCNT composites: (A) polymer ball milling; (B) ultrasonication of PEEK/SWCNT dispersion in ethanol; (C) melt blending.

Homogeneous films can be prepared in a hot-press at 380°C under 130 bar and cooled to room temperature between aluminium plates.

10.5 Characterization of PEEK/Carbon Nanotube Nanocomposites

10.5.1 Morphology

To achieve a good dispersion of the CNTs in the polymer matrix and strong nanotube-matrix interfacial bonding are the keys to fabricate composites with enhanced thermal and mechanical properties. This is commonly a difficult task because carbon nanotubes, especially SWCNTs due to their high specific surface area, have strong tendency to gather and form bundles or micron-sized agglomerates, which adversely affect the mechanical properties of the nanocomposites. Moreover, their large aspect ratio (length/diameter) causes extremely high viscosity in the melt or dissolved polymers, which in turn would affect their uniform dispersion. On the other hand, the interfacial bonding strengths among nanotubes and with the matrix are highly dependent on the type and size of the filler. MWCNTs generally stay as an individual tube with some degree of entanglement and thus they are easier to disperse.

Scanning electron microscopy (SEM) is frequently used to observe the surface morphology of nanocomposite films and qualitatively visualize the state of dispersion of carbon nanotubes in the matrix. To improve the crystallinity of the polymer and the visualization of the fillers, samples are fractured in liquid nitrogen and then annealed in an oven for a few hours at 200°C. Figure 10.8 shows typical micrographs of different PEEK/SWCNT systems, illustrating the dispersion of the carbon nanotubes, which appear as bright spots. In the composite prepared by direct integration of 0.5 wt% raw arc-grown SWCNTs, (Figure 10.8A), the nanotubes are relatively well dispersed through the matrix, and present an average bundle diameter of ~55 nm. Similar nanocomposite, fabricated with the aid of mechanical pre-treatments in ethanol, containing 0.5 wt% arc-purified SWCNTs can be observed in Figure 10.8B. In this case, the size of the domains of the filler phase is smaller, and the nanotubes possess approximately half the diameter of a bundle of as-received arc SWCNTs, meaning that purified fillers are more disentangled and better integrated in the matrix, which confirms the efficiency of the pre-mixing stage

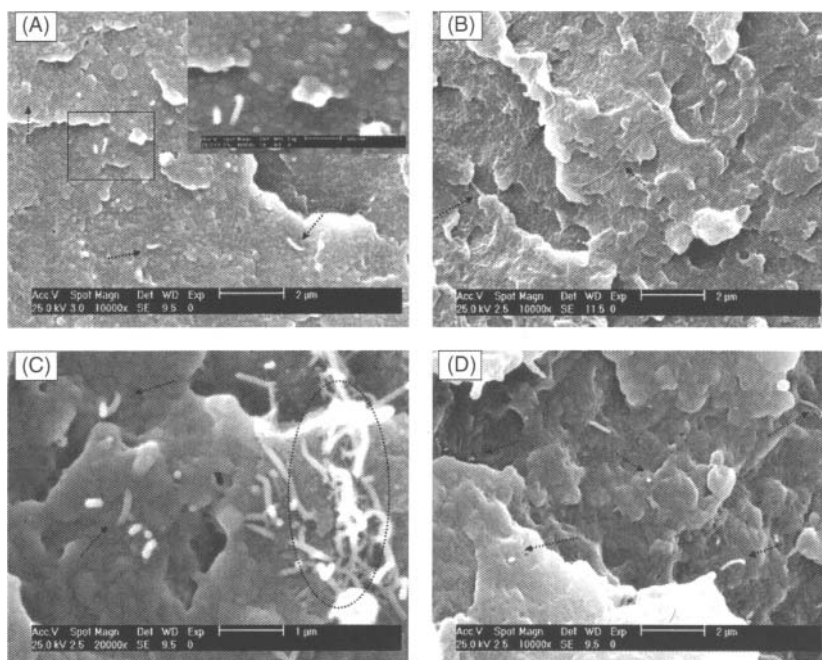


Figure 10.8. SEM micrographs from fractured surfaces of different types of PEEK/SWCNT nanocomposites, obtained with an acceleration voltage of 25 kV and an intensity of $9 \cdot 10^{-9}$ A. (A) PEEK/arc-grown SWCNT 0.5 wt%; (B) PEEK/arc-purified SWCNT 0.5 wt%; (C) PEEK/laser-grown SWCNT 1.0 wt%; (D) PEEK/laser-grown SWCNT dispersed in PEI 1.0 wt%. The arrows indicate randomly distributed nanotube bundles throughout the matrix. (A) and (C) correspond to composites prepared by direct mixing, whereas composites shown in (B) and (D) were prepared following a pre-processing based on mechanical treatments in ethanol (see explanation in the text). The inset in (A) is a magnification to show the shape of the filler phase. The dashed circle in (C) shows a small region of agglomerated CNT. From ref 10.

in alcohol. Samples including both types of SWCNTs show a good interfacial adhesion between the filler and matrix phases, as no open ring holes are found around the nanotubes.

Figures 10.8C and 10.8D compare composites with 1 wt% laser-grown SWCNTs; the former was prepared by direct mixing, and the latter, including PEI as compatibilizer, followed a pre-processing in organic solvent. As it can be clearly observed, the SWCNTs are quite agglomerated in the non-compatible sample (see the circle marked on the image), forming a highly entangled interconnected structure. However, the compatibilized nanocomposite displays a random and improved dispersion of the reinforcing phase; addition of the compatibilizer induced CNT disentanglement and

debundling, leading to a reduction of the organic filler domains. This results in larger effective contact area and thus stronger CNT-PEEK interfacial adhesion, reflected in more efficient load transfer under stress conditions.

10.5.2 Thermogravimetric Study

The thermal stability of nanocomposites, a key parameter for their technological applications, can be evaluated by means of thermogravimetric analysis (TGA), under oxidative and inert atmospheres. The following characteristic temperatures are selected to compare the stability of the different samples: T_i , initial degradation temperature obtained at 2% weight loss; T_{10} , temperature corresponding to the 10% weight loss and T_{mr} , temperature of maximum rate of weight loss.

The degradation curves of pure PEEK and different nanocomposites containing 1 wt% SWCNTs are displayed in Figure 10.9. The thermal stability of these composites is strongly influenced by the type of atmosphere: the decomposition under oxidative conditions (Figure 10.9A) occurs in two consecutive stages, leading to the total decomposition of the material at temperatures between 600–650°C; under inert environment (Figure 10.9B), all samples present a single degradation step, with approximately 45% weight loss at 650°C. The incorporation of SWCNTs shifts the matrix curve toward higher temperatures, being this stabilization effect qualitatively similar to that observed for other polymer/CNT nanocomposites (44,45). The temperature

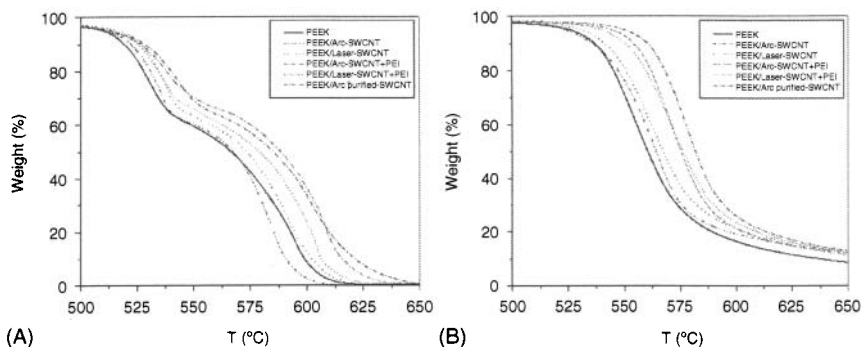


Figure 10.9. TGA curves for different types of 1 wt% PEEK/SWCNT composites under dry air (A) and nitrogen (B) atmospheres, at a heating rate of 10°C/min. The measurements were performed under dynamic conditions, from room temperature to 900°C, with a gas purge of 150 mL/min. For the sake of comparison, only the temperature range between 500 and 650°C is plotted. Reprinted with permission from ref 11. Copyright 2009 IOP publishing.

increment depends considerably on the type of SWCNT: composites containing arc-purified CNTs exhibit the highest degradation temperatures (under nitrogen conditions, T_i and T_{mr} increased by about 20 and 25°C, respectively). This is consistent with the results obtained from TGA study of the SWCNTs (see Table 10.1), which shows that these nanotubes are more resistant to the oxidation process, probably due to a lower content in metal impurities that catalyze their decomposition (46). Moreover, the decomposition temperatures of samples incorporating laser-grown SWCNTs are slightly higher than those of nanocomposites containing raw arc-grown fillers, which seems reasonable taking into account the improved quality and higher interfacial area (aspect ratio) of the formers (see Table 10.1).

The preparation procedure also affects to the decomposition process. Samples prepared with the aid of mechanochemical pre-treatments present higher thermal stability than those obtained by direct mixing; a more uniform and fine dispersion of the SWCNTs improves the interfacial adhesion between the CNTs and the matrix and restricts the thermal motion of the PEEK chains, leading to composites thermally more stable. In general, the compatibilizer (PEI) maintains or increases slightly the thermal stability of these nanocomposites. This can be explained considering that, although PEI exhibits lower degradation temperatures than pure PEEK, it improves the dispersion of the CNTs and enhances the interfacial interactions CNT-matrix. Well dispersed nanotubes hinder the diffusion of the degradation products from the bulk of the polymer to the gas phase and thereby delay the degradation temperatures.

Table 10.2 illustrates the effect of the SWCNT content on the thermal behaviour of different PEEK/SWCNT systems. The incorporation of increasing CNT loading progressively enhances the stability of the matrix. The observed stabilization may be attributed to the above mentioned barrier effect of CNTs, combined with the higher thermal conductivity of the composite that facilitates heat dissipation.

10.5.3 Differential Scanning Calorimetry

From a technological point of view, the dynamic crystallization of composites is of a great interest, because most of processing routes take place under these conditions. Generally, the crystallization and melting behaviour of polymer/CNT nanocomposites is analyzed by differential scanning calorimetry (DSC) analysis; the transition temperatures are taken as the peak maximum or minimum in the

Table 10.2. Characteristic temperatures of different PEEK/SWCNT nanocomposites obtained from TGA measurements under nitrogen and dry air atmospheres at heating rate of 10°C/min

Mat. (% SWCNT)	Nitrogen			Dry air		
	T _i (°C)	T ₁₀ (°C)	T _{mr} (°C)	T _i (°C)	T ₁₀ (°C)	T _{mr} (°C), II
PEEK	521	544	558	472	520	530, 592
PEEK/arc-grown (0.1)	520	545	560	472	521	529, 583
PEEK/arc-grown (0.5)	521	547	562	474	522	532, 585
PEEK/arc-grown (1.0)	523	548	565	476	525	533, 587
PEEK/arc-purified (0.1)	536	550	564	481	523	537, 597
PEEK/arc-purified (0.5)	540	558	574	483	527	542, 602
PEEK/arc-purified (1.0)	543	564	578	485	531	545, 606
PEEK/arc+PEI (0.1)	535	549	562	476	523	536, 598
PEEK/arc+PEI (0.5)	537	553	571	479	525	540, 604
PEEK/arc+PEI (1.0)	539	558	574	481	529	543, 609

The displayed temperatures are: T_i: initial degradation temperature obtained at 2% weight loss; T₁₀: temperature for 10% weight loss; T_{mr}: temperature(s) of maximum rate of weight loss, determined from the peaks of the first derivative of TGA curve.

calorimetric curves and the apparent enthalpies are calculated as normalized integrals of the corresponding peaks. The levels of crystallinity (X_c) of the nanocomposites can be determined using the relation: $X_c = \Delta H_c / (\Delta H_c^\circ \times w_{\text{polymer}})$, where ΔH_c is the apparent crystallization enthalpy of the matrix, w_{polymer} is the weight fraction of the matrix and ΔH_c° is the extrapolated value of the enthalpy corresponding to a 100% crystalline polymer (e.g. 130 J/g for PEEK (47)).

Figure 10.10 shows the non-isothermal DSC runs for different PEEK/SWCNT composites containing 1 wt% CNT loading. The incorporation of SWCNTs leads to a significant shift of the

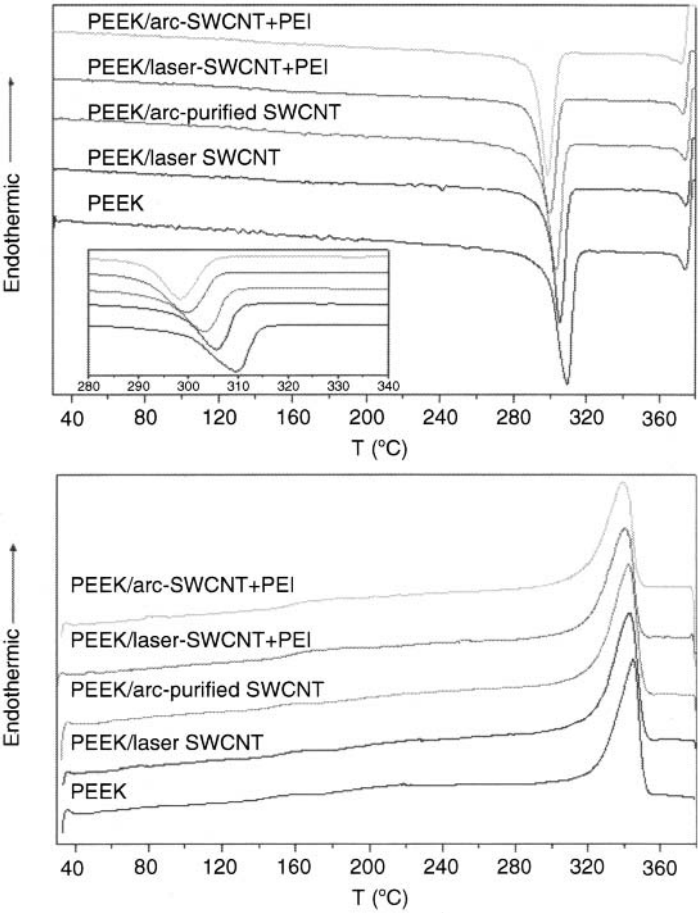


Figure 10.10. Non-isothermal DSC scans of different PEEK/SWCNT nanocomposites containing 1 wt% CNT loading, from 30 to 380°C, at rates of 10°C/min. Top: crystallization thermograms; Bottom: heating thermograms. The inset is a magnification showing the T_c decrease in the nanocomposites. From ref 10 and 11.

crystallization peak (T_c) toward lower temperatures, (see the inset in Figure 10.10), whereas does not significantly modify the apparent crystallization enthalpy ΔH_c , hence the level of crystallinity of the composites. These observations indicate that the nanotubes reduce the crystallization rate of the PEEK matrix, which can be explained by a nanoconfinement effect (48): CNT network imposes a confinement on polymer chain diffusion and crystal growth which slows down the overall crystallization process, leading to lower values of T_c for the composites. These results are consistent with the behaviour described by Shaffer *et al.* (7) on DSC analysis of vapour grown carbon-nanofibre/PEEK composites. A small T_c decrease was observed for samples with nanofibre loading up to 5 wt%, and this effect was attributed to interactions between the matrix and the filler occurring during the crystallization process.

With regard to the influence of the type of SWCNT, it is found that composites including wrapped CNTs present the lowest T_c values, decreasing the matrix T_c by about 10°C. This could be explained taking into account that the compatibilizer (PEI) is an amorphous polymer miscible with the matrix which perturbs its crystallization. The mentioned behaviour is a common attribute of miscible and compatible blends containing one non-crystallizing polymer (49), and the most likely explanation is the reduction in chain mobility imposed by the strong interactions between the components, that take place between the oxygen ion-pair electrons of the ether group in PEEK and the electron-deficient imide rings in PEI. On the other hand, samples with improved degree of dispersion of the SWCNTs present slightly higher T_c than those obtained by direct mixing; in the latter the existence of small agglomerates makes the indicated confinement effect more significant, and the crystallization occurs at lower temperatures. However, no significant differences are found within samples containing arc and laser-grown SWCNTs, hinting that the purity and quality of the nanotubes affect slightly to the crystallization process. The influence of the CNT content on the crystallization of the PEEK matrix is illustrated in Table 10.3. With increasing the filler loading, T_c decreases progressively, due to the intensification of the restrictions on the crystal growth. In general, differences between the levels of crystallinity of the composites are quite small, lower than 5%. This behaviour differs from that found for carbon-nanofibre/PEEK composites prepared by injection moulding (6), where the presence of the nanoscale reinforcement lead to an increase in the overall degree of crystallinity.

Table 10.3. DSC crystallization and melting data of different PEEK/SWCNT nanocomposites

Mat. (% SWCNT)	T_m (°C)	ΔH_m (J/g)	T_c (°C)	ΔH_c (J/g)	αX_c (%)	βX_c (%)	D_{110} (nm)
PEEK	344.2	58.2	309.1	55.3	42.5	43.6	20.9
PEEK/arc-purified (0.1)	343.9	58.6	308.1	58.2	44.8	43.8	22.5
PEEK/arc-purified (0.5)	343.2	57.5	306.6	57.0	44.1	43.0	21.3
PEEK/arc-purified (1.0)	342.6	56.6	304.3	54.6	42.4	41.9	18.6
PEEK/laser-grown (0.1)	343.4	58.3	307.7	56.4	43.4	45.1	21.5
PEEK/laser-grown (0.5)	343.0	58.0	305.8	55.6	42.9	44.2	20.7
PEEK/laser-grown (1.0)	342.8	55.8	304.9	53.9	41.8	42.5	19.4
PEEK/arc+PEI (0.1)	343.0	57.2	305.9	56.0	43.0	43.9	21.9
PEEK/arc+PEI (0.5)	341.9	56.1	303.4	54.8	42.4	42.8	19.8
PEEK/arc+PEI (1.0)	340.3	54.9	299.5	52.7	40.9	41.5	18.6

The displayed data are: T_c : crystallization temperature; ΔH_c : apparent crystallization enthalpy; T_m : melting temperature; ΔH_m : apparent melting enthalpy; X_c : degree of crystallinity, obtained by DSC (a) and WAXS experiments. D_{110} : crystallite size perpendicular to the diffraction plane (110).

In the case of the melting process, the addition of SWCNTs does not significantly change the melting temperature T_m or the apparent melting enthalpy ΔH_m of the matrix (see bottom of Figure 10.10). This is consistent with the observations reported by Shaffer et al., where the melting behaviour of PEEK remained merely unaffected by the presence of the nanofibres (7). It is also important to notice that a small variation of the specific heat associated to the glass transition of the matrix in the nanocomposites can be visualized in the heating thermograms. The presence of the nanotubes shifts this transition toward higher temperatures; this phenomenon will be discussed in detail according to DMA measurements.

10.5.4 X-ray Diffraction Analysis

The crystalline structure of polymer composites depends strongly on their thermal history and their manufacturing process. To assess their crystal structure and degree of crystallinity, wide angle X-ray diffraction (WAXS) experiments are frequently performed. Figure 10.11 shows the room temperature diffraction patterns of different PEEK/

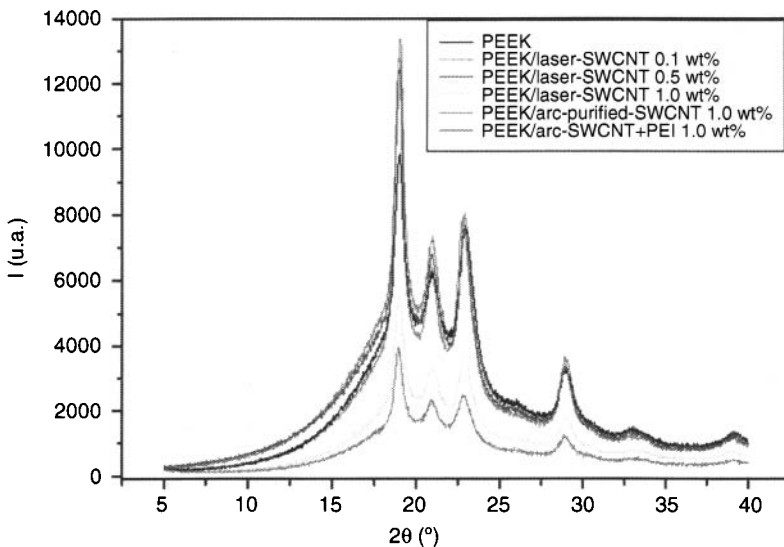


Figure 10.11. Room temperature wide angle X-ray diffractograms (WAXS) of pure PEEK and different PEEK/SWCNT film samples in the angular region of $2\theta = 5 - 40^\circ$, obtained using $\text{CuK}\alpha$ ($\lambda = 0.15418 \text{ nm}$) radiation, with a scan speed of 0.2s and angular increment of 0.02° .

SWCNT film samples, in the angular region $2\theta = 5\text{--}40^\circ$. Four main peaks can be observed at 2θ values of 18.8° , 20.7° , 22.9° and 28.9° , which correspond to the diffraction of the (110), (111), (200) and (211) crystalline planes (50), respectively, of the orthorhombic unit cell. All composites exhibit similar diffractogram to the PEEK matrix, with no shift in the position of the Bragg reflections. As the SWCNT content increases, peaks became wider and with decreased intensity. Composites prepared by dispersion in ethanol show narrower peaks than those obtained by direct mixing.

The degree of crystallinity X_c of the samples can be calculated from WAXS diffractograms using the following relation: $X_c = I_c / (I_c + I_a)$, being I_c and I_a the integrated intensities of the crystalline and amorphous phases, respectively. The values obtained for different PEEK nanocomposites are collected in Table 10.3; these data are in very good agreement with those derived from DSC thermograms.

The crystallite size perpendicular to the diffraction (hkl) plane, D_{hkl} can be obtained from the diffractograms using the Scherrer expression: $D_{hkl} = K \lambda / \beta \cos \theta$, where β is the half-width of the experimental peak, k is the Scherrer factor ~ 1 , and 2θ the Bragg angle. In the case of PEEK/SWCNT composites, D_{110} increases with the addition of SWCNTs until a concentration of 0.1 wt% is reached, and then slightly decreases (see Table 10.3). This behaviour can be explained based on the aforementioned nanoconfinement effect and the T_c decrease observed from DSC thermograms. As the SWCNT loading rises, the formation of a strong nanotube network restricts the crystal growth and the dimension is thus decreased. Moreover, it is found that samples containing purified SWCNTs present the highest D_{110} values, and that the procedure of dispersion in ethanol leads to larger crystals.

10.5.5 Mechanical Properties

One of the main goals of the development of polymer/CNT composites is to attain materials with enhanced mechanical properties. These properties depend on many factors, including the size and degree of dispersion of the filler and the adhesion at the CNT-matrix interface. To achieve an efficient load transfer, a homogeneous nanotube distribution free from agglomerates and entanglements as well as good compatibility SWCNT-matrix are required. Dynamic mechanical analysis (DMA) tests are performed over a wide range of temperatures and frequencies, providing information about the

transitions and relaxation processes of the matrix in the composites. The most important parameters obtained from these experiments are the storage modulus E' , which gives an idea of stiffness behaviour and load bearing capability of the sample, loss modulus E'' , which is proportional to the amount of energy dissipated as heat, and the damping coefficient $\tan \delta$, ratio of the loss to storage modulus, related to the degree of molecular mobility in the polymeric material. The glass transition temperature (T_g) can be defined as the peak maximum in the loss modulus or loss tangent curve.

Figure 10.12 shows the temperature dependence of the storage moduli E' and loss moduli E'' of different PEEK/SWCNT nanocomposites incorporating 1 wt% CNT content, at the frequency of 1 Hz. E' decreases progressively with increasing temperature, showing a very strong decay in the temperature range between 138–170°C, which correlates with the glass transition of the material. This fall in the modulus is attributed to an energy dissipation phenomenon involving cooperative motions of the polymer chains

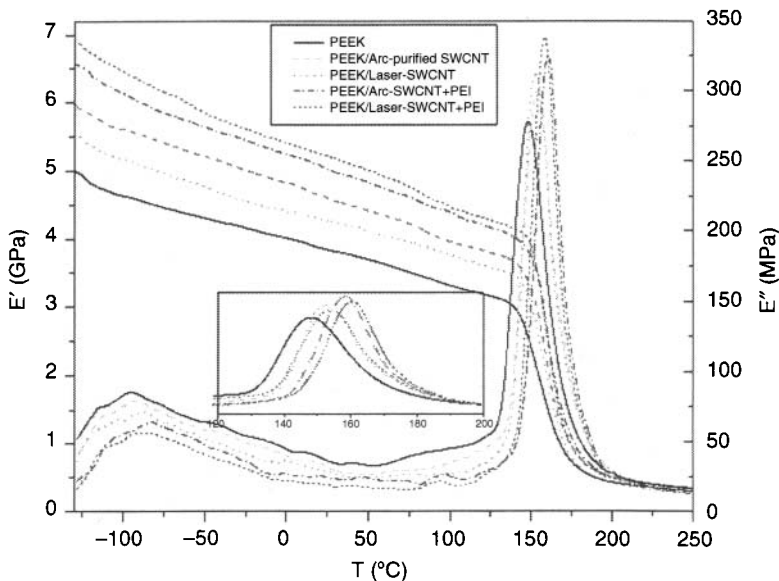


Figure 10.12. Temperature dependence of the storage modulus E' and loss modulus E'' of different PEEK/SWCNT nanocomposites with 1 wt% CNT content, obtained from DMA measurements performed in the tensile mode at frequency 1 Hz and heating rate of 2°C/min. The inset is a magnification showing the increment in T_g for the nanocomposites. From ref 11.

(51). The incorporation of SWCNTs induces a remarkable increase in the storage modulus of the matrix at temperatures below the glass transition, which becomes worthless at higher temperatures. The increase in E' is more pronounced for the compatibilized samples, attributed to their improved CNT dispersion and interfacial adhesion between the filler and matrix interfaces.

Experimental data reveal a non-linear growth of E' with CNT content, the increase being more pronounced at low concentrations. Thus, at 25°C, composites containing 0.1, 0.5 and 1 wt% laser-grown SWCNTs increased E' by approximately 16, 23 and 27% respectively. These results are not consistent with the predictions of continuum-based volume additivity models (52). E' of samples with 0.1 wt% SWCNTs exceeded the theoretical calculations, whereas those of higher compositions were lower than expected. At very low concentrations, the nanotubes are well dispersed and E' increases rapidly with SWCNT content. However, when the concentration becomes higher, the nanotubes interact and form small aggregates, leading to E' values which fell appreciably below theoretical predictions. The aforementioned results are in contrast to the study of vapour-grown carbon nanofibres/PEEK composites (7) prepared by injection moulding, which revealed a linear increase in stiffness with increasing nanofibre loading. This contradiction can be explained based on the large aspect ratio, high mass density and low flexibility of carbon nanofibres compared to CNTs (4) and on the processing routes employed that play a key role in the resulting properties of these materials.

The development of the loss modulus of PEEK as a function of temperature, Figure 10.12, exhibits a low broad peak (centred around -95°C), attributed to the β relaxation (21), associated with local motions of the ketone groups, and an intense sharp peak (at 148.3°C), denominated the α relaxation (53), whose maximum corresponds to the glass transition temperature (T_g) of the polymer. The addition of SWCNTs results in a reduction of the magnitude of E'' at temperatures below T_g . Furthermore, β relaxation was broadened, smoothed and shifted to higher temperatures; this suggests that the presence of SWCNTs act as a barrier for the local movements of the ketone groups. Moreover, the CNTs restrict rotational motion within the polymer chains, causing small increases in T_g , hence in the stiffness of these systems. Such effects have been observed in other PEEK systems reinforced with inorganic nanoparticles (54).

The processing routes and the type of SWCNT have strong influence on the mechanical response of the composites. As expected, samples prepared following the procedure of dispersion in ethanol, which present a more homogeneous distribution of the nanotubes, exhibit higher E' and T_g than those obtained by direct mixing. Moreover, for similar CNT loadings, the highest E' were found among samples including laser-grown SWCNTs. This is not surprising since the purity, quality, aspect ratio and nature of impurities, hence the source of SWCNTs are determining factors in the final properties of CNT based composites. The laser process produces CNTs with high quality (few defects, high crystallinity) and very large aspect ratio (>10000) (55). The acid treatments used to purify the arc-grown SWCNTs are known to shorten the CNTs and induce defects on their side walls; it has recently been shown that defects have detrimental effects on mechanical properties of SWCNTs (56).

Deng *et al.* (8) investigated the tensile properties of PEEK/MWCNTs, and found increases in the elastic modulus and yield strength at temperatures above and below T_g ; at 25°C, the tensile modulus increased by ~90% for composites including 15 wt% MWCNTs, and the increment reached ~160% at 200°C. According to those results, the improvement of MWCNTs in the mechanical behaviour of the matrix is more effective at higher temperatures. Experimental results do confirm that the overall mechanical performance of PEEK/CNT nanocomposites is well above the required for potential aircraft applications.

10.5.6 Electrical and Thermal Conductivity

Polymer composites incorporating carbon nanotubes are frequently used in the electronic and aerospace industries to dissipate heat and prevent the build up of static charge. Pure PEEK is an insulating polymer ($\sigma < 10^{-13}$ S/cm), and becomes electrically conductive with the incorporation of CNTs. In the case of PEEK/SWCNT nanocomposites, room temperature conductivity values increased up to 10^{-2} S/cm for 1 wt% filler loading (dashed lines in Figure 10.13), enhancement only been reported in the literature for composites incorporating loosely entangled and uniformly distributed CNTs (57). Song *et al.* (9) also reported a similar electrical conductivity improvement when buckypaper SWCNTs were embedded at the surface of the PEEK polymer. However, no significant changes are observed with increasing CNT concentration, which indicates that the percolation threshold (57) in these systems is below 0.1 wt%

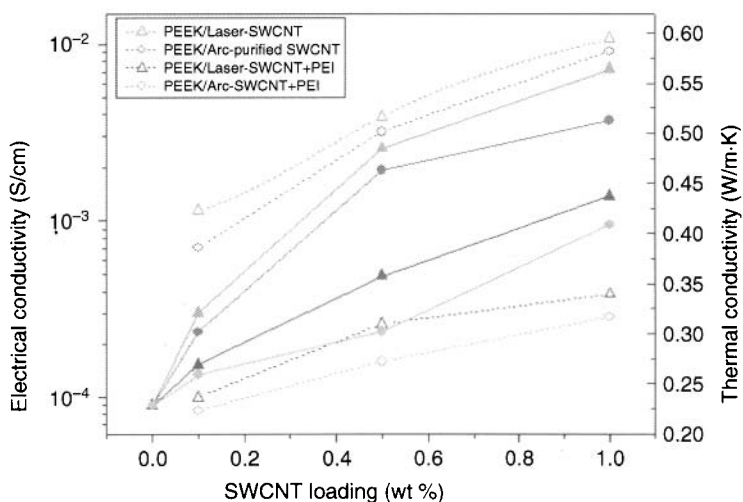


Figure 10.13. Room temperature DC volume conductivity (dashed lines) and thermal conductivity (solid lines) as a function of CNT loading for different types of PEEK/SWCNT nanocomposites. Reprinted with permission from ref 11. Copyright 2009 IOP publishing.

CNT loading. Samples including compatibilizer show conductivity values about one order of magnitude lower than those non-compatible, since the wrapping leads to a decrease in the number of contacts between the tubes, hence a reduction in the conductivity. On the other hand, for the same CNT concentration, small differences were found among conductivity data of composites reinforced with laser-grown and arc-grown SWCNTs.

The thermal conductivity of PEEK (0.23 W/mK) also improves considerably by the incorporation of carbon nanotubes (solid lines in Figure 10.13). At 0.1, 0.5 and 1 wt% CNT content, the increment was about 40, 115 and 150%, respectively, for composites including laser-grown SWCNTs, whereas for the corresponding compatibilized samples the increase was reduced to 23, 60 and 90%. Taking into account the exceptionally high thermal conductivity of SWCNTs ($\sim 10^3$ W/mK) (4), the values cited above are considerably below the predictions by the rule of mixtures, probably due to the small thermal conductance of the nanotube-matrix interface. Nevertheless, this improvement in thermal conductivity is higher than the attained for sandwich like SWCNT paper/PEEK composites (9), which confirms once again the effectiveness of the methods described for integration of CNTs in the PEEK matrix.

10.6 Concluding Remarks

This review provides an extensive outlook of the research in PEEK/single-walled carbon nanotube nanocomposites and insights to the factors that ultimately control their properties. A complete characterization at nano(micro)-scopic and macroscopic scales is fundamental to obtain information about the changes induced in the polymer with the addition of CNTs. Different strategies have been developed to efficiently incorporate these fillers in the PEEK matrix, including purification, wrapping in compatibilizing agents and covalent functionalization of the nanotubes, as well as polymer ball milling and mechanochemical pre-treatments in organic solvent. The composites exhibit higher degradation temperatures than the matrix, and their thermal stability is found to increase with better dispersion, higher loading and improved purity and quality of the nanotubes. The compatibilizers maintain the level of thermal stability attained in the binary composites. The crystallization temperature of the nanocomposites decreases with increasing SWCNT content, whereas the melting temperature remains almost constant. This behaviour can be explained by a confinement effect of the polymer chains within the CNT network, which delays the crystallization process. Compatibilized samples present the lowest crystallization temperature, since the compatibilizer perturbs the crystallization of the matrix; however, the level of crystallinity of these systems is not affected by the type or concentration of the filler. The storage modulus of non-compatibilized composites shows a non-linear growth with increasing SWCNT content, and fell appreciably below theoretical predictions at high nanotube loadings. This phenomenon can be attributed to weaker nanotube-matrix interphase adhesion taking place when a larger concentration regime is reached. The compatibilizer improves this interfacial interaction, hence the stress transfer ability, leading to a larger enhancement in the modulus. SWCNTs restrict molecular mobility and consequently increase the glass transition temperatures. In general, improved mechanical properties are found among composites incorporating laser-grown SWCNTs, probably due to the high quality of this type of filler. The incorporation of CNTs results in a drastic enhancement of the matrix conductivity. Samples including compatibilizer present conductivity values lower than non-compatibilizer, since the wrapping leads to a decrease in the number of contacts between the tubes. PEEK/SWCNT composites are interesting multifunctional materials for potential technological applications, particularly for the aircraft industry.

Acknowledgements

Financial support from a coordinated project between the National Research Council of Canada (NRC) and the Spanish National Research Council (CSIC) is gratefully acknowledged.

Glossary of Abbreviations

CNTs	Carbon nanotubes
D	Average bundle diameter
DMA	Dynamic mechanical analysis
DMF	N, N-Dimethylformamide
DMSO	Dimethyl Sulfoxide
DSC	Differential scanning calorimetry
MWCNTs	Multi-walled carbon nanotubes
NIR	Near infrared spectroscopy
E'	Storage modulus
E''	Loss modulus
ΔH_c	Crystallization enthalpy
ΔH_m	Melting enthalpy
PAEKs	Poly(aryl ether ketone)s
PEEK	Poly(ether ether ketone)
PEI	Polyetherimide
PPA	Polyphosphoric acid
PTFE	Politetrafluoretileno
RBM	Radial breathing modes
SDS	Sodium dodecyl sulphate
SEM	Scanning electron microscopy
SWCNTs	Single-walled carbon nanotubes
T_c	Crystallization temperature
TEM	Transmission electron microscopy
T_g	Glass transition temperature
TGA	Thermogravimetric analysis
T_i	Initial degradation temperature
T_m	Melting temperature
T_{mr}	Temperature of maximum rate of weight loss
WAXS	Wide angle X-ray diffraction
X_c	Degree of crystallinity

References

1. L. Dai, and A.W.H. Mau, *Advanced Materials*, Vol. 13, p. 99, 2001.
2. X.L. Xie, Y.-W. Mai, and X.-P. Zhouet, *Materials Science and Engineering R*, Vol. 49, p. 89, 2005.
3. E.T. Thostenson, Z. Ren, and T.-W. Chou, *Composites Science and Technology*, Vol. 61, p. 1899, 2001.
4. M. Moniruzzaman, and K.I. Winey, *Macromolecules*, Vol. 39, p. 5194, 2006.
5. B. Valter, M.K. Ram, and C. Nicolini, *Langmuir*, Vol. 18, p. 1535, 2002.
6. J. Sandler, A.H. Windle, P. Werner, V. Altstadt, M.V. Es, and M.S.P. Shaffer, *Journal of Materials Science*, Vol. 38, p. 2135, 2003.
7. J. Sandler, P. Werner, M.S.P. Shaffer, V. Demchuck, V. Altstadt, and A.H. Windle, *Composites A*, Vol. 33, p. 1033, 2002.
8. F. Deng, T. Ogasawara, and N. Takada, *Key Engineering Materials*, Vols. 334–335, p. 721, 2007.
9. L. Song, H. Zhang, Z. Zhang, and S. Xie, *Composites A*, Vol. 38, p. 388, 2007.
10. A.M. Díez-Pascual, M. Naffakh, M.A. Gómez, C. Marco, G. Ellis, M.T. Martínez, A. Ansón, J. M. González-Domínguez, Y. Martínez-Rubi, and B. Simard, *Carbon*, Vol. 47, p. 3079, 2009.
11. A.M. Díez-Pascual, M. Naffakh, M.A. Gómez, C. Marco, G. Ellis, M.T. Martínez, A. Ansón, J. M. González-Domínguez, Y. Martínez-Rubi, B. Simard, and B. Ashrafi, The influence of a compatibilizer on the thermal and dynamic mechanical properties of PEEK/Carbon Nanotube Composites, *Nanotechnology*, Vol. 20, p. 315707, 2009.
12. P.A. Staniland, "Poly(ether ketone)s" in G. Allen and J.C. Bevington, eds., *Comprehensive Polymer Science*; Pergamon Press: New York, Vol. 5, pp. 484–497, 1989.
13. K.J. Dahl, and V. Jansons, in *Polymers and Other Advanced Materials: Emerging Technologies and Business Opportunities*, P.N. Prasad ed., Plenum Press: New York, pp. 69–81, 1995.
14. W. H. Bonner, US Patent 3,065,205 (1962).
15. R.N. Johnson, A.G. Farnham, R.A. Clendinning, W.F. Hale, and C.N.J. Merriam, *Journal of Polymer Science, Part A: Polymer Chemistry*, Vol. 5, p. 2375, 1967.
16. T.E. Attwood, P.C. Dawson, J.L. Freeman, L.R. Hoy, J.B. Rose, and P.A. Staniland, *Polymer*, Vol. 22, p. 1096, 1981.
17. O.B. Searle, and R.H. Pfeiffer, *Polymer Engineering and Science*, Vol. 25, p. 474, 1985.
18. D.P. Jones, D.C. Leach, and D.R. Moore, *Polymer*, Vol. 26, p. 1385, 1985.
19. M. Naffakh, M.A. Gómez, G. Ellis, and C. Marco, *Polymer International*, Vol. 52, p. 1876, 2003.
20. P. Cebe, S.Y. Chung, and S.D. Hong, *Journal of Applied Polymer Science*, Vol. 33, p. 487, 1987.
21. C.M. Hsiung, M. Cakmak, and J.L. White, *Polymer Engineering and Science*, Vol. 30, p. 967, 1990.
22. C.T. Kingston, Z.J. Jakubek, S. Dénomée, and B. Simard, *Carbon*, Vol. 42, p. 1657, 2004.

23. C. Journet, W.K. Maser, P. Bernier, A. Loiseau, M. Lamy de la Chapelle, S. Lefrant, P. Deniard, R. Lee, and J.E. Fischer, *Nature*, Vol. 388, p. 756, 1997.
24. M.T. Martinez, M.A. Callejas, A.M. Benito, M. Cochet, T. Seeger, A. Ansón, J. Schriber, C. Gordon, C. Mahric, O. Chauvet, J.L.G. Fierro, and W.K. Maser, *Carbon*, Vol. 41, p. 2247, 2003.
25. M.T. Martinez, M.A. Callejas, A.M. Benito, M. Cochet, T. Seeger, A. Ansón, J. Schriber, C. Gordon, C. Mahric, O. Chauvet, and W.K. Maser, *Nanotechnology*, Vol. 14, p. 691, 2003.
26. M.T. Martínez, M.A. Callejas, A.M. Benito, W.K. Maser, M. Cochet, J.M. Andrés, J. Schreiber, O. Chauvet, and J.L.G. Fierro, *Chemical Communications*, p. 1000, 2002.
27. J. Li, and Y. Zhang, *Physica E*, Vol. 28, p. 309, 2005.
28. J.M. González-Domínguez, P. Castell, A. Ansón, W.K. Maser, A.M. Benito, and M.T. Martinez, *Journal of Nanoscience and Nanotechnology*, Vol. 9, p. 6104, 2009.
29. S. Arepalli, P. Nikolaev, O. Gorelik, V.G. Hadjiev, W. Holmes, B. Files, and L. Yowell, *Carbon*, Vol. 42, p. 1783, 2004.
30. M.R. Smith, S.W. Hedges, R. LaCount, D. Kern, N. Shah, and G.P. Huffman, *Carbon*, Vol. 41, p. 1221, 2003.
31. S.M. Bachilo, M.S. Strano, C. Kittrell, R.H. Hauge, R.E. Smalley, and R.B. Weisman, *Science*, Vol. 298, p. 2361, 2002.
32. M.E. Itkis, D. Perea, R. Jung, S. Niyogi, and R.C. Haddon, *Journal of the American Chemical Society*, Vol. 127, p. 3439, 2005.
33. J. Chen, M.A. Hamon, H. Hu, Y. Chen, A.M. Rao, and P.C. Eklund, *Science*, Vol. 282, p. 95, 1998.
34. J.Q. Pham, C.A. Mitchell, J.L. Bahr, J.M. Tour, R. Krishnamoorti, and P.F. Green, *Journal of Polymer Science*, Vol. 41, p. 3339, 2003.
35. H.J. Barraza, F. Pompeo, E.A. O'Rea, and D.E. Resasco, *Nano Letters*, Vol. 2, p. 797, 2002.
36. S.S. Bafna, T. Sun, and D.G. Baird, *Polymer*, Vol. 34, p. 708, 1993.
37. S.J. Oh, H.J. Lee, D.K. Keum, S.W. Lee, D.H. Wang, S.Y. Park, L.S. Tan, and J.B. Baek, *Polymer*, Vol. 47, p. 1132, 2006.
38. J.Y. Choi, S.W. Han, W.S. Huh, L.S. Tan, and J.B. Baek, *Polymer*, Vol. 48, p. 4034, 2007.
39. I.Y. Jeon, L.S. Tan, J.B. Baek, *Journal of Polymer Science, Part A: Polymer Chemistry*, Vol. 46, p. 3471, 2008.
40. M.-R. Baaba, J.-L. Bantignies, L. Alvarez, P. Parent, F. Le Normand, M. Gulas, J.M. Mane, and B.P. Doyle, *Journal of Nanoscience and Nanotechnology*, Vol. 7, p. 3463, 2007.
41. S.D. Hudson, D. Davis, and A.J. Lovinger, *Macromolecules*, Vol. 25, p. 1759, 1992.
42. G. Grevecoeur, and G. Groeninckx, *Macromolecules*, Vol. 24, p. 1190, 1991.
43. A. Thess, R. Lee, P. Nikolaev, H. Dai, P. Petit, J. Robert, C. Xu, Y. H. Lee, S.G. Kim, A.G. Rinzler, D.T. Colbert, G.E. Scuseria, D. Tománek, J.E. Fischer, and R.E. Smalley, *Science*, Vol. 273, p. 483, 1996.
44. G.-X. Chen, H.-S. Kim, B.H. Park, and J.-S. Yoon, *Polymer*, Vol. 47, p. 4760, 2006.
45. H. Xia, and M. Song, *Soft Matter*, Vol. 1, p. 386, 2005.

46. L.S.K. Pang, J.D. Saxby, and S.P. Chatfield, *Journal of Physical Chemistry*, Vol. 97, p. 6941, 1993.
47. D.J. Blundell, and B.N. Osborn, *Polymer*, Vol. 24, p. 953, 1983.
48. L. Li, C.Y. Li, C. Ni, L. Rong, and B. Hsiao, *Polymer*, Vol. 48, p. 3452, 2007.
49. S. Bicakci, and M. Cakmak, *Polymer*, Vol. 43, p. 149, 2002.
50. J.N. Hay, D.J. Kemmish, J.I. Langford, and A.M.I. Rae, *Polymer Communications*, Vol. 25, p. 175, 1994.
51. S. Kumar, T. Rath, R.N. Mahaling, C.S. Reddy, C.K. Das, K.N. Pandey, R.B. Srivastava, and S.B. Yadaw, *Materials Science and Engineering B*, Vol. 141, p. 61, 2007.
52. J.C. Halpin, and J.L. Kardos, *Polymer Engineering and Science*, Vol. 16, p. 344, 1976.
53. A. Mehta, and A.I. Isayev, *Polymer Engineering and Science*, Vol. 31, p. 963, 1991.
54. M.C. Kuo, C.M. Tsai, J.C. Huang, and M. Chen, *Materials Chemistry and Physics*, Vol. 90, p. 185, 2005.
55. J.N. Coleman, U. Khan, W.J. Blau, and Y.K. Gunko, *Carbon*, Vol. 44, p. 1624, 2006.
56. R.W. Haskins, R.S. Maier, R.M. Ebeling, C.P. Marsh, D.L. Majure, and A.J. Bednar, *Journal of Chemical Physics*, Vol. 127, p. 74708, 2007.
57. J. Li, P.C. Ma, W.S. Chow, C.K. To, B.Z. Tang, and J.-K. Kim, *Advanced Functional Materials*, Vol. 17, p. 3207, 2007.

This Page Intentionally Left Blank

Synthesis and Properties of PVA/ Carbon Nanotube Nanocomposites

C. Mercader, P. Poulin and C. Zakri

*University of Bordeaux, Centre de Recherche Paul Pascal,
CNRS, Avenue Schweitzer Pessac, France*

Abstract

This chapter is an overview of the synthesis and properties of PVA/nanotube composites. Various films and fibers have been processed from carbon nanotube and PVA dispersions. Compared to other polymers, PVA exhibits particularly strong interaction with single-walled as well as multiwalled carbon nanotubes. This leads to unique properties which are not observed in other nanotube polymer nanocomposites. In particular, this literature review confirms that nanotubes can promote PVA crystallization in the vicinity of their interface. This yields improvements of mechanical stress transfer. This effect can be enhanced with the surface functionalization of carbon nanotubes, in particular with hydroxyl or carboxyl groups, which display hydrogen bonds with PVA. Beyond the usual mechanical and electrical performances, this review also points out the emergence of other original properties, like the remarkable capability of some nanotube/PVA composites to absorb mechanical energy and shape memory phenomena that differ from traditional behaviors of other polymers. These features are opening new investigation fields, in which several fundamental questions will have to be solved. But they also offer new opportunities for a variety of applications like smart or protective clothing, helmets, bullet proof vests, or active composites.

Keywords: poly(vinyl) alcohol, carbon nanotubes, composite, processing, reinforcement, conductivity.

11.1 Introduction

Since their discovery, and due to exceptional physical and chemical properties, carbon nanotubes (CNTs) have generated a lot of

scientific activities. Combining at the same time mechanical, electrical, thermal or even electrochemical performances, nanotubes are often considered as ideal materials for a wide range of applications. They are particularly suitable as additive fillers in various composites, and among them, in polymer-based nanocomposites. In addition to their remarkable physical properties, they exhibit a low density and a high aspect ratio useful to bring conductivity at very low percolation thresholds, or considerable reinforcement of the polymer matrices.

Poly(vinyl) alcohol (PVA) is a semi-crystalline polymer, which is already widely used for various applications, either under the form of films or fibers. Compared to other polymers, as it is water-soluble at high temperature, it is easy to process from aqueous solutions. Carbon nanotubes can also be dispersed or solubilized in water via different functionalization approaches. It was quite natural for researchers to try to mix carbon nanotubes and PVA to improve the properties of the neat polymer. In this chapter, we will first examine the different methods that have been used to process CNT/PVA composites. The structures and the particular interaction between the polymer and the nanotube surface have been characterized in several works. Then we will consider the composite mechanical properties, which have been extensively investigated in the literature. Despite the number of publications in the field, we will see that a lot of work is still to be done for achieving the most of the exceptional reinforcement potential of carbon nanotubes.

11.1.1 Mechanical and Electrical Properties of Carbon Nanotubes

Due to unprecedented mechanical, electrical and chemical properties, CNTs have been considered as an ideal material for various applications as well as for new fundamental investigations (1,2). In this review chapter, we will only discuss mechanical and electrical properties. In most composite structures, nanotubes are used as mechanical reinforcing agents or conductive fillers. This is also the case of PVA/nanotubes nanocomposites.

The first measurements of nanotube mechanical properties were performed on multiwalled nanotubes (MWNTs) using transmission electron microscopy (3). This was achieved by analyzing the amplitude of thermal vibrations of the nanotubes. This measurement has been followed by a number of others, either on MWNTs (4–6),

or on single walled nanotube (SWNTs) (7,8) via direct or indirect methods. All these measurements led to results with a broad range of values. Overall it is accepted that the nanotube Young modulus should be within 0.5 and 4 TPa and the tensile strength between 10 and 60 GPa. These huge strength values allowed nanotubes to be defined as the strongest material on earth. However, these values were obtained on high quality SWNTs and MWNTs, mainly synthesized by arc-discharge methods. Chemical vapour deposition (CVD) synthesis is probably today the best method to produce large quantities of nanotubes and has already emerged in the industrial world, with a production of several tens of kilograms per day by some companies. CVD nanotubes could realistically be a solution for the composite market where large amounts will be necessary. But these nanotubes still display some structural or chemical defects. These defects tend to downgrade mechanical properties with a decrease of modulus and strength (7,8). However, with still high strength values, low density and excellent bending resistance, nanotubes remain excellent candidates for mechanical reinforcement in nanocomposites.

In addition to the mechanical properties described above, electrical properties of carbon nanotubes are also of great interest. At low temperature, an ideal infinite and straight SWNT would behave like a quantum wire in which the electrons move without being scattered. The conduction regime in these conditions is termed "ballistic". But in practice structural defects tend to scatter electrons. The SWNT transport behaviour varies from metallic to semiconducting, depending on the chirality of the nanotubes. MWNTs are, on the other hand, metallic. Typically metallic nanotubes have a resistivity of 10^{-4} – 10^{-2} Ωcm , whereas the room temperature resistivity of semiconducting SWNTs is about 10^1 Ωcm (1). Thus, despite the defects which tend to decrease the nanotube conductivity, the values are still very good and make nanotubes interesting materials to be used in composites where electrical conductivity is targeted.

11.1.2 Why Use Nanotubes in Nanocomposites?

Mechanical properties – Numerous theoretical works have been done to predict the mechanical properties of reinforced composites. Some of these models are more sophisticated, but in order to understand why nanotubes are ideal reinforcement particles, the rule of

mixture given by Krenchel (9), describing the mechanical properties of fiber reinforced composites, contains the basic requirements for an effective reinforcement. This model defines the Young modulus of the composite as:

$$E_c = (\eta_0 \eta_l E_f - E_m) \Phi_f + E_m$$

In this expression, E_f and E_m are the Young modulus of respectively the fiber and the matrix, and Φ_f is the fiber volume fraction. η_0 is the fiber orientation factor: this factor is equal to 1 for perfectly oriented fibers and 1/6 for a random orientation. η_l is the so-called effective length coefficient (10), which mainly depends on the aspect ratio of the fiber. Indeed:

$$\eta_l = 1 - \frac{\text{Tanh}(a.L/d)}{a.L/d}$$

L and d respectively are the length and the diameter of the fiber, and

$$a = \sqrt{\frac{-3E_m}{2E_f \ln \Phi_f}}$$

This factor approaches 1 for aspect ratios above 10, pointing out the importance of using high aspect ratio fillers.

A very similar expression can be derived to calculate the composite strength:

$$\sigma_c = (\eta_s \sigma_f - \sigma_m) \Phi_f + \sigma_m$$

In which η_s is the strength efficiency coefficient. This factor is related to the length of the fiber. It is a comparison between the length of the fiber and a critical length above which the stress transfer between the matrix and the fiber is high enough to break the fiber. So, fibers longer than this critical length will break at large applied stress. Shorter fibers will not ensure a good stress transfer and the composite matrix will break with pulling out of the fiber.

This model shows that the requirements for a good reinforcement are: a high volume fraction of very well oriented fibers and with high aspect ratios. Nanotube aspect ratios are varying, but are very large, from at least 50 for the shorter and thicker nanotubes to sometimes more than 1000 for the longer and thinner ones.

Moreover, the carbon nanotube density is low. Thus, there is a considerable interest in using nanotubes to fabricate composite materials from the point of view of mechanical reinforcement. However, the above models assume a perfect adhesion of the nanotubes to the matrix. In practice, the interface can fail. Of course, this lowers the stress transfer and the reinforcement by the nanotubes. This is why controlling the surface chemistry of the nanotubes and their interactions with a polymer matrix are also critical challenges.

Electrical properties – Insulating matrices are loaded with conductive particles to make them electrically conductive. The conductivity occurs above the so-called percolation threshold. The percolation is a statistical concept that describes the formation of an infinite cluster of connected particles or pathways in the composite. Lowering the percolation threshold is a critical issue to reduce the cost and facilitate the processing of such composites. A route towards this goal is based on the use of rod-like particles. These particles exhibit an excluded volume larger than that of spheres of the same weight. As a result, they form percolated networks at concentrations lower than spherical particles (11,12). As carbon nanotubes are conductive rods with large aspect ratios, they are ideal particles to bring conductivity to an insulating polymer at low concentration. However, the dispersion state of the nanotubes in the composite matrix is the critical point to control the electrical conductivity of the material. In particular, it has been shown that the interactions between the CNTs in the dispersion are important to control the spatial structure and thus the percolation threshold in the composite (13–15). These interactions depend on several factors, such as the type of the polymer matrix, the surface chemistry of nanotubes and the presence of additives in the composite.

11.1.3 Poly(vinyl) Alcohol

Since its discovery, at the beginning of the last century, PVA has become a polymer broadly used in various fields. Adhesives, water-soluble packaging, fishing nets or marine cables are some examples of the different applications of PVA. The polymer is generally synthesized from the radical polymerization of vinyl acetate, leading to polyvinyl acetate. A final hydrolysis step is necessary to obtain PVA. The number of remaining acetyl groups after this step determines the so called “hydrolysis rate” of PVA. This rate and the final molecular weight of the polymer are determining factors

for the properties of PVA. Depending on the synthesis process, the structure of PVA can vary from simple 1,3 glycol type structures to branched structures (16). In all cases, due to their polarity, the PVA chains strongly tend to locally align. This tendency leads to the presence of crystalline domains, the size of which depends on the hydrolysis rate: the presence of residual acetyl groups limits the chain orientation and thus the crystallinity of PVA (17). A high hydrolysis rate corresponds to weak acetyl content and to a better crystallinity of the polymer. PVA is a semi-crystalline polymer, with a glass transition temperature (T_g) between 40 and 80°C and a melting transition between 180 and 240°C, depending on the origin and on the thermal history of the PVA. Moreover, this polymer is water-soluble at high temperature. Nevertheless, thermal treatments of PVA with high hydrolysis rate leads to highly crystalline materials that exhibit excellent water and moisture resistance (17).

11.2 Synthesis Methods and Structural Properties of Nanotubes/PVA Composites

11.2.1 Films

In this section, we present different approaches that have been used to produce various forms of PVA/nanotube composite films and the morphological studies that have been performed to enlighten the interactions between PVA and nanotubes.

Most of PVA/CNT composites are processed under the form of films. Generally, films are casted and dried from water-based PVA and nanotube dispersions. Different types of water-based dispersions have been used. Carbon nanotubes come from various production sources and can be covalently functionalized. The PVA molecular weight and hydrolysis rate can also be varied as well as the nanotube fraction. This is why comparisons between all the contributions in the literature can sometimes be difficult. Nevertheless some general and important features can still be deduced from all the studies reported on this topic.

In 1999, M. Shaffer and A. Windle reported the first study of the thermo-mechanical and electrical properties of PVA/MWNT composite films (18). In this work, a high hydrolysis rate PVA was used (98–99%), with a large range molecular weight (between 85,000 and 146,000 g/mol). Water solutions of PVA were prepared at 90°C.

This temperature is commonly used to solubilize PVA in water. CVD grown MWNTs were used as starting material. The nanotubes were then oxidized to graft -COOH groups at their surface. This allowed their dispersion in water at basic pH (19). The nanotube and PVA dispersions were carefully mixed and casted into Teflon troughs, where water gently evaporated. Final composite films were obtained, containing a wide range of nanotube loadings between 0 and 60wt%, and a quasi constant thickness of about 50 μm . The films were characterized by a combination of electron microscopy, small angle X-ray scattering (SAXS), dynamical mechanical measurements (DMA) and thermo gravimetric analysis (TGA). The authors observed a good homogeneity of the films, even for large amounts of MWNTs. The nanotubes were completely disoriented in the films. Thermal analyses indicated that the presence of nanotubes implies a small retardation of the onset of PVA decomposition, which could likely be attributed to the adsorption of free radicals during polymer decomposition by the activated carbon surface. However the effect was small, even with the largest amounts of nanotubes.

This simple film forming method was also used by other groups, with variants of the nanotube types and mixing methods. Cadek et al. directly added a raw arc discharge MWNT soot to a PVA solution (20). No precision was given about the used PVA. By contrast to the previous work of Shaffer et al., no functionalization, neither covalent nor non-covalent, was used to disperse the nanotubes into the polymer suspension. The aim was to compare the structural and mechanical properties of composites made of PVA, which is semi-crystalline, to composites made of PVK (poly(9-vinyl carbazole), which is totally amorphous. Films were formed on a glass substrate by drop casting of PVA solutions or by spin coating multiple layers from PVK solutions. The amount of MWNTs inside the films was varied from 0 to 8 wt%, much less than in the systems studied by Schaffer et al. From differential scanning calorimetry (DSC) measurements, the authors clearly observed that the MWNTs increased the crystallinity of the PVA: from 14% to 27% when only 1 wt% nanotubes were added. Thus, nanotubes can promote the crystallization of the polymer, acting as nucleation sites. In other words, a layer of highly crystallized PVA could be formed at the MWNT surface and be involved in the stress transfer between the matrix and the nanotubes. This structural observation is of primary importance because it helps understanding why nanotubes/PVA composites exhibit very good mechanical properties, as described in the

next section. In contrast to PVA, no crystallization was observed in PVK even in the presence of nanotubes.

In 2004, Probst et al. (21) also confirmed the promotion of PVA crystallinity by SWNTs. The used PVA was highly hydrolyzed (98–99%) and had a molecular weight of about 150,000 g/mol. In this work, the nanotubes were catalytic CoMoCAT™ SWNTs. They were dispersed in water with sodium dodecylbenzenesulfonate (NaDDBS), and added to PVA aqueous solutions. The mixtures were spin casted onto plates, thus forming films containing 0.1 or 1wt% SWNTs. TGA (thermal gravimetric analysis) experiments showed that thermal degradation of PVA was enhanced by the presence of nanotubes, even at only 1wt%. However, provided a careful control of heating rates during DSC (differential scanning calorimetry) measurements, this degradation did not prevent an increase of PVA crystallinity in the 1% wt loaded film. This finding is in good agreement with the work done by Cadek et al., who used raw MWNTs.

Nevertheless, the increase in crystallinity of PVA by nanotubes is still an open and controversial question: Indeed, consecutively to Cadek's work, Zhang et al. (22) prepared composite films from PVA (hydrolysis rate 99%, molecular weight 124,000–186,000 g/mol) aqueous solutions and SWNTs (HiPco) aqueous dispersions. In these suspensions, nanotubes were stabilized by sodium dodecyl sulphate (SDS) and poly(vinyl pyrrolidone) (PVP). The SWNT dispersions were centrifuged to keep only individual nanotubes, covered by a SDS-PVP association. 30 μm thick films containing between 1 and 5 wt% of SWNTs were then obtained by casting the solution into Teflon dishes. Optical micrographs of 1% wt nanotube films did not show any aggregates. Unlike the previous authors, Zhang et al. did not observe any improvement of the PVA crystallinity in the presence of nanotubes. On the contrary, the addition of 5 wt% of SWNT decreased the crystallinity of pure PVA by 13%, whereas the mechanical stress transfer did not seem to be affected (see next section). These discrepancies from previous studies could be due to the presence of PVP. This polymer adsorbed at the nanotube interface can presumably screen the interactions between the PVA and the nanotubes.

In order to achieve deeper understanding of the interaction between nanotubes and PVA, the influence of the nature of the CNTs was examined by Cadek et al. (23). Free standing composite films were prepared from PVA and raw nanotube soot, again with no surfactant. Six different sources of nanotubes were studied.

DSC measurements allowed the calculation of the polymer crystallinity rate. It was nicely shown that the latter linearly increases with the nanotube content in all the composites, as shown in Figure 11.1. The linearity suggests that nanotubes are coated with a layer of crystalline PVA. The thickness of this layer which should be constant for each nanotube type was estimated between 10 and 29 nm. This result is important because it means that PVA can actually crystallize at the surface of various types of nanotubes. In particular, the graphitization state of the nanotubes, or the number of defects, which differs from a type to another, does not seem critical. On the other hand, among the different nanotubes studied, the one inducing the best crystallinity are those with the smallest diameter, including double walled nanotubes as long as they do not form bundles. This suggests that the crystallinity rate is proportional to the total surface area developed by the nanotubes.

Note that PVA is not the only polymer whose crystallinity can be enhanced by nanotubes. Other studies (24–28) have indeed shown that carbon nanotubes can act as nucleating sites for several other polymers. It is also important to note that most studies were focused on composites with a low fraction of carbon nanotubes. When the nanotube content increases in the composite, the control

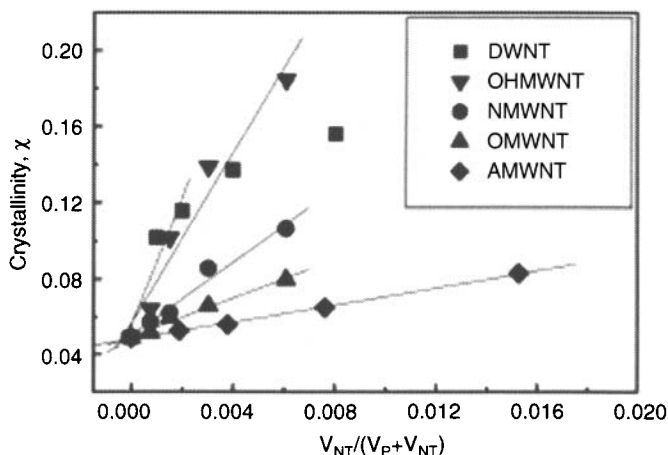


Figure 11.1. Crystallinity of PVA-nanotubes composites versus carbon nanotube volume fraction, for various types of nanotubes (DWNT= double-walled nanotubes, OHMWNT= hydroxylated MWNTs, NMWNT= catalytic Nanocyl S.A. MWNTs, OMWNT=catalytic MWNTs from Orléans, AMWNT=Arc grown MWNTs produced in the author's laboratory. Reprinted with permission from reference (23)).

of their dispersion becomes critical. This is illustrated in the work of Bin et al. (29): the authors showed that, depending on the filler content, the interaction between the nanotubes and the polymer varies a lot. In particular, they opined that a large amount of filler may obstruct the crystallization of the matrix instead of promoting it.

11.2.2 Fibers

The rule of mixture given above predicts a very strong effect of the nanotube alignment in the composite reinforcement. In addition, recent models also predicted an exponential improvement of the Young's modulus with the orientation of pure nanotube assemblies (30). Thus, fibers and yarns are among the most promising forms to use nanotubes on the macroscopic scale. Indeed, in analogy with polymer fibers, they allow nanotubes to be aligned. A number of methods have been proposed to produce fibers. The systems include composite fibers with a fraction of nanotube of a few wt% to fibers solely comprised of nanotubes (31–36). In 2000, Vigolo et al. (37) proposed a simple method to process nanotubes into PVA composite fibers. The method consists of dispersing nanotubes into water using SDS. The homogeneity of the dispersion is controlled by optical microscopy. The dispersion is then spun in the co-flowing stream of an aqueous solution of PVA. PVA induces the coagulation of nanotubes and the process results in the spontaneous formation of wet fibers. The fibers can be washed and drawn as conventional polymer fibers. Once extracted from the washing or coagulation bathes, the fibers can be dried. The fraction of nanotubes can be controlled by varying the spinning and washing conditions. This fraction can be particularly high; typically it can be varied from 10 wt% up to 70 wt%. Figure 11.2(a) shows a long nanotube fiber collected on a small winder. The diameter of the fiber is of about 30 μm .

The average alignment of nanotubes (assuming a Gaussian distribution and taking for the average the full width at half maximum of the distribution) and of PVA chains, measured by small angle X-ray scattering (38) is $\pm 30^\circ$, compared to the fiber axis. It can be largely improved using hot-drawing. Figure 11.2(b) shows a scanning electron micrograph (SEM) of such a stretched fiber. It clearly shows the composite structure, with a dense network of aligned nanotubes embedded into the polymer. The polymer is strongly confined inside the CNT network. In a more recent paper,

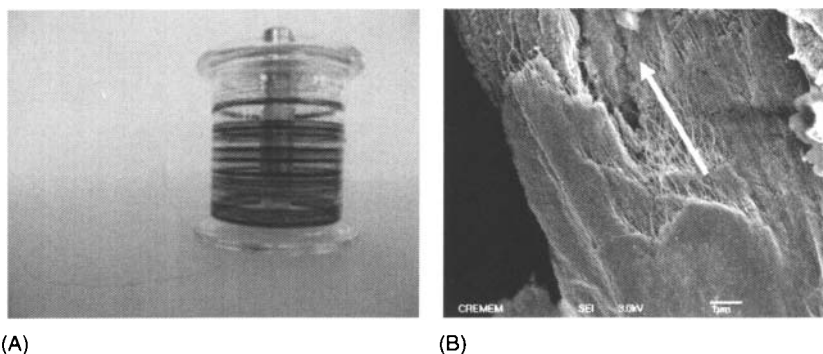


Figure 11.2. (a) PVA/carbon nanotube fibers collected on a winder, produced by wet-spinning (b) Scanning Electron Micrograph of a stretched fiber. The white arrow indicates the fiber axis.

the authors showed that for a SWNT hot stretched fiber, the average alignment is significantly more pronounced, with an orientation of $\pm 4^\circ$ for the PVA chains and $\pm 6^\circ$ for the nanotubes (39). Moreover, the crystallinity of PVA is increased compared to raw fibers. This particular structure leads to new mechanical properties, as described in section 11.3.

In 2004, fibers were produced via a gel-spinning process from a mixture of SWNTs, PVA, dimethyl-sulfoxide (DMSO) and water (40). In this DMSO solution, PVA seems to assist the dispersion of nanotubes, like surfactants in other systems. The dispersion is extruded into a methanol bath at -25°C , thus forming a gel fiber. In order to ensure a good coagulation, the fiber remains in methanol for 2 days and is then dried during 3 days. This method is inspired from the traditional PVA fiber spinning technology used to produce pure high strength PVA fibers (17). In Zhang's work, nanotubes are successfully added to the initial dope. The obtained fibers, with a diameter in the range 5–45 μm , are compared to pure PVA fibers made with the same process (41). The X-ray scattering pattern is almost isotropic in the case of pure PVA fibers, meaning that the alignment of the PVA chains is very poor. In contrast, PVA/SWNT fibers are more oriented. At the same time, the crystallinity of the polymer is increased from 48 to 84% when SWNTs are added to the PVA, without any fiber annealing or drawing. Raman polarized spectroscopy gives an average orientation of 38° for the SWNTs, compared the fiber axis. In summary, the nanotubes seem to template the orientation of the polymer in the fiber.

Fibers containing high fractions of MWNTs have been produced in 2007 (42) by another wet-spinning process, in which a PVA/CNT dispersion is injected in a static bath of sodium sulfate coagulating solution. The PVA/CNT dispersion precipitates and forms gel-fibers that can be extracted from the bath. The fibers have large diameters (0.5 mm) and contain up to 40 wt% of nanotubes. However, according to the authors, they are rather inhomogeneous: unfortunately this tends to degrade the final mechanical and electrical properties of the composite.

PVA is also one of the most studied polymers to produce fibers by electrospinning. PVA/CNTs electrospun fibers have first been reported in 2005 (43) and the interaction between PVA and nanotubes in these particular fibers was studied in 2007 (44). A mixture of purified MWNTs and water is sonicated and then added to a PVA solution. The resulting dispersion is electrospun via a voltage of 20 kV. This leads to the production of very thin fibers of typically 300 nm in diameter, as shown in Figure 11.3.

These fibers show higher crystallinity than the neat PVA fibers which are electrospun for comparison. The orientation of PVA or nanotubes is not mentioned in this work. In a very recent article, another group also investigated electrospun PVA/MWNTs fibers. The nanotubes and PVA were dispersed into a water/ethanol mixture in the presence of lignosulfonic acid sodium (45).

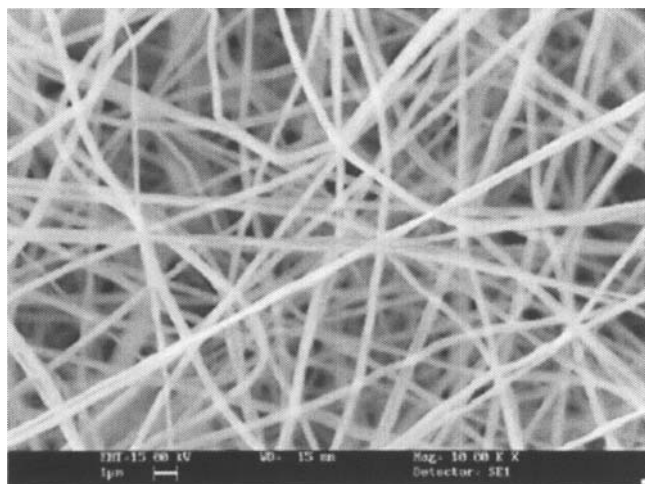


Figure 11.3. SEM image of PVA/MWNT electrospun fibers. The scale bar is 1 μ m. Reprinted with permission from reference (44).

This method also produces thin fibers with diameters of less than 300 nm.

Overall it can be concluded that it is difficult to achieve composite PVA fibers with high fractions of carbon nanotubes. Traditionnal spinning approaches use a starting material mixture of nanotubes and PVA. But PVA tends to destabilize the nanotubes and causes their aggregation. It is therefore only possible to achieve homogeneous dispersions at low nanotube fractions (25). On the other hand, when a high amount of nanotubes is mixed with the polymer, the dope material contains aggregates, which lead to non-uniform and fragile fibers. So far the only method that allowed high nanotube fraction and uniformity to be combined consists in using co-flowing streams (37). In this method the PVA is not mixed with the initial nanotube dispersions. Instead the PVA solution serves as a coagulating agent to form the fibers. Nevertheless, this method is more complicated as it requires the control of the flows of different liquids (the dope and the coagulating solutions) in confined geometries. Research is still needed to find simple spinning processes using static coagulating bathes and large nanotube fractions. For this it will be necessary in the future to achieve stable and concentrated dispersions of nanotubes in PVA solutions. And more importantly the resultant mixture has to remain spinnable; meaning that the PVA and the nanotubes can still be coagulated in another fluid. The combination of all these conditions is far from being straightforward and still a great challenge for future research.

11.3 Mechanical Properties of the Composites

Globally, carbon nanotubes have a positive effect on the mechanical properties of all the composites with PVA matrices described in the previous sections. However, the enhancement of mechanical properties differs substantially from a material to another, depending on the type of nanotubes, or on the process used to manufacture the composite. The Young's modulus and the strength are deduced from usual tensile experiments. As depicted in Figure 11.4, PVA/nanotube composites generally follow the same tensile behavior, with a short elastic regime on the first percent strain, followed by a more or less extended plastic behavior.

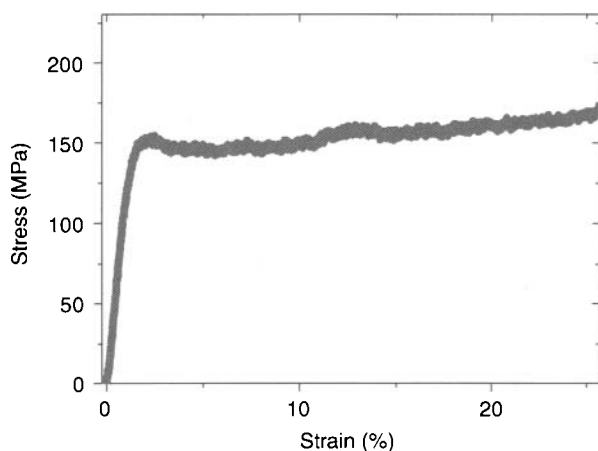


Figure 11.4. Typical stress-strain curve of a PVA/nanotube composite. The material is a fiber containing 25wt% of MWNTs in a PVA matrix (molecular weight 195 000, 99% hydrolized).

11.3.1 Reinforcement

From a general point of view, the Young's moduli and the strengths measured in PVA/nanotube composites are lower than those expected in the frame of an ideal reinforcement. As explained above, this can arise from the small aspect ratios of the nanotubes, the weak adhesion of the nanotubes to the matrix, the presence of defects in the nanotubes, or to a poor alignment. In addition, most of the composites that have been processed contain only a small fraction of carbon nanotubes. The mechanical properties of composites described in the previous section, are summarized in Table 11.1. Concerning films, there are no clear trends when the type of PVA is changing. For example, it is very difficult to extract any influence of the PVA molecular weight from these data. In films, the best Young's modulus enhancements are obtained for raw MWNTs directly mixed with PVA without the help of surfactant or covalent functionalization (46). Very interestingly, Cadek et al. (23) also showed that the Young's modulus is directly related to the total surface area of nanotubes in the composite. This is, of course, also connected to the improvement of crystallinity of PVA as described in section 11.2.1. In other words, the smallest diameter nanotubes should lead to the best composite Young's modulus. In this frame, SWNTs should be the best candidates. However, the measured

Table 11.1. Comparison of reinforcement for various PVA/nanotube composites reported in literature. Y/Y_p is the ratio between the Young's modulus of the composite and the Young's modulus of the neat PVA. σ/σ_p is the ratio between the strength of the composite and the strength of the neat PVA

Composite	Nanotube type	Nanotube cont.	PVA mol weight	Y/Y_p	σ/σ_p	Reference
Film	COOH-MWNT	50 wt%	85000–146000	1.6	/	Shaffer 99
Film	Arc MWNT	1 wt%		1.8	/	Cadek 02
Film	HipCo SWNT (SDS+PVP)	5 wt%	124000–186000	2.1	2.1	Zhang 03
Film	Catal. MWNT	0.5 wt%	/	2.1	/	Cadek 04
Film	OH-SWNT (HipCo)	0.8 wt%	/	1.8	1.44	Liu 05
	HipCo SWNT (SDS)	0.5 wt%	50000–85000	1.25	0.93	
Film	Catal. MWNT	0.6 wt%	30000–70000	3.6	7	Coleman 04
Film	Catal. MWNT	1 wt% 5 wt%	30000–70000	5.8 Loss	1.9 Loss	Ryan 07
Oriented film	MWNT	3 wt%	2000	3.5	1.4	Bin 06
Oriented film	Arc SWNT in DMSO	1 wt%	84000–124000	1.45	3	Wang 07
Raw gel-spun fiber	HipCo SWNT in DMSO	3 wt%	20000	1.4	1.2	Zhang 04
Raw wet-spun fibers	Arc SWNT (SDS)	30 wt%	195000	2.2		Vigolo 04
Hot-stretched wet-spun fibers	HipCo SWNT, MWNT, (SDS)	30 wt%	195000	6.5		Miaudet 05
Electrospun fibers	Purified MWNT	4.5 wt%	146000–186000	/	1.4	Naebe 07

reinforcement was found to be smaller for SWNTs than for thin MWNTs. This was ascribed to the presence of bundles of SWNTs, in which the nanotubes are sliding when stress is applied to the composite. Thus, the authors conclude that the best candidates are CVD-MWNTs of small diameters. One remaining question is: is it possible to add more nanotubes in the matrix under their pristine form?

According to Ryan et al. (46), with 1 wt% of nanotubes, the Young's modulus of the composite can increase by a factor 5.8 compared to pure PVA. This is already very promising for a small fraction of CNTs. But the same authors showed that, for 5 wt% of MWNTs added to the matrix, there is an opposite effect and a loss of mechanical properties. This is very problematic because the Young's modulus of the composite is expected to be proportional to the filler volumic fraction. This holds of course as long as the nanotubes can be homogeneously dispersed. Unfortunately it is difficult to achieve homogeneous dispersions of nanotubes and therefore good mechanical properties at high volume fraction.

Nanotube functionalization is performed in other examples listed in Table 11.1. In 1999, Shaffer et al. used carboxylated MWNTs. By contrast to studies described in the followings, this allows to the achievement of homogeneous composites with a large nanotube fraction of about 50 wt%. However, the improvement of the Young's modulus is still weak, particularly if we consider the large amount of CNTs included in the matrix. Liu et al. (47) reported an improvement of mechanical properties with SWNTs which are covalently functionalized by OH groups, compared to the same neat nanotubes simply dispersed with SDS.

Gel-spun and electrospun fibers do not contain much higher contents of fillers than the films described above, and the orientation of the nanotubes, when measured, are not better than $\pm 35\text{--}38^\circ$ compared to the fiber axis. As a consequence, and not surprisingly, the mechanical reinforcement is not improved when compared with composite films. However, wet spun fibers of Vigolo et al. (37) have nanotube fractions of at least 30 wt%. They exhibit slightly better improvement of Young's modulus and strength. But the major effect is achieved by hot-stretching the fibers, as detailed in section 11.2.2. Hot stretching induces a much better alignment of the structure, from $\pm 30^\circ$ to $\pm 6^\circ$ for the nanotubes, while, at the same time, PVA becomes also more aligned and crystalline.

11.3.2 Stress Transfer Efficiency

The Young's modulus of defect free nanotubes is very high. As indicated above, this makes nanotubes particularly promising for mechanical reinforcement. However, several other factors have to be considered to actually manifest this reinforcement. The stress transfer efficiency is a key point. There are different methods to evaluate the stress transfer between a polymer matrix and carbon nanotubes. A pioneering work was performed in 2003 by D.H. Wagner and his team (48). The authors measured the adhesive interactions between a single CNT and polymer matrix using a nano-pullout technique. This technique measures the force necessary to extract a single nanotube, attached to an AFM tip, from a polymer. The separation force is found to be remarkably high, indicating that carbon nanotubes are effective at reinforcing the polymer. These experiments were not performed with PVA, but with polyethylene-butene. They confirmed that the stress transfer between a MWNT and a polymer matrix can be as high as 50 MPa. This method is a direct measurement of the interfacial stress, but it is rather difficult to be standardized because the manipulation of a single nanotube is a delicate work.

Other indirect methods are possible to estimate the stress transfer. One of them consists in analyzing the mechanical properties of composites and comparing them with those expected from a rule of mixture. In the different models of rules of mixture, equations are often derived by assuming a perfect stress transfer. If we consider high values of the nanotube Young's modulus, typically around 1 TPa, the aspect ratio becomes a fitting parameter and can be adjusted in these equations. This was done by Cadek et al. (20), using the Halpin-Tsai equations (49). Depending on the matrix, PVA or PVK, (L/d) values of respectively 800 or 40 were obtained. This is unexpected because the same batch of MWNTs is used in both cases, with an actual aspect ratio of about 100, as measured by electron microscopy. According to the authors, this aspect ratio mismatch is a strong indication that the stress transfer is actually not perfect. Thus, the full potential of carbon nanotubes can never be addressed. Anyway, the results also prove that the stress transfer is far better between nanotubes and PVA than between nanotubes and PVK. According to these authors and to others, this good stress transfer between PVA and nanotubes is related to the presence of crystalline PVA layers at the nanotube surface.

Another elegant and quantitative method to evaluate the stress transfer between the nanotubes and the matrix consists in following a particular resonant mode of the nanotubes by Raman spectroscopy. Zhang et al. (22) used this method to monitor the load transfer from PVA to SWNTs. The D^* band reflects a breathing vibration mode of the carbon atoms in the graphene sheet plane of the nanotube. This mode is very sensitive to any axial deformation of the nanotubes and thus to any stress applied to the nanotube by the polymer matrix. As a consequence, it is very efficient to evaluate the stress transfer in composites. In Zhang's work, in PVA/PVP/SCS/SWNT composite films, the D^* band peak of SWNTs was measured as a function of strain. The results are represented in Figure 11.5(a), and compared with the related stress-strain curve in Figure 11.5(b). The D^* band shift is very similar to the stress-strain curve for the corresponding composite film: it seems that there is a very good stress transfer between the PVA and the SWNTs, even if the last are covered by PVP and if, as explained in section 11.2.2, no induced crystallization is observed in this composite. Note that the D^* band shift is stronger in the elastic regime of the tensile load curve and much weaker in the plastic regime above a few percent strain.

More recently, Liu et al. (47), compared OH- covalently functionalized SWNTs to SDS stabilized SWNTs. The authors used Raman spectroscopy to understand why the improvements of the Young's modulus and strength are greater for covalently functionalized nanotubes. The Raman shift was plotted versus the tensile strain in the two composites: PVA/OH-SWNTs and PVA/SDS dispersed SWNTs, in the elastic regime (for strain values below 1.2%). The shift is linear in this regime, and a larger slope is measured

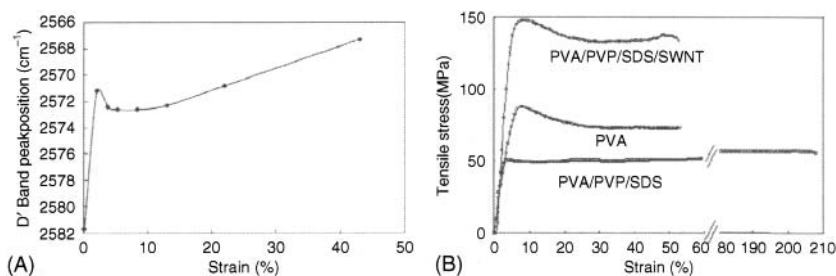


Figure 11.5. (a) Raman D^* band shift versus strain for PVA/PVP/SDS/SWNT composite films containing 5wt% of nanotubes. (b) Tensile load curves for the same composite film (upper curve), compared to pure PVA or PVA/SDS/PVP films. Reprinted with permission from reference (22).

in PVA/OH-SWNT composite; reflecting of a better stress transfer. The lateral OH-groups can form hydrogen bonds and improve the interfacial adhesion between the PVA and the modified nanotubes, leading thereby to better mechanical properties.

Another interesting example of the evaluation of interfacial stress using Raman spectroscopy was reported for carboxylated nanotubes (50). The D^* band shift is measured in SWNT/PVA fibers made by wet-spinning. Due to a stronger interfacial adhesion, stronger shifts are measured when the nanotubes are functionalized by carboxylic groups. However, in this case, and despite a better stress transfer, a degradation of the mechanical properties is observed when nanotubes are carboxylated, in comparison to raw nanotubes. Additional Raman analyses indicate that this mechanical degradation can be attributed to the degradation of the nanotubes mechanical properties.

11.4 Electrical Properties

In 1999, Shaffer and Windle (18) observed that the addition of MWNTs to PVA increases, as expected, the conductivity of the polymer. They measure a percolation threshold lying between 5 and 10 wt% of nanotubes. This threshold is rather high and the values of conductivity are rather low compared to other sets of composites. For example, smaller amounts of nanotubes are added to epoxy resins for achieving high electrical conductivity. Minus et al. (41) compared the electrical properties of PVA/VGCF (vapour-grown carbon fibers) and PVA/MWNT films, both prepared by the same method. As depicted in Figure 11.6, the electrical conductivity of the PVA/MWNT composite increases drastically with a small amount of nanotubes. The percolation threshold is below 1 wt%. The electrical conductivity of a composite with 3 wt% of MWNTs is the same than that of a composite with 20 wt% of VGCFs. It has to be noted that the percolation threshold is amazingly high for VGCFs. This is rather surprising because even if the aspect ratio of VGCFs is smaller than that of nanotubes, such particles still exhibit a rod-like morphology. The differences of MWNTs from VGCFs can clearly not be ascribed only to differences of aspect ratio. Instead, the dispersion of the particles and their interactions with the polymer can also play an important role. The morphology of the nanotubes and the carbon fibers is also very different and can affect

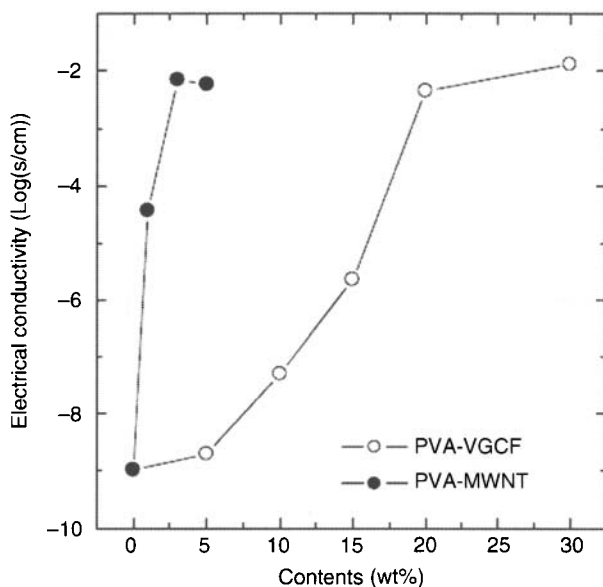


Figure 11.6. Electrical conductivity of MWNT/PVA and VGCF/PVA films, as a function of the filler content. Reprinted with permission from reference (29).

the conductivity of the material. MWNTs are more tortuous than the rigid and straight VGCFs. When drawn, nanocomposite films often lose electrical conductivity. However this decrease is more pronounced with VGCFs than with carbon nanotubes. According to the authors, this could be due to the waviness of the nanotubes and to their ability to form conductive networks within the composite, even when the nanotubes align in response to the drawing of the composite.

More recently, a similar percolation threshold of 0.67 wt% was also measured in a composite containing MWNTs. The composites were prepared by gelation/crystallization from solutions in the mixture solvent of dimethyl-sulfoxide (DMSO) and water (51).

Thermo-electrical properties of PVA composite fibers with a large fraction of carbon nanotubes were studied by Miaudet et al. (52,53). Low temperature conductivity measurements showed that the conductivity depends on several factors: the electronic properties of the nanotubes (54), the number and properties of intertube contacts, like in other polymer composites (55). The authors investigated also the behavior at high temperature. A strong increase of conductivity is observed in the vicinity of the glass transition of

PVA, close to 80°C. The polymer chains become mobile at the glass transition, allowing a partial re-organization of the nanotubes in the matrix and a modification of the conducting network. The polymer mobility allows some relaxation in the structure with possible better intertube contacts and loss of nanotube alignment which favors the contact probability. Both mechanisms can explain improvements of conductivity at the glass transition of the polymer.

11.5 Other Original Properties of PVA/ Nanotube Composites

As seen in the previous sections, carbon nanotubes can improve mechanical properties and bring electrical conductivity to PVA materials. Moreover, other original properties of PVA/nanotube composites have been reported over the last years. Among them, we can cite the remarkable capability of some nanotube/PVA composites to absorb mechanical energy and shape memory phenomena that differ from traditional behaviors of other polymers.

11.5.1 Energy Absorption

Vigolo et al. developed in 2000 a simple method to spin nanotube suspension into PVA coagulating solutions, leading to PVA/CNT composite fibers containing up to 30%wt of nanotubes (37). In 2003, Dalton et al. produced similar fibers out of high quality nanotubes. The authors also proposed improvements to produce longer fibers. The authors achieved a significant breakthrough with fibers that exhibit a tensile strength of about 1.8 GPa. These fibers also exhibit a high strain to failure and an exceptional toughness, up to 570 J/g (56); the toughness being the energy needed to break the fiber. This value was by far superior to the toughness of any other synthetic or natural materials known so far. In 2005 Miaudet et al. (39), still using the same process achieved fibers with an energy absorption of almost 900 J/g. The achieved progresses can likely be explained by the improvement of the spinning process but also by the quality of the nanotubes, which has kept increasing since 2000. Figure 11.7(a) shows the stress-strain curve of such high toughness wet-spun PVA/SWNT fiber. The absorption of energy is directly calculated from the area under the stress-strain curve. The very large strain, up to 300%, associated to a good stiffness yields materials

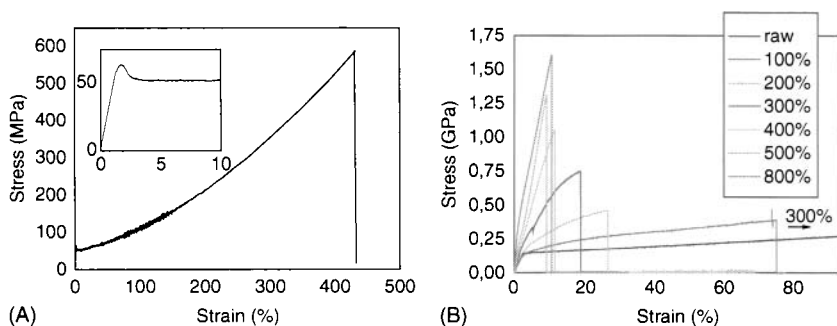


Figure 11.7. (a) Stress-strain curve of a raw wet-spun fiber (the inset focuses on the elastic regime). (b) stress-strain curves of wet-spun fibers that have been hot-stretched at 180°C, at various draw-ratios, from 0 (raw) to 800%.

with a very high toughness. Very interestingly, MWNTs can also be used to make composite fibers of very high toughness (39). As for most synthetic polymer fibers, it is also possible to modify the mechanical properties of the fibers by hot-stretching the fibers at a temperature above the glass temperature transition of the PVA.

Figure 11.7(b) shows the stress-strain curves for fibers that have been hot-stretched at 180°C for different draw ratios, from 0 (raw fiber) to 800%. The mechanical behavior is drastically changing when the draw-ratio is modified. At the extreme stretching ratio of 800%, the fibers exhibit a much higher Young's modulus and the tensile strength raises to about 1.6 GPa. The strain to failure is reduced to about 11%. These fibers still exhibit a large toughness of 55 J/g. In comparison, Kevlar® fibers, made of pure crystallized poly(aramide), are characterized by a maximum toughness of 35 J/g. The hot-stretched fibers could thus be competitive with the current industrial fibers used for energy absorption applications (composites, protective clothings, bullet proof vests). The mechanical properties of the composite fibers can be tuned by varying the hot-stretching ratio, as depicted in Figure 11.7b and summarized in Table 11.2, where the Young's modulus, the strength, the strain to failure and the energy absorption are given as a function of the draw-ratio. The fibers progressively display a better reinforcement when stretching is increased. At the same time, the toughness is decreasing, but the absorbed energy at a given strain is actually increasing.

This behavior seems to be related to the already discussed strong interactions between the nanotubes and the PVA. Indeed, as shown in (39), hot-stretching induces the orientation of the PVA and

Table 11.2. Mechanical properties of wet-spun fibers, hot-stretched at different draw-ratios. The fibers are drawn at 180°C and contain a fraction of 25wt% nanotubes. The PVA is 195000 g/mol and 99% hydrolyzed

Hot-stretching ratio (%)	0	100	200	300	400	500	600	800
Young's modulus (GPa)	7	12	17.2	20	24	32	42.6	46
Strength (GPa)	0.60	0.39	0.66	0.70	0.99	1.32	1.28	1.60
Strain to failure (%)	300	76.6	27.5	17.3	13	11	10.7	10.4
Toughness (J/g)	650	157	82	71	60.1	42	48.7	55

of the nanotubes along the fiber axis. At the same time, the PVA crystallinity increases. When polymer chains are strongly oriented, a stress along this orientation direction will directly apply on the covalent bonds of the chains, which are stronger than the lateral inter-chain bonds: this effect modifies the mechanical response of the polymer (57). For neat PVA fibers in particular, some studies have already shown the improvement of the stiffness when the polymer fibers are hot-stretched (17). The values of Young's modulus and strength are already very good in these neat fibers and it is particularly interesting to see that they can still be increased with the addition of nanotubes.

11.5.2 Shape Memory Effect

Shape memory materials (58) are usually made of polymers (59,60) or metallic alloys. They have been investigated for more than 30 years and find applications in packaging, heat-shrink tubing or deployable structures. Shape memory polymers are deformed at high temperature and then cooled down under a fixed strain to trap the deformed polymer chains. Thus, the polymer store mechanical energy. When they are reheated, in the vicinity of their glass transition, the polymers can relax and revert to their initial shape, then generating a so-called recovery stress. This recovery stress is a growing function of the energy that was absorbed during the deformation step at high temperature (61,62). For that reason, high energy to failure, or large toughness, is needed for achieving strong

shape-memory materials. Shape-memory polymers can exhibit large strain when they revert towards their initial shape. But this large strain is usually associated with a low stress recovery from a few tenths of MPa to a few tens of MPa (59,60,63). We have seen above that wet-spun PVA-nanotube composite fibers can absorb a large amount of mechanical energy when they are hot-stretched (39). They also exhibit good so-called shape fixity. This means that the fibers don't relax when they are cooled down under tensile load. Instead they keep their extended shape by storing mechanical energy. When reheated the polymer chains become mobile and the fibers shrink to revert to their initial shape. If the strain is fixed and the fiber linked to a force sensor, a mechanical stress is measured as the temperature is raised. The stress generated by PVA-nanotube composite fibers in these conditions is particularly strong with a maximum at a well-defined temperature (64). The peak of recovery stress is a common feature of many shape memory polymers which exhibit a shape recovery at their glass temperature transition (T_g). Surprisingly, the peak of stress recovery for nanotube fibers doesn't systematically occur at the PVA glass transition, but at the temperature at which the composite fibers was initially deformed. This reflects a unique feature: hot-stretched fibers can memorize the temperature at which they have been deformed (T_d). The peak of recovery stress can be observed up to 180°C, which is ~100°C above the glass transition of the neat PVA. In addition, it was observed that the maximal stress generated by the fiber is close to 150 MPa. This value is from one to two orders of magnitude greater than the stress generated by conventional shape-memory polymers. It is obtained for fibers that have been deformed at 70° and 90°C, temperatures that are in the vicinity of the glass transition of the neat PVA. These temperatures correspond to the conditions for which the greatest energy is supplied during the initial deformation. Nanotubes reinforce the PVA matrix, leading to a high storage modulus and to a large stress recovery that exceeds 100 MPa. In addition and as already reported, nanotubes favor the stabilization of PVA crystalline domains. This could contribute to the locking of mechanical constraints and to the strong shape memory effects. However, the origin of the temperature memory is less clear. It could likely be arising from a broad glass transition with the contribution of confined polymers at the interface of nanotubes or crystalline domains (64). It has been shown that significant gradients of T_g can develop at the interface of nanoparticles (65). Amorphous polymer shells

around the CNTs or around crystalline domains largely overlap and percolate, such as the CNTs themselves; meaning that there is a distribution of polymer-CNT or amorphous polymer-crystallites distances which ranges from molecular contact to several nanometers. This distribution of confinement results in a wide broadening of the relaxation time spectrum and specifically the glass transition through a distribution of polymer fractions which exhibit different T_g . This property could be responsible for peaks of stress recovery well above the T_g of the neat polymer. Indeed, when the material is stretched at T_d , the polymer fractions that have lower glass transition temperatures (far from the interface) can quickly relax and don't efficiently participate to the storage of mechanical energy. In contrast, polymer fractions with glass transition temperatures close to T_d dominate the behavior by storing and restoring mechanical energy. We also note that composites treated in the vicinity of T_g still exhibit higher toughness and generate greater stress recovery. This indicates that the fractions of amorphous polymer with un-shifted or slightly shifted glass transition temperatures remain the major components of the composite. This scenario is still speculative and further research is needed to clarify the microscopic origin of the temperature memory. In particular, if it would indeed be arising from a broadening of the glass transition and to confined polymers at the interface of nanotubes or crystallites, this temperature memory should take place in other nanocomposites and even in neat semi-crystalline polymers which exhibit a sufficient fraction of crystalline domains. Such predictions call for future investigations to be validated. They would be of great interest for applications since temperature memory allows tuning shape memory phenomena via material treatments without varying its chemical composition.

11.6 Conclusion

This chapter is an overview of the synthesis and properties of PVA/nanotube composites. Various films and fibers have been processed from carbon nanotube and PVA dispersions. Compared to other polymers, PVA exhibit particularly strong interaction with single-walled as well as multiwalled carbon nanotubes. This leads to unique properties which are not observed in other nanotube polymer nanocomposites. In particular, this literature review confirms

that nanotubes can promote PVA crystallization in the vicinity of their interface. This yields improvements of mechanical stress transfer. This effect can be enhanced with the surface functionalization of carbon nanotubes, in particular with hydroxyl or carboxyl groups, which display hydrogen bonds with PVA. On the other hand, the overriding problem of dispersion is also being progressively solved using functionalization and controlling the interactions between the nanotubes and the PVA matrix. Despite these progresses made over the last years, there are nevertheless some obstacles to overcome. For example, it is always challenging to obtain composites loaded with high fractions of oriented nanotubes: solutions will have to be found to improve the existing processes or to invent new ones to overcome this difficulty. Better controlled chemical functionalization routes will also have to be developed to improve the interfacial interaction between nanotubes and PVA. Hardening of the polymer matrix could be investigated too, using, for example, acetylation processes (17,42).

Beyond the usual mechanical and electrical performances, this review also points out the emergence of other original properties, like the remarkable capability of some nanotube/PVA composites to absorb mechanical energy and shape memory phenomena that differ from traditional behaviors of other polymers. These features are opening new investigation fields, in which several fundamental questions will have to be solved. But they also offer new opportunities for a variety of applications like smart or protective clothing, helmets, bullet proof vests, or active composites.

References

1. R. Saito, G. Dresselhaus, and M.S. Dresselhaus, *Physical Properties of Carbon Nanotubes*, Imperial College Press, 1998.
2. R.H. Baughman, A.Z. Zakhidov, and W.A. de Heer, *Science*, Vol. 297, p. 787, 2002.
3. M.M.J. Treacy, T.W. Ebbesen, and J.M. Gibson, *Nature*, Vol. 381, p. 678, 1996.
4. P. Poncharal, Z.L. Wang, D. Ugarte, and W.A. de Heer, *Science*, Vol. 283, p. 1513, 1999.
5. M.R. Falvo, G.J. Clary, R.M. Taylor, V. Chi, F.P. Brooks, S. Washburn, and R. Superfine, *Nature*, Vol. 389, p. 582, 1997.
6. J.P. Salvetat, A.J. Kulik, J.M. Bonard, G.A.D. Briggs, T. Stockli, K. Metenier, S. Bonnamy, F. Beguin, N.A. Burnham, and L. Forro, *Advanced Materials*, Vol. 11, p. 161, 1999.
7. J.P. Salvetat, G.A.D. Briggs, J.M. Bonard, R.R. Bacsá, A.J. Kulik, T. Stockli, N.A. Burnham, and L. Forro, *Physical Review Letters*, Vol. 82, p. 944, 1999.

8. M.F. Yu, B.S. Files, A. Arepalli, and R.S. Ruoff, *Physical Review Letters*, Vol. 84, p. 5552, 2000.
9. H. Krenchel, *Fibre reinforcement*, Akademisk Forlag, Copenhagen, Denmark, 1964.
10. H.L. Cox, *Br. Journal of Applied Physics*, Vol. 3, p. 72, 1952.
11. I. Balberg, N. Binenbaum, and N. Wagner, *Physical Review Letters*, Vol. 52, p. 1465, 1984.
12. F. Carmona, P. Prudhon, and F. Barreau, *Solid State Communications*, Vol. 51, p. 255, 1984.
13. B. Vigolo, C. Coulon, M. Maugey, C. Zakri, and P. Poulin, *Science*, Vol. 309, p. 920, 2005.
14. T. Schilling, S. Jungblut, and M.A. Miller, *Physical Review Letters*, Vol. 98, p. 10, 2007.
15. A. Kyrlyuk, and P. van der Schoot, *PNAS*, Vol. 105, p. 8221, 2008.
16. H. Staudinger, K. Frey, and W. Starck, *Ber. Dtsch. Ges.*, Vol. 60, p. 1782, 1927.
17. I. Sakurada, *International Fiber Science and Technologies Series* 6, 1985.
18. M.S.P. Shaffer, and A.H. Windle, *Advanced Materials*, Vol. 11, p. 937, 1999.
19. M.S.P. Shaffer, X. Fan, and A.H. Windle, *Carbon*, Vol. 36, p. 1603, 1998.
20. M. Cadek, J.N. Coleman, V. Barron, K. Hedicke, and W.J. Blau, *Applied Physics Letters*, Vol. 81, p. 5123, 2002.
21. O. Probst, E.M. Moore, D.E. Resasco, and B.P. Grady, *Polymer*, Vol. 45, p. 4437, 2004.
22. X. Zhang, T. Liu, T.V. Sreekumar, S. Kumar, V.C. Moore, R.H. Hauge, and R. Smalley, *Nano Letters*, Vol. 3, p. 1285, 2003.
23. M. Cadek, J.N. Coleman, K.P. Ryan, V. Nicolosi, G. Bister, A. Fonseca, J.B. Nagy, K. Szostak, F. Béguin, and W.J. Blau, *Nano Letters*, Vol. 4, p. 353, 2004.
24. B.P. Grady, F. Pompeo, R.L. Shambaugh, and D.E. Resasco, *Journal of Physical Chemistry B*, Vol. 106, p. 5852, 2002.
25. A.R. Bhattacharyya, T.V. Sreekumar, T. Liu, S. Kumar, L.M. Ericson, R.H. Hauge, and R.E. Smalley, *Polymer* Vol. 44, p. 2373, 2003.
26. L. Valentini, J. Biagiotti, J.M. Kenny, and M.A.L. Manchado, *Journal of Applied Polymer Science*, Vol. 89, p. 2657, 2003.
27. E. Assouline, A. Lustiger, A.H. Barber, C.A. Cooper, E. Klein, E. Wachtel, and H.D. Wagner, *Journal of Applied Polymer Science*, Vol. 87, p. 20, 2003.
28. J. Sandler, G. Broza, M. Nolte, K. Schulte, Y.M. Lam, and M.S.P. Shaffer, *Journal of Macromolecular Science*, Vol. 42, p. 479, 2003.
29. Y. Bin, M. Mine, A. Koganemaru, X. Jiang, and M. Matsuo, *Polymer*, Vol. 47, p. 1308, 2006.
30. T. Liu, and S. Kumar, *Nano Letters*, Vol. 3, p. 647, 2003.
31. H.H. Gommans, J.W. Alldredge, H. Tashiro, J. Park, J. Magnuson, and A.G. Rinzler, *Journal of Applied Physics*, Vol. 88, p. 2509, 2000.
32. H.W. Zhu, C.L. Xu, D.H. Wu, B.Q. Wei, R. Vajtai, and P.M. Ajayan, *Science*, Vol. 296, p. 884, 2002.
33. K. Jiang, Q. Li, and S. Fan, *Nature*, Vol. 419, p. 801, 2002.
34. Y. Li, I.A. Kinloch, and A.H. Windle, *Science*, Vol. 304, p. 276, 2004.
35. L.M. Ericson et al., *Science*, Vol. 305, p. 1447, 2004.

36. M. Zhang, K.R. Atkinson, and R.H. Baughman, *Science*, Vol. 306, p. 5700, 2004.
37. B. Vigolo, A. Penicaud, C. Coulon, C. Sauder, R. Pailler, C. Journet, P. Bernier, and P. Poulin., *Science*, Vol. 290, p.1331, 2000.
38. P. Poulin, B. Vigolo, and P. Launois, *Carbon*, Vol. 40, p. 1741, 2002.
39. P. Miaudet, S. Badaire, M. Maugey, A. Derré, V. Pichot, P. Launois, P. Poulin, and C. Zakri, *Nano Letters*, Vol. 5, p. 2212, 2005.
40. X. Zhang, T. Liu, T.V. Sreekumar, S. Kumar, X. Hu, and K. Smith, *Polymer*, Vol. 45, p. 8801, 2004.
41. M.L. Minus, H.G. Chae, and S. Kumar, *Polymer*, Vol. 47, p. 3705, 2006.
42. P. Xue, K.H. Park, X.M. Tao, W. Chen, and X.Y. Cheng, *Composite Structures*, Vol. 78, p. 271, 2007.
43. W. Zhou, Y. Wu, F. Wei, G. Luo, and W. Qian, *Polymer*, Vol. 46, p. 12689, 2005.
44. M. Naebe, T. Lin, W. Tian, L. Dai, and X. Wang, *Nanotechnology*, Vol.18, p. 225605, 2007.
45. K.K.H. Wong, M. Zinke-Allmang, J.L. Hutter, S. Hrapovic, J.H.T. Luong, and W. Wan, *Carbon*, Vol. 47, p. 2571, 2009.
46. K.P. Ryan, M. Cadek, V. Nicolosi, D. Blod, M. Ruether, G. Armstrong, H. Swan, A. Fonseca, et al., *Composite Science and technology*, Vol. 67, p. 1640, 2007.
47. L. Liu, A.H. Barber, S. Nuriel, and D.H. Wagner, *Advanced Functional Materials*, Vol. 15, p. 975, 2005.
48. A.H. Barber, S.R. Cohen, and H.D. Wagner, *Applied Physics Letters*, Vol. 82, p. 4140, 2003.
49. J.C. Halpin, and J.L. Kardos, *Polymer Engineering and Science*, Vol.16, p. 344, 1976.
50. N. Lachman, C. Bartholome, P. Miaudet, M. Maugey, P. Poulin, and H.D. Wagner, *Journal of Physical Chemistry C*, Vol. 113, p. 4752, 2009.
51. J. Zhang, M. Min, D. Zhu, and M. Matsuo, *Carbon*, Vol. 47, p. 1311, 2009.
52. P. Miaudet, C. Bartholome, A. Derré, M. Maugey, G. Sigaud, C. Zakri, and P. Poulin, *Polymer*, Vol. 48, p. 4068, 2007.
53. C. Bartholome, P. Miaudet, A. Derré, M. Maugey, O. Roubeau, C. Zakri, and P. Poulin, *Composites Science and Technology*, Vol. 68, p. 2568, 2008.
54. S. Badaire, V. Pichot, C. Zakri, P. Poulin, P. Launois, J. Vavro, et al., *Journal of Applied Physics*, Vol. 96, p. 7509, 2004.
55. E. Kymakis, and G.A.J. Amaratunga, *Journal of Applied Physics*, Vol. 99, 2006.
56. A.B. Dalton, S. Collins, E. Munoz, J.M. Razal, V.H. Ebron, J.P. Ferraris, J.N. Coleman, B.G. Kim, and R.H. Baughman, *Nature*, Vol. 423, p. 703, 2003.
57. N.E. Nielsen, *Mechanical properties of polymers and composites*, Vol. 2, Marcel Dekker INC., NY, 1974.
58. E. Hornbogen, *Advanced Engineering Materials*, Vol. 8, p. 101, 2006.
59. A. Lendlein, S. Kelch, *Angewandte Chemie International Edition*, Vol. 41, p. 2034, 2002.
60. C. Liu, H. Qin, P.T. Mather, *Journal of Materials Chemistry*, Vol. 17, p. 1543, 2007.
61. B.K. Kim, S.Y. Lee, and M. Xu, *Polymer*, Vol. 37, p. 5781, 1996.
62. K. Gall, C.M. Yakacki, Y. Liu, R. Shandas, N. Willett, and K.S. Anseth, *Journal of Biomedical Materials Research Part A*, Vol. 73, p. 339, 2005.

63. A. Lendlein, and R. Langer, *Science*, Vol. 296, p.1673, 2002.
64. P. Miaudet, A. Derré, M. Maugey, C. Zakri, P.M. Piccione, R. Inoubli, and P. Poulin, *Science*, Vol. 318, p. 1294, 2007.
65. J. Berriot, H. Montes, F. Lequeux, D. Long, and P. Sotta, *European Physical Letters*, Vol. 64, p. 50, 2003.

This Page Intentionally Left Blank

Elastomers Filled with Carbon Nanotubes

Liliane Bokobza

*E.S.P.C.I., Laboratoire PPMD,
10 rue Vauquelin, 75231 Paris Cedex, France*

Abstract

This paper represents an overview of investigations carried out in carbon nanotube / elastomeric composites with an emphasis on the factors that control their properties. Carbon nanotubes have clearly demonstrated their capability as electrical conductive fillers in nanocomposites and this property has already been commercially exploited in the fabrication of electronic devices. The filler network provides electrical conduction pathways above the percolation threshold. The percolation threshold is reduced when a good dispersion is achieved. Significant increases in stiffness are observed. The enhancement of mechanical properties is much more significant than that imparted by spherical carbon black or silica particles present in the same matrix at a same filler loading, thus highlighting the effect of the high aspect ratio of the nanotubes.

Keywords: elastomers, filler dispersion, interfacial adhesion, reinforcement, mechanical properties, thermal stability.

12.1 Introduction

Elastomers require, in most applications, to be reinforced by fillers in order to improve their mechanical properties. Carbon black and silica have been used for a long time in the rubber industry to prepare composites with greatly improved properties such as strength, stiffness and wear resistance. These conventional fillers must be used at high loading levels to impart to the material the desired properties (1). The state of filler dispersion and orientation

in the matrix, the size and aspect ratio of the particles as well as the interfacial interactions between the organic and inorganic phases have been shown to be crucial parameters in the extent of property improvement (2,3).

The last few years have seen the extensive use of nanoparticles because of the small size of the filler and the corresponding increase in the surface area, allowing to achieve the required mechanical properties at low filler loadings. Nanometer-scale particles including spherical particles such as silica or titanium dioxide generated *in-situ* by the sol-gel process (4–8), layered silicates (9–12), carbon (13) or clay fibers (14,15), single-wall or multiwall carbon nanotubes (16,17) have been shown to significantly enhance the physical and mechanical properties of rubber matrices.

The recognition of the unique properties of carbon nanotubes (CNTs) has stimulated a huge interest in their use as advanced filler in composite materials. In particular, their superior mechanical, thermal and electrical properties are expected to provide much higher property improvement than other nanofillers (18–22). For example, as conductive inclusions in polymeric matrices, CNTs shift the percolation threshold to much lower loading values than traditional carbon black particles.

Although most efforts have been devoted to the use of carbon nanotubes in glassy polymers, some studies have reported strong reinforcing effects of CNTs in elastomeric matrices such as butyl (23), natural (17,24–27) and styrene-butadiene rubbers (28–31) as well as styrene-butadiene and butadiene rubber blends (32).

All the results obtained by incorporation of CNTs in hydrocarbon rubbers remain far below the expected values and factors such as weak interfacial bonding, poor dispersion and degradation of the CNTs during processing are often cited to explain the discrepancy between experimental and predicted results. Moreover, a reduction in the efficiency of peroxide vulcanization of ethylene-propylene-diene terpolymer has been reported by addition of functionalized carbon nanotubes (33). Nevertheless, an outstanding affinity of carbon nanotubes towards poly(dimethylsiloxane) has been demonstrated (34–39). Tiny amounts of multiwall carbon nanotubes have been shown to bring significant changes in the mechanical, electrical and thermal properties of silicone rubbers. This chapter is intended to review some recent advances in processing and characterization of elastomers filled with multiwall carbon nanotubes.

12.2 Composite Processing

The main factor that controls the performance of the composites is the state of dispersion of CNTs in the matrix. Carbon nanotubes can easily form bundles and this aggregation decreases their aspect ratio thus reducing their efficiency as fillers. So, all processing methods used to prepare polymer nanotube composites aim to improve dispersion of CNTs in order to fully exploit the potential of these materials.

Different approaches have been used to optimize the dispersion of CNTs in the polymeric medium. Composites can be prepared by different techniques including *in-situ* polymerization, solution mixing, surfactant-assisted processing and melt compounding.

Solution blending seems one of the common method for the preparation of polymer nanotube composites since it leads to a de-aggregation of the bundles especially under ultrasonication (40,41). The sonication conditions must be determined in such a way not to degrade the nanotubes. As seen in Figure 12.1, ultrasonication for a long period of time (120 min) shortens the nanotube length which could be detrimental to the performance of the resulting composite. Magnetic stirring or shear mixing have also been used to disperse the nanotubes but as it will be shown below yield poorer dispersions than sonication.

Preparing an elastomeric nanotube composite requires several steps which can be summarized as follows: dispersion of the nanotube in a suitable solvent by ultrasonication during 30 min, mixing of nanotubes suspension and polymer in solution by further sonication for 30 min followed by agitation under magnetic stirring until evaporation of the solvent. Total removal of any remaining solvent is achieved under vacuum overnight at 50°C before the cross-linking process and film formation.

In solution mixing, solvent plays an important role in determining the properties of polymer nanocomposites. The choice of the solvent used to disperse the nanotubes is often based on the solubility of the polymer. But both solvents might be either the same or of different types, the polymer can be dissolved in one solvent, the filler particles in a second one. Toluene is a good solvent for rubbers and has also been shown to yield homogeneous dispersion of nanotubes (40–43). Nevertheless in a previous study (38), we have tested different solvents and shown that dispersing the nanotubes in isopropyl alcohol with a ultrasonication probe (Bioblock Vibra-cell, 500 W, working at 40% of its power) gives a stable dispersion one week after the preparation (Figure 12.2). Sonication in alcoholic

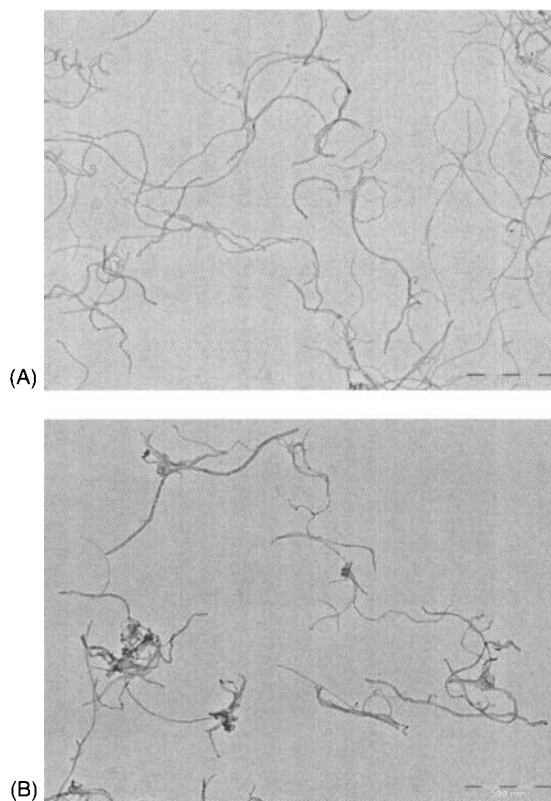


Figure 12.1. TEM images of MWNTs previously sonicated in toluene for: 30 min (A), 120 min (B).

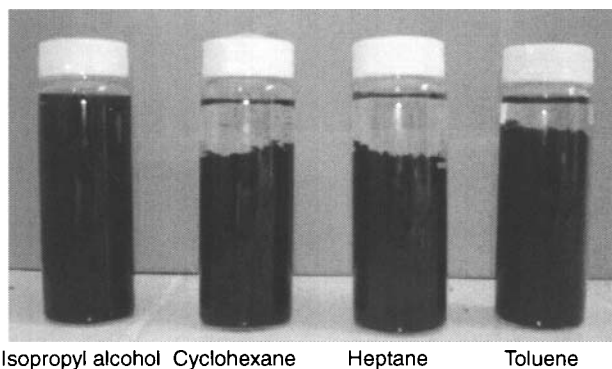


Figure 12.2. MWNTs dispersions at 0.01 wt% in various solvents one week after their preparation. [Reproduced by permission of Kautschuk Gummi Kunststoffe from L. Bokobza and M. Rahmani: "Carbon nanotubes: Exceptional reinforcing fillers for silicone rubbers", KGK, 62, 112, 2009].

media have been shown to deagglomerate the bundles in order to get an homogeneous distribution in the polymer matrix (28,44). Figure 12.3 shows typical TEM images of a toluene suspension of multiwall carbon nanotubes (MWNTs) previously sonicated before being put onto copper grids for observation. These nanotubes produced via a catalytic carbon deposition (CCVD) process were used without further purification. Their average diameter and length are around 10 nm and 1.5 μm respectively and their surface area between 250 and 300 $\text{m}^2\cdot\text{g}^{-1}$. Figure 12.3a shows entangled nanotubes revealing their exceptional flexibility and Figure 12.3b magnifies individual nanotubes with their tubular shape and their hollow core.

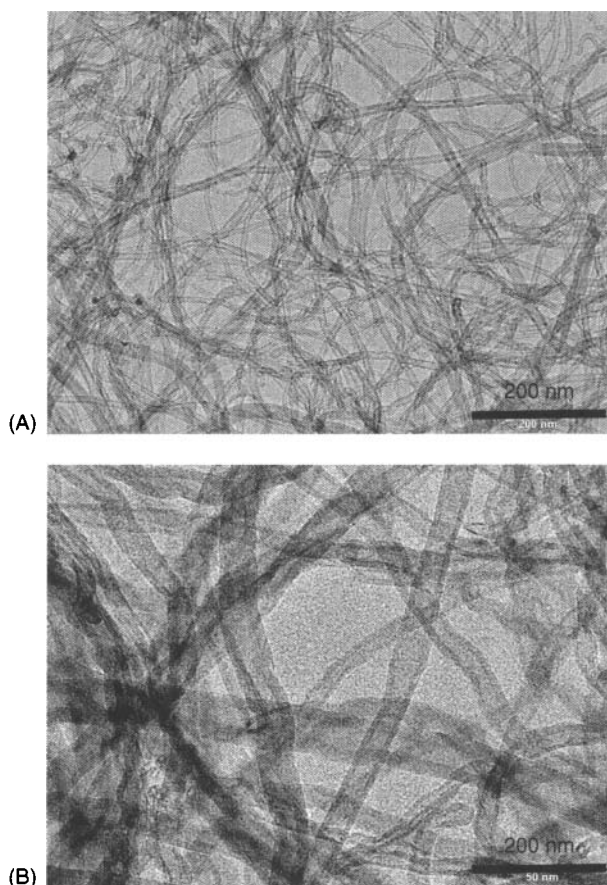


Figure 12.3. TEM images of a suspension of MWNTs in isopropyl alcohol at two magnification levels.

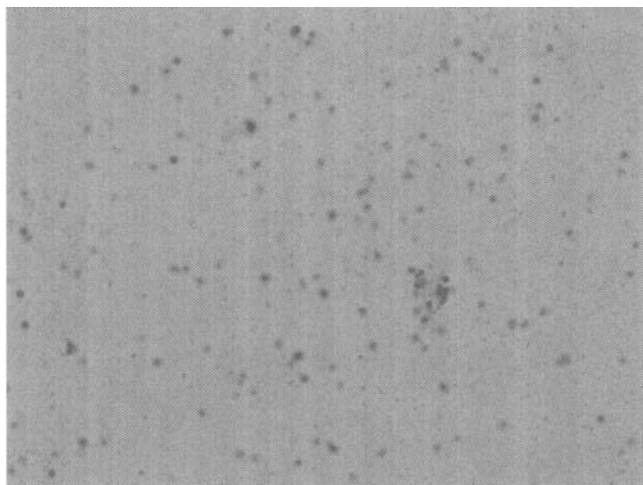


Figure 12.4. Optical microscopy of a dispersion of MWNTs in natural rubber. Vertical dimension of the picture: 140 μm .

Optical microscopy can be used to assess the dispersion quality of the nanotubes during the different steps of the composite processing. Figure 12.4 shows a uniform distribution of particles on macroscopic and microscopic scales after adding an isopropyl suspension of MWNTs to a solution of natural rubber (NR). Considering the resolution limit of optical microscopy, we deduce the absence of aggregates larger than one micrometer.

12.3 Electrical Properties

Most polymers are usually electrical insulators but need to be conductive for many engineering applications. Incorporation of conductive filler particles into the polymeric medium remains an interesting way to produce an electrically conducting polymer. Carbon materials provide electrical conduction and lead to a change in resistivity with increasing filler volume fraction in the polymer matrix.

The electrical conduction process depends on several parameters, mainly on filler concentration. But filler morphology such as particle size and structure as well as filler-filler and filler-matrix interactions which determine the state of dispersion and filler orientation are key factors in determining the electrical properties. On the other hand, processing techniques also influence the electrical conductivity of

the final material. At a given amount of conductive particles (carbon black or carbon nanotubes), called the percolation threshold (45,46), a continuous network of filler is formed across the matrix and the material undergoes a sudden transition from an insulator to a conductor. For composites containing conventional conducting fillers such as carbon black (CB), carbon nanofibers or graphite, depending on the structural properties of the particles, the percolation threshold is achieved for a filler content as high as 10 – 50 wt% (47–49), which may result in a composite with poor mechanical properties and high density. Thongruang et al. (50) showed that the percolation-threshold concentration in composites is around 10 – 15 wt% for carbon fiber and high structure carbon black and around 40 – 50 wt% for low structure carbon black and graphite. Carbon nanotubes are expected to yield adequate conductivity at a much lower filler content on account of their high aspect ratios thus retaining the desired mechanical properties of the resulting material.

Figure 12.5a shows the effect of filler loading on the volume resistivity of MWNTs and CB (CB: Ensaco 250G from Timcal) filled composites based on insulating styrene-butadiene rubber. The styrene-butadiene rubber contains 25 w% of styrene units. The microstructure of the butadiene phase is the following: 10% cis, 17% trans, 73% 1,2. It was compounded with sulfur (1.1 phr), cyclohexyl benzothiazole sulfenamide (1.3 phr), diphenyl guanidine (1.45 phr), stearic acid (1.1 phr), zinc oxide (1.82 phr) (phr = parts per hundred parts of rubber). The unfilled and filled samples are cured into films (around 200 μm thick) at 170°C during 10 min under a pressure of 150 bar in a standard hot press.

Electrical resistivity measurements were determined on samples of $10 \times 20 \times 0.2 \text{ mm}^3$ by measuring their resistance on a high resistance meter (Keithley 6517A) between two conductive rubber electrodes with an alternative voltage of 1 V. This alternative voltage is needed to avoid a background current effect. The measured resistances R were then converted into volume resistivity ρ by using this equation:

$$\rho = \frac{RS}{d}$$

where S is the cross-sectional area perpendicular to the current and d the thickness of the sample between the two electrodes.

As seen in Figure 12.5a, the continuous network is formed at a lower filler loading of the nanotube bundles with MWNTs than

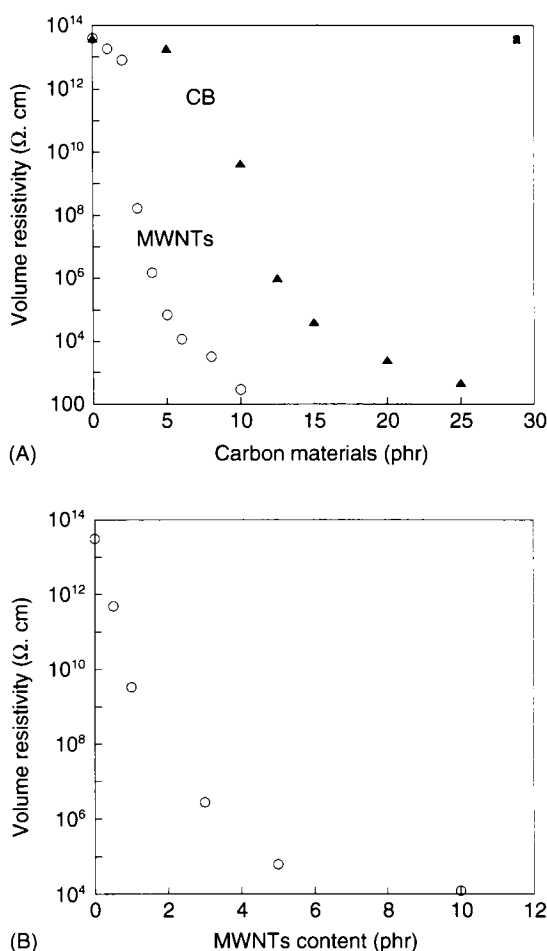


Figure 12.5. Volume resistivity against filler loading for SBR composites filled with carbon black (CB : Ensaco 250G from Timcal) and MWNTs. [Figure 5A is reprinted from L. Bokobza, M. Rahmani, C. Belin, J.-L. Bruneel, N.-E. El Bounia: "Blends of carbon blacks and multiwall carbon nanotubes as reinforcing fillers for hydrocarbon rubbers", *Journal of Polymer Science: Part B: Polymer Physics*, 46, 1939, 2008, permission from John Wiley and Sons].

with CB. The higher aspect ratio of the nanotube bundles which increases the probability of particle-particle contacts explain the low percolation threshold (between 2 and 3 phr). Results displayed in Figure 12.5a are related to composites prepared by dispersing the nanotubes in toluene by means of a high shear mixer (Ultra-Turrax) operating at 13,000–16,000 rpm.

As mentioned above, an important factor that controls the performance and especially the electrical properties of CNTs-reinforced composites is the state of dispersion of CNTs. Ultrasonication has been shown to be more effective in dispersing the nanotubes without the need for surfactants or other chemical treatments. Figure 12.5b presents electrical results of samples prepared by using a different composite processing. MWNTs were dispersed in this case in cyclohexane by ultrasonication and the MWNTs suspension was then mixed into a cyclohexane solution of SBR. Mixing was achieved by a further sonication for 30 minutes. Cyclohexane has been chosen in this case on account of the solubility of the rubbers in this solvent. As revealed in Figure 12.5b, the percolation threshold is shifted to a lower nanotube content and from this point of view, measurements of electrical resistivity appears as an indirect tool to evaluate the state of dispersion.

A method of incorporating simultaneously hybrid fillers of CB and MWNTs into a polymeric matrix has also been used to enhance the electrical conductivity of composites because the CB particles link the gaps between the unconnected MWNTs thus improving the formation of connected structures (51,52). In fact the synergistic effects arising between the two different fillers improve the dispersion of MWNTs in the polymer matrix.

Adding carbon nanotubes to SBR containing a constant CB content and MWNTs reduces the resistivity and the percolation threshold to a lower content than that obtained with samples only filled with MWCNTs making clear the formation of connected structures (Figure 12.6a). A TEM image of a SBR matrix containing a dual filling : 5 phr of CB + 5 phr of MWNTs, shows individual carbon nanotubes connecting carbon black aggregates to form conducting paths in the polymer matrix which can explain the improvement in the electrical properties (Figure 12.6b).

Because the resistivity is very sensitive to any change in filler distribution, electrical properties of composite filled with conductive particles should be affected by a mechanical deformation. Significant changes in electrical conductivity against degree of elongational strain have already been reported in the literature (53–55).

Typical strain dependences of volume resistivity are shown in Figure 12.7: the results are related to an ethylene-propylene-diene rubber (EPDM) (supplied by ExxonMobil Chemical under the trade name Vistalon 5601) filled with 6 phr of MWNTs that is at a filler content well above the percolation threshold (determined around

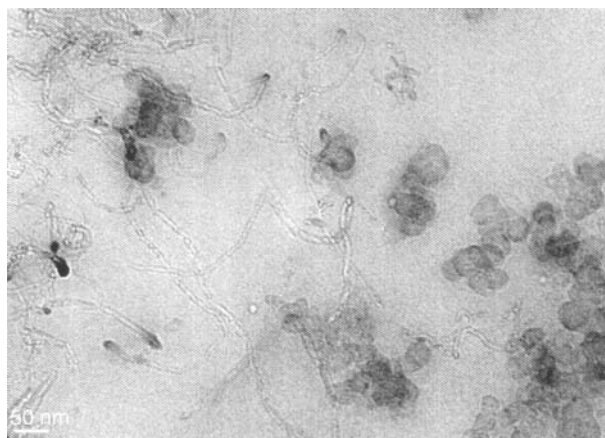
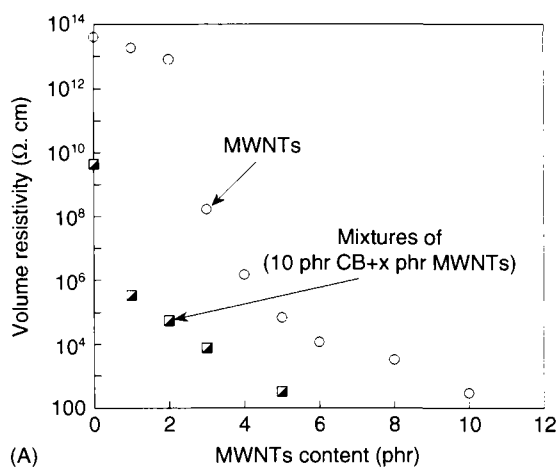


Figure 12.6. Volume resistivity against filler loading for SBR composites filled with MWNTs and mixtures (10 phr CB + x phr (MWNTs) (A) and TEM image of a styrene-butadiene copolymer (SBR) containing a dual filling (5 phr CB + 5 phr MWNTs) (B). [Reprinted from L. Bokobza, M. Rahmani, C. Belin, J.-L. Bruneel, N.-E. El Bounia: "Blends of carbon blacks and multwall carbon nanotubes as reinforcing fillers for hydrocarbon rubbers", *Journal of Polymer Science: Part B: Polymer Physics*, 46, 1939, 2008, permission from John Wiley and Sons].

0.5 phr of filler). A gradual increase in resistivity is obtained as result of a breakdown of the conductive networks and of an orientation of the nanotubes. After total unloading of the sample, the resistivity is much higher than that observed for the undeformed material thus showing that the filler network is not reformed after removal

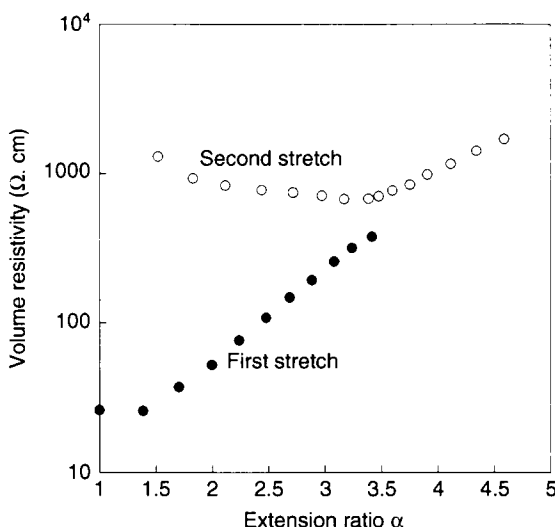


Figure 12.7. Strain dependence of the electrical resistivity for the EPDM filled with 6 phr of MWNTs.

of the stress. Measurements were made at about 5 min after each elongation step. A second stretching leads to a decrease in resistivity attributed to the formation of new conductive pathways.

The strain dependence of electrical resistivity was carried out on strips (size: 40 mm \times 6 mm \times 0.3 mm) stretched with a manual stretching machine. The film under study is clamped between the jaws of the stretching machine and two copper plates attached to the jaws of the machine are connected to the high-resistance meter (Figure 12.8).

12.4 Mechanical Properties

12.4.1 Tensile and Swelling Behaviors

The incorporation of reinforcing particles in an elastomeric matrix leads to an enhancement of the mechanical properties. Tensile tests are thus widely used to evaluate the extent of reinforcement imparted to the polymeric matrix by a filler. Tensile curves representing the nominal stress (force divided by the undeformed area of the sample) against strain are given in Figure 12.9a for the pure polymer (NR) and for NR composites filled with carbon nanotubes (MWNTS) at different loadings and stress at 100% strain is given in Figure 12.9b.

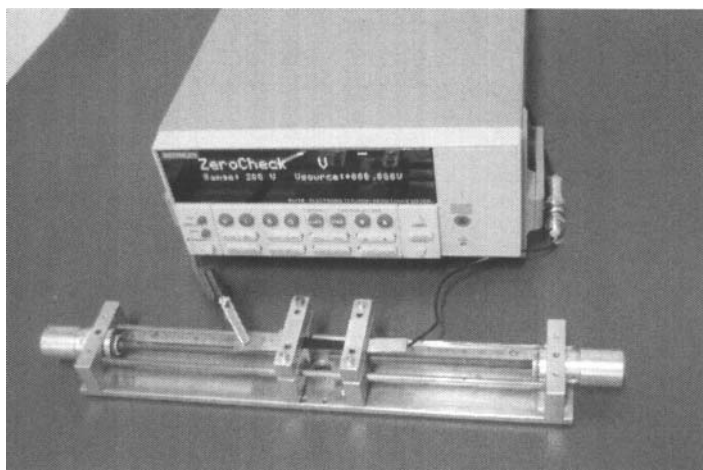


Figure 12.8. Stretching device for electrical measurements under uniaxial extension.

The strain-stress measurements were carried out at room temperature on strips of $50 \times 5 \times 0.3 \text{ mm}^3$ between two clamps by means of a sequence of increasing weights attached to the lower clamp. The distance between two marks on the sample was measured with a cathetometer after allowing sufficient time (10 min after adding a weight) for equilibration.

The stress-strain curve for unfilled NR exhibits a large increase in stress at higher deformations. NR displays, due to its uniform microstructure, a very unique important characteristic, that is, the ability to crystallise under strain, a phenomenon known as strain-induced crystallization. This phenomenon is responsible for the large and abrupt increase in the reduced stress observed at higher deformation corresponding, in fact, to a self-toughening of the elastomer because the crystallites act as additional cross-links in the network. This process can be better visualized by using a Mooney-Rivlin representation, based on the so-called Mooney-Rivlin equation:

$$[\sigma^*] = \sigma / (\alpha - \alpha^2) = 2C_1 + 2C_2 \alpha^{-1}$$

where σ is the nominal stress, α is the extension ratio (ratio of the final length in the direction of stretch to the initial length before deformation) and $2C_1$ and $2C_2$ are constants independent of α . The curves of the unfilled and filled vulcanizates display, at higher deformations, upturns in the modulus ascribed to the strain-induced crystallization of polymer chains (Figure 12.10). Only the composite

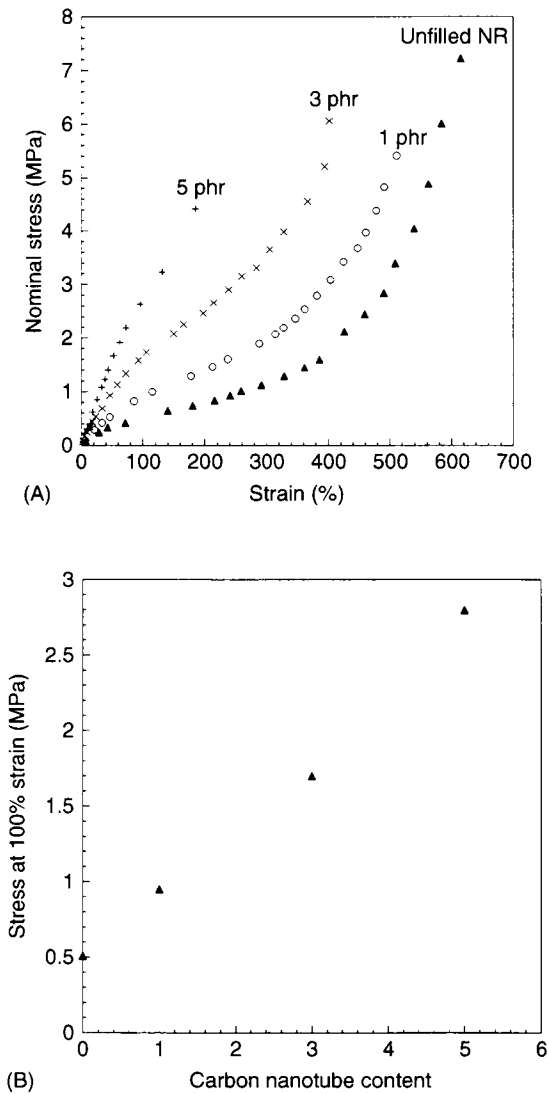


Figure 12.9. Stress-strain curves (A) and stress at 100% for pure NR and MWNTs composites (B).

filled with 1 phr has been presented in Figure 12.10 because the reduction in the stress and strain at rupture for the other composites does not allow the observation of the tensile behaviour at high deformations. Unfortunately, the rupture properties are negatively affected by the nanotubes probably on account of the presence of

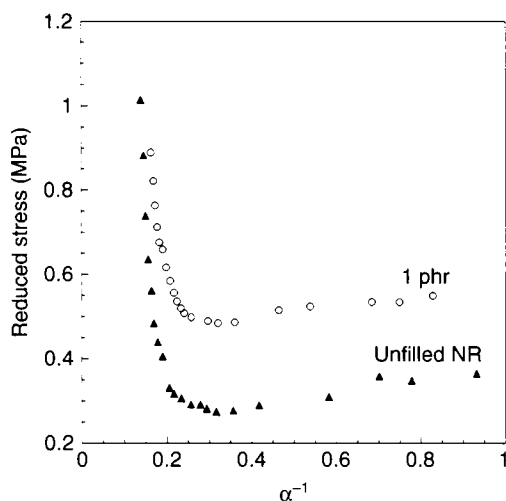


Figure 12.10. Mooney-Rivlin plots for pure NR and 1 phr MWNTs/NR composite.

some agglomerates which act as failure points and lead to a degradation of the mechanical properties of the materials.

The stress at 100% deformation is seen to increase linearly with the MWNTs loading (Figure 12.9b). With regard to the pure polymer, 1 phr of MWNTs almost doubles the strain at 100% strain while a 450% increase is observed for the 5 phr content. These observed improvements are higher than those previously obtained in the literature for the same polymer (17,24–27).

Such increases in stiffness are not observed for similar loading fractions of spherical carbon black or silica particles in the same matrix, thus highlighting the effect of the high aspect ratio (length/diameter) of the nanotubes. In conventional composites, the increase in the modulus has been ascribed to a hydrodynamic effect arising from the inclusion of rigid particles in the soft matrix and to an increase in the cross-linking density created by polymer-filler interactions (2,3,56–62). But the anisometry of the filler structures as well as the quality of their dispersion can greatly affect the composite performance. The latter point is especially true for entangled MWNTs in which the occluded rubber trapped inside the bundles and partially shielded from deformation, increases the effective filler concentration.

To interpret the variation of stiffness of the polymeric composites with the MWNTs amount, the 100% modulus results are fitted to

two models intended to predict the mechanical properties of fibre reinforced composites. The Guth equation (63) only based on the aspect ratio, f , and volume fraction, ϕ , of filler, predicts a strong increase in modulus at high volume fraction: :

$$E = E_0 (1 + 0.67f\phi + 1.62f^2\phi^2), \quad (1)$$

(E and E_0 are the moduli of the composite and the unfilled elastomer respectively).

The Halpin-Tsai model (64) yields, for aligned fibre composites and in conditions where the modulus of the fiber, E_f , is much higher than that of the unfilled matrix (as in elastomeric composites) :

$$E = E_0 (1 + 2f\phi) / (1 - \phi) \quad (2)$$

The experimental values are compared with the Guth and Halpin-Tsai predictions using the respective aspect ratios of 70 and 90 to fit the data (Figure 12.11). These values are lower than expected from the average dimensions of the MWNTs but much higher than those previously published for MWNTs for hydrocarbon rubber / MWNTs composites (22,31) which is a result from a better filler dispersion.

The degree of adhesion between polymer chains and filler particles can be evaluated from equilibrium swelling of the composites

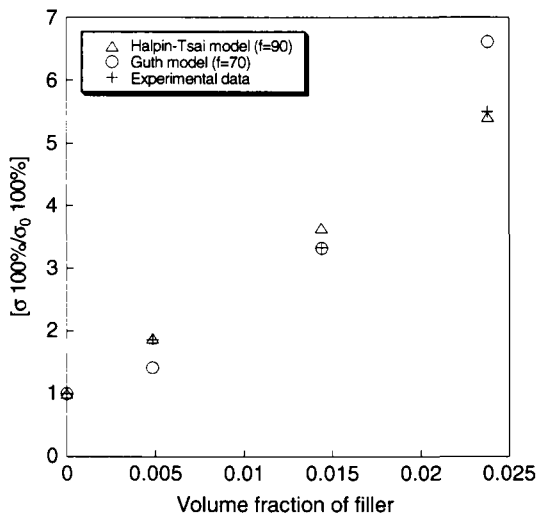


Figure 12.11. Dependence of the stress at 100% strain of NR / MWNTs composites on the filler volume fraction and comparison with predictions of theoretical models.

in good solvents. The extent of swelling at equilibrium is reduced in the case of adsorption of polymer chains on particle surfaces and may be enhanced with non-adhering fillers due to a dewetting of the particles and vacuole formation (65). For these experiments, a sample around 20 mm × 10 mm × 0.3 mm was put into cyclohexane. After 72h at room temperature, the length and width of the sample were measured with a caliper square. The equilibrium swelling ratio, Q , of the composite ($Q = V / V_d$, V being the volume of the swollen sample and V_d that of the dry sample) was determined from the lengths of the sample in the unswollen and swollen states. The equilibrium swelling ratio of the rubber alone, Q_r , is equal to $(Q - \phi) / (1 - \phi)$, where ϕ is the volume fraction of filler in the dry state. As seen in Figure 12.12 for NR/MWNTs composites, the equilibrium swelling ratio of the rubber phase in cyclohexane, Q_r , decreases with increasing amount of carbon nanotubes, indicating a pronounced restriction in swelling in the filled samples. Such experiments are generally used to estimate the total cross-linking density and the polymer-filler attachments. An alternative explanation to the swelling restriction would be to consider occluded rubber in addition to the actual volume occupied by the carbon nanotubes. This interpretation is not unrealistic because during the composite processing, a certain amount of polymer could be entrapped inside the nanotube bundles.

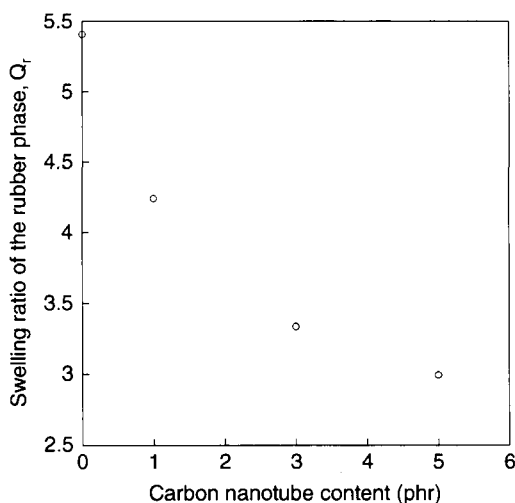


Figure 12.12. Dependence of rubber phase swelling of NR / MWNTs composites on the amount of carbon nanotubes.

12.4.2 Dynamic Mechanical Analysis (DMA) and Differential Scanning Calorimetry (DSC)

In conventional composites filled with carbon black or silica, the increase in stiffness is mainly associated with a change in the structure and dynamics of the polymer at the filler surface. On account of the enormous surface-to-volume ratio of the particles, the polymer in the interfacial region represents a significant fraction of the materials and its behavior significantly affects or even governs the properties of the composite.

The temperature dependences of the storage modulus G' are given in Figure 12.13 for unfilled and filled EPDM. The dynamic mechanical experiments were conducted from -100 to 150°C at a frequency of 1 Hz in tensile mode using a DMA (TA 2980). Heating rate was $5^{\circ}\text{C}/\text{min}$.

As already reported by several authors, the addition of carbon nanotubes did not affect the storage modulus in the glassy region, nevertheless a strong increase with the filler content is observed in the rubbery region. In conventional composites, this increase is mainly attributed to interfacial interactions leading to introduction of additional cross-links into the network by the filler. These interfacial interactions contribute to the formation of an adsorption layer whose thickness has been estimated around 2 or 3 nm and where

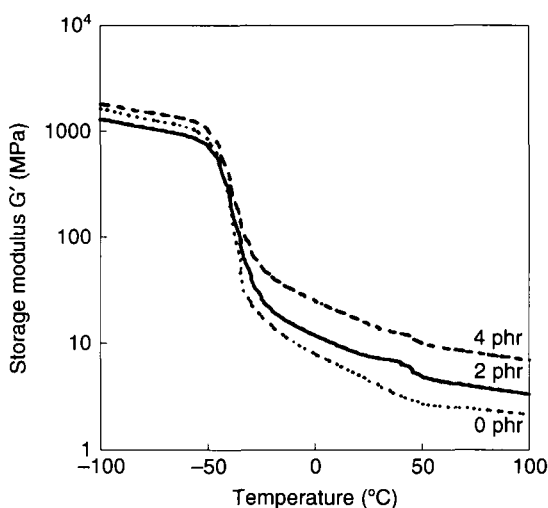


Figure 12.13. Temperature dependence of the storage modulus for EPDM-MWNTs composites.

motions of chain units are more restricted than those in the mobile phase. Surprisingly, even at high degrees of reinforcement, the glass transition temperature of these materials was not found to change significantly with the filler content. The presence of the interfacial layer was evidenced by dielectric or solid state NMR spectroscopies (66,67). The incorporation of MWNTs in EPDM as well as in any other elastomeric matrix investigated in this study does not lead to an appreciable change in the glass transition temperature, T_g , (determined around -40°C at the maximum of the loss modulus and $\tan \delta$), in agreement with differential scanning calorimetry results. With regard to conventional elastomeric composites where an almost unchanged value of T_g was observed despite the existence of strong interfacial interactions, no clear conclusion on the interfacial adhesion can be drawn from the examination of the DMA data. It has to be mentioned that López-Manchado et al. (68) report increase in T_g values going from -49.4°C for pristine NR to -45.7°C for NR-10 phr SWNTs composite and conclude to a strong interfacial interaction between the filler and the matrix. Gauthier et al. (69) observe a shift of around 3° between an unfilled styrene-butadiene rubber and the same matrix filled with 7 wt% of vapor grown carbon fibres. The authors believe that the carbon fibres may slightly modify the cross-linking reaction of the elastomeric matrix. Nevertheless, these reported changes in T_g observed by the incorporation of carbon nanotubes in elastomers remain rather low with regard to those obtained in other matrices. For composites of poly(methyl methacrylate) (PMMA) and unmodified or amide-functionalized SWNTs, $\tan \delta$ peak broadens but the peak is at the 105°C value of bulk polymer (70). The amide-functionalized PMMA composite displays a $\tan \delta$ peak shifted to a higher temperature by 30°C with regard to the pure polymer. The authors suggest the existence of discrete interphase regions with unmodified SWNTs due to clustering of tubes while the functionalized composite system has a stronger interfacial bonding via the covalent linkages between the two phases leading to the formation of an extensive region with altered properties. From SEM analysis of MWNTs-polycarbonate composites, Pötkke (71) and Ding (72) observe tube diameters larger than those of the pristine MWNTs used in the sample preparation and suggest the existence of an adsorbed layer of polymer on the tubes surface but unfortunately do not mention if a shift in T_g is associated with the tube coating. Additionally, a dependence of the nanotube content on the glass transition temperature was observed

for MWNTs/epoxy-composites with a stronger increase in T_g for samples containing amino-functionalized nanotubes (73).⁸ The authors do not exclude a possible effect of the additional functional groups on the curing reaction of the epoxy matrix. So unclear picture arises from the numerous studies dedicated to the glass transition temperature of CNTs composites. This point is discussed by Allaoui and El Bounia (74) in a very recent paper dealing with the effect of carbon nanotubes on the cure kinetics and glass temperature of carbon nanotube / epoxy composites. The authors reviewed and analyzed the literature results but no clarification could be drawn due to a lack of information such as purity of carbon nanotubes (catalyst particles can affect cure reaction), glass transition temperature along with the corresponding cure degree (to isolate the true potential effect of CNTs from curing variations).

If the presence of filler has no noticeable effect on the glass transition temperature of the different elastomeric matrices investigated in this present study, one interesting point regarding the thermal properties is the influence of carbon nanotubes on the crystallization process of crystallizable polymers and especially poly(dimethylsiloxane) (PDMS). Besides a very low glass transition temperature (-126°C), -the lowest reported for any polymer-, PDMS exhibits an exothermic peak at -68°C ascribed to crystallization. The addition of silica particles (a conventional reinforcing filler for silicone rubbers) to PDMS has been shown to decrease the temperature of crystallization as well as the degree of crystallinity (area under the peak) (8,75). This effect is related to an increase in the cross-linking density by polymer-filler interactions, it is more difficult for a polymer with a high cross-linking density, to carry out the crystallization process. This interpretation is close to that reached by Patel et al. (76) in a study on the effect of the network cross-linking density on the crystallisation characteristics of PDMS. Filling PDMS with very small amounts of MWNTs also leads to a decrease in the temperature of crystallization as in high reinforcing silicas (Figure 12.14). The PDMS network has been obtained by the hydrosilylation reaction (i.e., the addition of a silyl function $-\text{SiH}$ of precursor chains of hydride-terminated PDMS ($M_w=17,200 \text{ g mol}^{-1}$) to an unsaturated $\text{C}=\text{C}$ bond of the cross-linking molecule (77). The nanotubes are predispersed in isopropyl alcohol by sonication before being added to the PDMS. After total evaporation of the solvent, the cross-linking agent (1,3,5,7-tetravinyl-1,3,5,7-tetramethylcyclotetrasiloxane) then the catalyst (i.e., platinum-divinyltetramethyldisiloxane)

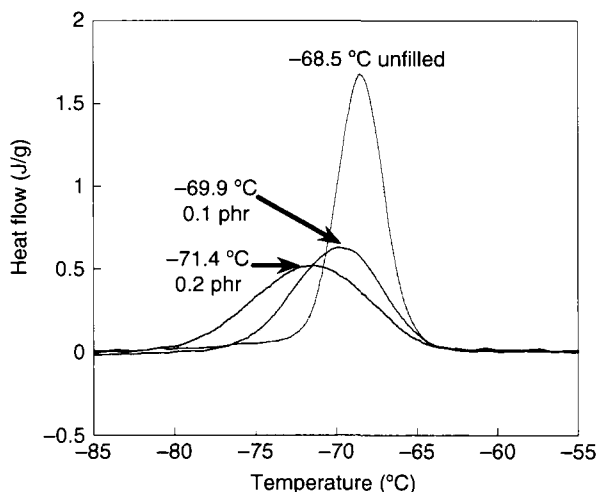


Figure 12.14. Dependence of the crystalline peak of PDMS on the amount of carbon nanotubes. [Reproduced by permission of Kautschuk Gummi Kunststoffe from L. Bokobza and M. Rahmani: "Carbon nanotubes: Exceptional reinforcing fillers for silicone rubbers", KGK, 62, 112, 2009].

are introduced under magnetic stirring. The uncured mixture is then poured into a manual applicator for film casting on a glass plate recovered with Teflon. The film is left at 80°C for one night for complete curing.

Differential scanning calorimetry experiments were performed on a TA DSC 2920 instrument from room temperature to -150°C with a cooling rate of 1.5°C/min under N₂ atmosphere.

12.5 Spectroscopic Characterization

Since the mechanical properties of the composites are intimately related to the filler structure and especially to the tube surface, techniques able to bring information at a molecular level are required for a further insight into the structure/property correlation.

Raman scattering has been used for a long time for the characterization of carbon-based materials. The pioneering study was made by Tuinstra and Koenig who showed that single crystals of graphite exhibit one single Raman line at 1575 cm⁻¹ (78). The authors observed an additional line near 1355 cm⁻¹ for other graphitic materials like activated charcoal, carbon black, and vitreous carbon. The intensity of this band increases with an increase in the amount of

“unorganized” carbon in the samples and with a decrease in the graphitic crystal size. Later, several Raman studies were carried out on various carbon materials. Cuesta et al. (79) tried to rationalize the dependence of Raman spectra on the degree of structural order in materials exhibiting a broad variation in graphitization. The band originally observed at 1355 cm^{-1} and designated as D band (after defects) has been shown to display a strong dependence in frequency and intensity on excitation energy whereas the characteristic band at 1585 cm^{-1} called G band (after graphite) remains practically independent (80). Matthews et al. (81) showed that the frequency of the related overtone of the D band, the so-called second-order G' band (observed at about 2700 cm^{-1} using 488 nm laser excitation) also shifts with changing laser energy. In spite of its early discovery, the origin of the D band is still controversial. Osswald et al. (82) observed in the Raman spectra of double-wall carbon nanotubes (DWNs) recorded with 514 nm laser excitation, a complete disappearance of the D band during heating. They conclude that the D band originates from amorphous carbon present in the sample and not from defects in the tube walls. But the decrease or disappearance has not been observed in MWNTs, where defects in tube walls generate a much stronger D band signal compared to DWNs. Chang et al. (83) observe that after annealing single-wall carbon nanotubes (SWNTs), the relative intensity of the D-band decreases slightly, indicating some removal of amorphous carbons. The authors also used Raman scattering for an evaluation of the state of dispersion of SWNTs in polystyrene and of the quality of the load transfer from the polymer matrix to the nanotubes.

As a typical example, Figure 12.15 shows the Raman spectra of an unfilled ethylene-propylene-diene rubber (EPDM). The Raman spectra of pure MWNTs, pure CB and of a EPDM / MWNTs composite are also given. The D, G and G' bands are respectively located at 1348 , 1577 and 2684 cm^{-1} in the Raman spectrum of the multi-wall carbon nanotubes. The Raman spectrum of pure carbon black (CB) remains dominated by the bands associated with the D and G modes at 1354 and 1589 cm^{-1} respectively, even when the carbons do not have particular graphitizing ordering (Figure 12.11). This fact has been widely discussed by Robertson (84) and Filik (85). Amorphous carbons are mixtures of sp^3 (as in diamond) and sp^2 (as in graphite) hybridised carbon. The π bonds formed by the sp^2 carbons being more polarisable than the σ bonds formed by the sp^3 carbons, the authors conclude that the Raman spectrum is dominated by the sp^2 sites.

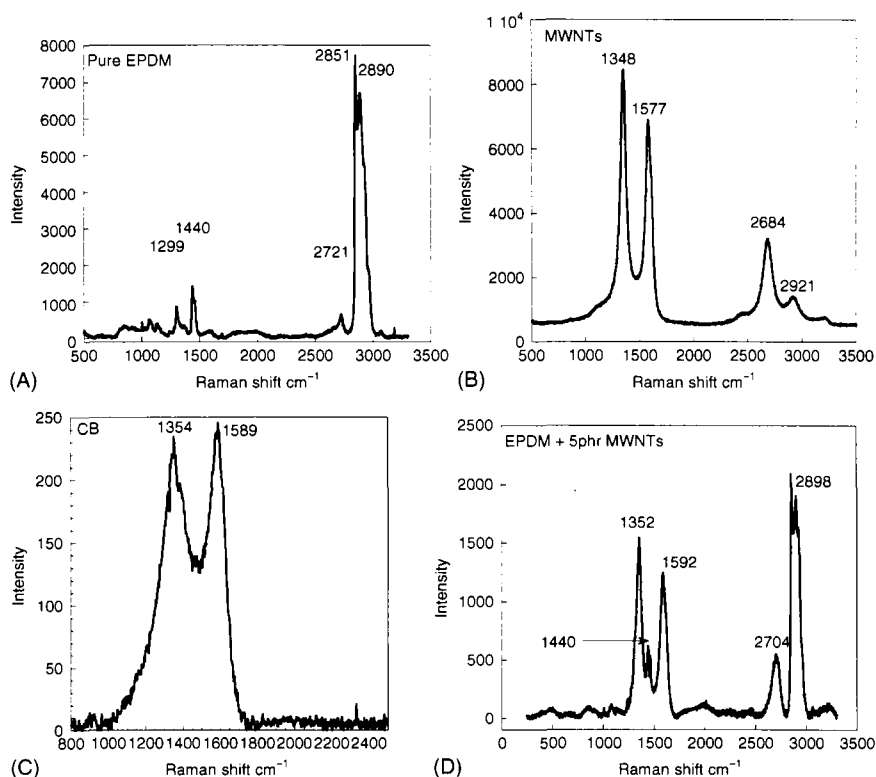


Figure 12.15. Raman spectra of pure polymer, pure MWNTs and CB and of a EPDM/MWNTs composite.

The G mode would not only mean “graphite” but would arise from the stretching vibration of any pair of sp^2 sites, whether in $\text{C}=\text{C}$ chains or in aromatic rings while the D mode would be associated with the breathing mode of sp^2 sites only in rings, not in chains. In a contribution reviewing recent achievements in characterization of carbon black aggregates – the aggregate being the mono-unit of carbon black that cannot be broken-, Gerspacher (86) shows that the shell surface of an aggregate is formed by graphitic crystallites and some regions rich in highly disordered structures that are referred to as amorphous carbon. The author assigns the two main peaks at 1300 and 1550 cm^{-1} to the crystallites and the shoulder observed around 1500 cm^{-1} to the amorphous regions on the CB surface.

Examination of the Raman spectra of EPDM filled with MWNTs, shows that the bands of MWNTs shifts to higher frequencies when carbon nanotubes are incorporated into the elastomeric matrix

(Figure 12.15). In the case of MWNTs, the shift to higher frequencies was explained by a disentanglement of the carbon nanotubes and a subsequent dispersion in the polymer as a consequence of polymer penetration into the bundles during solution mixing. An up-shift of 17 cm^{-1} for the G band, obtained on addition of 1 wt% MWNTs in a polyethylene matrix, was considered as a consequence of strong compressive forces associated with polymer chains on MWNTs (87).

The Raman spectra were recorded in the backscattering geometry on a Labram I (Jobin-Yvon, Horiba Group, France) microspectrometer in conjunction with a confocal microscope. To avoid any thermal photochemical effect, we have used a minimum intensity laser power on sample of $370\text{ }\mu\text{W}$ with the 514.5 nm incident line from an Ar-Kr laser from Spectra Physics. Detection was achieved with an air cooled CCD detector and a 1800 grooves/mm , giving a spectral resolution of 4 cm^{-1} . An acquisition time of 120 s was used for each spectrum. The confocal aperture was adjusted to $200\text{ }\mu\text{m}$ and a $50\times$ objective of 0.75 numerical aperture was used.

12.6 Thermal Stability

Thermogravimetric analysis (TGA) is widely used to study the thermal stability of a polymer and to evaluate the effect of adding filler particles on the thermal degradation of the elastomers.

Thermogravimetric analysis (TGA) was conducted using a TA Instrument (SDT Q600). Samples of weight around 6 and 8 mg were ramped at $10^\circ\text{C}/\text{mn}$ from room temperature to 800°C under nitrogen atmosphere with a flow rate of $100\text{ mL}/\text{min}$ and a purge time of 20 min .

A thermogravimetric analysis is performed in order to evaluate the effectiveness of adding the filler particles on the thermal properties of the composite.

TGA of unfilled NR and of MWNTs/composites are shown in Fig. 12.16. Pyrolysis occurs typically at about 377°C (temperature of the derivative peak: Figure 12.16b) for the neat polymer and produces a small percentage of residual weight arising most probably from some ingredients of formulation. The residual weight increases of course with the increasing amount of the CNT but the presence of carbon nanotubes does not show significant effect on the thermal stability of NR. One would expect a slower degradation of the polymer close to the nanotubes and thereby a delay

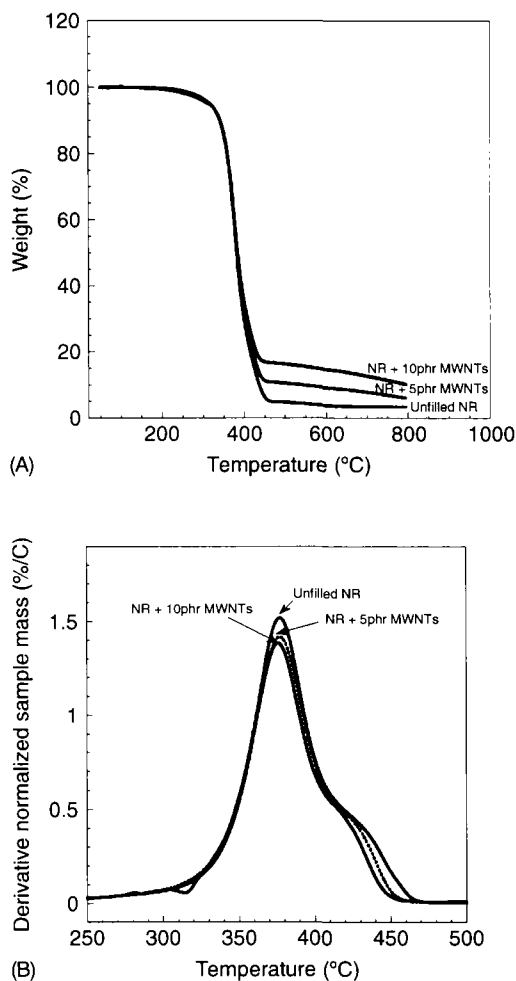


Figure 12.16. TGA thermograms of pure natural rubber (NR) and of NR composites, under a nitrogen atmosphere (a) and derivative mass loss rates (b).

in the overall polymer decomposition as in the case for clay fillers where the reduction of the pyrolysis rate has been attributed to barrier effects. No effect on the thermal stability was also found for PMMA/SWNTs composites (88) but measurements of the heat release have shown that the sample with relatively good nanotube dispersion burns much slower than the pure polymer. The formation of a continuous network structured layer from the tubes which acts as a thermal shield is the mechanism proposed by the authors for significant reduction in heat release and slowing down of thermal

degradation of the polymer. From this point of view, carbon nanotubes have potential as flame retardants but a good dispersion is required to modify the flammability properties of the composites.

12.7 Conclusions

This paper represents an overview of investigations carried out in carbon nanotube / elastomeric composites with an emphasis on the factors that control their properties. It is clear that the state of filler dispersion and the interfacial adhesion between the nanotube and the polymer matrix remain major issues to fully realize the reinforcing potential of CNTs. Carbon nanotubes have clearly demonstrated their capability as electrical conductive fillers in nanocomposites and this property has already been commercially exploited in the fabrication of electronic devices. The filler network provides electrical conduction pathways above the percolation threshold. The percolation threshold is reduced when a good dispersion is achieved. Significant increases in stiffness are observed. The enhancement of mechanical properties is much more important than that imparted by spherical carbon black or silica particles present in the same matrix at a same filler loading, thus highlighting the effect of the high aspect ratio of the nanotubes. In conclusion, although the full potential of nanotube composites has not been reached, encouraging results have been reported that build the foundation for years to come.

References

1. L. Bokobza, and O. Rapoport, *Journal of Applied Polymer Science*, Vol. 85, p. 2301, 2002.
2. L. Bokobza, *Macromolecular Materials and Engineering*, Vol. 289, p. 607, 2004.
3. L. Bokobza, *Journal of Applied Polymer Science*, Vol. 3, p.2095, 2004.
4. D.W. McCarthy, J.E. Mark, and D.W. Schaffer, *Journal of Polymer Science: Part B: Polymer Physics*, Vol. 36, p. 1167, 1998.
5. S. Kohjiya, K. Murakami, S. Iio, T. Tanahashi, and Y. Ikeda, *Rubber Chemistry and Technology*, Vol. 74, p. 16, 2001.
6. K. Yoshikai, T. Ohsaki, and M. Firukawa, *Journal of Applied Polymer Science*, Vol. 85, p. 2053, 2002.
7. A. Bandyopadhyay, M. De Sarkar, and A.K. Bhowmick, *Journal of Polymer Science: Part B: Polymer Physics*, Vol. 43, p. 2399, 2005.
8. L. Dewimille, B. Bresson, and L. Bokobza, *Polymer*, Vol. 46, p. 4135, 2005.

9. M. Arroyo, M.A. López-Manchado, and B.Herrero, *Polymer*, Vol. 44, p. 2447, 2003.
10. S. Varghese, and J. Karger-Kocsis, *Polymer*, Vol. 44, p. 4921, 2003.
11. S. Sadhu, and A.K. Bhowmick, *Journal of Applied Polymer Science*, Vol. 92, p. 698, 2004.
12. M. Liao, J. Zhu, H. Xu, Y. Li, and W. Shan, *Journal of Applied Polymer Science*, Vol. 92, p. 3430, 2004.
13. C. Gauthier, L. Chazeau, T. Prasse, and J.Y. Cavaillé, *Composites science and Technology*, Vol. 65, p. 335, 2005.
14. L. Bokobza, and J.-P. Chauvin, *Polymer*, Vol. 46, p. 4144, 2005.
15. L. Bokobza, A. Burr, G. Garnaud, M.Y. Perrin, and S. Pagnotta, *Polymer International*, Vol. 53, p. 1060, 2004.
16. M.A. López-Manchado, J. Biagiotti, L. Valentini, and J.M. Kenny, *Journal of Applied Polymer Science*, Vol. 92, p. 3394, 2004.
17. L. Bokobza, and M. Kolodziej, *Polymer International*, Vol. 55, p. 1090, 2006.
18. R. Andrews, and M.C. Weisenberger, *Current Opinion in Solid State and Materials Science*, Vol. 8, p. 31, 2004.
19. Y. Hu, O.A. Shenderova, Z. Hu, X.W. Padgett, and D.W. Brenner, *Reports on Progress in Physics*, Vol. 69, p. 1847, 2006.
20. M. Moniruzzaman, and K.I. Winey, *Macromolecules*, Vol. 39, p. 5194, 2006.
21. J.N. Coleman, U. Khan, W.J. Blau, and Y.K. Gun'ko, *Carbon*, Vol. 44, p. 1624, 2006.
22. L. Bokobza, *Polymer*, Vol. 48, p. 4907, 2007.
23. L. Bokobza, and N.-E. El Bounia, *Composite Interfaces*, Vol. 15, p. 9, 2008.
24. M. Kolodziej, L. Bokobza, and J.-L. Bruneel, *Composite Interfaces*, Vol. 14, p. 215, 2007.
25. A. Fakhru'l-Razi, M.A. Atieh, N. Girun, T.G. Chuah, M. El-Sadig, and D.R.A. Biak, *Composite Structures*, Vol. 75, p. 496, 2006.
26. S. Bhattacharyya, C. Sinturel, O. Bahloul, M.-L. Saboungi, S. Thomas and J.-P. Salvetat, *Carbon*, 46 (2008) 1037-1045
27. F. Cataldo, O. Ursini, and G. Angelini, *Fullerenes, Nanotubes and Carbon Nanostructures*, Vol. 17, p. 38, 2009.
28. A. De Falco, S. Goyanes, G.H. Rubiolo, I. Mondragon, and A. Marzocca, *Applied Surface Science*, Vol. 254, p. 262, 2007.
29. L. Bokobza, and C. Belin, *Journal of Applied Polymer Science*, Vol. 105, p. 2054, 2007.
30. F. Cataldo, O. Ursini, and G. Angelini, *Fullerenes, Nanotubes and Carbon Nanostructures*, Vol. 17, p. 55, 2009.
31. L.D. Perez, M.A. Zuluaga, T. Kyu, J.E. Mark, and B.L. Lopez, *Polymer Engineering and Science*, Vol. 49, p. 866, 2009.
32. A. Das, K.W. Stöckelhuber, R. Jurk, M. Saphiannikova, J. Fritzsche, H. Lorenz, M. Klüppel, and G. Heinrich, *Polymer*, Vol. 49, p. 5276, 2008.
33. F. Barroso-Bujans, R. Verdejo, M. Pérez-Cabero, S. Agouram, I. Rofriguez-Ramos, A. Guerrero-Ruiz, and M.A. López-Manchado, *European Polymer Journal*, Vol. 45, p. 1017, 2009.
34. M.D. Frogley, D.R. Ravich, and H.D. Wagner, *Composites Science and Technology*, Vol. 63, p. 1647, 2003.

35. I.-S. Park, K.J. Kim, J.-D. Nam, J. Lee, and W. Yim, *Polymer Engineering and Science*, Vol. 47, p. 1396, 2007.
36. J.X. Xu, M. Razeeb, and S. Roy, *Journal of Polymer Science: Part B: Polymer Physics*, Vol. 46, p. 1845, 2008.
37. A. Beigbeder, M. Linares, M. Devalckenaere, P. Degée, M. Claes, D. Beljonne, R. Lazzaroni, and P. Dubois, *Advanced Materials*, Vol. 20, p. 1003, 2008.
38. L. Bokobza, and M. Rahmani, *Kautschuk Gummi Kunststoffe*, Vol. 62, p. 112, 2009.
39. L. Bokobza, *Silicon*, Vol. 1, p. 141, 2009.
40. D. Qian, E.C. Dickey, R. Andrews, and T. Rantell, *Applied Physics Letters*, Vol. 76, p. 2868, 2000.
41. B. Safadi, R. Andrews, and E.A. Grulke, *Journal of Applied Polymer Science*, Vol. 84, p. 2660, 2002.
42. J.Q. Pham, C.A. Mitchell, J.L. Bahr, J.M. Tour, R. Krishnamoorti, and P.F. Green, *Journal of Polymer Science: Part B: Polymer Physics*, Vol. 41, p. 3339, 2003.
43. F. Barroso-Bujans, R. Verdejo, M. Pérez-Cabero, A. Guerrero-Ruiz, and M.A. López-Manchado, *European Polymer Journal*, Vol. 45, p. 1017, 2009.
44. S. Bal, *Journal of Scientific and Industrial Research*, Vol. 66, p. 752, 2007.
45. R. Schueler, J. Petermann, K. Schulte, and H.-P. Wentzel, *Macromol. Symp.*, Vol. 104, p. 261, 1996.
46. C. Klason, D.H. McQueen, and J. Kubát, *Macromol. Symp.*, Vol. 108, p. 247, 1996.
47. L. Karásek, B. Meissner, S. Asai, and M. Sumita, *Polymer Journal*, Vol. 28, p. 121, 1996.
48. L. Flandin, A. Chang, S. Nazarenko, A. Hiltner, and E. Baer, *Journal of Applied Polymer Science*, Vol. 76, p. 894, 2000.
49. Z. Li, J. Zhang, and S. Chen, *Journal of Electrostatics*, Vol. 67, p. 73, 2009.
50. W. Thongruang, C.M. Balik, and R.J. Spontac, *Journal of Polymer Science: Part B: Polymer Physics*, Vol. 40, p. 1013, 2002.
51. L. Bokobza, M. Rahmani, C. Belin, J.-L. Bruneel, and N.-E. El Bounia, *Journal of Polymer Science: Part B: Polymer Physics*, Vol. 46, p. 1939, 2008.
52. P.-C. Ma, M.-Y. Liu, H. Zhang, S.-Q. Wang, R. Wang, K. Wang, Y.-K. Wong, B.-Z. Tang, S.-H. Hong, K.-W. Paik, and J.-K. Kim, *Applied Materials & Interfaces*, Vol. 1, p. 1090, 2009.
53. N.C. Das, T.K. Chaki, and D. Khastgir, *Polymer International*, Vol. 51, p. 156, 2002.
54. K. Yamaguchi, J.J.C. Busfield, and A.G. Thomas, *Journal of Polymer Science: Part B: Polymer Physics*, Vol. 41, p. 2079, 2003.
55. J.J.C. Busfield, A.G. Thomas, and K. Yamaguchi, *Journal of Polymer Science: Part B: Polymer Physics*, Vol. 42, p. 2161, 2004.
56. G. Kraus, *Reinforcement of Elastomers*, Wiley, New York, 1965.
57. E.M. Dannenberg, *Rubber Chemistry and Technology*, Vol. 48, p. 410, 1975.
58. M.P. Wagner, *Rubber Chemistry and Technology*, Vol. 49, p. 703, 1976.
59. A. Voet, *Journal of Polymer Science : Macromolecular Reviews*, Vol. 15, p. 327, 1980.
60. D.C. Edwards, *Journal of Materials Science*, Vol. 25, p. 4175, 1990.
61. S. Ahmed, and F.R. Jones, *Journal of Materials Science*, Vol. 25, p. 4933, 1990.

62. S. Wolff, *Rubber Chemistry and Technology*, Vol. 69, p. 325, 1996.
63. E. Guth, *J. Appl. Phys.*, Vol. 16, p. 20, 1945.
64. J.C. Halpin, *Journal of Composite Materials*, Vol. 3, p. 732, 1969.
65. G. Kraus, *Advances in Polymer Science*, Vol. 8, p. 155, 1971.
66. V.M. Litvinov, Poly(dimethylsiloxane chains at a silica surface. In: *Organosilicon Chemistry II, From molecules to Materials*, N. Auner and J. Weiss, Editors, Weinheim: VCH, pp.779-814, 1996.
67. D. Fragiadakis, P. Pissis, and L. Bokobza, *Polymer*, Vol. 46, p. 6001, 2005.
68. M.A. López-Manchado, J. Biagiotti, L. Valentini, and J.M. Kenny, *Journal of Applied Polymer Science*, Vol. 92, p. 3394, 2004.
69. C. Gauthier, L. Chazeau, T. Prasse, and J.Y. Cavaille, *Composites Science and Technology*, Vol. 65, p. 335, 2005.
70. T. Ramanathan, H. Liu, and L.C. Brinson, *Journal of Polymer Science: Part B: Polymer Physics*, Vol. 43, p. 2269, 2005.
71. P. Pötschke, T.D. Fornes, and D.R. Paul, *Polymer*, Vol. 43, p. 3247, 2002.
72. W. Ding, A. Eitan, F.T. Fisher, X. Chen, D.A. Dikin, R. Andrews, L.C. Brinson, L.S. Schadler, and R.S. Ruoff, *Nano Letters*, Vol. 3, p. 1593, 2003.
73. F.H. Gojny, and K. Schulte, *Composites Science and Technology*, Vol. 64, p. 2303, 2004.
74. A. Allauoui, and N. El Bounia, *eXPRESS Polymer Letters*, Vol. 3, p. 588, 2009.
75. M.I. Aranguren, *Polymer*, Vol. 39, p. 4897, 1998.
76. M. Patel, P.R. Morrell, and A.R. Skinner, *Macromolecular Symposia*, Vol. 180, p. 109, 2002.
77. S. Besbes, I. Cermelli, L. Bokobza, L. Monnerie, I. Bahar, B. Erman, and J. Herz, *Macromolecules*, Vol. 25, p. 1949, 1992.
78. F. Tuinstra, and J.L. Koenig, *Journal of Chemical Physics*, Vol. 53, p. 1126, 1970.
79. A. Cuesta, P. Dhamelincourt, J. Laureyns, A. Martínez-Alonso, and J.M.D. Tascón, *Carbon*, Vol. 32, p. 1523, 1994.
80. I. Pócsik, M. Hundhausen, M. Koós, and L. Ley, *Journal of Non-Crystalline Solids*, Vol. 227, p. 1083, 1998.
81. M.J. Matthews, M.A. Pimenta, G. Dresselhaus, M.S. Dresselhaus, and M. Endo, *Physical Review B*, Vol. 59, p. R6585, 1999.
82. S. Osswald, E. Flahaut, H. Ye, and Y. Gogotsi, *Chemical Physics Letters*, Vol. 402, p. 422, 2005.
83. T.-E. Chang, A. Kisliuk, S.M. Rhodes, W.J. Brittain, and A.P. Sokolov, *Polymer*, Vol. 47, p. 7740, 2006.
84. J. Robertson, *Materials Science and Engineering*, Vol. R37, p. 129, 2002.
85. J. Filik, *Spectroscopy Europe*, Vol. 17, p. 10, 2005.
86. M. Gerspacher, *Kautschuk Gummi Kunststoffe*, Vol. 59, p. 609, 2006.
87. T. McNally, P. Pötschke, P. Halley, M. Murphy, D. Martin, S.E.J. Bell, G.P. Brennan, D. Bein, P. Lemoine, and J.P. Quinn, *Polymer*, Vol. 46, p. 8222, 2005.
88. T. Kashiwagi, F. Du, K.I. Winey, K.M. Groth, J.R. Shields, S.P. Bellayer, H. Kim, and J.F. Douglas, *Polymer*, Vol. 46, p. 471, 2005.

Specific Interactions Induced Controlled Dispersion of Multiwall Carbon Nanotubes in Co-Continuous Polymer Blends

Suryasarathi Bose, Arup R. Bhattacharyya,
Rupesh A. Khare and Ajit R. Kulkarni

*Department of Metallurgical Engineering and Materials Science,
Indian Institute of Technology Bombay, Powai, Mumbai-400076, India*

Abstract

Blends of polyamide6/acrylonitrile-butadiene-styrene copolymer (PA6/ABS) with multiwall carbon nanotubes (MWNTs) were prepared by melt mixing in order to develop conducting composites. To control the dispersion and to selectively restrict MWNTs in the PA6 phase of the blends, MWNTs were pre-treated with two different modifiers viz. sodium salt of 6-amino hexanoic acid and octadecyl tri-phenyl phosphonium bromide. These modifiers were found to differ in their molecular length scales and architectures and could play a key role in debundling the MWNTs mediated by specific interactions like 'cation- π ' or ' π - π ' with the extended delocalized ' π -electron' clouds of MWNTs. Further, these modifiers could also take part in melt-interfacial reactions and facilitate selective localization of MWNTs. Raman spectroscopy and transmission electron microscopy has been performed to get insights into the role of these modifiers in debundling the MWNTs. The state of dispersion of MWNTs was assessed using AC electrical conductivity measurements, scanning electron microscopy and solution experiments. This strategy was further extended to PA6 based multi-component blends.

Keywords: blends, MWNTs, electrical conductivity, morphology.

13.1 Introduction

Blending of polymers is an economic way of preparing new materials with the existing polymers. The final properties of a multi-phase

blend typically depend on the constituent blend components, the interface and the morphology developed during processing. Most polymer blends are immiscible which gives rise to wide range of microstructures during processing. One of the classical strategies to reduce the interfacial tension between the components and stabilize the morphology during processing is employing a suitable compatibilizer like block copolymers (1). Alternatively, the concept of using nanofillers to stabilize the blends morphology has received a great deal of interest in recent years (2). Besides stabilizing the morphology of the blends, the fillers also offer a synergistic combination of properties.

The discovery of carbon nanotubes (CNTs) promises new opportunities in the material world especially in the field of polymer based nanocomposites (3). Large aspect ratio (L/D , where L is the length and D is the diameter of CNTs) enables CNTs to form a 'network-like' structure corresponding to percolation threshold. This also enables CNTs to improve the bulk electrical conductivity of the nanocomposites at a much lower content. However, CNTs exist as either ropes/bundles (in case of single wall carbon nanotubes) or as entangled network (in case of multiwall carbon nanotubes, MWNTs) and hence its effective dispersion in the matrix dictates the overall performance of the nanocomposites. Over the years different approaches have been attempted to debundle the CNTs and render homogeneous dispersion in the matrix polymer. These approaches can be broadly classified into two categories; covalent and non-covalent pre-treatments. The former involves covalent attachment of functional groups on the CNT surface by acid treatments and the later enables adsorption of molecules with hierarchical structure on the CNT surface (4,5). Both the opportunities and the limitations of these pre-treatments are widely addressed in the literature. For instance, improved interactions between the functional moieties on the CNT surface with the available functional groups in the matrix enable the covalent treatment to result in substantial improvements in the structural properties of the nanocomposites (6). On the other hand this strategy also perturbs the extended π -conjugation of electrons which results in loss of intrinsic electronic properties of CNTs (7). Alternatively, the non-covalent approach provides a synergistic combination in the properties as it preserves the integrity of the tubes and further enhances the interfacial adhesion on account of various levels of interaction with the polymer chains. Hence a perfect balance in these approaches would result in optimal macroscopic properties.

Selective filling of conducting fillers in one of the phases or at the interface of co-continuous binary immiscible blends has generated profound interest especially in context to designing conducting polymer composites. In addition, it has been reported that selective localization of filler in co-continuous blends also broadens the phase inversion regime and further manifests in finer ligament size of the phases in binary blends (8). The changes in the phase morphology of the blends typically depend on the concentration, shape, type and dimensions of the filler. It is well understood that selective localization of the filler in binary blends typically depends on various factors like thermodynamic, kinetic and melt viscosity of the components (9,10). For instance, thermodynamic factors govern the localization of filler in a particular phase depending on the differences in surface free energy (SFE) values between the matrix and the filler whereas kinetic factors dominate the migration of the filler towards the preferred phase during processing. The melt viscosity factor promotes the localization of filler in less viscous phase in the blends. However, there are certain evidences in the literature reporting that the filler has been found to localize in a particular phase though not favourable by either one of these factors (11). In context to polymer blends with CNTs, it has been realized that selectively restricting them at the interface is quite intricate and with few exceptions (12) they are mostly found to be localized in one of the phases of the blends (13). This is presumably due to large length scales of CNTs which are often larger than the phase dimensions of the blends.

Two issues deserve attention in this chapter. Effective disentanglement of MWNTs prior to compounding and selective localization in a specific phase during processing in 50/50 polyamide6/acrylonitrile-butadiene-styrene (PA6/ABS) blends. To accomplish this we employed a unique strategy viz. specific interaction in combination with melt-interfacial reaction. This was facilitated by utilizing two modifiers viz., sodium salt of 6-amino hexanoic acid (Na-AHA) and octadecyl tri-phenyl phosphonium bromide (OTPB), which had a difference in their molecular length scales and architectures. It is expected that both these modifiers can play a key role in debundling the MWNTs mediated by specific interactions like 'cation- π ' or ' π - π ' with the extended delocalized ' π -electron' clouds of MWNTs. Further, these modifiers can also take part in melt-interfacial reactions with the available functional groups of PA6 during melt-mixing and selectively restrict the MWNTs in the

PA6 phase of the blends. This approach was further extended to PA6 based ternary and quaternary blends in an attempt to find the applicability of this strategy. Raman spectroscopy and transmission electron microscopy (TEM) have been performed to get more insights into the role of these modifiers in debundling the MWNTs. AC electrical conductivity measurements have been carried out to assess the state of dispersion of MWNTs in the blends. Further, the phase microstructures and the localization of MWNTs in the blends have been investigated using scanning electron microscopy (SEM).

13.2 Experimental

13.2.1 Materials

Polyamide6 (PA6) was obtained from GSFC, Gujarat, India (Gujlon M28RC, relative viscosity 2.8, M_v is 38642 in 85% formic acid). Polypropylene (PP, H110MA) and high density polyethylene (HDPE, Relene M60075) was obtained from Reliance Industries Ltd., Mumbai, India. ABS copolymer (Absolac-120, with composition as: acrylonitrile 24 wt %, styrene 59.5 wt % and rubber content 16.5 wt %) was obtained from Bayer India Ltd. Continuous carbon vapor deposition (CCVD) synthesized purified multiwall carbon nanotubes (p-MWNTs) were obtained from Nanocyl CA Belgium (NC-3100, average length: 1.5 μm , average diameter: 9.5nm, purity>95 %).

13.2.2 Preparation of the Modifiers

6-aminohexanoic acid (AHA) (Sigma Aldrich, M_w = 132.18; purity: 98%) was neutralized using sodium hydroxide (Sisco Research Laboratories, India, purity: 98%) to obtain Na-AHA. The following procedure was adopted to prepare Na-AHA modified MWNTs. p-MWNTs were initially sonicated in distilled water for 20 min and then required amount of Na-AHA solution was added to p-MWNTs (corresponding to 1:1, wt/wt) and again sonicated for 10 min. The Na-AHA modified MWNTs solution was then subjected to evaporation. The obtained dry powder was then left in a vacuum oven at 80°C to ensure the complete removal of moisture. OTPB was synthesized by reacting triphenyl phosphine with the corresponding alkyl halides. In a round bottom flask n-octadecyl bromide (16.65 gm,

0.05 mol) and triphenyl phosphine (15.71 gm, 0.06 mol) were mixed at 80°C for 10 hr under nitrogen atmosphere. Final product obtained was washed with petroleum ether and dried overnight in a vacuum oven at 50°C. OTPB modified MWNTs were prepared by sonicating p-MWNTs and OTPB in required ratios (1:1 wt/wt) in ethanol for 15 min. Subsequently, excess ethanol was evaporated. In order to check the thermal stability of the modifiers we carried out the thermal gravimetric analysis (TGA) of both Na-AHA and OTPB. TGA analysis showed that Na-AHA and the OTPB were stable up to 375°C and 290°C respectively.

13.2.3 Melt Blending

Neat blends of 50/50 PA6/ABS and blends with various MWNTs were prepared by melt-mixing in a conical twin-screw microcompounder (Micro 5, DSM Research, Netherlands) at 260°C with a rotational speed of 150 rpm for 15 min. A specific mixing sequence was adopted where p-MWNTs were melt mixed with PA6 initially (for 10 min) followed by ABS (without interrupting the mixing process). Few compositions involving ternary (40/30/30, PA6/PP/ABS) and quaternary blends (30/25/25/20, PA6/PP/ABS/HDPE) with various MWNTs were also prepared by melt-mixing technique. For these compositions, masterbatches of PA6 and MWNTs (without or with pre-treated OTPB) were prepared (under the same extrusion conditions mentioned above except for the mixing time which was fixed at 10 min) prior to compounding with the other constituents. Required amount of the masterbatch was then subsequently diluted further in the next step of melt mixing under the same extrusion conditions mentioned above except for the mixing time which was fixed at 10 min. All the components were pre-dried in vacuum oven at 80°C for at least 24 h. All the experiments were performed under nitrogen atmosphere in order to prevent oxidative degradation of the components. Injection-moulded samples (according to ASTM D 638, Type V) were prepared using mini injection-moulding machine from DSM Research Netherlands. The injection-moulding parameters maintained for all the compositions were injection pressure 3 bar, melt temperature 260°C, mold temperature 60°C, holding time 60 sec and cooling time 2–3 min. The codes with detail compositions and the compounding procedure adopted during melt-mixing used in this study are shown in Table 13.1.

Table 13.1. Sample codes and compositions

Sample	Codes
Purified multiwall carbon nanotubes	p-MWNTs
Polyamide 6	PA6
Acrylonitrile butadiene styrene	ABS
Polypropylene	PP
High density polyethylene	HDPE
50/50 blends of PA6 and ABS	N50A50
50/50 blends of PA6 and ABS with 2 wt% of p-MWNTs	N50T2A50*
40/30/30 PA6/PP/ABS blends with 2 wt% p-MWNTs by masterbatch dilution technique	N40P30A30T2 ⁺
30/25/25/20 PA6/PP/ABS/HDPE blends with 2 wt% p-MWNTs by masterbatch dilution technique	N30P25A25E20T2 ⁺
50/50 PA6/ABS blends with 2 wt% MWNTs (pre-treated with Na-AHA in 1:1 wt ratio)	N1M1T2A*
50/50 PA6/ABS blends with 2 wt% MWNT (pre-treated with OTPB in 1:1 wt ratio)	N1O1T2A*
40/30/30 PA6/PP/ABS blends with 2 wt% MWNT (pre-treated with OTPB in 1:1 wt ratio)	N40P30A30O1T2 ⁺
30/25/25/20 PA6/PP/ABS/HDPE blends with 2 wt% MWNT (pre-treated with OTPB in 1:1 wt ratio)	N30P25A25E20O1T2 ⁺

* by specific mixing sequence

* by masterbatch dilution technique

13.2.4 Characterization

Raman spectroscopy was performed using Jobin Yvon (HR 800 micro-Raman) on powder samples of MWNT and solid mixtures of MWNT/modifiers over a scanning range of 200 to 2000 cm^{-1} with incident laser excitation wavelength of 514 nm. Transmission electron microscopy (TEM) analysis was performed with Philips CM 200, operated at 200 kV. FTIR spectroscopic analysis was carried out with Nicolet, MAGNA 550 for composite powder samples using KBr pellets in the scanning range of 400 to 4000 cm^{-1} .

The AC electrical conductivity measurements were performed on the injection molded samples (across the thickness) in the frequency range between 10^{-1} and 10^6 Hz using Alpha high resolution analyzer coupled to a Novocontrol interface (broad band dielectric converter). The phase morphology of the blends were investigated by scanning electron microscopy (SEM). Extrudate samples were cryofractured in liquid nitrogen and etched with either formic acid or tetrahydrofuran (THF) to selectively etch the PA6 and the ABS phases respectively. The etched surface was gold sputtered to avoid charging of the sample. These samples were then observed under SEM using Hitachi S3400N.

13.3 Results and Discussion

13.3.1 Specific Interactions: Spectroscopic and Microscopic Evidences

Raman spectroscopy is an important tool to get insights into the existence of specific interactions between the modifiers and the MWNTs. The p-MWNTs displayed two characteristic peaks, the first at $\sim 1345\text{ cm}^{-1}$ assigned to the D band and derived from disordered graphite structures and the second centered at $\sim 1585\text{ cm}^{-1}$ assigned to the G band and associated with tangential C–C bond stretching (14). The strong up-shifts in the G-band intensities in the solid mixtures of MWNT and the modifiers manifest the existence of specific interactions (Figure 13.1). Such observations were also reported for poly(acrylic acid) wrapped MWNT where up shifts in G band intensity were correlated with the hydrophilic attractions between poly(acrylic acid) and MWNTs (15). It is worthy to mention here that with increase in the molecular length scale of the modifiers the peak intensity related to G-band increases. This is manifested in higher peak intensity of the G-band in case of OTPB modified MWNTs as compared to Na-AHA modified MWNTs.

In order to study the suspension stability of various MWNTs investigated here the following procedure was followed. Fixed amounts of MWNTs were added to each vial containing deionized water, resulting in a fixed concentration of 20 mg/L and were sonicated for 20 min. Figure 13.2 illustrates the TEM of various MWNTs and the inset shows the photographs of the vials (taken more than 2

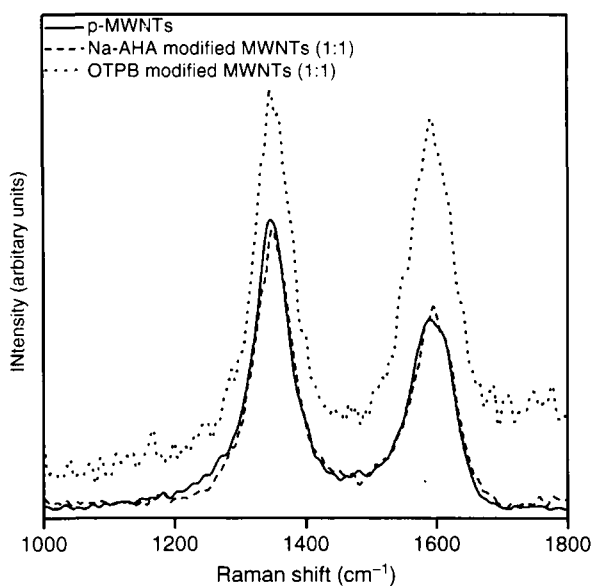


Figure 13.1. Raman spectra for various MWNTs.

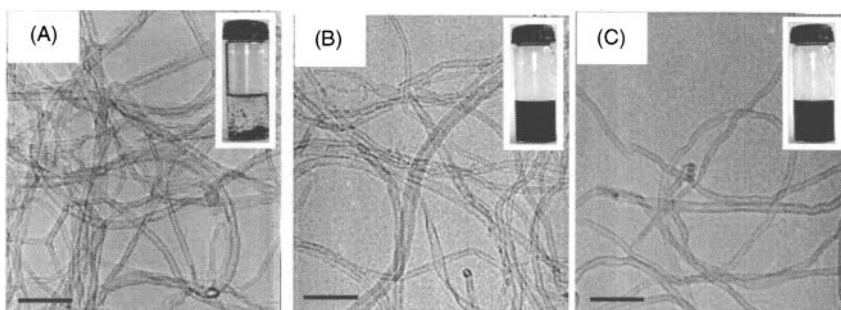


Figure 13.2. TEM images of a) p-MWNTs; 1:1 mixtures of b) Na-AHA modified MWNTs; c) OTPB modified MWNTs (scale bar: 100 nm). Inset showing the dispersion of (1:1) respective mixtures of modifier/MWNT in deionized water following sonication.

weeks after the initial sonication process) of the respective MWNTs solution. From the TEM micrographs of p-MWNTs (Figure 13.2a) one can clearly observe a highly entangled 'network-like' structure whereas in case of the modified MWNTs (at the same scale) a substantial exfoliation can be seen in case of Na-AHA (Figure 13.2b) and OTPB modified MWNTs (Figure 13.2c). The respective solutions (see inset

of Figure 13.2) clearly support the state of dispersion of MWNTs as observed from TEM as well. The vial representing p-MWNTs clearly demonstrate the aggregated nature of MWNTs with largely settled at the bottom of the vial (see inset of Figure 13.2a). In case of Na-AHA modified MWNTs (see inset of Figure 13.2b), though the solution appears to be black similar to OTPB modified MWNTs (see inset of Figure 13.2c), large amount of MWNTs are settled at the bottom of the vial (difficult to distinguish from this figure). This presumably indicates a mixture of smaller bundles together with few individual tubes in case of Na-AHA modified MWNTs as compared to OTPB modified MWNTs.

13.3.2 AC Electrical Conductivity Measurements: Assessing the State of Dispersion of MWNTs

Figure 13.3a shows the frequency dependent AC electrical conductivity of 50/50 PA6/ABS blends with p-MWNTs and MWNTs modified with different modifiers. The AC electrical conductivity increased linearly with frequency for control PA6 as well as for blends with 2 wt% p-MWNTs. On incorporating Na-AHA and OTPB modified MWNTs (2 wt%, 1:1) the electrical conductivity remains constant up to a critical frequency (ω_c), above which the conductivity increased linearly with frequency manifesting in the formation of percolating 'network-like' structure at this concentration. This is consistent with the 'Jonscher's Universal Power Law' behavior for frequency dependent conductivity of solids (16). It is evident that blends with OTPB modified MWNTs showed orders of magnitude higher electrical conductivity as compared to both Na-AHA and p-MWNTs. This explains clearly the role of OTPB in efficiently disentangling the MWNTs aggregates and facilitating 'network-like' structure in the blends. This is further supported by substantial increase in ω_c . It is worth pointing out that these observations are closely related to the molecular length scales and the architectures of the modifiers investigated here. It is apparent that the large organic tail length of OTPB facilitated in more efficient debundling of MWNTs as compared to Na-AHA and manifested in higher electrical conductivity in the blends at a fixed concentration of MWNTs. In order to get more insight into the type of conduction mechanism in the composites, we analyzed the charge transport properties obtained by fitting the power law equation ($\sigma_{AC} = \sigma_{DC} + A\omega^n$, $0 < n < 1$; A is the constant dependent on the temperature and n

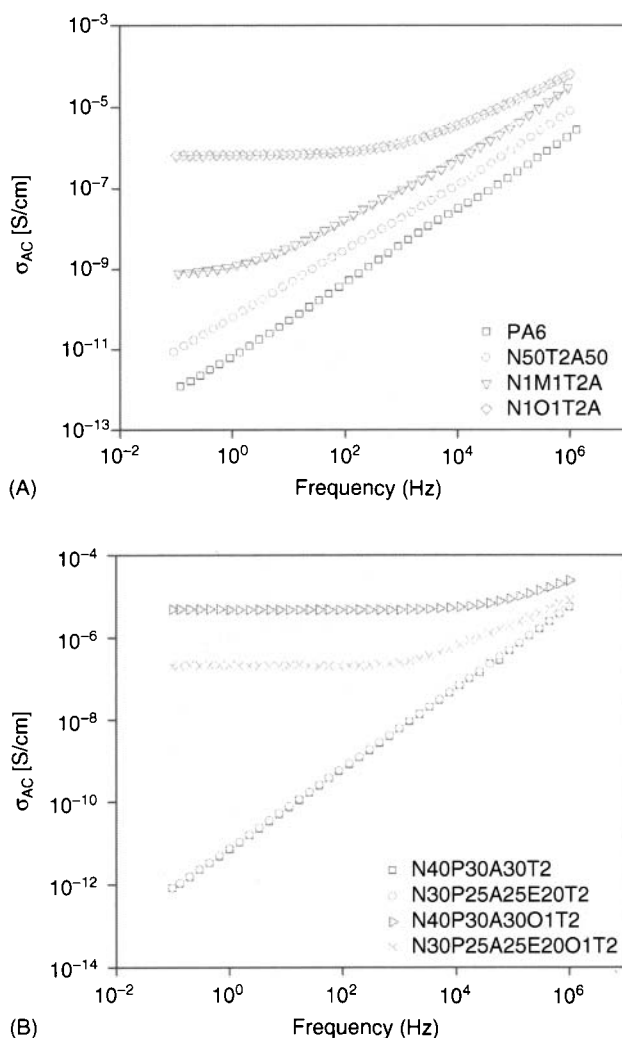


Figure 13.3. AC electrical conductivity of a) 50/50 PA6/ABS blends; b) multi-component blends with various MWNTs.

is an exponent dependent on both frequency and temperature, solid lines in Figure 13.3). It has been reported that the value of 'n' in the range of $0.8 < n < 1.0$ characterizes tunneling/hopping mechanism of charge transfer in a disordered material (17). The value of 'n' in case of blends with Na-AHA modified MWNT is close to 0.83 indicating the charge transfer by either hopping or tunneling mechanism whereas the value of 'n' in case of blends with OTPB lies in the range of 0.7 which indicates charge transfer through polarization effects

between small clusters of MWNTs. In the next section we closely analyze the morphological and spectroscopic details which would provide further insights into the state of dispersion of MWNTs in the blends and possible interactions between the modified MWNTs and the polymer chains.

In an attempt to further extend this strategy to PA6 based multicomponent blends, we prepared few compositions of ternary (40/30/30, PA6/PP/ABS) and quaternary (30/25/25/20, PA6/PP/ABS/HDPE) blends involving OTPB modified MWNTs. Instead of directly compounding the modified MWNTs with the components, we employed masterbatch dilution approach which is an often used technique to disperse filler in multicomponent systems. For this purpose, we prepared a masterbatch of OTPB modified MWNTs with PA6 and subsequently diluted in the multicomponent blends. Figure 13.3b shows the AC electrical conductivity measurements as a function of frequency for multicomponent blends with OTPB modified MWNTs prepared by masterbatch dilution approach. For comparison, we also prepared two compositions viz. ternary blends (40/30/30, PA6/PP/ABS/HDPE) and quaternary blends (30/25/25/20, PA6/PP/ABS/HDPE) with p-MWNTs utilizing masterbatch dilution technique. Both these compositions showed insulating behavior even when compounded by masterbatch dilution technique. This observation clearly suggests that without any pre-treatment the MWNTs are rather dispersed as aggregates and affect adversely the bulk electrical conductivity of the system. The multicomponent blends with OTPB modified MWNTs showed orders of magnitude higher conductivity as compared to blends with p-MWNTs with a substantial increase in ω_c . In multicomponent blends the continuity of MWNT rich phase dictates the overall conductivity of the blends. From the morphological analysis we found that the PA6 phase was continuous in both ternary and the quaternary blends with OTPB modified MWNTs (discussed in detail in ref. (18)). In this context, the slight decrease in conductivity in quaternary blends as compared to ternary blends have been correlated with the continuity of MWNTs rich phase (here PA6) (18).

13.3.3 Phase Morphology and Selective Localization of MWNTs in the Blends

SEM of cryofractured and THF etched surfaces of 50/50 PA6/ABS blends with or without MWNTs are illustrated in Figure 13.4.

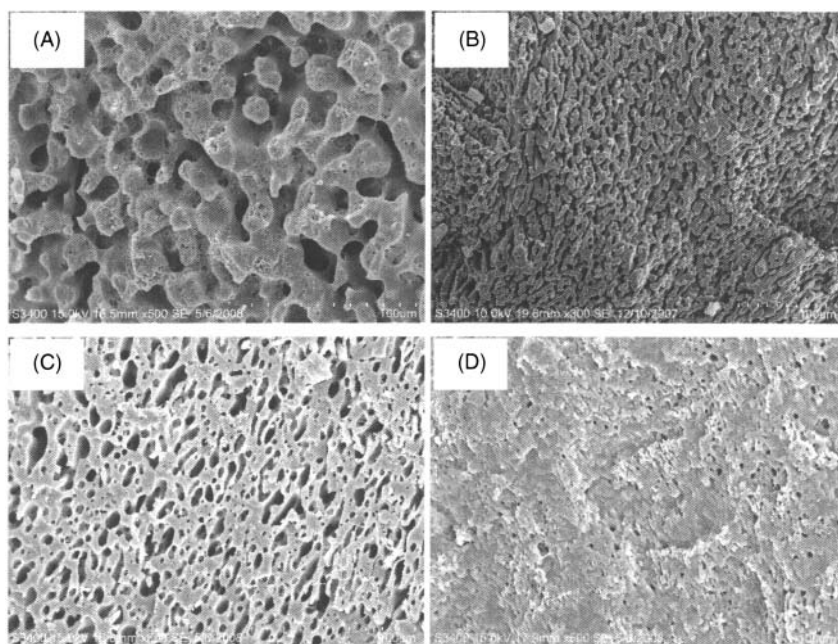


Figure 13.4. SEM micrographs of a) 50/50 PA6/ABS blends; blends with 2 wt% b) p-MWNTs; c) Na-AHA modified MWNTs (1:1) and d) OTPB modified MWNTs (1:1).

50/50 PA6/ABS blends exhibit coarse co-continuous morphology (see Figure 13.4a); a characteristic of incompatible blends. In addition, one can also observe sub-inclusions of ABS in the PA6 ligaments. Addition of MWNT results in significant change in the morphology of the blends. Blends with MWNTs (either modified or p-MWNTs) reveal much finer co-continuous morphology. Such changes are associated with either the changes in the melt viscosity of the constituents or the interfacial tension between the components. Interestingly, incorporating Na-AHA modified MWNTs resulted in a sea-island type of morphology (Figure 13.4c) whereas blends with OTPB modified MWNTs showed significant refinement in the phase morphology (see Figure 13.4d). Figure 13.5 shows higher magnification SEM images of 50/50 PA6/ABS blends with p-MWNTs (Figure 13.5a), Na-AHA modified MWNTs (Figure 13.5b) and OTPB modified MWNTs (Figure 13.5c). One can clearly observe MWNTs (as white dots) in the remaining PA6 phase in both 50/50 PA6/ABS blends with p-MWNTs and Na-AHA modified MWNTs. Interestingly blends with OTPB modified MWNTs show a hierarchical 'network-like' structure of MWNTs in the remaining

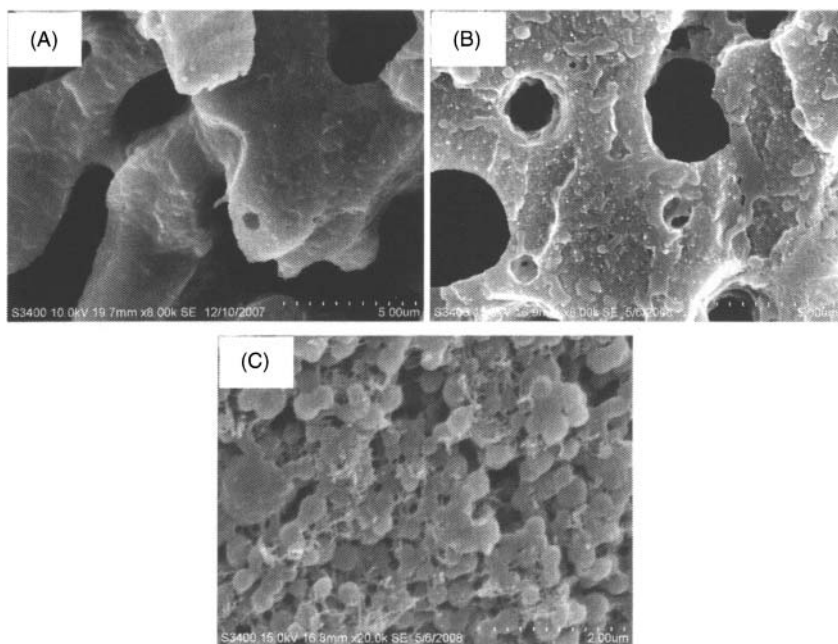


Figure 13.5. High magnification SEM micrographs of 50/50 PA6/ABS blends with 2 wt% a) p-MWNTs; b) Na-AHA modified MWNTs (1:1) and c) OTPB modified MWNTs (1:1).

PA6 phase of the blends (see Figure 13.5c). These morphological observations can be well correlated with the observed changes in the AC electrical conductivity measurements where OTPB modified MWNTs showed dramatic improvements as compared to p-MWNTs and Na-AHA modified MWNTs.

Figure 13.6a shows the SEM of cryofractured and etched (with THF and xylene to remove the ABS and PP phases respectively) surfaces of ternary blends with OTPB modified MWNTs. Figure 13.6b shows the SEM of cryofractured and etched (with THF and hot xylene to remove ABS, PP and HDPE phases respectively) surfaces of quaternary blends. In both these SEM images one can clearly observe the remaining continuous PA6 phase. Further, the strands were observed to be intact even after extracting ABS and PP (in case of ternary blends); and ABS, PP and HDPE (in case of quaternary blends). This clearly manifests the co-continuous nature of the blends. The morphologies of the multicomponent blends with OTPB modified MWNTs and the solution experiments are discussed in detail in ref. 18. Both the ternary and the quaternary

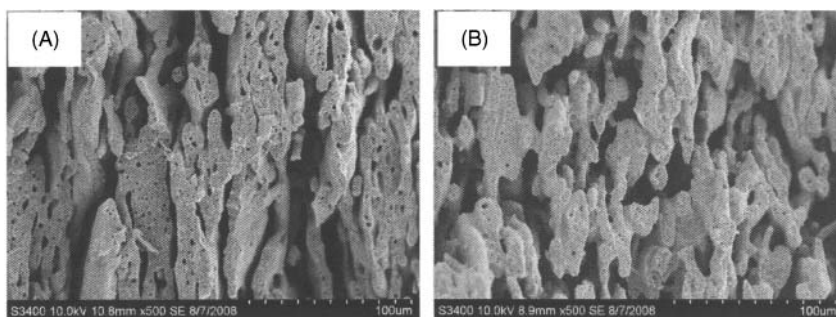


Figure 13.6. SEM micrographs of a) ternary 40/30/30 PA6/PP/ABS; b) quaternary 30/25/25/20 PA6/PP/ABS/HDPE blends.

blends with OTPB modified MWNTs also showed co-continuous type of microstructure with MWNTs selectively localized in the PA6 phase. However, the % continuity of the PA6 phase has been observed to be slightly lower in quaternary blends as compared to the ternary blends and this presumably resulted in a moderate decrease in the bulk electrical conductivity of quaternary blends. Solution experiments further supported the selective localization of MWNTs in the PA6 phase of the blends (18).

13.3.4 Melt-Interfacial Interactions

Figure 13.7 shows the FTIR spectra of pure PA6, PA6/ABS blends with Na-AHA and OTPB modified MWNTs. Peak at 1641 cm^{-1} represents carbonyl ($\text{C}=\text{O}$) stretching vibration ($\nu_{\text{C}=\text{O}}$), which is for amide I band. Peaks at 1543 cm^{-1} and 1264 cm^{-1} are for amide II band and amide III band respectively, which are both assigned to nitrogen-hydrogen (N-H) bending vibration and carbon-nitrogen (C-N) stretching vibration ($\delta\text{N-H} + \nu\text{C-N}$), band at 3091 cm^{-1} is the characteristic double frequency absorption of amide II band. A weak band $\sim 3300\text{ cm}^{-1}$ corresponding to the N-H stretching vibration (as indicated in Figure 13.7) is also seen in the FTIR spectra of neat PA6. This band is also observed in the blends with Na-AHA and OTPB modified MWNTs. In addition, blends with OTPB modified MWNTs show an additional band around $\sim 3450\text{ cm}^{-1}$, corresponding to NH_3^+ (as indicated in Figure 13.7). Since the central phosphonium is surrounded by phenyl groups, it is likely that there can be ' π - π ' type of interaction between MWNTs and OTPB. Since, ' π - π ' type of interaction is weaker in nature, some of the phosphonium

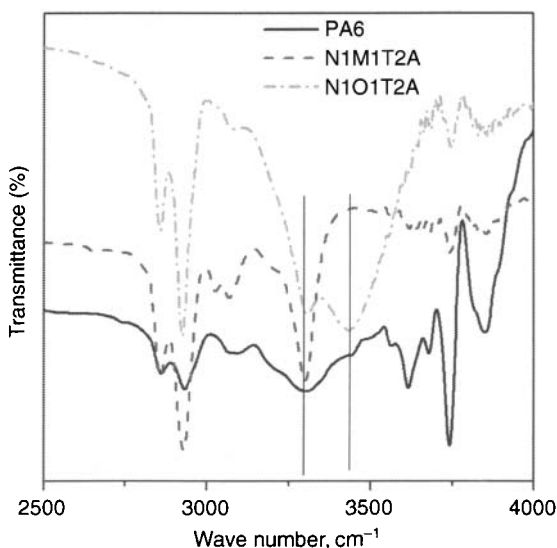


Figure 13.7. FTIR spectra of pure PA6 and PA6/ABS blends with various MWNTs.

ions are likely to dissociate and form a complex with the lone pair of electrons of nitrogen; either from the terminal -NH_2 groups or from -CONH groups in PA6 (19). Such complex interactions can facilitate selective localization of MWNTs in the PA6 phase. However, the possibility of 'cation- π ' type of interaction between OTPB and MWNTs could not be ruled out completely. Further, in case of blends with Na-AHA modified MWNT, an increase in the intensity of the peaks corresponding to amide I (1635 cm^{-1}) and amide II (1537 cm^{-1}) has been observed. The reaction between amine groups of Na-AHA and acid groups of PA6 may be the plausible reasons behind an increase in the intensity of peaks corresponding to amide groups.

13.4 Summary

Co-continuous polymer blends of 50/50 polyamide6/acrylonitrile-butadiene-styrene copolymer (PA6/ABS) involving multiwall carbon nanotubes (MWNTs) were prepared by melt mixing technique in order to develop conducting composites utilizing the concept of 'double-percolation'. To control the dispersion and to selectively restrict MWNTs in the PA6 phase of the blends, MWNTs were pre-treated with two modifiers which differ in their molecular length scales and

architecture; sodium salt of 6-amino hexanoic acid (Na-AHA) and octadecyl tri-phenyl phosphonium bromide (OTPB). The ionic moieties present on the modifiers enable them to establish specific interactions with the delocalized π -electron clouds of MWNTs. Raman spectroscopy and transmission electron microscopy supported the role of these modifiers in debundling the MWNTs mediated by various types of specific interactions. FTIR analysis provided insights into various types of interactions between the modified MWNTs and the available functional groups on PA6. This further led to selective localization of MWNTs in the PA6 phase of the blends. PA6/ABS blends with OTPB modified MWNTs resulted in dramatic improvements in the bulk electrical conductivity of the blends as compared to unmodified p-MWNTs and Na-AHA modified MWNTs. Scanning electron microscopic analysis of the blends revealed co-continuous type of microstructure wherein MWNTs were observed selectively in the PA6 phase of the blends. In addition, this strategy was also proven to be successful in PA6 based multicomponent blends.

Acknowledgements

'ARB duly acknowledges the financial support from the Department of Science & Technology (DST), India (Project No. 08DST016). The authors would also like to thank Microcompounder Central Facility, SAIF and CRNTS, IIT Bombay.'

References

1. Y.S. Lipatov, A.E. Nesterov, *Thermodynamics of polymer blends*, Lancaster-Basel, Technomic, 1997.
2. F. Fenouillot, P. Cassagnau, and J. Majesté, *Polymer*, Vol. 50, p. 1333, 2009.
3. P.J.F. Harris, *International Materials Review*, Vol. 49, p. 31, 2004.
4. D.E. Hill, Y. Lin, A.M. Rao, L.F. Allard, and Y.P. Sun, *Macromolecules*, Vol. 35, p. 9466, 2002.
5. C. Richard, F. Balavoine, P. Schultz, T.W. Ebbesen, and C. Mioskowski, *Science*, Vol. 300, p. 775, 2003.
6. T. Ramanathan, H. Liu, and L.C. Brinson, *Journal of Polymer Science, Part B: Polymer Physics*, Vol. 43, p. 2269, 2005.
7. K. Kamaras, M.E. Itkis, H. Hu, B. Zhao, and R.C. Haddon, *Science*, Vol. 301, p. 1501, 2003.
8. S. Bose, A.R. Bhattacharyya, A.P. Bondre, A.R. Kulkarni, and P. Pötschke, *Journal of Polymer Science, Part B: Polymer Physics*, Vol. 46, p. 1619, 2008.

9. F. Gubbels, R. Jerome, E. Vanlathem, R. Deltour, S. Blacher, and F. Brouers, *Chemistry of Materials*, Vol. 10, p. 1227, 1998.
10. M. Sumita, K. Sakata, Y. Hayakawa, S. Asai, K. Miyasaka, and M. Tanemura, *Colloid and Polymer Science*, Vol. 270, p. 134, 1992.
11. P. Pötschke, S. Pegel, M. Claes, and D. Bonduel, *Macromolecular Rapid Communications*, Vol. 29, p. 244, 2007.
12. D. Wu, Y. Zhang, M. Zhang, and W. Yu, *Biomacromolecules*, Vol. 10, p. 417, 2009.
13. S. Bose, A.R. Bhattacharyya, A.R. Kulkarni, and P. Pötschke, *Composites Science and Technology*, Vol. 69, p. 365, 2009.
14. R. Saito, G. Dresselhaus, and M.S. Dresselhaus, *Physical properties of carbon nanotubes*, London, Imperial College Press, 1998.
15. A. Liu, I. Honma, M. Ichihara, and H. Zhou, *Nanotechnology*, Vol. 17, p. 2845, 2006.
16. A.K. Jonscher, *Nature*, Vol. 267, p. 673, 1977.
17. C. Rajagopal, and M. Satyam, *Journal of Applied Physics*, Vol. 49, p. 5536, 1978.
18. S. Bose, A.R. Bhattacharyya, R.A. Khare, S.S. Kamath, and A.R. Kulkarni, The role of molecular interactions and selective localization of multiwall carbon nanotubes on the electrical conductivity and phase morphology of multicomponent polymer blends (*manuscript in preparation*).
19. S. Bose, A.R. Bhattacharyya, R.A. Khare, A.R. Kulkarni, T.U. Patro, and P. Sivaraman, *Nanotechnology*, Vol 19, p. 335704, 2008.

This Page Intentionally Left Blank

Effect of Structure and Morphology on the Tensile Properties of Polymer/Carbon Nanotube Nanocomposites

Jingjing Qiu

*Department of Construction and Engineering Technology,
Texas Tech University, USA*

Shiren Wang

Department of Industrial Engineering, Texas Tech University, USA

Abstract

In this chapter, different morphologies of CNTs during fabrication were investigated, including isolated CNTs, short CNTs and CNT membranes. The effect of morphologies and structures on tensile properties was discussed in detail. Generally, the addition of CNTs into polymer matrix indicated improvement in tensile modulus and tensile strength if good dispersion and strong interfacial bonding are achieved. Especially, tensile properties improved substantially via chemical or physical functionalization due to the enhanced reactivity on CNT sidewalls and the improved interfacial bonding. It should be noted that film-impregnated CNT/polymer composites were readily handled compared with the conventional casting or melting-processed CNT/polymer composites. The improved interfacial bonding strongly enhances the effectiveness of load-transfer and makes it possible to take full advantage of the exceptional performance of CNTs.

Keywords: morphology, structure, tensile properties, dispersion, aspect ratio, impregnation, load transfer, casting.

14.1 Background

Carbon nanotubes (CNTs) are the strongest fibers that are currently known. They demonstrate amazing mechanical, thermal and electrical properties, while a low density and a very high aspect ratio (1–5). A lot

of studies have shown that effective incorporation of CNTs into polymer significantly enhances polymer tensile modulus and tensile strength with an addition of small amounts of CNTs (6–13). In CNT/polymer composite, the polymer matrix transfers the load via shear to the CNT reinforcement. The high aspect ratio of CNTs compensates for the low modulus of the polymer matrix (14). Moreover, mechanical properties are enhanced due to reduced critical flaws and insensitivity to flaws at the nanoscale. Since mechanical properties depend on defect concentrations, the addition of nanoscale particles can generate a number of novel effects through quantum confinement, or through the dramatic increase in interfacial area (14). Therefore, reinforcement of polymers using CNTs as novel modifiers will also improve electrical conductivity, thermal conductivity and fire-retardant properties of composites (15–16).

Crucially, structure of CNTs and polymers plays a key role on mechanical properties and load-transfer of nanocomposites. Efficient load-transfer is only possible when adequate interfacial bonding strength is available. Interfacial failure may compromise the reinforcement effect and then the full potential of CNTs may not be realized (11). Therefore, it is of great importance to understand the effect of molecular structure, interfacial structure and morphology characteristics on the tensile properties of nanocomposite materials.

14.2 Structure and Morphology Characterization

In the last ten years, a great deal of experimental work has been presented about the tensile properties of CNTs/polymer composites in the literature. However, it is difficult to generalize across these studies because of the large number of parameters that can influence the effective properties, including size and structure of the CNT, CNT/polymer interaction, processing techniques and processing conditions. In this chapter, the effect of structure and morphology on the properties of the nanocomposites will be focused and discussed.

14.2.1 Structure and Mechanical Properties of CNTs

CNTs are formed from pure carbon bonds through SP^2 covalent bonds (17–21). Wrapping two-dimensional graphite sheets into cylinders and joining the edges, a tube of graphite is formed, called SWNT, as shown in Figure 14.1. The graphite sheet may be rolled in different orientations along any two-dimensional lattice vector (m, n). The orientation of the graphite lattice relative to the axis

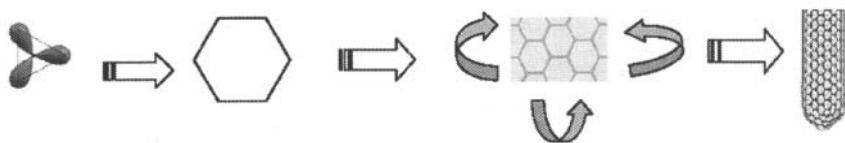


Figure 14.1. Structure of carbon nanotube.

defines the chirality or helicity of CNT. MWNTs consist of two or more coaxial cylinders, each rolled out of single sheets, separated by approximately the interlayer spacing in graphite.

CNT sidewall consists of hexagonal rings which are seamlessly arranged, and so it is rather inert in chemistry. This stable chemical characteristic of CNTs makes it difficult to achieve strong interfacial bonding between CNTs and polymer matrix. That is, in order to achieve high tensile strength and tensile modulus, structure modification is desired to improve the reactivity.

Most initial work studying the mechanical properties of CNTs has come from computational methods including molecular dynamics and *ab initio* models. Typically these computational studies have found nominal values for the axial Young's modulus on the order of 1 TPa, with values for the Poisson ratio approximately 0.20 to 0.30 for the SWNTs (21–23). The calculation of empirical force-constant method indicated that elastic modulus of individual SWNTs was approximately 1.23 TPa, while SWNT bundles were between 0.4 and 0.8 TPa, and modulus were found to be very dependent on the diameter of the individual tubes (24). Because strength is closely related to the presence of defects within a material, it has been hypothesized that CNTs (particularly low defect CNTs formed via carbon arc and laser vaporization methods) may approach theoretical limits in terms of strength. Molecular mechanics simulation suggested that CNT fracture strains were between 10 and 15%, with corresponding tensile stresses on the order of 65 to 93 GPa (31). Above computations were based on the assumption of defect-free CNTs. But actual CNTs with a significant number of defects, especially those produced via CVD methods, are expected to have much lower modulus values, for example, 640 GPa (25–26). More recently, some progress has been made in the manipulating and testing of individual CNTs and CNT bundles through AFM and TEM experiments (27–30). These measurements of CNT mechanical properties have been carried out by assuming CNTs as elastic beams. In general, the experimental results have validated the computational predictions.

A summary of these experimental results is given in Table 14.1. For SWNT bundles, the maximum tensile strain was estimated to be 5.3%, and the tensile strength of the individual SWNTs was estimated to be ~52 GPa (27). As a comparison, the tensile strength of CNTs has been estimated to be 3.6 GPa for CVD-grown 2mm MWNT ropes. The decrease in strength is attributed to an increase in defects (26). The fracture strengths were found to range from 13 to 52 GPa and the modulus from 320 to 1470 GPa when assuming the load is carried only by the SWNTs on the perimeter of rope (28). The tests on MWNTs found that failure occurred at tensile strains up to 12%, with the tensile strength of the outer shell of the MWNT estimated to be between 11 and 63 GPa and the tensile modulus values ranged from 270 to 950 GPa (29). Recent experimental measurement found that the maximal tensile strain was about $5.8 \pm 9\%$ and the tensile stress was about $47 \pm 8 \text{ GPa}$ (30). Typical values of Young's modulus are shown and compared in Table 14.2.

Table 14.1. Experimental values for the Young's modulus of CNTs

Synthesis method	Test methods	Experiment Value
Laser ablated SWNTs	Amplitude of thermal vibration within TEM	~1.3TPa
Laser ablated SWNTs	Nanostressing within SEM	~1TPa
HiPco SWNTs bundles	Beam bending via AFM	~1TPa for small ropes <3nm diameter
Laser ablated MWNTs bundles	Electrimechanical deflection and resonance within TEM	~TPa for small ropes <10nm diameter

Table 14.2. Mechanical properties of current reinforcement fibers

Fiber	Diameter (μm)	Density (g/cm ³)	Tensile strength (GPa)	Young's Modulus (GPa)
Carbon	7	1.66	2.4~3.1	120~170
Glass	14	2.5	3.4~4.6	90
Aramid	12	1.44	2.8	70~170
Boron	100~140	2.5	3.5	400
Quartz	9	2.2	3.4	70
SiC	10~20	2.3	2.8	190
CNTs	0.001~0.1	1.33	50~200	~1000

Theoretically, tension and compression behavior of CNTs are mainly governed by in-plane σ -bonds, while pure bending is influenced by out-of-plane π -bonds. However, for such nanostructures, conventional continuum elasticity theory is not appropriate to model the mechanical behaviors. Therefore, some efforts have been tried on theoretical investigation of tensile properties for CNTs (31). It was found that abrupt changes in CNT morphology under axial loads strongly depend on CNT length (31). For MWNTs, although the outer layers are stressed in tension, all layers contribute under compression (32). Generally, the strength of CNTs depends on the distribution of defects on CNTs and the dispersion state of CNTs, as well as interlayer interactions for MWNTs. Usually, good dispersion, high aspect ratios and few defect concentrations contribute to a high CNT tensile strength. That is the reason why some have suggested that individually dispersed SWNTs should be the ideal reinforcement (26,27).

14.2.2 Characterization of CNTs/Polymer Composites

Polymer based composites reinforced by CNTs have been extensively studied and researchers have utilized both computational and experimental techniques to determine their mechanical properties. The superior mechanical properties of the CNTs alone do not ensure mechanically superior composites because the composite properties are strongly influenced by the mechanics that govern the CNT-polymer interface (33). The mechanical load transfer from the polymer matrix to the CNT and the bonding of the interface are dependent on the structure and morphology. In order to realize the full potentials of CNTs in polymer-based composites, strong interface and perfect bonding are desired. If the interface is weak, the interface fails or the load is not effectively transferred to CNT when the composites are under external load (33). In this chapter, effects of structure and morphology on tensile properties are discussed. A better understanding of the structure and morphology will help tailor the interface for superior mechanical properties of CNTs/polymer composites.

The main experimental methodology used is to directly characterize the tensile properties of CNTs/polymer composites by conventional pull tests (e.g. with Instron tensile testers). Similarly, dynamic mechanical analysis (DMA) and thermal mechanical analysis (TMA) were also applied to investigate the tensile strength and tensile modulus. With these tensile tests, the ultimate tensile strength, tensile modulus and elongation to break of composites can be determined from the tensile strain-stress curve.

Raman spectroscopy was used to analyze the tensile properties. For CNTs/epoxy polymer composite, shifts in CNT peaks can be observed in Raman spectroscopy during straining of the sample (34). Experimental evidences of the high strength and good bonding between polymer matrix and CNTs can also be presented in microscopy tests, such as scanning electron microscopy (SEM) and transmission electron microscopy (TEM). In some studies, it was noticed that good bonding exists if there is good wetting or sheathing of CNT surrounded by polymer matrix on the fracture surface.

All the previous literatures indicated that the superior mechanical properties of CNTs can be maintained in the well-dispersed composite system. Or else, the large CNT aggregates act as the defect sites and become the potential stress concentrators. Such aggregates also adversely influence other physical properties of composites. Hence, good CNT dispersion is necessary for effective reinforcement. Moreover, the chemistry of the bonding between CNTs and polymer is also crucial, especially the nature of the bonding (e.g. covalent or non-covalent and electrostatic). In addition, the effect of functionalization for CNTs/polymer interface bonding and the resultant tensile strength of composites were also broadly investigated. 50% increase was observed in PP fiber modulus with the addition of 5 wt% carbon nanofibers (35), and 60% increase in PBO fiber tensile strength with the addition of 10 wt% SWNT (36). It was found that fibers processed with high catalytic impurity resulted in lower tensile strength (37). Some researchers have tried to correlate the obvious enhancement in tensile properties with the micro-mechanic theories or Kelly Tyson shear lag model (37,38).

It is highly desired that in situ experiments and measurements may be performed on tensile properties, so that a better understanding will be obtained by incorporating local microscopy observation with macroscopic tensile tests.

14.2.3 Structure and Tensile Properties of CNTs/ Polymer Composites

Given the modulus and strength values that have been predicted and measured for CNTs, they are potentially an ideal reinforced material for high performance polymer composites with outstanding specific modulus and specific strength with only low concentrations of CNTs (11, 39–42). However, one issue of practical importance for nanocomposite is the separation and dispersion of the CNTs within the matrix,

which is critical as CNTs tend to assemble into ropes or bundles due to van der Waals interactions. Till now, most researchers directly dispersed as-received CNTs into the thermoplastic polymer or thermosetting polymer precursors. The viscosity and processing difficulties remarkably increased with the increment of CNT concentrations due to their high aspect ratio, aggregation and the resulting cluster network. These issues result in modest augment or even reduction in tensile strength and the strain to failure. Different approaches have been explored to prevent the CNTs aggregation and avoid high viscosity during the dispersion process. Ultra-sonication, high-speed stirring are often followed to improve the dispersion. While separating individual CNTs from the bundles can be obtained via ultrasound and polar solvents, maintaining separated CNTs during the processing of nanocomposites is still the subject of ongoing work.

Recently a great deal of experimental work has been presented in the literature to improve the properties of polymers reinforced with CNTs. Vacuum-assisted processing is also applied to reduce defects in the composites (43,44). Some researchers applied functionalization to pre-treat CNTs before dispersion in surfactants or matrices, and then curing agent was added (45–48). Some researchers controlled the morphology and structure of CNTs before they were introduced into polymer matrix system so that strong bonding may be obtained (49,50). A number of efforts have been focused on innovative manufacturing processes to fabricate film-impregnated CNT/polymer composite structure or CNT-integrated fiber/polymer composite structure (51,52). However, it is difficult to cover all of them across these studies because of the large number of parameters that can influence the tensile properties. In this chapter, effect of CNT morphology on tensile properties is discussed. For casting- or melting-processed CNTs/polymer composites, CNTs were dispersed as isolated CNT molecules. For shorten CNTs/polymer composites, caps of pristine CNTs were removed and tube lengths were controlled by different cutting techniques. For film-impregnated CNTs/polymer composites, CNTs were distributed as small ropes in the buckypaper membranes. The improvements in the tensile properties of the composites after the addition of CNTs will be introduced.

14.2.3.1 *Casting- or Melting-Processed CNTs/Polymer Composites*

Solution-based casting methods provide an advantage through low viscosities, which facilitate mixing and dispersion of the CNTs (11).

Many studies have used these methods for processing of both thermosetting and thermoplastic polymers. Y. Liao (53) dissolved epoxy in a well-dispersed, ultra-sonicated CNT suspension. The solvent was evaporated, and the epoxy was subsequently cured to form a nanocomposite in which the good CNT dispersion was achieved. Jin et al. (54) produced various types of polymer-coated and polymer-grafted MWNT solutions, in some cases evaporating the solvent and subsequently melt-mixing with another polymer. Yudasaka et al. (55) used a mixture of SWNTs and PMMA in monochlorobenzene (MCB) for dispersion, purification and subsequent spin-casting of the material.

Melt-mixing of CNTs into thermoplastic polymers using conventional processing techniques, such as extrusion, internal mixing, injection molding and blow molding, are particularly desirable, because of the speed, simplicity and availability of these processes in the plastics industry. These methods are also beneficial because they are free of solvents and contaminants, which are present in solution processing methods and *in-situ* polymerization (56). Nanomaterials have less fiber breakage in thermoplastic compounding and molding. Moreover, a high aspect ratio can be maintained for CNTs in contrast to larger, microscale carbon fibers. Application of high-shear mixing and longer processing times may enhance dispersion, and may yield aligned CNTs when coupled with elongation flow. The increase in viscosity with composition is much higher for CNTs than larger-diameter fibers or carbon black, so high shear mixing is needed to overcome high viscosities of the CNTs/polymer mixtures (57).

For both casting-process and melting-process, CNTs are dispersed into polymer as single CNTs or CNT bundles. When mechanical properties are concerned, optimal tensile properties will only be achieved if the orientation of the CNTs within the polymer can be controlled. A few CNT aligning techniques have been developed (58). Especially, controlling the alignment is possible by using several melt-mixing methods. Spinning of extruded melt samples is one way of making well-aligned CNT/polypropylene (PP) composites with good CNT dispersion. Aligned CNTs can be achieved in CNTs/PP composites by increasing the residence time in the die channel, or altering the die design to control the orientation of the CNTs (59). Injection molding was also found to induce significant alignment in CNT/PP samples, as demonstrated by coefficient of thermal expansion and electrical resistivity measurements (60). One group found that cutting thin slices (on the order of 100 nm) of a CNT-reinforced epoxy film introduced

preferential orientation via shear flow (61). An alternative method to achieve alignment for larger samples is applying tensile loading on the nanocomposite at temperatures above the glass transition temperature of the polymer (62,63). A combination of solvent casting and melt mixing was also found to produce a high degree of CNT alignment (64). While individual SWNTs and SWNT ropes have been aligned in the presence of electric (65) and magnetic fields (66,67), this method has yet to be extended to CNT-reinforced polymers under consideration of the large friction force from high viscosity of polymer resin.

However, when casting-processing or melting-processing was applied, the stable chemical characteristics of CNTs make it difficult to achieve a strong interfacial bonding and effective load transfer between tubes and polymer matrix. Therefore, modest improvements were observed for the tensile strength and tensile modulus after the addition of CNTs. Tensile test of the resultant SWNT/epoxy composite was usually conducted according to the ASTM D638. For the neat resin, the average tensile strength and Young's modulus were found to be 72.6 MPa and 2.0 GPa, respectively. When the pristine SWNTs (p-swnts) were used to reinforced epoxy composite, the test results indicated that the average strength and modulus were 71.5 MPa and 2.3 GPa. Obviously the tensile strength did not show any improvement while modulus was enhanced slightly.

Functionalization has been suggested to be one of the most effective methods in improving the dispersion and surface properties of CNTs (11). It was reported that the most amazing improvement was demonstrated when chemical functionalization was introduced (47). The oxidation of CNTs was the easiest functionalization method and was often carried out to form the -COOH functional group before CNTs were dispersed into polymer matrix. Because the reactivity of oxygen-containing group is greater than pristine CNTs, better interfacial bonding and load transfer between CNTs and polymer matrix will be obtained. Similarly, fluorination and amino-grafting were also widely applied in CNT/polymer composites (64–66). After these different sidewall functionalization methods, both tensile strength and tensile modulus was significantly enhanced (48,49). For instance, after acid treatment and fluorination, SWNTs were integrated into epoxy composites through the formation of strong covalent bonds in the course of epoxy ring-opening esterification and curing chemical reactions (Figure 14.2). The Young's modulus of fluorinated SWNT reinforced epoxy composite increased by 30% and the tensile strength increased by 18% with only 1 wt% of functionalized SWNT (47). Another example is that grafted

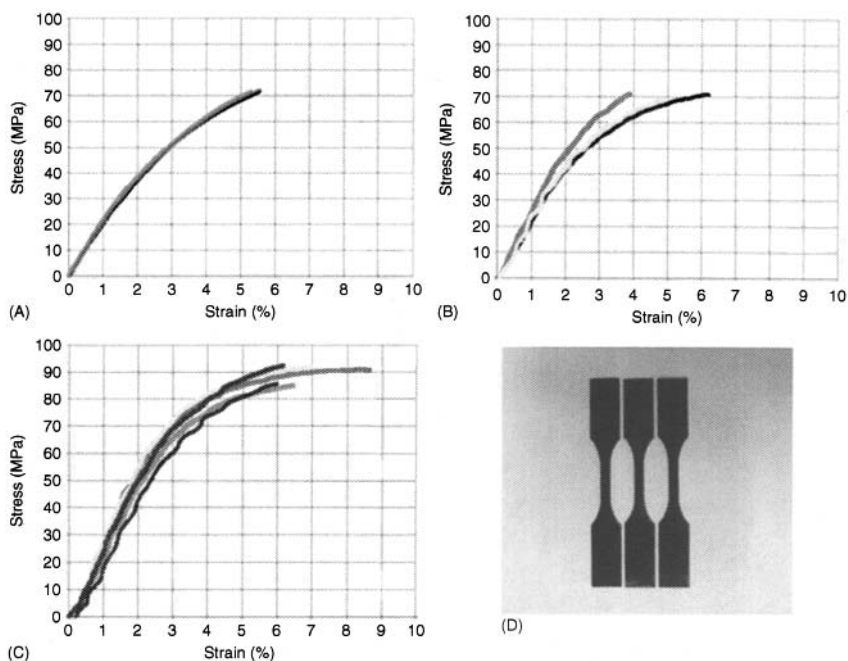


Figure 14.2. The mechanical properties of 0.5 wt% SWNT/Epoxy composites (a) tensile test of neat epoxy resin; (b) tensile test of pristine-SWNT/epoxy; (c) tensile test of amino grafted-SWNT/Epoxy; (d) tensile test samples.

amino-groups enhanced the polarity and also participated in the latter curing behavior of epoxy polymer. So when the amino-grafted SWNTs were applied in the composite, the average tensile strength was increased to 88.5 MPa by about 21.9% enhancement. The average modulus was enhanced to 2.5 GPa in contrast to the neat resin (11). The noticeable improvement of the tensile strength suggested that the functionalization of SWNTs has substantially enhanced interfacial bonding so that improved load transfer was achieved.

Especially, epoxy-grafting functionalization enables cross-linking reactions with amines, carboxylic acids, anhydrides and hydroxyl-containing polymers, and thus attracted more attentions in the recent years (11). The TEM images of pristine and epoxy-grafted SWNT are showed in Figure 14.3 (11). For the pristine, SWNT, the sidewall is quite smooth. However, for the epoxy-grafted SWNT, some molecular cluster can be clearly seen in the sidewalls, appearing like a number of buds growing on the SWNT surface. These TEM results suggest functionalization has attached some specific chemical groups to the CNTs.

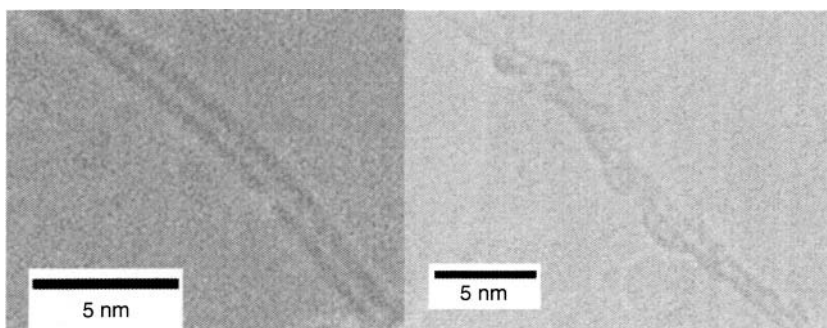


Figure 14.3. TEM images of epoxy-grafted SWNTs (a) pristine SWNT and (b) epoxy-grafted SWNT [11].

The morphology of the interface between CNTs and polymer matrix can be investigated by characterizing the fracture cross-section through SEM. In the pristine-SWNT/epoxy composite, CNTs tended to form cluster and big agglomerations, as shown in Figure 14.4(a). As a comparison, epoxy grafted-SWNTs were well dispersed in the epoxy resin and embedded in the epoxy matrix. No cluster of SWNTs was found in the fracture surface. Most of the CNTs were embedded in the matrix, and few of them were pulled out, as shown in Figure 14.4(b) (11). It demonstrated that the functionalization effectively improves the dispersion and interfacial bonding in SWNTs reinforced polymer composite.

Correspondingly, the stress-strain curves of the neat resin and epoxy-grafted CNT enhanced nanocomposites are shown in the Figure 14.5. When the epoxy-grafted SWNTs were applied in the composite with 0.5 wt% loading, the average tensile strength was increased to 92.3MPa, about 27.1% enhancement (Figure 14.6). The average modulus was enhanced to 2.6GPa in contrast to the neat resin. Further, 1 wt% loading x-SWNT/epoxy composite samples were fabricated and characterized. The tensile strength was found to enhance to 101.9MPa, about 40.3% increase. The Young's modulus was enhanced to 3.2GPa, about 60% improvement in contrast to the neat resin (11). The noticeable improvement of the tensile strength suggested that the functionalization of SWNTs substantially enhanced interfacial bonding so that improved load transfer was achieved.

These efforts indicated that the sidewall functionalization effectively enhances the tensile strength and tensile modulus by improving dispersion and interfacial bonding in SWNTs reinforced polymer composite.

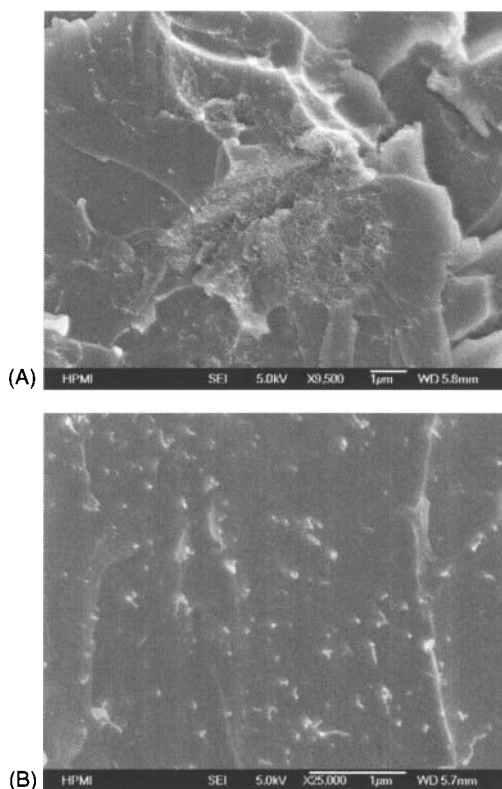


Figure 14.4. SEM images of pristine and epoxy grafted SWNT reinforced nanocomposites (a) pristine SWNT/epoxy composite and (b) epoxy grafted SWNT/epoxy composite (11).

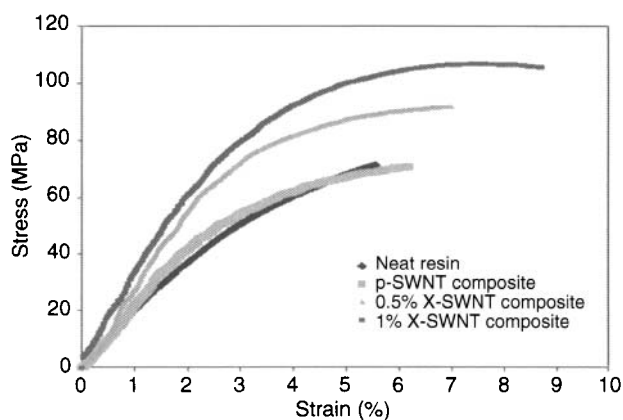


Figure 14.5. Tensile curve of the neat resin and SWNT reinforced nanocomposites (a) neat resin, (b) p-SWNT composite, (c) 0.5 wt% epoxy grafted-SWNT composite, (d) 1 wt% epoxy grafted-SWNT composite (11).

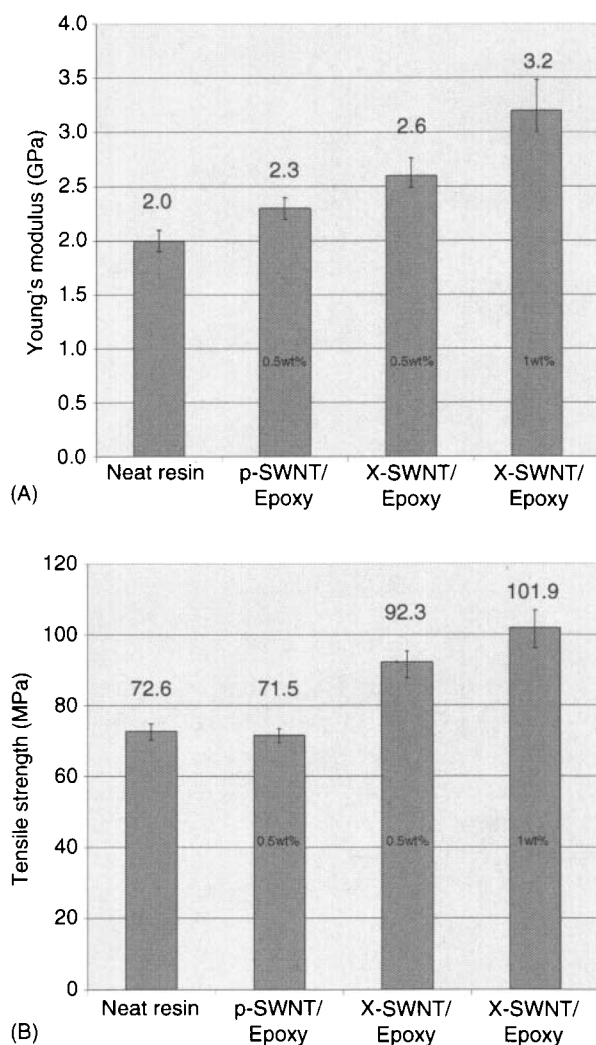


Figure 14.6. Summarized modulus and strength of the nanocomposites (a) neat resin, (b) p-SWNT composite, (c) 0.5 wt% epoxy grafted-SWNT composite, (d) 1 wt% epoxy grafted-SWNT composite (11).

14.2.3.2 Short-CNTs/Polymer Composites

In the past years, great efforts have been tried on interfacial structure of both CNTs and polymers through covalent modification on the sidewall of CNTs and polymer molecule. There are several classical ways of surface treatment, which improve the colloidal stability of CNTs and the interaction between CNT and

polymer matrix. In addition to the surface modification, another typical functionalization approach is CNT chopping because shortened single-walled CNTs (SWNTs, $<1\ \mu\text{m}$) are expected to have rich chemistry and they are promising one-dimensional building blocks for constructing advanced nanoscale structures and materials (68). For instance, shortened SWNT becomes an open-end tube when the caps in the ends are removed during sectioning. As a result the resin molecules will fill into SWNTs so that in SWNTs/epoxy mixture, partial resin molecules are inside tubes and partials are outside. Both of the epoxy molecules inside tubes and outside tubes could form chemical bonding during curing as shown in Figure 14.7. This provides extra bonding between SWNTs and epoxy resin, and then improves the interfacial bonding. In the following paragraphs, some different cutting methods are reviewed. The basic cutting techniques include acid cutting (69–73), fluorination cutting (74), and ultrasonic cutting (75–77).

Although ultrasonic treatment is a kind of standard procedure in dispersing SWNT into solvent and resin matrix and it can also shorten SWNTs (75), ultrasonic treatment would cause mechanic defects such as buckling, bending of CNTs and finally lead to the formation of amorphous carbon. The problem is that sonication sometimes makes holes on the CNTs sidewalls, resulting in “worm-eaten look” tubes (76). Long time sonication may permanently damage the CNTs structure and lead to the modest improvement of tensile strength (77).

Since SWNTs length distribution can be represented by a specific Weibull distribution (11), Cox-Krench shear-lag model, as expressed in equation (1) and (2) (78), was applied to compute SWNT/epoxy composite tensile strength based on the SWNT lengths distribution and random alignment. The Young's modulus and tensile strength of SWNTs were specified as 1TPa and 100GPa, respectively (11). For epoxy resin, Young's modulus $E_m = 2.0\text{GPa}$, tensile strength

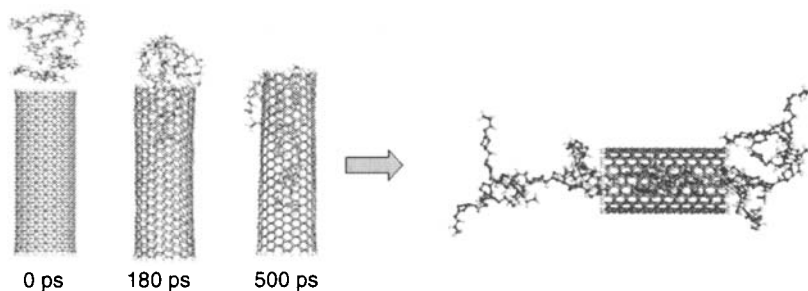


Figure 14.7. Simulation of epoxy and EPI cure molecules filling into CNTs.

$\sigma_m = 72.6 \text{ MPa}$ and Poisson ratio $\nu_m = 0.3$. The Weibull distribution parameters were $a = 8 \times 10^{-7}$, $b = 2.2$. Young's modulus and tensile strength of nanocomposites were estimated by the shear-lag model (1~6) and computational results are shown in the Figure 14.8.

$$E_{com} = \chi_1 \chi_2 E_f V_f + E_m (1 - V_f) \quad (14.1)$$

$$\sigma_{com} = \chi_1 \chi_2 \sigma_f V_f + \sigma_m (1 - V_f) \quad (14.2)$$

$$\chi_1 = \frac{1}{l_{mean}} \int_{l_{min}}^{l_{max}} \left[1 - \frac{\tanh(\beta l / 2)}{\beta l / 2} \right] f(l) dl = \frac{1}{l_{mean}} \int_{l_{min}}^{l_{max}} \left[1 - \frac{\tanh(\beta l / 2)}{\beta l / 2} \right] a b l^b \exp(-a l^b) dl \quad (14.3)$$

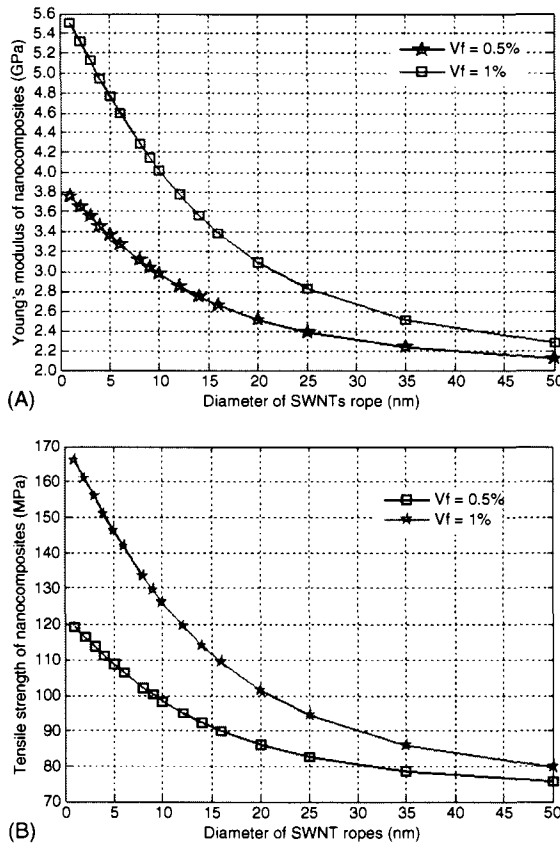


Figure 14.8. The effect of dispersion on the nanocomposites modulus and strength.

$$\beta = \left[\frac{2G_m}{E_f r^2 \ln(R/r)} \right]^{1/2} = \left[\frac{2 \times \frac{E_m}{2(1+\nu_m)}}{E_f r^2 \ln(R/r)} \right]^{1/2} = \left[\frac{E_m}{E_f (1+\nu_m) r^2 \ln(R/r)} \right]^{1/2} \quad (14.4)$$

$$\ln\left(\frac{R}{r}\right) = \frac{1}{2} \ln\left(\frac{2\pi}{\sqrt{3}V_f}\right) \quad (14.5)$$

$$\chi_2 = \int_0^{\pi/2} [(\cos\theta)^2 - \nu_{12}(\sin\theta)^2](\cos\theta)^2 g(\theta) d\theta \quad (14.6)$$

where:

E_{com} ----- Young's modulus of nanocomposite;

σ_{com} ----- Tensile strength of nanocomposite;

χ_1 ----- Length effect factor for discontinuous fibers;

χ_2 ----- Orientation effect factor, equal to 1/5 for 3D plane random, 3/8 for 2D random;

E_f ----- Young's modulus of reinforced fiber;

E_m ----- Young's modulus of resin matrix;

σ_f ----- Tensile strength of fiber;

σ_m ----- Tensile strength of resin matrix;

V_f ----- Reinforced fiber volume fraction;

r ----- Reinforced fiber radius.

R ----- Average separation for the reinforced fiber norm to the length.

The negative effect of rope diameter on the nanocomposites was also observed in the Figure 14.8. When rope diameter was less than 25 nm, especially close to the individual tube, the slight improvement in the dispersion would lead to considerable increase in the modulus and strength. These observations indicate that the SWNTs should be dispersed as well as possible to get isolated SWNTs so that maximal contribution of the SWNTs to composite properties would be acquired. The effect of CNTs aspect ratio on the reinforcement in the nanocomposites was shown in Figure 14.9 (11).

It was found in both experiments and simulation results that the aspect ratio of the CNTs plays a significant role. Usually it is believed that the chirality of CNTs have minor effects on the mechanical properties of the CNT/polyethylene composite. While the increased orientation ordering leads to an enhancement of the mechanical modulus of the nanocomposite materials, and such

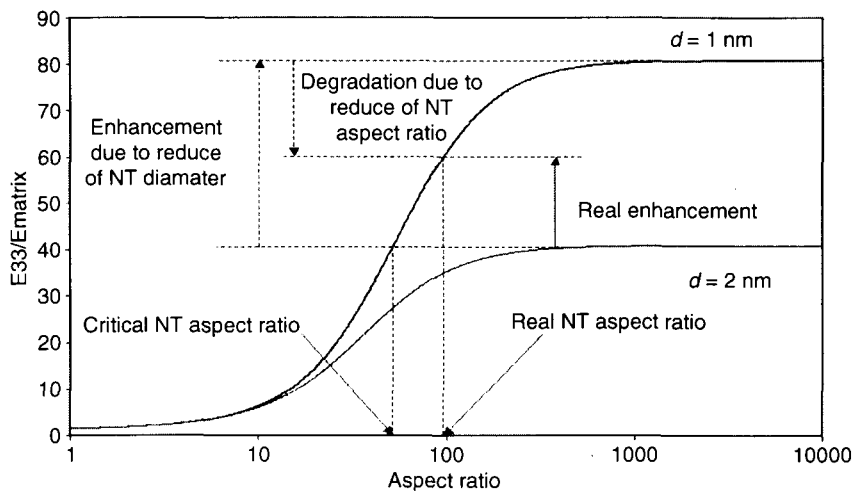


Figure 14.9. Effect of CNTs aspect ratio on the reinforcement

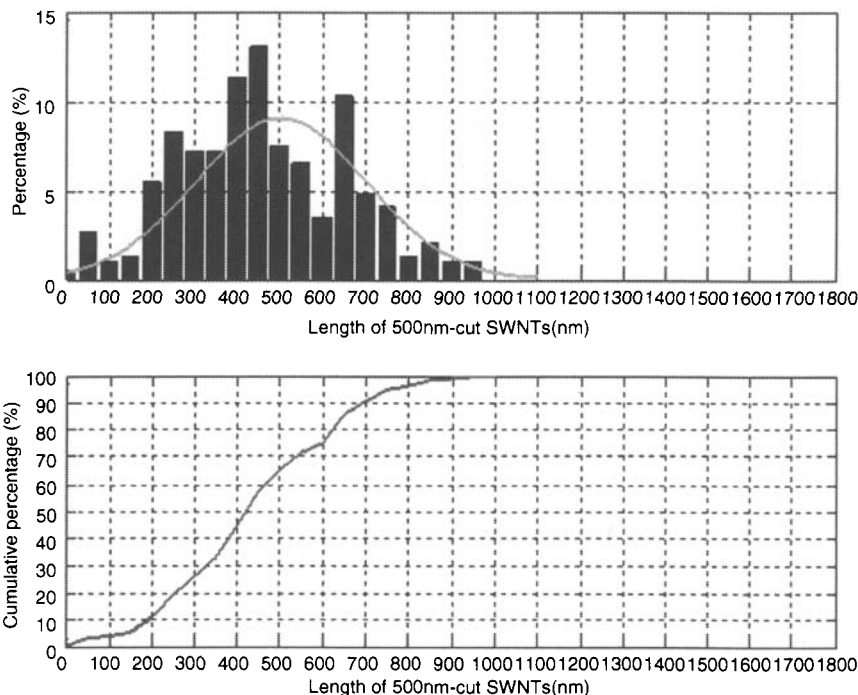


Figure 14.10. Length distributions of 500 nm-cut SWNTs.

structural ordering also plays an important role in the yielding behavior of the materials. The enhanced modulus is denoted as E_{33} and the resin matrix modulus is denoted as E_{matrix} . So the reinforcement is investigated as a function of aspect ratio. The reduction of

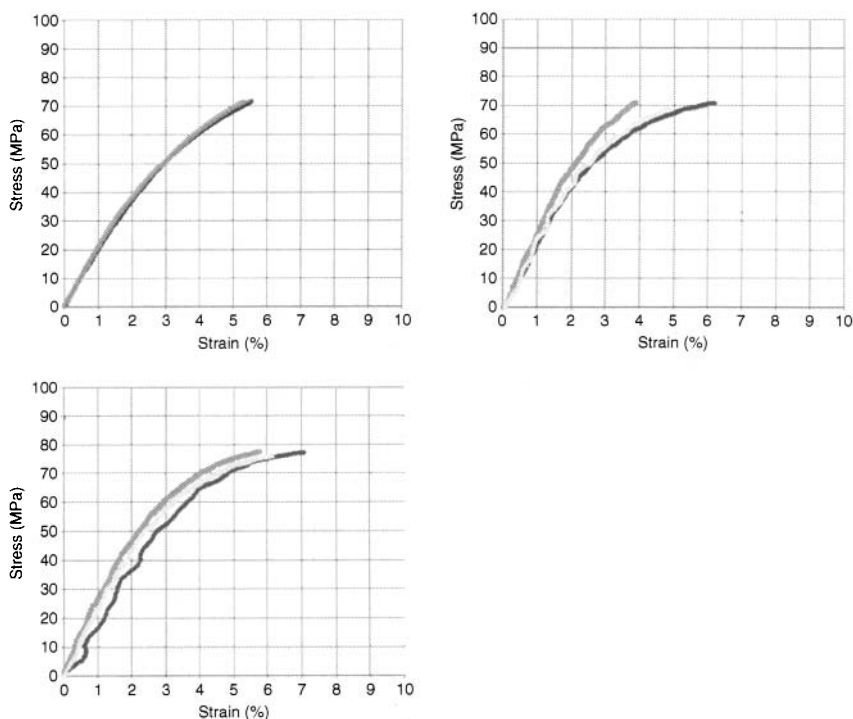


Figure 14.11. Tensile strength of CNT/Epoxy composites with the 0.5 wt% SWNT loading (a) neat epoxy resin, (b) pristine SWNT/epoxy, (c) cut-SWNT/epoxy (11).

aspect ratio will reduce the reinforcement, while the improved dispersion and interfacial bonding will enhance the reinforcement. The proper trade-off will be made to acquire the desired enhancement in the tensile properties of resultant composites.

Because of these issues, the reasonable cutting length needs to be decided to maximize the reinforcement. The length distribution of the 500 nm-cut SWNTs was shown in the Figure 14.10. There was about 65% SWNTs shorter than 500 nm. The average length was about 504 nm. In comparison, the pristine SWNTs' average length was about 580 nm and about 50% SWNTs were below 500 nm.

A large number of experimental efforts have been conducted on cut-CNT/polymer composites. For instance, samples of 0.5 wt% SWNTs reinforced epoxy composites were prepared. It was reported that the experimental average tensile strength was increased to 77.6 GPa, about 7% enhancement when the cut-SWNTs were applied in the composite. The average modulus was enhanced to 2.4 GPa,

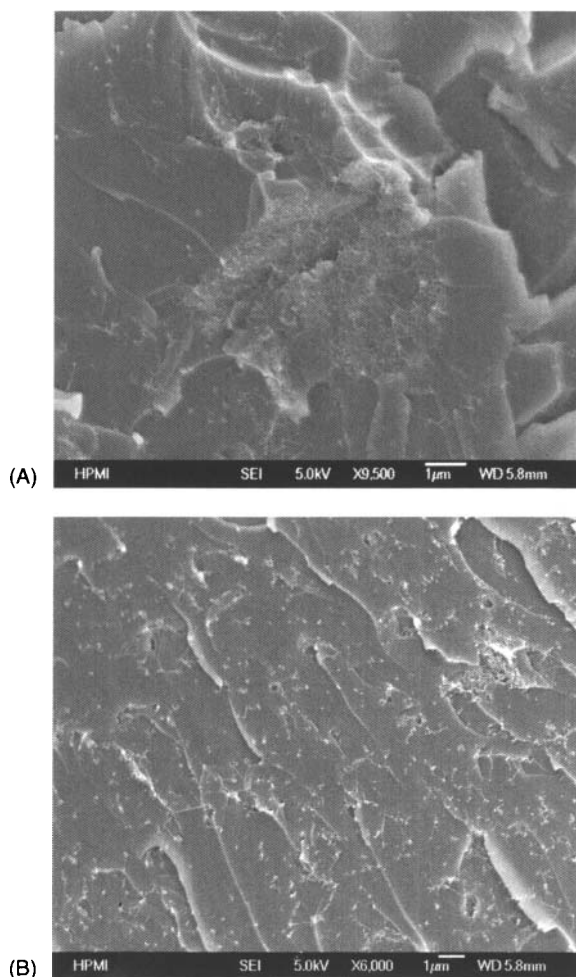


Figure 14.12. SEM images of CNT/Epoxy composites with the 0.5 wt% SWNT loading (a) pristine SWNT/epoxy, (b) cutting-SWNT/epoxy [11].

about 20% in contrast to the neat resin (11). The improvement of the tensile strength and modulus suggested that the cutting SWNTs have enhanced dispersion and interfacial bonding so that improved load transfer was achieved (Figure 14.11).

The cross-section of the nanocomposites was examined by SEM (JSM-7401F) and shown in the Figure 14.12. For the p-SWNT/epoxy composite, the CNTs tend to aggregate together and form large-diameter ropes. The phenomena of pullout can be observed. However, cut-SWNTs were well dispersed in the epoxy resin and

embedded in the epoxy matrix. Adhesion enhanced because of the increased true contact area. Therefore, the cutting enhanced the tensile strength and modulus by improving dispersion and interfacial bonding in SWNTs reinforced polymer composite.

14.2.3.3 *Film Impregnated-CNTs/Polymer Composites*

Since fabricating CNT-reinforced composites with good CNT dispersion and high CNT loading is a great challenge, an effective method was developed to fabricate nanocomposites with preformed CNT networks and high CNT loading. Buckypaper is such a macroscopic aggregate of CNT networks. It was produced by direct synthesis or multi-step filtration of aqueous dispersed CNTs. Then buckypaper was soaked into polymer resin (78) or filtrated with polymer resin (79), followed by drying and hot-pressing. These CNT buckypapers may find potential applications in micro-devices and electronic packaging with tailored properties and functions.

If pristine CNTs are directly fabricated into membranes through filtration process and then impregnated by polymer resin, they are called pristine CNT film based composites. High loading nanocomposites can be produced with outstanding tensile strength by effectively incorporating CNT buckypapers into matrix materials. For example, polycarbonate (PC) is a widely used engineering thermoplastic with high melting temperature and viscosity. These properties make it difficult to fabricate high-quality CNTs/PC composites through conventional injection or extrusion molding processes. Therefore, resin-infiltration technique was utilized. SEM characterization results revealed the controlled nanostructure in the resultant nanocomposites, as shown in Figure 14.13 and Figure 14.14 (79).

Figure 14.14 indicated that the impregantion of polycarbonate solution through buckypaper yielded controlled nanostructure in the nanocomposite. CNT ropes were homogeneously spread in the PC, and continuous intercalation networks formed in the resultant composite. With this technique, thermoplastic or thermosetting based nanocomposites with high CNT loading can be achieved by adjusting the viscosity of polymer solution.

Dynamic mechanical property tests indicated that the storage modulus of the resulting nanocomposites at 20 wt% CNTs loading was improved by a factor of 3.4 compared with neat PC material, as shown in Figure 14.15. It was reported that PC/buckypaper samples

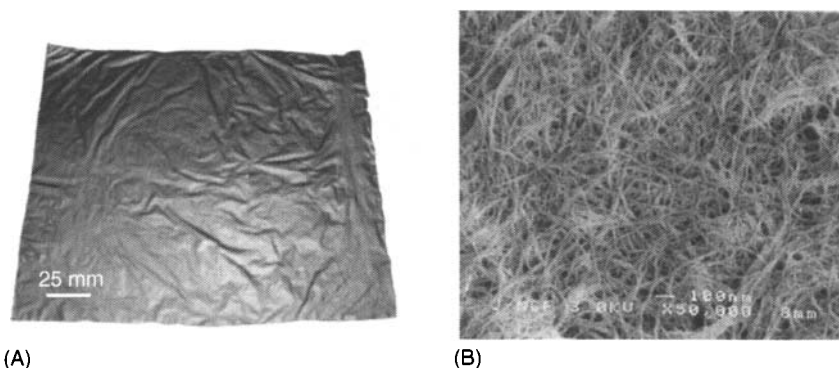


Figure 14.13. SWNT buckypaper (a) Buckypaper sample, (b) SEM image (79).

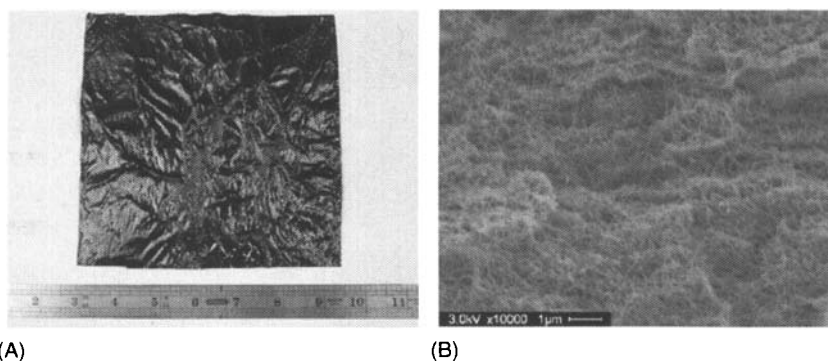


Figure 14.14. Impreganated buckypaper: (a) impreganated buckypaper sample, (b) SEM image of a cross-section of impreganated buckypaper (79).

exhibit higher tensile modulus (up to 122%), tensile strength (up to 203%), and elongation-to-fracture (up to 174%) than neat buckypaper samples (80). These results suggest the developed approach is an effective way to fabricate thermoplastic nanocomposites with good dispersion and high SWNT loading.

In comparison, electron beam irradiation was also utilized to crosslink isolated CNTs or their ropes of thin SWNT films in order to transform them into high-strength and multifunctional fabrics. It also provides a practical means to mass production of strong CNT membrane materials. Usually, SWNT membranes can be irradiated with electron accelerators. Figure 14.16 shows the effects of

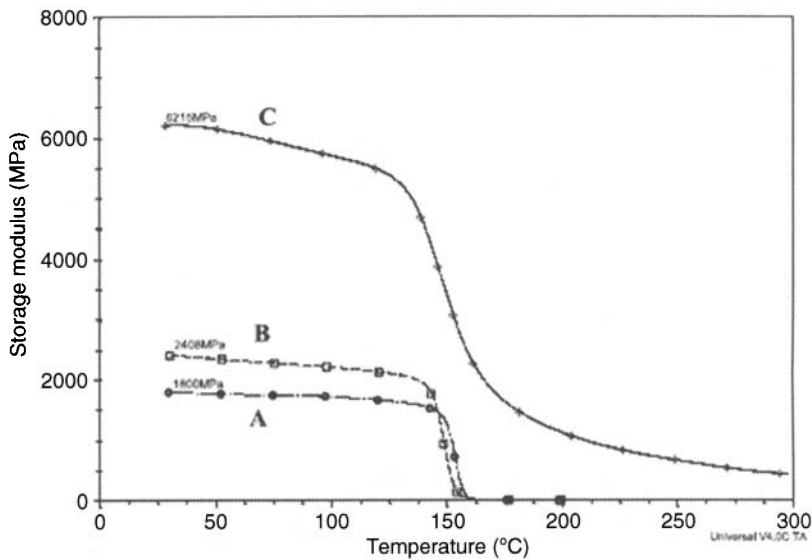


Figure 14.15. Dynamic mechanical analysis of SWNT reinforced PC composites: (A) pristine PC, (B) 2 wt% SWNTs/PC composite, (C) 20 wt% SWNT-buckypaper/PC composite [79].

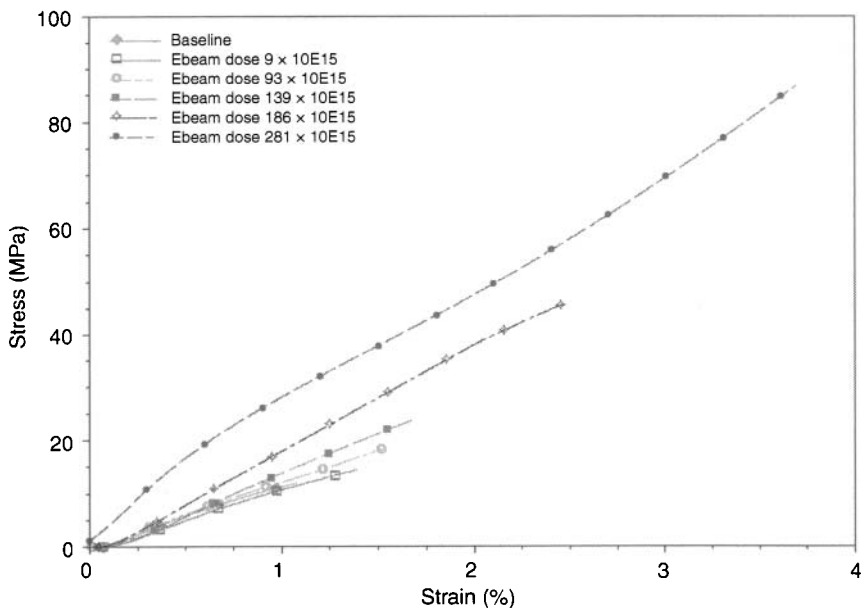


Figure 14.16. Tensile test curve of pristine and irradiated SWNT membrane.

irradiation doses on tensile properties of the SWNT membranes. From observations, it was concluded that the mechanical properties of the irradiated SWNT membranes were significantly improved.

Figure 14.17(a) indicated that there also existed a critical irradiation dose level for Young's modulus, above which substantial property improvement in Young's modulus was observed. Young's modulus of the SWNT membrane was not substantially

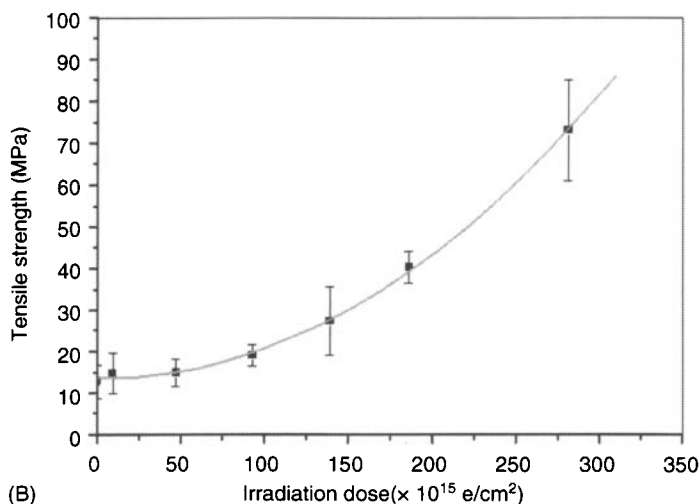
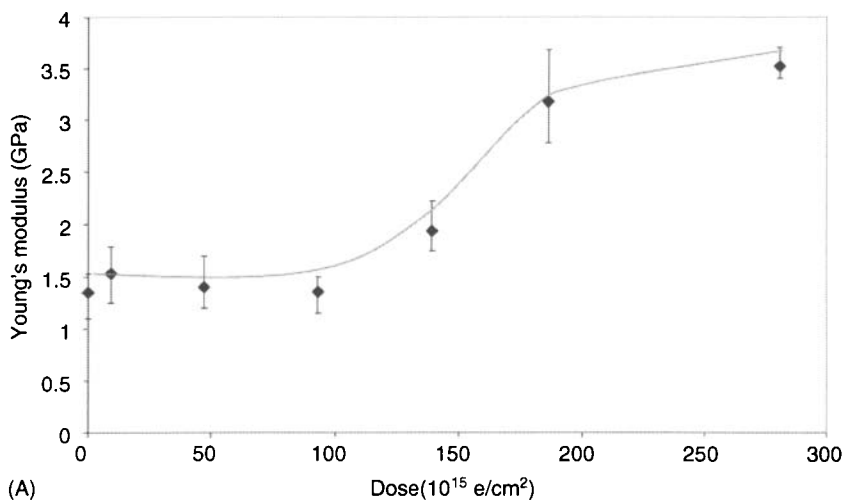


Figure 14.17. Young's modulus and tensile strength of SWNT membrane as a function of irradiation dose.

enhanced until the irradiation dose increased to a threshold value, $1.86 \times 10^{16} \text{ e/cm}^{-2}$.

On the other hand, the tensile strength of the irradiated membrane increased first gradually and then dramatically with the increase of irradiation dosage, as shown in Figure 14.17(b). High irradiation doses enhanced the strength of the thin membrane by a factor of about 6, making it as high as 80 MPa. This significant enhancement of properties indicated that SWNTs in the membranes were covalently bridged with each other, so that the interaction between tubes was transformed from non-covalent bonding forces (Van der Waals and electrostatic forces) to a combination of both covalent bonding and non-covalent bonding forces. Since SWNT membrane is a single-phase material consisting of anisotropic discontinuous fullerene tubes, its tensile strength is heavily dependent upon the interactions between isolated CNTs. It was almost approximately proportional to the interaction potential energy among these tubes. Induced cross-linkage noticeably raised the existing interaction energy, resulting in an exponential increase in strength. Regression analysis suggests that the tensile strength was approximated to the quadratic function of the irradiation dosage. Since tensile strength was almost proportional to the density of CNT cross-linkage in the membrane before intensive devastation caused by irradiation occurred, the cross-linkage density of the treated fabrics was approximately a quadratic function of irradiation doses.

Inter-tube covalent bonding can be confirmed with TEM images. For as-produced tube bundles, the walls of SWNTs were straight and clear. After electron beam irradiation, the sidewalls were etched and some atoms were knocked-out, as shown in Figure 14.18. Cross-linkage also significantly changed the CNT morphologies. Dangling carbons, which ended up with mobile interstitials, were coupled with counterparts and blurred the previously clear and straight tube walls.

The irradiated CNT buckypaper with porous structure can be applied to fabricating the nanocomposites. The porous structure composed by small CNT ropes allow for the resin infiltration when the polymer molecular is smaller than the pore dimension. In order to avoid squeezing out too much resin from impregnated CNT buckypapers, low pressure (such as 200Psi) was usually applied during the hot-pressing. For instance, the loading of SWNTs was 12.3 wt% and 13.5 wt% for pristine and irradiated CNT buckypaper/epoxy composite, respectively. Then the tensile test of the hot-pressed

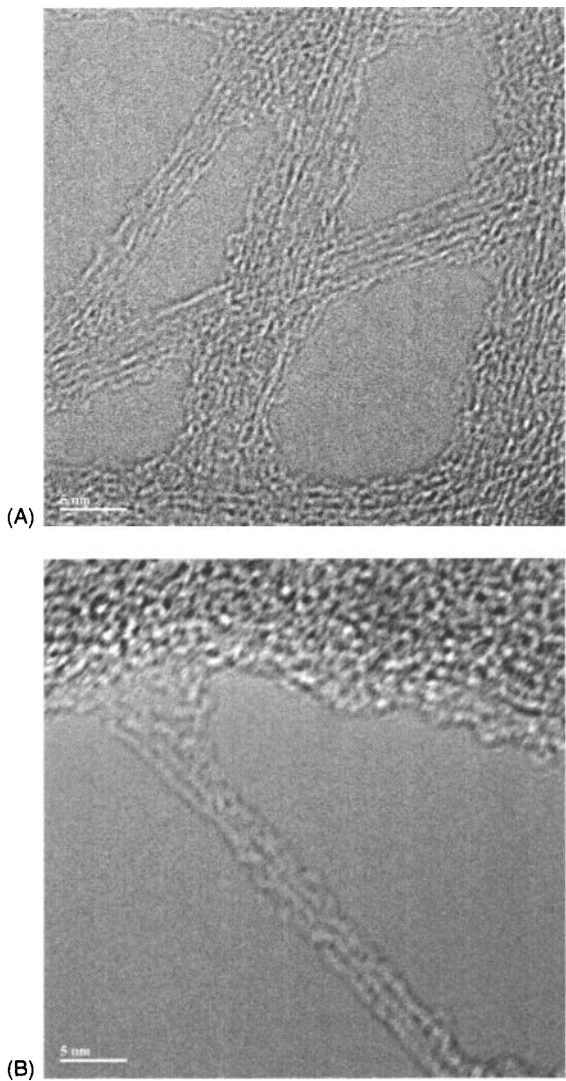


Figure 14.18. TEM images of cross-linkage in the irradiated SWNT membrane.

CNT buckypaper/epoxy composites was conducted. The tensile test results are shown in the Figure 14.19, and tensile properties were summarized in Figure 14.20.

For the neat resin, the Young's modulus was about 2GPa and strength 72.5 MPa. For the pristine buckypaper composite, the Young's modulus increased to 4 GPa with the increment of one fold while the tensile strength decreased to 51 MPa with about 13%

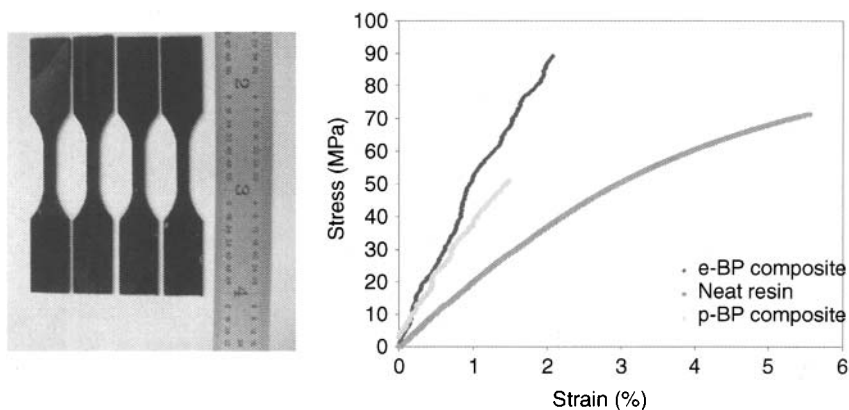


Figure 14.19. Typical samples and curves of the tensile tests for buckypaper (BP) composites. (p-BP composite: pristine CNT buckypaper composites, e-BP composite: electron beam treated CNT buckypaper composites (11).)

reduction. For the e-beam treated buckypaper composite, not only the modulus enhanced by 1.35 folds, but also the tensile strength increased by 17.4%. These enhancements should arise from the improvement of the interfacial bonding within ropes and between CNTs and epoxy matrix.

The experimental results indicated that the irradiated buckypaper can be applied to fabricate nanocomposites and showed certain improvement in both modulus and strength, which decreased in the un-irradiated buckypaper composites. However, the enhancement was not as striking as expected. More significant improvement should be achieved by increasing the interfacial bonding through removing the unwanted surfactant before e-beam treatment.

Obviously, all the typical chemical modification methods used on pristine CNTs including oxidization, grafting via carboxyl, *in-situ* polymerization, fluorination, cutting and subsequent functionalization may also be applied on CNT buckypaper. If chemical functionalization was applied during the fabrication of buckypapers, the integrated functionalized-buckypaper /polymer composites will provide more significant improvement in tensile properties. These methods enhance the reactivity of CNTs and make it possible to obtain a stronger chemical bonding between CNTs and polymer matrix. The covalent bonding makes it possible to provide strong interfacial shear stress and effective load transfer. It was demonstrated that both mechanical and electrical properties were remarkably enhanced if CNT were chemically functionalized before resin infiltration (81).

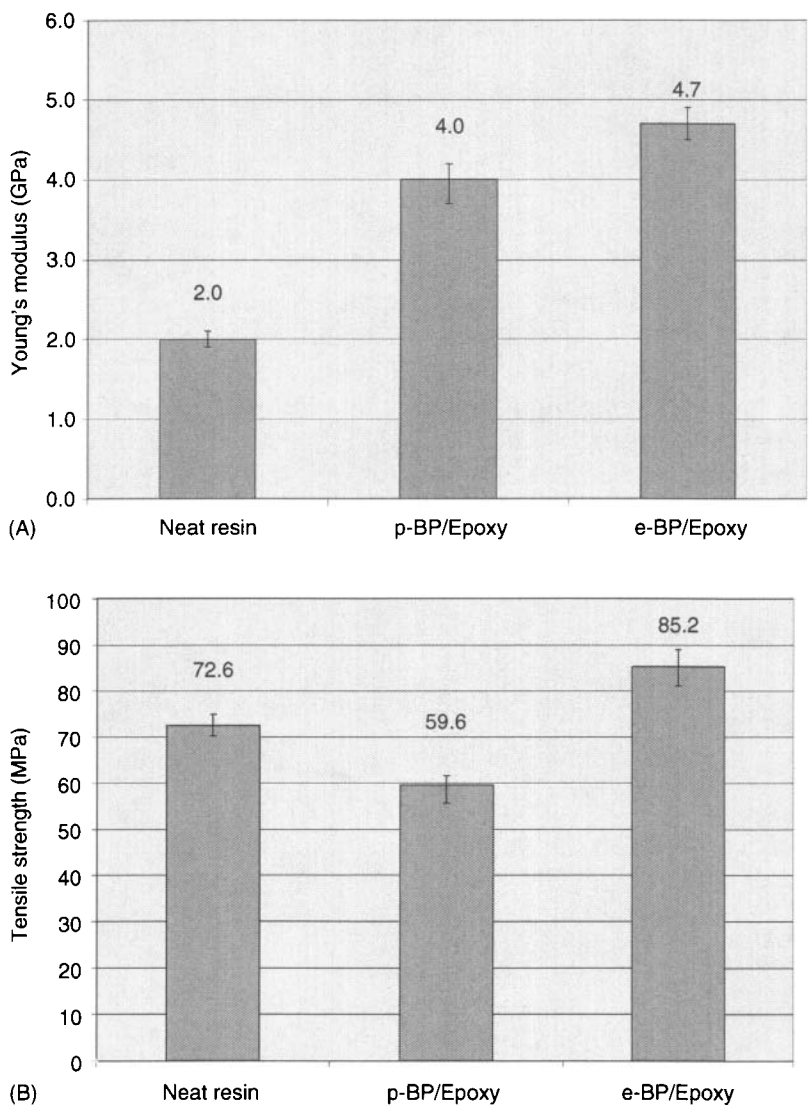


Figure 14.20. Tensile test results of the NBP composites (a) Histogram graph of the Young's modulus. (b) Histogram graph of the tensile strength (11).

14.3 Concluding Remarks

In this chapter, different morphologies of CNTs during fabrication were investigated, including isolated CNTs, short CNTs and CNT networks. The effect of morphologies and structures on tensile

properties was discussed in details. Generally, the addition of CNTs into polymer matrix resulted in improvement in tensile modulus and tensile strength if good dispersion and strong interfacial bonding are achieved. Compared with pristine CNT/polymer composites, enhanced tensile modulus and strength may be obtained for shorten CNT/polymer composites by precise sectioning of CNT through ultra-microtome. However, the high aspect ratio of CNTs was sacrificed. Especially, tensile properties were substantially improved via chemical or physical functionalization due to the enhanced reactivity on CNT sidewalls and the improved interfacial bonding. It should be noted that film-impregnated CNT/polymer composites were readily handled compared with the conventional casting or melting-processed CNT/polymer composites. Therefore, the improved interfacial bonding strongly enhanced the effectiveness of load-transfer and makes it possible to take full advantage of the exceptional performance of CNTs.

References

1. M.M.J. Treacy, T.W. Ebbesen, and T.M. Gibson, *Nature*, Vol. 381, p. 678, 1996.
2. E.W. Wong, P.E. Sheehan, and C.M. Lieber, *Science*, Vol. 277, p. 1971, 1997.
3. E. Dujardin, T.W. Webbese, A. Krishan, P.N. Yianilos, and M.M.J. Treacy, *Physical Review B*, Vol. 58, p. 14013, 1998.
4. M.R. Falvo, G.J. Clary, R.M. Taylor, V. Chi, F.P. Brooks, and S. Washburn, *Nature*, Vol. 389, p. 582, 1997.
5. S. Wang, Z. Liang, B. Wang, and C. Zhang, *Nanotechnology*, Vol. 17, p. 634, 2006.
6. S. Wang, R. Liang, B. Wang, and C. Zhang, *Chemical Physics Letters*, Vol. 457, p. 371, 2008.
7. C. Bower, R. Rosen, L. Jin, J. Han, and O. Zhou, *Applied Physics Letters*, Vol. 74, p. 3317, 1999.
8. E.T. Thostenson, and T.-W. Chou, *Journal of Physics, D: Applied Physics*, Vol. 36, p. 573, 2003.
9. S. Wang, R. Liang, B. Wang, and C. Zhang, *Carbon*, Vol. 47, p. 53, 2009.
10. H.W. Zhu, C.L. Xu, D.H. Wu, B.Q. Wei, R. Vajtai, and P.M. Ajayan, *Science*, Vol. 296, p. 884, 2002.
11. S. Wang, "Functionalization of Carbon Nanotubes: Characterization, Modeling and Composite Application", Doctoral Dissertation, Florida State University, 2006.
12. L. Zhu, and K.A. Narh, *Polymer International*, Vol. 53, p. 1461, 2004.
13. J. Xiong, Z. Zheng, X. Qiu, M. Li, H. Li, and X. Wang, *Carbon*, Vol. 44, p. 2701, 2006.
14. D. Shi, X. Feng, Y. Huang, K. Hwang, and H. Gao, *Journal of Engineering Materials and Technology, Transactions of the ASME*, Vol. 126, p. 250, 2004.

15. F. Buffa, G.A. Abraham, B.P. Grady, and D. Resasco, *Journal of Polymer Science, Part B: Polymer Physics*, Vol. 45, p. 490, 2007.
16. C. Wei, and D. Srivastava, *Nano Letters*, Vol. 4, p. 1946, 2004.
17. S. Iijima, *Nature*, Vol. 354, p. 56, 1991.
18. D.S. Bethune, C.H. Kiang, M.S. Devries, G. Gorman, R. Savoy, and J. Vazquez, *Nature*, Vol. 363, p. 605, 1993.
19. S. Iijima, and T. Ichihashi, *Nature*, Vol. 363, p. 603, 1993.
20. M.M.J. Treacy, T.W. Ebbesen, and T.M. Gibson, *Nature*, Vol. 381, p. 678, 1996.
21. E.W. Wong, P.E. Sheehan, and C.M. Lieber, *Science*, Vol. 277, p. 1971, 1997.
22. Y. Guo, and W. Guo, *Journal of Physics, D: Applied Physics*, Vol. 36, p. 805, 2003.
23. S. Portal, E. Artacho, J.M. Soler, A. Rubio, and P. Ordejón, *Physical Reviews B*, Vol. 59, p. 2678, 1999.
24. J.P. Lu, *Physical Reviews Letters*, Vol. 79, p. 1297, 1997.
25. J.P. Salvetat, , A.J. Kulik, J.M. Bonard, G.D.A. Briggs, T. Stöckli, K. Métierier, S. Bonnamy, F. Béguin, N.A. Burnham, and L. Forró, *Advanced Materials*, Vol. 11, p. 161, 1999.
26. S. Xie, W. Li, Z. Pan, B. Chang, and L. Sun, *Journal of Physics and Chemistry of Solids*, Vol. 61, p. 1153, 2000.
27. M.F. Yu, B.S. Files, S. Arepalli, and R.S. Ruoff, *Physical Review Letters*, Vol. 84, p. 5552, 2000.
28. M.F. Yu, T. Kowalewski, and R.S. Ruoff, *Physical Review Letters*, Vol. 85, p. 1456, 2000.
29. M.F. Yu, O. Lourie, M. Dyer, K. Moloni, T.F. Kelly, and R.S. Ruoff, *Science*, Vol. 287, p. 637, 2000.
30. D.A. Walters, L.M. Ericson, M.J. Casavant, J. Liu, D.T. Colbert, K.A. Smith, and R.E. Smalley, *Applied Physics Letters*, Vol. 74, p. 3803, 1999.
31. B.I. Yakobson, C. J. Brabec, and J. Bernholc, *Physical Review Letters*, Vol. 76, p. 2511, 1996.
32. L.S. Schadler, S.C. Giannaris, and P.M. Ajayan, *Applied Physics Letters*, Vol. 73, p. 3842, 1998.
33. A.V. Desai, and M.A. Haque, *Thin-Walled Structures*, Vol. 43, p. 1787, 2005.
34. C.A. Cooper, R.J. Young, and M. Halsall, *Composites: Part A: Applied Science and Manufacturing*, Vol. 32, p. 401, 2001.
35. S. Kumar, H. Doshi, M. Srinivasrao, J.O. Park, and D.A. Schiraldi, *Polymer*, Vol. 43, p. 1701, 2002.
36. S. Kumar, T.D. Dang, F.E. Arnold, A.R. Bhattacharyya, B.G. Min, X. Zhang, R.A. Vaia, C. Park, W.W. Adams, R.H. Hauge, R.E. Smalley, S. Ramesh, and P.A. Willis, *Macromolecules*, Vol. 35, p. 9039, 2002.
37. J. Gou, B. Minaie, B. Wang, Z. Liang, and C. Zhang, *Computational material Science*, Vol. 31, p. 225, 2004.
38. E.T. Thostenson, and T.-W. Chou, *Journal of Physics, D: Applied Physics*, Vol. 35, p. 77, 2002.
39. K. Kordas, T. Mustonen, G. Toth, H. Jantunen, M. Lajunen, C. Soldano, S. Talapatra, S. Kar, R. Vajtai, and P.M. Ajayan, *Small*, Vol. 2, p. 1021, 2006.
40. J.N. Coleman, U. Khan, and Y.K. Gunko, *Advanced Materials*, Vol. 18, p. 689, 2006.

41. T.V. Sreekumar, T. Liu, B.G. Min, H. Guo, S. Kumar, R.H. Hauge, and R.E. Smalley, *Advanced Materials*, Vol. 16, p. 58, 2004.
42. E.T. Thostenson, and T.-W. Chou, *Advanced Materials*, Vol. 18, p. 2837, 2006.
43. J. Qiu, C. Zhang, B. Wang, and R. Liang, *Nanotechnology*, Vol. 18, p. 275708, 2007.
44. P.M. Ajayan, L.S. Schadler, C. Giannaris, and A. Rubio, *Advanced Materials*, Vol. 12, p. 750, 2000.
45. S. Wang, Z. Liang, T. Liu, B. Wang, and C. Zhang, *Nanotechnology*, Vol. 17, p. 1551, 2006.
46. S. Wang, R. Liang, B. Wang, and C. Zhang, *Carbon*, Vol. 45, p. 3042, 2007.
47. J. Zhu, J.D. Kim, H. Peng, J.L. Margrave, V.N. Khabashesku, and E.V. Barrera, *Nano Letters*, Vol. 3, p. 1107, 2003.
48. Z. Gu, H. Peng, R.H. Hauge, R.E. Smalley, and J.L. Margrave, *Nano Letters*, Vol. 2, p. 1009, 2002.
49. S. Wang, Z. Liang, B. Wang, C. Zhang, and Z. Rahaman, *Nanotechnology*, Vol. 18, p. 055301, 2007.
50. J. Chen, *Journal of the American Chemical Society*, Vol. 123, p. 6201, 2001.
51. X. Gong, J. Liu, S. Baskaran, R.D. Voise, and J. S. Young, *Chemistry of Materials*, Vol. 12, p. 1049, 2000.
52. V.P. Veedu, A. Cao, X. Li, K. Ma, C. Soldano, S. Kar, P.M. Ajayan, and M.N. Ghasemi-Nejhad, *Nature Materials*, Vol. 5, p. 457, 2006.
53. X. Song, S. Liu, Z. Gan, Q. Lv, H. Cao, and H. Yan, *Microelectronic Engineering*, Vol. 86, p. 2330, 2009.
54. Y.-H. Liao, O. Marietta-Tondin, Z. Liang, C. Zhang, and B. Wang, *Materials Science and Engineering A*, Vol. 385, p. 175, 2004.
55. Z. Jin, X. Sun, G. Xu, S. Goh, and W. Ji, *Chemical Physics Letters*, Vol. 318, p. 505, 2000.
56. M. Yudasaka, M. Zhang, C. Jabs, and S. Iijima, *Applied Physics, A: Materials Science and Processing*, Vol. 71, p. 449, 2000.
57. O. Breuer, and U. Sundararaj, *Polymer Composites*, Vol. 25, p. 630, 2004.
58. P. Potschke, T.D. Fornes, and D.R. Paul, *Polymer*, Vol. 43, p. 3247, 2002.
59. R. Andrews, D. Jacques, M. Minot, and T. Rantell, *Macromolecular Materials and Engineering*, Vol. 287, p. 395, 2002.
60. J.C. Kearns, and R.L. Shambaugh, *Journal of Applied Polymer Science*, Vol. 86, p. 2079, 2002.
61. D.J. Burton, D.G. Glasgow, M.L. Lake, C. Kwag, and J.C. Finegan, 46th International SAMPE Symposium and Exhibition: Materials and Processes Odyssey, Long Beach, California, May 2001.
62. P.M. Ajayan, O. Stephan, C. Colliex, and D. Trauth, *Science*, Vol. 265, p. 1212, 1994.
63. L. Jin, C. Bower, and O. Zhou, *Applied Physics Letters*, Vol. 73, p. 1197, 1998.
64. C. Bower, R. Rosen, J. Lin, J. Han, and O. Zhou, *Applied Physics Letters*, Vol. 74, p. 3317, 1999.
65. X.Q. Chen, T. Saito, H. Yamada, and K. Matsushige, *Applied Physics Letters*, Vol. 78, p. 3714, 2001.
66. B.W. Smith, Z. Benes, D.E. Luzzi, J.E. Fischer, D.A. Walters, M.J. Casavant, J. Schmidt, and R.E. Smalley, *Applied Physics Letters*, Vol. 77, p. 663, 2000.

67. J. Casavant, D.A. Walters, J.J. Schmidt, and R.E. Smalley, *Journal of Applied Physics*, Vol. 93, p. 2153, 2003.
68. J. Liu, A. G.Rinzler, H. Dai, J.H. Hafner, R.K. Bradley, P.J. Boul, A. Liu, T. Iverson, K. Shelimov, C.B. Huffman, F. Rodriguez-Macias, Y.S. Shon, T.R. Lee, D.T. Colbert, and R.E. Smalley, *Science*, Vol. 280, p. 1253, 1998.
69. J. Chen, M.A. Hamon, H. Hu, Y.S. Chen, A. M. Rao, P.C. Eklund, and R.C. Haddon, *Science*, Vol. 282, p. 95, 1998.
70. A. Javey, P. Qi, Q. Wang, and H. Dai, *PNAS*, Vol. 101, p. 13408, 2004.
71. E. Farkas, M.E. Anderson, Z. Chen, and A.G. Rinzler, *Chemical Physics Letters*, Vol. 363, p. 111, 2002.
72. J. Chen, *Journal of the American Chemical Society*, Vol. 123, p. 6201, 2001.
73. D.-H. Oh, and Y.H. Lee, *Physics Reviews B*, Vol. 58, p. 7407, 1998.
74. Z. Gu, H. Peng, R.H. Hauge, R.E. Smalley, and J.L. Margrave, *Nano Letters*, Vol. 2, p. 1009, 2002.
75. M. Yudasaka, M. Zhang, C. Jabs, and S. Iijima, *Applied Physics A*, Vol. 71, p. 449, 2000.
76. H. Yanagia, E. Sawada, A. Manivannan, and L.A. Nagahara, *Applied Physics Letters*, Vol. 78, p. 1355, 2001.
77. M. Zhang, M. Yudasaka, A. Koshio, C. Jabs, T. Ichihashi, and S. Iijima, *Applied Physics A*, Vol. 74, p. 7, 2002.
78. C.J. Frizzell, M. in het Panhuis, D.H. Coutinho, K.J. Balkus, A.I. Minett, W.J. Blau, and J.N. Coleman, *Physical Reviews B*, Vol. 72, p. 245420, 2005.
79. S. Wang, Z. Liang, G. Pham, Y.B. Park, B. Wang, C. Zhang, L. Kramer, and P. Funchess, *Nanotechnology*, Vol. 18, p. 095708, 2007.
80. G.T. Pham, Y.-B. Park, S. Wang, Z. Liang, B. Wang, C. Zhang, P. Funchess, and L. Kramer, *Nanotechnology*, Vol. 19, p. 325705, 2008.
81. S. Wang, R. Liang, Y. Xue, B. Wang, and C. Zhang, "Functionalization of SWNT buckypapers through electron-beam irradiation", 39th ISTC – Cincinnati, OH, 2007.

This Page Intentionally Left Blank

Polymer Nanotube Composites: Promises and Current Challenges

Amal M.K. Esawi and Mahmoud M. Farag

*Department of Mechanical Engineering
The American University in Cairo, New Cairo Campus
AUC Avenue, P.O. Box 74 New Cairo 11835, Egypt*

Abstract

Designing a new composite is a lengthy process and involves high costs. Being aware of the strengths and weaknesses of the new composite is thus critical. In this chapter, we compare predicted upper bounds for mechanical and electrical properties of CNT composites to published experimental data. It is highlighted that the experimental values are falling short of the values predicted by theory. The chapter highlights the factors leading to such discrepancies.

Two case studies are presented in which polymer nanotube composites are proposed as replacements for conventional materials. We evaluate the technical and economic feasibility of using them as smart materials for strain gauges; thus, exploiting their electrical properties, and as structural materials for aircraft panels; bringing into play their mechanical properties. Our analysis shows that as new strain gauge materials, polymer nanotube composites offer many advantages. As a possible replacement for aluminum in an aircraft panel, it is found that a hybrid composite of (Epoxy 33% carbon fabric + 30% carbon fibers + 3% CVD-MWNT) is an attractive candidate.

Keywords: polymer matrix composites; carbon nanotubes; cost; materials substitution.

15.1 Carbon Nanotubes

15.1.1 Background

In view of their excellent properties, carbon nanotubes (CNTs) have been in the spotlight since their discovery in 1991. They have been labeled the “material for the 21st century” (1). They are structures of nano-dimensions made up of rolled sheets of graphite. Nanotubes are classified as either single-walled nanotubes (SWNTs) or multi-walled nanotubes (MWNTs). Their properties are a mix of diamond and graphite: strong, thermally conductive like diamond; electrically conductive like graphite. CNTs can be either metallic or semi-conducting depending on their chirality. With typical diameters of 1 – 140 nm and lengths in the μm scale, they have very high aspect ratios. They are also light and flexible.

Carbon nanotubes are being heavily researched. Their electrical, electronic and thermal properties have been the focus of the researchers’ interests (1–12). They have been used or else are being considered for many applications such as conductive polymers for use in the automotive industry (for car body panels that can be electro-statically painted), anti-static semi-finished products based on PEEK, and in the aerospace industry (to protect from lightning strikes as well as shield against electromagnetic interference); sensors and actuators; field emission displays; replacing silicon in microcircuits; multilevel chips; probes for SPM (scanning probe microscopy); membrane materials for desalination and gas separation; energy storage/conversion devices such as batteries and solar cells; packaging of computer chips.

Being rolled up graphite sheets, their mechanical properties are expected to be equal to or greater than the value for a graphene sheet. Qualitative and quantitative TEM and AFM studies have been performed on individual tubes and have confirmed their extraordinary strength and stiffness (2–6). The Young’s modulus of a defect-free CNT is over 1 TPa. Its estimated tensile strength is over 50 GPa. Values for commercially available CNTs are, however, much lower due to their structural defects. Their high elastic modulus and strength has led to enthusiasm toward CNTs as reinforcements for advanced composite materials (1–12). Heavy research efforts are being conducted in this respect. Commercial applications in the sports equipment industry are continually emerging (ice-hockey sticks, baseball bats, tennis racquets, surfboards, etc.).

Potential applications in remote-controlled flying cameras, rotor blades of wind power plants, as well as replacing conventional metal and ceramic-based composites in automotive and aerospace components are under development.

15.1.2 Synthesis of CNTs

Both chemical and physical methods are used to synthesize CNTs (1–12). Electric Arc Discharge is the classic technique in which an arc is created between a graphite cathode and a graphite anode. By adding a catalyst (Co, Ni, Fe and Y powder), CNTs condense on the surface of the cathode. Although the yield of this process is low, it produces nanotubes with few structural defects. In Laser Ablation, carbon nanotubes form in the plume of carbon vapour evaporated by a laser from a graphite target held at 1200°C. Adding metal dispersions to the target results in the formation of SWNTs. Chemical Vapour deposition (CVD) (catalytic methods) is the most common method in which a controlled reaction of the decomposition of a hydrocarbon gas (methane, carbon monoxide or acetylene) on a metal catalyst such as Ni, Fe or Co produces multiwalled CNTs (MWNT). The three techniques described above produce random SWNTs and MWNTs. A variant of CVD: Plasma Enhanced CVD (PECVD) can produce aligned arrays of CNTs with controlled diameter and length but is more costly. Because large quantities are required for reinforcing composites, of the current synthesis methods, CVD is believed to offer the best potential for scaling up since the carbon source is a flowing gas. Another technique - flame synthesis - seems to hold promise for low-cost synthesis of SWNTs (13).

Until recently, the exorbitant prices of CNTs meant that they were only used in limited quantities; mainly in applications in high-tech fields such as the optics/electronics fields. We have reported in our previous paper (12) that CNTs cost between 5 to 800 \$/g depending on their type (SWNT/MWNT), synthesis process (Arc/CVD), diameter, purity and defect density and stressed that to continue to encourage wider applications of CNTs, efficient novel processing routes, which could be scaled up for commercial production, should be explored. In fact, compared to three years ago, new CNT suppliers have appeared in the market offering CNTs at much lower prices than was previously the case. Table 15.1 lists some suppliers of MWNTs and SWNTs and the 2009 prices and specifications of their products (13–18). Prices given are based on kg quantities,

whenever available. The availability of kg quantities of MWNTs, purities reaching 99% as well as the prices which are more than ten times cheaper than in 2006 is worth-noting. One example is the Bayer MaterialScience Company who has recently patented a catalytic chemical vapour deposition (CCVD) process that allows industrial scale production of low cost MWNTs, with plans for increasing their production capacity in the near future to cope with the forecasted growing market (16). It is also worth reporting that the cheapest commercially available SWNTs currently cost 13,000 \$/kg and thus their potential use in reinforcing composites on a large scale is limited.

Although a few research groups, for example, the US Department of Energy Los Alamos National Lab and the University of Cincinnati (UC) are developing nanotubes with lengths in the mm to cm range for specific applications, commercially available nanotubes have lengths in the tens of microns range as seen in Table 15.1. In our previous paper (12), we have stressed that for effective load transfer from the polymer matrix to the CNTs, their lengths have to exceed a certain critical length l_c and we concluded from our analysis that longer nanotubes than what was available commercially at the time were needed for effective strengthening and stiffening in composites. This point is further stressed here although it seems that producers can currently produce longer CNTs than was the case previously. It is also noted that our earlier analysis assumed a CNT strength of 60 GPa which is typical for SWNT or Arc MWNT. CVD MWNTs, on the other hand, which are more likely to be used to reinforce composites have strength values of around 10 GPa and therefore the estimated critical length would be more in line with the commercially available lengths especially for smaller diameter CNTs which are well bonded to the polymeric matrix.

15.1.3 Fabrication of CNT Polymer Composites

Various research groups have used both SWNTs and MWNTs in different weight fractions to fabricate Polymer Nanotube Composites. A variety of methods have been investigated for mixing CNTs with the polymer powder including direct mixing which is used for thermosetting resins; *in-situ* polymerization in which CNTs are mechanically dispersed in an un-polymerized solution containing the polymer monomer then the nanotubes are locked into the polymer matrix by polymerization; and melt processing which involves

Table 15.1. Comparison between 2009 prices of different types of commercially available MWNTs and SWNTs (13–18)

Supplier (Product)	CNT type	Purity (% nanotubes)	Diameter (nm)	Length (μm)	Density (g/cc)	Price*
Cheaptubes.com	CCVD-MWNT	95 %	8-50 nm OD	10–50	0.27 bulk 2.1 true	400–1500 \$/kg
Bayer MaterialScience (Baytubes®)	Catalytic - MWNT	95–99 %	13–16 nm	1–>10	140–230 kg/m ³ bulk	560–700 \$/kg
Thomas Swan (Elicarb)	High Purity MWNT	70–90%	10–12 nm	tens of microns		32–80 \$/g
Arkema (Graphistrength®C100)	Catalytic CVD	> 90 %	10–15	0.1–10	2.1 g/ml	11–18 \$/g
MER	Catalytic MWNT	> 90 %	140 + / - 30	7 \pm 2	0.1 powder 1.9 bulk	10–20 \$/g (5000 \$/kg)
MER	Catalytic MWNT	> 90 %	35 + / - 10	30	1.9	35–60 \$/g
MER	Arc MWNT	30–40 %	6–20	1–5	0.7 powder	15–25 \$/g
Cheaptubes.com	CCVD-SWCNT	60–90 %	1–2 nm OD		0.14 bulk 2.1 true	45–95 \$/g (13,000 –32,000 \$/kg)
Thomas Swan (Elicarb)	High Purity SWCNT	> 70 %	< 2 nm			163–327 \$/g

* Price depends on quantity purchased, CNT diameter, and purity.

mechanically dispersing the CNTs into the polymer melt using a mixer (2,3,7,8,10–12,19). Melt processing using conventional polymer processing techniques such as extrusion and injection moulding has become a very popular technique for the fabrication of CNT-polymer composites due to its low cost and availability. Additionally, shear forces during melt mixing (or melt processing), have been reported to disentangle the CNT aggregates and thus aid the dispersion of the CNTs within the polymer matrix (7,11,19,20). However, careful control of the process parameters must be exercised in order to avoid polymer degradation and also to take into account the increased viscosity of the CNT-polymer mix. Shortening of the CNTs was also reported in one study and was attributed to high shear rates (20).

There seems to be an agreement among researchers, irrespective of the technique used, that the main challenges facing the production of composites with enhanced behavior are dispersion, alignment and interfacial load transfer (2–12,19,20). Dispersion has been a particularly critical factor and thus improving dispersion by employing different techniques has been heavily researched (11,12,19). Several research teams have used the solvent method (or solution processing) in which a solvent dissolves the solid thermoplastic polymer to which the CNTs are added and then the mixture is sonicated. Alternatively, the CNTs are first dispersed in the solvent before adding the polymer or polymer solution. Upon achieving dispersion of the CNTs in the polymer, the solvent is evaporated and the polymer is re-solidified forming a composite film. Alternatively, the CNT polymer mix, thus formed, is further processed by conventional melt processing techniques (21). Often a surfactant is used to aid the dispersion of pristine CNTs in the chosen solvent. Due to its proved effectiveness, the solvent method is becoming the most common method for dispersing CNTs in soluble polymers. However, there is concern that the solvents influence the mechanical performance of the composite (22–24) and that the sonication energy tends to break the CNTs into shorter lengths (25). Additionally, given that the technique requires the evaporation of large amounts of solvent, it doesn't hold promise for low-cost large scale-production (26).

The use of surfactants and the chemical functionalization of CNT surfaces have also been investigated in efforts to improve CNT dispersion as well as enhance the CNT-polymer interfacial bond (10,27–29). However, although chemical functionalization can lead

to a stronger interface between the CNT and the polymer matrix, reduction in mechanical properties of composites based on functionalized CNTs has been reported (25,30).

Although aligning the CNTs within the polymer matrix hasn't received as much attention as dispersion and chemical functionalization, possibly due to it being considered a less critical issue for effective mechanical reinforcement (11), the use of an electric field (31) or alternatively melt-drawing an extruded film or rod of the CNT-polymer composite have been reported to achieve alignment of CNTs (32,33). Rather than bulk composites, melt processing of composite fibers using extrusion, drawing or fiber spinning was also reported to produce highly aligned nanotubes (34–36).

15.1.4 Electrical Properties of CNT Polymer Composites

In view of their possession of electrical conductivities comparable to copper, CNTs have been the subject of substantial research aiming at making conductive polymers. Researchers have found that CNTs can impart conductive properties to polymers provided the minimum percolation threshold – or minimum amount of CNTs at which a continuous network of CNTs is formed – is reached. This parameter depends on a number of factors: CNT type (SWNT or MWNT), its aspect ratio, synthesis technique (arc evaporation, CVD, laser, etc.), degree of dispersion, alignment and polymer matrix. Many researchers have focused on investigating the electrical percolation thresholds of a variety of CNT-reinforced polymers. Percolation thresholds were generally found to be much lower than other conductive fillers such as metal particles and carbon black due to the high aspect ratios of CNTs and their nanoscale dimensions (37). Significant variations, however, were reported even for the same polymer matrix. Additionally, the use of different CNT types, different synthesis methods and different treatments has led to additional difficulties in interpreting the results. A recent review by Bauhofer and Kovacs (38) concluded that the type of polymer and dispersion method play a bigger role in defining the minimum percolation threshold than the type and production method of CNT.

As noted by Ashby (39), calculating the exact values of properties of composites is difficult, even on a macroscopic scale, so bounds or limits are often used. The value of the property cannot exceed or

fall below the bound. Subject to certain assumptions, the electrical conductivity of a CNT-polymer parallel to the CNT direction can be derived simply from the rule-of-mixtures.

$$S_c = V_{\text{CNT}} S_{\text{CNT}} + (1 - V_{\text{CNT}}) S_m \quad (15.1)$$

where S_c , S_{CNT} and S_m are electrical conductivities of the composite, CNT and matrix, respectively.

V_{CNT} is the volume fraction of CNT.

In order to estimate the theoretical upper bounds for the electrical conductivities of polymer nanotube composites, equation (15.1) was used to calculate conductivity values for model composites based on both SWNT and MWNT. The values are included in Table 15.2 together with the electrical conductivities of individual CNTs; as reported in the literature. Although arc-synthesized MWNTs are likely to possess higher conductivities than CVD-grown ones, no distinction is made in the present analysis between the two types due to the unavailability of reliable data. An electrical conductivity of 1E^{-9} S/m is taken to represent the conductivity of a typical polymer matrix.

The model composites in Table 15.2 contain either 1 vol% if using SWNT, or 20 vol% in the case of MWNT. This is the maximum possible CNT loading that the polymer matrix can accommodate such that every polymer strand is within 5 nm of the CNT, as proposed by Coleman et al. (11). Since the electrical conductivity of a composite is proportional to the volume fraction of the CNTs in it, the predicted conductivity of a polymer composite based on MWNTs is higher by one order of magnitude than that of one based on SWNTs. Equation 15.1 assumes that the CNTs are well dispersed and aligned and thus gives the idealized upper bound. However, processing problems such as agglomeration of CNTs, segregation of CNTs and matrix, and non-uniform distribution become more significant as the volume fraction increases. The high viscosity of

Table 15.2. Electrical conductivities of different types of CNTs and the maximum conductivities of their composites

CNT type	V_f (%)	S_{CNT} (S/m)	S_c^* (S/m)
SWNT	1	3E^{+9}	3E^{+7}
MWNT	20	1E^{+9}	2E^{+8}

*Calculated using equation 15.1.

the matrix and the difficulty in manipulating the small size of the nanotubes also put an upper limit on the maximum achievable volume fraction. In addition, in practice CNTs are not easily aligned in any one direction, and the bond between the CNT and the polymer matrix, if not perfect, creates a barrier to electrical conductance. Thus electrical conductivities of CNT-polymers are expected to be much lower than the values given in Table 15.2.

Figure 15.1 is a graph of electrical conductivity against price for conventional polymers and polymer composites (40). Boxes comparing both published experimental data and calculated upper bounds for CNT-based composites were superimposed on the figure. Due to the huge amount of data available in the literature (about 200 publications) (38), a box encompassing all the published values is used. It is clear from Figure 15.1 that although various researchers have been successful in fabricating conductive polymers, the reported data is falling short of predicted values. It is reported that the homogeneous distribution of the CNTs in the matrix strongly affects the measured conductivity values (38) although it has been conversely reported that composites with some entangled CNTs give good results. Contradicting results have also been reported concerning the dependence of the percolation threshold on the aspect ratio and alignment since minimum resistivity was found for a partially aligned rather than a perfectly

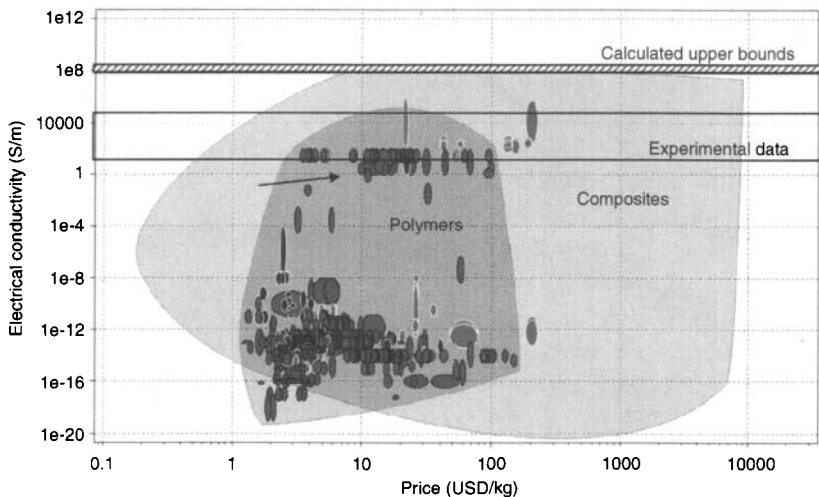


Figure 15.1. Electrical conductivity against price for conventional polymers and polymer composites (40). Boxes representing both published experimental data and calculated upper bounds for CNT - composites were superimposed on the figure.

aligned nanotube film in one case (38). Therefore, it seems that the factors contributing to the electrical conductivities of polymer nanotube composites are still not well-established and thus more research is required in order to produce polymers with controlled electrical conductivities.

15.1.5 Mechanical Properties of CNT Polymer Composites

Though numerous groups have fabricated CNT-polymer composites, mechanical behaviour has not been the main focus of such studies. The bulk of the work has focused on studying the effect of the addition of CNT on the crystallization behaviour and on the electrical conductivity and improving dispersion by employing different techniques, as described earlier.

With regard to mechanical behaviour, to-date reports on improvements in mechanical properties have been inconsistent and appear to depend on the matrix used, the type of CNT, its diameter, its surface treatment, and the processing technique. Some investigations, for example: Bhattacharyya et al. (41), Jia et al. (42) and Xiong et al. (43) have reported either reductions in mechanical properties or very modest increases when adding CNTs to various polymer matrices. Structural enhancements were reported in other investigations, for example: Alloui et al. (44), Gojny et al. (45), Xiao et al. (46) and Machado et al. (47). The strengthening was, however, usually accompanied with noticeable reductions in failure strain. In spite of the enhancements, reductions in mechanical properties were usually observed when adding CNT wt fractions above 2% and were attributed to the agglomeration of the CNTs as their amounts increase (21,24,47). An extensive review of over 150 papers focused on the mechanical properties of CNT-polymer composites (11) has reported that, in general, both melt-processed CNT reinforced polymers and CNT-epoxy composites showed modest enhancements in modulus and very poor strength results.

It is concluded from the above that the mechanical characteristics of CNT composites are not yet well established. In order to have a better insight into the expected performance, idealized upper bounds for various mechanical properties would be useful to have. Although many sophisticated models for predicting the mechanical properties of fiber-reinforced polymers exist, the two most common and simplest ones are the rule of mixtures and the Halpin-Tsai

equations (11). In line with recent studies (11–12), the upper bounds of the mechanical properties of CNT composites can be easily calculated using a special form of the rule of mixture in which:

$$P_c = K_1 K_2 V_{\text{CNT}} P_{\text{CNT}} + (1 - V_{\text{CNT}}) P_m \quad (15.2)$$

where P_c , P_{CNT} and P_m are property values (Young's modulus or strength) of the composite, CNT and matrix, respectively.

V_{CNT} is the volume fraction of CNT.

K_1 is the CNT length efficiency factor; taken as 1 since l/D is > 10 for most types of CNT.

K_2 is an orientation efficiency factor.

Equation 15.2 is used to calculate the maximum feasible values (upper bounds) for stiffness and strength for different types of CNT. The results are summarized in Table 15.3.

The values in Table 15.3 were calculated using the maximum possible CNT loading for each type of CNT, as proposed in Coleman et al. (11). The values also assume the composite is aligned, the CNTs are well dispersed and their lengths are a few times the critical length so that both the orientation efficiency factor and the length efficiency factor are equal to 1. It is very clear from Table 15.3 that when using CVD-MWNT, the enhancements in modulus and strength are significantly lower than when using the more defect-free Arc-MWNT. The maximum volume fraction of CNTs (1% for SWNT and 20% for MWNT) that can be incorporated in the composite affects the maximum achievable enhancement. It is anticipated that careful functionalization of the CNTs – in addition to its effect in strengthening the bond between the CNT and the polymer matrix – also enhances the dispersion of the CNTs within the matrix and thus allows more CNTs to be incorporated.

Table 15.3. Mechanical properties of different types of CNTs and the maximum mechanical properties of their composites

CNT type	V_f (%)	E_{CNT}	σ_{CNT} (GPa)	E_c^* (GPa)	σ_c^* (GPa)
SWNT	1	1 TPa	50	10	0.5
Arc- MWNT	20	1 TPa	50	200	10
CVD- MWNT	20	300 GPa	10	60	2

*Calculated using equation 15.2

A recent review by Coleman et al. (11), which reviewed the mechanical properties of carbon nanotube-polymer composites, compared the mechanical properties of CNT-polymer composites processed using different preparation techniques: solution processing, melt processing, thermoset composites, *in-situ* polymerization as well as the effect of the use of functionalized CNTs. It was concluded that the best mechanical enhancements are achieved when using chemically modified CNTs which seem to be easier to disperse and more effective in load transfer. It is also noted that among the various preparation techniques, the solution based method gave the best results. Melt processed polymers, on the other hand, showed modest enhancements. Similarly, composites based on epoxy showed limited enhancements. In addition to the different preparation techniques employed, the investigations reviewed by Coleman et al. (11) used different matrices, different types of CNT and different weight fractions. As for the effect of CNT type (SWNT vs MWNT), it was found that in general better results were obtained with MWNT composites. In addition to the modest enhancements in modulus, strength enhancements were in general found to be very poor.

Figure 15.2 compares predicted and published Young's modulus values of various polymer CNT composites to those of

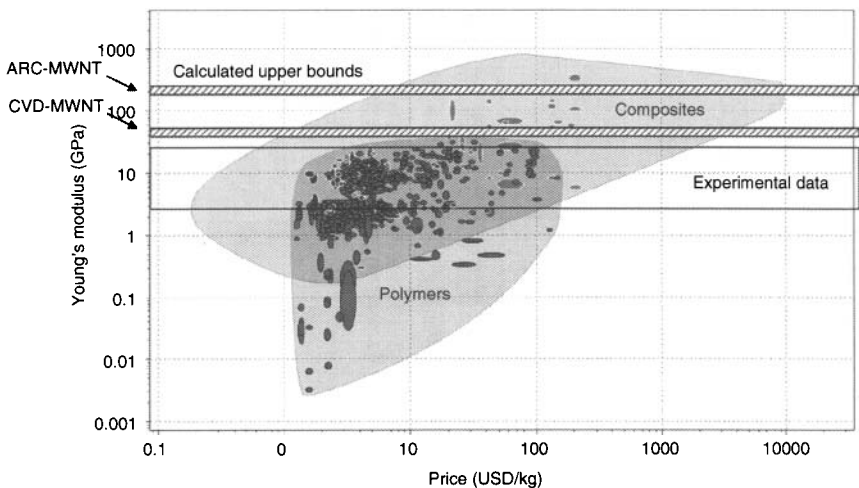


Figure 15.2. Young's modulus against price for conventional polymers and polymer composites (40). Boxes representing both published experimental data and calculated upper bounds for CNT-composites were superimposed on the figure.

conventional polymers and their composites. A box encompassing all the published values for CNT composites is used due to the large amount of data available. It is clear that there is a large discrepancy between the values which could be achieved and what various investigators have been successful in attaining. As noted earlier in the section on electrical properties, the need for higher CNT contents, uniform dispersion, controlled alignment and improved interfacial bonds between the CNTs and the polymer matrix are critical issues that need to be addressed in order to push the properties of CNT polymer composites closer to predicted values. The need to improve the graphitization and thus the mechanical properties of CVD grown CNTs is also essential.

15.2 Case Studies

15.2.1 Case Study: CNT-Based Strain Sensor

Introduction

Smart materials are materials that change properties easily when external forces such as temperature, stress, light, or voltage are applied. They are heavily researched and some are already used in products. Current smart materials have limitations such as high current and voltage requirements and small range of strain sensitivity. Recently CNT based materials are being considered as promising nanoscale smart materials that could overcome such limitations. Several applications are under development (48): electrochemical actuation, piezoresistive strain sensor for structural health monitoring, harvesting power from structural vibrations and a bioelectric sensor. In this case study, the focus will be on CNT-based strain sensors. We will attempt to evaluate the added advantage of using such novel materials and weigh their cost against the added benefits.

Conventional Strain Sensor Materials

A strain gauge is designed to give accurate and reliable strain measurements under specific operating conditions. In addition, it should be easy to install and of low cost. The resistance-type foil strain gauge is one type of strain gauges in common use. It consists of a photo-etched metal foil pattern mounted on a plastic backing material. Printed circuit techniques are used to photo-etch the gauge pattern on a specially treated foil of the appropriate alloy

which is rolled to exact thickness (0.003–0.005 mm) and adhered to a polymer backing layer (49).

One of the most important requirements for a strain gauge material is its gauge factor (strain sensitivity). The most widely used alloy for strain gauges is constantan alloy known to have the best overall combination of properties such as high strain sensitivity, insensitivity to strain level and temperature, high fatigue life and high elongation capability (50). Other requirements of a strain gauge material include minimum temperature-induced strain over a wide temperature range, self temperature compensation to match the test material's thermal expansion coefficient, the ability to measure very large strains 5% (50,000 $\mu\epsilon$), high fatigue life for dynamic applications, and excellent stability for accurate static strain measurements over long periods of time. Variations of the constantan alloy are available for such demanding applications. Although commercially available strain gauges offer wide static, dynamic and temperature ranges, they exhibit relatively low and narrow range of gauge factors (2–3.2). They also lack versatility and flexibility as they only measure strain at the location where they are bonded and along the direction of the grid (37).

CNT-Based Strain Sensors

CNT is being considered as a potential strain sensor because of its structural and electrical characteristics. A long continuous CNT based sensor is envisaged to measure strain over a large structure and thus can be used for structural health monitoring. As a strain gauge material, many forms of CNT have been considered. For example, a SWNT buckypaper sensor was made but was found to be fragile, and slippage between the CNT bundles occurred above strains of 500 $\mu\epsilon$ in tension (51). Better interfacial bonding was achieved by using a polymer such as PMMA as the binding material to reduce slip and increase strain transfer to the CNTs. The strain response of composite film strain sensors containing up to 10 % SWNT showed lower sensitivity compared to the buckypaper sensor but demonstrated a linear symmetric strain response in tension and compression. Gauge factors were found to range from 1 to 5 (48). In another study, MWNT was used in order to reduce cost and also for easier dispersion in the polymer matrix. A PMMA + 1 wt% MWNT strain gauge was developed with a gauge factor approaching 15 (37). In spite of initial successes, growing longer nanotubes,

controlling chirality, improving dispersion and enhancing bonding to the polymer matrix still need to be addressed to produce better performance CNT-based strain sensors.

Cost-Benefit Analysis of Conventional Foil Gauges vs. CNT-Based Composite Gauges

The gauge sensitivity to changes in strain (gauge factor, G) represents the major selection criteria for a strain gauge material when evaluating the technical performance of one material relative to another. Therefore, for the purpose of this analysis, the incremental relative performance index ($\Delta\gamma$), representing the increase in performance when using the new CNT-based gauge, will be defined as:

$$\Delta\gamma = ((G)_{\text{CNT}} - (G)_{\text{base}}) / (G)_{\text{base}} \quad (15.3)$$

The relative incremental cost (ΔC), representing the increased cost due to the more expensive CNT-based gauge, is taken as:

$$\Delta C = (C_{\text{CNT}} - C_{\text{base}}) / C_{\text{base}} \quad (15.4)$$

where C_{CNT} and C_{base} are the costs of the CNT-based gauge and the conventional gauge, respectively.

The Benefit/Cost can be measured as:

$$\Delta\gamma\alpha_T / \Delta C\alpha_c \quad (15.5)$$

where α_T is a weighting factor to account for technical performance and α_c is a weighting factor to account for the importance of cost. For the CNT-based gauge to be competitive relative to current gauge materials, the value of $\Delta\gamma\alpha_T / \Delta C\alpha_c$ needs to be greater than 1.

When seeking a polymer material for a CNT-based strain gauge, ductility and ease of processing are the key requirements. For that reason, polymethyl methacrylate (PMMA) and polyethylene (PE) are two candidate materials. Studies on the electrical conductivities of CNT-PMMA composites reported minimum percolation thresholds ranging from 0.084 to 1.3 wt% which depend on the type of CNT (SWNT or MWNT) and the dispersion technique. Such values are much lower than percolation thresholds reported for CNT-PE which rise up to 15 wt% (38). As a consequence, much higher conductivity values were reported for CNT-PMMA composites. For this reason, a PMMA matrix will be considered for the current

study. Two CNT types will be evaluated: a SWNT content of 10 wt% which was reported in the literature to give the highest electrical conductivity for composites of SWNT and PMMA (52) and a gauge factor of 5. Another candidate is a 1 wt% MWNT-PMMA film produced by the solvent-mixing technique, found by Pham (37) to have a gauge factor exceeding 15.

The proposed CNT-based composite gauge in this case study is assumed to be a thin film of a flexible thermoplastic polymer to which the CNTs are added and dispersed using the techniques described in (37,48). The produced thin film is then cut into small dimensions equivalent to those of conventional foil gauges. The cost of CNT-based film strain gauge is based on the material cost of a film of 15 mm x 50 mm x approximately 0.15 mm thickness using a density of PMMA = 1.2 g/cc, density of SWNT = 1.4 g/cc and density of MWNT = 1.9 g/cc. Table 15.4 summarizes the properties of the materials used.

C_p is the gauge fabrication cost which at this stage of their development is difficult to estimate. However, it is anticipated that this cost will be low since traditional melt processing techniques such as extrusion can be used for producing the gauge film. The cost of the CNT dispersion step which could involve solvent mixing and the cost of painting of the electrodes on the film surface as well as other secondary costs will, however, make the total cost higher. Figure 15.3 shows the variation in the acceptable relative cost of the CNT-based gauge to the conventional foil gauge, for when different importance is given to performance and cost. For example, in applications in which technical performance is of prime importance (e.g. $\alpha_T / \alpha_c = 5$), the cost of the CNT-based gauge, C_{CNT} , can be equal to almost 25 times the cost of a conventional gauge, C_{base} , if its gauge factor is 6 times that of the conventional one, or 5 times the cost of a conventional gauge if the gauge factor is only twice. On the other hand, if

Table 15.4. Properties of strain gauges used in this case study

Material	Gauge factor	Price (\$ per foil gauge)
Conventional foil gauge	2 – 3.2	1
PMMA-10 wt% SWNT gauge (48)	5	$0.6^* + C_p$
PMMA-1 wt% MWNT gauge (37)	15	$0.0014^* + C_p$

*Calculated using the rule of mixture.

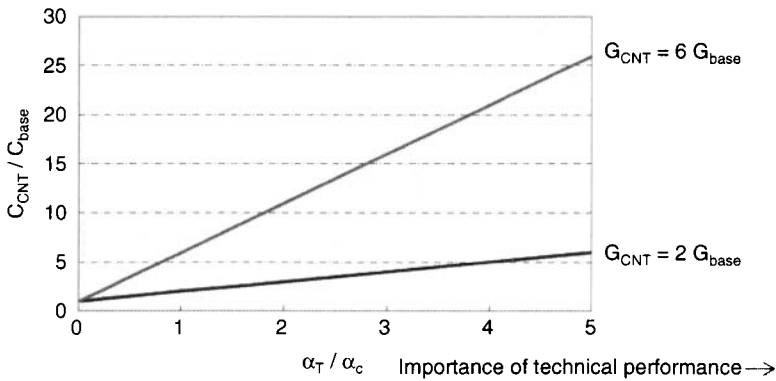


Figure 15.3. Effect of relative importance of performance to cost on the competitive cost of the CNT gauge for gauges with $G_{CNT} = 5$ and 15. The solid lines represent limits on the cost of the CNT-based gauge.

cost is a key factor, for example, when using such gauges over large surfaces ($\alpha_T / \alpha_c < 1$), the acceptable C_{CNT} for the CNT gauge to be viable is much lower ($C_{CNT} / C_{base} < 2$ for when $G_{CNT} = 2 G_{base}$ and < 6 for when $G_{CNT} = 6 G_{base}$).

Findings of the Case Study

The analysis above shows that although still under development and while their full potential to enhance the performance of strain gauges has not yet been realized, CNT-based composite gauges compete favorably with the commercially available metallic foil gauges. It is envisaged that as the cost of CNTs continues to go down and problems of dispersion are overcome, they will become more competitive and could be used as a conductive coating to measure strains over large areas. The CNT composite strain gauge has the added advantages that its strain sensitivity can be tuned by varying the CNT loading (37) and that it can measure strain in all directions since the CNTs are randomly dispersed within the polymer matrix. Conversely, as the long-term behavior of the new materials is not well established, careful attention should be given to the effect of temperature since their thermal expansion coefficients are expected to be very different from that of metallic surfaces. In addition, their fatigue life and their long-term stability should be characterized for when they are needed for dynamic applications or for when accurate static strain measurements over a long period of time are required.

15.2.2 Case Study: Technical and Economic Feasibility of Using CNT-Based Composites in Aerospace Applications

Introduction

The main driving force for materials substitution in aerospace industry is weight reduction at a reasonable cost while maintaining reliability and safety standards. Reducing the weight of the structure allows lifting a greater payload and/or reducing fuel consumption. This case study gives an analysis of the different factors involved in materials substitution in aerospace industry. The merits and drawbacks of substituting carbon fiber reinforced plastics (CFRP) and carbon nanotubes reinforced plastics (CNTRP) for the traditionally used aluminum alloys are examined. A panel in the upper wing surface of a civilian aircraft will be discussed here. Similar analysis may be used for other parts of the structure of the aircraft.

Aluminum alloys in the 5xxx, 2xxx and 7xxx series are normally used for panel applications in the aerospace industry. Aluminum panels can be joined either by riveting or welding. Carbon fiber reinforced plastics (CFRP) are being increasingly used in view of their superior strength/weight and stiffness/weight. In low production volumes, composite panels containing continuous fibers can be made by stacking the required number of layers of preimpregnated fibers, prepregs, in the form of tapes or fabrics and then shaping them in matched dies. Stacking of the prepregs can be done manually or using tape-laying machines.

Carbon nanotubes can be used in reinforcing polymer matrix composites in two ways: a) as the sole reinforcing phase (CNTRP), or b) as an additional reinforcing phase in conjunction with carbon fibers (CF+CNT) in a hybrid composite. Carbon nanotubes reinforced plastics (CNTRP) can be prepared by several methods, as described in section 15.1.3. Both CFRP and CNTRP composite structures can be joined using structural adhesives but machining and drilling are difficult as a result of the widely different properties of their constituents.

Required Mechanical Properties

Body panels of an aircraft can be subjected to a variety of loading conditions depending on their position and function. For example, the loading conditions on the wing of an airplane in flight can be

approximately represented by a uniformly distributed load acting in the upward direction on a cantilever beam. In such case, the load on a panel in the upper wing surface can be approximated to uniform in-plane compression. A major requirement for such panel is resistance to buckling. For such panels, it can be shown that $(E^{1/3}/\rho)$ is the major design parameter for comparing the candidate materials, where E is modulus of elasticity and ρ is density (53). It can also be shown that the weight of the panel is proportional to $(\rho/E^{1/3})$ (53). In addition to the in-plane compression, some transverse and torsional loading may occur in maneuvering the aircraft or as a result of unfavorable weather conditions. Such secondary loads are not serious when isotropic materials, such as aluminum alloys, are used for the panel. CFRP, however, is not isotropic, and if all the fibers are oriented in the direction of the compressive load, the panel could easily fail under relatively small loads at right angles to the fibers. This can be avoided by placing some of the fibers at 90° or arranging them in the $+45^\circ/-45^\circ$ directions, depending on the required degree of isotropy. With the random orientation of CNTs in CNTRP anisotropy is not expected to present a major problem.

The rule of mixtures can be used to estimate upper bound values to the different properties (P_c) of the resulting composites as follows:

$$P_c = K_1 V_1 P_1 + K_2 V_2 P_2 + (1 - (V_1 + V_2)) P_m \quad (15.6)$$

where:

V_1 and V_2 are volume fractions of phases 1 and 2, representing carbon nanotubes and carbon fibers respectively.

P_1 and P_2 are properties of phases 1 and 2, representing carbon nanotubes and carbon fibers respectively.

P_m is property of the polymer matrix.

K_1 is the CNT efficiency parameter.

K_2 is the CF efficiency parameter, which is equal to 1 for continuous aligned fibers in the direction of alignment, as is the case here.

In calculating the upper bound values here, K_1 will be assumed equal to 1. It should, however, be noted that in the great majority of cases a value of K_1 which is much lower than unity needs to be assumed in the case of CNT if the calculated values are to match

experimentally measured values. This is particularly true in the case of mechanical properties and elastic modulus.

From Farag 2008 (53), the mass of an aluminum panel that can bear the load in a civilian aircraft is 20.25 kg. The masses of CFRP and CNTRP panels of equivalent stiffness can be estimated from the proportionality of the weight to $(\rho / E^{1/3})$ and the values in Tables 15.5 and 15.6. The values for the aluminum alloy and Epoxy 33% carbon fabric+30% carbon fibers are based on (53). The calculated values are given in Table 15.7. The calculations show that, with the exception of Epoxy+1 wt% CVD-MWNT and Epoxy+0.1 wt % MWNT (54), the aluminum panel is heaviest. The cost of material in a panel is calculated from its mass and the cost of material per kg, from Table 15.5. The results show that, with the exception of Epoxy+0.1 wt% MWNT, the aluminum panel is the least expensive.

Cost savings in fuel consumption, or the extra payload, as a result of reducing the weight of aircraft by one kg is estimated at \$1000, see (53). This value is used to calculate the cost saving due to a lighter panel in Table 15.7. The net cost saving as a result of substituting a composite material for the aluminum panel is given in Table 15.7.

Table 15.5. Assumptions made in calculating the values in Table 15.6

Parameter	Value used in calculations
E of epoxy matrix	2.4 GPa
E of SWNT	1000 GPa
E of ARC-MWNT	1000 GPa
E of CVD-MWNT	300 GPa
Price of epoxy matrix	2.3\$ per kg
Price of SWNT is	13,000\$ per kg (purity is 60%, cheapest available)
Price of ARC-MWNT	15,000\$ per kg and purity is 30-40%
Price of CVD-MWNT	400\$ per kg – cheapest available.
Density of epoxy matrix	1.26 g/cc
Density of SWNT	1.4 g/cc
Density of MWNT	1.9 g/cc

Table 15.6. Calculated (and actual) properties of different model composites

Material	E_c (GPa)	Density ρ_c (g/cc)	$(E_c^{1/3}/\rho_c)$	Cost C_c^* (\$/kg)
Aluminum alloy (average of 2xxx and 7xxx series)	71	2.7	1.53	4.3
Epoxy 33% carbon fabric + 30% carbon fibers	100	1.61	2.88	110
Epoxy+1%SWNT	12.376	1.26	1.82	218.9
Epoxy+20%ArcMWNT	201.92	1.39	4.15	8573.3
Epoxy+20%CVD-MWNT	61.92	1.39	2.81	81.84
Epoxy+0.1wt%CVD-MWNT (54)	2.7 (5)	1.26	1.1	2.75
Epoxy+6wt%CVD-MWNT (55)	20.26 (4.1)	1.34	2.03	26.16
Epoxy+5wt%SWNT (56)	52.28 (7)	1.274	2.94	1085.7
Epoxy+1%CVD-MWNT (57)	5.38 (2.4)	1.27	1.38	6.28
Epoxy 33% carbon fabric + 30% carbon fibers + 1% SWNT	110	1.61	2.98	325.6
Epoxy 33% carbon fabric + 30% carbon fibers + 3% SWNT	130	1.61	3.15	756.7
Epoxy 33% carbon fabric + 30% carbon fibers + 1% CVD-MWNT	102	1.62	2.88	112.9
Epoxy 33% carbon fabric + 30% carbon fibers + 3% CVD-MWNT	106	1.62	2.92	118.7

Findings of the Case Study

The results of Table 15.7 show that the hybrid composite (Epoxy 33% carbon fabric + 30% carbon fibers + 3% CVD-MWNT) gives the maximum cost saving and is, therefore, given top ranking. Of the two second best materials (Epoxy+20% CVD-MWNT and Epoxy+33%carbon fabric+30% carbon fibers) the latter is a more

Table 15.7. Feasibility of panel material substitution

	Mass of panel (kg)	Cost of material in panel (\$)	Additional cost due to more expensive material (\$)	Cost saving due to lighter panel (\$)	Net cost saving per panel (\$)	Ranking
Aluminum alloy (average of 2xxx and 7xxx series)	20.25	87.1	–	–	–	Base material
Epoxy 33% carbon fabric + 30% carbon fibers	10.77	1184.7	1079.6	9480	8400.4	2
Epoxy+1%SWNT	17.02	3725.7	3645.2	3230	-415.2 *	reject
Epoxy+20%ArcMWNT	7.47	64042.6	63955.5	12680	-51275.5	reject
Epoxy+20%CVDMWNT	11.03	902.7	815.6	9220	8404.4	2
Epoxy+0.1wt%MWNT (54)	28.17	77.46	-9.6	-7920	-7833	reject
Epoxy+6wt%CVD-MWNT (55)	15.26	399.2	311.9	4990	4678.1	5
Epoxy+5wt%SWNT (56)	10.54	11441.4	11354.3	9710	-1644.3	reject
Epoxy+1wt%CVD-MWNT (57)	22.45	141	53.9	-2200	-2253.9	reject
Epoxy 33% carbon fabric + 30% carbon fibers + 1% SWNT	10.39	3382.98	3295.88	9860	6564.1	4
Epoxy 33% carbon fabric + 30% carbon fibers + 3% SWNT	9.84	7445.93	7358.83	10410	3051.17	6
Epoxy 33% carbon fabric + 30% carbon fibers+1% CVD-MWNT	10.76	1214.56	1127.56	9490	8362.44	3
Epoxy 33% carbon fabric + 30% carbon fibers + 3% CVD-MWNT	10.61	1259.46	1172.36	9640	8467.64	1

likely contender. This is because CNT composite manufacturing techniques have to be considerably improved in order to incorporate 20% CNT, which cannot be achieved at present. Also, a value K_1 in Equation 15.6 approaching unity is not achievable with the current preparation techniques. The third best material is the hybrid composite (Epoxy 33% carbon fabric + 30% carbon fibers+1% CVD-MWNT). The above ranking shows that CVD-MWCNT are more cost effective in reinforcing composites than SWNT. With the available preparation techniques and at their current prices they can be effectively used as an additional strengthening phase in hybrid composites.

As the long-term behavior of the new materials is not well established, the present design codes require higher factors of safety in design and extensive testing programs when adopting CNT composites for critical components. This adds to the economic disadvantage of CNTs. Such difficulty can only be solved gradually because engineers need to be more familiar with the unusual behavior of the new materials and to gain more confidence in their long-range performance.

15.3 Conclusions

Since their discovery, CNTs have been the subject of substantial research. Although envisaged as reinforcing fibers for superstiff/superstrong composites, nanotube composites still face several challenges. The realization that uniform dispersion, alignment and a strong interfacial bond are critical has led many research groups to focus on resolving these issues. In addition, the recently reduced cost of CVD-CNT is expected to signal new development potential and more interest from the industrial community.

In this chapter, we have investigated the use of a novel CNT-polymer composite in two completely different applications exploiting both their electrical and mechanical properties: a strain gauge and an aerospace panel. As a strain gauge, our analysis shows that a CNT-based gauge is a viable alternative to conventional foil gauges. Additionally, polymer-CNT composite gauges can offer many advantages: high gauge factor, anisotropic performance and possibility of being made into very long gauges. For a CNT-polymer composite aerospace panel to be mechanically competitive the analysis has assumed that a composite can be fabricated

with a minimum of 20 vol % MWNTs which are aligned and well dispersed; and that there is efficient load transfer from the matrix to the CNTs. Judging from the still large discrepancy between actual mechanical performance values reported by researchers and theoretical upper bounds predicted by theory, such a composite may still be far from reality. The technique of fabricating CNT-composites should be reconsidered so as to accommodate higher volume fractions of CNTs and also allow tighter control over nanotube orientation. For the time being, a hybrid of a CNT-CF is more realistic for such an application.

References

1. P.J.F. Harris, *Carbon Nanotubes and Related Structures: New Materials for the Twenty-first Century*, Cambridge University Press, 2001.
2. E.T. Thostenson, C. Li, and T.-W. Chou, *Composites Science and Technology*, Vol. 65, p. 491, 2005.
3. K.-T. Lau, and D. Hui, *Composites: Part B*, Vol. 33, p. 263, 2002.
4. J.-P. Salvetat-Delmotte, and A. Rubio, *Carbon*, Vol. 40, p. 1729, 2002.
5. R.S. Ruoff, D. Qian, and W.K. Liu, C. R. *Physique*, Vol. 4, p. 993, 2003.
6. C. Li, and T.-W. Chou, *Composites Science and Technology*, Vol. 63, p. 1517, 2003.
7. E.T. Thostenson, Z. Ren, and T.-W. Chou, *Composites Science and Technology*, Vol. 61, p. 1899, 2001.
8. O. Breuer, and U. Sundararaj, *Polymer Composites*, Vol. 25, p. 630, 2004.
9. J. Robertson, *Materials Today*, p. 46, 2004.
10. M. Shaffer, and I.A. Kinloch, *Composites Science and Technology*, Vol. 64, p. 2281, 2004.
11. J.N. Coleman, U. Khan, W.J. Blau, and Y.K. Gunko, *Carbon*, Vol. 44, p. 1624, 2006.
12. A.M.K. Esawi, and M.M. Farag, *Materials & Design*, Vol. 28, p. 2394, 2007.
13. <http://www.nano-c.com/>
14. <http://www.cheaptubes.com>
15. <http://www.mercorp.com>
16. <http://www.baytubes.com>
17. <http://www.thomas-swan.co.uk>
18. <http://www.sigmaaldrich.com>
19. X.-L. Xie, Y.M. Mai, and X.P. Zhou, *Materials Science and Engineering R*, Vol. 49, p. 89, 2005.
20. R. Andrews, D. Jacques, M. Minot, and T. Rantell, *Macromolecular Materials and Engineering*, Vol. 287, p. 395, 2002.
21. A.M.K. Esawi, H.G. Salem, H.M. Hussein, and A.R. Ramadan, *Polymer Composites*, doi 10.1002/pc.20859, 2009.

22. K.-T. Lau, "Recent research in nanotube/nanoclay related polymer composites", Proceedings of the Twelve International Conference on Composites/Nanoengineering, ICCE-12, August 1 – 6, 2005, Tenerife, Spain.
23. K.Q. Xiao, L.C. Zhang, and I. Zarudi, *Composites Science and Technology*, Vol. 67, p. 177, 2007.
24. M.A.L. Manchado, L. Valentini, J. Biagiotti, and J.M. Kenny, *Carbon*, Vol. 43, p. 1499, 2005.
25. R. Andrews, and M.C. Weisenberger, *Current Opinion in Solid State & Materials Science*, Vol. 8, p. 31, 2004.
26. W. Tang, M.H. Santare, and S.G. Advani, *Carbon*, Vol. 41, p. 2779, 2003.
27. C. Velasco-Santos, A.L. Mart nez-Hernandez, F.T. Fisher, R. Ruoff, and V.M. Castano, *Chemistry of Materials*, Vol. 15, p. 4470, 2003.
28. L. Chen, X.J. Pang, M.Z. Qu, Q.O.T. Zhang, B. Wang, B.L. Zhang, and Z.L. Yu, *Composites: Part A*, Vol. 37, p. 1485, 2006.
29. B. Fiedler, F.H. Gojny, M.H.G. Wichmann, M.C.M. Nolte, and K. Schulte, *Composites Science and Technology*, Vol. 66, p. 3115, 2006.
30. A. Garg, and S.B. Sinnott, *Chemical Physics Letters*, Vol. 295, p. 273, 1998.
31. A. Sharma, S. Kumar, B. Tripathi, M. Singh, and Y.K. Vijay, *International Journal of Hydrogen Energy*, Vol. 34, p. 3977, 2009.
32. E.T. Thostenson, and T.-W. Chou, *Journal of Physics, D: Applied Physics*, Vol. 35, p. L77, 2002.
33. R.E. Gorga, and R.E. Cohen, *Journal of Polymer Science, Part B: Polymer Physics*, Vol. 42, p. 2690, 2004.
34. R. Haggemueller, H.H. Gommans, A.G. Rinzler, J.E. Fischer, and K.I. Winey, *Chemical Physics Letters*, Vol. 330, p. 219, 2000.
35. J.C. Kearns, and R.L. Shambaugh, *Journal of Applied Polymer Science*, Vol. 86, p. 2079, 2002.
36. J.K.W. Sandler, S. Pegel, M. Cadek, F. Gojny, M. van Es, J. Lohmar, W.J. Blau, K. Schulte, A.H. Windle, and M.S.P. Shaffer, *Polymer*, Vol. 45, p. 2001, 2004.
37. G.T. Pham, Y.-B. Park, Z. Liang, C. Zhang, and B. Wang, *Composites, Part B: Engineering*, Vol. 39, p. 209, 2008.
38. W. Bauhofer, and J.Z. Kovacs, *Composites Science and Technology*, Vol. 69, p. 1486, 2009.
39. M.F. Ashby, *Encyclopedia of Materials: Science and Technology*, pp. 1357–1361, 2008.
40. CES software, The Cambridge Engineering Selector, Granta Design, Rustat House, 62 Clifton Road, Cambridge CB1 7EG, UK (www.grantadesign.com).
41. A.R. Bhattacharyya, T.V. Sreekumar, T. Liu, S. Kumar, L.M. Ericson, R.H. Hauge, and R.E. Smalley, *Polymer*, Vol. 44, p. 2373, 2003.
42. Z. Jia, Z. Wang, C. Xu, J. Liang, B. Wei, D. Wu, and S. Zhu, *Materials Science and Engineering A*, Vol. 271, p. 395, 1999.
43. J. Xiong, Z. Zheng, X. Qin, M. Li, H. Li, and X. Wang, *Carbon*, Vol. 44, p. 2701, 2006.
44. A. Allaoui, S. Bai, H.M. Cheng, and J.B. Bai, *Composites Science and Technology*, Vol. 62, p. 1993, 2002.
45. F.H. Gojny, M.H.G. Wichmann, B. Fiedler, and K. Schulte, *Composites Science and Technology*, Vol. 65, p. 2300, 2005.
46. K.Q., Xiao, L.C. Zhang, and I. Zarudi, *Composites Science and Technology*, Vol. 67, p. 177, 2007.

47. M.K. Seo, J.R. Lee, and S.J. Park, *Materials Science and Engineering A*, Vol. 404, p. 79, 2005.
48. I. Kang, Y.Y. Heung, J.H. Kim, J.W. Lee, R.G.S. Subramaniam, S. Narasimhadevara, D. Hurd, G.R. Kirikera, V. Shanov, M.J. Schulz, D. Shi, J. Boerio, S. Mall, and M. Ruggles-Wren, *Composites Part B: Engineering*, Vol. 37, p. 382, 2006.
49. A.L. Window, *Strain Gauge Technology*, 2nd Edition, Elsevier Applied Science. Springer, 1992.
50. www.vishaymg.com
51. I. Kang, M.J. Schulz, J.H. Kim, V. Shanov, and D. Shi, *Smart Material Structures*, Vol. 15, p. 737, 2006.
52. V. Skákalová, U. Dettlaff-Weglikowska, and S. Roth, *Synthetic Metals*, Vol. 152, p. 349, 2005.
53. M.M. Farag, *Materials & Process Selection for Engineering Design*, 2nd edition, CRC Press, 2008.
54. X. Xu, M.M. Thwe, C. Shearwood, and K. Liao, *Applied Physics Letters*, Vol. 81, p. 2633, 2002.
55. Y. Breton, G. Désarmot, J.P. Salvetat, S. Delpeux, C. Sinturel, F. Béguin, and S. Bonnamy, *Carbon*, Vol. 42, p. 1027, 2004.
56. X.D. Li, H.S. Gao, W.A. Scrivens, D.L. Fei, X.Y. Xu, M.A. Sutton et al., *Nanotechnology*, Vol. 15, p. 1416, 2004.
57. J. Bai, *Carbon*, Vol. 41, p. 1325, 2003.

Index

- ABS/clay/MWNTs, flame retardation, 102–104
- Acid-functionalized CNTs, 189
 - Acid-treated SWCNTs, 293
- Adhesion, 117
- AFM *see* Atomic force microscopy (AFM)
- Agglomeration, 152
- Airy disc, 52
- Alignment, 19–20, 126, 146, 151
- Amino-grafting, 401
- Amorphous polymers, 144–145
- Arc discharge method, 57
- Arc-grown SWCNTs, 285–286
- Arc-purified SWCNTs, 285–286
- Aspect ratio, 19, 295
- Atomic force microscopy (AFM),
 - 48–49, 151
 - and CNT composites, 50–52
 - contact mode, 49
 - electrostatic force microscope, 49–50
 - resonating mode, 49
 - tapping mode, 49
- AzoPU-MWNTs, 150, 168
- Ball milling, 290
- Ballistic, 317
- Bayer Material Science Company, 428
- Behaviour laws, 45
- Bio-nanocomposites, 253, 277
- Biobased plastics, 252
- Buckypaper, 410–411
 - sample, 413
- Samples and curves of tensile tests, 418
- SEM image, 413
- Butadiene styrene rubber nanocomposites, 32
- Calendering approach, 183
- Carbon based nanofillers, 46
- Carbon black, 345, 351
- Carbon fiber reinforced plastics (CFRP), 442
- Carbon fibers, 1, 4, 177, 190, 200, 346
- Carbon nanofibers, 351
- Carbon nanotubes (CNTs), 46, 177, 221–222, 256–257
 - additive fillers, 316
 - applications, 256
 - arc-discharge methods, 317
 - aspect ratio, 374
 - bending resistance, 317
 - chemical vapour deposition synthesis, 317
 - chirality, 2
 - conductive filler, 86, 316
 - conductivity, 7
 - de-aggregation and dispersion, 145
 - elastic modulus, 256
 - electric conductivity, 256
 - electric-current-carrying capacity, 144
 - electrical properties, 144, 317

- electronic properties, 6–7
- functionalization methods, 116
- low density and high aspect ratio, 316
- mechanical properties, 5, 316–317
- metals and semiconductors, 2
- modulus, 5
- multi-walled, 3, 143
- nanotube properties, 58
- nanotube structure, 56–57
- properties, 4, 114
- quantification of diameter distribution, 57–58
- reactive sites, 7
- reinforcement, 46, 89, 114, 153
- single-walled, 3, 143
- surface functionalization, 11
- surface modification, 115–117
- synthesis, 8–12
- tensile modulus, 143
- tensile strength, 143
- thermal conductivity, 144
- thermal properties, 144
- Carbon nanotubes reinforced plastics (CNTRP), 442
- Carboxylic-functionalization, 266
- Casting/melting-processed CNTs/polymer composites, 399–403
- Catalytic carbon deposition (CCVD), 349
- Catalytic chemical vapour deposition (CCVD), 9, 428
- Cellulose whiskers, 46
- Chain-extendors, 254
- Charge contrast imaging mode (CCI), 71
- Chemical functionalization, 149, 431
- Chemical surface functionalization, 116
- Chemical treatment of CNT, advantages, 181
- Chemical vapor deposition, 8–9, 146, 427
 - ordered nanotube arrays, 11
- Chemically modified CNTs, 436
- Chitosan/CNT-clay composites, 90–93
 - interactions and networks, 93
 - morphology, 93
 - tensile strength, 91
 - XRD pattern, 92
- Chitosan nanocomposites, 26–27
- Chopped carbon fibers, 159
- Clay fibers, 346
- Clumping, 117
- CNT-based composites in
 - aerospace applications, 442
 - Aluminium alloys, 442
 - required mechanical properties, 443–447
- CNT-based gauge, 447
- CNT based nanocomposites, 46–47
- CNT-based strain sensor, 437
 - conventional strain sensor materials, 437–438
 - cost-benefit analysis of conventional foil gauges *vs.* composite gauges, 439–441
- CNT chopping, 406
- CNT/Epoxy composites, SEM images of, 412
- CNT/HDPE composites, mechanical properties, 127
- CNT-polyethylene nanocomposites
 - material characterization, 126–135
 - preparation methods, 119–123
 - CNT-HDPE composite, 121–122
 - CNT-low density PE composites, 123
 - combined solution mixing technique and melt processing, 122
 - direct mixing, 119

- electrostatic technique, 123
- in-situ* polymerization, 119
- melt processing, 119, 120
- solution processing, 119, 120
- twinscrew extruder, 120
- CNT/polymer compatibility, 149, 189
- CNT polymer composites, 431
 - electrical properties of, 431
 - fabrication of, 428–431
 - mechanical properties of, 434–436
- CNT/polymer matrix interface, 195
- CNT-polymer mix, 430
- CNT/polypropylene (PP)
 - composites, 400
- CNT shortening, 118
- CNT-UHMWPE composites,
 - mechanical properties, 128, 129
- CNTRP anisotropy, 443
- CNTs *see* Carbon nanotubes
- Co-flowing streams, 327
- Coated fabrics, 167–168
- Compatibilizers, 188, 196, 290, 292
- Compatibilizing agent, 292–294
- Compression molding, 183
- Condensation, 167
- Condensation polymerization, 146
- Conductive polymers, 425, 431
- Conductive fillers, 86, 158, 179, 198, 316
- Conductive polymer composites (CPCs), 86
- Conductivity, 58
- Constantan alloy, 438
- Controlled polymerization
 - methods, 21
- Conventional polymers *vs.* polymer composites, 433, 437
- Cosolvent, 188
- Covalent chemical
 - functionalization, 189, 190
- Covalent functionalization, 149, 292
- Covalent grafting, 291
- Covalent pre-treatments, 374
- Covalent surface modification, 12
- Cox-Krench shear-lag model, 406
- Crystalline structure, 303
- Current reinforcement fibers,
 - mechanical properties of, 396
- Cutting-SWNT/Epoxy, 412
- D-band, 289
- 3D CNT-clay hybrid fillers, 97–98
- DC arc discharge, 8
- Deagglomeration, 182
- Degradation temperature, 34–36
- Differential scanning calorimetry, 298–303, 361–364
- Dispersibility, 89
- Dispersion of CNTs in polymer matrix, 117–119, 149–151
- Dispersion polymerization, 228
- Dispersion quality, 118
- Double-percolation, 387
- Double-wall carbon nanotubes (DWCNT), 222
- Drop casting, 183
- Dynamic mechanical analysis (DMA), 266, 304, 361–364, 397
- Elastomeric/CNT composite
 - composite processing, 347–350
 - dispersion and mixing of nanotube, 347
 - dispersion of MWNTs in natural rubber, 350
 - solution mixing, 347, 349
 - toluene suspension of MWNTs, 348, 349
 - electrical properties, 350–355
 - volume resistivity, 351–352

- mechanical properties
 - differential scanning calorimetry, 361–364
 - dynamic mechanical analysis, 361–364
 - tensile and swelling behaviors, 355–360
 - spectroscopic characterization, 364–367
 - thermal stability, 367–369
- Elastomers, 345
 - applications, 158
- Electric arc-discharge, 285, 427
- Electrical conductivity, 37, 39–40
- Electrochemical method, 116
- Electromagnetic interference
 - shielding, 168–169, 200–204
- Electron Energy-Loss Spectroscopy (EELS), 55
- Electron microscopy, 233
- Electron tomography (EFTEM), 56, 60–61, 73
- Electrorheological fluids, 236, 243
- Electrorheological phenomenon, 243, 244
- Electrorheology, 240, 243
- Electrospinning, 148, 326
- Electrospun fibers, 330
- Electrostatic Force Microscope (EFM), 49–50
- Elongation at break, 27–28, 34
- Emulsion polymerization, 225
- Energy Dispersive Spectroscopy (EDS), 55
- Energy Filtered TEM, 55, 151
- Energy Los Alamos National Lab, 428
- Entanglement, 117–118
- Environmental scanning electron microscopy (ESEM), 72
- Epoxy/clay/CNTs composite, 87
 - electrical conductivity, 87
 - SWNT-clay interaction, 89
- Epoxy-grafted CNT enhanced nanocomposites *vs.* neat resin, 403
- Epoxy grafted SWNT/epoxy composite, 403, 404
- Epoxy-grafting functionalization, 402
- Epoxy nanocomposites, 30, 33–34, 37, 39–40
- Exfoliated clay-CNTs hybrid (E-MMT), 98
- Extrusion, 290
- FIB slicing, drawbacks, 75
- Fibers, 324–327
 - gel-spinning process, 325
 - gel-spun, 326, 330
 - hot-stretching, 330
 - mechanical properties, 337
 - PVA/CNTs electrospun, 324–325, 326
 - PVA/MWNT electrospun, 326
 - stress-strain curves, 336
 - stretched, 325
 - wet spun, 330
- Field emission scanning electron microscopy (FESEM), 241
- Film impregnated-CNTs/polymer composite, 410–418
- Films, 320–324
- Flame pyrolysis, 10
- Flame retardants, 156, 222
- Fluorination, 401
- Friedel-Crafts acylation, 283
- FTIR analysis, 378
- Fullerenes, 46
- Functionalisation, 20–21, 67, 293, 294, 311, 401
- Functionalized CNTs, 117, 149
- Future work, 108, 170–171
- G-Band, 289
- Gas phase decomposition, 9
- Gel-effect, 225

- Gel-spinning process, 325
- Gel-spun fibers, 330
- Glass transition temperature, 305
- Grafting, 20–21
- Grafting, 67, 76
- Graphene sheets, 1, 46, 56, 143, 222
- Graphite, 3, 4, 351

- HAADF mode(High Angle Annular Dark Field mode), 55
- High density polyethylene (HDPE), 114
- High-power ultrasonication, 146
- High resolution electron microscopy, 151
- High Resolution TEM, 55
- High shear mixer cum twin screw extruder, 183
- High shear mixing, 149
- HiPco method (high pressure carbon monoxide), 9
- HNBR/clay/CNTs, thermal degradation, 105
- Hybrid filler, 96–97

- Impreganated buckypaper, 413
- In-situ* polymerization, 146–147, 430
- In-situ* radical polymerization, 185, 221
- In-situ* spectroscopy, 76
- Individualization of tubes from CNT bundles, 149, 180
- Induced controlled dispersion of multiwall CNTs
 - characterization, 378–379
 - materials, 376
 - melt blending, 377
 - preparation of modifiers, 376–377
 - results and discussion
 - AC electrical conductivity measurements, 381–383
 - melt-interfacial interactions, 386–387
 - phase morphology and selective localization, 383–386
 - spectroscopic and microscopic evidences, 379–381
- Injection and blow moulding, 290
- Inner tubes of DWCNTs, 10
- Interface polymer fraction, 16
- Interface strength, 89–90, 124
- Interfacial adhesion, 123, 290, 292, 296–297, 298
- Interfacial adhesion strength, 65, 117
- Interfacial bonding, 123–126
- Interfacial failure, 123
- Interfacial phonon scattering, reduction, 154–155
- Interfacial stress, 127
- Interfacial stress transfer, 117, 126–127, 331, 333
- Irradiated SWNT membrane, 417
 - tensile test curve of, 414
- 3-isocyanatopropyltriethoxysilane (IPTES), 38

- Kelly Tyson shear lag model, 398
- Kelly–Tyson approach, 123
- Kevlar® fibers, 336

- Laboratory mixing molder, 183
- Laser ablation, 427
- Laser ablation, 8
- Laser-grown SWCNTs, 285
- Latex technology, 148
- Layered silicates, 346
- Load transfer, 123–126, 282, 304
- Loss modulus, 305, 306
- Low-pressure oxygen plasma treatment, 116

- Magnetic stirring, 181–182
- Mechanical dispersion
 - methods, 149

- Mechanical reinforcement, requirements, 126
- Mechanochemical method, 116, 298
- Melt-blending, 183
 - advantages, 290
- Melt-mixing, 144–145
- Metallic flakes, 159
- Methylene-bis-ortho-chloroaniline (MOCA), 147
- Microemulsion polymerization, 186
- Microscopy techniques, 47, 69
- Microspheres, applications of, 236
- Microstructure, 47
- Mild sonication, 146
- Miniemulsion approach, 20
- Modulated differential scanning calorimetry, 154
- Molecular simulation, 153
- Morphology, 16, 17, 30
- Multi-wall carbon nanotubes (MWCNT), 2, 46, 222
 - stretching process, 5–6
 - tensile test, 5–6
- Multistep melt-mixing, 184
- Multiwalled nanotubes (MWNT)
 - see* MWNT
- MWCNT-PMMA composites
 - EMI shielding effectiveness, 200–201
 - properties, 206–215
 - variation of EMI shielding effectiveness, 202–203
- MWCNT *see* Multi walled carbon nanotubes (MWCNT)
- MWNT, 395, 396–397
 - vs SWNT, 436
- Nano-clays, 46
- Nano composites
 - CNTs and polymers role in, 394
 - effect of dispersion on, 407
 - modulus and strength of, 405
- Nano-pullout technique, 331
- Nanocomposites, 4–5
 - filler geometries, 5
- Nanofillers, 253
- Nanohorns, 222
- Nanoscrolls, 222
- Nanotube composites, 425
- Nanotube nanocomposites, 17
- Nanotubes use in nanocomposites
 - electrical properties, 319
 - mechanical properties, 317–319
- NBP composites, tensile test results of, 419
- Near-edge X-ray absorption, 151
- Near field microscopy, 47
 - AFM and CNT composites, 50–52
 - nanotubes, 50
 - STM and AFM, principles of, 48–50
- NIR spectroscopy, 289, 290
- Non-covalent functionalization, 188
- Non-covalent surface modifications, 11
- Noncovalent adsorption, 149
- Noncovalent interaction, 150–151
- Noncovalent pre-treatments, 374
- Octadecyl tri-phenyl phosponium bromide (OTPB), 376–377
- Onion-like carbon, 222
- Organoclay, 100
- PA6/CNT-clay composite, 96–97
- PE and MWCNT-PE
 - nanocomposites, mechanical properties, 132
- PEEK/CNT nanocomposites
 - aeronautic and aerospace applications, 282
 - characterization of SWCNTs, 287–290
 - covalent grafting, 291–292
 - differential scanning calorimetry, 298–303

- characteristic temperatures, 299
- crystallization and melting data, 302
- non-isothermal, 300
- electrical and thermal conductivity, 307–308
- mechanical properties, 304–307
- melt blending approach, 290–291, 294–295
- morphology, 295–297
- pre-mixing stage, 294–295
- synthesis and purification of arc-grown SWCNTs, 285–286
- synthesis of laser-grown SWCNTs, 285
- thermal stability, 297
- thermogravimetric study, 297–298
- wrapping of SWCNTs, 292–294
- X-ray diffraction analysis, 303–304
- PEEK *see* Poly(ether ether ketone) (PEEK)
- Percolating network, 46, 76–77, 77
- Percolation, 319
- Percolation threshold, 86, 159, 200, 319, 351
- Petroleum based plastics, 251–252
- Plasma Enhanced CVD (PECVD), 427
- Plasma treatment, functionalization, 116
- PMMA/CNTs nanocomposites
 - electrical conductivity, 198–200
 - electromagnetic interference shielding, 200–204
 - fabrication/processing
 - chemical modification of CNTs, 189–190
 - co-solvent, 188–189
 - coagulation method, 186–188
 - compatibilizers, 188–189
 - in-situ* polymerization
 - processing, 185–186
 - melt-processing, 183–185
 - solution processing, 181–183
 - solvent casting and compression molding, 184
 - solvent casting and melt-mixing, 184
 - surfactant, 188–189
 - homogeneous dispersion, 182
 - mechanical properties, 190–198
 - elastic modulus, 191, 192
 - flexural strength, 193–194
 - fracture toughness, 193
 - storage modulus, 196–198
 - tensile strength, 190–193
 - thermal properties, 204–215
- PMMA *see* Polymethylmethacrylate
- Polarized Raman spectroscopy, 151
- Poly (3-hexylthophene) (P3HT)-graft-PMMA, 188
- Poly (ether ether ketone) (PEEK), 283
 - applications, 283–284
 - characteristics, 284
 - structure and properties, 283–284
 - synthesis, 283–284
 - extrusion and compression moulding, 283
 - Friedel-Crafts acylation, 283
- Poly(3-hexylthiophene) nanotube nanocomposites, 35–36
- Poly(acrylonitrile) nanotubes, 28
- Polyamide nanocomposites, 26, 36
- Polyamide6 (PA6), 376
- Poly(aryl ether ketone)s (PAEKs), 283
- Poly(arylene ether sulfone)s, 283
- Poly(butylene succinate) nanocomposites, 32–33, 39
- Poly(butylene terephthalate) nanocomposites, 28, 37
- Polycarbonate nanocomposites, 33

- Polyetherimide (PEI), 292
- Polyethylene nanocomposites, 36
- Polyhydroxyalkanoates (PHAs), 252
- Polyimide nanocomposites, 27
 - surface and volume resistivity, 38
- Poly lactide-based CNT nanocomposites
 - applications, 277
 - biodegradability, 276–277
 - carbon nanotubes, 256–257
 - electrical conductivity, 275–276
 - mechanical properties, 271–274
 - strain-at-break, 271–272
 - tensile strength, 271–273
 - toughness, 272–273
 - Young's modulus, 271, 273
 - preparation, 257–266
 - "grafting to" technique, 257–258
 - melt-compounding, 261, 263–264
 - microcellular
 - injection-molding, 261–262
 - microcellular processing technology, 261
 - one-step condensation synthesis, 266
 - solution-mixing and precipitation method, 260–261
 - two-step method, 257
 - thermal degradation, 274
 - thermal properties, 270–271
 - viscoelastic properties, 266–270
 - complex viscosity, 268–269
 - storage modulus, 266–269
 - tan- δ , 267–268
- Poly lactide (PLA), 251
 - aliphatic polyester, 254
 - biodegradable and biobased polymers, 252
 - effects of plasticizers/fillers on properties, 253
 - limitations, 252
 - medical applications, 252
 - physical properties, 252
 - synthesis, 254–256
 - azeotropic condensation polymerization, 254
 - condensation polymerization, 254
 - high-molecular weight PLA, 255
 - ring opening polymerization, 254
- Poly(m-phenylene vinylene-co-2,5-dioctoxy-p-phenylene vinylene), 42
- Polymer blends, 50/50
 - polyamide6/acrylonitrile-butadiene-styrene (PA6/ABS), 375
- Polymer/CNT composites, 15, 58–59, 393, 426
 - agglomeration, 433, 434
 - aspect ratio on reinforcement, 409
 - characterization of, 397–398
 - chirality of, 408, 426
 - composite manufacturing techniques, 447
 - 2D apparent nanotube curvature radius, 62
 - 3D nanotube network, 62
 - degradation temperature, 34–36
 - electric properties of, 425
 - electrical conductivities, 432
 - electrical conductivity, 37, 39–40
 - electrical properties, 34–42
 - elongation at break, 27, 33, 34
 - experimental values for Young's modulus of, 396
 - functionalizing, 436
 - glass transition temperature, 37–38, 40–41

- in-situ* polymerization, 20–22
- incorporation into polymer, 394
- interfacial adhesion strength, 65–67
- mechanical properties, 25–34
- mechanical properties of
 - different types of, 435
- melt mixing, 22–25
 - advantages and limitations, 22
 - combined use of solution mixing and, 25
 - kneader and injection molding, 25
 - poly(butylene succinate) synthesis, 24
 - poly(butylene terephthalate) synthesis, 24
- melt-mixing into thermoplastic polymers, 400
- nanotube dispersion state, 59–63
- nanotube orientation state, 63–64
- preferential orientation via shear flow, 401
- Raman spectroscopy, 398
- segregation, 433
- simulation of epoxy and EPI
 - cure molecules filling into, 406
- solution mixing, 18–20
 - advantages and disadvantages, 18
 - epoxy nanocomposites synthesis, 19
 - polycarbonate nanocomposites synthesis, 18
- structure and mechanical properties of, 394–397
- structure and tensile properties of, 398–418
- structure of, 395
- synthesis, 427–428
- tensile modulus, 27–29, 31–34
- tensile strength, 26–29, 33
- thermal properties, 34–42
- Polymer crystallization method, 116
- Polymer degradation, 430
- Polymer matrix composites, 442
- Polymer nanocomposites
 - clay and carbon natubes
 - electrical properties, 86–89
 - flame properties, 100–106
 - mechanical properties, 89–100
 - synergistic effect, methods, 107
 - thermal properties, 100–106
- Polymer nanotube composites, 425–448
- Polymer reinforcing additive, 177–178
- Polymer wrapping, 116, 117
- Polystyrene-grafted nitrogen-doped multiwalled nanotubes, 65
- Polystyrene nanocomposites, 30–32, 37
- Polytrimethylene terephthalate (PTT), 252
- Polyurethane, 141
 - applications, 143
 - distinguishing criterion, 142
 - hard-segment domain, 143
 - melt viscosity, increase of, 157–158
 - segmented PU, 142
 - soft-segment matrix, 143
 - urethane-bonded interphase, 143
- Polyurethane/CNT nanocomposites
 - applications
 - electromagnetic interference, 168–169
 - nanowebs, 169
 - photoresponsive, 168
 - tissue-engineering scaffolds, 169–170
 - vapor sensitive response, 168
 - bio-applications, 165–166

- dispersion morphology, 148–151
- electrical conductivity, 158–161
- fire retardancy, 156–157
- functionalization, 148–151
- homogeneous dispersion, 145, 147, 149, 158
- interfacial interactions, 153
- mechanical properties, 151–153
- micro-/nano-structures, 148–151
- microwave absorption, 166–167
- preparation methods
 - in-situ* polymerization, 146–147
 - melt-mixing, 144–145
 - sol-gel process, 147–148
 - solution casting, 145–146
- rheological properties, 157–158
- shape memory, 162–165
- tensile modulus and strength, 152
- thermal conductivity, 154–155
- thermal stability and degradation, 155–156
- UV-protection, 167–168
- viscosity, 157
- water vapor transport properties, 161–162
- Polyurethane garments, 167
- Poly(vinyl) alcohol, 25–26, 316, 319–320
 - applications, 319
 - hydrolysis rate, 319
- Poly(vinylidene fluoride), 188
- Pristine and PEI-wrapped arc-SWCNTs, 293
- Pristine CNT, 411
- Pristine CNT film based composites, 411
- Pristine EP and composites, 98–99
- Pristine SWNT, 403
- Pristine-SWNT/epoxy composite, 403, 404, 412
- Pristine SWNT membrane, tensile test curve of, 414
- PU *see* Polyurethane
- Pull-out experiments, 123–124
- PVA/CNT nanocomposites
 - electrical properties, 333–335
 - energy absorption, 335–337
 - mechanical properties
 - reinforcement, 328–330
 - stress transfer efficiency, 331–333
 - shape memory effect, 337–339
 - synthesis and structural properties
 - fibers, 324–327
 - films, 320–324
- PVA crystallization, 322–323, 325, 340
- PVA *see* Poly(vinyl) alcohol
- Pyrolysis, 367
- Radial breathing modes, 289
- Radical addition, 231
- Radical polymerization, 146
- Raman peak shift, 124–125
- Raman scattering, 364
- Raman spectroscopy, 123, 124, 288–289, 378, 379
- Raw nitrogen-doped multiwalled nanotubes, 65
- Recovery stress, 337
- Reinforcement, 293, 303, 328–329
- Resin-infiltration technique, 411
- Resistivity, 38–39
- Rheological measurements, 234
- Roping and wrapping method, 116
- Rule-of-mixtures, 432, 435, 443
- Scanning electron microscopy (SEM), 67, 146, 287, 379
 - application, 68–69
 - CNT/polymer nanocomposites, 69–72
 - high resolution, 68
- Scanning probe microscopy (SPM), 70, 426

- Scanning tunneling microscope (STM), 48
 - continuous current mode, 48
- Scattering, 47, 151
- Secondary Electrons Imaging (SEI), 67–68
- Segmented polyurethanes (SPU), 169
- Semi-crystalline polymers, 145
- Shape fixity, 338
- Shape memory effect, 162–163
- Shape memory polymers, 162
 - applications, 337
- Shear mixing, 183
- Short-CNT/polymer composites, 405–410
- Shortened SWNT, 406
- Silane modified nanotubes, 38
- Silica, 345
- Single-wall carbon nanotubes (SWCNT), 1, 2, 46, 222, 394, 395, 397
 - characterization, 287–290
 - epoxy-grafted, TEM images of, 403
 - length distributions of 500 nm-cut, 410
 - mechanical properties, 46
 - prices of different types of
 - commercially available, 429
 - synthesis
 - arc-grown, 285–286
 - laser-grown, 285
 - tensile strength, 152
 - thermal conductivity, 154–155
 - unique properties, 282
 - vs MWNT, 436
 - Young's modulus, 152
 - Young's modulus and tensile strength of, 415
- Slippage, 152
- Sodium salt of 6-amino hexanoic acid (Na-AHA), 376–377
- Sol-gel process, 147–148, 346
- Solar furnace, 10
- Solution blending method, 90
- Solution casting, 145–146
- Solution-intercalation/mixing method, 93
- Solution polymerization, 225
- Solvent casting, 181, 182
- Solvent method, 430
- Sonochemical polymerization method, 228
- Spin casting, 183
- Starch plastics, 252
- STM *see* Scanning tunneling microscope (STM)
- Stone Waals defect, 5
- Strain gauges, 438
- Strain-induced crystallization, 356
- Stress transfer property, 17
- Stretching device, 356
- Structure and morphology on
 - tensile, effect of, 393–394
 - characterization, 394–418
- Surface modification, 235
- Surfactants, 149, 151, 188–189
- Suspension polymerization, 221, 235–243
- SWNT buckypaper, 413
- SWNT/epoxy composite, 401
 - mechanical properties of, 402
- SWNT reinforced PC composites,
 - dynamic mechanical analysis of, 414
- SWNT *see* Single-walled nanotube (SWNT)
- Synergistic effect, 85–86, 89, 90, 94, 97, 100, 104, 106
- TEM *see* Transmission Electron Microscopy (TEM)
- Tensile testing machine, 271
- Tensile tests, 66, 272, 355
- Thermal mechanical analysis (TMA), 397

- Thermally induced phase separation, 148
- Thermo-extruder, 294
- Thermogravimetric analysis, 35, 155, 287, 297, 367
- Thermogravimetric analyzer, 274
- Thermoplastic polyurethane (TPU), 143, 144
- Thermosetting resins, 430
- Thermotropic liquid crystalline polymer nanocomposites, 29–30, 37
- Toluene, 347
- Tomo-STEM, 73–75
- Transmission Electron Microscopy (TEM), 52, 287, 378
 - advantages, 52
 - bright field imaging mode, 53, 54
 - dark field mode, 54
 - environmental mode, 56
 - HAADF mode, 55
 - high resolution, 55
 - principles, 52–56
- Trifluoroacetic acid (TFA), 188
- Twin-screw extruders, 145, 183
- Ultra-sonicated CNT suspension, 400
- Ultrahigh molecular weight polyethylene (UHMWPE), 114–115
- Ultramicrotomy, 65
- Ultrasonication, 145, 149, 181–182
- Ultrasonication-induced nanotube cutting, 232
- UV radiation, 167
- UV-Visible-NIR absorption spectroscopy, 287
- Vacuum-assisted processing, 399
- Vapor grown carbon fibers, 46
- Victrix PEEK, 284
- Vinyl polymer/ CNT nanocomposites
 - bulk polymerization, 225
 - disadvantages, 225
 - electrorheology, 243–246
 - free radical polymerization, 223–225
 - initiation, 223–224
 - propagation, 224
 - termination, 224
 - in-situ* radical polymerization in presence of CNT
 - addition of radicals onto CNT, 229–232
 - additional analyses, 233–235
 - CNT degradation, 232–233
 - polymer matrix, 228–229
 - in-situ* suspension polymerization, 243–246
 - microspheres
 - CNT material adsorbed onto polymer microspheres, 239–243
 - suspension polymerization, 225–228
 - advantages and disadvantages, 226
- Wet-spinning, 325, 326
- Wet-STEM, 72, 73
- Wettability, 233
- Wide angle X-ray diffraction (WAXS), 303
- Wrapping, 149, 292
- X-ray diffraction, 151
- Yarns, 324
- Zeolite grown, 10

Also of Interest

Check out these published and forthcoming related titles from Scrivener Publishing

Introduction to Industrial Polyethylene: Properties, Catalysts, Processes by Dennis P. Malpass. Published 2010. ISBN 978-0-470-625989.

Demystifies the largest volume manmade synthetic polymer by distilling the fundamentals of what polyethylene is, how it's made and processed, and what happens to it after its useful life is over.

A Concise Introduction to Additives for Thermoplastic Polymers by Johannes Karl Fink. Published 2010. ISBN 978-0-470-60955-2.

Written in an accessible and practical style, the book focuses on additives for thermoplastic polymers and describes 21 of the most important and commonly used additives from Plasticizers and Fillers to Optical Brighteners and Anti-Microbial additives. It also includes chapters on safety and hazards, and prediction of service time models.

Handbook of Engineering and Specialty Thermoplastics

Volume One: Polyolefins and Styrenics by Johannes Karl Fink. Published 2010. ISBN 978-0-470-62483-5.

Volume Two: Polyethers and Polyesters edited by Sabu Thomas and Visakh P.M. Forthcoming late 2010.

Volume Three: Nylons edited by Sabu Thomas and Visakh P.M. Forthcoming late 2010.

Volume Four: Water Soluble Polymers edited by Johannes Karl Fink. Forthcoming 2011.

Miniemulsion Polymerization Technology edited by Vikas Mittal. Forthcoming summer 2010.

The book is a ready reference for the background information as well as advanced knowledge regarding the applications of miniemulsion polymerization technology.

A Guide to Safe Material and Chemical Handling by Nicholas P. Cheremisinoff and Anton Davletshin. Published 2010. ISBN 978-0-470-62582-8

The volume provides an assembly of useful engineering and properties data on materials of selection for process equipment, and the chemical properties, including toxicity of industrial solvents and chemicals.